

# Polysaccharide Applications

Downloaded by on July 3, 2011 | <http://pubs.acs.org>  
Publication Date: August 20, 1999 | doi: 10.1021/bk-1999-0737.fw001

Downloaded by on July 3, 2011 | <http://pubs.acs.org>  
Publication Date: August 20, 1999 | doi: 10.1021/bk-1999-0737.fw001

ACS SYMPOSIUM SERIES 737

# Polysaccharide Applications

## Cosmetics and Pharmaceuticals

**Magda A. El-Nokaly**, EDITOR  
*The Procter and Gamble Company*

**Helena A. Soini**, EDITOR  
*The Procter and Gamble Company*



**American Chemical Society**  
American Chemical Society, Washington, DC  
**Library**  
**1155 16th St., N.W.**  
**Washington, D.C. 20036**

In Polysaccharide Applications; El-Nokaly, M., et al.;  
ACS Symposium Series; American Chemical Society: Washington, DC, 1999.

**Polysaccharide applications  
: cosmetics and**



**Library of Congress Cataloging-in-Publication Data**

Polysaccharide applications : cosmetics and pharmaceuticals / Magda A. El-Nokaly, Helena A. Soini, editors.

p. cm.—(ACS symposium series, ISSN 0097-6156 : 737)

Includes bibliographical references and index.

ISBN 0-8412-3641-0

1. Polysaccharides—Industrial applications Congresses.
2. Cosmetics Congresses.
3. Pharmaceutical chemistry Congresses.

I. El-Nokaly, Magda A., 1945– II. Soini, Helena A., 1956– . III. Series.

TP979.5.P6P65 1999  
661'.8—dc21

99-30375  
CIP

The paper used in this publication meets the minimum requirements of American National Standard for Information Sciences—Permanence of Paper for Printer Library Materials, ANSI Z39.48-94 1984.

Copyright © 1999 American Chemical Society

Distributed by Oxford University Press

All Rights Reserved. Reprographic copying beyond that permitted by Sections 107 or 108 of the U.S. Copyright Act is allowed for internal use only, provided that a per-chapter fee of \$20.00 plus \$0.50 per page is paid to the Copyright Clearance Center, Inc., 222 Rosewood Drive, Danvers, MA 01923, USA. Republication or reproduction for sale of pages in this book is permitted only under license from ACS. Direct these and other permissions requests to ACS Copyright Office, Publications Division, 1155 16th Street, N.W., Washington, DC 20036.

The citation of trade names and/or names of manufacturers in this publication is not to be construed as an endorsement or as approval by ACS of the commercial products or services referenced herein; nor should the mere reference herein to any drawing, specification, chemical process, or other data be regarded as a license or as a conveyance of any right or permission to the holder, reader, or any other person or corporation, to manufacture, reproduce, use, or sell any patented invention or copyrighted work that may in any way be related thereto. Registered names, trademarks, etc., used in this publication, even without specific indication thereof, are not to be considered unprotected by law.

PRINTED IN THE UNITED STATES OF AMERICA

**American Chemical Society  
Library**

**1155 16th St., N.W.**

**Washington, D.C. 20036**

# Advisory Board

## ACS Symposium Series

**Mary E. Castellion**  
ChemEdit Company

**Arthur B. Ellis**  
University of Wisconsin at Madison

**Jeffrey S. Gaffney**  
Argonne National Laboratory

**Gunda I. Georg**  
University of Kansas

**Lawrence P. Klemann**  
Nabisco Foods Group

**Richard N. Loepky**  
University of Missouri

**Cynthia A. Maryanoff**  
R. W. Johnson Pharmaceutical  
Research Institute

**Roger A. Minear**  
University of Illinois  
at Urbana-Champaign

**Omkaram Nalamasu**  
AT&T Bell Laboratories

**Kinam Park**  
Purdue University

**Katherine R. Porter**  
Duke University

**Douglas A. Smith**  
The DAS Group, Inc.

**Martin R. Tant**  
Eastman Chemical Co.

**Michael D. Taylor**  
Parke-Davis Pharmaceutical  
Research

**Leroy B. Townsend**  
University of Michigan

**William C. Walker**  
DuPont Company



# Foreword

**T**HE ACS SYMPOSIUM SERIES was first published in 1974 to provide a mechanism for publishing symposia quickly in book form. The purpose of the series is to publish timely, comprehensive books developed from ACS sponsored symposia based on current scientific research. Occasionally, books are developed from symposia sponsored by other organizations when the topic is of keen interest to the chemistry audience.

Before agreeing to publish a book, the proposed table of contents is reviewed for appropriate and comprehensive coverage and for interest to the audience. Some papers may be excluded in order to better focus the book; others may be added to provide comprehensiveness. When appropriate, overview or introductory chapters are added. Drafts of chapters are peer-reviewed prior to final acceptance or rejection, and manuscripts are prepared in camera-ready format.

As a rule, only original research papers and original review papers are included in the volumes. Verbatim reproductions of previously published papers are not accepted.

ACS BOOKS DEPARTMENT

# Preface

Polysaccharides are very important and much neglected ingredients in Nature. Proteins and biopolymers, from DNA to collagen, and presently even lipids, have had much positive publicity. But polysaccharides, and their special capacities for self organization, have remained by and large in *terra incognita*. They are very important molecules in cell adhesion as well as in the glycolipids of the brain and in plants. They are contained in most of the foods we eat, such as whole grains and vegetables. Although much recent academic interest has been shown, most research has resided in the hands of the formulators of industry. Research on products applications and performance are still very much an art form. The work, not less interesting because of that, is mainly unpublished. Polysaccharides are mostly biodegradable, derived from renewable resources, and commonly used in most cosmetics and pharmaceutical products, where they are the work horse molecules of the thickeners, fillers, gellants, delivery systems, film formers, and so on. The specialized researches on these materials (theoretical, chemical, physical, biological, and technological) have often been conducted in almost complete isolation of each other.

The purpose of the volume is to consolidate some current work in the subject of polysaccharide chemistry to bring synergism and interaction between researchers in the fields of cosmetic and pharmaceutical applications. We hope that by doing so, other researchers such as those in foods and pesticides will also derive some benefits.

International authors representing academia, industry, and governmental research centers have provided a balanced perspective in their presentations on the diverse facets of polysaccharides pertaining to their applications.

Several chapters cover modification of polysaccharides to optimize their performance, for example, in drug and vaccine delivery. The field is in its infancy. Immunologists have only recently begun to realize that adsorption of proteins on adjuvants such as aluminum hydroxide particles are essential to vaccine effectiveness. Presentation of proteins and antigens at the cell surface in the right structural form and environment is clearly the key to recognition, which must be through the polysaccharide coating of all surfaces. Hence presentation of agents within cell surface compatible polysaccharide vehicles must be a promising area of some importance. Chapter 1 presents information on an alginate microparticles for vaccine delivery, whereas Chapter 2 covers gene delivery via quaternary chitosan. Cyclodextrin-drug complexation in the presence of soluble polymers and their performance in percutaneous transport is discussed in Chapter 3. Some remarkable new molecular tubes and other peculiar structures that can be tailored at will for host-guest systems are presented in Chapter 4. Chapter 5 introduces research on cyclodextrin-linked chitosan technologies, whereas Chapter 6 covers chitin-PEG systems for drug



delivery. Silicified microcrystalline cellulose as a novel pharmaceutical material is discussed in Chapter 7 and thermoreversible sucrose hydrogel in Chapter 8.

These chapters present the state of the art in this obviously important area. Another group of chapters form a nice complement to Chapters 1–8. They are concerned with a fundamental question related to the first—What is the microstructure of surfactant-polysaccharide, or polysaccharide–other polymer self-assembled aggregates? Chapters here span a diversity of mixed systems—chitosan–pluronic networks and protein transport within them in Chapter 12. Those systems form the basis of emerging bacterial-resistant membrane technologies, an area of much activity, which has not been publicized previously. Chapters 13–15 deal with the physical chemistry and microstructure of polysaccharide-surfactant gels. Chapters 16 and 17 address the rheology of emulsions, and the wide range of properties that can be accessed with polysaccharide polymers. Then to complement these, in turn, we have a further group of contributions showing new usable analytical techniques for characterization of these systems. These include ultrasonic techniques (Chapter 18) for concentrated polymer dispersions, fluorescence microscopic studies of polysaccharide adsorption (Chapter 19), small-angle neutron scattering (Chapter 20), gel-permeation chromatography combined with multi-angle light scattering applied to characterization of polysaccharides (Chapter 21), and finally, capillary electrophoresis in starch analysis (Chapter 22). The final group of chapters (Chapters 18–22) deals with some new explorations of polysaccharide hydration (a core issue, hardly researched so far). Therefore, any progress toward understanding the recognition specificity of carbohydrate isomers is important. The novel work of Chapters 9 and 10 and the major review in Chapter 11 on cellulosic liquid crystals contribute to the issue as well.

We believe, the chapters provide a nice complementary balance, which will be of value not only to experts but also to workers who wish to enter this field. In spanning so wide a range of applications the contributions provide a ready access to a scattered literature that is very difficult for even specialists to locate.

Although the editors worked hard to present a comprehensive view of the field, the resulting collection reflects the fact that most application studies have not been published. We hope this volume will stimulate more exchange, dialogue, and learning between academia and industry.

## Acknowledgments

We thank the American Chemical Society's (ACS) Cellulose, Paper, and Textile Division and Macromolecular Secretariat for sponsoring the symposium and the Procter and Gamble Company for their financial support. Special thanks are due to Procter and Gamble Managers Fernando Benvegnu, R&D, Corporate Re-

search and Development; Grover Owens, Recruiting Office; Ken Smith, Food and Beverage Technology; Mark Grote, OTC–Health Care Technology; and Charles Hong, Corporate New Ventures.

We thank each of the contributing authors for their cooperation, without which there would be a book. Many thanks to the editorial staff of the ACS Books Department, especially Anne Wilson, for her professional support. Last, but not least, we acknowledge with many thanks the secretarial and other support of Pat Ehrhardt.

MAGDA A. EL-NOKALY  
The Procter and Gamble Company  
Miami Valley Laboratory  
P.O. Box 538707  
Cincinnati, OH 45253–8707

HELENA A. SOINI  
The Procter and Gamble Company  
Miami Valley Laboratory  
P.O. Box 538707  
Cincinnati, OH 45253–8707

## Chapter 1

# Alginate Microparticles for Vaccine Delivery

M. A. Suckow<sup>1</sup>, L. Siger<sup>2</sup>, T. L. Bowersock<sup>3</sup>, J. J. Turek<sup>2</sup>, D. Van Horne<sup>2</sup>,  
D. Borie<sup>2</sup>, A. Taylor<sup>4</sup>, H. Park<sup>4</sup>, and K. Park<sup>4</sup>

<sup>1</sup> Freimann Life Science Center, University of Notre Dame, Notre Dame, IN 46556

<sup>2</sup> School of Veterinary Medicine, Purdue University, West Lafayette, IN 47907

<sup>3</sup> Pharmacia & Upjohn, Inc., Kalamazoo, MI 49001

<sup>4</sup> School of Pharmacy, Purdue University, West Lafayette, IN 47907

Many pathogens initially establish infection on the mucosal surfaces lining the respiratory and gastrointestinal tracts in both man and animals. Although immunization against infectious pathogens is frequently effective, efficacy could be enhanced if directed specifically to the mucosal surfaces. Oral immunization in particular would be advantageous, since large numbers of individuals could be quickly and easily immunized, possibly through the feed or drinking water. Efforts at oral immunization are hampered by dilution and destruction of antigens within the harsh environment of the gastrointestinal tract. Encapsulation of antigen in alginate microparticles was examined as a means to orally immunize rabbits against the important bacterial pathogen, *Pasteurella multocida*. Initial studies in mice showed that the bacterial load of microparticles could be reduced by a factor of  $10^3$  by boiling, but that this process diminished the immunogenicity of a potassium thiocyanate extract of *P. multocida* (PTE) incorporated into the microparticles. Studies in rabbits showed that incorporation of PTE into alginate microparticles allowed effective immunization through the drinking water. Alginate microparticles can be used for immunization against infectious disease; however, alternative methods for sterilization will need to be pursued.

Infectious disease related to viruses, bacteria, fungi, and parasites is a major cause of morbidity and mortality in animals and humans worldwide. An example in an animal model is *Pasteurella multocida*, which is the most common bacterial pathogen of domestic rabbits. Although infection may be subclinical, disease characterized by rhinitis, pneumonia, abscessation of viscera and subcutaneous sites, metritis, orchitis, septicemia, and otitis interna may occur (1). Losses due to *P. multocida*-related disease pose a serious problem for those using rabbits in research and for production of food and fiber.

Although efficacious therapeutic measures have been developed for many such diseases, including lapine Pasteurellosis (2,3), specific treatment is hampered by expense, limited supply of some antimicrobial compounds, and noncompliance by patients with respect to scheduled self-medication. Rather, vaccination is widely viewed as a means to induce lasting immunity to large numbers of individuals at relatively little expense and without the need for self-medication.

Standard vaccination methods have typically relied on parenteral immunization, usually by intramuscular injection of the vaccine. Such methods stimulate the humoral arm of the immune system to produce antibody, a glycoprotein which is created in response to immunogenic stimulation and which may interact with specific antigens. If the antigen represents a key epitope of the infectious agent, the interaction with antibody can facilitate inactivation of the agent. A number of antigenic preparations have been examined as potential vaccine candidates for immunization of rabbits against Pasteurellosis, including lipopolysaccharide (4), outer membrane proteins (5), and potassium thiocyanate extracts (6,7) by intramuscular or subcutaneous routes of administration.

Although spectacularly successful for protection against some infectious agents, parenteral immunizations has several limitations. First, injection site reactions may occur. In the case of feline leukemia virus vaccination, injection site reactions have been associated with eventual development of sarcoma (8,9). Second, injection of vaccine can be painful for some individuals, leading many to avoid participation in vaccination programs. Third, parenteral immunization typically stimulates elaboration of serum antibody by plasma cells, particularly IgG. In contrast, many infectious agents, including *P. multocida*, initially access the body at mucosal surfaces, such as those lining the gastrointestinal, respiratory, and genitourinary tracts.

Immunization by delivery of vaccine directly at mucosal surfaces has been shown to be a promising alternative to parenteral vaccination. At mucosal sites, secretory IgA (sIgA) is the predominant antibody isotype present. Elaboration of sIgA at mucosal surfaces represents, then, a first-line immunological defense against many infectious agents. For example, presence of sIgA specific to epitopes on influenza virus on surfaces of the upper respiratory tract following

vaccination strongly correlate with resistance of individuals to challenge with infectious influenza (10,11).

There are many examples of the use of locally administered vaccines that stimulate a protective immune response to bacterial pathogens. These include use of a temperature-sensitive mutant of *Bordetella bronchiseptica* administered intranasally to dogs to induce protection against the bacterial component of kennel cough (12); aerosolization of *P. multocida* to chickens (and inhalation of the inhaled vaccine) is a practical as well as effective method of vaccinating a large number of birds against that pathogen (13); and an attenuated *Salmonella choleraesuis* var. *kunzendorf* vaccine used to prevent disease in swine when administered either orally or intranasally (14).

Induction of immunity at mucosal surfaces requires administration of antigen directly to a mucosal site. Interestingly, the mucosal immune system is linked, such that exposure to an immunogen at one mucosal surface can result in secretion of sIgA onto other mucosal surfaces. This phenomenon is due to stimulated antigen-specific B lymphocytes (plasma cell precursors) entering the lymphatic and general circulation from the stimulated mucosal site and dispersing to distant mucosal sites. In transit, these cells enter local draining lymph nodes, such as the mesenteric lymph nodes that drain the gastrointestinal tract, where they undergo further differentiation and maturation. Most of the differentiated plasma cells preferentially home back to the originating mucosal tissue; however a significant number also migrate to the other mucosal sites. Although the homing of lymphocytes to mucosal sites is not fully understood, special receptors on endothelial venule cells and lymphocytes (selectins and integrins) are thought to interact to allow extravasation of lymphocytes selectively into the lamina propria of mucosal sites (15). The lamina propria is the effector site of the mucosal immune system where plasma cells produce primarily IgA, and T cell-mediated response occur.

Mucosal immunization by oral administration of vaccines is a particularly appealing potential method for stimulating protective immunity. Theoretically, vaccines could be administered in the feed or drinking water by this means. Oral vaccination has the advantages of limited possibility of reaction to the vaccine, high acceptability by patients, ease of administration, and low cost. In the case of rabbits, a vaccine delivered in the drinking water would allow quick immunization of a large number of animals and with little stress or risk of handling-related injury to both animals and handlers. Despite these advantages, development of oral vaccines has been slow. Primary among the limitations to development is the degradation of important vaccine components by bacteria, enzymes, and low pH within the gastrointestinal tract. Furthermore, dilution and loss of antigen in ingesta as well as poor diffusion through the mucus layer on intestinal villi prevent antigen from being taken up by the lymphoid tissue.

Microencapsulation is a unique way to protect antigens and stimulate their

uptake by Peyer's patches, sites of lymphoid tissue in the gastrointestinal tract (16). Incorporation of antigen into microparticles has been shown to be an effective means of inducing serum and secretory antibody responses following oral immunization (17). One of the most common materials used to encapsulate antigens is poly-(D,L-lactide-co-glycolide) (DL-PLG). Although DL-PLG particles are readily taken up by Peyer's patches, where the antigen is then processed by the immune system, their production requires organic solvents and high temperatures which could threaten the integrity of fragile antigens.

Sodium alginate is a natural polysaccharide extracted from the brown seaweed, *Macrocystis pyrifera*. Alginic acid is an unbranched (1-4)-linked glycuronan. The linear copolymer is composed of two monomeric units, D-mannuronic acid and L-guluronic acid. The monomers are arranged within the alginate molecule as a series of block structures which may be homopolymeric, heteropolymeric, or alternating sequences.

Alginate block structures are all polyionic and will form intermolecular bonds with d- or multi-valent cations. These polyvalent cations react and crosslink the alginate polymer. Zinc is particularly effective at inducing gel formation, because it increases gel strength by non-selectively cross-linking MM and GG blocks in adjacent alginate polymers (18). As the concentration of polyvalent ion in the solutions increases, the alginate polymer increases in viscosity, and eventually gels into a solid material. The resulting gel consists of polymerized alginate in a three dimensional egg crate-like lattice (18). Alginate microspheres can be produced at room temperature and in the absence of organic solvents or other harsh conditions which might damage protein immunogens prior to encapsulation. Alginate has been used for incorporation living beta-islet cells for the experimental treatment of diabetes mellitus (19) as well as immunogens for delivery to lymphoid tissues in a variety of species (20). Because it readily forms gels and is non-toxic, alginate is a common additive (thickener) in many food and pharmaceutical products.

## Materials and methods

**Preparation of antigen.** Potassium thiocyanate extract (PTE) of *P. multocida* (serotype 3,12,15:D) prepared as previously described (7) was used as the antigen in this study. Briefly, *P. multocida* was grown to confluence on tryptic soy agar containing 5% sheep blood and harvested in 6 ml of equal parts saline and 1.0 M KSCN. Following incubation at 37° C for 6 hours, whole cells were removed by centrifugation at 8000 g for ten minutes, and the supernatant was dialyzed extensively against 0.01 M Tris-hydrochloride-0.32 M NaCl-0.01% NaN<sub>3</sub> buffer (pH 8.0). The extract was then concentrated with a Centriprep-10 concentrator (Amicon, Inc., Beverly, MA, USA) and sterilized by passage through a 0.22 μm filter.

**Production of microparticles.** Alginate microparticles were prepared as

previously described (21) to contain either 100  $\mu\text{g}$  or 5 mg per ml of a potassium thiocyanate extract of the bacteria *Pasteurella multocida* (6). Briefly, sodium alginate, medium viscosity (Keltone LV<sup>®</sup>, Monsanto, St. Louis, MO) was dissolved in distilled water at a 2% w/v concentration with constant stirring. PTE was added to the alginate solution to create a final alginate concentration of 1.2% w/v. An additional batch was similarly prepared but with no added protein. The mixture was placed in a syringe pump (Pump 44; Harvard Instruments, Inc., South Natick, MA) and infused into an atomizer (Turbotak, Inc., Ontario, Canada). The alginate/PTE mixtures were then sprayed into a 1.5% w/v  $\text{CaCl}_2$  solution placed approximately 40 cm from the tip of the atomizer. Particles were separated from the  $\text{CaCl}_2$  solution by low-speed centrifugation and placed in a 0.05% solution of poly-L-lysine (MW 100,000; Sigma Chemical Co., St. Louis, MO) with stirring for 30 minutes at room temperature. The size of the alginate particles ranged from 1  $\mu\text{m}$  to larger than 50  $\mu\text{m}$  in diameter, with 70% of the particles less than 10  $\mu\text{m}$  in diameter as measured by a Microtrak Series 9200 particle analyzer (Leeds and Northrup Co., Northwales, PA).

Portions of each batch of microparticles containing either 100  $\mu\text{g}$  of PTE/ml or no added protein were boiled in an attempt to sterilize the material. In this regard, microparticles were brought to a temperature of 100° C by placing a glass tube containing the microparticles in a beaker of boiling water for a period of 10 minutes. After cooling, an aliquot of microparticles was subjected to bacteriological culture and the rest used to immunize mice. Microparticles containing 5 mg of PTE/ml were not boiled and were used to immunize rabbits.

Enumeration of the microparticle bacterial load was performed on microparticles before and after boiling by decanting fluid once the microparticles had settled to the bottom of a 15-ml conical centrifuge tube. Fifty  $\mu\text{l}$  of microparticles were added to 950  $\mu\text{l}$  of phosphate buffered saline (pH 7.4) with 0.1 M EDTA. The suspension was thoroughly mixed on a high speed vortex for 3 min, and the microparticles allowed to settle to the bottom of the tube over 30 min. One hundred  $\mu\text{l}$  of the supernatant was then plated for lawn growth on tryptic soy agar with 5% sheep blood. After 24 hours of incubation at 37°C, bacterial colony forming units were counted on each plate.

**Electron microscopy of microparticles.** Microparticles were prepared for electron microscopy using previously described methods (22). Briefly, 100  $\mu\text{l}$  of microparticles were allowed to settle to the bottom of a 1.5 ml microcentrifuge tube. The supernatant  $\text{CaCl}_2$  solution was removed and replaced with 1% of  $\text{OsO}_4$  in distilled water. The microparticles were gently dispersed in the  $\text{OsO}_4$  by shaking every 10 minutes and held at 20°C for 1 hour. The microparticles were then allowed to settle by gravity followed by centrifugation at 200  $\times g$  for 1 minute. Supernatant was removed and the particles were washed twice with distilled water. For preparation for scanning electron microscopy, particles were dehydrated through a 30-100% ethanol gradient, washed twice in freon-113, and

then pipetted onto a nucleopore filter for mounting on a specimen stub. The particles were sputter coated with gold and viewed on a scanning electron microscope (Model ISI-100A, Topcon Technologies, Inc., Paramus, NJ). Electron micrographs were taken of typical fields.

**Animals.** All animal studies were approved by the Institutional Animal Care and Use Committee and conducted in a manner consistent with regulatory policy. Rabbits used were *Pasteurella*-free New Zealand White males, weighing 2.0-2.4 kg (Covance, Inc., Kalamazoo, MI). Ten to twelve week-old female Balb/c mice obtained from the Purdue University Biological Sciences Breeding Colony were used in these studies. Each experimental group was housed in a separate cage.

**Mouse immunization studies.** Groups of five mice were immunized subcutaneously with 500  $\mu$ l of either nonboiled or boiled microparticles containing 100  $\mu$ g/ml of PTE. All mice were immunized initially and boosted 21 days later. Serum was harvested by retroorbital venipuncture prior to and 28 days following initial immunization. Blood collection was performed on mice which were anesthetized by inhalation of methoxyflurane (Metofane<sup>®</sup>, Pitman-Moore, Inc., Mundelein, IL). Mice were humanely euthanized 28 days after initial immunization. Serum samples were frozen at -20° C until used for enzyme-linked immunosorbent assay.

**Rabbit immunization and challenge studies.** Groups of five rabbits were immunized by placing 5.0 ml of microparticles with either no added protein or 5 mg of PTE protein/ml in the drinking water on days 0, 7, and 14. In addition, a group of rabbits was provided on those same days with drinking water that was mixed with 25 mg of PTE protein not incorporated into microparticles. A fourth group was provided with fresh water containing no added materials. Water was withheld for 12 hours prior to immunization, and microparticles were mixed in 20 ml of tap water to ensure that the full dose of vaccine would be ingested. All rabbits ingested the full dose of vaccine within 2 hours and were then offered *ad libitum* access to additional fresh water. Serum and nasal lavage samples were collected from the rabbits on days 0 (day of initial immunization), 10, 16, and 21.

Additional groups of five rabbits were immunized as described above and inoculated intranasally on Day 16 with  $1.0 \times 10^6$  colony forming units (CFUs) of live *P. multocida* in 1.0 ml of sterile saline. In addition, a nonimmunized, nonchallenged group was included in the study. One week after challenge with *P. multocida*, rabbits were humanely euthanized with an intravenous overdose of sodium pentobarbital. The lungs, liver, and nasopharynx were cultured for *P. multocida* at 37° C on tryptic soy agar (TSA) with 5% sheep blood. For quantitative comparison, bacteriologic evaluation of lungs was performed by macerating a 1 gram sample from the apical portion of the left cardiac lobe in 2.0 ml of sterile saline and the number of *P. multocida* present enumerated by



culturing 100  $\mu$ l of 1:10 to 1:10,000 10-fold dilutions of this suspension on plates of TSA with 5% sheep blood. The nasopharynx was vigorously swabbed, the swab vortexed at high speed for 15 seconds in 2.0 ml of sterile saline, and the number of *P. multocida* present quantified by culturing 100  $\mu$ l of 1:10 to 1:10,000 10-fold dilutions of this suspension. Colony forming units of *P. multocida* were counted following 24 hours of growth. The cut-surface of the liver was aseptically swabbed and cultured non-quantitatively for the presence of *P. multocida*.

**Enzyme-linked immunosorbent assay.** Serum and nasal lavage samples were assayed for anti-PTE IgG or IgA antibody activity as previously described (7). Briefly, wells of a polystyrene microtiter plate (Immulon 2, Dynatech Laboratories, Chantilly, VA) were each coated with either 0.5  $\mu$ g of PTE protein per well for assay of mouse samples or 10  $\mu$ g of PTE protein diluted in phosphate buffered saline (PBS, pH 7.4) per well for assay of rabbit samples. Immediately before testing samples, PTE was removed and the wells washed with PBS containing 0.05% (v/v) Tween 20 followed by a 1-hour incubation at room temperature with 0.1% gelatin (Sigma Chemical Co.) to block non-specific binding.

Mouse sera were serially diluted from 1:25 to 1:25,600 and added at 50  $\mu$ l per well, in triplicate. Rabbit nasal lavage samples were added to wells undiluted, while rabbit serum samples were diluted 1:20 in PBS-Tween 20 and added to wells. After incubation and washing of wells, 50  $\mu$ l of peroxidase conjugated goat antibodies to mouse IgG or IgA (Bethyl Laboratories, Montgomery, TX) were added to each well that had contained mouse sera, whereas peroxidase conjugated sheep anti-rabbit IgA (Accurate Chemical and Scientific, Inc., Westbury, NY) or peroxidase conjugated goat anti-rabbit IgG (Sigma Chemical Co.) was added to wells that had contained samples from rabbits.

Following further incubation and washing of wells, substrate (0-phenylaminediamine, Sigma Chemical Co.) was added to each well and optical density at 490 nm measured 30 minutes later in a Vmax microplate reader (Molecular Devices, Inc., Menlo Park, CA). Data are presented for mouse samples as the greatest dilution with detectable activity at least three standard deviations greater than the negative control wells, and for rabbits as optical density at 490 nm after 30 minutes of incubation.

## Results and Discussion

**Bacterial load of microparticles.** Results from bacterial culture of microparticles showed that non-boiled microparticles had a bacterial load of  $2 \times 10^7$  CFUs/ml, while the bacterial load of boiled microparticles was  $2 \times 10^4$  CFUs/ml. Thus, while boiling was unable to completely sterilize the microparticles, it did achieve a 1000-fold reduction in the overall bacterial load. None of the bacteria cultured demonstrated colony morphology suggestive of *P. multocida*.

**Electron microscopy.** Most unboiled microparticles had generally smooth surfaces and minimal aggregation of spheres (Figure 1). In contrast, boiled microparticles demonstrated uneven surfaces with moderate pitting and aggregation (Figure 2), however they appeared to be intact with no rupture or destruction of the microparticles.

**Enzyme-linked immunosorbent assay.** Results for ELISA tests of mouse sera are shown in Table 1. These data indicate that boiling of the microparticles greatly diminishes the immunogenicity of incorporated PTE. This may or may not be the case for other antigens, although other strategies for reduction of bacterial load, such as gamma irradiation or greater control for sterile procedures during the production process might be of greater use. Because the gastrointestinal tract is not a sterile environment, the need for sterility of orally administered compounds is of less consequence compared to those administered parenterally. For this reason, and because of the potential for damage to incorporated PTE, non-boiled microparticles were used for oral immunization trials in rabbits.

**Table 1. Anti-PTE IgG activity in mouse sera of boiled and non-boiled microparticles<sup>a</sup>**

| Treatment Group                 | Average Positive Titer Before Immunization ( $\pm$ S.D.) | Average Positive Titer After Immunization ( $\pm$ S.D.) |
|---------------------------------|--|---|
| Microparticles + PTE, nonboiled | 300 ( $\pm$ 3)   | 22,800 ( $\pm$ 11)                                      |
| Microparticles + PTE, boiled    | 163 ( $\pm$ 3)   | 388 ( $\pm$ 4)  |

<sup>a</sup>No appreciable anti-PTE IgA activity was detected in any samples. Values shown are average titers measured at 490 nm following 30 minutes incubation with substrate (ortho-phenylaminediamine).

Results for ELISA testing of rabbit serum and nasal lavage samples are shown in Figures 3 and 4, respectively. Immunization of rabbits with PTE incorporated into microparticles stimulated significantly greater anti-PTE IgG activity in the serum (Figure 3) and IgA activity in nasal lavage samples (Figure 4) than any of the other treatments. Appreciable serum anti-PTE IgA nor nasal lavage IgG were not detected in samples from any rabbits. These results show that incorporation of PTE into microparticles significantly improves specific antibody activity against *P. multocida*.

**Rabbit challenge studies.** Mean numbers of *P. multocida* CFUs cultured from the lungs and nasopharynx of rabbits are shown in Figure 5. Significantly

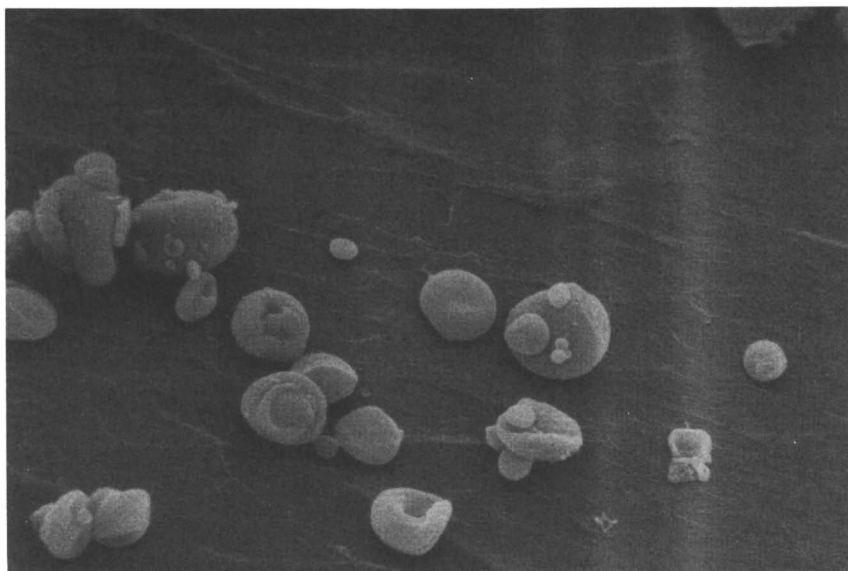


**Figure 1.** Scanning electron micrograph of unboiled microparticles (magnification 3000X).

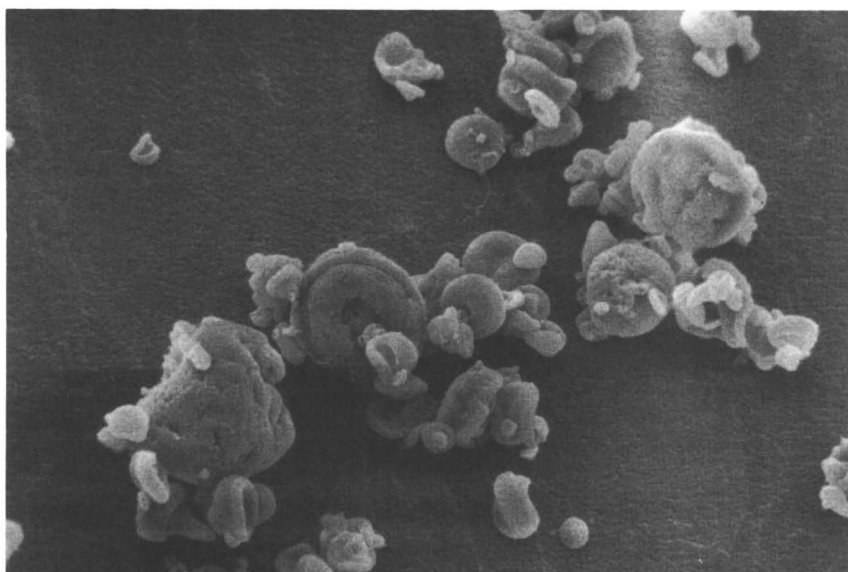


**Figure 2.** Scanning electron micrograph of boiled microparticles (magnification 3000X).

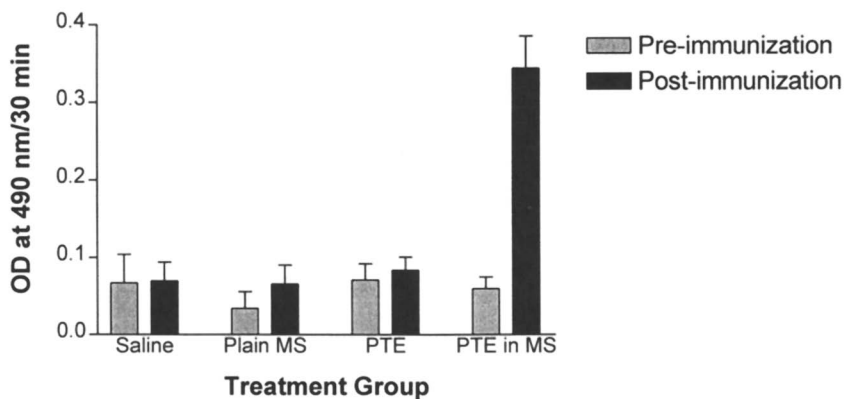


**Figure 3.** Anti-PTE IgG activity in rabbit serum samples.

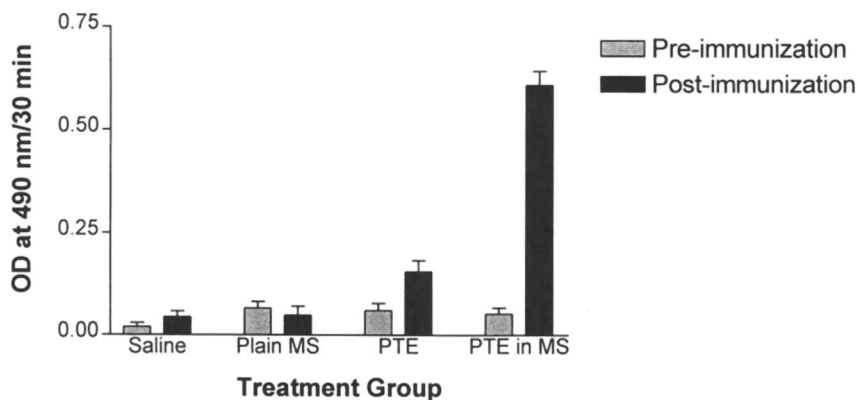


**Figure 4.** Anti-PTE IgA activity in rabbit nasal lavage samples.

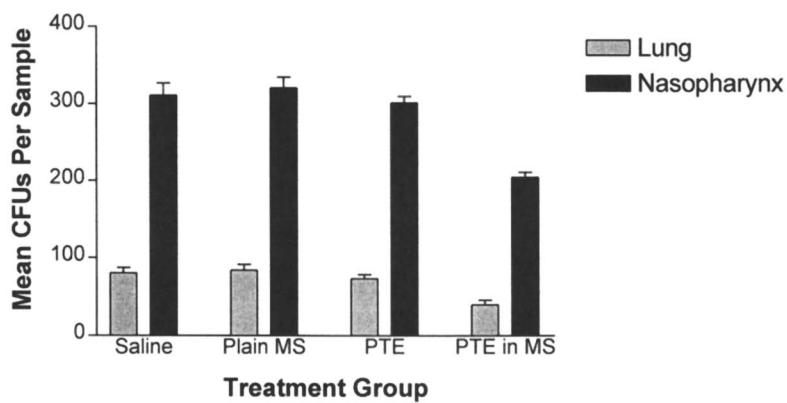


**Figure 5.** Mean *P. multocida* colony forming units (CFUs) cultured from challenged rabbits.

fewer CFUs were cultured from both sites in rabbits immunized with PTE in microparticles compared to rabbits in all other treatment groups. There were no other significant differences between groups. *P. multocida* was cultured from 2/5 livers from rabbits immunized with microparticles with no added protein and from 1/5 livers from rabbits immunized with PTE not in microparticles. *P. multocida* was not cultured from the livers of rabbits in either of the remaining treatment groups. These results demonstrate that oral immunization of rabbits with PTE incorporated into microparticles stimulates significant protective immunity to challenge with live *P. multocida*.

### Summary

Oral vaccination is a simple, efficient means of inducing immunity to infectious pathogens such as *P. multocida* which colonize mucosal surfaces. Effective oral vaccines must overcome problems related to destruction and dilution of the antigen in the harsh environment of the gastrointestinal tract. We have shown that encapsulation of vaccines into alginate microparticles is an effective method for delivery of an oral vaccine.

Rabbits immunized with PTE incorporated into microparticles developed a strong antibody response which was associated with protection against challenge with live *P. multocida*. It seems likely that the alginate microparticles served to protect PTE as it traversed through the gastrointestinal tract to lymphoid tissues such as Peyer's patches. It is also possible that particles such as alginate microparticles are taken up by lymphoid tissues to a greater extent than soluble substances such as PTE. Uptake of particles by gastrointestinal lymphoid tissues is greatest when particles are less than 10  $\mu\text{m}$  in diameter (23, 24). The number and concentration of Peyer's patches likely varies between species and ages, thus additional work will need to be conducted to determine the utility of oral vaccination using alginate microparticles in other species.

Boiling of alginate microparticles containing PTE reduced the bacterial load by a factor of  $10^3$ , however bacterial contamination was still great. Furthermore, the process of boiling apparently destroyed the immunogenicity of incorporated PTE, as evidenced by greatly reduced antibody responses of mice following subcutaneous immunization. Taken together, these results argue against boiling of alginate microparticles as a means to prepare sterile vaccines. As temperature increases from 25 - 80° C, the viscosity of alginate in solution decreases. However, exposure of the microparticles to temperatures exceeding 80° C did not appreciably alter the polymerized microparticles; they were still intact, did not lose their polymerized state, and can retain antigens other than that reported in this study. This emphasizes the need to examine the stability of each antigen when the microparticles are exposed to such extremes in conditions. In subsequent experiments, we have successfully encapsulated antigens without bacterial contamination by sterilizing all equipment and handling the materials in

a controlled aseptic environment. Such care would eliminate the need for post-production sterilization. One advantage of oral delivery of vaccines is that such preparations would not need to be completely sterile since the gastrointestinal tract already contains considerable microbial flora.

The difficulty with sterilization of polymerized material, specifically alginate, has been investigated by others (25). In that study, chlorine was investigated as a means of reducing the number of bacteria entrapped within alginate gels. Although the purpose of the study was to use alginate as a model to determine the ability of chlorine to penetrate bacterial biofilms, it did show that alginate could not be well penetrated by chlorine to kill bacteria.

In conclusion, the results support the concept that oral immunization with alginate-microencapsulated vaccine may be a practical and effective means of immunizing rabbits, and possibly other animals or humans, against infectious disease.

## References

1. DeLong, D.; Manning, P.J. *The Biology of the Laboratory Rabbit*; Academic Press, Inc.: Orlando, FL; **1994** Chapter 8, pp131.
2. Broome, R.L.; Brooks, D.L. *Lab. Anim. Sci.*, **1991**, *41*, 572.
3. Suckow, M.A.; Martin, B.J.; Bowersock, T.L.; Douglas, F.A. *Vet. Microbiol.*, **1996**, *51*, 161.
4. Manning, P.J. *Infect. Immun.*, **1985**, *44*, 502.
5. Lu, Y.S.; Afendis, S.J.; Pakes, S.P. *Infect. Immun.*, **1988**, *56*, 1532.
6. Ringler, D.H.; Peter, G.K.; Chrisp, C.E.; Keren, D.F. *Infect. Immun.*, **1985**, *49*, 498.
7. Suckow, M.A.; Bowersock, T.L.; Nielsen, K.; Grigdesby, C.F. *Lab. Anim.*, **1996**, *30*, 120.
8. Hendrick, M.J.; Kass, L.D.; McGill, L.D.; Tizard, I.R. *J. Nat. Cancer Inst.*, **1994**, *86*, 341.
9. Doddy, F.F.; Glickman, L.T.; Glickman, N.W.; Janovitz, E.B. *J. Comp. Pathol.*, **1996**, *114*, 165.
10. Walmann, R.H.; Stone, J.; Bergmann, K.C.; Khakoo, R.; Lazell, V.; Jacknowitz, A.; Walman, E.R.; Howard, S. *Am. J. Med. Sci.*, **1986**, *292*, 367.
11. Bergmann, K.C.; Walmann, R.H.; Tischner, H.; Pohl, W.D. *Int. Arch. Allergy Appl. Immunol.*, **1986**, *80*, 107.
12. Keil, D.J.; Fenwick, B. *J. Am. Vet. Med. Assoc.*, **1998**, *212*, 200.
13. Hofacre, C.L.; Glisson, F.R.; Kleven, S.H. *Avian Dis.*, **1987**, *31*, 260.
14. Kramer, T.T.; Roof, M.B.; Matheson, R.R. *Am. J. vet. Res.*, **1992**, *53*, 444.
15. Butcher, E. *Curr. Top. Microbiol. Immunol.*, **1986**, *128*, 85.
16. Eldridge, J.H.; Stass, J.K.; Meulbroek, J.A.; McGhee, J.R.; Tice, T.R.; Gilley, R.M. *Mol. Immunol.*, **1991**, *28*, 287.

17. Mathowitz, E.; Jacobs, J.S.; Jong, Y.S.; Carino, G.P.; Chickering, D.E.; Chaturvedi, P.; Santos, C.A.; Vijayaraghavan, K.; Montgomery, S.; Bassett, M.; Morrell, C. *Nature*, **1997**, *386*, 410.
18. Smidsrod, O. *Faraday Disc.*, **1974**, *57*, 263.
19. Lim, F.; Sun, A.M. *Science*, **1980**, *210*, 908.
20. Bowersock, T.L.; HogenEsch, H.; Suckow, M.; Porter, R.E.; Jackson, R.; Park, H.; Park, K. *J. Control. Rel.*, **1996**, *39*, 209.
21. Kwok, K.K.; Groves, M.J.; Burgess, D.J. *Pharmaceut. Res.*, **1991**, *8*, 341.
22. Bowersock, T.L.; HogenEsch, H.; Suckow, M.A.; Turek, J.; Davis-Snyder, E.; Borie, D.; Jackson, R.; Park, H.; Park, K. *Hydrogels and Biopolymers for Bioapplications*; American Chemical Society Symposium Series, Washington, D.C., **1996**, Vol. 627, Chapter 6, pp 58-66.
23. Eldridge, J.H.; Gilley, R.M.; Stass, J.K. *Curr. Top. Microbiol. Immunol.*, **1989**, *146*, 58.
24. Porter, R.E.; Suckow, M.A.; Macri, N.P.; Bowersock, T.L. *Avian Dis.*, **1997**, *41*, 981.
25. Xu, X.; Stewart, P.S.; Chen, X. *Biotech. Bioengineer.*, **1996**, *49*, 93.



## Chapter 2

# Gene Delivery by Quaternary Chitosan with Antennary Galactose Residues

Tatsuro Ouchi, Jun-ichi Murata, and Yuichi Ohya

Department of Applied Chemistry, Faculty of Engineering,  
Kansai University, Suita, Osaka 564-8680, Japan

Chitosan is a non-toxic and biocompatible amino-type of polysaccharide. Quaternary chitosan can form polyelectrolyte complexes with DNA. Theoretically, it could be used as a carrier of DNA in gene delivery systems. However, chitosan itself has no recognizable efficacy. On the other hand, it is well known that polysaccharides play important roles in biological recognition on cellular surfaces. The "cluster effect" has been recently noted in biological recognition by carbohydrate-receptor binding in relation to cell-cell interaction. Therefore, a multi-antennary sugar chain may be effective in the application for cellular recognition devices. In order to achieve an effective gene delivery *via* receptor-mediated endocytosis, we designed *N,N,N*-trimethyl(TM)-chitosan/tetragalactose antenna conjugate (TC-Gal4A). The interaction between the TC-Gal4A conjugate and RCA<sub>120</sub> lectin was investigated as a simple model experiment by using a biosensor based on surface plasmon resonance. In order to investigate specific delivery of DNA by the TC-Gal4A conjugate, the expression of  $\beta$ -galactosidase activity by the TC-Gal4A/DNA (pSV $\beta$ Gal plasmid) complex was evaluated in HepG2 cells. The conjugate showed high binding affinity against RCA<sub>120</sub> and the complex expressed significant  $\beta$ -galactosidase activity.

It has been suggested that the "cluster effect", an increase in the binding strength beyond that expected from the increase in galactose concentration, is dependant on the maximum spatial inter-galactose distance, the flexibility of the arm connecting galactosyl residue, and the branch point (1, 2). Consequently, a multi-antennary sugar chain is expected to be very effective in the application for cellular recognition device.

Recently, the gene therapy involving the delivery of genes to target cells has become a topic in medical chemistry. The gene-transfer methods that adopt natural receptor-mediated endocytosis pathways for the delivery of DNA into target cells have been developed. Ligands for cellular receptors, such as transferrin (3, 4), viral

proteins (5), insulin bound to albumin (6), and asialoorosomuroid (7, 8) have been used for the import of the DNA molecule. For this purpose, these ligands have been conjugated to DNA-binding compounds, such as a polycation and an intercalating agent. Incubating DNA with these protein conjugates generates ligand-coated DNA which can bind receptors to the cellular surface and is subsequently internalized.

Chitosan is a cationic natural polysaccharide capable of forming polyelectrolyte complexes with DNA. However, chitosan itself has no recognizable efficacy as a carrier of DNA in gene delivery systems. Also it is sparingly soluble in water, except at acidic pH. In order to achieve an efficient gene delivery *via* receptor-mediated endocytosis (Figure 1), we have designed quaternary chitosan conjugates with galactose residues, *N,N,N*-trimethyl(TM)-chitosan/galactose conjugates (9), and quaternary chitosan conjugate with antennary galactose residues, TM-chitosan/tetragalactose antenna conjugate (10). In this paper, we discuss the polyelectrolyte complex formation with DNA, the cellular recognition ability of these conjugates, and the specific gene delivery by the polycation-DNA complex. Moreover, we describe the cluster effect of tetra-antennary galactose residues and the effect of local galactose concentration on these conjugates.

## Experimental

**Materials and methods.** Chitosan was provided by Kimitsu Chemical Industries, Ltd. pSVluc and Maker 1 (Lambda phage DNA/Hind III digest) were purchased from Wako Pure Chemical Industries. Biotin labeled lectin from Ricinus communis agglutinin-120 (RCA<sub>120</sub>) was purchased from SIGMA Chemical Company, and pSVβGal was purchased from Promega. HepG2 and Hela cells were maintained in Dulbecco's modified Eagle's medium (DMEM) (Nissui Seiyaku Co.) containing 10 % heat-inactivated fetal calf serum (FCS) (HAZELETON Biologics, Inc.), 4 mM of L-glutamine, 36 mM of sodium bicarbonate, and 60 mg/l of kanamycin at 37°C in a humidified atmosphere containing 5 % CO<sub>2</sub> in air. The cells used in each test were cultured in 96-well flat-bottomed plates (CORNING Laboratory Sciences Company) using 200 ml of the culture medium.

**Synthesis of 6-O-carboxymethyl-TM-chitosan 1.** The synthesis of the 6-O-carboxymethyl(CM)-TM-chitosan **1** was prepared from chitosan according to the method described by Domard *et al.* (11). Two different 6-O-carboxymethyl(CM)-TM-chitosans with different carboxymethylation were synthesized by changing the ratio of monochloroacetic acid to TM-chitosan in the reaction.

**Synthesis of N-lactonoyl-1,6-hexanediamine 2.** The synthesis of N-lactonoyl-1,6-hexanediamine **2** was performed through three reaction steps shown in Scheme 1. Lactonoyl lactone was prepared from lactose according to the method described by Kobayashi *et al.* (12).

**Synthesis of N-[Tetragalactose antenna]-1,6-hexanediamine 3.** The synthesis of the tetragalactose antenna residue was performed as shown in Scheme 2. *N*-[Tetragalactose antenna]-1,6-hexanediamine **3** was prepared according to the following method. *N*-[Antenna]-*N*-Z-1,6-hexanediamine•4HCl (760mg, 973μmol), which was

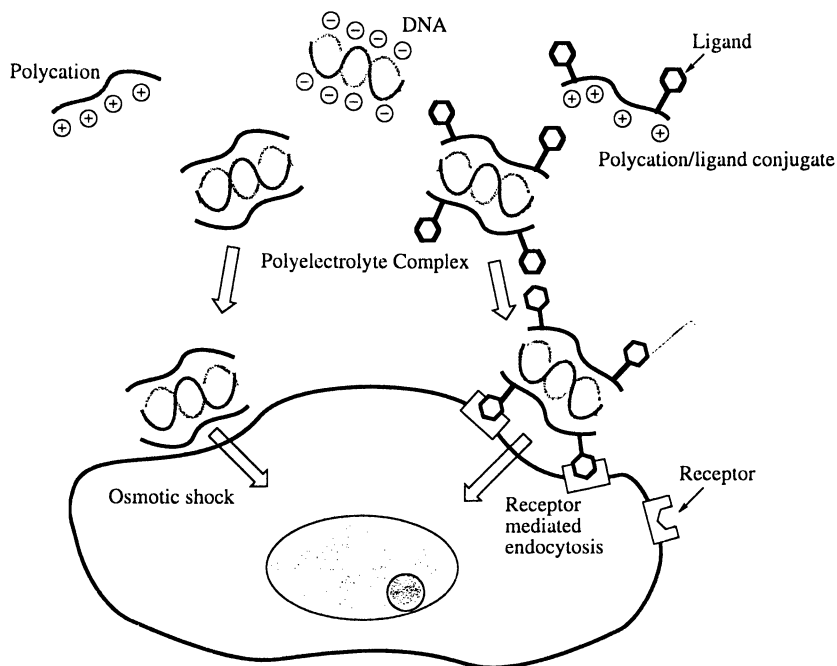
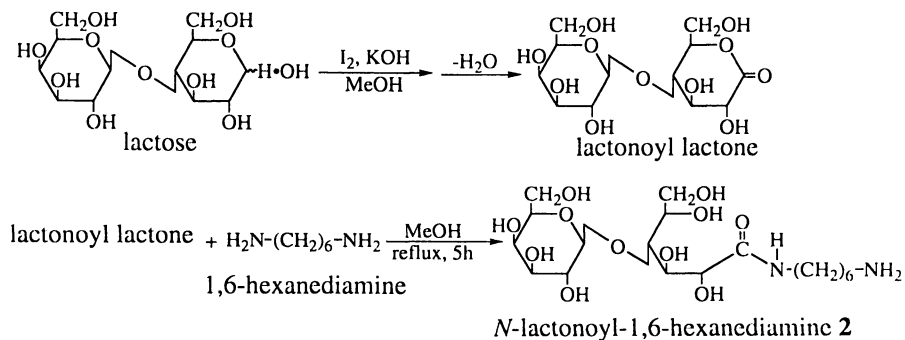
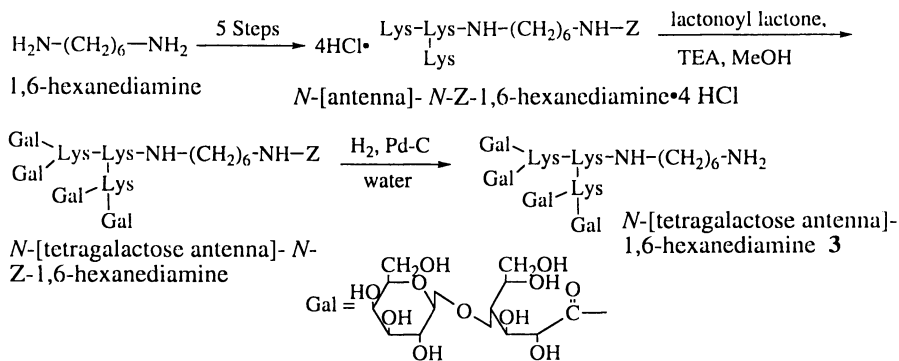


Figure 1. Gene delivery by polycation-DNA complex.

synthesized through five reaction steps according to the method by Shinohara *et al.* (13), and lactonoyl lactone (1.60g, 4.71mmol) were dissolved in methanol. TEA (600 $\mu$ l, 4.29mmol) was added and refluxed for 5 h. This reaction mixture was evaporated and then reprecipitated from water and ethanol (963mg, 483 $\mu$ mol, yield : 49.6%). The *N*-[tetragalactose antenna]-*N*-Z-1,6-hexanediamine (424mg, 213 $\mu$ mol) was dissolved in water and hydrogenolyzed in the presence of palladium black (40mg) at room temperature for 24h. After removal of the catalyst by filtration, the filtrate was evaporated under reduced pressure. *N*-[Tetragalactose antenna]-1,6-hexanediamine was isolated by ion-exchange chromatography (SP-Sephadex, conditioning : water, eluent : 0.1M ammonium bicarbonate), and freeze-dried. The powder, 378mg, 202 $\mu$ mol corresponded to a yield of: 95.0%.

Scheme 1. Synthesis of galactose residue **2**.Scheme 2. Synthesis of tetragalactose antenna **3**.

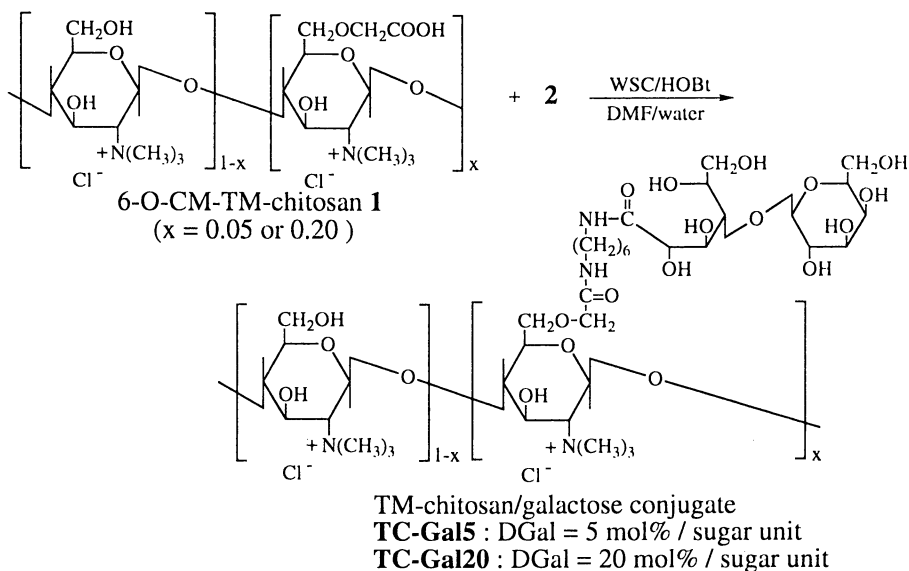
**Synthesis of TM-chitosan/galactose conjugate.** The synthesis of TM-chitosan/galactose conjugate was performed as shown in Scheme 3. In the case of TM-chitosan/galactose conjugate (degree of substitution of galactose group per sugar unit (DGal)= 5 mol%/sugar unit : **TC-Gal5**), **1** (DCM = 5 mol%/sugar unit, 0.2 g, 842  $\mu\text{mol/sugar}$ , 42  $\mu\text{mol/COOH}$ ) was dissolved in DMF/water (1:1 v/v) and WSC (15 mg, 79  $\mu\text{mol}$ ) and HOBt (11 mg, 82  $\mu\text{mol}$ ) were added at 0°C for 1 h. And then **2** was added and stirred at room temperature over night. After this reaction mixture was evaporated, dissolved in water and ultrafiltrated to remove unreacted reagents. The above reaction was repeated to remove residual carboxyl groups. TM-chitosan/galactose conjugate (DGal=20 mol%/sugar unit: **TC-Gal20**) was synthesized by the same method as that of **TC-Gal5**.

**Synthesis of TM-chitosan/tetragalactose antenna conjugate.** The synthesis of TM-chitosan/tetragalactose antenna conjugate (the degree of substitution of tetragalactose antenna residue per sugar unit (DGal4A)=20 mol%/sugar unit: **TC-Gal4A20**) was performed as shown in Scheme 4. Compound **1** (DCM = 20 mol%/sugar unit, 50.4mg, 201 $\mu\text{mol/sugar}$ , and 40.1 $\mu\text{mol/COOH}$ ) were dissolved in DMF/water (1:1 v/v) and WSC (11.5mg, 59.9 $\mu\text{mol}$ ) and HOBt (6.7mg, 49.6 $\mu\text{mol}$ ) were added at 0°C for 1 h. Then **3** (90.9mg, 48.9 $\mu\text{mol}$ ) was added and stirred at room temperature over night. After this reaction mixture was evaporated, dissolved in water and it was ultrafiltrated to remove unreacted reagents. The above reaction was repeated to remove residual carboxyl groups. The objective conjugate was isolated by gel filtration chromatography (HW-40,  $\phi 2 \times 27\text{cm}$ , eluent : water) and freeze-dried to be afforded as powder, 31.2mg.

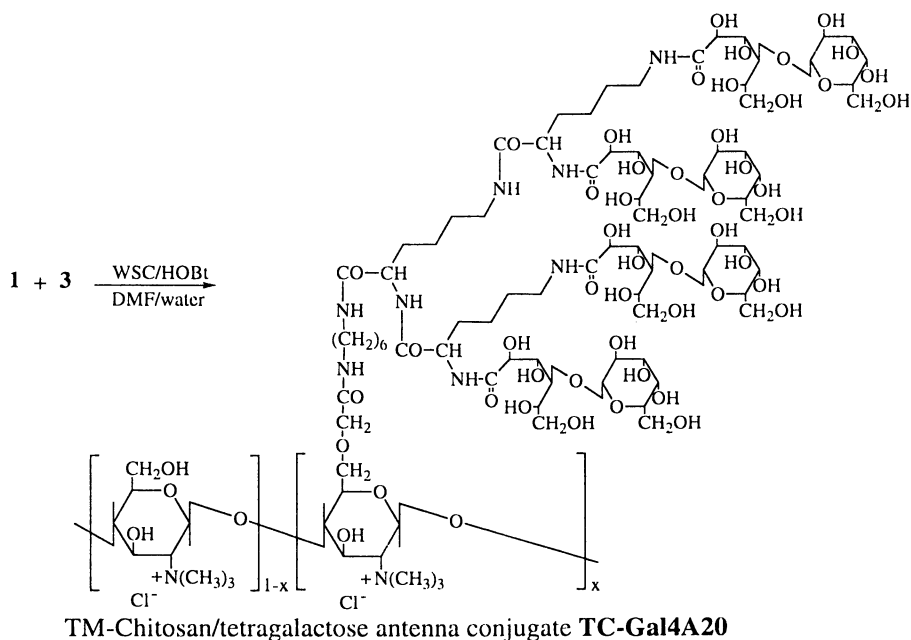
**Evaluation of formation of polyelectrolyte complex with DNA.** Each polyelectrolyte complex with DNA (pSVluc : 6046 bp) was electrophoresed on 1 % agarose gel at 50 V for 45 min and stained with ethidium bromide to be visualized.

**Interaction of conjugates with lectin.** The interaction of polysaccharides with RCA<sub>120</sub> lectin was evaluated using a biosensor based on surface plasmon resonance (BIAcore system, Pharmacia Biotech) (13). The biotin labeled RCA<sub>120</sub> lectin solution was injected onto the streptavidin pre-immobilized surface of a sensor chip, and various concentrations of polysaccharides were injected to measure sensorgrams. The obtained sensorgrams were used to carry out kinetic analysis of the interaction between RCA<sub>120</sub> and polysaccharides; the apparent affinity constants of polysaccharides were calculated.

**Assay of  $\beta$ -galactosidase activity.** In order to evaluate the specific delivery of corded DNA, the  $\beta$ -galactosidase activity of cationic polysaccharide/DNA(pSV $\beta$ Gal plasmid) complex was measured against HepG2 human hepatoma cells *in vitro*. The tumor cell suspension containing  $1 \times 10^4$  cells in DMEM containing 10% FCS was distributed in a 96-well microplate and incubated in a humidified atmosphere containing 5% CO<sub>2</sub> at 37°C for 24 h. After adding a fresh medium containing 100 $\mu\text{M}$  chloroquine and incubating in a humidified atmosphere containing 5% CO<sub>2</sub> at 4°C for 1 h, the suspension was changed into FCS free DMEM containing 5mM CaCl<sub>2</sub> and/or 50mM lactose for the inhibition test and added to each sample. After incubating at 4°C for 1h, it was changed into FCS free DMEM and incubated for 48 h. After adding X-gal solution (14), it was incubated for 48 h and measured using a microplate reader at 420 nm.



Scheme 3. Synthesis of TM-chitosan/galactose conjugate.



Scheme 4. Synthesis of TM-chitosan/tetragalactose antenna conjugate.

## Results and Discussion

**Synthesis of TM-chitosan/galactose and TM-chitosan/tetragalactose antenna conjugate.** The synthesis of TM-chitosan/galactose conjugates was carried out through reaction steps shown in Schemes 1 and 3. By repetition of the reaction of conjugation, the objective TM-chitosan/galactose conjugate having no residual carboxyl group was obtained. We could synthesize TM-chitosan/galactose conjugates having two values of DGal, **TC-Gal5**, and **TC-Gal20** through the coupling reaction of **2** with 6-O-CM-TM-chitosan **1**. For efficient binding to galactose receptors on the surface of hepatocyte, a tetra-antennary ligand having four  $\beta$ -D-galactosyl residues, *N*-[tetragalactose antenna]-1,6-hexanediamine, was designed. The synthesis of TM-chitosan/tetragalactose antenna conjugate was carried out through the reaction steps shown in Schemes 2 and 4. By the usual method, the *N*-[antenna]-*N*-Z-1,6-hexanediamine•4HCl having hetero terminal groups was made from 1,6-hexanediamine. *N*-[tetragalactose antenna]-1,6-hexanediamine having hetero terminal groups, antennary tetragalactose residue, and amine, was isolated by ion-exchange chromatography. By repetition of the reaction of conjugation, the objective TM-chitosan/tetragalactose antenna conjugate having no residual carboxyl group was obtained.

**Formation of polyelectrolyte complex with DNA.** The results of electrophoresis suggested that the neutral polyelectrolyte complex of cationic polysaccharides with plasmid DNA (pSVluc) was formed when the ratio of cationic group to base pair was 2 : 1 in each polycation. Thus, this ratio was utilized in all subsequent experiments.

**Interaction of conjugates with RCA<sub>120</sub> lectin.** In order to evaluate the affinity of obtained conjugates to hepatocyte, the interaction between polysaccharides and RCA<sub>120</sub> lectin was investigated as a simple model experiment. The measurement of interaction between polysaccharides and RCA<sub>120</sub> lectin was carried out by the use of a biosensor based on surface plasmon resonance (BIAcore system, Pharmacia Biotech). RCA<sub>120</sub> lectin is well known to recognize  $\beta$ -D-galactose and  $\beta$ -D-*N*-acetylgalactosamine residues. The results of the interaction of polysaccharides with RCA<sub>120</sub> lectin are shown in Figure 2. The apparent affinity constant of TM-chitosan was the same level as that of DEAE-dextran. **TC-Gal5** and **TC-Gal20** showed a higher apparent affinity constant than TM-chitosan. The **TC-Gal4A20** conjugate showed the highest apparent affinity constant among these tested polysaccharides. These results suggested that the high apparent affinity constant per galactose residue of **TC-Gal4A20** was caused by the "cluster effect" referred to by Lee *et al.* as branches. It could be expected that novel polysaccharides with a high affinity to hepatocyte could be synthesized.

**Effective genetic transfection by TC-Gal4A20/DNA complex in HepG2 cells.** In order to investigate the specific delivery of DNA by the **TC-Gal4A20** conjugate, the expression of  $\beta$ -galactosidase activity by the polycation-corded DNA (pSV $\beta$ Gal plasmid) complex in HepG2 cells was carried out. Furthermore, in order to make sure that the specific delivery of DNA by the **TC-Gal4A20** conjugate was caused by receptor-mediated endocytosis, the inhibition test was performed. The results of effect of the inhibitor on the expression of  $\beta$ -galactosidase activity by polycation-corded DNA complex in HepG2 cells are shown in Figure 3. In the absence of the inhibitor, the  $\beta$ -galactosidase activity of TM-chitosan was similar as that of DEAE-dextran. **TC-Gal5** and **TC-Gal20** conjugates showed higher  $\beta$ -galactosidase activity

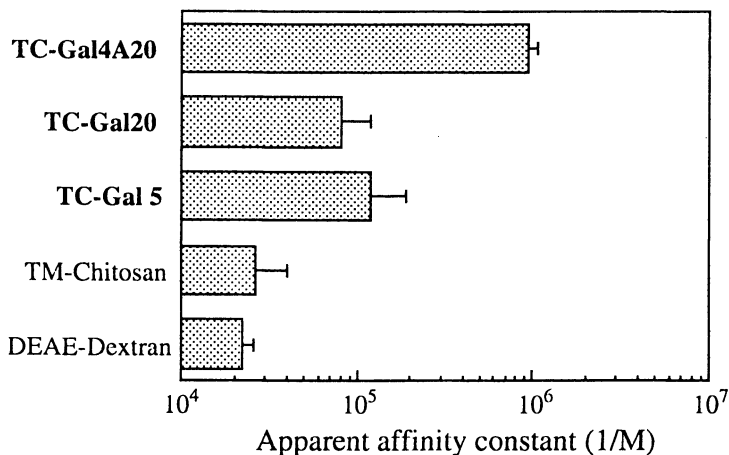


Figure 2. Apparent affinity constant of polysaccharides against agglutinin RCA 120 (10). (Reproduced with permission from reference 10. Copyright 1997 Elsevier Science.)

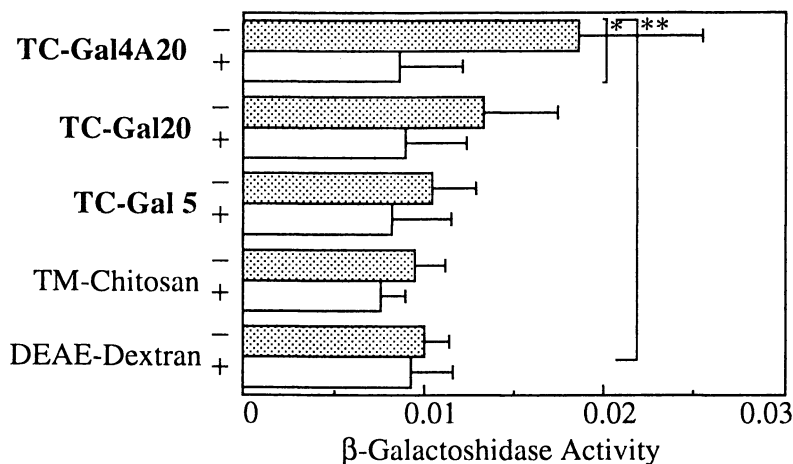


Figure 3. Effects of inhibitor on expression of  $\beta$ -galactosidase by polycation-DNA complexes in HepG2 cells (10).

DNA (pSV $\beta$ Gal plasmid) dose = 0.5 $\mu$ g/well. Ratio of polycation / DNA = 2 cationic group / 1 bp. - : in the absence of inhibitor(lactose 50 $\mu$ M), + : in the presence of inhibitor(lactose 50 $\mu$ M).

\* :  $p < 0.05$ , \*\* :  $p < 0.01$ . (Reproduced with permission from reference 10. Copyright 1997 Elsevier Science.)



than TM-chitosan and DEAE-dextran. The **TC-Gal4A20** conjugate showed the highest  $\beta$ -galactosidase activity among these polysaccharides. When the amount of galactose residues in the conjugates was increased, the  $\beta$ -galactosidase activity of the conjugates increased.

In the presence of the inhibitor, the  $\beta$ -galactosidase activities of DEAE-dextran and TM-chitosan were hardly affected. On the contrary those of **TC-Gal5**, **TC-Gal20** and **TC-Gal4A20** conjugates were significantly decreased by the addition of lactose. These results suggested that the increase of  $\beta$ -galactosidase activity of **TC-Gal5**, **TC-Gal20** and **TC-Gal4A20** conjugates were caused by the specific internalization *via* the galactose receptor on the cellular surface of HepG2 cells and the "cluster effect" of multi-galactose residues.

## References

1. Lee, Y. C. *Carbohydr. Res.* **1978**, 67, 509.
2. Lee, R. T.; Lin, P.; Lee, Y. C. *Biochemistry.* **1984**, 23, 4255.
3. Cotten, M.; Langle-Rouault, F.; Kirlappos, H.; Wanger, E.; Mechtler, K.; Zenke, M.; Beug, H.; Birnstiel, M. L. *Proc. Natl. Acad. Sci. U.S.A.* **1990**, 87, 4033.
4. Wagner, E.; Zenke, M.; Cotten, M.; Beug, H.; Birnstiel, M. L. *Proc. Natl. Acad. Sci. U.S.A.* **1990**, 87, 3410.
5. Cotten, M.; Wagner, E.; Birnstiel, M. L. *Methods Enzymol.* **1993**, 217, 618.
6. Hockett, B.; Ariatti, M.; Hawtrey, A. O. *Biochem. Pharmacol.* **1990**, 40, 253.
7. Wu, G. Y.; Wu, C. H. *J. Biol. Chem.* **1987**, 262, 4429.
8. Wu, C.; Wilson, J.; Wu, G. *J. Biol. Chem.* **1989**, 264, 16985.
9. Murata, J.; Ohya, Y.; Ouchi, T. *Carbohydr. Polym.* **1996**, 29, 69.
10. Murata, J.; Ohya, Y.; Ouchi, T. *Carbohydr. Polym.* **1997**, 32, 105.
11. Domard, A.; Rinaudo, M.; Terrassin, C. *Int. J. Biol. Macromol.* **1986**, 8, 105.
12. Kobayashi, K.; Sumitomo, H.; Ina, Y. *Polym. J.* **1985**, 17, 567.
13. Shinohara, Y.; Sota, H.; Kim, F.; Shimizu, M.; Gotoh, M.; Tosu, M.; Hasegawa, Y. *J. Biochem.* **1995**, 117, 1076.
14. Takai, T.; Ohmori, H. *Biochim. Biophys. Acta* **1990**, 1048, 105.

## Chapter 3

# Drug–Cyclodextrin Complexation in the Presence of Water-Soluble Polymers: Enhanced Solubility and Percutaneous Transport

Már Mátsson and Thorsteinn Loftsson<sup>1</sup>

Department of Pharmacy, University of Iceland, Hofsvallagata 53,  
105 Reykjavik, Iceland

For variety of reasons, including production capabilities, toxicology and cost, the amount of cyclodextrin that can be used in drug and cosmetic formulations will be limited. In order to use less cyclodextrin the complexation efficacy ( $K_c[S_o]$  or  $[D \cdot CD]/[CD]$ ) must be increased. We have shown that the complexation efficacy of various lipophilic drugs can be significantly increased by heating cyclodextrin drug solution up to 120–130 °C for 20–40 minutes in the presence of small amount of water soluble polymers. At least 30% enhancement in complexation efficacy is common and in some cases over 200% increase is observed. Phase-solubility studies revealed that this was due to an apparent increase in the complexation stability constant ( $K_c$ ). The percutaneous transport through hairless mouse skin *in-vitro* from drug-cyclodextrin solutions was increased up to 200% by addition polymer and *in-vivo* studies showed that the bioavailability of for example dexamethasone from eye-drop solutions could be increased about four fold. Formulation of drugs with cyclodextrins and polymers can thus enhance the attractive properties of cyclodextrins as pharmaceutical excipients

The formulation of a drug can present several challenges. The first step in the drug absorption is often diffusion across a biological membrane such as the intestinal mucosa, skin or eye cornea. Only small non-ionic hydrophilic compounds or relatively lipophilic compound will be efficiently transported across such membranes by passive diffusion. However the passive diffusion is driven by high activity of the drug in aqueous membrane exterior, which would require the same compound to be highly water soluble.

Successful formulation of relatively lipophilic drug will maintain sufficiently high concentration at the surface of the lipophilic membrane in order to get the drug absorbed at an acceptable rate. Another approach to achieve this goal is to synthesize

<sup>1</sup> Corresponding author.

a water soluble pro-drug from the parent compound. The former approach is usually favored in order to avoid the process of registering a new drug compound which can be costly and delay marketing for years.

Highly lipophilic drugs are often formulated into emulsions with surfactants, or into solution using organic solvents. However in some cases neither acceptable solubility nor availability can be achieved in such formulations, or the formulations are not acceptable due safety considerations, irritation of sensitive tissues or bad taste.

Application of cyclodextrins in various formulations is currently being investigated by both academic and industrial researchers. Although the cyclodextrins (CDs) were discovered more than 100 years ago (1) they have only recently been produced in sufficient quantities, and at reasonable cost, to merit consideration as industrial excipients. The cyclodextrins are oligosaccharides with the unique properties in solubilizing drugs and other compounds through formation of inclusion complexes. The hydrophilic CDs are not readily adsorbed through biological membranes (2-4). However the complex formation is fully and rapidly reversible and therefore the availability of poorly soluble drugs can be increased from cyclodextrins solutions.

The pharmaceutical usage of cyclodextrin is rapidly expanding as new cyclodextrin formulated drugs are introduced to the market (5). However solubilizing the drug may require more cyclodextrin than is acceptable due to cost and other requirements for a particular product. The present chapter describes some of the basic properties of cyclodextrin and how the cyclodextrin concentration in a formulation can be reduced by augmenting the solubility and bioavailability through the use of water soluble polymers.

### **Cyclodextrins and cyclodextrin derivatives.**

Cyclodextrins (CDs) are cycloamylose oligosaccharides produced by enzymatic degradation of starch. The common natural CDs are  $\alpha$ -cyclodextrin ( $\alpha$ CD)  $\beta$ -cyclodextrin ( $\beta$ CD) and  $\gamma$ -cyclodextrin ( $\gamma$ CD), consisting of 6,7 and 8 ,1-4 $\alpha$  linked glucopyranose units, respectively. Cyclodextrins smaller than  $\alpha$ CD should not exist due to steric factors and CDs larger than  $\gamma$ CD are only formed in small amounts and will generally exhibit poorer complexing properties than  $\alpha$ CD,  $\beta$ CD and  $\gamma$ CD (6-8). The CDs are slightly conical or doughnut shaped molecules. The outer surface is somewhat hydrophilic, while the interior of the cavity is hydrophobic. The unique property of cyclodextrins is their ability to form inclusion complexes with other molecules.

The ability to form complexes with a particular type of molecule will vary the size of the cyclodextrin cavity. The  $\alpha$ -CD will form the most stable complexes with linear aliphatic and unsubstituted aromatic moiety,  $\beta$ CD with complexes with aromatic, monocyclic and bicyclic moiety and  $\gamma$ CD with bicyclic, tricyclic and larger moieties (9).

Although the  $\beta$ CD can form complexes with moieties which are the most common in small drug molecules (Mw 100-1000) its use is often limited by the poor aqueous solubility of  $\beta$ CD and its complexes. The crystal structure of  $\beta$ CD is rather stable and the aqueous solubility of the pure compound is no more than 19 mg/ml at room

temperature. Partially due to these limitations in solubility the CD derivatives have been preferred to the parent compounds. The CD derivatives, which have been used as pharmaceutical excipients, are produced as highly soluble amorphous mixtures of isomeric compounds. Numerous derivatives have been reported in the literature (10) but the three derivatives listed in Table 1 are available for pharmaceutical use and have been used in clinical investigations.

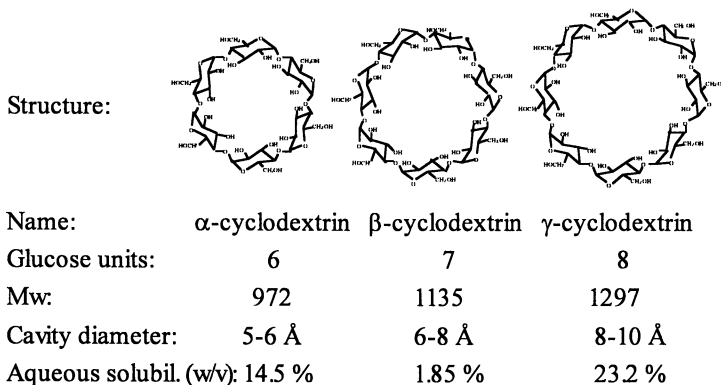
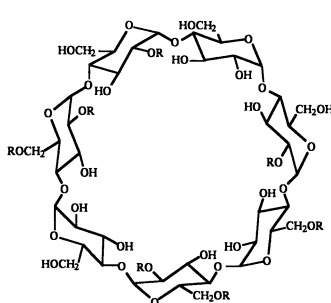


Figure 1. Structure and some data for the three most common cyclodextrins produced by the enzymatic degradation of starch. (Adapted from ref. 2)

**Table 1. Structure of the three most common cyclodextrin derivatives used in pharmaceutical applications.**



| Cyclodextrin                            | R   | D.S | Toxicity             |
|---|---|-----|----------------------|
| HP $\beta$ CD<br>(Hydroxypropyl-)       | OH<br>-CH <sub>2</sub> CHCH <sub>3</sub>                      | 0.7 | Non-toxic.           |
| SB $\beta$ CD<br>(Sulfobutylether-)     | -(CH <sub>2</sub> ) <sub>4</sub> SO <sub>3</sub> <sup>-</sup> | 0.9 | Non-toxic.           |
| RM $\beta$ CD<br>(Randomly methylated-) | -CH <sub>3</sub>  | 1.8 | Hemolytic reactions. |

Both sulfobutylether  $\beta$ CD (SB $\beta$ CD) and hydroxypropyl  $\beta$ CD (HP $\beta$ CD) can be considered non-toxic even when used in high dosage (11, 12) and have been studied for, parental, oral and topical usage.

Randomly methylated  $\beta$ CD (RM $\beta$ CD) is highly soluble but has more hydrophobic character than the other two derivatives and will generally form more stable complexes. This molecule is somewhat surface active and will cause hemolysis at low concentrations (12). The RM $\beta$ CD is therefore not suitable for parenteral usage and its oral applications may be limited. However, RM $\beta$ CD may be valuable for

topical applications and it has been shown that it will enhance the nasal absorption of many compounds, especially small peptides (13, 14).

### Increased solubility of drugs and other compounds through complexation with cyclodextrins.

When a 1:1 complex between drug (or other molecule) and cyclodextrin is formed the equilibrium between the concentration of drug in complex  $[D \cdot CD]$ , free cyclodextrin  $[CD]$  and free drug  $[D]$  is described by the stability constant  $K_c$ . (Equation 1). If the solution is saturated with drug then  $[D]$  is equal to the intrinsic solubility of the drug ( $s_0$ ). The solubility of the drug will then increase linearly with cyclodextrin concentration as described by  $A_L$  type of phase-solubility diagram (Figure 2). Non-linear phase solubility diagrams are distinguished as  $A_P$ , typical for a drug which also can form 1:2 ( $D \cdot CD_2$ ) complexes and  $A_N$  which is typical for drug that can also form 2:1 complexes ( $D_2 \cdot CD$ ) (15). The  $B_S$  type of diagram describes the case when the complex has limited solubility and  $B_I$  the case when the complex has less solubility than the free drug.

$$K_c = \frac{[D \cdot CD]}{[D][CD]} \quad (1)$$

$$K_c = \frac{\text{slope}}{s_0(1 - \text{slope})} \quad (2)$$

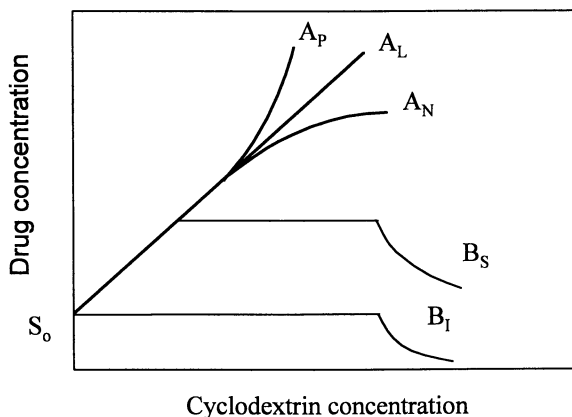


Figure 2. Phase solubility types.  $S_0$  is solubility of drug in absence of CD. Phase solubility types  $A_P$ ,  $A_L$ , and  $A_N$  when very soluble complexes are formed;  $B_S$  when complexes of limited solubility are formed and type  $B_I$  when insoluble complexes are formed. (Adapted from ref. 2)

The  $K_c$  value can be obtained from the slope of the phase solubility diagrams by using the Equation 2 derived from Equation 1. Example of this approach is shown in Figure 3. The phase solubility can be linear at very high CD concentrations because a small molecule cannot be included in more than one CD molecule.

The linear nature of the phase solubility diagram is in marked contrast with generally non-linear nature of solubilization in organic solvents. CD solutions, containing 1:1 complexes can be diluted without precipitation. When CD formulation is applied the drug should therefore remain in aqueous solution until it is absorbed.

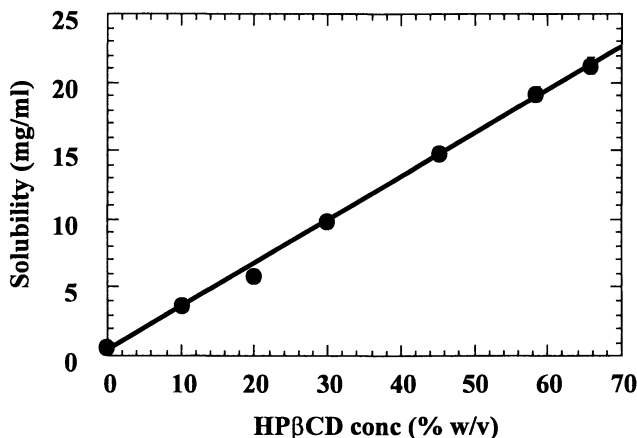


Figure 3. Solubility of acetazolamide in aqueous HPβCD solutions (Adapted from ref. 31).

### Increased aqueous stability of drugs in cyclodextrin solutions

The aqueous formulation of a drug may not be possible due to limited stability of the drug. When a drug molecule is included in the cyclodextrin cavity the reactive part of the molecule is sometimes shielded from interaction with water molecules and hydrolysis. More than 5 fold stabilization of the drug is common (10, 16-20) and a more than a 1000 fold decrease in the degradation rate has been reported (21). In other cases complexation with CD will have little effect, especially when the reactive group is located far from the part included in the cavity. Catalysis of degradation reaction can also be present where the hydroxyl group lining the rim of the cyclodextrin cavity participate in the reaction. CDs will, for example, accelerate the degradation of β-lactam antibiotics at high pH (22).

The observed degradation rate constant ( $k_{obs}$ ) in aqueous CD solution consists of the intrinsic degradation rate ( $k_0$ ) for the free drug and the degradation rate constant for the drug within the complex ( $k_c$ ) and the relative concentrations of free and complexed drug which determined by the  $K_C$  value. (Figure 4). The  $K_C$  and  $k_c$  values can then be obtained from data fitting of  $k_{obs}$  vs. the CD concentration (Figure 5).

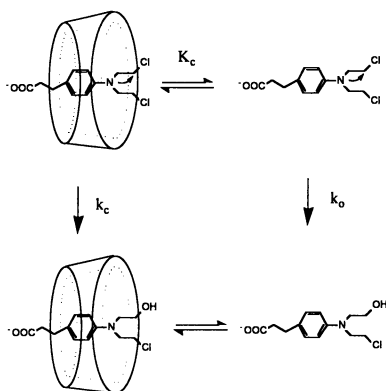


Figure 4. Degradation pathways for chlorambucil in CD solutions. (Adapted from ref. 19)

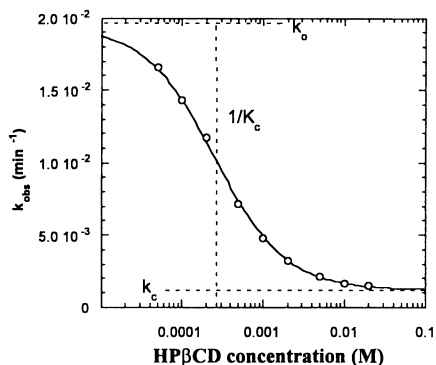


Figure 5. Chlorambucil degradation rates in HP $\beta$ CD solutions (pH 7.5, 30 °C). The broken lines indicate  $1/K_c$ ,  $k_c$  and  $k_o$ .

### Availability of drugs from aqueous CD formulations

Lipophilic drugs which are solubilised through CD complexation must first be brought from the solution to the surface of skin, cornea, buccal, nasal or intestinal mucosa or other biological membrane. The drug will partition from the aqueous surface layer into the membrane surface and diffuse across the membrane, driven by the concentration gradient. The equilibrium between the aqueous surface layer and the membrane surface is determined by the partition coefficient ( $K_p$ ). Thus the diffusion rate should increase proportionally with increase in aqueous concentration and also proportionally with increase in  $K_p$ . Although the solubility of the drug will increase dramatically in CD solution the partition coefficient (determined by the solubility in the aqueous and the membrane phase) will fall to the same degree and the driving force for flux through the membrane should remain constant. The increased availability observed with increased drug concentration CD solutions can therefore best be explained in terms of increased aqueous diffusion rate. Diffusion through an aqueous diffusion layer at the membrane surface will be assisted by CDs. Schematic representation of this system is shown in Figure 6. The flux can be described by a relatively simple mathematical equation (Equation 3). In this equation the  $P_M$  is the maximum permeability and  $M_{1/2}$  is equal to the CD concentration when the drug flux is half of the maximum flux (23). The mucosal membranes are covered by relatively viscous mucus which will contribute to an aqueous barrier to drug diffusion. Significant portion of a lipophilic drug can be transported through the hair follicles on the skin surface (24, 25) and these can function as dermal aqueous diffusion barrier.

$$J_D = \frac{(P_M/K_d)[D \cdot CD]_d}{M_{H2} + [CD]_d} \quad (3)$$

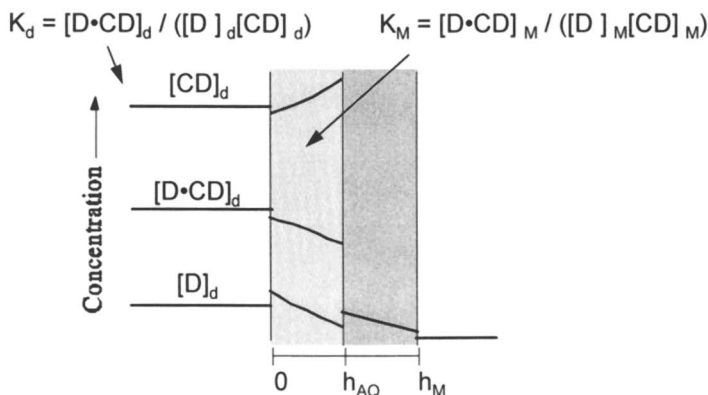


Figure 6. Schematic representation of the diffusion of drug (D) from CD solution through skin. The light gray area indicates the aqueous diffusion layer and the dark gray are indicates the lipophilic part of the membrane. (Adapted from ref. 23)

In-vitro studies of the drug diffusion through skin are often performed with the Franz-diffusion cell setup. The CD formulation is placed in the donor chamber and the drug concentration with set time intervals in the acceptor phase. Steady-state conditions are maintained in the experiment, so that only small portion of the drug in the donor chamber diffuses through skin during the experiment. Experiments with hairless mouse skin (23, 26) show that the drug flux will increase with CD concentrations, as long as some drug remains in suspension (Figure 7) However when an excess of CD is added, relative to what is needed to solvate the drug, the drug flux will decrease. Similar results have been obtained for rabbit eye cornea (27) and nasal mucosa (14). The experimental results are in agreement with theory were the predicted increase is due to increase in the aqueous diffusion rate and the decrease, when excess CD is added, is due to decreasing partition coefficient. Cellophane membrane can be used to optimize the release from topical formulations (Figure 8). In this case Equation 3 can also be fitted to the relationship between flux and CD concentration.

Penetration enhancers are frequently used in dermal and other topical formulations. Dermal penetration enhancers will affect the barrier function in the stratum corneum (28, 29). According to Equation 3 a co-operative effect between penetration enhancers and CDs should be expected and this has been demonstrated by experiment (30).



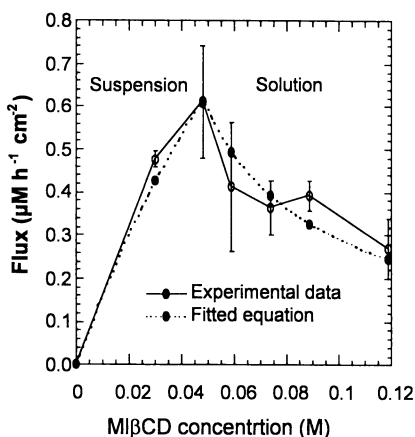


Figure 7. Hydrocortisone flux, through hairless mouse skin. The broken line show the result of fitting to Equation 3. (Adapted from ref 23)

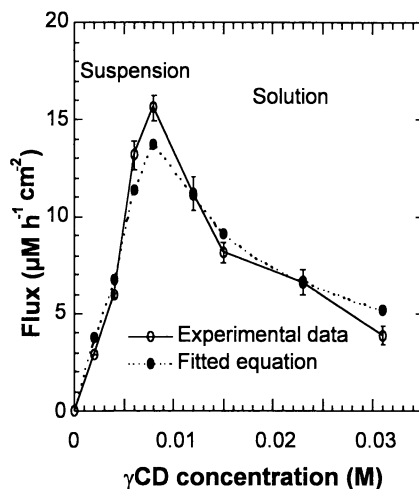


Figure 8. Triamcinolone acetonide flux through cellophane membrane. The broken line shows the results of fitting to Equation 3.

### CD complexation efficacy

Small drug compounds forming 1:1 complexes with CD are generally of the molecular weight in the range 100 to 1000 g / mole. The molecular weight of CD and CD derivatives is in the range 1000 to 2000. Excess CD is needed to fully complex the drug (Equation 1) and therefore the formulation of drug with CD can result in 4- to 10-fold increase in the weight of dry material. Isotonic aqueous solution cannot contain more than 20 to 25 % (w/v) CD. Viscosity of such solutions is similar to that water, but in concentrations above 40% (w/v) the viscosity increases rapidly with CD concentration up to a value of 70 mPa s in 60% solutions (31). High complexation efficacy, i.e. the equilibrium ratio of  $[D \cdot CD]$  to  $[CD]$  or  $K_{c,s_0}$ , can therefore be critical to successful drug formulation.

The most common approach to increase the complexation efficacy is to ionize the drug through pH changes (32). The stability constant of the complexation will usually decrease but this will be offset by the increase in the intrinsic solubility. Therefore the overall complexation efficacy ( $K_{c,s_0}$ ) can be expected to increase. However there are several limitations to this approach as the drug compound may not be ionizable, it might be unstable at the pH range where the drug is in the ionized form, or the required pH range may be unacceptable for the intended application. For some drugs the complexation efficacy can be increased through ion pairing or salt formation with acetate (33) or fruit acid anions (34). Ionic strength of the solution will have little effect on the complexation efficacy.

The intrinsic solubility of drugs can be increased through addition of organic solvents. However the affinity for the CD cavity will decrease, so that the overall

complexation efficacy should not improve. Furthermore the organic solvent will often compete with the drug in the CD cavity and complexation efficacy will therefore decrease (35). Generally it is therefore not advisable to include organic solvents in CD formulations.

Recently it has been shown that heating in the presence of water soluble polymer will increase the CD complexation efficacy with various drug compounds (36). This method to increase drug solubility and bioavailability will be discussed in some detail in the following sections.

### **Increasing complexation efficacy through cyclodextrin formulation with water soluble polymers.**

Water soluble polymers are widely used in pharmaceutical systems as emulsifying agents, flocculating agents, adjuncts, suspending materials, coating materials and binders. The polymers are chemically inert but do have some ability to complex with drug compounds (37, 38). Solubility of drugs can therefore be notably increased by formulation with polymers.

Polymers can also affect the precipitation rates and they have, for example, been shown to stabilize supersaturated solutions of the experimental drug, RS-8358 for few minutes or few hours (39). These effects are apparently due to direct interaction between the polymer and drug compound.

Addition of water soluble polymers can increase the solubilizing effect of surfactants (40). Investigation of laurylsulfate-polyvinyl pyrrolidone (PVP) mixtures have shown that solubilizing effect of polymer (PVP) was synergistic with the solubilizing effect of the surfactant, i.e. that the solubilizing effect of the mixture was much larger than could be expected from an additive effect (40). Some type of polymer-surfactant complex has been proposed for these systems where the polymers interact with the surfactant micelles and link them together on a long string or as a large web (41). The direct interaction of the polymers with the surfactant has also shown to cause dehydration of the micellar surface (42).

Adding polymer to a cyclodextrin solution will produce little effect on the solubilization of drugs (43, 44). However a considerable increase in the solubilization of drugs can be achieved through heating the drug/polymer/cyclodextrin mixture in an autoclave (121 °C) for 20 to 40 minutes (45) or by heating in a sonicator (e.g. 70 °C for one hour). The effect is synergistic, as in the case of polymer surfactant interactions, with an apparent increase in the observed  $K_c$  value (Figure 9). The effect cannot be satisfactorily explained as supersaturation as the samples were equilibrated at room-temperature for 3 days or longer before filtration to remove precipitated drug (46). Increased solubility was also observed when a large excess of crystalline drug had been added, after autoclaving, to promote precipitation (47). Stability studies have shown that drug/cyclodextrin/polymer preparations can be stable (48). Presently we have stored some formulations for more than 5 years without any precipitation.

The solubilizing effect of the polymer is optimized at relatively low polymer concentrations. When hydrocortisone suspensions in 10% HP $\beta$ CD in the presence of PVP the solubility is increases 30 percent, but little increase in solubility is observed

in polymer concentrations above 0.01% w/v, with maximum solubility in the range 0.1% to 0.25% (Figure 10)

Similar observations were made with other drugs and other polymers (26, 49, 50) with maximum solubility observed in the concentration range 0.05%–0.25% (46) and sometimes a gradual decrease in solubility with higher polymer concentrations. Similarly when the polymer is interacting with surfactants, a maximum effect is produced at relatively low polymer concentrations.

The effect of carboxymethyl cellulose sodium salt (CMC) and PVP on the solubilization by HP $\beta$ CD is shown in Table 2. The increased in solubilization after heating suspensions of HP $\beta$ CD and polymer was in the range 5% to 57% in with CMC and 12% to 129% in the case of PVP (46). Similarly the solubilization effect on hydrocortisone by various CDs was increased 19% to 156% after heating in the presence of water soluble polymer (46).

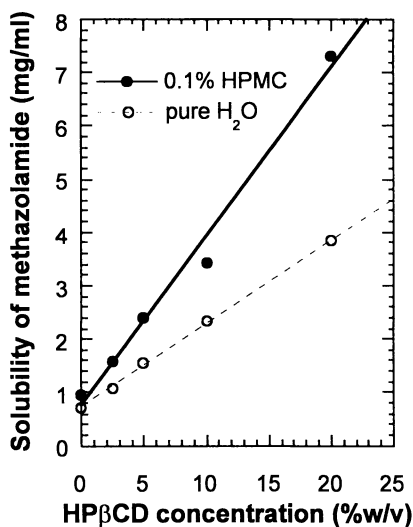


Figure 9. Phase solubility diagram for methazolamide in aqueous HP $\beta$ CD solution. The apparent  $K_c$  increases, relative to the value for pure water ( $\circ$ ), when 0.1 % HPMC ( $\bullet$ ) is added to the solution. Both solutions were heated in an autoclave. (From ref. 46)

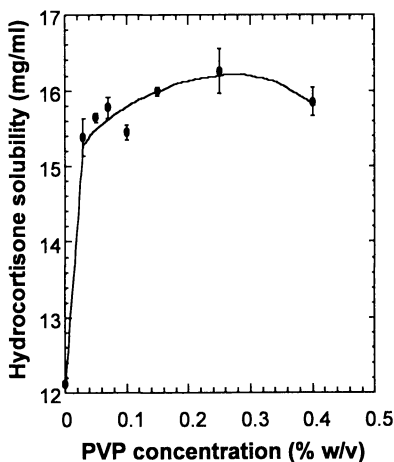


Figure 10. Hydrocortisone solubility relative to PVP concentration in a 10% aqueous HP $\beta$ CD solution (after autoclaving). (Adapted from ref. 46)

**Table 2.** The effect of adding 0.25 % (w/v) CMC or 0.25% (w/v) PVP to aqueous 10% (w/v) HP $\beta$ CD.  $S_o$ : the intrinsic solubility of the drug,  $S_p$ : the solubility of the drug in polymer solution,  $S_{co}$  : solubility of the drug in CD solution,  $S_{cp}$ : solubility of the drug in CD solution containing polymer\*.

| Drug                  | $S_o$<br>(mg/ml) | $S_p$<br>(mg/ml) | $S_{co}$<br>(mg/ml) | $S_{cp}$<br>(mg/ml) | $S_{cp}/S_{co}$ |
|-----------------------|------------------|------------------|---------------------|---------------------|-----------------|
| <u>CMC</u>            |                  |                  |                     |                     |                 |
| Acetazolamide         | 0.70             | 0.84             | 2.52                | 3.11                | 1.23            |
| Alprazolam            | 0.07             | 0.18             | 1.28                | 1.55                | 1.21            |
| Carbamazepine         | 0.11             | 0.20             | 7.00                | 9.20                | 1.31            |
| Clotrimazole          | 0.00             | 0.00             | 1.20                | 1.40                | 1.17            |
| Dexamethasone         | 0.20             | 0.33             | 8.43                | 8.75                | 1.04            |
| Diazepam              | 0.69             | 0.81             | 9.14                | 9.70                | 1.06            |
| Econazole             | 0.57             | 0.60             | 5.03                | 7.41                | 1.47            |
| 17 $\beta$ -Estradiol | 0.01             | 0.17             | 5.10                | 5.35                | 1.05            |
| Ethoxzolamide         | 0.04             | 0.07             | 1.36                | 1.66                | 1.22            |
| Hydrocortisone        | 0.36             | 1.10             | 12.88               | 17.02               | 1.32            |
| Miconazole            | 0.04             | 0.06             | 1.98                | 2.50                | 1.26            |
| Oxazepam              | 0.03             | 0.04             | 0.90                | 1.42                | 1.57            |
| Prednisolone          | 0.38             | 0.53             | 13.60               | 15.30               | 1.13            |
| Progesterone          | 0.00             | 0.00             | 4.39                | 6.11                | 1.39            |
| Sulfamethoxazole      | 0.36             | 0.69             | 10.01               | 12.60               | 1.26            |
| Temazepam             | 0.60             | 0.65             | 3.10                | 3.48                | 1.16            |
| <u>PVP</u>            |                  |                  |                     |                     |                 |
| Acetazolamide         | 0.70             | 1.05             | 2.52                | 3.92                | 1.56            |
| Carbamazepine         | 0.11             | 0.31             | 7.00                | 8.50                | 1.21            |
| Clotrimazole          | 0.00             | 0.00             | 1.20                | 1.80                | 1.50            |
| Dexamethasone         | 0.26             | 0.33             | 7.53                | 8.80                | 1.17            |
| Econazole             | 0.57             | 0.64             | 5.03                | 5.65                | 1.12            |
| Ethoxzolamide         | 0.04             | 0.06             | 1.36                | 2.72                | 2.00            |
| Progesterone          | 0.00             | 0.00             | 4.39                | 5.71                | 1.30            |
| Sulfamethoxazole      | 0.36             | 86               | 10.01               | 14.80               | 1.48            |
| Trimethoprim          | 0.82             | 1.35             | 2.83                | 6.47                | 2.29            |

Adapted from ref. 45

### Physiochemical properties linked to the drug/CD/polymer co-complexes.

The increased solubility of drugs with polymer is explained largely in terms of increase in the apparent  $K_c$  for the CD complexation. With hydrocortisone and PVP the  $K_c$  value for HP $\beta$ CD will increase with PVP concentration up to 0.10% (w/v) and then gradually decrease (46) (Table 3).

The entropy of CD complexation is generally negative and with addition of polymers the entropy and enthalpy of complexation will become more negative, indicating a more ordered complex (45). The association of polymer and cyclodextrin is also indicated by reduced mobility of cyclodextrin after preparation of the complex (51) These observation have lead to similar conclusions as have been reached for the polymer-surfactant micelle systems. That is, due to a significant association between the cyclodextrin (or micelles) and the polymer, there is a formation of a co-complex, leading to modification of the complexing properties which will enhance the solubility. However like in the case of the micelles the exact structure of the complex is not known.

**Table 3. The effect of PVP (MW 360,000) on the stability constant ( $K_c$ ) of the hydrocortisone HP $\beta$ CD MS 0.6 complex at room temp. (23°C)**

| PVP concentration (% w/v) | Slope | Corr. | $K_c M^{-1}$ |
|---------------------------|-------|-------|--------------|
| 0.000                     | 0.502 | 0.988 | 1010         |
| 0.010                     | 0.528 | 0.972 | 1120         |
| 0.025                     | 0.532 | 0.994 | 1140         |
| 0.050                     | 0.544 | 0.977 | 1190         |
| 0.100                     | 0.591 | 0.999 | 1450         |
| 0.150                     | 0.577 | 0.999 | 1390         |
| 0.200                     | 0.548 | 0.999 | 1290         |
| 0.500                     | 0.544 | 0.998 | 1190         |
| 0.700                     | 0.543 | 0.999 | 1190         |

### Increasing the solubility of $\beta$ CD and $\beta$ CD complexes through use of polymers.

The "natural"  $\beta$ CD was the first cyclodextrin to become widely available and complexes of this cyclodextrin have been extensively studied for the last two decades (9).  $\beta$ CD is non-toxic in oral and topical formulations. Some food products

containing  $\beta$ CD are available and drug formulations of  $\beta$ CD are also on the market (4). Monograph for  $\beta$ CD has been included in both the US and European Pharmacopoeia. Although  $\beta$ CD is an attractive excipient due to its low cost, the limited solubility of this compound severely limits its application, especially in aqueous formulations.

Many drug/ $\beta$ CD complexes have low aqueous solubility but the formation of inclusion complexes between the water soluble salicylic acid and the relatively insoluble  $\beta$ CD will lead to increase in the  $\beta$ CD solubility from 1.9% to approximately 20% (46). However this increase, when observed, is much smaller with less soluble drugs such as carbamazepine, methazolamide and sulfamethoxazole (Figure 11). When the suspension of these drugs was heated in the presence of 0.1% HPMC the  $\beta$ CD solubility was further increased by further 20% to 100%. The maximum enhancement by the polymer was, as in the case of CD derivative, reached at relatively low polymer concentrations. In the case of acetazolamide the solubility increased sharply to a maximum solubility between 0.01% (w/v) and 0.2 % (w/v) polymer concentrations (46) (Figure 12). At these concentrations the solubility of acetazolamide was comparable to that obtained for 5% HP $\beta$ CD solution. Similar effect of the polymer concentration on the solubility of  $\beta$ CD complexes of other drugs was also observed (51).

### **Increased availability of drugs form cyclodextrin/polymer solutions.**

The increased solubility of the drugs in polymer/cyclodextrin formulation is accompanied by increased availability of the drug. The maximum flux of hydrocortisone from RM $\beta$ CD solutions, through hairless mouse skin was increased 100% when the solutions were prepared in the presence of 0.25% PVP (Figure 13). As predicted by the theory the maximum flux was obtained when the drug was transformed from suspension to solution.

The oral availability from lyophilized CD complexes can also be increased by formulation with polymers. Savolainen et al. (52) showed that, by preparing glibenclamide/SB $\beta$ CD/HPMC by sonication at 70 °C, the use of SB $\beta$ CD could be reduced by 80%, as compared to complexes prepared without polymer, without affecting the oral bioavailability of glibenclamide in dogs (HPMC: hydroxymethyl propyl cellulose)

Further examples of increased bioavailability are presented below, where the development of individual drug formulations is discussed.

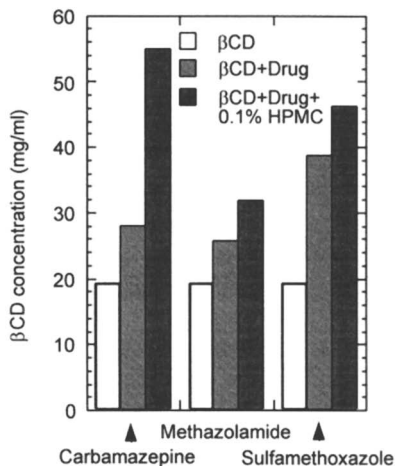


Figure 11. The effect of drug compounds and HPMC polymer on the aqueous solubility of  $\beta$ CD at room temperature (23 °C). (Adapted from ref. 46)

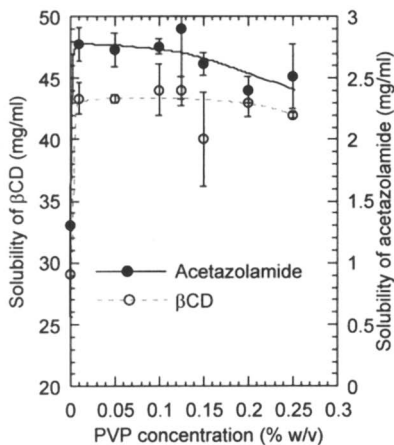


Figure 12. The effect of PVP concentration on the aqueous solubility of  $\beta$ CD ( $\circ$ ) and acetazolamide ( $\bullet$ ). The aqueous suspension was heated in an autoclave. (Adapted from ref. 46)

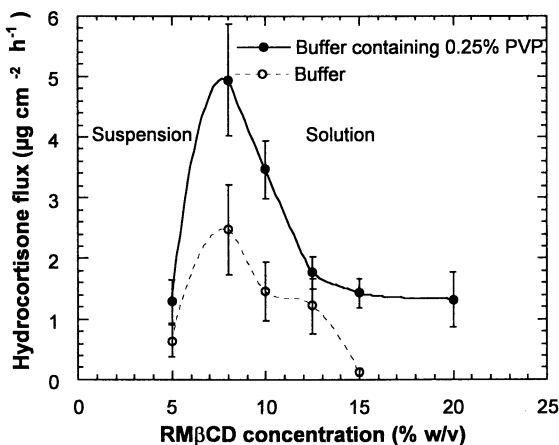


Figure 13. Flux from RM $\beta$ CD solutions through hairless mouse skin. Comparing solutions prepared without polymer ( $\circ$ ) and solutions prepared after addition of 0.25% (w/v) PVP ( $\bullet$ ). (Adapted from ref. 23)

## Development and in-vivo evaluations of drug/cyclodextrin/polymer formulations.

Drug formulations must be optimized with all their constituents included. Some components may interfere with the CD interactions and the polymer CD interaction. Following are three examples of pre-formulation optimization, release and bioavailability studies. In all cases the CD complexation efficacy and the release characteristic were improved through heating the drug cyclodextrin formulation in an autoclave in the presence of a polymer.

### Acetazolamide eye-drop solutions (46, 53).

Acetazolamide is a carbonic anhydrase inhibitor and one of the first medicines introduced to reduce intraocular pressure (IOP) associated with glaucoma (54). To obtain effective lowering of IOP large doses have to be administered, but this will also lead to some systemic side effects of the drug. Recently some water soluble carbonic anhydrase inhibitors have been introduced (55). These can be administered in eye drop solutions, avoiding many of the systemic side effects of the previously orally administered drugs. Acetazolamide has previously not been considered suitable for eye-drop formulation (55) due to its low water solubility ( $< 1$  mg/ml).

Our studies showed that acetazolamide can form inclusion complex with HP $\beta$ CD and the required concentration of the CD could be reduced by for as much as 60% by heating the suspension in an autoclave in the presence of 0.1% HPMC (Figure 14).

The pH value of the eye-drop solution was adjusted to 4.5 to maintain acetazolamide in a unionized form. Other constituents beside acetazolamide and HP $\beta$ CD, where 0.1 % (w/v) HPMC, 0.01 % (w/v) benzalconium chloride preservative, 0.05 % (w/v) sodium EDTA, and sufficient NaCl to make the solution isotonic with the tear fluid. Phase solubility study for this formulation showed that 16-17% (w/v) HP $\beta$ CD was required to solubilize 1% (w/v) acetazolamide, which was the desired drug concentration. In the final formulation the HP $\beta$ CD concentration was in approximately 10% excess or 18% (w/v) in order to prevent possible precipitation on storage. The shelf life of these solutions was more than two years (53).

Release study, done with cellophane membrane in Franz-diffusion cell, showed that the concentration of HP $\beta$ CD in the final formulation allowed maximum availability of the drug (Figure 15).

The efficacy of the 1% acetazolamide eye-drop solution was tested in vivo, first in animals and then in humans. In humans the IOP lowering activity was similar to that obtained for the commercially available 2% dorzolamide eye drop solution (Figure 16).



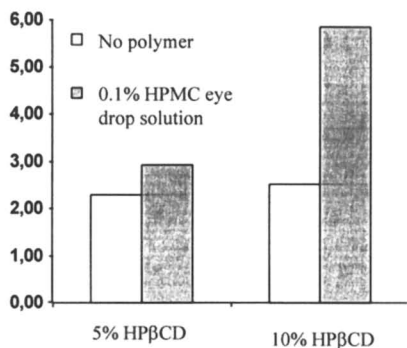


Figure 14. The solubility of acetazolamide in eye drop solutions prepared with and without polymer. (Adapted from ref. 53)

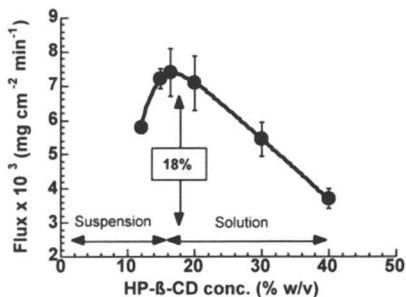


Figure 15 Release of acetazolamide through semi-permeable cellophane membrane (Adapted from ref. 53)

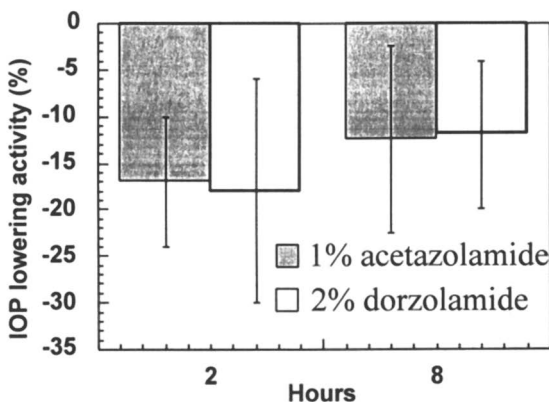


Figure 16 The mean IOP lowering activity of 1% acetazolamide CB-DDS eye-drop solution (n=9) and 2% dorzolamide HCl eye-drop solution. (Adapted from ref 53)

### Dexamethasone eye-drop formulation (56-58).

Corticosteroids which are used for treatment of inflammatory disease of the eye are administered topically or systemically. Dexamethasone is a water insoluble compound and can only be included in eye drop solution as aqueous suspension or as water soluble prodrugs, e.g. dexamethasone phosphate. Due to low availability the

topical administration is mostly used to treat the outer and anterior segments of the eye. Treatment of the posterior segment of the eye will usually require oral administration (59). Topical administration with increased bioavailability could eliminate the need for oral administration and reduce the potential side effects. Following is the description of the development and testing of dexamethasone eye drop solution formulated with HP $\beta$ CD and polymer in order to increase bioavailability.

The dexamethasone eye drop solution was developed in similar steps as the acetazolamide eye-drop solution. The dexamethasone eye drop contained dexamethasone in 1.3%, 0.67% or 0.32% concentration, HP $\beta$ CD in a 10% excess of what was needed to solvate dexamethasone, 0.1 % (w/v) HPMC, 0.01 % (w/v) benzalconium chloride, 0.05 % (w/v) sodium EDTA and sufficient NaCl to make the solution isotonic with the tear fluid. The phase solubility study revealed a relatively small increase in the solubility (6%) when formulation with polymer was compared to formulation without polymer. Similarly the maximum release through cellophane membrane was obtained for the HP $\beta$ CD concentrations used in the final formulations but there was only a small increase when polymer was included in the solution.

Patients scheduled to undergo cataract surgery were recruited for human bioavailability study. One drop (50  $\mu$ l) of eye-drop solution was administered to the eye prepared for cataract surgery and at predetermined time points and before opening of the anterior chamber a 0.1 ml sample of the aqueous humor was withdrawn with a small needle and a syringe. The solubility and in-vitro release studies had only shown small improvements in the formulation after a drug/CD/polymer co-complex had been prepared. To investigate the effectiveness of the co-complex, 0.67 % solutions of dexamethasone/HP $\beta$ CD/polymer co-complex was prepared by heating in autoclave and the bioavailability was compared to a solution where the constituents were the same but the heating procedure had been omitted. Significant increase in the dexamethasone bioavailability at all time points was detected for the co-complex formulation, with about 4 fold increase in the relative bioavailability (area under the curve) (Figure 17). The availability from dexamethasone eye drop solution (0.32 %) was compared to commercially available alcoholic suspension of dexamethasone (Maxidex). The bioavailability from the HP $\beta$ CD/polymer solution was twice the value determined for the alcoholic suspension (Figure 18).

### **Estradiol sublingual tablets (46, 60)**

The steroid, 17 $\beta$ -estradiol is used in hormone replacement therapy (HRT) in post-menopausal women. Good clinical results have been obtained after oral administration of microdosed 17 $\beta$ -estradiol. However bioavailability is low due to first-pass effect and therefore large doses must be administered. First-pass effects can

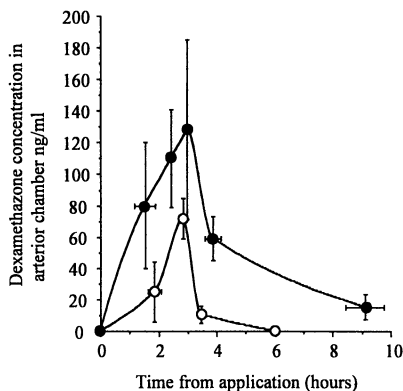


Figure 17 Dexamethasone concentration in aqueous humor after administration of 1) heated (●) 0.67% dexamethasone-HP $\beta$ CD-HPMC and unheated (○) 0.67% dexamethasone-HP $\beta$ CD. Mean concentration  $\pm$  s.e.m. after administration of the eye drops. (Adapted from ref. 58)

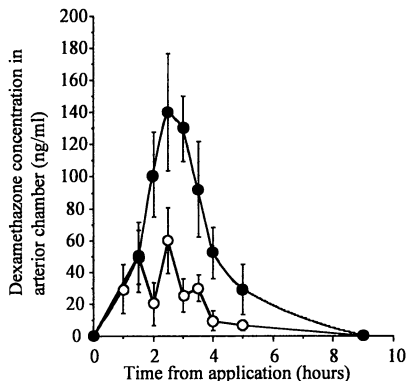


Figure 18. Dexamethasone concentration ( $\pm$  s.e.m.) in the aqueous humor of humans after administration of 0.32% (●) dexamethasone in an aqueous HP $\beta$ CD-HPMC solution or (○) 0.1% dexamethasone alcoholic suspension (Maxidex<sup>®</sup>) (Adapted from ref. 58)

be avoided by adsorption through various non-intestinal membranes of the body. The buccal mucosa of the oral cavity is an easily accessible and convenient side for such delivery. It is continuously exposed to various foreign substances and is therefore relatively robust.

Following is the description of formulation of 17 $\beta$ -estradiol with HP $\beta$ CD and polymers into sublingual tablets and clinical evaluation of bioavailability.

Solubility study showed that significant enhancement in the complexation efficiency was achieved with addition of CMC. The dissolution rates were determined for three different formulations: 1) tablets containing physical mixture of drug and CD, 2) tablets containing lyophilized drug-HP $\beta$ CD without addition of CMC and 3) tablets containing lyophilized drug-HP $\beta$ CD complex where the complexation efficacy had been enhanced through addition of CMC. The fastest dissolution was observed for the drug-HP $\beta$ CD/CMC formulation (Figure 19). The release, i.e. final concentration of the drug, was also higher. Thus the tablets containing the drug-HP $\beta$ CD/CMC were chosen for clinical evaluation.

A supraphysiologic peak of 17 $\beta$ -estradiol was observed 15 minutes after sublingual administration (Figure 20.). The half-life of the absorption was estimated to be 7 minutes, which indicated that 90% of the total dose was absorbed in 25 minutes.

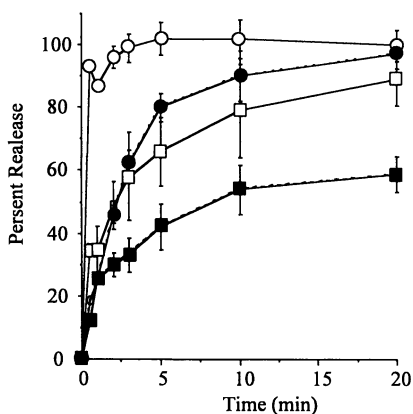


Figure 19 The dissolution rate profiles of  $17\beta$ -estradiol from sublingual tablets. Tablets containing pure  $17\beta$ -estradiol (■), tablets containing physical mixture of  $17\beta$ -estradiol and HP $\beta$ CD (□), tablets containing lyophilized  $17\beta$ -estradiol-HP $\beta$ CD inclusion complex with excess of HP $\beta$ CD (●), and tablets containing lyophilized  $17\beta$ -estradiol-HP $\beta$ CD without excess of HP $\beta$ CD (○).

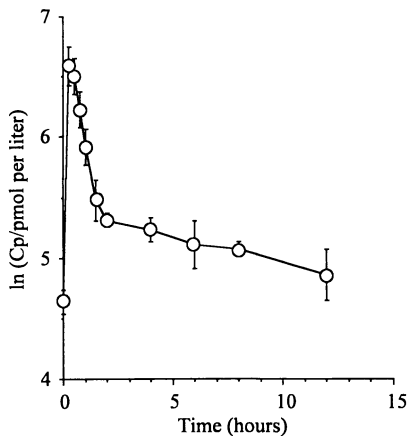


Figure 20 The  $17\beta$ -estradiol concentration ( $\ln C_p$ ) versus time, after sublingual administration of  $100\mu\text{g}$  of  $17\beta$ -estradiol. Mean values from 6 women

## Conclusion.

The CDs have many attractive properties which make them unique as pharmaceutical excipients. They solvate drugs into aqueous formulation through inclusion complexation. Formulations containing 1:1 complexes of the drug can be diluted without precipitation of the drug. The drug is often protected in the cyclodextrin cavity and thus the stability of chemically unstable drugs is dramatically increased. The complex formation is rapidly reversible and the availability of drugs can therefore be increased by formulation in CD solutions. The bioavailability enhancement by CDs can be combined with classical permeation enhancers to further increase the drug availability.

The first pharmaceutical products have been introduced to the market with more than twenty CD formulations approved in the United States, Europe and Japan. The acceptance of the relative safety of these compounds is also growing among industry

and regulatory authority. The use of CDs in pharmaceutical applications is therefore rapidly expanding.

The main obstacle to wider use of CDs is the large increase in the bulk of dry material in the formulations. Even under the most ideal conditions the increase will be 4 to 10 fold.

By heating drug/CD solution in the presence of small amount of polymer the complexation efficacy can be increased, allowing less CD to be used. In some case a more than 2-fold increase in solubility of the drug, with the same concentration of CD, is observed. The solubility of  $\beta$ CD complexes could also be increased. Furthermore, the bioavailability from drug/CD/polymer formulations can be significantly increased. For example, the 0.1% HPMC formulation of dexamethasone with HP $\beta$ CD resulted in 4-fold increase in the drug bioavailability. The polymer enhancement of drug solubility and bioavailability is independent of its physicochemical properties. Thermodynamic investigation and other studies indicated that the polymer interacted directly with the drug/CD complex. Formulation of drugs with CDs and polymer can therefore further enhance the attractive properties of CDs as excipients

## References

- (1) Villers, A. C. *R. Acad. Sci.* **1891**, *112*, 536-538.
- (2) Fromming, K. H.; Szejtli, J. *Cyclodextrins in pharmacy*; Kluwer Academic Publishers: Dordrecht, 1994.
- (3) Loftsson, T.; Ólafsson, J. H. *Int. J. Dermatol.* **1998**, *37*, 241-246
- (4) Rajewski, R. A.; Stella, V. J. *J. Pharm. Sci.* **1996**, *86*, 1142-1168.
- (5) Stella, V.; Rajewski, R. A. *Pharm. Res.* **1997**, *14*, 556-567.
- (6) Miyazawa, I.; Ueda, H.; Nagase, H.; Endo, T.; Kobayashi, S.; Nagai, T. *Eur. J. Pharm. Sci.* **1995**, *3*, 153-162.
- (7) Endo, T.; Nagase, H.; Ueda, H.; Kobayashi, S.; Nagai, T. *Chem. Pharm. Bull.* **1997**, *45*, 532-536.
- (8) Ueda, H.; Endo, T.; Nagase, H.; Kobayashi, S.; Nagai, T.; in: Szejtli, J.; Szente, L., (Eds.): *Proceedings of the Eighth International Symposium on Cyclodextrins*, Budapest 1996; Kluwer Academic Publishers; pp. 17-20.
- (9) Szejtli, J. *Cyclodextrin Technology*; Kluwer Academic Publishers: Dordrecht, 1988.
- (10) Loftsson, T.; Brewster, M. E. *J. Pharm. Sci.* **1996**, *85*, 1017-1025.
- (11) Thompson, D. O. *CRC Crit. Rev. Ther. Drug Carrier Syst.* **1997**, *14*, 1-104.
- (12) Irie, T.; Uekama, K. *J. Pharm. Sci.* **1997**, *86*, 147-162.
- (13) Schipper, N. G.; Verhoef, J. C.; Romeijn, S. G.; Merkus, F. W. *Calcif. Tiss. Int.* **1995**, *56*, 280-282.
- (14) Kublik, H.; Bock, T. K.; Schreier, H.; Muller, B. W. *Eur. J. Pharm. Biopharm.* **1996**, *42*, 320-324.
- (15) Higuchi, T.; Connors, K. A. *Adv. Anal. Chem. Instrum.* **1965**, *4*, 117-212.
- (16) Jarho, P.; Urtti, A.; Järvinen, T. *Pharm. Res.* **1995**, *12*, 1371-1375.

- (17) Loftsson, T.; Jónsdóttir, B.; Baldvinsdóttir, J.; Fridriksdóttir, H. S. *T. P. Pharma Sci.* **1994**, *4*, 354-358.
- (18) Loftsson, T. *Drug Stability* **1995**, *1*, 22-33.
- (19) Másson, M.; Loftsson, T.; Jónsdóttir, S.; Fridriksdóttir, H.; Petersen, D. S. *Int. J. Pharm.* **1998**, *164*, 45-55.
- (20) Pop, E.; Loftsson, T.; Bodor, N. *Pharm. Res.* **1991**, *8*, 1044-1049.
- (21) Jarho, P.; Urtti, A.; Jarvinen, K.; Pate, D. W.; Jarvinen, T. *Life Sciences* **1996**, *58*, 181-185.
- (22) Loftsson, T.; Ólafsdóttir, B. J. *Int. J. Pharm.* **1991**, *67*, 5-7.
- (23) Másson, M.; Másson, G.; Loftsson, T.; Stefánsson, E.; *J. Contr. Rel.* (in press)
- (24) Meidan, M. V.; Docker, M.; Walmsley, A. D.; Irwin, W. J. *Pharm. Res.* **1998**, *15*, 85-92.
- (25) Illel, B.; Schaefer, H.; Wepierre, J.; Doucet, O. *J. Pharm. Sci.* **1991**, *80*, 424-427.
- (26) Loftsson, T.; Sigurdardottir, A. M. *Eur. J. Pharm. Sci.* **1994**, *2*, 297-301.
- (27) Jarho, P.; Jarvinen, K.; Urtti, A.; Stella, V. J.; Jarvinen, T. *Int. J. Pharm. Pharmacol.* **1996**, *48*, 264-270.
- (28) Ruddy, S. B.; In *Percutaneous Penetration Enhancers*; Smith, E. W., Maibach, H. I., Eds.; CRC Press, Inc.: N.Y., 1995, pp 245-258.
- (29) Smith, E. W.; Maibach, H. I.; In *Percutaneous Penetration Enhancers*; Smith, E. W., Maibach, H. I., Eds.; CRC Press, Inc.: N.Y., 1995, pp 1-4.
- (30) Loftsson, T.; Masson, M.; Sigurdsson, H. H.; Magnusson, P.; Goffic, F. L. *Pharmazie* **1997**, *53*, 137-139.
- (31) Loftsson, T.; Másson, M.; Sigurjónsdóttir, J. F.; Fridriksdóttir, H.; *Proceedings of the 17th Pharmaceutical Technology Conference and Exhibition*, Dublin, Ireland 1998; pp. .
- (32) Loftsson, T.; Petersen, D. S. *Drug Dev. Ind. Pharm.* **1998**, (in print)
- (33) Loftsson, T.; Bodor, N. *Acta Pharm. Nord.* **1989**, *1*, 185-193.
- (34) Piel, G.; Evrard, B.; Fillet, M.; Llabres, B.; Delattre, L. *Int. J. Pharm.* **1998**, *169*, 15-22.
- (35) Connors, K. A. *Chem. Rev.* **1997**, *97*, 1325-1357.
- (36) Loftsson, T. : *UP 5,472,954*, 5 dec. **1995**.
- (37) Riley, C. M.; Rytting, J. H.; Kral, M. A. *Equilibria and Thermodynamics*; Allen Press: Lawrence (Kansas), 1991.
- (38) Loftsson, T.; Fridriksdóttir, H.; Gudmundsdóttir, T. K. *Int. J. Pharm.* **1996**, *127*, 59-66.
- (39) Usui, F.; Maeda, K.; Kusai, A.; Nishimura, K.; Yamamoto, K. *Int. J. Pharm.* **1997**, *154*, 59-66.
- (40) Attwood, D.; Florence, A. T. *Surfactant Systems. Their Chemistry, Pharmacy and Biology*; Chapman and Hall: London, 1983.
- (41) Myers, D. *Surfactant Science and Technology*; VCH Publishers: New York, 1988.
- (42) Heyuhas, D.; Lichtenberg, D. *Biophys. J.* **1996**, *71*.

- (43) Loftsson, T.; Sigurdardóttir, A. M.; *Proceedings of the Eighth International Symposium on Cyclodextrins*, Budapest 1996; Kluwer Academic Publishers; pp. 403-406.
- (44) Loftsson, T.; Stefánsson, E.; Fridriksdóttir, H.; Kristinsson, J. K. Szejtli, J.; Szente, L., (Eds.): *Proceedings of the Eighth International Symposium on Cyclodextrins* Budapest 1996; Kluwer Academic Publishers; pp. 407-412.
- (45) Loftsson, T.; Fridriksdóttir, H.; Sigurdardóttir, A. M.; Ueda, H. *Int. J. Pharm.* **1994**, *110*, 169-177.
- (46) Fridriksdóttir, H. Ph. D. Thesis, University of Iceland, Reykjavik, Iceland, 1997.
- (47) Loftsson, T.; Petersen, D. S. *Drug Dev. Ind. Pharm.* **1998**, *24*, 365-370
- (48) Loftsson, T.; Stefansson, E.; Kristinsson, J. K.; Fridriksdóttir, H.; Sverrisson, T.; Gudmundsdóttir, G.; Thorisdóttir, S. *Pharm. Sci.* **1996**, *6*, 277-279.
- (49) Fridriksdóttir, H.; Loftsson, T.; Stefánsson, E. *J. Contr. Rel.* **1997**, *44*, 95-99.
- (50) Loftsson, T.; Gudmundsdóttir, T. K.; Fridriksdóttir, H. *Drug Dev. Ind. Pharm.* **1996**, *22*, 401-405.
- (51) Loftsson, T.; Fridriksdóttir, H. *Int. J. Pharm.* **1998**, *163*, 115-121.
- (52) Savolainen, J.; Jarvinen, K.; Taipale, H.; Jarho, P.; Loftsson, T.; Jarvinen, T. *Pharm. Res.* **1998**, *15*, 1696-1701
- (53) Loftsson, T.; Fridriksdóttir, H.; Stefansson, E.; Thorisdóttir, S.; Gudmundsson, O.; Sigthorsson, T. *J. Pharm. Pharmacol.* **1994**, *46*, 503-504.
- (54) Backer, B. *American Journal of Ophthalmology* **1954**, *13*, 13-15.
- (55) Maren, T. H. In *United States Patent*; University of Florida: U.S.A., 1986, pp 6.
- (56) Loftsson, T.; Fridriksdóttir, H.; Thórisdóttir, S. u.; Stefánsson, E. *Int. J. Pharm.* **1994**, *104*, 181-184.
- (57) Loftsson, T.; Stefansson, E. *Drug Dev. Ind. Pharm.* **1997**, *23*, 473-481.
- (58) Kristinsson, J. K.; Fridriksdóttir, H.; Thórisdóttir, S.; Sigurdardóttir, A. M.; Stefánsson, E.; Loftsson, T. *Invest. Ophthalmol. & Vis. Sci.* **1996**, *37*, 1199-1203.
- (59) Gordon, D. M. *Am. J. Ophthalmol.* **1959**, *48*, 656-660.
- (60) Fridriksdóttir, H.; Loftsson, T.; Gudmundsson, J. A.; Bjarnasson, G. J.; Kjeld, M.; Thorsteinsson, T. *Pharmazie* **1996**, *51*, 39-42.

## Chapter 4

# Preparation of Polyrotaxanes and Molecular Tubes for Host–Guest Systems

Pierandrea LoNostro<sup>1</sup>, Massimo Ceccato, and Piero Baglioni

Department of Chemistry and CSGI, University of Florence,  
via Gino Capponi 9, 50121 Firenze, Italy

Linear polymers, such as long chain aliphatic alcohols or polyethyleneoxide derivatives, can form peculiar structures (called "polyrotaxanes"), when mixed with molecules that contain a suitable cavity, for example cyclodextrins and crowns. Polyrotaxanes can be converted into stable structures called "molecular necklaces" and "molecular tubes", that keep the hosting properties of their precursors, and that can be used to entrap small molecule or ions in their cavities. These products are relevant in the study of several biological structures (ribosomes, membranes, DNA complexes), and for the development of industrial processes in which the main factor is the uptake and removal of an undesired product, or its transfer from one environment to another medium. We report some studies carried out by kinetics, UV and NMR measurements on the structure and properties of some cyclodextrin-based host molecules, and their capacity to include ions or small molecules.

Cyclodextrins form a great number of inclusion compounds with low-molecular weight molecules and ions, that have already been studied and characterized (1-5). Depending on the number of glucose moieties, the most common oligomers are  $\alpha$ -,  $\beta$ -, and  $\gamma$ -cyclodextrin (see Figure 1). Long linear or branched molecules, such as polyethylene glycols and aliphatic alcohols (6-10), produce threaded complexes with cyclodextrin (CD) that are called "polyrotaxanes" (1,2,6,7,11), from "rota" (Latin for wheel), and

<sup>1</sup> E-mail: [LONOSTRO@hotmail.com](mailto:LONOSTRO@hotmail.com). Voice: +39 (055) 275-7567. Fax: +39 (055) 24.08.65. Internet: <http://mac.chim.unifi.it>



"axis" (Latin for axle). Figure 2 schematically shows the formation of a polyrotaxane main chain: these structures are obtained upon threading of some cyclic molecules over a linear chain that penetrates into their empty cavities (11-17). The formation of these host-guest systems is driven by the stabilization of the final product, where strong non-covalent interactions are established between the host and the guest. Polyrotaxanes can be obtained from a number of different chemicals: besides cyclodextrins, crowns, and porphyrins, other macrocyclic ligands have been used as host molecules, while several different kinds of long chain alkyl derivatives have been checked as linear guests (18-23).

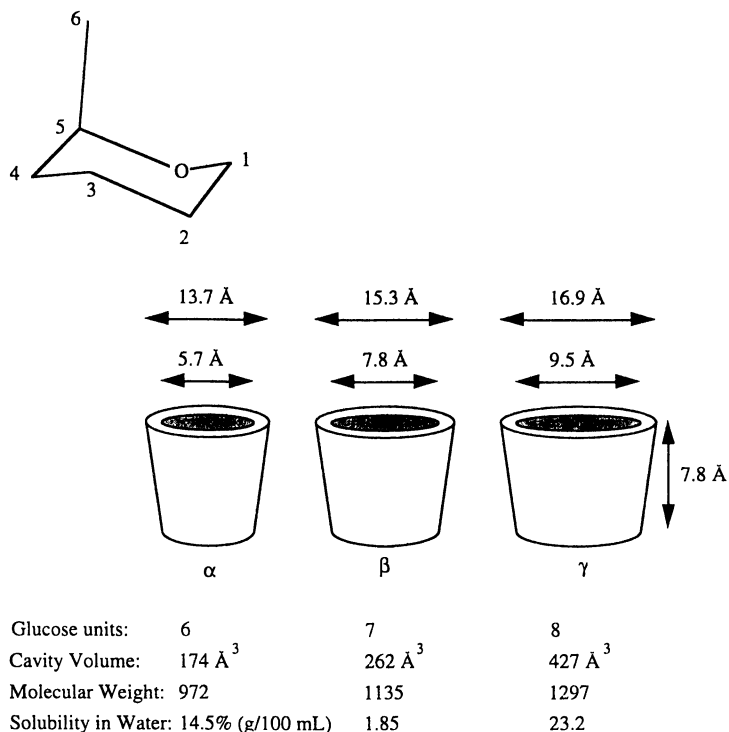
The addition of bulky stoppers at both the ends of the linear chain keeps the host molecules around the guest component, and avoids the threaded units from sliding away. The kinetics of the threading process significantly depends on the nature of the solvent where the polyrotaxane formation takes place, and on temperature (24). The threading process does not occur if PEG is replaced with propylene glycol, because of the presence of branched methyl groups in the chain that increase the cross-section of the linear polymer (11). Similarly, the formation of the molecular necklace (MN) is avoided when  $\alpha$ -CD is substituted with one of its larger homologues,  $\beta$ - or  $\gamma$ -CD, that possess larger cavities, and cannot properly interact with the polymer. Removal of the PEG chain from the adduct results in the final MT, that can act as a host for reversible binding of organic molecules and ions (11,22). Besides their interest in Topological Chemistry (2,25), polyrotaxanes are an important model for the study of the structure and properties of relevant biological systems such as membranes, ribosomes and enzyme complexes that result from the aggregation of relatively simple subunits (4,11).

Harada and coworkers (11,13) reported the formation of a threaded molecular structure, named *molecular necklace* (shortly MN) formed by  $\alpha$ -CD and 2,4-dinitrobenzene-PEG, and the synthesis of the so-called *molecular tube* (shortly MT), obtained upon cross-linking with epichlorohydrin of  $\alpha$ -CD that form the MN, and then the removal of the linear PEG chain (11). MT is a rod-like, rigid molecule that keeps the same internal hydrophobic cavities of  $\alpha$ -CD.

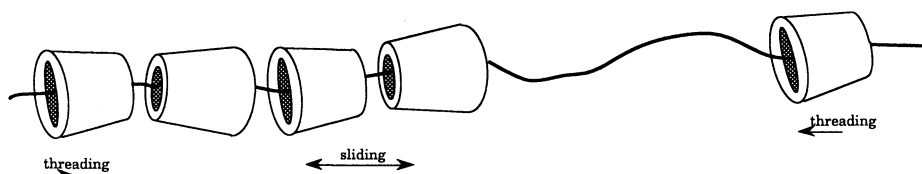
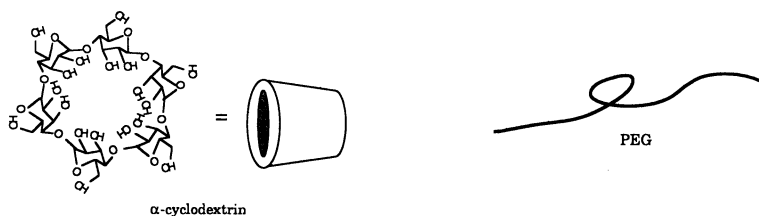
In the recent past the study of molecular recognition, operated by relatively small ligands that selectively bind ions and organic molecules, has been the object of several works (26-31). However, very large host-guest systems are required for the study of more complicated biological complexes such as enzyme-substrate, antigen-antibody, DNA, RNA, and cell adhesion systems (22).

The entrapment of ions and organic molecules is very important with the perspective of using host species also as molecular cages in enantiomeric enrichment, isomer separation, molecular recognition, for the removal of undesired compounds from industrial products (32), in drug delivery and other biomedical applications (33).

In this paper we report a study on the threading process involved in the formation of the  $\alpha$ -CD/PEG<sub>3350</sub> polyrotaxane, carried out at different temperatures and in different solvents, and we propose a model for the interpretation of the threading phenomenon. Moreover we investigated the dynamic properties of free  $\alpha$ -CD, MN, PEG-MT, and MT (see Figure 2) by <sup>13</sup>C-NMR at different temperatures in d<sup>6</sup>-DMSO. The experimental findings indicate that in MT,  $\alpha$ -CD rings are indeed aligned



### 1. Structure and properties of $\alpha$ -, $\beta$ -, and $\gamma$ -cyclodextrin.



2. Formation of the polyrotaxane: the PEG linear chain penetrates the free empty cavity of several  $\alpha$ -CD rings that move towards the center of the stretched polymer.

and linked like the coaches of a train, and that MT shows a faster re-orientational motion with respect to  $\alpha$ -CD, MN, and PEG-MT. Finally, we found evidence for the formation of a host-guest inclusion complex when an aqueous solution of  $I_3^-$  or caffeine is added to a water dispersion of the molecular tube, by recording UV spectra.

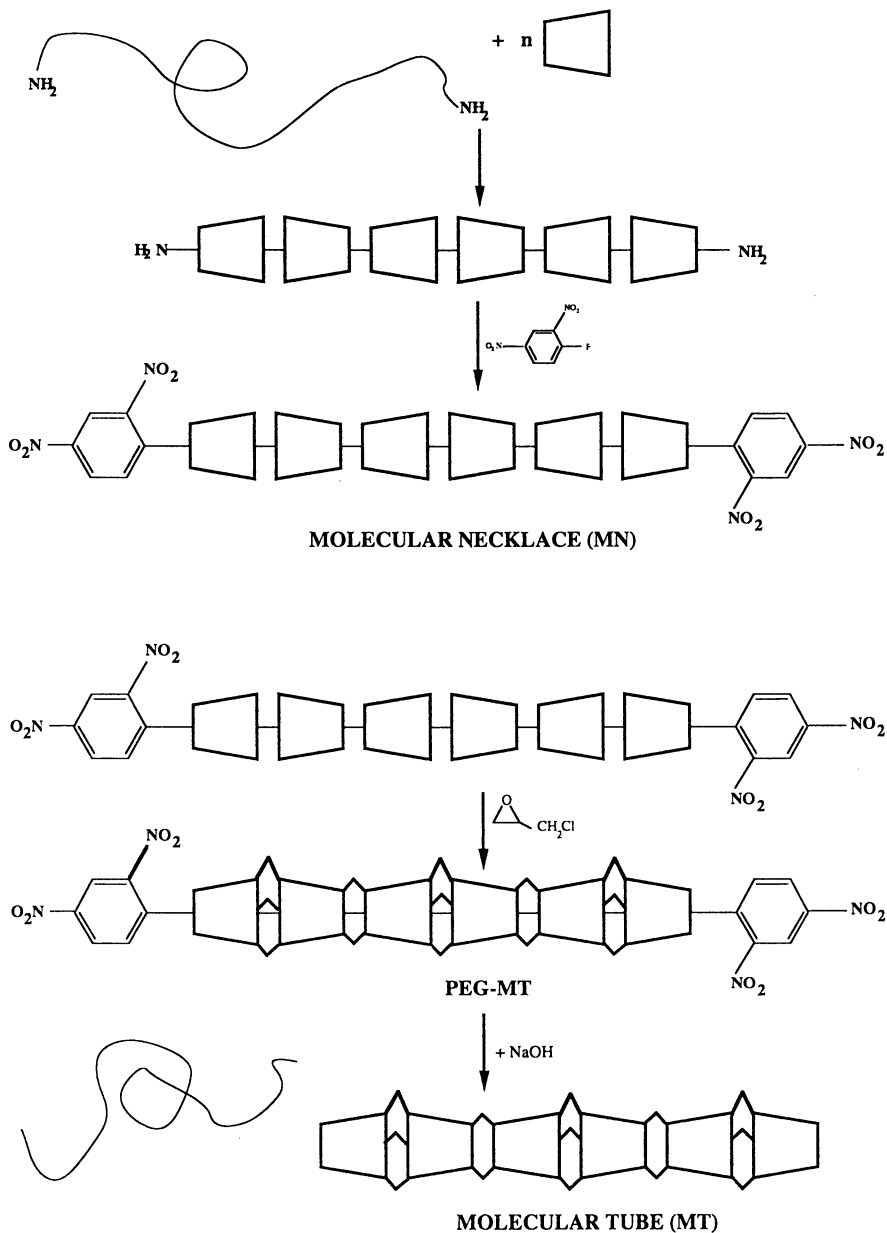
### Materials and Methods

$\alpha$ -CD, 2,4-dinitro-fluorobenzene, dimethylsulfoxide, N,N-dimethylformamide, epichlorohydrin, and PEG<sub>3350</sub>-bis-amine were purchased from Sigma-Aldrich Srl (Milan, Italy). Hydrochloric acid, sodium hydroxide, diethylether, deuterium oxide, caffeine and deuterated dimethylsulfoxide were from Fluka (Milan, Italy). All chemicals were used as received. For all experiments we used bidistilled water purified with a MilliQ system (Millipore) to remove colloidal impurities.

**Synthesis.** The synthesis of the MT is a four step procedure (11,13) and is schematically depicted in Figure 3. NMR, polarimetry, and LC chromatography were used to isolate, purify, and characterize the reaction intermediates and the final products as well.

A water solution of  $\alpha$ -CD (14%) and an aqueous solution of polyethylene-glycol-bis-amine (PEG-BA) (12%) are mixed at room temperature (molar ratio  $\approx$  30). After an hour a thick solid gel is formed. The gel is presumably due to aggregation of polyrotaxanes that entrap a large amount of solvent in the free cavities. The gel is then filtered under reduced pressure and stored in a dessiccator under vacuum in the presence of 96%  $H_2SO_4$  (yield = 90%). The product is then dissolved in DMF, a large excess of 2,4-dinitro-fluorobenzene is added and the solution stirred at room temperature for 24 hours. Eventually the addition of diethylether will precipitate a yellow solid that is filtered under vacuum, washed, and stored in a dessiccator in the presence of 96%  $H_2SO_4$  (yield = 70%). Unreacted  $\alpha$ -CD and PEG are removed by washing with water. Column chromatography (Sephadex G-50, DMSO) is used to purify the product by checking the absorbance spectrum and the optical solution of each eluted portion. UV/VIS spectrum shows the presence of the molecular necklace in the first elution peak, and of unreacted 2,4-dinitro-fluorobenzene that appears in another peak. After removing the solvent, the solid is dissolved in 10% aqueous solution of NaOH, and treated with an excess of epichlorohydrin that binds two adjacent molecules of  $\alpha$ -CD by cross-linking hydroxyl groups. The mixture is stirred at room temperature for 36 hours. After neutralization of the solution with HCl and evaporation of the solvent under vacuum, a viscous yellow oil is obtained, and the hydrolysis of the dinitro-benzene residues from the PEG chain is achieved by treating the product with aqueous 25% NaOH for 24 hours at room temperature, and then neutralizing with HCl. The final solution is eluted through a chromatography column (Sephadex G-25, water) so that all sub-products are removed from the solution.

UV/VIS spectra were recorded with a Lambda 5 Spectrophotometer (Perkin-Elmer), using a thermostatted bath to control the temperature of the cuvette ( $\pm 0.1^\circ C$ ). Fixed volumes of aqueous solutions of  $\alpha$ -CD and PEG were mixed in the cuvette (185 mg of  $\alpha$ -CD and 11 mg PEG in 3 mL of solvent), and the absorbance measurement (at



3. Synthesis of the molecular necklace (MN) and of the molecular tube (MT) by using bulky, benzene-based, stoppers to prevent the sliding of  $\alpha$ -CD from PEG, then cross-linking  $\alpha$ -CD with epichlorohydrin, and finally with an alkaline hydrolysis.

$\lambda=400$  nm) was started immediately after, until a thick solid, white gel was formed. The reference sample was pure water.

For NMR experiments we used Varian XL200 and Bruker AMX600 instruments. The carbon-spin-lattice relaxation rate of  $0.16 \text{ mol dm}^{-3}$  solution of  $\alpha$ -CD in  $d^6$ -DMSO and  $7 \cdot 10^{-3} \text{ mol} \cdot \text{dm}^{-3}$  solutions of PEG-MT and MT (to obtain the same number of carbon atoms in all cases) have been measured in the temperature range 25-70 °C.  $^{13}\text{C}$ -NMR experiments were performed to determine the rate constant of relaxation  $r_1$  with sequence  $(180^\circ\text{-}\tau\text{-}90^\circ\text{-t})_n$ , modified to remove the scalar coupling between  $^1\text{H}$  and  $^{13}\text{C}$  nuclei. The proton decoupling "broad-band" induced an increment in the  $^{13}\text{C}$  signal, due to the Nuclear Overhauser Effect (NOE). The value of  $r_1$  was calculated from the following equation:

$$A_\infty - A_\tau = 2A_\infty \cdot \exp(-\tau \cdot r_1) \quad (1)$$

where  $A_\infty$  is the integral of absorbance line before the perturbation, and  $A_\tau$  is the integral of absorbance line at time  $\tau$ . Experimental errors for  $r_1$  were  $\pm 5\%$ . In these conditions we observed that the only effective relaxation mechanism was the dipolar interaction. In fact, other mechanisms can be excluded according to NOE results.

The dipolar interaction in solution, modulated by Brownian motion, results in a magnetic field swinging, that can produce relaxation. Therefore, from carbon spin-lattice relaxation rate measurements we obtained a complete description of the dynamic properties of PEG-MT and MT at different temperatures. For protonated carbon nuclei (the proton-carbon distance being constant and known), the following equations hold:

$$R_1^{DD} = r_1 \cdot \chi^{DD} \quad (2)$$

$$\chi^{DD} = \frac{NOE_{exp.}}{NOE_{theor.}} \quad (3)$$

$$R_1^{DD} = \frac{1}{10} \frac{h^2 \gamma_H^2 \gamma_C^2}{r_{C-H}^6} \left[ \frac{3 \tau_c}{1 + \omega_C^2 \tau_c^2} + \frac{6 \tau_c}{1 + (\omega_H + \omega_C)^2 \tau_c^2} + \frac{\tau_c}{1 + (\omega_H - \omega_C)^2 \tau_c^2} \right] \quad (4)$$

these equations calculate the effective correlation time  $\tau_c$ .  $R_1^{DD}$  is the dipolar contribution to the experimental spin-lattice relaxation rate;  $\chi^{DD}$  is the dipolar fraction term obtained from the ratio between the experimental and theoretical broad-band proton-carbon nuclear overhauser effect (NOE);  $\gamma_H$ ,  $\gamma_C$  and  $\omega_H$  and  $\omega_C$  are the proton and carbon magnetogyric ratios and Larmor frequencies respectively;  $r_{C-H}$  is the proton-carbon internuclear distance and  $\tau_c$  is the effective rotational correlation time.

## Results and Discussion

The results obtained from the study of the kinetic of the threading process, of the dynamics of the  $\alpha$ -CD/PEG adducts, and of the host-guest properties will be discussed separately.

### Kinetic study.

The threading and sliding of  $\alpha$ -CD on a linear PEG molecule (see Figure 2), and the precipitation of large aggregates occur when the two compounds are mixed in water, result in the appearance of strong turbidity in the sample, and eventually in the formation of a thick gel. The nature of the solvent and temperature strongly affect the process.

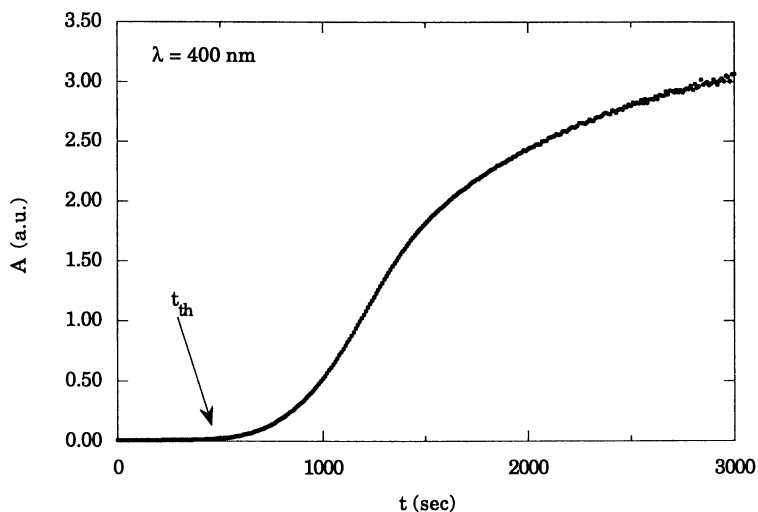
Assuming that the PEG chain threads  $\alpha$ -CD units until it is completely covered, the total number of  $\alpha$ -CD around the PEG molecule can be predicted in two ways: from the fully-stretched length of polyethylene glycol and the depth of  $\alpha$ -cyclodextrin (7.8 Å), and by measuring the molecular weight of the final polyrotaxane (13). In both cases about 20-25 molecules of  $\alpha$ -CD are expected to be threaded by a single linear PEG<sub>3350</sub> molecule, therefore the estimated total length of the final product with 20-25 aligned  $\alpha$ -CD molecules is about 150 to 200 Å. According to the polyrotaxane's size, and recalling that the Rayleigh scattering occurs when particles are bigger than  $\lambda/20$  (where  $\lambda$  is the wavelength of incident light) (14), we measured the absorbance of the  $\alpha$ -CD/PEG solution as a function of time (t) at  $\lambda=400$  nm (see Figure 4), where neither  $\alpha$ -CD, nor PEG, absorb. The A/t curve shows three regions: in the first part, for  $0 < t < t_{th}$ , absorbance remains almost constant, and we assume that during this time the threading phenomenon takes place. After that time, A increases rapidly, as a result of polyrotaxanes' aggregation and precipitation, and finally it reaches an asymptotic average value.

We studied in detail the first part of the curve, where the formation of polyrotaxanes occurs, and defined the time required to record a detectable increment in absorbance as *threading time* ( $t_{th}$ ), for the reaction:

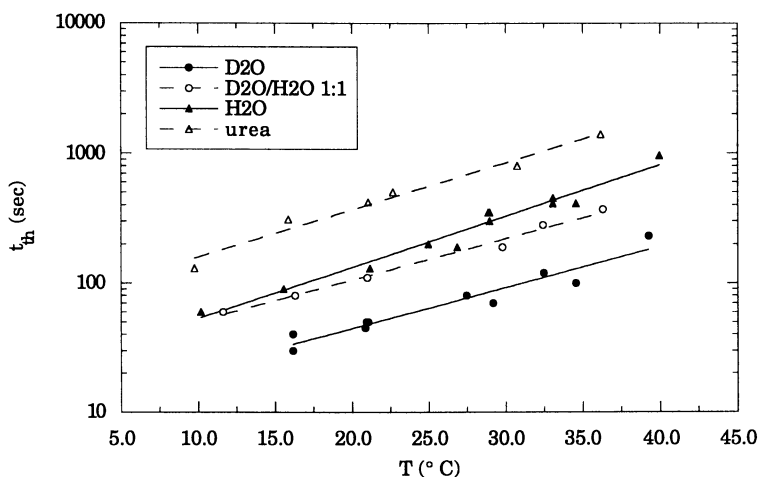


Since for  $t > t_{th}$  the absorbance rapidly increases, as a result of the aggregation of several polyrotaxanes, we assume that the whole threading process occurs during  $t_{th}$ . In order to study the threading phenomenon and to propose a model for its interpretation, we investigated the effect of temperature, solvent composition, and dilution of the solution on  $t_{th}$ , using a large excess of  $\alpha$ -CD with respect to PEG.

Figure 5 shows the variation of  $t_{th}$  with temperature between 10 and 40 °C, for four different solvents: water, heavy water, a 1:1 H<sub>2</sub>O/D<sub>2</sub>O mixture, and urea (0.1 M in water). These solvents possess different hydrogen bonding networks (15-17,34); in fact the strength of hydrogen bonds decreases in the order D<sub>2</sub>O>H<sub>2</sub>O>urea. The trend indicates that the reaction is strongly affected by T, with a significant increase in  $t_{th}$  when temperature increases. Moreover, the reaction depends on the solvent composition with a relevant increment of  $t_{th}$  in going from D<sub>2</sub>O to H<sub>2</sub>O/D<sub>2</sub>O 1:1, to H<sub>2</sub>O and to urea for each T value.



4. Variation of absorbance ( $A$ ) with time ( $t$ ) at  $\lambda = 400$  nm after mixing  $\alpha$ -CD and PEG aqueous solutions;  $t_{th}$  is defined as the time required for  $A$  to increase from the initial zero value.



5. Variation of  $t_{th}$  as a function of temperature for four different solvents possessing different hydrogen bonding networks.

Thirdly, we checked the dilution of the two reactants in the solvent, keeping their molar ratio  $\alpha$ -CD/PEG constant (about 56). Figure 6 reports  $\ln(t_{th})$  versus the PEG molar concentration ( $c$ ); the plot clearly shows that the reaction goes faster as  $c$  increases.

Harada has shown that the threading process rate depends on the PEG chain length, and reaches a maximum when the linear polyethylene glycol molecule has a molecular weight of about 3000 (11).

In order to explain our experimental data and the findings reported by the literature (10) regarding the effect of the PEG chain length on the threading process, we propose a model at the microscopic level that takes into account five different steps in which the whole phenomenon can be divided:

- a) diffusion of the two reactants in the solvent
- b) initial threading of PEG ends into  $\alpha$ -CD cavities
- c) sliding of  $\alpha$ -CD over the PEG chain
- d) de-threading of  $\alpha$ -CD from the PEG chain
- e) precipitation of the final large aggregate.

a) When  $\alpha$ -CD and PEG are dissolved in the solvent, they will randomly move by diffusion. Some of the  $\alpha$ -CD molecules will be located in the proper position for the threading to occur. The diffusion process is expected to be ruled by temperature and solvent, with a lowering of  $t_{th}$  (faster process) when  $T$  increases and when the solvent possesses weaker hydrogen bonds. The experimental data show that  $t_{th}$  increases as  $T$  increases and with a weakening of the solvent structure, and thus indicate that the diffusion is not the main step of the whole threading process.

b) When the  $\alpha$ -CD cavity is correctly oriented in front of the PEG chain, the initial threading may occur. The initial threading is favoured and driven by the attractive interactions between the  $\alpha$ -CD internal cavity and the  $-O-CH_2-CH_2-$  units of the linear PEG chain. This step is favoured by low temperatures and highly structured solvents, that is when the random thermal motion of the two reactants is reduced.

c) When further  $\alpha$ -CD molecules approach the PEG ends, the previous cyclodextrin rings will be pushed along the linear chain, moving towards the center of the PEG molecule. This process requires the unfolding and stretching out of the coiled PEG molecules, and therefore will be favoured by low temperatures and strong hydrogen bonding in the solvent.

d) When the PEG molecule is almost fully covered with  $\alpha$ -CD, a de-threading of cyclodextrins from the polyrotaxane ends is possible, particularly when the PEG has a high mobility due to an increment in  $T$ , or to a lower hydrogen bonding strength of the solvent.

e) When the polyrotaxane is finally obtained, attractive interactions are established between different particles and produce large aggregates that precipitate from the solution and form a white gel, that entraps large amounts of solvent.

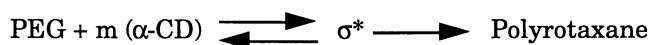
This model depicts the whole process in terms of five different steps, and explains the changes of  $t_{th}$  as a function of temperature and solvent structure. It explains the experimental results that we found in our studies, as well as Harada's



observation regarding the effect of the PEG molecular weight on the threading process. In fact, according to our model, the main factors that rule over the whole process are the initial threading of the PEG end into the  $\alpha$ -CD unit, and the following sliding of the threaded cyclic molecules toward the center of the polyethylene glycol chain. The entire process occurs with a significant stabilization of the final inclusion compound, due to the strong interactions between the  $-O-CH_2-CH_2-$  units of PEG with the hydrophobic cavity of  $\alpha$ -CD.

The data clearly show that the threading process is favoured by low temperatures and when the solvent possesses a highly ordered molecular network. The temperature and solvent effects on each step agree with the experimental findings, and confirm that the process is not determined by the diffusion of PEG and  $\alpha$ -CD in the solution, but by the energy stabilization of the final polyrotaxane.

In order to calculate the thermodynamic parameters related to the threading phenomenon, we applied the transition state equation (35). If  $\sigma^*$  represents the activated complex in the formation of the polyrotaxane, the reaction can be written as:



where the rate step is the formation of  $\sigma^*$ .

$$\frac{d[\sigma^*]}{dt} = k^*[\sigma^*] = k^*K^\ddagger[\text{PEG}][\alpha\text{-CD}]^m \quad (5)$$

where  $k^*$  is the rate constant,  $K^\ddagger$  is the equilibrium constant, and  $m$  is the number of  $\alpha$ -CD rings that participate in the formation of  $\sigma^*$ . Since the polyrotaxane is produced as soon as the activated state is formed, according to Eyring theory (18) we can write:

$$\frac{d[\sigma^*]}{dt} = \frac{d[\text{Polyrotaxane}]}{dt} = C[\text{PEG}] \quad (6)$$

$$C = \frac{k_B T}{h} \cdot [\alpha\text{-CD}]^m \cdot \exp\left(-\frac{\Delta G^\ddagger}{RT}\right) \quad (7)$$

where  $k_B$  is the Boltzmann constant,  $T$  is the absolute temperature (K),  $h$  is the Planck constant,  $R$  is the universal gas constant,  $[\alpha\text{-CD}]$  is the concentration of  $\alpha$ -cyclodextrin in the solution, and  $\Delta G^\ddagger$  is the Gibbs free energy change of activation (in kJ/mol).  $C$  is only a function of temperature and contains the two fitting parameters  $m$  and  $\frac{\Delta G^\ddagger}{R}$ . Since  $\alpha$ -cyclodextrin is in large excess with respect to PEG, we assume that  $[\alpha\text{-CD}]$  is equal to its initial value,  $6.2 \cdot 10^{-2}$  mol/L. At time  $t$ , the concentration of polyrotaxane is given by:

$$[\text{Polyrotaxane}] = [\text{PEG}]_0 - [\text{PEG}] \quad (8)$$

where  $[\text{PEG}]_0$  and  $[\text{PEG}]$  represent the concentrations of PEG at the beginning of the reaction and at time  $t$ , respectively.

$$\frac{d[\text{Polyrotaxane}]}{dt} = -\frac{d[\text{PEG}]}{dt} = C[\text{PEG}] \quad (9)$$

the integration gives:

$$\int_{[\text{PEG}]_0}^{[\text{PEG}]} \frac{d[\text{PEG}]}{[\text{PEG}]} = -C \int_0^t dt \quad (10)$$

from which:

$$\ln \left( \frac{[\text{PEG}]}{[\text{PEG}]_0} \right) = -C t \quad (11)$$

but, since  $[\text{PEG}] < [\text{PEG}]_0$ , the approximation gives:

$$\ln \left( \frac{[\text{PEG}]}{[\text{PEG}]_0} \right) \approx - \left( 1 - \frac{[\text{PEG}]}{[\text{PEG}]_0} \right) - \frac{1}{2} \left( 1 - \frac{[\text{PEG}]}{[\text{PEG}]_0} \right)^2 + \dots = -Ct \quad (12)$$

from which we obtain:

$$[\text{PEG}] = \left[ 2 - (1 + 2Ct)^{\frac{1}{2}} \right] [\text{PEG}]_0 \quad (13)$$

Inserting eq. 13 into eq. 9, integrating between 0 and  $t_{th}$ , and considering that the final concentration of polyrotaxane can be assumed to be equal to  $[\text{PEG}]_0$ , we obtain:

$$\int_0^{t_{th}} d[\text{Polyrotaxane}] = [\text{PEG}]_0 = C \cdot [\text{PEG}]_0 \cdot \int_0^{t_{th}} \left[ 2 - (1 + 2Ct)^{\frac{1}{2}} \right] dt \quad (14)$$

from which:

$$\frac{1}{t_{th}} \approx \frac{3C}{2} = \frac{3k_B T}{2h} \cdot [\alpha - CD]^m \cdot \exp \left( -\frac{\Delta G^\ddagger}{RT} \right) \quad (15)$$

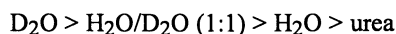
and then the final equation:

$$\ln\left(\frac{1}{T \cdot t_h}\right) = 24.17 - 2.78m - \frac{\Delta G^\ddagger}{RT} \quad (16)$$

From which  $\Delta G^\ddagger$  and  $m$  can be calculated by using the data reported in Figure 4, and are shown in Figure 7 as a function of the different tested solvents.

The number of  $\alpha$ -CD molecules that take part in the formation of the activated complex ( $m$ ) does not depend strongly on the solvent, and is in good agreement with the predicted number of  $\alpha$ -CD units that are threaded by each single chain of PEG, between 20 and 25, as discussed previously (13).

$\Delta G^\ddagger$  is always negative, indicating that the reaction is spontaneous. Since the enthalpic factor is practically zero ( $t_h$  increases with temperature), the phenomenon is essentially ruled by the entropic term.  $\Delta S$  is positive in all cases and is to be related to the release of a large number of solvent molecules from PEG and  $\alpha$ -CD before the two reactants form the host-guest complex.  $\Delta G^\ddagger$  increases in going from  $D_2O$  to  $H_2O$  and to urea; the value for the  $H_2O/D_2O$  (1:1) mixture is about the average of the values for water and pure heavy water.  $\Delta G^\ddagger$  is related to the interactions established between PEG and  $\alpha$ -CD with the solvent and within the solvent molecules, according to the sequence:



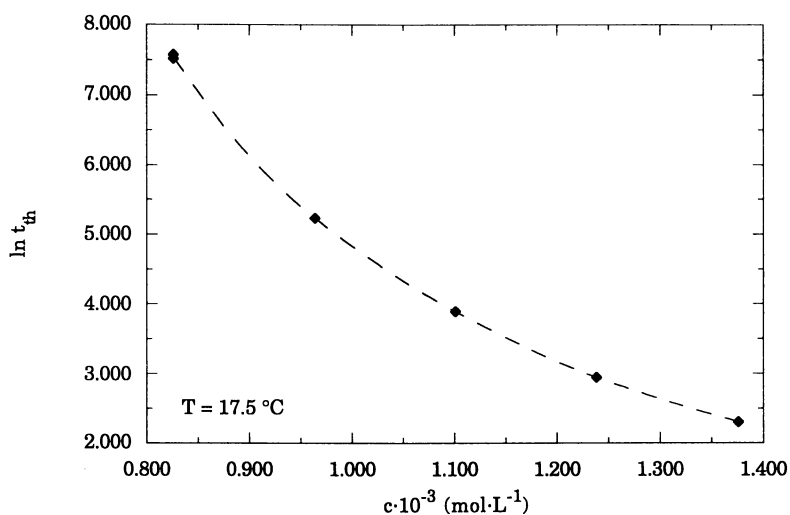
that reflects the hydrogen bonding strength in these liquids.

#### Dynamics study.

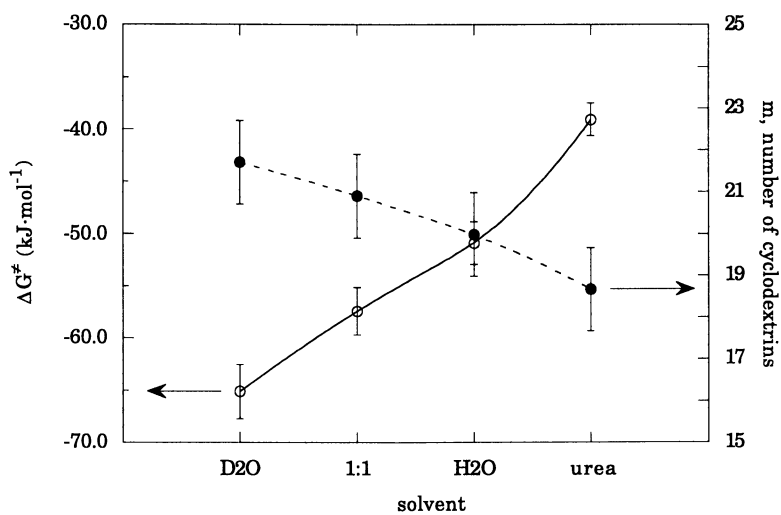
In the experimental conditions that we used, the  $^1H$ - $^{13}C$  dipolar interaction is the only effective relaxation mechanism that can contribute to the experimental value of  $R_1$  ( $\chi^{DD} \geq 0.95$ ).  $^1H$ - $^{13}C$  relaxation rate measurements on  $\alpha$ -CD, MN, PEG-MT and MT were carried out at different temperatures, to study the dynamic properties of these molecules. In fact the temperature dependence of  $R_1$  reveals whether the molecular re-orientational dynamic is fast ( $\omega_0\tau_c \ll 1$ ) or slow ( $\omega_0\tau_c \gg 1$ ): in the case of fast motion,  $R_1$  decreases with  $T$ , due to the decrement of  $J(\omega)$  at  $\omega = \omega_0$ .

$R_1$  always lowers as  $T$  increases, and therefore all molecules show fast motions.  $\alpha$ -CD, MN, PEG-MT and MT possess fast dynamics in solution, in spite of their high molecular weight. The average correlation times over all carbons ( $\tau_c$ ), calculated from the relaxation rate  $R_1$ , are  $7.5 \cdot 10^{-10}$ ,  $6.5 \cdot 10^{-10}$ ,  $1.5 \cdot 10^{-10}$ , and  $1.8 \cdot 10^{-10}$  s, for  $\alpha$ -CD, MN, PEG-MT and MT respectively (24,36). According to these data, the dynamics of  $\alpha$ -CD and MN in solution are much slower than those of PEG-MT and MT, in spite of their lower molecular weight, due to the presence of a main internal axis in both PEG-MT and MT molecules. In the case of MN, the PEG chain is not able to force  $\alpha$ -CD molecules to rotate simultaneously around the preferential symmetry axis, therefore its dynamic is slow.

The values of  $\tau_c$  for the  $C_5$  and  $C_6$  signals (see Figure 1) are reported in Figures 4a-d, along with the calculated  $\tau_j$  at different temperatures and for  $\alpha$ -CD, MN, PEG-MT and MT. The fact that  $\tau_c$  for  $C_5$  and  $C_6$  atoms are different is due to the jump



6. Dilution effect: the overall concentration of  $\alpha$ -CD and PEG in the solution affect the  $t_{th}$  value at a fixed temperature.



7.  $\Delta G^\ddagger$  and  $m$  are calculated according to a model for the four different solvents.

motion ( $\tau_j$ ) of the  $-\text{CH}_2\text{OH}$  group around the  $\text{C}_5\text{-C}_6$  bond, affecting the dynamics of  $\text{C}_6$ .  $\tau_j$  is obtained from the following equation (37-39):

$$\tau_c^{-1}(\text{C}_6) = \tau_c^{-1}(\text{C}_5) + \tau_j^{-1} \quad (17)$$

$\alpha\text{-CD}$ . The data reported in Figure 8a show that  $\ln(\tau_c)$  is proportional to  $T^{-1}$ , meaning that cyclodextrins' correlation time can be actually described in terms of activation energy in an Arrhenius' expression. The dynamic analysis shows a limited distribution of  $\tau_c$  along the sugar chain, in particular  $\tau_c$  for  $\text{C}_1$  and  $\text{C}_4$  is always larger than that for  $\text{C}_2$ ,  $\text{C}_3$ , and  $\text{C}_5$  at all temperatures. This behavior is related to the fact that the ring formed by  $\text{C}_1$ ,  $\text{C}_4$  and the anomeric oxygens that link adjacent molecules of  $\alpha\text{-CD}$  is rigid. On the other hand  $\text{C}_2$ ,  $\text{C}_3$ , and  $\text{C}_5$  are subject to a bending with respect to the  $\text{C}_1\text{-C}_4$  axis, and therefore their re-orientation is faster, since they have one more component of motion. Nevertheless, since the  $\omega_0\tau_c \ll 1$  condition holds a less efficient longitudinal relaxation, the  $-\text{CH}_2\text{-OH}$  group contributes with another rotation to the motions that are typical for cyclo-pyranose. In fact, for the primary alcoholic residue there is a rotation around the  $\text{C}_5\text{-C}_6$  bond, that allows this group to have a faster dynamic. According to eq. 17, we calculated  $\tau_c(\text{C}_5) = 7.715 \cdot 10^{-10}$  s, and  $\tau_j = 19.8 \cdot 10^{-10}$  s for  $\alpha\text{-CD}$ ; these values show that the re-orientational rotation around the  $\text{C}_5\text{-C}_6$  bond contributes to the relaxation only at a little extent.

*Molecular necklace*. This system is very similar to cyclodextrin however the differences in  $\tau_c$  of the different carbon atoms are smaller. It is interesting to note that in this case the calculation of the correlation times for the relaxation of the  $-\text{CH}_2\text{-OH}$  group gives  $\tau_c(\text{C}_5) = 6 \cdot 10^{-10}$  s, and  $\tau_j = 22.6 \cdot 10^{-10}$  s.

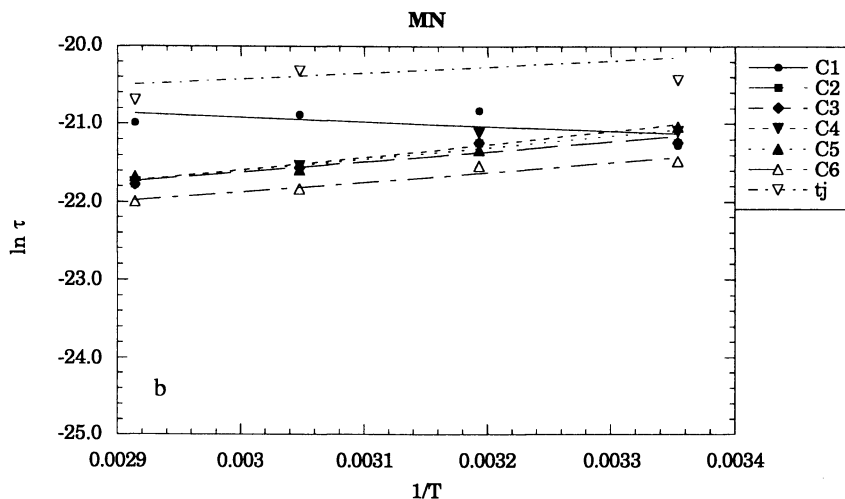
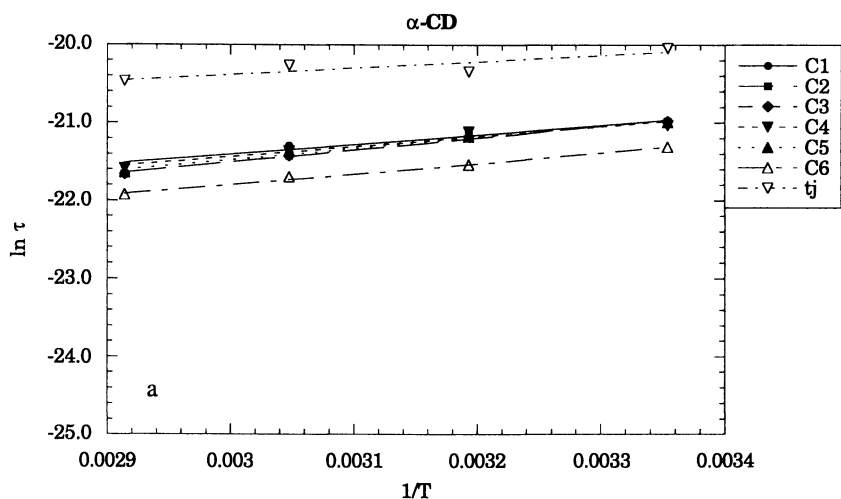
*PEG-molecular tube*. The calculation of the correlation times for the relaxation of the primary alcoholic group gives  $\tau_c(\text{C}_5) = 4.37 \cdot 10^{-11}$  s, and  $\tau_j = 22.5 \cdot 10^{-11}$  s.

*Molecular tube*. In the case of MT we observed a new signal corresponding to the  $\text{C}_6$  atom, at 60.8 ppm, that links adjacent cyclodextrins, while the signal for the free  $\text{C}_6$  appears at 63.04 ppm. This information shows that  $\alpha\text{-CD}$  are really condensed throughout  $-\text{OH}$  groups.

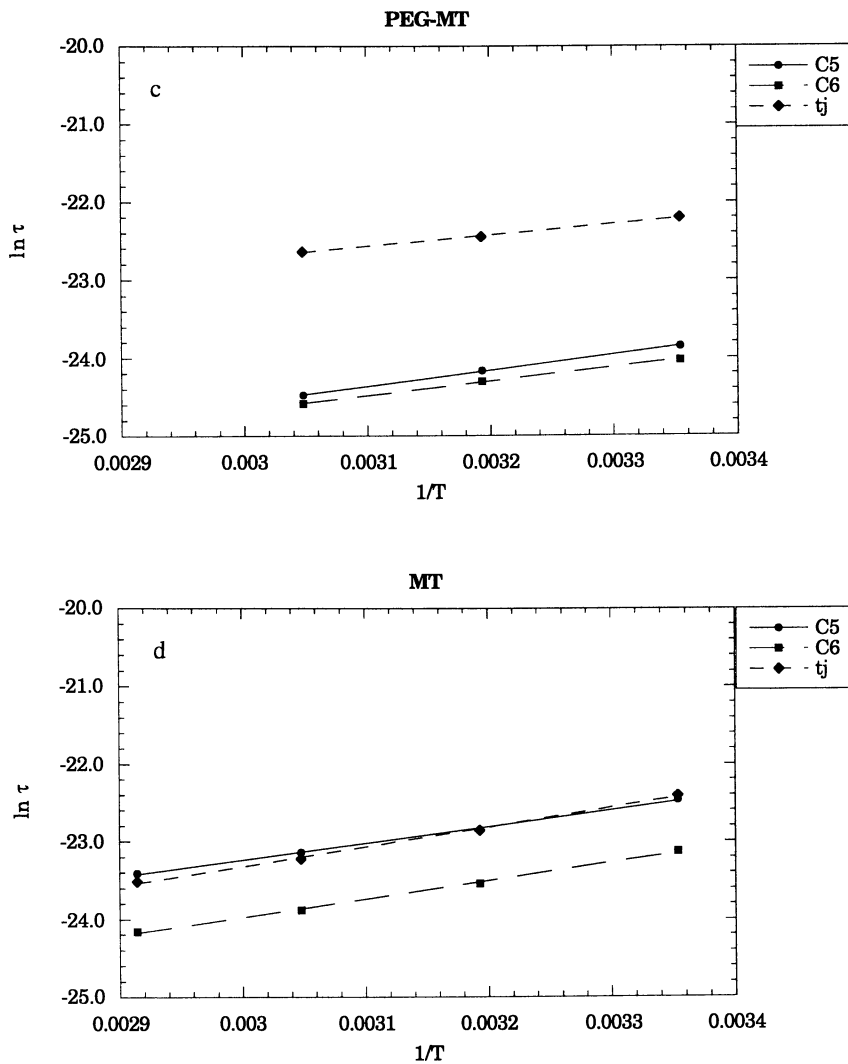
The analysis of the temperature dependence of  $\tau_c$  is important in order to determine the energy barrier for the re-orientation of the system in solution. As previously suggested,  $\tau_c$  can be written in the following form (40):

$$\ln\left(\frac{\tau_c}{\tau_c^0}\right) = \frac{E_a}{RT} \quad (18)$$

where  $E_a$  is the activation energy for the re-orientational motion. When no phase transition occurs in the solvent in the considered temperature range, the Arrhenius plot  $\ln(\tau_c)$  vs.  $T^{-1}$  is linear, and eq. 18 can be used to study the dynamics of  $\alpha\text{-}$



8.  $\ln \tau_c$  versus  $1/T$  for  $\alpha$ -CD (a), MN (b), PEG-MT (c), and MT (d). Almost in all cases an Arrhenius' plot of the data indicates the presence of an activation energy in the re-orientational motion. The legends show the different carbon atoms that have been studied by NMR experiments (see Figure 1 for the numbering of the carbon atoms in glucose).

Figure 8. *Continued.*

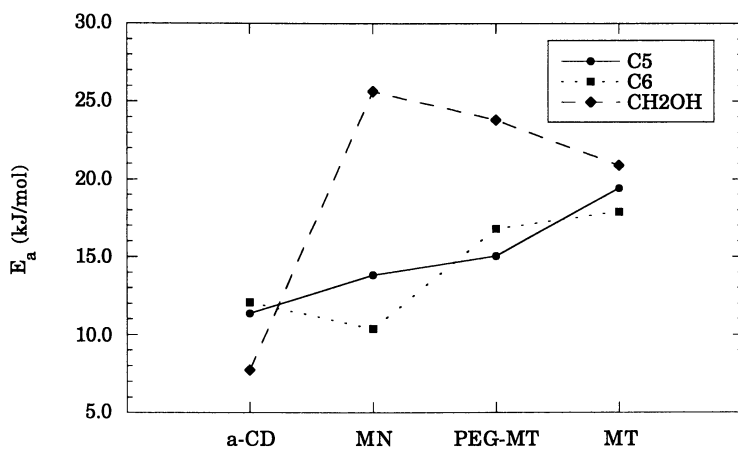
CD/MN/PEG-MT/MT. Any deviation of the experimental values from eq. 18 can be ascribed to an internal molecular re-arrangement, due to the temperature effect on the molecular motions. A large discrepancy between the slope of the fitting curve and the expected theoretical value indicates the presence of impurities in the sample. Plotting the values shown in Figures 8a-d, and calculating the activation energy for each case, we obtained the results for  $E_a$  reported in Figure 9. The data show that no conformation changes occur due to the temperature increment, and therefore that as  $T^{-1}$  decreases, the motion becomes faster and faster, but it remains of the same kind. MT is characterized by an  $E_a$  value that is larger than that for the other compounds, and particularly with respect to  $\alpha$ -CD (see the data for  $C_6$  and  $C_5$ ); such behavior can be explained by considering that MT's mass is at least twenty times bigger than that of cyclodextrin, and thus the inertia for the re-orientation of the molecular tube is larger. This means that for MT the initial re-orientation is more difficult, but the correlation time is shorter, because of the higher activation energy.  $E_a$  for the internal orientation of the  $-\text{CH}_2\text{-OH}$  group is larger for MN than for cyclodextrin. This evidence can be explained by considering that many close threaded cyclodextrins produce a steric hindrance, and therefore a slower motion with respect to free cyclodextrin molecules in solutions.

### Host-guest interactions.

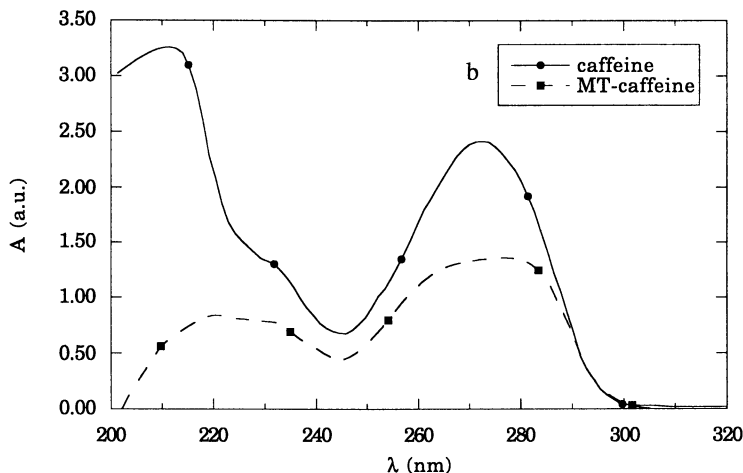
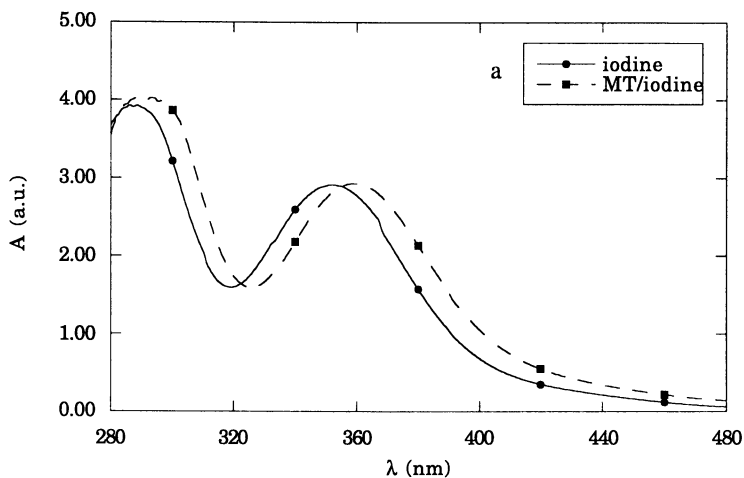
In order to study the capability of MT to include ions or small molecules in its empty cavity, we investigated the inclusion compound formed from MT and an aqueous solution of  $\text{I}_3^-$  or of caffeine by recording UV spectra. Figure 10a reports the absorbance spectra of  $\text{I}_3^-$  and of a MT/ $\text{I}_3^-$  mixture, and shows a significant shift of the  $\lambda_{\text{max}}$  value. This change is comparable to the wavelength shift recorded for the MT/ $\text{I}_3^-$  system found by Harada (12), using a shorter molecular tube, and that has been related to the formation of a host-guest inclusion complex. Our finding confirms the formation of the MT/iodine inclusion complex even for a much longer nanotube, with an estimated length of about 150-200 Å. Further studies are being carried out at this moment for testing the host properties of MT towards organic molecules, for their potential industrial applications.

Figure 10b shows the case of the inclusion compound made up of MT and caffeine. The addition of caffeine to the molecular tube solution results in a prompt clarification of the dispersion, meaning that an adduct between the MT and the organic molecule has been formed. In this case a slight shift of the absorption peak at  $\lambda=272$  nm is observed, as well as a significant reduction of the absorbance around 220 nm. UV data show that the kinetics of the formation of the caffeine-MT complex is very slow, in fact a significant difference between the two spectra can be observed only after 4 days after the mixing of the host and guest solutions. In this form, caffeine remains unaltered in the aqueous solution even for a long time.





9. Activation energy ( $E_a$ , kJ/mol) for the different compounds ( $\alpha$ -CD, MN, PEG-MT, and MT), and for the different carbon atoms.



10. UV spectra reveal the formation of a host-guest inclusion system between MT and  $I_3^-$  ions (a), and between MT and caffeine (b). The straight lines refer to the pure hosts in water solution, while the dashed lines represent the absorbance spectra of their complexes with the molecular tube.

## Conclusions

When  $\alpha$ -CD and PEG are mixed together, a peculiar threading process takes place, with the formation of a polyrotaxane, that eventually precipitates and forms a thick gel. This paper reports a study on the mechanism of the threading of  $\alpha$ -cyclodextrin rings ( $\alpha$ -CD) around a polyethylene glycol molecule (PEG<sub>3350</sub>), and on the dynamics of the molecular tube obtained upon cross-linking of  $\alpha$ -CD with epichlorohydrin. The temperature and solvent effect on the kinetics of the threading process have been studied, and lead us to propose a microscopic model for this phenomenon, that can be depicted as a five-step process, basically ruled by the threading and sliding of  $\alpha$ -CD rings over the PEG chain.

Transition state theory provides a way to calculate two important parameters: the  $\Delta G^\ddagger$  value related to this process and the number of  $\alpha$ -CD molecules ( $m$ ) that participate in the formation of the polyrotaxane. The value of " $m$ " calculated according to our model is in good agreement with the value found in the literature, and does not change with the solvent composition. On the other hand, our findings show that  $\Delta G^\ddagger$  depends on the nature of the solvent and is related to the interactions of PEG and  $\alpha$ -CD with the solvent molecules.

<sup>1</sup>H NMR studies confirmed the cylindrical structure of MT, whereas <sup>13</sup>C NMR experiments have been used to study the dynamics of  $\alpha$ -CD,  $\alpha$ -CD/PEG complexes and of the final molecular tube (MT). The study of the dynamics of  $\alpha$ -CD and of its derivatives is relevant in order to clarify the structural stability and the selective uptake performances of these compounds. The experiments show that, in spite of its large molecular weight, MT possesses a faster re-orientational motion than  $\alpha$ -CD and of its precursors, due to the main rotation axis in its structure. The minor influence of local motions observed in the case of MT with respect to  $\alpha$ -CD and its derivatives, suggests a conservative almost linear arrangement of the  $\alpha$ -CD moieties in the nanotube. The effect of this peculiar behavior on the uptake inclusion properties is an important issue that needs to be further studied. In fact, depending on the dynamics of the molecular tube, ions or organic molecules with an appropriate size can be either transported and stored in the tube's free hydrophobic cavity, or absorbed at the two ends of the rod structure, or they can remain confined on its external surface.

By recording UV spectra we also showed the formation of a host-guest inclusion compound between MT and I<sub>3</sub><sup>-</sup> ions or caffeine in water solution; this finding is particularly relevant for further studies on the inclusion properties of the molecular tube towards ions and organic molecules for scientific and industrial applications.

## Acknowledgments

The Authors are thankful to the Italian Ministry of University (M.U.R.S.T.) and to the "Consorzio Interuniversitario per lo Studio dei Sistemi a Grande Interfase" (C.S.G.I.) for partial financial support.

## References

1. Lipatov, Y. S.; Lipatova, T. E.; and Kosyanchuk, L. F. *Adv. Polymer Sci.* **1989**, *88*, 49-76.
2. Gibson, H. W.; Bheda, M.; Engen, P. T.; Shen, Y. X.; Sze, J.; Wu, C.; Joardar, S.; Ward, T. C.; and Lecavalier, P. R. *Makromol. Chem., Macromol. Symp.* **1991**, *42/43*, 395-407.
3. Rao, T. V. S.; and Lawrence, D. S. *J. Am. Chem. Soc.* **1990**, *112*, 3614-15.
4. Stryer, L. "Biochemistry", 3<sup>rd</sup> Ed., W. H. Freeman & Co., New York, 1988, Chapters 12 and 30.
5. Szejtli, J. *Chem. Rev.* **1998**, *98*, 1743-53.
6. Agam, G.; Graiver, D.; and Zilkha, A. *J. Am. Chem. Soc.* **1976**, *98*, 5206-14.
7. Chambron, J.-C.; Heitz, V.; Sauvage, J.-P. *Bull. Soc. Chim. Fr.* **1995**, *132*, 340-47.
8. Isnin, R.; and Kaifer, A. E. *J. Am. Chem. Soc.* **1991**, *113*, 8188-90.
9. Wenz, G.; von der Bey, E.; and Schmidt, L. *Angew. Chem., Int. Ed. Engl.* **1992**, *31*, 783-85.
10. Wenz, G.; and Keller, B. *Angew. Chem., Int. Ed. Engl.* **1992**, *31*, 197-99.
11. Harada, A.; and Kamachi, M. *Macromolecules* **1990**, *23*, 2821-23.
12. Harada, A.; Li, J.; and Kamachi, M. *Nature* **1993**, *364*, 516-18.
13. Harada, A.; Li, J.; and Kamachi, M. *Nature* **1992**, *356*, 325-27.
14. Rabek, J. F. "Experimental Methods in Polymer Chemistry", J. Wiley & So., New York, 1980, page 191.
15. Lo Nostro, P.; Stubicar, N.; and Chen S.-H. *Langmuir* **1994**, *10*, 1040-43.
16. Chou, S. I.; and Shah, D. O. *J. Coll. Interface Sci.* **1981**, *80*, 49-57.
17. Baglioni, P.; Rivara-Minten, E.; Dei, L.; and Ferroni, E. *J. Phys. Chem.* **1990**, *94*, 8218.
18. Cooper, A. *J. Am. Chem. Soc.* **1992**, *114*, 9208..
19. Saenger, W.; "Structural Aspects of Cyclodextrins and their Inclusion Complexes" in "Inclusion Compounds", vol. 2, Atwood J.L., Davies J.E.D., MacNicol D.D. Editors, Academic Press, London, 1984, 231-59.
20. Mc Mullan, R.K.; Saenger, W.; Fayos, J.; and Mootz, D. *Carbohydr. Res.* **1973**, *31*, 37.
21. Born, M.; and Ritter, H. *Adv. Mater.* **1996**, *8*(2), 149.
22. Harada, A. *Coord. Chem. Rev.* **1996**, *148*, 115.
23. Wenz, G.; and Keller, B. *Macromol. Symp.* **1994**, *87*, 11.
24. Ceccato, M.; LoNostro, P.; and Baglioni, P. *Langmuir* **1997**, *9*, 2436-39.
25. Gibson, H.W.; Liu, S.; Lecavalier, P.; Wu, C.; and Shen, Y.X. *J. Am. Chem. Soc.* **1995**, *117*, 852.
26. Pedersen, C.J. *J. Am. Chem. Soc.* **1967**, *89*, 2495.
27. Lehn, J.M. *Angew. Chem. Int. Ed. Engl.* **1988**, *27*, 89.
28. Baglioni, P.; Bencini, A.; Dei, L.; Gambi, C.M.C.; Lo Nostro, P.; Chen, S.H.; Liu, Y.C.; Teixeira, J.; and Kevan, L. *Coll. & Surf. A* **1994**, *88*, 59.
29. Cram, D.J. *Nature* **1992**, *356*, 29.
30. Lo Nostro, P.; Casnati, A.; Bossoletti, L.; Dei, L.; and Baglioni, P. *Coll. & Surf. A* **1996**, *116*, 203.

31. Dei, L.; Casnati, A.; Lo Nostro, P.; Pochini, A.; Ungaro, R.; and Baglioni, P. *Langmuir*, **1996**, *12*, 1589.
32. Hedges, A. R. *Chem. Rev.* **1998**, *98*, 2035-44
33. Uekama, K.; Hirayama, F.; and Irie, T. *Chem. Rev.* **1998**, *98*, 2045-76.
34. Baglioni, P.; Ferroni, E.; and Kevan, L. *J. Phys. Chem.* **1990**, *94*, 4296.
35. Laidler, K. Y. "Chemical Kinetics", McGraw-Hill Book Co., New York, 1965, page 89.
36. Ceccato, M.; LoNostro, P.; Rossi, C.; Bonechi, C.; Donati, A.; and Baglioni, P. *J. Phys. Chem. B* **1997**, *101* (26), 5094-99.
37. Wittbort, R.J.; and Szabo, A. *J. Chem. Phys.* **1978**, *69*, 1722.
38. London, R.E.; and Avitabile, J. *J. Am. Chem. Soc.* **1977**, *99*, 7765.
39. Hertz, H.G. *Prog. Nucl. Magn. Reson. Spectr.* **1982**, *26*, 115.
40. Dwek, K. A. "NMR in Biochemistry", Clarendon Press, Oxford 1973, 178

## Chapter 5

# Cyclodextrin-Linked Chitosan: Synthesis and Inclusion Complexation Abilities

Nobuo Sakairi<sup>1</sup>, Norio Nishi<sup>1</sup>, and Seiichi Tokura<sup>2</sup>

<sup>1</sup> Graduate School of Environmental Earth Science, Hokkaido University, Sapporo 060-0810, Japan

<sup>2</sup> Faculty of Engineering, Kansai University, Suita, Osaka 564-0073, Japan

Novel polysaccharide derivatives capable of forming inclusion complexes with various organic compounds have been synthesized by coupling chitosan with cyclodextrins. Two methods were established for the coupling reactions: condensation of carboxymethylated cyclodextrin with chitosan oligomers, and reductive amination of (formylmethyl)-cyclodextrins with chitosan. The latter method was applicable to the synthesis of high molecular weight (>250,000) cyclodextrin-linked chitosan in a homogeneous reaction system. The degree of substitution (D.S.) varied from 7 to 75% depending on the amount of the starting cyclodextrin derivative used. Derivatives with D.S. >30% were soluble in water under neutral or alkaline conditions. Preliminary spectroscopic analyses using model guest compounds suggested that their ability to form inclusion complexes (as measured by their dissociation constants) was almost identical with that of the uncoupled cyclodextrin. Furthermore, insoluble cyclodextrin-linked chitosan with a highly porous structure was prepared by a similar coupling method using cross-linked chitosan beads. Preliminary experiments were conducted to assess the utility of these polymeric host compounds for reversed-phase chromatography, as adsorbents for controlled release applications, as pseudostationary phase in capillary electrophoresis, and as additives in cosmetics to protect skin from chemical damage.

Chitosan is  $\beta(1\rightarrow4)$ -2-amino-2-deoxyglucan prepared by basic removal of *N*-acetylation of chitin, which is known as one of the most abundant polysaccharides found in the shells of crustaceans such as crab, shrimp, and insects (1). Because chitosan has highly reactive hydroxyl and amino groups, it has been used as a multifunctional polymer for various purposes—for example, as a chelating agent for heavy metal ions (2), as an ion exchanger (3), and as an antifungal agent (4). Furthermore, to introduce novel functions into this biopolymer, numerous investigations on chemical modification of chitosan have also been carried out (5).

Cyclodextrins (CDs) are cyclic carbohydrates which also have received much attention in the pharmaceutical industry and in what is now referred to as the

nutraceutical industry (6). As the cyclic oligosaccharides consist of more than six D-glucopyranose moieties with  $\alpha(1\rightarrow4)$  glycosidic linkages, their most remarkable feature is ability to complex various organic compounds into their hydrophobic cavities. Due to this quite unique property, CDs have been singled out for studies on host-guest chemistry (7). A considerable amount of excellent research has involved the use of CDs and their derivatives in studies of artificial enzyme (8). In the course of our ongoing project to synthesize new types of cyclodextrin analogs, so-called neo-cyclodextrins (9), we undertook to create a chitosan-based supramolecular species through condensation of cyclodextrin and chitosan.

We describe below the synthesis of CD-linked chitosan through two different reactions: condensation to form amide bond linkages (10), and reductive amination of CD derivatives with an aldehyde functional group (11,12). We also describe the physical properties of the CD-linked chitosan, including solubility in water and inclusion ability. In addition to these basic studies, we have examined the applicability of the CD-linked chitosan as a versatile functional material for purposes of separation, controlled release applications, and protection of the skin from chemical irritants.

### Preparation of Cyclodextrin-Linked Chitosans

We targeted the reactive amino group at the C-2 position of chitosan **1** in the coupling reaction with CD derivatives and developed new methods for preparing two types of cyclodextrin-linked chitosans that have an amide-containing linker **4** and an amino-containing linker **5**, as shown in the Figure 1. In the following section, we describe the details of the syntheses.

**Coupling with a Carboxymethylated Cyclodextrin Derivative 2.** Previously, we have examined the synthesis of CD-linked chitosan by condensation of the amino group and carboxymethylated  $\beta$ -CD (**2 $\beta$** ) (10). One of the problems in this synthesis was thought to be the low solubility of chitosan in water. Although high molecular weight chitosan ( $M_w = 10^4$ - $10^6$ ) is soluble in water when it forms a salt with an organic acid, such as formic acid or acetic acid, the high viscosity and acidity of such solutions restrict its chemical modification. To carry out the condensation in aqueous solution under neutral conditions, we chose low molecular weight chitosan, which is soluble in water and has low viscosity, as a substrate for the reaction. We have established a method for a large-scale preparation of low molecular weight chitosan using a modified procedure for nitrous acid degradation of chitosan (13). Chitosan oligomers with an average molecular weight of 7300 were obtained by fractional precipitation using solvent systems of 1:10 v/v water-methanol.

The low molecular weight chitosan was found to be a good substrate for the next condensation with **2 $\beta$** , which was prepared by Satomura's procedure (14). When we employed water-soluble carbodiimide (WSC) as the condensing agent, the expected formation of peptide linkages proceeded smoothly in water, giving  $\beta$ -CD-linked chitosan (**4 $\beta$** ). The degree of separation (D.S.) of **4 $\beta$**  was estimated from the ratio between the H-1 signals of the  $\beta$ -CD moiety ( $\delta$  5.59, 5.78) and chitosan ( $\delta$  5.18) from the  $^1\text{H-NMR}$  spectrum recorded in deuterium oxide. As a result, the ratio of glucosamine residues and  $\beta$ -CD units introduced was calculated to be 4:1. Unfortunately, any attempts to apply this procedure to chitosan with a higher molecular weight failed because its extremely low solubility in water.

**Typical Procedure for the Synthesis of 4 $\beta$ .** An aqueous solution (50 mL) of sodium nitrite (4.88 g, 70.8 mmol) was added dropwise to an ice-cold solution of commercial chitosan (50 g) with degree of deacetylation of 80% in 5% acetic acid (1000 mL). The mixture was stirred for 9 h at 0-4 °C and then neutralized with

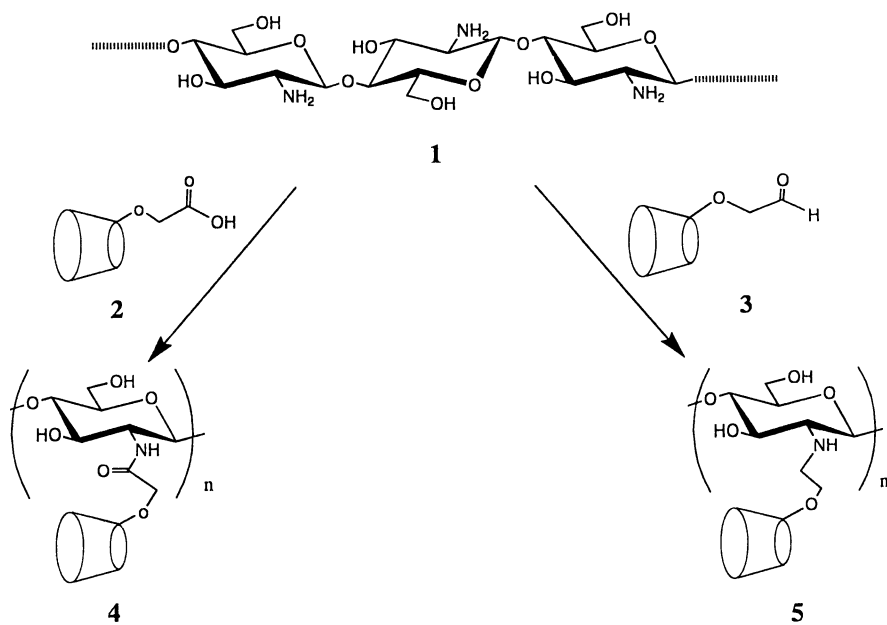


Figure 1. Preparation of CD-linked chitosans with different linkages.



aqueous concentrated ammonia. Portions of sodium borohydride (total 5.35 g, 149 mmol) were added to the resulting solution with stirring at 4 °C. The mixture was stirred at room temperature overnight, and concentrated to 250 mL under reduced pressure. After addition of methanol (750 mL), the precipitate was removed by centrifugation at 6000 rpm. The supernatant was concentrated to 120 mL, and reprecipitated with methanol (1.2 L); the second precipitate was collected by centrifugation. The residue was successively washed with methanol, acetone, and diethyl ether, and air-dried to give chitosan oligomer with molecular weight of 7300 (13.6 g). A solution of 1-ethyl-3-(3-dimethylaminopropyl)carbodiimide (WSC; 0.96 g) in water (1.5 mL) was added dropwise to a solution of the chitosan oligomer (0.87 g) and carboxymethylated  $\beta$ -CD **2 $\beta$**  (4.0 g) in water (8 mL). The mixture was stirred at 0-4 °C for 40 h and then dialyzed with water for 9 days. Lyophilization of the resulting solution gave the  $\beta$ -CD-linked chitosan **4 $\beta$**  with a D.S. of approximately 20% (1.23 g).

**Table I. Preparation and Physical Properties of  $\alpha$ - and  $\beta$ -Cyclodextrin-linked Chitosan<sup>a</sup>**

| Starting Material           | Ratio CD : Chitosan | D.S. (%) | C/N   | H/N  | $[\alpha]_D^{25}$ <sup>b</sup> |
|-----------------------------|---------------------|----------|-------|------|--------------------------------|
| <b>3<math>\alpha</math></b> | 1 : 1               | 11       | 8.59  | 1.37 | 74                             |
|                             | 2 : 1               | 15       | 10.12 | 1.60 | 103                            |
|                             | 3 : 1               | 27       | 13.90 | 2.18 | 115                            |
|                             | 5 : 1               | 59       | 24.45 | 3.92 | 130                            |
| <b>3<math>\beta</math></b>  | 1 : 3               | 7        | 7.29  | 1.13 | 28                             |
|                             | 5 : 1               | 37       | 18.66 | 2.68 | 107                            |
|                             | 10 : 1              | 75       | 29.54 | 4.31 | 118                            |

<sup>a</sup> Coupling reactions were carried out in acetate buffer (pH 4.4) at room temperature.

<sup>b</sup> Measured in 2% aqueous acetic acid (c = 0.2 g/dL) at 300K.

**Coupling with a Formylmethylated Cyclodextrin Derivative 3.** The above-mentioned condensation procedure was not applicable to the synthesis of polymeric CD-linked chitosan. Surveying new coupling reactions between CD derivatives and polymeric chitosan, we found that reductive amination was effective for the synthesis of polymeric CD-linked chitosan (11,12). The starting material, a CD derivative with an aldehyde functional group, was prepared according to Hanessian's report (15) concerning the preparation of various aminated CD derivatives. Thus,  $\beta$ -CD was treated with allyl bromide-lithium hydride in the presence of lithium iodide to give a mixture of allylated derivatives, from which the monoallyl derivative was isolated by reversed phase chromatography on Diaion HP-20 in 30-35% yield. Removal of multi-allylated derivatives from the mixture was crucial in carrying out the next coupling reaction smoothly. The C-C double bond of the allyl group was oxidized with ozone, yielding a CD derivative **3 $\beta$**  with an aldehyde functional group. Chitosan is readily soluble in acidic media, and the formation of a Schiff's base, a key intermediate in reductive amination, is accelerated at lower pH. Therefore, the reductive coupling between the formylmethylated  $\beta$ -CD **3 $\beta$**  and the high molecular weight chitosan was conducted in acetate buffer at pH 4.4. The Schiff's base formed was directly subjected to reduction with sodium cyanoborohydride to give the  $\beta$ -CD-linked chitosan **5 $\beta$**  (12). In a similar way,  $\alpha$ -CD-linked chitosan **5 $\alpha$**  was synthesized from the corresponding

$\alpha$ -CD derivative **3 $\alpha$**  (13). The D.S. was dependent on the ratio of **3** and the chitosan used. Physical data of **5 $\alpha$**  and **5 $\beta$**  with different degrees of separation (7-75%) are summarized in Table I.

The structure of **5 $\beta$**  was characterized by  $^1\text{H}$ - and  $^{13}\text{C}$ -NMR spectroscopy in  $\text{D}_2\text{O}$  at 60 °C, as shown in Figure 2. In the  $^{13}\text{C}$ -NMR spectrum, the signals assignable to the anomeric carbons of the CD moiety and chitosan were observed at  $\delta$  103-104 and 100.6 ppm, respectively. In addition, the two methylene carbons linking the cyclodextrin and glucosamine residues appeared at  $\delta$  32.7 and 58.0 ppm. The  $^1\text{H}$ -NMR spectrum showed the anomeric protons of  $\alpha$ -D-glucopyranosyl residues in the  $\beta$ -CD moiety at  $\delta$  5.5-5.6 ppm and that of 2-amino-2-deoxy- $\beta$ -D-glucopyranosyl residues in the chitosan skeleton at  $\delta$  4.9-5.1 ppm. The D.S. of CD residue calculated on the basis of integration of these peaks showed good agreement with that from elemental analysis. Furthermore, values of optical rotation increased incrementally with their D.S. because of the strongly dextrorotatory nature of  $\alpha$ - or  $\beta$ -CD units. This data is in agreement with the expected structures of the products.

**Typical Procedure for the Synthesis of 5 $\beta$ .** Chitosan with an average of molecular weight of 50,000 (200 mg) was dissolved in 0.2 M acetate buffer at pH 4.4 (100 mL). A solution of **3 $\beta$**  prepared from monoallylated  $\beta$ -CD (1 g) in the same buffer (50 mL) was added by portions to the chitosan solution. After stirring at room temperature for 1 h, sodium cyanoborohydride (260 mg) was added to the resulting solution. The mixture was stirred for 4 days at room temperature, and then neutralized with 5% ammonia. The solution was subjected to ultrafiltration through a membrane (molecular weight cut-off, 10,000), and lyophilized to give the  $\beta$ -CD-linked chitosan **5 $\beta$**  (0.86 g, 57% yield) with a D.S. of 37%.

**Preparation of CD-Linked Chitosan Beads.** The reductive amination strategy was found to be effective for introducing CD residues into chitosan beads. The starting beads were synthesized by dropping an acetic acid solution of chitosan into aqueous sodium hydroxide through a hypodermic needle followed by cross-linking with 10% molecular equivalents of hexamethylene diisocyanate in DMF. Introduction of  $\alpha$ -CD to the beads was carried out in a similar way to that described for the homogeneous system. That is, the beads were treated with **3 $\alpha$**  in acetate buffer at pH 4 to form the Schiff's base, which was reduced by sodium cyanoborohydride to give  $\alpha$ -CD-linked chitosan beads. On the basis of elemental analyses of the starting chitosan beads and CD-linked products, D.S. was calculated to be 16%. The diameter of the white bead product was 2.5-3.0 mm and its dried and hydrated weights were 0.28 g/mL and 1.66 g/mL, respectively. The water content of the beads was 83%. Scanning electron microscopy (SEM) revealed a highly porous structure (see Figure 3) with an average pore size of 0.5-1.0  $\mu\text{m}$  both on the surface and inside the beads.

### Physical Properties of CD-Linked Chitosan

**Solubility.** Chitosan is known to be insoluble in water under neutral and basic conditions, whereas solubility of  $\beta$ -CD is slightly higher in alkaline than in acidic conditions. Solubility of our newly synthesized chitosan derivatives was examined before proceeding with the characterization of their utility. Similar to the original chitosan, the  $\beta$ -CD-linked chitosan **5 $\beta$**  with a D.S. of 7% was soluble in water only under acidic conditions. By contrast, a swelling gel was formed when **5 $\beta$**  with a D.S. of 20% was suspended in water. Furthermore, **5 $\beta$**  with a D.S. of 37% was found to be soluble in distilled water, or even in alkaline solutions such as aqueous ammonia and aqueous sodium hydroxide, as well as in acidic solutions. The large steric hindrance of the CD residue may restrict the formation of inter-residual hydrogen bonding that makes the structure of chitosan rigid.

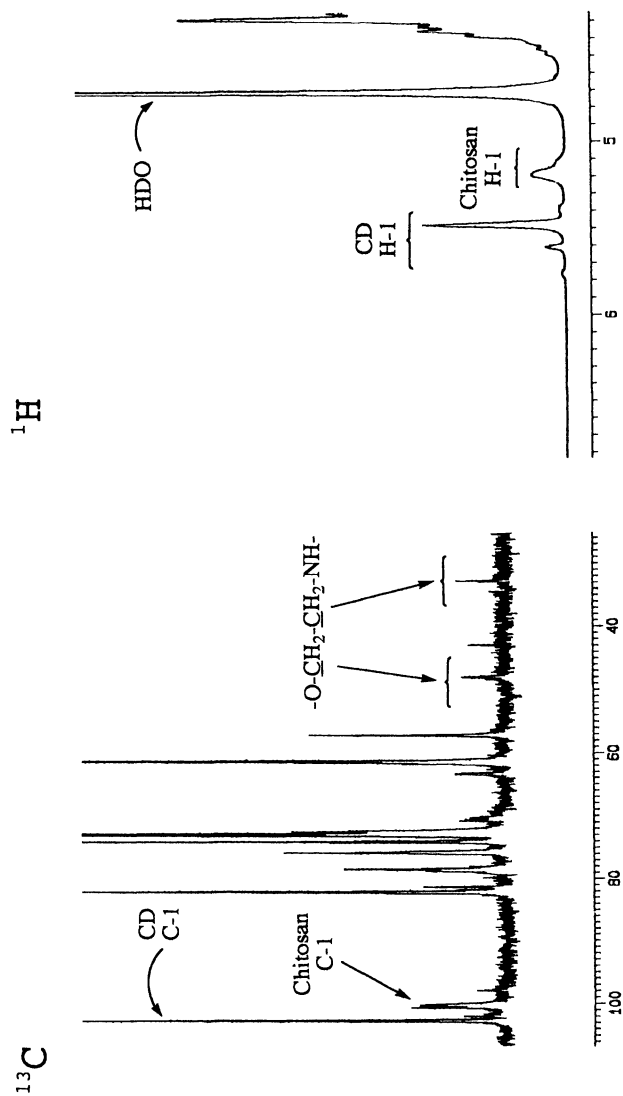


Figure 2.  $^{13}\text{C}$ - and  $^1\text{H}$ -NMR spectra of  $\beta$ -CD-linked chitosan  $5\beta$  with D.S. of 37% recorded in  $\text{D}_2\text{O}$  at 60  $^\circ\text{C}$ .

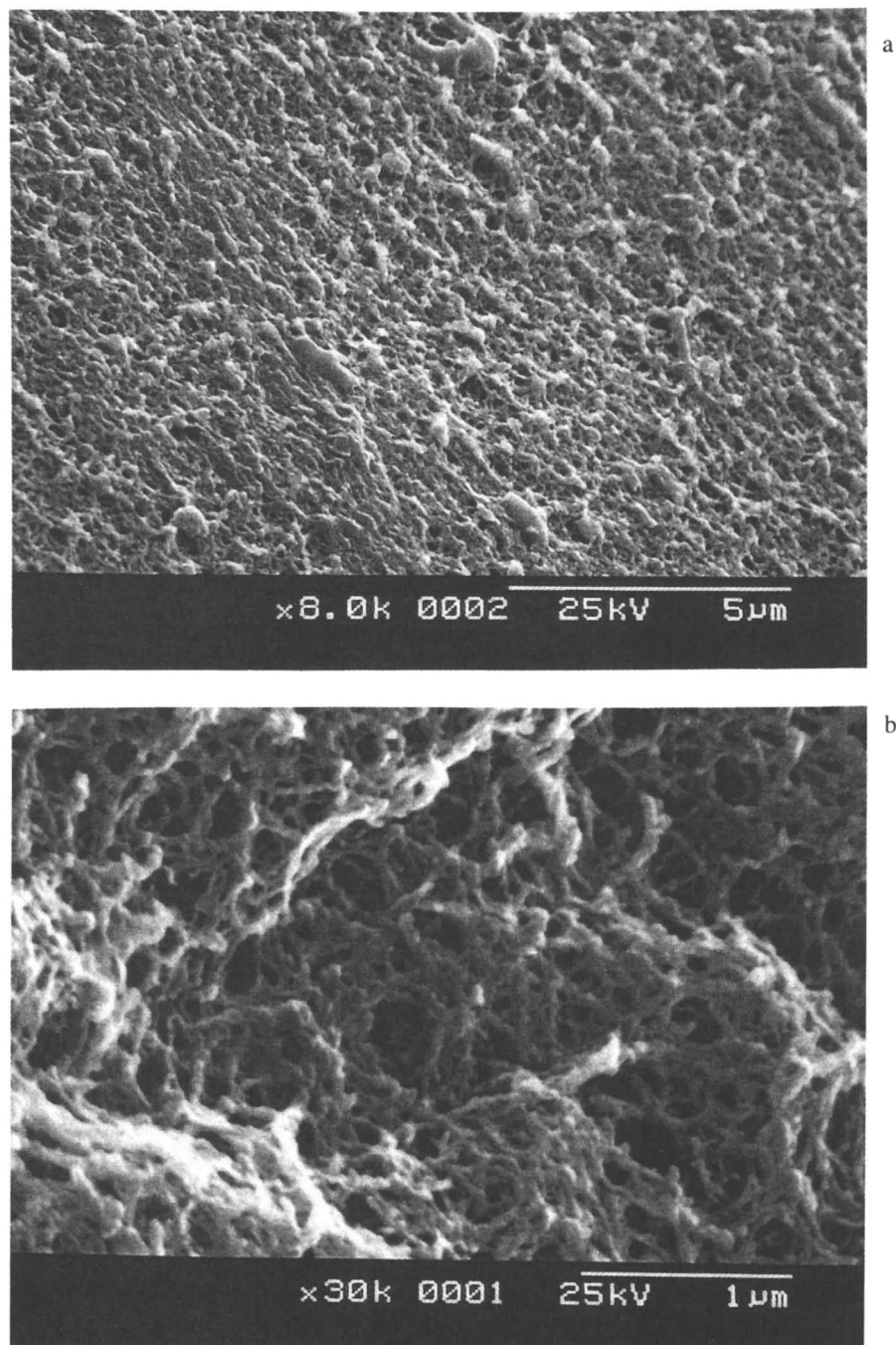


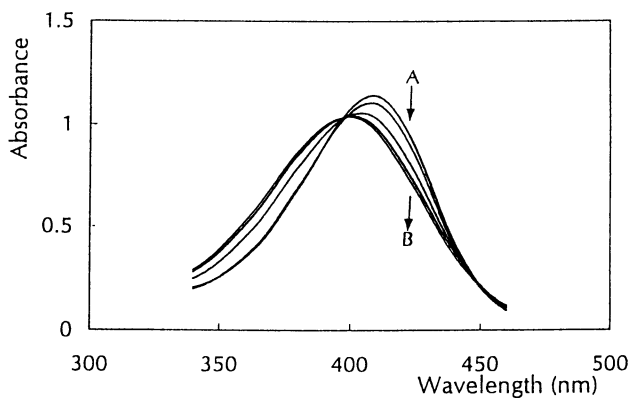
Figure 3. Scanning electron microscope (SEM) photograph of an  $\alpha$ -CD-linked chitosan bead; surface of the bead (a) and cut surface (b) cross-section.

**Inclusion Ability.** Given that the most remarkable characteristic of CDs is that they form host-guest complexes with various organic compounds, we next focused on determining whether our CD-linked chitosan possesses the inclusion ability of the original CDs. The formation of inclusion complexes was examined by spectroscopic procedures as follows.

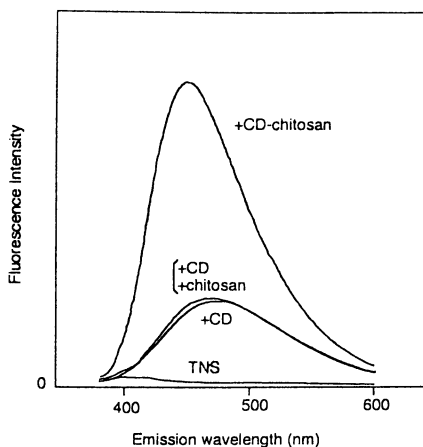
**UV-Visible Spectroscopy.** The inclusion ability of  $\alpha$ -CD-linked chitosan **5 $\alpha$**  with a D.S. of 50% was examined by means of UV-visible spectroscopy using *p*-nitrophenolate (PNP) as a guest compound in a phosphate buffer at pH 8.7. When the concentration of **5 $\alpha$**  increased, a bathochromic shift was observed in the UV-visible spectrum of PNP and isosbestic points were observed at 397 and 451 nm as shown in Figure 4 (A) (spectroscopic titration). This phenomenon indicates that host-guest complexes form between chitosan-linked CD and PNP, and, as with the original  $\alpha$ -CD, equilibrate with the free substrates. Knowing the amount of  $\alpha$ -cyclodextrin residues in **5 $\alpha$**  and having measured the change of absorption, we were able to use the Benesi-Hildebrand equation (16) to calculate that the dissociation constant of the host-guest complex with **5 $\alpha$**  and PNP was  $7.54 \times 10^{-4}$  M. In a similar way, the dissociation constant of PNP and the  $\beta$ -CD-linked chitosan **5 $\beta$**  with a D.S. of 37% was found to be  $1.49 \times 10^{-3}$  M. These values were comparable to that of the parent  $\alpha$ - and  $\beta$ -CD ( $K_D = 2.21 \times 10^{-4}$  M and  $1.50 \times 10^{-3}$  M, respectively), indicating that the ability of original CDs to form inclusion complexes is maintained after coupling with chitosan.

**Fluorescence Spectroscopy.** TNS, 6-(*p*-toluidino)-2-naphthalene-6-sulfonate, is one of a family of aminonaphthalenesulfonates which have been frequently used as fluorescent probes for structural elucidation of biopolymers, because the quantum yield increases as the micro-environmental polarity decreases (17). The fluorescence spectra of TNS in the presence of  $\beta$ -CD and  $\beta$ -CD-linked chitosan **4 $\beta$**  in phosphate buffer (pH 3.5) are shown in Figure 4 (B). The relative fluorescence intensity of TNS in the absence of any host compounds was very weak. Whereas addition of  $\beta$ -CD caused a 25-fold increase in fluorescence intensity. When **4 $\beta$**  was added to the solution, the fluorescence intensity increased 90-fold. One explanation for this phenomenon may be that the TNS molecule penetrates readily into the cavity of CD, which is relatively hydrophobic due to the high density of C-H and C-O-C groups. The chitosan backbone of **4 $\beta$**  may increase its hydrophobicity. Fluorometric titration is known to be an effective tool for analyzing stoichiometric relationships between host and guest molecules (18). The double reciprocal plots for the titration of TNS with **4 $\beta$**  indicated the presence of 1:1 complex under our experimental conditions; the equilibrium constant was calculated to be  $1.68 \times 10^3$  M<sup>-1</sup>.

**Circular Dichroism Spectroscopy.** Since the pioneering work on the chiro-optical effect of the inclusion complexation by Sense and Cramer (20), numerous experiments have focused on optical rotatory dispersion (ORD) spectra and circular dichroism (CD) spectra of host-guest complexes. Those complexes formed from chiral but non-absorbing cyclodextrins and a chiral but light-absorbing dye must be both chiral and light-absorbing. It is assumed that the main reason for this highly induced optical activity is that the guest molecule takes up a time-averaged preferential conformation in the chiral environment of the cyclodextrin cavity. For this reason, complexation of our  $\alpha$ -CD-linked chitosan **5 $\alpha$**  was examined by circular dichroism spectroscopy using PNP as the guest molecule. The large induced circular dichroism effect was observed at 400 nm, as shown Figure 4 (C). These results suggest that CD-linked chitosan may be applicable for chiral recognition and for a catalyst in asymmetric synthesis.

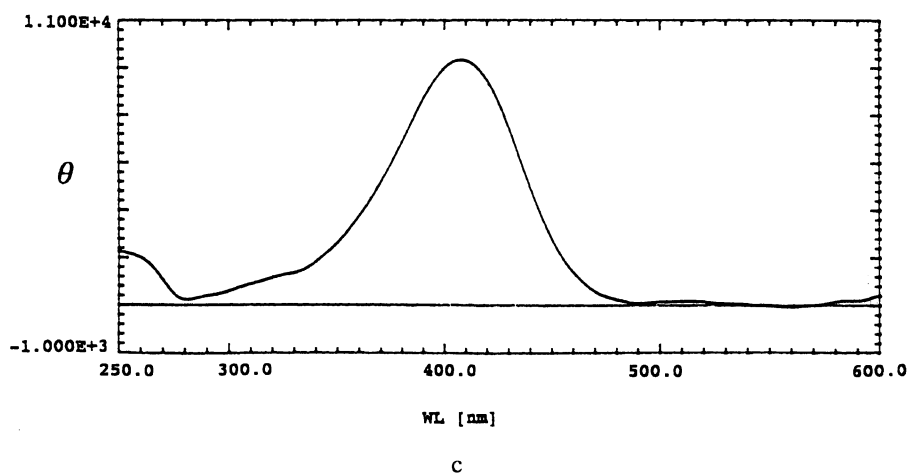


a



b

Figure 4. Spectroscopic examination of the inclusion ability of CD-linked chitosan: (A) UV-visible spectra of *p*-nitrophenol ( $5 \times 10^{-5}$  M) in 0.1 M phosphate buffer at pH 11.0 (concentrations of  $\alpha$ -CD-chitosan with D.S. of 50% were 0,  $5 \times 10^{-5}$ ,  $5 \times 10^{-4}$ ,  $5 \times 10^{-3}$ , and  $5 \times 10^{-2}$  M); (B) fluorescent spectra of TNS in 0.1 M phosphate buffer at pH 3.5 in the presence of  $\beta$ -CD-chitosan ( $1 \times 10^{-3}$  M),  $\beta$ -CD ( $1 \times 10^{-3}$  M), chitosan ( $5 \times 10^{-3}$  M); (C) Circular dichroism spectrum of *p*-nitrophenol ( $5 \times 10^{-5}$  M) in 0.05 M phosphate buffer at pH 8.7 in the presence of  $\alpha$ -CD-chitosan.

Figure 4. *Continued.*

## Some Applications of CD-Linked Chitosan

As we indicated above, CD-linked chitosan is readily prepared by coupling reactions of CD derivatives and chitosan. Furthermore, it can form inclusion complexes with specific organic compounds. Accordingly, it is reasonable to assume that CD-linked chitosan may be useful in the fields of analytical and pharmaceutical chemistry including the new nutraceutical industry. To assess its practical utility, we carried out several preliminary experiments.

**Selective Adsorption.** Recently the use of cyclodextrin and their derivatives in high-performance liquid chromatography (HPLC) has achieved spectacular success. For example, CD-modified silica gels have been demonstrated to be exceptionally useful in resolving various kind of geometric and enantiomeric isomers (20-23). In addition, CD-linked polymers have been used successfully as a stationary phase in affinity chromatography for separating such biopolymers as amylase (24) and fibroblast growth factor (25). These precedents prompted us to use our highly porous  $\alpha$ -CD-linked chitosan beads to develop a new type of separation system. As a first step, we examined the adsorption properties of nitrophenols to the beads. We used *p*-nitrophenol (PNP) and 3-methyl-4-nitrophenol (MPNP) as the model guest molecules because the dissociation constants of inclusion complexes of NPN and MPNP with  $\alpha$ -CD are reported to be  $4.1 \times 10^{-4}$  and  $4.1 \times 10^{-2}$  M, respectively (26). Although these two guest molecules have very similar structures, the methyl group of the latter strongly inhibits the formation of an inclusion complex. For this reason, we subjected a mixture of PNP and MPNP to column chromatography on  $\alpha$ -CD-linked chitosan beads; the chromatogram recorded by absorbance at 401 nm is shown in Figure 5. Eluting from the column with phosphate buffer at pH 11.0, MPNP showed less affinity to  $\alpha$ -CD and a band of PNP stayed on the top of the column. PNP was eluted after the mobile phase was changed to a less hydrophobic aqueous methanol solution. These results suggest that the  $\alpha$ -CD-linked chitosan beads may be useful as selective adsorption systems for organic compounds through differential molecular complexation.

**Controlled Release.** Recently, a number of novel drug delivery and control release approaches have been studied in order to enhance the effectiveness of the medicine and decrease its harmful side reactions. These approaches involve drug entrapment in small vesicles or polymer matrixes as well as the drug modification by chemical means. As PNP binds strongly to  $\alpha$ -CD-linked chitosan beads, our interest turned toward examining the controlled release of organic molecules entrapped within  $\alpha$ -CD-linked chitosan beads. After dipping the beads in a PNP solution, we allowed them to stand in a phosphate buffer at pH 9.0; the buffer solution was replaced every 30 min. The time course of the change in absorbance of the supernatant was recorded at 401 nm (Figure 6). In contrast to this data, chitosan beads, with little ability to form inclusion complexes, released almost all of the PNP within several hours. Our spectroscopic data indicated that PNP may become entrapped within  $\alpha$ -CD-linked chitosan beads and may be released slowly into the buffer. More than 40% of the PNP may remain in the beads after 30 changes of the buffer. These experiments suggested that CD-linked chitosan may serve as an adsorbent for controlled release of drugs and aromatics.

**Capillary Electrophoresis.** Capillary electrophoresis (CE) is a powerful microanalytical technique for analyzing pharmaceuticals and compounds of biological importance (26). Nowadays, CE is applied to electrically neutral



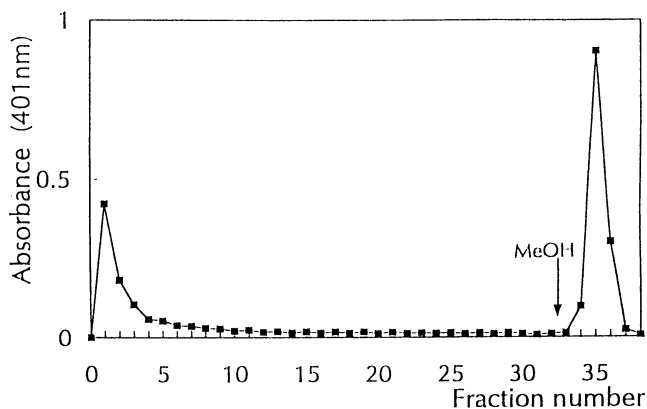


Figure 5. Chromatogram of nitrophenols: a solution of a mixture of *p*-nitrophenol and 3-methyl-4-nitrophenol was subjected to a column of  $\alpha$ -CD-linked chitosan beads and the column was washed with 0.1 M phosphate buffer at pH 11.0 and then 9:1 v/v methanol-buffer. The flow rate was 1 mL/min and fractions (10 mL each) were collected. The chromatogram was obtained by measuring absorbance at 401 nm.

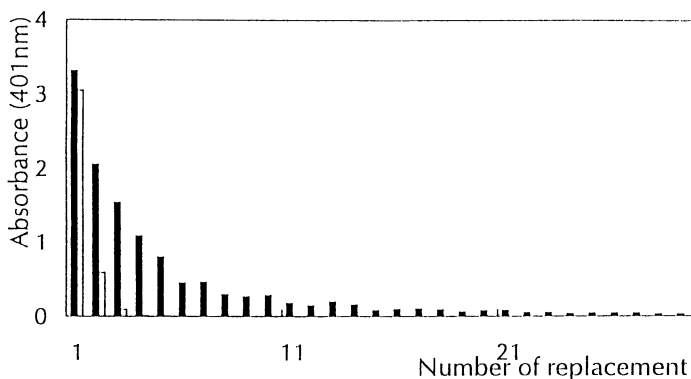


Figure 6. Release of *p*-nitrophenol from  $\alpha$ -CD-linked chitosan beads (black) and form chitosan beads (white) using 0.1 M phosphate buffer at pH 11.0. The buffer solution was changed every 30 min and absorbance at 401 nm was recorded.

analytes using a pseudostationary phase *e.g.*, a micellar solution as a running buffer. This popular technique is known as micellar electrokinetic chromatography (MEKC) (27). Furthermore, direct separation of enantiomers has been successfully accomplished by employing cyclodextrin and its derivatives as a pseudostationary phase (CDKC) (28). Because hydrophobic interaction between analytes and micelles is essential for separation, the development of new phases is a very active area of research. For the foregoing reasons we decided to test our CD-linked chitosan, which has both cationic and hydrophobic properties, as a pseudostationary phase for the CE analysis.

One preliminary example is shown in Figure 7, where *o*-, *m*-, and *p*-nitrophenols are used as analytes. Without  $\alpha$ -CD-linked chitosan, three peaks were shown in the electrogram but separation of the *o*- and *p*-isomers was not sufficient when 50 mM phosphate buffer at pH 9.3 was used as a running buffer. By contrast, a remarkable change was observed in the separation when  $\alpha$ -CD-linked chitosan **5a** was added to the running buffer. Migration times of the *o*- and *m*-isomers were almost the same as in the original electrogram, but that of *p*-isomer was much faster. This phenomenon may indicate differential formation of inclusion complexes with  $\alpha$ -CD-linked chitosan during the separation. Among these analytes, only the *p*-isomer is thought to form a tight inclusion complex with  $\alpha$ -CD-linked chitosan, and the complex, being cationic, moves faster than the uncomplexed analytes toward the cathode. A similar tendency was observed in the separation of regioisomers of chlorophenols and catechols. This simple example suggests that, for difficult separations, CD-linked chitosan may be used effectively as a pseudostationary phase in CE.

**Protection of Skin from Chemical Penetration.** Finally, we explored CD-linked chitosan in relation to cosmetics. Cosmetics, because they contain surfactants and antiseptic substances, can cause skin irritation in those with hypersensitive skin. The development of protective agents for this population is a high priority for the cosmetic industry. Considering that both chitosan and cyclodextrin, constituents of CD-linked chitosan, can be generally described as "biologically friendly," we decided to investigate their ability to protect the skin against certain chemical damage. We selected benzalkonium chloride (alkyldimethylbenzylammonium chloride), a cationic surface-active agent commonly used as a topical antiseptic, for purposes of this investigation. The irritating effects of this germicide, which are associated with the denaturation of skin mucosa, can be inhibited by certain polysaccharides. As shown in Figure 8, CD-linked chitosan effectively inhibited denaturation and was more potent than either hyaluronic acid or hydroxyethyl cellulose.

## Conclusion

We described the successful synthesis of  $\alpha$ - and  $\beta$ -cyclodextrin-linked chitosan in a homogeneous system. Because formation of the Schiff's base with the corresponding 2-formylmethyl derivatives and subsequent reduction with  $\text{NaBH}_4/\text{CN}$  was carried out in a one-pot manner, this methodology would appear suitable for large-scale preparations. The coupling procedure was applicable to cross-linked chitosan, which yielded highly porous CD-linked chitosan beads. The ability of these CD-linked chitosans to form inclusion complexes with various organic compounds was validated by spectroscopic examination, which revealed that the dissociation constants were approximately the same as those of the original CDs.

Some preliminary experiments were performed, where these CD-linked chitosans were used as polymeric host compounds. These experiments revealed the ability of the CD-linked chitosan to retain and differentially recognize the

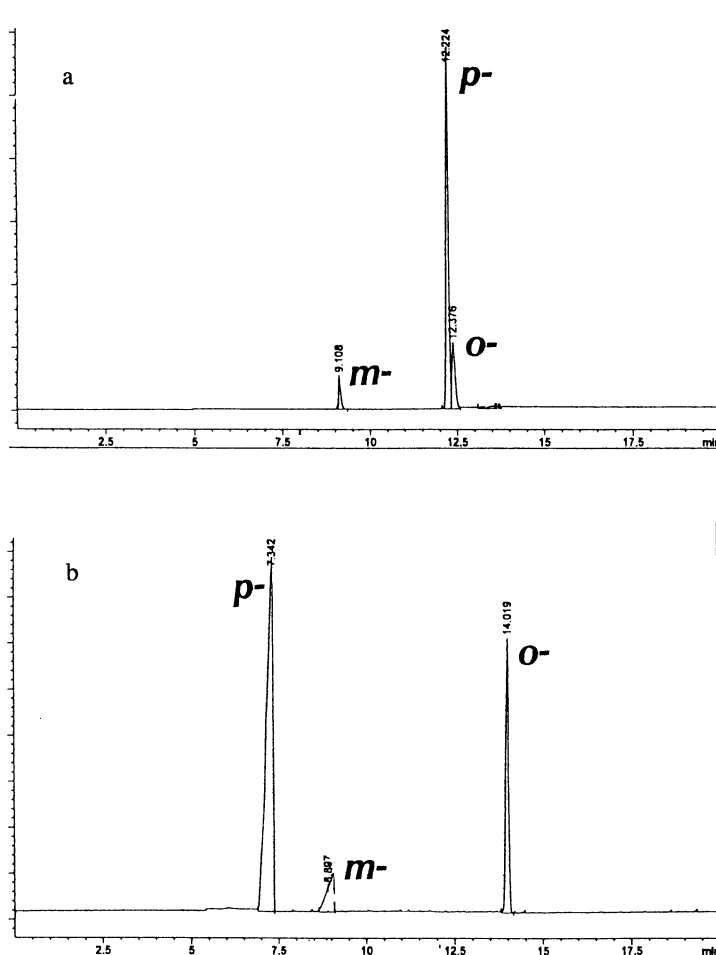


Figure 7. Separation of nitrophenols by capillary electrophoresis. Running solution (A) 50 mM phosphate buffer at pH 9.3 and (B) 50 mM phosphate buffer at pH 9.3 in the presence of  $\alpha$ -CD-linked chitosan  $S\alpha$  with D.S. 50%.

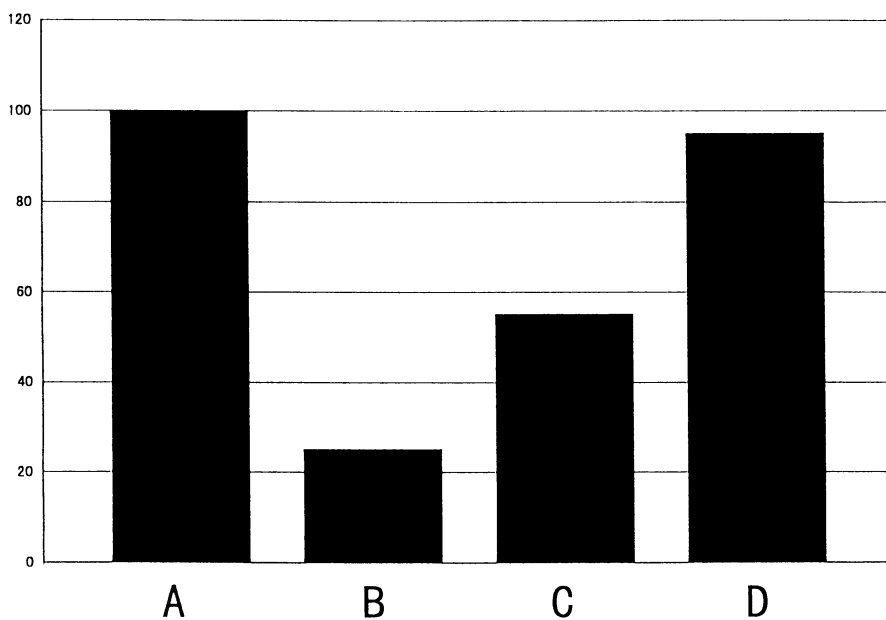


Figure 8. Inhibitory effect of polysaccharides on denaturation of skin mucosa induced by benzalkonium chloride (A: control, B: 0.3%  $\beta$ -CD-linked chitosan with D.S. of 37%, C: 0.3% hyaluronic acid, D: 0.3% hydroxyethyl cellulose). Y-axis indicates relative turbidity at 420 nm.

molecular shapes or the structure of guest compounds. They also confirmed their potential as a reverse-phase adsorption system, as an adsorbent in controlled release applications, as a pseudostationary phase in capillary electrophoresis, and as an additive in cosmetics to protect hypersensitive skin against chemical irritation.

This novel polymeric host compound with its carbohydrate skeleton shows potential in the production of biologically and/or environmentally friendly materials in a wide variety of fields. Further studies along this line are now in progress.

### Acknowledgments

We thank Dr. Kazuhiro Hamada and Mr. Haruyoshi Seino of Pias Corporation and Dr. Sang-Mun Han, Mr. Haruyoshi Seino, Ms. Etsuko Furusaki, Mr. Fusao Tanida, Mr. Hiroto Katsura, and Mr. Tomoya Tojima of Hokkaido University for their cooperation in this study. This work was partially supported by a Grant-in Aid for Scientific Research (B) (No. 09555290) and that for Priority Areas (No. 09240101) of the Ministry of Education, Science, Sports, and Culture of Japan.

### References

- Horton, D.; Lineback, D. R. In *Methods in Carbohydrate Chemistry*; Whistler R. L.; Academic Press: New York and London, 1965; Vol. 5, pp 403-406.
- Muzzarelli, R. A. A.; Rocchetti, R. *Anal. Chim. Acta.* 1974, 70, 283.
- Itoyama, K.; Tokura, S. *Sen-I Gakkaishi* 1994, 50, 118.
- Schlick, S. *Macromolecules* 1986, 19, 192.
- Kurita, K. In *Chitin in Nature and Technology*; Muzzarelli, R. A. A.; Jeuniaux, C.; Goody, G. W.; Plenum Press: New York, 1986; pp 287.
- Frank, S. G. *J. Pharm. Sci.* 1975, 64, 1585.
- Szejtli, J. *Cyclodextrin and Their Inclusion Complexs*; Akademiai Kaido: Budapest, 1982; Vogtle, F. *Supramolecular Chemistry: An Introduction*; John Wiley & Sons: West Sussex, 1989; Li, S.; Purdy, W. C. *Chem. Rev.* 1992, 92, 1457.
- Tabushi, I. *Acc. Chem. Res.* 1982, 15, 66; Bleslow, R. *Science* 1982, 218, 532; D'Souda, V. T.; Bender, M. L. *Acc. Chem. Res.* 1987, 20, 146.
- Sakairi, N.; Kuzuhara, H. *J. Chem. Soc., Chem. Commun.* 1993, 1875; Sakairi, N.; Wang, L.-X.; Kuzuhara, H. *J. Chem. Soc., Perkin Trans. 1* 1995, 437.
- Furusaki, E.; Ueno, Y.; Sakairi, N.; Nishi, N.; Tokura, S. *Carbohydr. Polym.* 1996, 29, 29.
- Tanida, F.; Tojima, T.; Han, S.-M.; Nishi, N.; Tokura, S.; Sakairi, N.; Seino, H.; Hamada, K. *Polymer* in press.
- Tojima, T.; Katsura, H.; Han, S.-M.; Tanida, F.; Nishi, N.; Tokura, S.; Sakairi, N.; *J. Polym. Sci., Part A: Polym. Chem.* 1998, 36, 1965.
- Nakao, N. *US Patent* 1992, 7,912,561.
- Satomura, S.; Omichi, K.; Ikenaka, T. *Carbohydr. Res.* 1988, 180, 137.
- Hanessian, S.; Benalil, A.; Laferriere, C. *J. Org. Chem.* 1995, 60, 4786.
- Benesi, H. A.; Hildebrand, J. H. *J. Am. Chem. Soc.*, 1949, 71, 2703.
- McClure, W. O.; Edelman, G. M. *Biochemistry*, 1966, 5, 1908; Yamaoka, Y. *Angew. Chem. Int. Ed. Engl.* 1977, 16, 137.
- Kondo, H.; Nakatani, H.; Hiromi, K. *J. Biochem.* 1976, 79, 393; Caneta, G. C.; Bright, F. V. *Anal. Chem.* 1989, 61, 905.
- Sensse, K.; Cramer, F. *Chem. Ber.* 1969, 102, 509.
- Beesley, T. E. *Am. Lab.* 1985, 17, 78.
- Armstrong, D. W.; DeMond, W.; Alak, A.; Hinze, W. L.; Riehl, T. E.; Bui, K. H. *Anal. Chem.* 1985, 57, 234.
- Han, S. M.; Armstrong, D. W. In *Chiral Separations by HPLC*; Krstulovic, A. M., Ed.; John Wiley & Sons: New York, 1989; p 208.

23. Armstrong, D. W. *J. Pharm. Biomed. Anal.* **1990**, *8*, 123.
24. Weselake, R. J.; Hill, R. D. *Carbohydr. Res.* **1982**, *108*, 153.
25. Sheng, Y.; Forkman, J.; Weisz, P. B.; Joullie, M. M.; Ewing, W. R. *Anal. Biochem.* **1990**, *185*, 108.
26. Monnlog, C. A.; Kennedy, R. T. *Anal. Chem.* **1994**, *66*, 280R.
27. McLaughlin, G. M.; Nolan, J. A.; Lindahl, J. L.; Palmieri, R. H.; Anderson, K. W.; Morris, S. C.; Morrison, J. A.; Bronzert, T. J. *J. Liq. Chromatogr.* **1992**, *15*, 961; Tanaka, M.; Ishida, T.; Araki, T.; Matsuyama, A.; Nakatsuji, Y.; Okahara, M.; Terabe, S. *J. Chromatogr.* **1993**, *648*, 469.
28. Tazaki, M.; Takagi, M.; Ueno, K. *Chem. Lett.* **1982**, 639; Yeo, S. K.; Ong, C. P.; Li, S. F. Y. *Anal. Chem.* **1991**, *63*, 2222; Fanali, S.; *J. Chromatogr.* **1991**, *545*, 437.

## Chapter 6

# Preparation of Inclusion Foams from Chitin and PEG–Chitin for the Drug Delivery System

S. Tokura <sup>1</sup>, H. Tamura <sup>1</sup>, T. Dohba <sup>2</sup>, K. Takahashi <sup>2</sup>, N. Sakairi <sup>2</sup>, and N. Nishi <sup>2</sup>

<sup>1</sup> Faculty of Engineering, Kansai University and HRC, Yamate-cho,  
Suita, Osaka 564–8680, Japan

<sup>2</sup> Graduate School of Environmental Earth Sciences, Hokkaido University,  
Sapporo 060–0012, Japan

Under mild and efficient chitin solubilization conditions, the molecular weight of chitin could be successfully estimated viscometrically using standard chitosan after reacylation of amino groups. Various dye were used as model compounds to test the use of chitin for the controlled drug release. An anionic dye tended to be adsorbed to chitin molecules tightly. Sulfonyl groups were the best functional groups for tight adsorption of dyes. The adsorption profile was changed by the introduction of hydrophilic polyethylene glycol (PEG) to chitin. This was likely due to formation of a micellar structure. Sulfonyl and nitro groups in the test compounds increased the inclusion into the chitin molecules.

Chitin, a naturally abundant mucopolysaccharide, is known to be biodegradable and its hydrolysates are susceptible to metabolic pathway in animals. Chitin is also known to accelerate the wound healing in animals(1). Chitin has been investigated as prospected biomedical material due to its several biological advantages. A disadvantage is its low solubility owing to the rigid crystalline structure of chitin molecules(2). Although solvents have been found for the regeneration of chitin, those solvents have been undesirable in the preparation of biomedical materials(3).

Calcium chloride dihydrate-saturated methanol was found as a mild and efficient solvent for chitin(4). Free amino groups in chitin molecule needed to be reacylated fully to obtain better solubility to calcium chloride dihydrate-methanol-water solvent. Chitosan was sparingly soluble also in anhydrous calcium chloride-methanol system. Since chitin solution in calcium chloride dihydrate-saturated methanol was stable for a long period at room temperature, a viscometric estimation of molecular weight of chitin was achieved successfully using N-reacylated standard chitosan which molecular weight was estimated by a well established viscosity equation(5). Chitin was recovered as a porous chitin gel by precipitation in large excess of water or methanol. On this paper the properties

of chitin gel has been investigated for drug inclusion using dyes as model compounds. The drug adsorption specificity was investigated by applying hydrophilic polyethyleneglycol(PEG) on the chitin molecule to increase a degree of molecular packing of chitin(Scheme 1).

## EXPERIMENTALS

**Chitin:** Chitin powder of under 200 mesh was prepared from Queen crab shells according to the method of Hackman(6) and sifted under 200 mesh following to grinding. The regenerated chitin (Chitin\*) was prepared from the standard chitosan (Degree of deacetylation:80% by IR method(7)) in which molecular weight was estimated by applying a viscosity equation for chitosan under the defined conditions(5).

**Preparation of PEG-chitin foam:** A 80% deacetylated chitin was applied to the acylation reaction with polyethylene glycol dicarboxylic chlorides(Mw =600) in methanol at pH 6-7 and 5°C under vigorous stirring for 24 h. The gel formed was rinsed extensively with deionized water and followed by lyophilization. The degree of PEG carboxylation was assumed both by elemental analysis and potentiometric titration. A gelous PEG-chitin within water insoluble fractions was applied to the study of dye inclusion.

**Chitin solution:** 2g of chitin powder and 85 g of calcium chloride dihydrate were suspended in 100ml of methanol and then refluxed for an hour to dissolve followed by filtration to obtain a clear chitin solution. The clear chitin solution was applied to the viscometric measurement to estimate molecular weight referring to the viscosity of Chitin\* using the Sakurada-Houwink's equation  $[\eta] = KM^\alpha$  where  $K=9.84 \times 10^4$  and  $\alpha=0.74(4)$ .

**Chitin foam included by dye:** Dye solutions in methanol were mixed with the chitin solution (Mw=  $3.1 \times 10^5$ , viscosity measurement) before casting on a glass plate. The cast dye-chitin mixed solution was then immersed into a mixed solution of ethylene glycol : aqueous sodium citrate solution(2N) = 1:1 (v/v) to remove calcium ions under gentle agitation. Resulted chitin gel was rinsed with deionized water to remove free dye and lyophilized to prepare porous chitin foam with a model compound. In the case of PEG-chitin, PEG-chitin gel was suspended in the dye solution of 50% aqueous methanol (v/v) followed by standing for 24 hr at room temperature under gentle stirring. The dye included PEG-chitin gel was rinsed with 50% aqueous methanol and deionized water to remove free dye followed by lyophilization after freezing in liquid nitrogen or freezing at -20°C (refrigerator) overnight.

**Controlled release of model drugs:** Dye release from chitin foam was carried out according to the method authorized by Japanese Pharmacopeia. Briefly, a square shaped portion of chitin or PEG-chitin foams(25-30mg) were applied into the cage and revolved (100 rpm) in 1,000ml of saline solution at various pHs and ionic strengths ranging from 0.01 to 1M to find the proper chemical structure of drugs to adsorb in chitin or the PEG-chitin gel. The amount of dye released was estimated by optical density using a spectrophotometer(Hitachi U-3200). The amount of dye included in chitin foam was also estimated by the optical density of the acid hydrolysate of chitin foam.



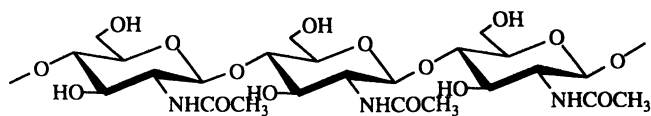
## RESULTS AND DISCUSSION

**Chitin solution:** The molecular weight of chitin was a significant factor to regulate solubility. For example, 2%(w/v) was the maximum concentration to dissolve in calcium chloride dihydrate-saturated methanol when molecular weight of chitin was around  $2 \times 10^5$ . Calcium chloride dihydrate-saturated methanol was the only effective solvent for chitin among the solvent systems tested as shown in Table 1. The crystalline structure seemed to be an important factor for chitin dissolution. For example,  $\beta$ -chitin solubility was lower than that of  $\alpha$ -chitin in calcium chloride dihydrate-saturated methanol.

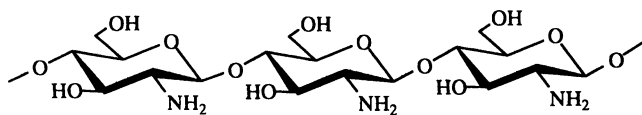
**Surface view of lyophilized chitin foam:** Porosity of chitin foam was found to depend on the freezing process after the removal of calcium ions as shown in Figure 1. A smaller pore size resulted on chitin foam, when a quick freezing process was applied using liquid nitrogen. Larger pore size resulted after slower freezing at  $-20^\circ\text{C}$  in refrigerator.

**Adsorption of dyes in chitin and PEG-chitin foams:** Time courses of dye release are shown in Figures 2-5. Release was significantly dependant on the anionic property of the dye (Scheme 2). Cationic dyes were unable to include into chitin molecules. The basicity of the amide bond was likely to regulate the adsorption of model drug into chitin molecule as shown in Figure 6, since pKa of the amino group of chitosan is reported to be 6.3-6.4 which is abnormally low value for an amino group in organic compounds. Anionic dye, Amido Black 10B, is shown to be included in a chitin molecule at pH 4.0 where protonation of amido group would be suppressed. Adsorbed dye appeared to get released slowly, as amido group might be protonated partially at pH 7.0. Release of the dye was almost complete at pH 11.0 where full protonation proceeds. The reversal of the tight inclusion of a model compound was observed after the change of ionic strength, urea concentration and an addition of a surface active reagent such as sodium dodecyl sulfate (SDS) (Figure 6). Therefore, an ionic binding was likely to contribute to the stacking of dyes to chitin molecules.

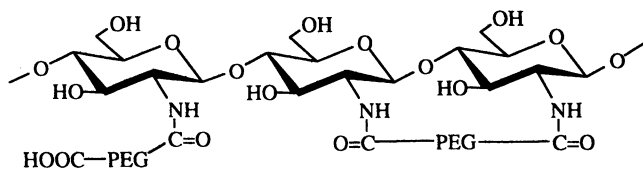
A similar tendency was shown with PEG-chitin where a part of amino groups remained without acylation with PEG bis carboxylic acid. However, there was a large difference on the stacking of Amido Black 10B between chitin (Figure 7) and PEG-chitin probably due to free amino groups in PEG-chitin molecule. The participation of nitro groups was shown by Eriochrome Black T and Eriochrome Blue Black B as shown in Figure 8. Amido Black 10B showed less affinity to PEG-chitin than to chitin, whereas Eriochrome Black A and Congo Red which have isolated sulfonyl groups associated with nitro or amino groups were stacked tightly as shown in Figure 9. These results would suggest the importance of the change of environment around the dye adsorption site through the introduction of hydrophilic side chain. Significant influence of the nitro group was shown in Figure 8 and 9 where nitro group would contribute to the strong stacking of dyes (Eriochrome Black A and Eriochrome Black T). The chitin molecule was assumed to pack tightly by the formation of a colloidal form in an aqueous solution due to hydrophilic PEG side chain and a relatively hydrophobic aminosugar chain. Similar biodegradability as with chitosan was still shown on regenerated chitin and PEG-chitin foams. Regulation of the test compound release from the complex was possible by changing the chemical structure of the compound, hydrophilicity of side chain and the porosity of chitin foam.



CHITIN



CHITOSAN



PEG - CHITIN

Scheme 1. Chemical structures of chitin and related polysaccharides

Table I. Solvent systems for chitin<sup>a</sup>

| Solution   | Solubility <sup>b</sup> |
|--|-------------------------|
| Saturated anhydrous CaCl <sub>2</sub> - MeOH                           | +                       |
| Saturated CaCl <sub>2</sub> · 2H <sub>2</sub> O - MeOH                 | +++                     |
| Saturated CaCl <sub>2</sub> · 2H <sub>2</sub> O - EtOH                 | +                       |
| Saturated MgCl <sub>2</sub> · 6H <sub>2</sub> O - MeOH                 | -                       |
| 100%(w/v) Ca(NO <sub>3</sub> ) <sub>2</sub> · 4H <sub>2</sub> O - MeOH | -                       |
| 100%(w/v) Mg(NO <sub>3</sub> ) <sub>2</sub> · 6H <sub>2</sub> O - MeOH | -                       |
| 200%(w/v) Ca(SCN) <sub>2</sub> · 4H <sub>2</sub> O - MeOH              | +                       |

0.5 g chitin was stirred in 50 ml each solution at r.t.

<sup>a</sup> Reproduced with permission from *Proceedings of the International Workshop on Green Polymers, Indonesian Polymer Association, 1996.*

<sup>b</sup> +++ transparent solution

+ partially soluble

- insoluble

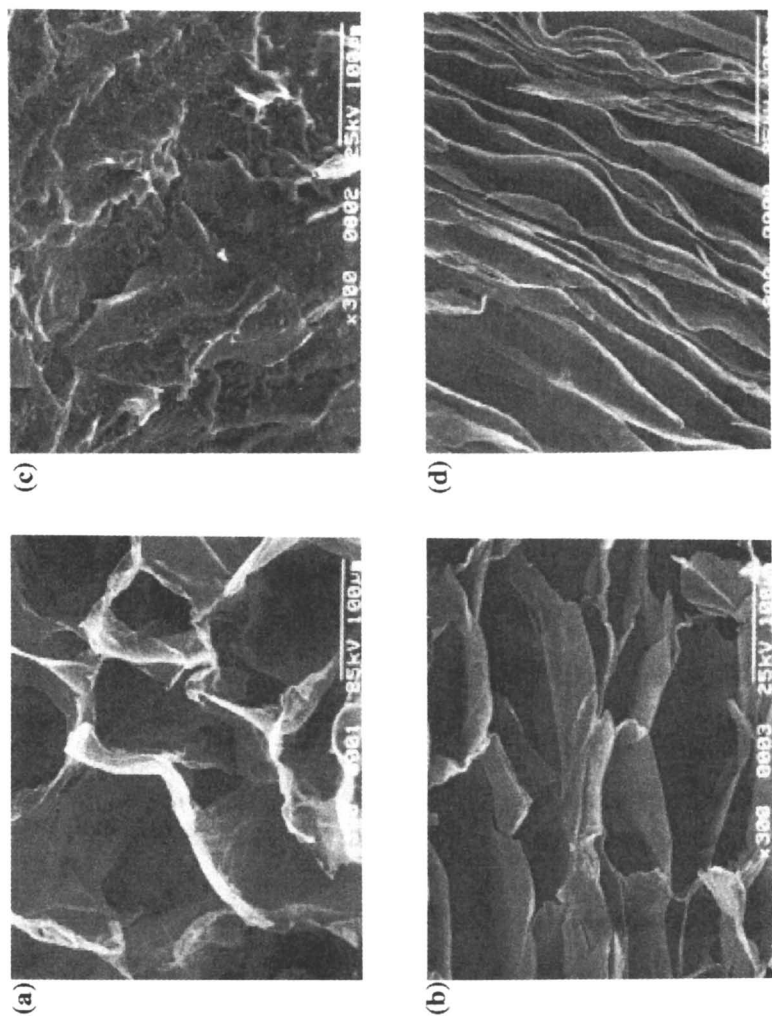


Fig. 1 SEM views of chitin foam lyophilized after freezing at  $-20^{\circ}\text{C}$  overnight : (a) surface, (b) cross section and chitin foam lyophilized after freezing by liquid nitrogen : (c) surface, (d) cross section.

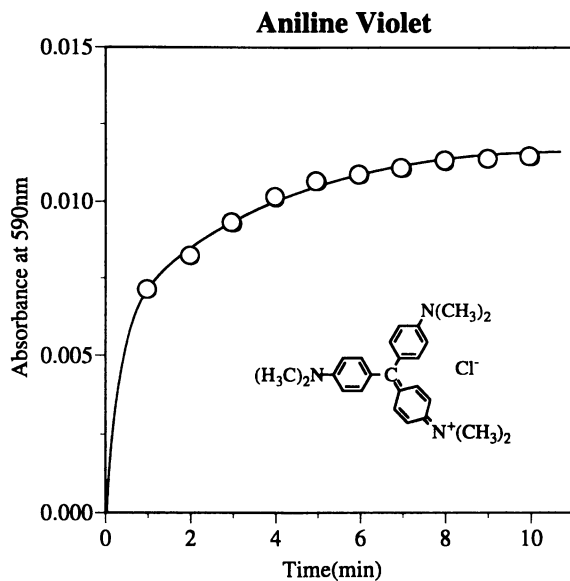


Fig.2 Time course of aniline violet release from chitin foam.

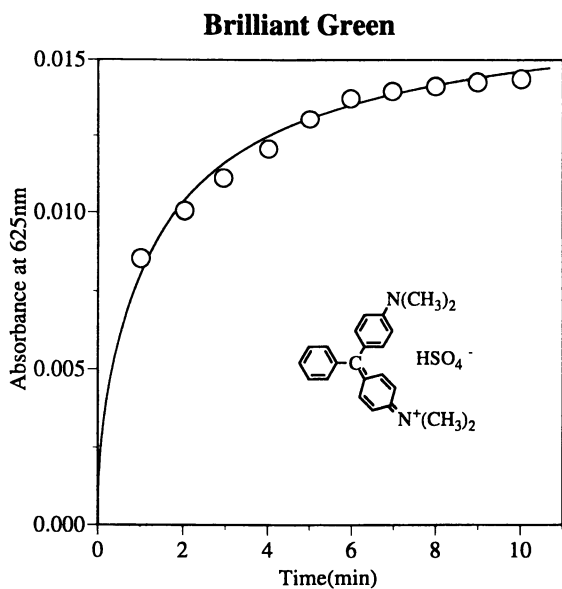


Fig.3 Time course of brilliant green release from chitin foam. Reproduced with permission from *Proceedings of the International Workshop on Green Polymers*, Indonesian Polymer Association, 1996.

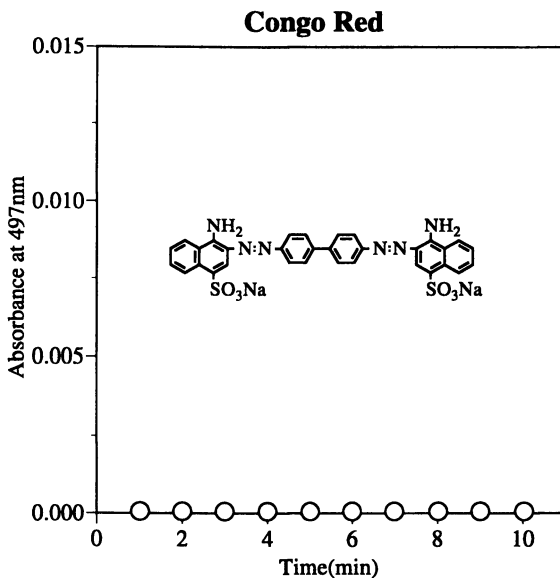


Fig.4 Time course of congo red release from chitin foam.

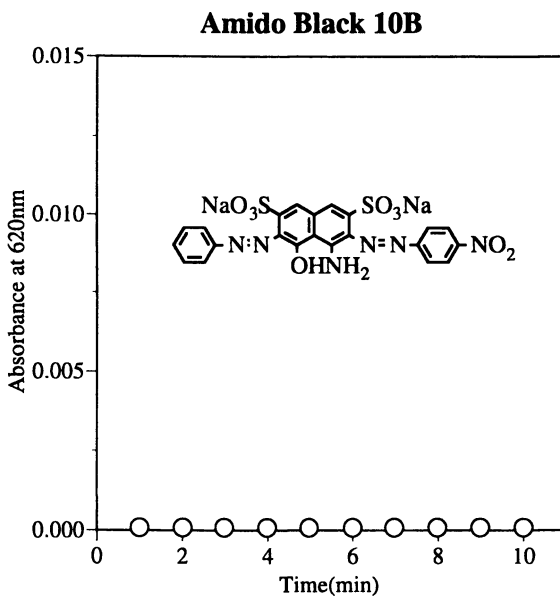


Fig.5 Time course of amido black 10B release from chitin foam. Reproduced with permission from *Proceedings of the International Workshop on Green Polymers, Indonesian Polymer Association, 1996.*

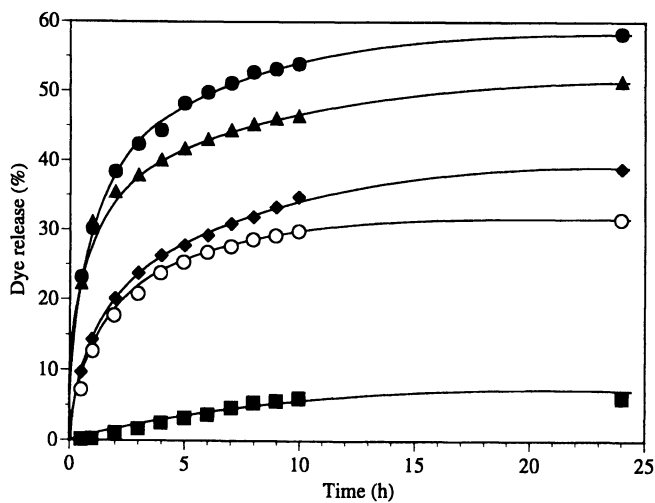
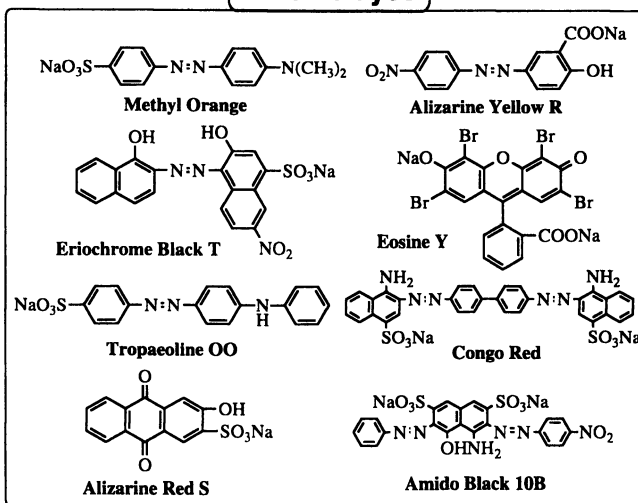
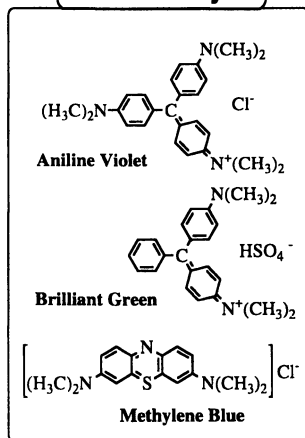


Fig. 6. Time course of amido black 10B release from chitin foam in SDS aqueous solution : (○) 0.1M; (◆) 0.05M; (▲) 0.02M; (●) 0.01M; (■) 0.001M.

### Anionic dyes



### Cationic dyes



Scheme 2. Chemical structures of various dyes. *Reproduced with permission from Proceedings of the International Workshop on Green Polymers, Indonesian Polymer Association, 1996.*

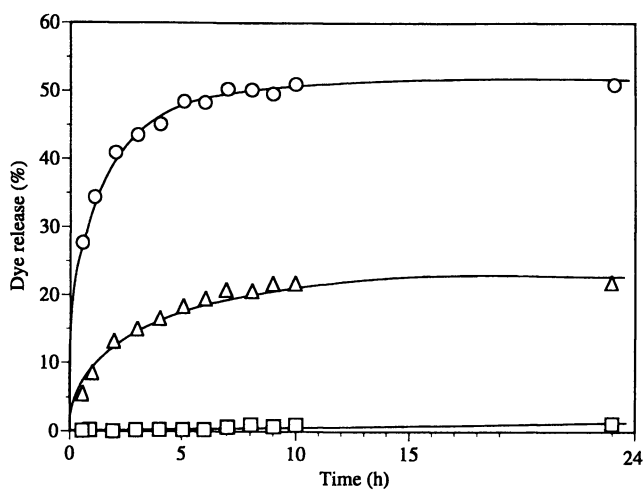


Fig.7 Time course of amido black 10B release from chitin foam at different pHs. ( $\square$ ) pH 4; ( $\Delta$ ) pH 7; ( $\circ$ ) pH 11.



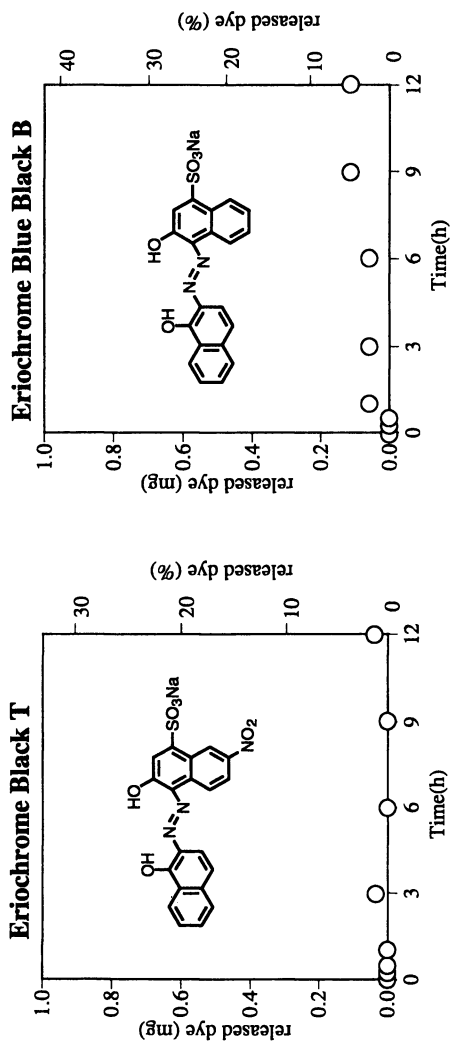


Fig.8 Time course of Eriochrome Black T and Eriochrome Blue Black B release from chitin foam.

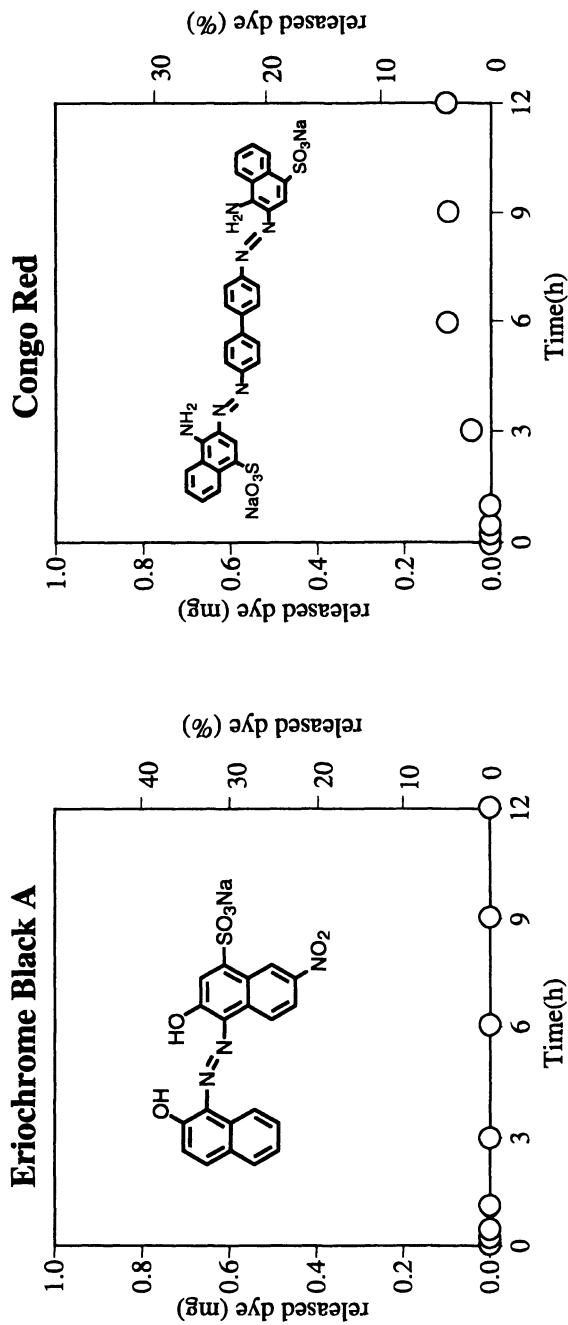


Fig.9 Time course of Eriochrome Black A and Congo Red release from PEG-chitin foam.

## REFERENCES

1. Prudden, J. F., and Nishihara, G., *Gynecology & Obstetrics*, **115**, 283-286 (1957).
2. Minke, R., and Blackwell, J., *J. Mol. Biol.*, **120**, 167-181 (1978).
3. "Chitin" Ed. by Muzzarelli, R. A. A., Pergamon Press, 1977, p58-62.
4. Tokura, S., and Nishi, N., *Chitin and Chitosan*, Ed. Zakaria, M. B. *et al.*( University Kebangsaan, Malaysia Press), 67-86 (1995).
5. Maghami, G. G., and Roberts, G. A. F., *Macromol. Chem.*, **189**, 195-200(1988).
6. Hackman, R. H., *Aust J. Biol. Sci.*, **7**, 168-178 (1958).
7. Domszy, J. G., and Roberts, G. A. F., *Macromol. Chem.*, **186**, 1671-1676 (1985).

## Chapter 7

# Polysaccharide Engineering: Silicified Microcrystalline Cellulose as a Novel High-Functionality Pharmaceutical Material

Stephen Edge, D. Fraser Steele, Michael J. Tobbyn, and John N. Staniforth<sup>1</sup>

Pharmaceutical Technology Research Group, Department of Pharmacy and Pharmacology, University of Bath, Bath, BA2 7AY, United Kingdom

Microcrystalline cellulose (MCC) is known to suffer loss of functionality following wet granulation. Research suggested that some of these losses could be attributed to quasi-hornification of MCC during manufacture and secondary processing. In order to address this a programme of polysaccharide engineering has been undertaken which indicated that silicon dioxide may act as an anti-hornification agent when combined with MCC. This silicified microcrystalline cellulose was found not only to resist loss of pharmaceutical functionality on wet granulation but also to have significantly improved performance compared with regular MCC in direct compression applications.

Microcrystalline cellulose (MCC) is one of the most widely used additives in tablet formulations. The material is a highly compressible pharmaceutical excipient and exhibits excellent compactibility, even at relatively low compression loads. Microcrystalline cellulose is a semi-crystalline polysaccharide which is prepared by partial hydrolysis of wood pulp using mineral acid and subsequent spray drying. It is produced by various manufacturers and is available in several grades based on particle size, density and water content. Equivalence between these manufacturers cannot be assumed, as significant differences in pulp and manufacturing processes may result in chemical and polymorphic changes which can, and do, lead to substantially different performance between materials (1,2).

Microcrystalline cellulose has many desirable properties but it does have some disadvantages such as loss of compactibility after wet granulation (3), poor flow (of the smaller particle size grades) and lubricant sensitivity. In order to try to address these problems manufacturers have produced even wider variations of MCC's such as high density grades (to improve flow), low moisture grades (for water sensitive drugs) and food grade materials produced from lower quality, less

<sup>1</sup> Corresponding author.

expensive pulps. However, in all reported cases improvement of one property invariably results in a detrimental effect in performance in another area. For instance, high density grades of MCC display improved flow but reduced compactibility. It has also been proposed that co-processing with  $\beta$ -cyclodextrin (4) or surface modification of MCC might improve some aspects of functionality during small scale manufacture (5-8).

Following a research programme aimed at reducing the susceptibility of MCC to loss of compactibility during wet granulation a new MCC, silicified microcrystalline cellulose, was developed. Silicified microcrystalline cellulose (SMCC) is produced by adding silicon dioxide to the MCC slurry upstream of the spray drying step of manufacture. This procedure produces a material which exhibits greater compactibility in wet granulation (resistance to 'quasi-hornification') and provides substantial additional tablet strength in direct compression (9). These advantages have been demonstrated in tablets containing only this excipient and also in an increasing number of formulated systems (10-12).

Even though SMCC offers improved performance over MCC the reasons for the substantially increased functionality have not been unequivocally explained. One of the major questions that must be addressed concerning SMCC is whether its properties can be considered as those of a simple composite material (MCC + silicon dioxide) providing a summation of the benefits of each component or whether a synergistic increase in performance can be demonstrated. It must also be discovered whether SMCC has to be classed as a new chemical entity or if any polymorphic changes in the cellulose have been induced. These are very important issues as these possibilities would lead to questions of regulatory acceptance and stability.

As part of our general pharmaceutical technology research program we have initiated a study of the structure/property relationships of MCC with a view to further understanding and improving the performance behaviour of SMCC and MCC.

## Materials and Methods

**Materials.** Microcrystalline cellulose (Emcocel 90M, MCC90 and Emcocel 50M, MCC50) and silicified microcrystalline cellulose (Prosolv90, SMCC90 and Prosolv50, SMCC50) were obtained from Penwest Pharmaceuticals Company, Patterson, NY, USA. Colloidal silicon dioxide (a 15%w/w aqueous dispersion, Cab-O-Sperse, ex Cabot Corporation, USA) was used as a source of silicon dioxide. To prepare silicon dioxide samples a quantity of the colloidal silicon dispersion was tray-dried using a convective oven (Gallenkamp) at 60°C and milled using laboratory mill (type Glen Creston DFH 48).

**Preparation of Samples.** Regular and silicified MCC's were used as received. Silicified microcrystalline celluloses have 2% w/w silicon dioxide concentration following silicification. A 'dry' mix consisting of 9.80g of Emcocel 90M and 0.20g dried silicon dioxide was prepared by trituration in a mortar and pestle or by low shear mixing.

**Scanning Electron Microscopy.** Scanning electron microscopy was performed after gold or carbon coating using a Jeol 6310 (Jeol Instruments, Tokyo, Japan).

**X-Ray Diffraction.** Diffraction patterns were obtained using an X-ray powder diffraction system (Phillips X-ray Analytical, Cambridge, UK). Each sample was analysed by a single sweep, step size  $0.05^\circ 2\theta$ , 13 second dwell time.

**Simple Powder Compaction.** Compacts of SMCC and MCC (25mm diameter, 6g) were prepared using a load of 100kN at a compression rate of 10mm/min and a dwell time of 1 minute using heat treated silver steel dies on an Instron 1185. Diametric tensile testing (13) was performed at 5mm/min and 0.05mm/min using an Instron 1125. Compression testing was performed using an Instron 1185 at 0.05mm/min.

**Compaction Simulator.** Compaction simulation studies were performed using an ESH machine (ESH testing, Brierly Hill, Midlands, UK). Compacts were produced using a single ended sawtooth profile, using 10mm flat faced F-tooling. An amount of material sufficient to produce a compact (at zero porosity) of  $0.25\text{cm}^3$  was added individually prior to compaction. The die walls were lubricated using 4% magnesium stearate suspended in acetone just prior to material addition. Analysis of Heckel plots was performed at a force previously determined by upper punch force/strength studies, with the chosen force in the upper range of compaction forces for that material. Yield strength was assessed by extrapolation from the linear portion (as determined by linear regression) of the Heckel plot (Tobyn, M.J., University of Bath, unpublished data).

### The Characterisation of MCC and SMCC Particles and Compacts

When considering the apparent benefits of silicification, in terms of material functionality, it is important to address possible reasons for any enhanced performance. This is particularly true for properties such as powder flow and (compacted) material strength. The difference in properties between MCC and SMCC must be due to differences in two general characteristics; the structural properties (physico-chemical characterisation) and/or the physical properties (material characterisation) of the materials.

In order for comparisons between the properties of MCC and SMCC to be made the properties of each "form" of MCC and SMCC need to be evaluated, *i.e.* as particles, as compacted particles and as tablets.

**Particle Properties.** Particle properties can also be used to describe the functional improvements of SMCC over MCC.

**True Density and Particle Size.** True density was measured by helium pycnometry and particle size using low angle laser light scattering. The true density and volume mean particle size data of MCC and SMCC ( $n=3$  for both samples and methods of analysis) were  $1.568\pm 0.003\text{g/cm}^3$ ,  $122\pm 3\mu\text{m}$  and  $1.576\pm 0.003\text{g/cm}^3$  and  $125\pm 3\mu\text{m}$  respectively (14). The data suggest that there is little change in the true

density of MCC during the silicification process. The results also suggest that no substantial change in the chemistry or crystallinity has occurred during silicification or subsequent processing. This is an important point since any modification of the crystallinity of MCC may affect stability or compactibility.

Additionally, the data also suggest that SMCC exhibits no significant change in particle size compared to unmodified MCC (14). The observed differences in particle size are well within the experimental error of this technique. As the particle size is not apparently altered it would be expected that there would be no decrease in the mixing capacity of the modified MCC. It is also apparent that any change in the flow properties of the material cannot readily be attributed to an increase in particle size (which would be expected to improve flow) and thus other explanations must be sought.

**Porosity.** The median pore size and overall pore distribution has been shown to be an important indicator of compactibility of plastically deforming solids. Porosity data suggested that bulk powders of MCC and SMCC90 exhibit similar pore size distributions (14). The porosity of plastically deforming materials, such as MCC, will influence compactibility since compact cohesion is dependent on *intra-* and *inter-* particulate contacts forming strong bonds. The apparent benefits attributed to SMCC cannot be explained by an increase in porosity, which would be apparent with a low density MCC. It has recently been shown, however, that the porosity of granulated samples differs significantly between MCC and SMCC, with SMCC retaining high porosity despite wetting (15).

**Morphology.** The morphology of MCC and SMCC has been studied using scanning electron microscopy (SEM) together with electron probe microanalysis (EPMA). In general, SMCC exhibited similar macroscopic morphology to MCC but different microscopic morphology (14-16). These studies suggest that there are small morphological features in the surface of SMCC90 which are absent in MCC90. Recently, a novel resin has been employed to study the internal structure of MCC using SEM/EPMA (17). This procedure has also been used to study the distribution of silicon dioxide in SMCC and suggested that silicon dioxide is present in the internal regions of some particles of SMCC (16). This is an important observation, especially in relation to compactibility studies.

**Flow.** The most widely used grade of MCC exhibits a primary particle size of *ca.* 50 $\mu$ m (*e.g.* Avicel PH101, Emcocel 50M). However, the relatively small particle size and the elongated shape of these particles makes this material unsuitable for many direct compression applications. This is because the relatively poor flow inhibits efficient mixing or consistent flow into the die of a high speed tablet press. For this reason manufacturers have produced larger particle size grades are which are generally used in direct compression. A grade with higher density, which should ensure more even flow into a tablet die, is also available (18). However, one drawback of the larger particle sized grades is that they do not show the same compactibility as the 50 $\mu$ m sized grades. In addition, there is evidence that the

200 $\mu\text{m}$  sized grade of MCC forms poorly ordered blends with a tendency towards segregation on standing or processing (19).

The flow of MCC's and SMCC's was tested using an Aeroflow device. This instrument, which measures the chaotic flow of powders on a dynamic basis, is becoming a standard device for testing the flow of pharmaceutical powders. In this type of analysis a low time between avalanches, where the powder cascades over itself, is indicative of low cohesive and adhesive properties, and thus good flow. The flow behaviour of SMCC and MCC following storage of the powders at a range of humidities is shown in Figure 1.

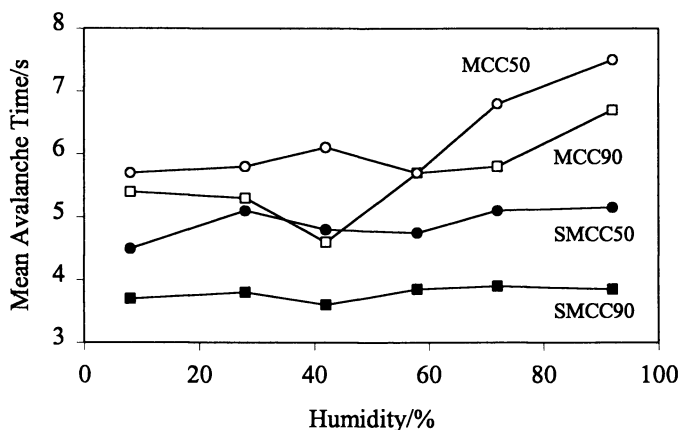


Figure 1. Aeroflow particle flow data of MCC and SMCC powders.

It can be seen from Figure 1 that the flow of grades of SMCC is significantly superior to the parent unmodified materials. Indeed, the flow of the 50 $\mu\text{m}$  size SMCC, SMCC50 appeared to be better than the 90 $\mu\text{m}$  sized MCC grade of regular unsilicified material. This is an important observation since MCC90 is preferred in direct compression due to its superior flow properties. Further observations suggested that SMCC90 grade was equivalent in flow to 200 $\mu\text{m}$  particle sized unmodified material, which exhibits excellent flow but relatively poor compactibility (20).

When unlubricated samples were tableted under power on a Manesty F-Press the relative standard deviation of tablet weight variations suggested that, once again, the SMCC samples displayed significantly improved flow. This performance is maintained on higher speed tableting presses (15).

The improved flow of SMCC samples opens up the possibility of using smaller particle size grades of material in situations where the flow of the formulation is critical, such as direct compression.



**Chemical Characterisation.** The chemical characterisation of materials can be divided into two distinct groups, surface structure and bulk structure. In terms of interfacial adhesion, surface structure is usually the more important characteristic.

In the evaluation of the characteristics of SMCC it is imperative that any chemical, or, polymorphic changes within the structure between the modified and unmodified materials are elucidated. A change in the amorphous nature of SMCC would have implications for the stability of blends and formulations containing MCC.

**X-Ray Diffraction.** It has previously been reported that polymorphic changes in the structure of MCC can lead to substantial differences in the functionality of these materials (1). In particular, the presence of cellulose polymorph II within the MCC structure has been reported to lead to very poor compactibility (21). X-ray diffraction (XRD) techniques have previously been shown to be capable of detecting polymorphic changes within MCC (21).

Samples of powders of SMCC and MCC were analysed using wide angle X-ray diffraction (14). The data suggested that both materials exhibit high crystallinity and that silicification has no significant affect on the crystallinity of MCC. Furthermore, the absence of a doublet at *ca.* 20-22° 2 $\theta$ , which is characteristic of cellulose II, suggested that the materials were composed primarily of cellulose I. No significant differences between the two materials were detected.

**Infrared Spectroscopy and <sup>13</sup>C, <sup>29</sup>Si NMR Spectroscopy.** Recently published results also suggest that there were no discernible differences between MCC and SMCC using solid state <sup>13</sup>C nuclear magnetic resonance (NMR) spectroscopy and attenuated total reflectance infrared spectroscopy (ATR FTIR) (14). The latter technique analyses only the outermost layers of a material and suggests that the structure of cellulose at the surface of the particles is retained during silicification, even if the silicified surface itself is morphologically different. Solid state <sup>29</sup>Si NMR suggested that SMCC contained (SiO)<sub>3</sub>SiOH, which is diagnostic for the presence of silicon dioxide (Edge, S., University of Bath, unpublished data).

**MCC and SMCC as Simple Compacted Powders.** The previous sections have undertaken to describe the physico-chemical characteristics and material properties of MCC and SMCC powders. The properties of compacts of MCC and SMCC was then investigated. The mechanical properties of compacts of MCC and SMCC were evaluated by tensile and compression testing.

**Tensile Strength.** The tensile strength of compacts of SMCC and MCC was determined using the diametric tensile test. Eight replicate samples of one batch were tested. The results are shown in Table I. It can be seen from Table I that, as expected, MCC50 produces stronger compacts than MCC90. Silicification of both materials produces powders whose compacts exhibit greater strength than their respective unmodified powders. Silicification appears to produce compacts of similar strength, at comparable silicon dioxide contents, of the two typical grades

tested. The strength benefit of silicification appears to be greater for the larger particle sized MCC90, under these specific conditions.

**Table I. Tensile Test Data for Compacts of MCC and SMCC (n=8)**

| <i>Sample</i> | <i>Tensile Strength/MPa</i> | <i>Density/gcm<sup>-3</sup></i> |
|---------------|-----------------------------|---------------------------------|
| MCC50         | 11.5 (+0.3, -0.4)           | 1.46 (+0.03, -0.03)             |
| SMCC50        | 12.9 (+0.4, -0.3)           | 1.42 (+0.03, -0.03)             |
| MCC90         | 10.5 (+0.2, -0.2)           | 1.45 (+0.02, -0.01)             |
| SMCC90        | 12.7 (+0.2, -0.1)           | 1.45 (+0.02, -0.03)             |

Numbers in parenthesis represent the highest and lowest measurements. Tested at 5mm/min.

Tensile test experiments were repeated at 0.05mm/min and the energies of failure during diametric tensile testing calculated for MCC90, SMCC90 and a dry blend of MCC90 and silicon dioxide (2%w/w). The results, together with the tensile test deflection data are given in Table II.

**Table II. Typical Tensile Strength and Failure Energies for MCC90, SMCC90 and a Dry Blend of MCC90/Silicon Dioxide (2%w/w)**

| <i>Sample</i> | <i>Deflection/mm</i> | <i>Tensile Strength/MPa</i> | <i>Failure Energy/J</i> |
|---------------|----------------------|-----------------------------|-------------------------|
| MCC90         | 0.86                 | 10.4 (+0.2, -0.1)           | 1.6                     |
| SMCC90        | 1.12                 | 12.8 (+0.1, -0.2)           | 2.6                     |
| Blend         | 0.66                 | 9.1 (+0.2, -0.2)            | 1.1                     |

Numbers in parentheses represent the highest and lowest measurements. Tested at 0.05mm/min.

It can be seen from Table II that silicification has a greater effect on the tensile strength and energy of failure of the larger particle sized MCC90 when tested at 0.05mm/min. In addition, the tensile strength, energy of failure and deflection of compacts of a dry blend of MCC90 and silicon dioxide (2%w/w) were significantly less than those for pure MCC90.

**Effective Stiffness.** The stiffness of compacts of the two materials was evaluated in two directions *i.e.* parallel to the compaction load (compression testing) and normal to the compaction load (diametric tensile testing) at 0.05mm/min test

rate. Compression testing suggested that the effective stiffness of compacts of SMCC90 and MCC90 and SMCC50 and MCC50 were similar (in this direction). The preliminary data for compacts of SMCC90 and MCC90 and SMCC50 and MCC50 which were subjected to diametric tensile testing are shown in Figure 2.

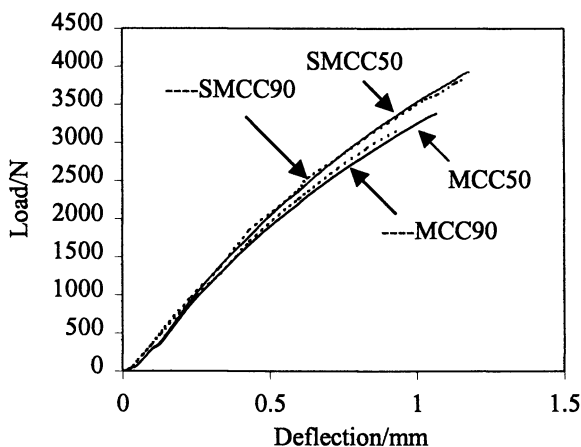


Figure 2. Tensile test load/deflection data of compacts of MCC and SMCC.

The data in Figure 2 suggest that silicification produces a material which, when compacted, exhibits a slightly greater stiffness normal to the compression direction, but that the apparent differences are not large.

### The Orientation of MCC and SMCC During Compaction

The direct compression of particles would be expected to produce anisotropic compacts in terms of density, structure (crystalline/amorphous orientation) and strength. This is particularly true for particles which have preferred orientations due to their shape. In order to detect any affect on orientation in MCC and SMCC failed compacts of MCC and SMCC were studied using X-ray diffraction. The directions of analysis are shown in Figure 3. The X-ray diffraction patterns of the failed MCC90 compacts (from the tensile test study, test rate 0.05mm/min) are shown in Figures 4-6.

Overall, these initial results suggest that compression of MCC and SMCC results in structurally anisotropic compacts in that the crystalline regions are predominately normal (direction X in Figure 3) to the direction of load. The other directions appear to be more amorphous. It has been reported that the tensile strength of MCC compacts is dependent on the direction of testing (22). These observations are in agreement with the swelling behaviour of MCC compacts (23).

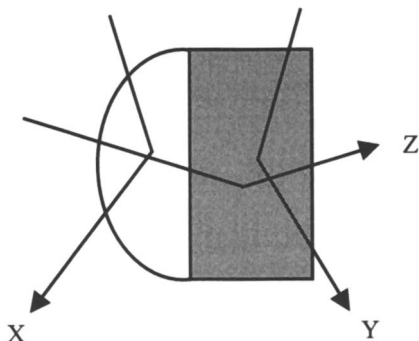


Figure 3. Directions of XRD analyses of failed compacts of MCC and SMCC.

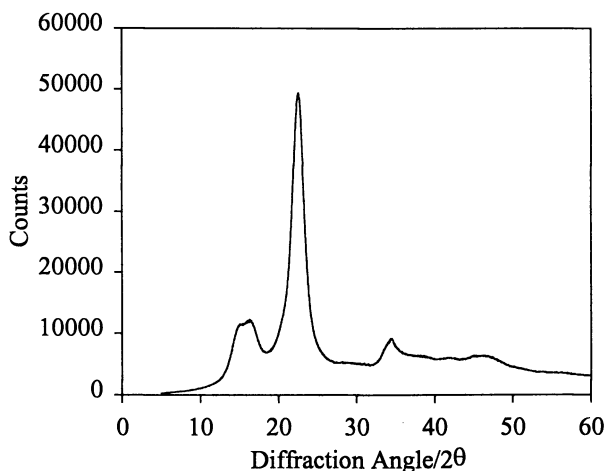


Figure 4. XRD pattern of failed MCC compact, direction X.

There also appear to be changes in the apparent ratio of diffraction lines at *ca.* 22° and 35° 2θ, again reflecting the ordering of MCC on compression. In addition, the ratio of diffraction lines at *ca.* 20.5 and 22.5° 2θ, previously assigned to cellulose

II and cellulose I respectively, appears to change on compaction. This is an interesting observation since, as previously stated, the presence of cellulose II has been reported to predict a decrease in compactibility of MCC.

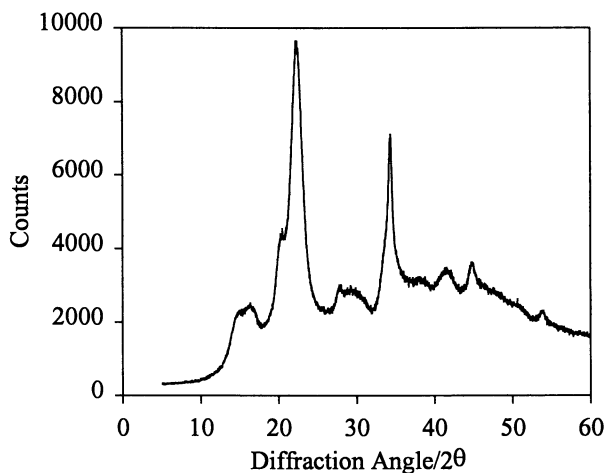


Figure 5. XRD pattern of failed MCC compact, direction Y.

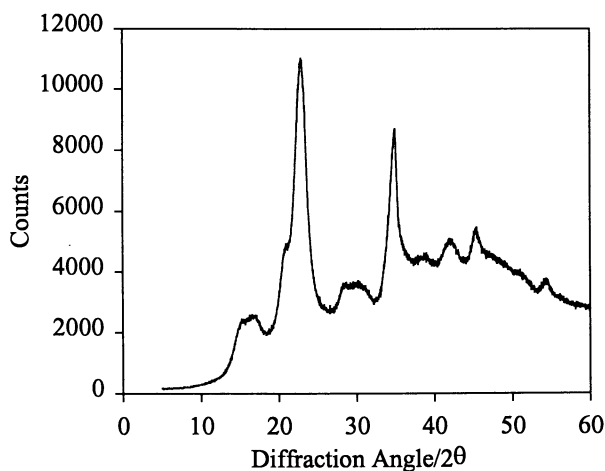


Figure 6. XRD pattern of failed MCC compact, direction Z.

Data obtained for SMCC90 appeared to be similar to the data obtained for MCC90 suggesting that orientation, in terms of crystallinity, is not significantly affected during compression.

Examination of the XRD patterns of MCC90 and SMCC90 and their respective compacts suggested that there were no significant differences in crystallinity between the two materials. In general, the mechanical properties of semi-crystalline polymers are governed by the crystalline phase. It would be expected that for this system, the crystallinity (crystal structure and degree) would be unaffected so long as dissolution and/or chemical modification of the crystalline regions did not occur during the silicification process. The present data suggest that this is the case and that the apparent differences in strength between MCC and SMCC are not due to any significant changes in bulk crystallinity.

### Tableting of MCC and SMCC

Initial simple compression of MCC and SMCC powders suggests that compact cohesion is significantly greater for SMCC. These materials have also been evaluated for tableting technology using a rotary tablet press and a compaction simulator. Although the primary design criterion for SMCC was retention of functionality in wet granulation its performance in direct compression was also evaluated.

**Direct Compression.** The variations of tablet strength with compaction pressure for MCC and SMCC has been reported recently (15). It was found that compacts of the silicified grades of material exhibited significantly greater strengths compared to untreated MCC during high speed rotary tableting. This result, although not expected, is highly significant. No previous modification of MCC had led to a material with higher direct compression strength. In development formulations the apparent increase in strength has proven to be useful by:

- a) Allowing higher drug loads for direct compression tableting.
- b) Improving the strength of friable tablet formulations.
- c) Allowing a reduction in the level of excipients (and thus reduction in tablet size) for direct compression formulations.

**Wet Granulation.** Samples of wet granulated MCC and SMCC were compacted and the tensile strength of the resulting tablets evaluated (15). The results suggested that SMCC maintained a much higher level of compactibility following wet granulation than the conventional material. Indeed the granulated SMCC had a compactibility equivalent to ungranulated conventional MCC.

**Lubricant Sensitivity.** Like many plastically deforming materials MCC forms much weaker compacts in the presence of hydrophobic lubricating agents such as magnesium stearate. It is thought that it is the hydrophobic nature of the lubricant which hinders the formation of hydrogen bonds at surfaces forced together during plastic deformation. These bonds strengthen the tablet matrix and form the primary means of cohesion in the compact. It has been shown that pre-mixing the

magnesium stearate with colloidal silica could reduce the deleterious effects of the former (24), but the additional processing steps and limited benefits of this approach have precluded its wide use.

However, no MCC, or other plastically deforming material, to date, has been reported to resist this problem without additional processing steps. The variation of tensile strength with compaction pressure for lubricated samples has been examined recently (15). It was found that SMCC resists the effects of magnesium stearate to an extent never previously demonstrated for MCC excipients.

**Compaction Simulator.** Further insights into the compaction behaviour of MCC and SMCC have been gained by the use of a compaction simulator. This machine uses hydraulics to mimic the compaction speeds of a high output tablet press but, since it is a single station machine, only requires a small amount of powder. The compaction simulator can, amongst other parameters, be used to elucidate the following:

- a) The yield pressure. This is determined *via* Heckel plot and gives an indication of the force required for a material to yield during compaction. For a plastically deforming material, which yields relatively easily, this value will generally be relatively low (*i.e.* <100MPa). However, for a compact which forms by brittle fracture this figure will be much higher, for example, for dicalcium phosphate it is >400MPa.
- b) The strain rate sensitivity. The strain rate sensitivity is a ratio of yield pressures at low and high tableting speeds. Plastically deforming materials, such as MCC, exhibit viscoelasticity on compression. In general, this means that they show a higher yield point (pressure) at higher compaction speeds. This manifests itself in practice by the formation of relatively weaker tablets at higher tableting speeds or failure due to capping or lamination (25).

Yield pressure data for typical batches of MCC and SMCC, 50 $\mu$ m and 90 $\mu$ m sized grades, are presented in Table III.

**Table III: Mean Yield Pressures and Strain Rate Sensitivities for MCC and SMCC (n=6)**

| Sample | Mean Yield Pressure/MPa |           | Strain Rate Sensitivity/% |
|--------|-------------------------|-----------|---------------------------|
|        | 1mm/sec                 | 100mm/sec |                           |
| MCC50  | 75.0                    | 87.1      | 16.7                      |
| SMCC50 | 83.0                    | 86.1      | 3.7                       |
| MCC90  | 78.1                    | 91.5      | 17.1                      |
| SMCC90 | 77.4                    | 82.4      | 6.5                       |

It can be seen from Table III that there is a small difference in yield pressure for SMCC's when compared to the parent materials at these speeds. However, these values are still well within the published range for MCC materials. The more significant data is the reduction in strain rate sensitivity for SMCC. The increased ductility of this material at higher speeds should provide additional functionality during large scale tablet manufacture and reduce problems attributed to the viscoelasticity of MCC's.

### Regulatory Status

The previous sections described the structure/properties relationships of MCC and SMCC. One important aspect of the development of pharmaceutical materials is regulatory acceptance. The lack of demonstrated chemical interaction between the two components of SMCC has led to it being classified, for regulatory purposes, as a combination product (in the same category as, for instance, MCC/calcium carbonate and MCC/lactose). Since the material contains pharmacopoeial grades of MCC and silicon dioxide and is manufactured by a previously established method it is considered that there are no additional regulatory considerations over MCC and silicon dioxide used singularly. This view has been established for new formulations being submitted to regulatory agencies and for formulations in which SMCC has been substituted for MCC in established formulations.

### Conclusions

The original aim of research into MCC was to reduce the dilatory effects of wet granulation on the compaction properties of MCC's. Whilst some evidence was obtained that the methods of wetting and drying could be used to ameliorate some of the loss of compactibility no processing method offered complete protection. Efforts to improve the functionality of MCC on wet granulation has led to the introduction of SMCC which, under controlled comparison conditions, retains compactibility on wet granulation and also appears to offer significant benefits in direct compression. Evidence suggests that SMCC has higher plasticity, higher intrinsic strength and shows a resistance to magnesium stearate compared to unmodified MCC. These are uniquely advantageous properties for a material based on MCC.

### Acknowledgment

We thank Penwest Pharmaceuticals Co. for financial support and Ahmed Khalaf for his help with the Aeroflow data.

### Literature Cited

1. Chatrath, M. and Staniforth, J.N. Source dependent polymorphism of microcrystalline cellulose. *J. Pharm. Pharmacol. Supp.*, **1991**, *43*, 4.
2. Landin, M, Martinez-Pachecho, R., Gomez-Amoza, J. L., Souto, C., Concheiro, A and Rowe, R.C. Comparison of batch variation and source of



- pulp on the properties of microcrystalline cellulose. *Int. J. Pharm.*, **1993**, *91*, 133-141.
3. Chatrath, M. PhD. thesis. The effect of wet granulation on the physico-mechanical characteristics of microcrystalline cellulose. University of Bath, **1992**.
  4. Tsai, T., Wu, J-S., Ho H-O. and Sheu, M-T. Modification of the physical characteristics of microcrystalline cellulose by codrying with beta-cyclodextrins. *J. Pharm. Sci.*, **1998**, *87*, 117-122.
  5. Nürnberg, E. and Wunderlich, J. Coating of cellulose products with highly dispersed silicic acid: Investigations on the improvement of tableting properties demonstrated in low-dose tablets. *Pharm. Ind.*, **1995**, *57*, 252-256.
  6. Nürnberg, E. and Wunderlich, J. Simple formulation optimization for extrusion-influence of particle size, source and preprocessing of microcrystalline celluloses. *Pharm. Ind.*, **1996**, *58*, 653-658.
  7. Nürnberg, E. and Wunderlich, J. Coating of cellulose products with colloidal silicon dioxide. Investigations to improve the tableting behaviour using low dose tablets as an example. *Drugs made in Germany*, **1996**, *39*, 104-107.
  8. Nada, A.H. and Graf, E. Evaluation of Vitacel M80K as a new direct compression vehicle. *Eur. J. Pharm. Biopharm.*, **1998**, *46*, 347-353.
  9. Staniforth, J.N., Sherwood, B.E. and Hunter, E.A. Towards a new class of high functionality tablet binders. II: Silicified microcrystalline cellulose (SMCC) for wet granulation. *Proceedings of the AAPS conference*, **1996**, PT6161.
  10. Sherwood, B.E., Hunter, E.A. and Staniforth, J.N. Silicified microcrystalline cellulose (SMCC): A new class of high functionality binders for direct compression tableting. *Proceedings of the AAPS conference*, **1996**, PT6164.
  11. Hunter, E.A., Sherwood, B.E. and Zeleznik, J.A. Silicified microcrystalline cellulose (SMCC) formulations: Use of a new class of high functionality binders for a high load acetaminophen tablet by direct compression. *Proceedings of the AAPS conference*, **1996**, PT6163.
  12. Riba, M. D., Segado, X. and Ferrer, F. Silicified microcrystalline cellulose: a comparative evaluation of this new high functionality direct compression excipient. *Proceedings of the AAPS conference*, **1997**, 1038.
  13. Fell, J.T. and Newton, J.M. Determination of tablet strength by diametrical compression test. *J. Pharm. Sci.*, **1972**, *59*, 688-691.
  14. Toby, M.J., McCarthy, G. P., Staniforth, J.N. and Edge, S. Physicochemical comparison between microcrystalline cellulose and silicified microcrystalline cellulose. *Int. J. Pharm.*, **1998**, *169*, 183-194.
  15. Sherwood, B.E. and Becker, J.W. A new class of high-functionality excipients: silicified microcrystalline cellulose. *Pharm. Tech.*, **1998**, *22*, 78-88.
  16. Edge, S., Potter, U.J., Steele, D.F., Toby, M.J. and Staniforth, J.N. The use of scanning electron microscopy and electron probe microanalysis for studying silicified microcrystalline cellulose. *Proc. 16<sup>th</sup> Pharmaceutical Technology Conference and Exhibition*, Dublin, Ireland, **1998**, *2*, 78-85.

17. Edge, S., Potter, U.J., Steele, D.F., Tobyn, M.J. and Staniforth, J.N. The use of a modified resin for studying the internal structure of microcrystalline cellulose. *Micron*, **1998**, *29*, 469-471.
18. Zeleznik, J.A., Virtanen, J. and Sherwood, B.E. Emcocel HD90, An enhanced high density grade of microcrystalline cellulose (MCC) exhibiting improved flow and greater compactibility. *Proceedings of the AAPS conference*, **1996**, PT6167.
19. Staniforth, J.N. and Tralhão, M. Blending characteristics of large particle size microcrystalline cellulose for direct compression. *Proceedings of the AAPS conference*, **1996**, PT6168.
20. Khalaf, A.S., Tobyn, M.J. and Staniforth, J.N. Measurement of the flow properties of silicified microcrystalline cellulose. *Proceedings of the AAPS conference*, **1997**, 2538.
21. Landin, M, Martinez-Pachecho, R., Gomez-Amoza, J. L., Souto, C., Concheiro, A and Rowe, R.C. Effect of country of origin on the properties of microcrystalline cellulose. *Int. J. Pharm.*, **1993**, *91*, 123-131.
22. Ek, R., Wormald P., Ostelius, J., Iverson, T. and Nyström, C. Crystallinity index of microcrystalline cellulose particles compressed into tablets. *Int. J. Pharm.*, **1995**, *125*, 257-264.
23. Khan, F., Pilpel, N. and Ingham, S. The effect of moisture on the density, compaction and tensile strength of microcrystalline cellulose. *Powder Technol.*, **1988**, *54*, 161-164.
24. Ahmed, H.A. and Staniforth, J.N. Influence of ternary components on compressibility of microcrystalline cellulose following blending with magnesium stearate. *J. Pharm. Pharmacol.*, **1986**, *38*, 50P.
25. Roberts, R.J and Rowe, R.C. The effect of punch velocity on the compaction of materials. *J. Pharm. Pharmacol.*, **1985**, *37*, 377-384.

## Chapter 8

# Synthesis and Characterization of Thermoreversible Sucrose Hydrogels (Sucrogels)

Seongbong Jo and Kinam Park

School of Pharmacy, Purdue University, West Lafayette, IN 47907

Sucrose-based monomers were synthesized for preparation of hydrogels with thermoreversible and degradable properties. New monomers synthesized were 6-(N-methacryloyl-6-aminocaproyl) sucrose (MACS), 6,6'-di(N-methacryloyl-6-amino caproyl) sucrose (DMACS), 6-(N-methacryloyl leucyl) sucrose (MLS), and 6-(N-methacryloyl-11-amino undecanoyl) sucrose (MAUS). They were prepared by Schotten-Bauman reaction and Mitsunobu reaction, and characterized by NMR spectroscopy, elemental analysis, and thin layer chromatography.

Modified sucrose monomers were copolymerized with other monomers such as poly(propylene glycol) methacrylate (PPGM) and poly(ethylene glycol) ethyl ether methacrylate (PEGEEM) to prepare sucrose hydrogels (sucrogels). DMACS, a bifunctional sucrose monomer, was used as a cross-linking agent. Prepared hydrogels showed inverse thermoreversible properties: they swelled at 5°C but shrank as the temperature increased up to 60°C. It took 2–3 days for the sucrogels to swell to equilibrium at 5°C. On the other hand, shrinking at 60°C requires only 2–4 h to complete. These sucrogels were degraded in both acidic (pH 2.0) and basic (pH 12.0) solutions. Degradation in acidic solution was quite slow but relatively fast in a basic environment. The sucrose monomers prepared in this study are useful in the synthesis of degradable, thermosensitive hydrogels for various applications including controlled drug delivery.

## Introduction

Hydrogels with the abilities to respond to changes in environmental factors, such as pH (1,2), temperature (3,4), electric field (5,6), magnetic field (7), or specific molecules (8,9), are useful in various applications including drug delivery, biotechnology, and biosensors. Of the many environment-sensitive hydrogels, temperature-responsive hydrogels have been used quite frequently for controlled drug delivery and bioseparation (10,11). The most widely used thermosensitive hydrogels are based on acrylamide derivatives such as N-isopropyl acrylamide. In this study, we synthesized various sucrose-based monomers which can be used to prepare thermoreversible hydrogels by copolymerization with hydrophobic monomers. Sucrose was chosen in this study, since it has unique properties. Specifically, sucrose is degradable and absorbable in the body. The hydroxyl groups of sucrose not only serve as good reaction sites for chemical modifications, but also make the carbohydrate very water-soluble. The design of thermoreversible hydrogels was focused on balancing the hydrophilic and hydrophobic properties so that the synthesized hydrogels exhibited inverse thermosensitivity resulting from the presence of lower critical solution temperature (LCST).

## Experimental

**Materials.** Methacryloyl chloride (90%), 6-amino caproic acid, 11-amino undecanoic acid, DL-leucine, anhydrous dimethylformamide, Hydrion buffers, triphenyl phosphine, diisopropyl azodicarboxylate, poly(propylene glycol) methacrylate (Mol. Wt. 350-389), poly(ethylene glycol) ethyl ether methacrylate (Mol. Wt. ~246), ammonium persulfate, N,N,N',N'-tetramethylethylenediamine (TEMED), and sucrose were purchased from Aldrich Chemical Co. (Milwaukee, WI). Methacryloyl chloride was purified with distillation at 150°C before use. Other organic solvents and chemicals used were reagent grade. Silica gel thin layer chromatography (TLC) plates (UNIPLATE) were obtained from Analtech, Inc (Newark, NJ). Charring agent for TLC (Sigma spray agent, sulfuric acid) was obtained from Sigma Chemical Co. (Milwaukee, WI).

**Synthesis of Sucrose Monomers.** Sucrose monomers were prepared by following the reactions in Fig. 1. Fig. 1-A shows modification of N-aminocarboxylic acids with methacryloyl chloride. N-methacryloyl-6-amino caproic acid and N-methacryloyl leucine were synthesized following the methods used by Kaczmar or Kulkarni (12,13). In a 250 ml round bottom flask, 0.1 mole of 6-aminocaproic acid or leucine was dissolved in 30 ml of deionized distilled water. In the case of leucine, 6 g of sodium hydroxide was added in advance. Then freshly distilled methacryloyl chloride and concentrated solution of sodium hydroxide (11.4 g of NaOH to 25 ml of deionized distilled water) were added dropwise to the mixture in an ice bath. During the addition of reagents, the temperature of reaction mixture was kept below 20°C and the pH at 8.5-9.5. After further reaction for 3 h, the solution was carefully acidified to pH 1-2 with 15% HCl solution and extracted with 150 ml of ethylacetate three times. The extract was dried with anhydrous magnesium sulfate, and crystallized with benzene and toluene. Final products were recrystallized with ethyl acetate. N-methacryloyl-11-aminoundecanoic acid (11-AUA) was prepared by the method outlined by Yeoh *et al.* (14). The purity of N-methacryloyl amino carboxylic acids was confirmed by TLC using a chloroform: methanol (10:1) mixture. The *rf* values in TLC and yields for N-methacryloyl-6-amino caproic acid, N-methacryloyl leucine, and N-methacryloyl-11-aminoundecanoic acid were 0.44 and 55%, 0.46 and 67%, and 0.54 and 48%, respectively.

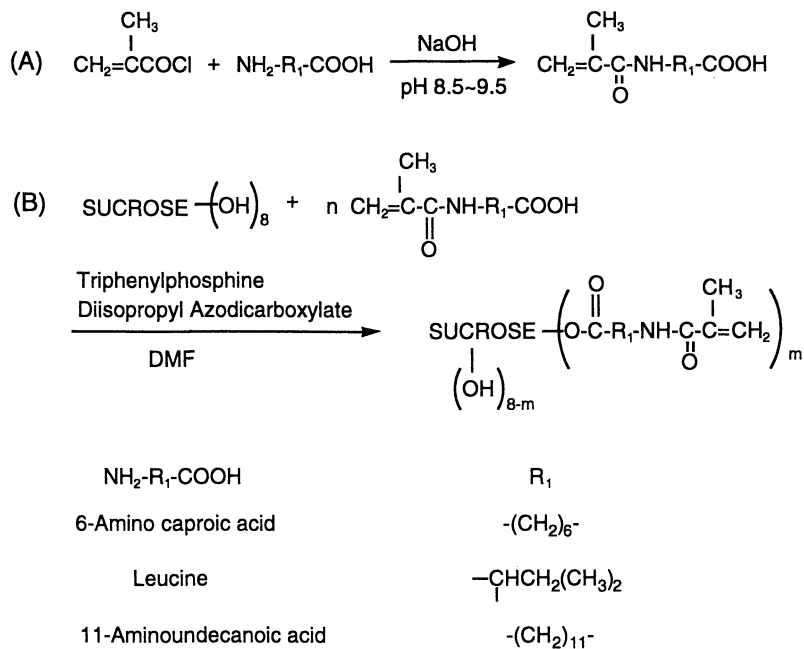


Figure 1. Synthetic reaction scheme of sucrose monomers. (A) Amino carboxylic acids were modified with methacryloyl chloride by Schotten-Bauman reaction at pH between 8.5~9.5. (B) Modified N-methacryloyl carboxylic acids were attached to sucrose by Mitsunobu reaction (B).  $m=1$  or  $2$ .

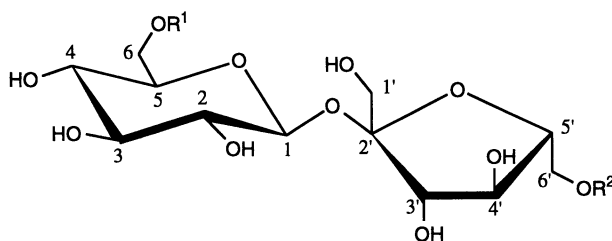
Sucrose was esterified with N-methacryloyl amino carboxylic acids by Mitsunobu reaction (Fig. 1-B). General synthetic procedure followed the method established by Abouhilale et al (15) with minor modifications. One equivalent of sucrose was reacted with N-methacryloyl amino carboxylic acid (1.5 eq. of N-methacryloyl caproic acid, and 1.0 eq. of N-methacryloyl leucine and N-methacryloyl-11-aminoundecanoic acid) in the presence of triphenylphosphine (1.7 eq. for N-methacryloyl-6-amino caproic acid, and 1.2 eq. for both N-methacryloyl leucine and N-methacryloyl-11-aminoundecanoic acid) and diisopropyl azodicarboxylate (same equivalent as triphenyl phosphine) using 200 ml of anhydrous dimethylformamide as solvent. The progress of the reaction was checked by TLC using chloroform:methanol (3:1) mixture. When the band of sucrose on TLC plate did not decrease further, the mixture was transferred to 1 L of hexane, and then chloroform was added to the mixture to precipitate sucrose monomers from the solvent mixture. The crude precipitates were purified further with gradient elution of chloroform-methanol eluents in the column chromatography. The chloroform:methanol ratios were 8:1, 6:1, and 4:1 for MACS, 10:1, 8:1, and 6:1 for DMACS and MLS, and 15:1, 12:1, and 10:1 for MAUS. Sucrose monomers were characterized by TLC using chloroform:methanol (3:1),  $^1\text{H}$ - and  $^{13}\text{C}$ -NMR with Bruker ARX 300 spectrometer in  $\text{CD}_3\text{OD}$ . Degree of substitution of DMACS was determined by quantitative  $^{13}\text{C}$ -NMR. For quantitation by  $^{13}\text{C}$ -NMR, chromium acetate, a NMR relaxation reagent for quantitative NMR analysis, was also dissolved in the sample to make its final concentration of 0.03 M. The quantitative  $^{13}\text{C}$ -NMR analysis was performed at 75 MHz with a 3-second pulse delay time. The gate-decoupled pulse sequence was also employed to suppress the NOE effect.

The yields of modified sucrose ranged from 9% to 19%. The *rf* values in TLC were 0.26 for MACS, 0.49 for DMACS, 0.39 for MLS, and 0.42 for MAUS, respectively. Structures of monomers used for the hydrogel synthesis are shown in Fig. 2.

**Elemental analysis.** Calculation for  $\text{C}_{22}\text{H}_{37}\text{O}_{13}\text{N}_1$  (MACS): C, 50.47; H, 7.12; N, 2.68. Found: C, 50.29; H, 7.45; N, 2.63. Calc. for  $\text{C}_{32}\text{H}_{52}\text{O}_{15}\text{N}_2$  (DMACS): C, 54.54; H, 7.44; N, 3.97. Found: C, 54.27; H, 7.94; N, 3.45. Calc. for  $\text{C}_{22}\text{H}_{37}\text{O}_{13}\text{N}_1$  (MLS): C, 50.47; H, 7.12; N, 2.68. Found: C, 48.54; H, 7.22; N, 2.42. Calc. for  $\text{C}_{27}\text{H}_{47}\text{O}_{13}\text{N}_1$  (MAUS): C, 54.63; H, 7.98; N, 2.36. Found: C, 54.27; H, 8.35; N, 2.69.

**Synthesis of Thermoreversible Hydrogels.** Sucrose monomers (MACS, MLS, DMACS, and MAUS) were copolymerized with PPGM or PEGEEM to prepare thermoreversible hydrogels. Solutions of 0.5M MACS, 0.5M MLS, 0.5M PPGM, 0.5M PEGEEM, 0.25M DMACS and 0.25M MAUS were prepared with 50% methanol as solvent. Various sucrogels were obtained by changing molar ratio of the sucrose monomers to comonomers from 1:1 to 1:2. The final volume of monomer solution was 6 ml. Total amount of monomers was 3.0 mmole for hydrogels made of MACS or MLS and 2.0 mmole for hydrogels containing MAUS. DMACS was used as a crosslinking agent and the amount of DMACS ranged from 0.5 to 10.0 mole% of total monomers. Sixty microliter of 10% ammonium persulfate solution in 50% methanol and 60  $\mu\text{l}$  of 10% tetramethylethylenediamine (TEMED) in 50% methanol were added to the monomer mixture as initiators. After mixing for 10 sec with a vortex mixer, the mixture was transferred into a mold to make films (7.5 cm x 7.5 cm x 0.3 cm). Polymerization was allowed for 10 h at room temperature. The prepared hydrogels were cut into discs with diameter of 1.5 cm for the investigation of swelling kinetics and 1.2 cm for degradation studies. Prepared hydrogel discs were washed once with ethanol and several times with cold deionized water. After the last washing, hydrogel discs were equilibrated for more than 1 day at 5°C.

## SUCROSE MONOMERS



|  | R <sup>1</sup>  | R <sup>2</sup>  |
|--|---|---|
| 6-(N-methacryloyl-6-amino caproyl) sucrose (MACS)        | $\begin{array}{c} \text{O} \\ \parallel \\ -\text{C}(\text{CH}_2)_5\text{NHCOC} \\   \\ \text{CH}_3 \\ \parallel \\ =\text{CH}_2 \end{array}$     | H   |
| 6,6'-di (N-methacryloyl-6-amino caproyl) sucrose (DMACS) | $\begin{array}{c} \text{O} \\ \parallel \\ -\text{C}(\text{CH}_2)_5\text{NHCOC} \\   \\ \text{CH}_3 \\ \parallel \\ =\text{CH}_2 \end{array}$     | $\begin{array}{c} \text{O} \\ \parallel \\ -\text{C}(\text{CH}_2)_5\text{NHCOC} \\   \\ \text{CH}_3 \\ \parallel \\ =\text{CH}_2 \end{array}$ |
| 6-(N-methacryloyl leucyl) sucrose (MLS)                  | $\begin{array}{c} \text{O} \\ \parallel \\ -\text{CCHNHCOC} \\   \\ \text{CH}_2\text{CH}(\text{CH}_3)_2 \\ \parallel \\ =\text{CH}_2 \end{array}$ | H   |
| 6-(N-methacryloyl-11-aminoundecanoyl) sucrose (MAUS)     | $\begin{array}{c} \text{O} \\ \parallel \\ -\text{C}(\text{CH}_2)_{10}\text{NHCOC} \\   \\ \text{CH}_3 \\ \parallel \\ =\text{CH}_2 \end{array}$  | H   |

## HYDROPHOBIC MONOMERS

|   |   |
|---|---|
| Poly (propylene glycol) methacrylate (PPGM)             | $\text{H}_2\text{C}=\text{C}(\text{CH}_3)\text{CO}_2\text{[CH}_2\text{CH}(\text{CH}_3)\text{O}]_n\text{H}$    |
| Poly (ethylene glycol) ethylether methacrylate (PEGEEM) | $\text{H}_2\text{C}=\text{C}(\text{CH}_3)\text{CO}_2\text{[CH}_2\text{CH}_2\text{O}]_n\text{CH}_2\text{CH}_3$ |

Figure 2. Structures of monomers used in the preparation of thermo-reversible sucrogels.

**Temperature Dependence of Swelling and Swelling Kinetics of Sucrogels.** Swollen gels previously equilibrated at 5°C were placed in a 60°C water bath. Changes in the swelling ratio of hydrogels were measured by the gravimetric method. The swelling ratio of hydrogels was calculated by dividing the weight of a swollen gel by the weight of a dried gel.

The temperature-dependent swelling kinetics was examined by first swelling the hydrogel to an equilibrium at 60°C and then changing the temperature to 5°C. To investigate thermosensitive swelling of sucrogels, previously swollen hydrogels were put into the water bath with temperature changing from 5°C to 60°C.

**Degradation of Thermoreversible Hydrogels.** Thermoreversible hydrogels with molar composition of PPGM:MLS:DMAC=5:4:1 and PPGM:MACS:DMACS = 5.00:4.95:0.05 were placed into beakers containing 100 ml of acidic solution (Hydrion buffer, pH 2.0) or basic solution (Hydrion buffer, pH 12.0). Solutions were kept at room temperature during experiments. Degradation of hydrogels was followed by measuring the weights of hydrogels and dividing it by the weight of the fully swollen gel at timed intervals.

## Results and Discussion

**Synthesis of Sucrose Monomers.** As shown in Fig. 1, sucrose monomers were prepared by first modifying N-aminocarboxylic acids with methacryloyl chloride by Schotten-Bauman reaction. The carbon length of N-aminocarboxylic acids determines the hydrophobicity of the substituents. One practical advantage of this approach is that various amino acids with different water solubility can be utilized for the preparation of hydrophobic sucrose monomers. N-methacryloyl amino carboxylic acids were then reacted with sucrose by Mitsunobu reaction. Since sucrose has 3 primary hydroxyl groups, sucrose derivatives with two polymerizable substituents or more could be used as a crosslinking agent in the synthesis of sucrose hydrogels.

<sup>13</sup>C-NMR spectrum of sucrose monomers showed that the most favorable site for esterification in sucrose was OH-6 (see Fig. 2). Reaction with 1:1 molar ratio mainly modified OH-6. This observation was consistent with the previous study by Abouhilale et al. who synthesized polyfluorinated 6-esters of sucrose by Mitsunobu reaction (15). All the carbon peaks and some proton peaks from sucrose were identified and assigned based on the results of Abouhilale et al. (15).

In the synthesis of DMACS, the molar ratio of sucrose:N-methacryl-6-amino caproic acid was 1:1.7. <sup>13</sup>C-NMR spectrum of purified DMACS showed that two N-methacryloyl-6-aminocaproyl groups were attached to C-6 and C-6'. The C-5' peak (83.9 ppm) and the C-6' peak (64.1 ppm) of sucrose shifted to upfield by 3 ppm and downfield by 2.7 ppm, respectively. These shifts were consistent with the results obtained by Jansson et al. (16) in the modification of glucose. Their results showed that the introduction of an O-acetyl group in any position of a glycopyranoside caused deshielding of the substituted carbon by 0.7-3.5 ppm and shielding of the carbons next to those carbons (b carbons) by 1.2-2.8 ppm. Another proof for the disubstitution of sucrose was <sup>13</sup>C-NMR spectrum of purified DMACS that showed two ester carbons peaks at 175.1 and 175.3 ppm.



Degree of substitution of DMACS was estimated by quantitative  $^{13}\text{C}$ -NMR integration (Fig. 3). By mixing chromium acetate, a NMR relaxation reagent,  $^{13}\text{C}$ -NMR peak could be integrated to provide quantitative information on the number of substituents. The integrated  $^{13}\text{C}$ -NMR peaks of DMACS showed that the integration values of carbon peaks from substituents were about twice those of sucrose. Fig. 4 shows  $^1\text{H}$ -NMR spectra of MACS and DMACS. An anomeric proton peak of sucrose appears at 5.3 ppm as doublet. In addition, two protons from  $=\text{CH}_2$  of substituents show clear two resonance peaks at 5.3 and 5.6 ppm (Fig. 4-B). The integration ratio between proton peak of 5.6 ppm to that of 5.3 were 1/2 and 2/3 for monosubstituted MACS and disubstituted DMAC, respectively. These integration ratios also proved disubstitution of sucrose. Elemental analysis also showed that the observed elemental compositions were close to theoretical values.

More hydrophobic sucrose monomers can be prepared by using functionalized hydrophobic polymers, such as poly(propylene glycol) and dihydroxy polybutadiene. Poly(propylene glycol) (meth)acrylate can also be coupled with sucrose after reaction with succinic anhydride. Sucrose modified with hydrophobic polymer can experience thermal gelation even without crosslinking.

**Temperature-Dependent Swelling Profiles.** Sucrose monomers were copolymerized with commercially available monomers, such as PPGM and PEGEEM, to make thermoreversible hydrogels. The formation of hydrogels was tested by polymerization of monomer mixtures with different amounts of DMACS, a crosslinking agent used in this study. The mixture of MACS and PPGM formed a gel at a low concentration (0.5 mole%) even in the absence of DMACS. This may be due to interdigitation of long side groups of MACS and PPGM. As the polymerization continued, side chains of PPGM and MACS might entangle each other significantly to crosslink polymer backbone even without DMACS. MLS that had bulky leucyl side groups ( $-\text{CH}_2\text{CH}(\text{CH}_3)_2$ ), however, needed a relatively large amount of DMACS to form a gel. This is probably because side groups were not linear and ineffective for entangling. At 5 mole% of DMACS, a very fragile hydrogel of poly(MLS-co-PPGM) was formed. In subsequent studies, MACS-containing sucrogels were crosslinked with 0.5 mole% of DMACS, while MLS-containing sucrogels were crosslinked with 10 mole% of DMACS for the formation of hydrogels with certain mechanical strength.

Sucrogels made of MACS and PPGM or DMACS and PPGM shrank as the temperature increased. As shown in Fig. 5, the volume decreased gradually as temperature increased until the temperature reached  $35^\circ\text{C}$ . The maximum of swelling ratio at  $5^\circ\text{C}$  was about 30, and the temperature-dependent volume change was slightly dependent on the amount of sucrose monomers used. As the amount of sucrose monomers in the gels increased from 33 mole% to 50 mole%, the maximum swelling ratio at  $5^\circ\text{C}$  decreased and the minimum swelling ratio at  $35^\circ\text{C}$  increased slightly without a clear change in the overall profile. This may be partially due to a slight loss of thermal sensitivity by the increase in hydrophilicity of sucrogels. When the concentration of DMACS was increased from 0.5 mole% to 5.0 mole%, swelling of sucrogels decreased while the overall thermosensitive swelling profiles remained very similar. Higher crosslinking density limited the swelling of hydrogels by forming tighter networks of polymer chains.

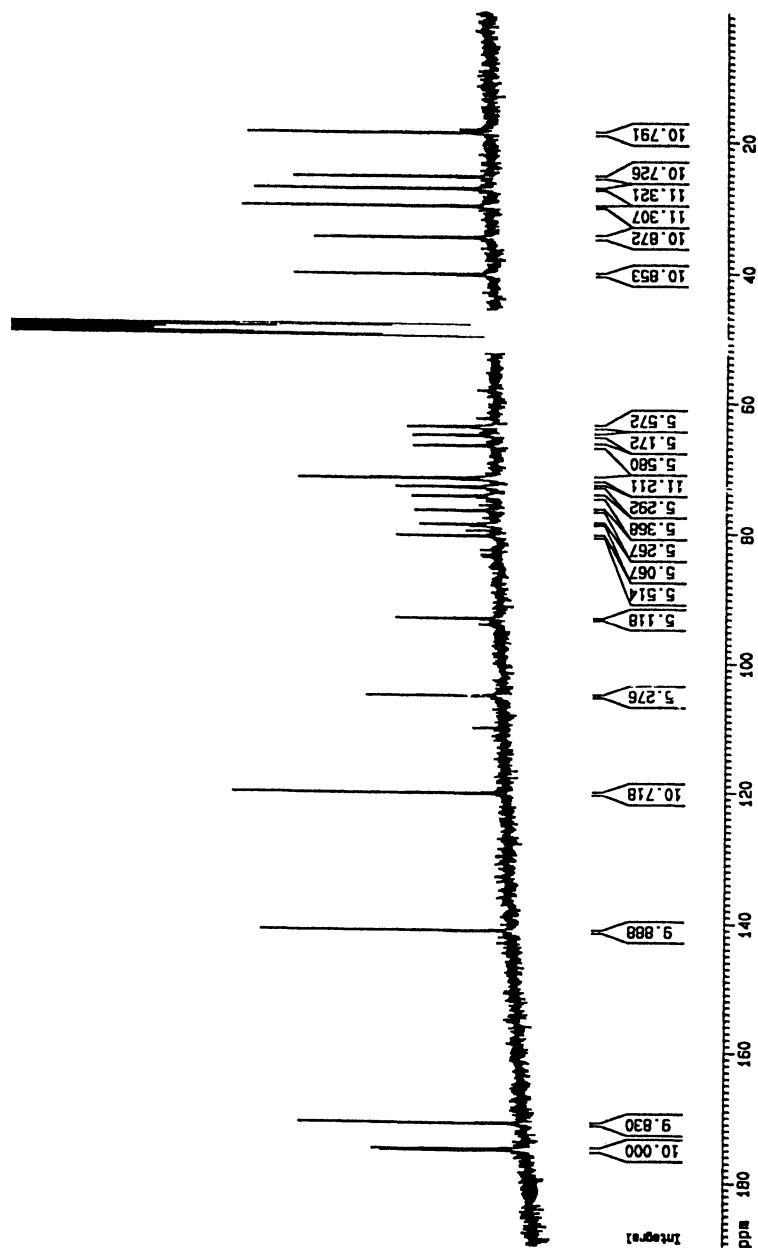


Figure 3. Degree of substitution of DMACS was determined using quantitative  $^{13}\text{C}$ -NMR Spectroscopy. All peaks from DMACS were integrated (18.27, 25.43, 27.25, 29.88, 34.58, 40.30, 63.73, 65.05, 66.46, 71.65, 72.92, 74.36, 76.54, 78.67, 80.42, 92.98, 105.16, 120.23, 141.19, 170.98, 175.00 ppm) and sucrose peaks were found at 63.73, 65.05, 66.64, 71.65, 72.92, 74.36, 76.54, 78.67, 80.42, 92.98, 105.16 ppm. The sucrose peak at 71.65 resulted from the overlap of two carbons (C4 and C-5).

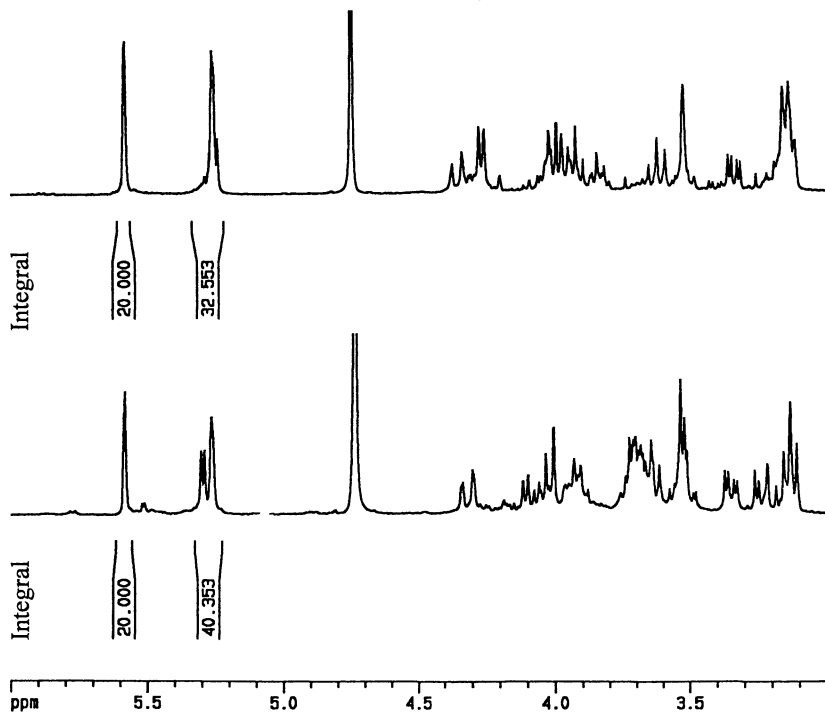


Figure 4.  $^1\text{H-NMR}$  spectra of MACS and DMACS were recorded in  $\text{CD}_3\text{OD}$ . Integration ratios of proton peak at 5.6 ppm (one of  $=\text{CH}_2$  protons) to proton peaks at 5.3 ppm (an anomeric proton peak of sucrose and the other  $=\text{CH}_2$  proton) were 2/3 (A) and 1/2 (B) for DMACS and MACS, respectively.

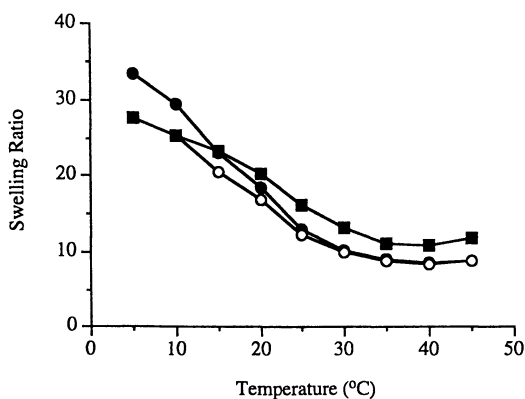


Figure 5. Thermosensitive volume change of sucrogels made of MACS and PPGM. The gels were cross linked with DMACS. The molar ratios of MACS:PPGM were 2:4 (●), 2:3 (○), and 2:2 (■).  $n=3$ . The error bars are smaller than the size of symbols.

Thermoresponsive hydrogels were also prepared by copolymerization of MACS and PEGEEM in the presence of DMACS. The thermosensitive property of MACS-PEGEEM sucrogels was quite unique in that a linear decrease in volume change was observed in the temperature range of 5°C to 50°C (Fig. 6). On the other hand, hydrogels of PEGEEM showed a thermosensitive property only until the temperature increased to 20°C and no thermosensitive property was observed above 20°C. The linear temperature dependence of the swelling ratio may be more useful than sigmoid temperature dependence.

Another type of thermosensitive sucrogels were synthesized by copolymerization of MLS and PPGM (or PEGEEM) with 10 mole% of DMACS as a crosslinking agent. The molar ratio of MLS:PPGM was either 1:1 or 2:1. Hydrogels made of PPGM only were not temperature sensitive at all and the swelling ratio was quite low (around 5) in the temperature ranging from 5°C to 60°C (Fig. 7). The MLS-PPGM and MLS-PEGEEM sucrogels, however, showed inverse thermosensitive properties in the same temperature range. The MLS-PPGM and MLS-PEGEEM sucrogels showed different thermosensitive profiles. The MLS-PPGM sucrogels had a rather clear volume transition between 15°C and 30°C, while the MLS-PEGEEM sucrogels showed almost linear volume transition between 10°C and 60°C. When the concentration of sucrose monomers in the sucrogels increased from 50 mole% to 67 mole%, the maximum swelling ratio of the gels increased dramatically from 30 to 90. The MLS hydrogel showed the obvious change in swelling ratio while the MACS did not. This difference between the two types of sucrogels may be due to the difference in side chains of monomers. A relatively long linear side chain of MACS (Fig. 2) may entangle each other as polymerization continued and prevented swelling of sucrogels regardless of increase in the amount of sucrose monomer. On the other hand, a bulky compact side group of MLS could avoid chain entanglement and formed less crosslinked gels. However, the overall thermosensitive profile did not change with the increase in the amount of sucrose monomer as shown in Fig. 7.

**Thermoreversible Properties of Sucrogels.** Thermoreversible swelling and shrinking of sucrogels were investigated by repetitive temperature changes. When fully swollen sucrogels at 4°C were placed into water at 60°C, sucrogels underwent volume decrease quite fast (Fig. 8). Shrinking of sucrogels at 60°C was much faster than swelling at 5°C. Sucrogels made of different sucrose monomers and different hydrophobic monomers showed the same behavior. In general, the shrinkage to an equilibrium at 60°C required only 2–6 h, while equilibrium swelling at 5°C took 2–3 days. The slow swelling compared to shrinking of hydrogels is observed for almost all hydrogels. This is probably due to the fact that swelling requires relaxation of entangled polymer chains. Of the three sucrose monomers examined, the MAUS-PEGEEM sucrogels showed this lowest swelling ratio under the same condition. The may be due to more chain entanglement by longer side chain and more hydrophobicity of MAUS than other sucrose monomers.

Studies on the swelling kinetics and the thermoreversible properties showed that the most important parameter controlling the thermosensitivity was the type of sucrose monomers. It appears that the thermosensitive properties of sucrogels result from combination of hydrophobic side chains of comonomers and hydrophilic and bulky sucrose moiety of sucrose monomers. The thermosensitivity of these sucrogels can be controlled by adjusting various factors such as length and the bulkiness of side chains of the polymer backbone. Thus, various amino acids can be used in the preparation of sucrose monomers and these will provide sucrogels with different thermosensitive properties.

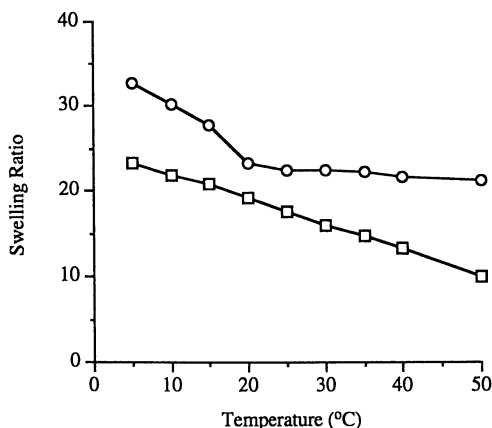


Figure 6. Thermosensitive changes in volume of hydrogels made of PEGEEM only (O) and MACS-PEGEEM copolymers (□). The molar ratio of MACS-PEGEEM was 1:1 and the sucrogels were formed using DMACS as a crosslinking agent.  $n=3$ . The error bars are smaller than the size of symbols.

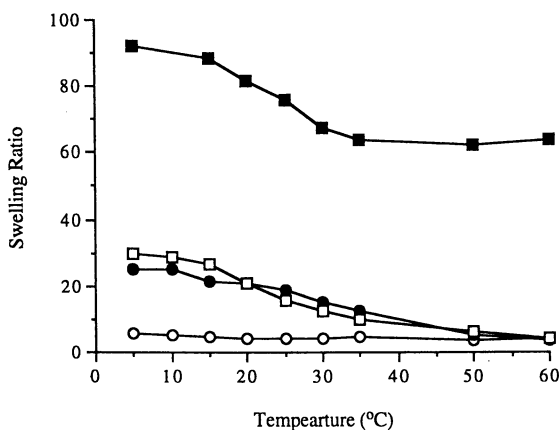


Figure 7. Thermosensitive changes in volume of hydrogels made of PPGM only (O), MLS-PPGM (□ and ■), and MLS-PEGEEM (●) copolymers. The molar ratios of MLS-PPGM were 1:1 (□) and 2:1 (■) and that of MLS-PEGEEM was 1:1. The sucrogels were formed using DMACS as a crosslinking agent.  $n=3$ . The error bars are smaller than the size of symbols.

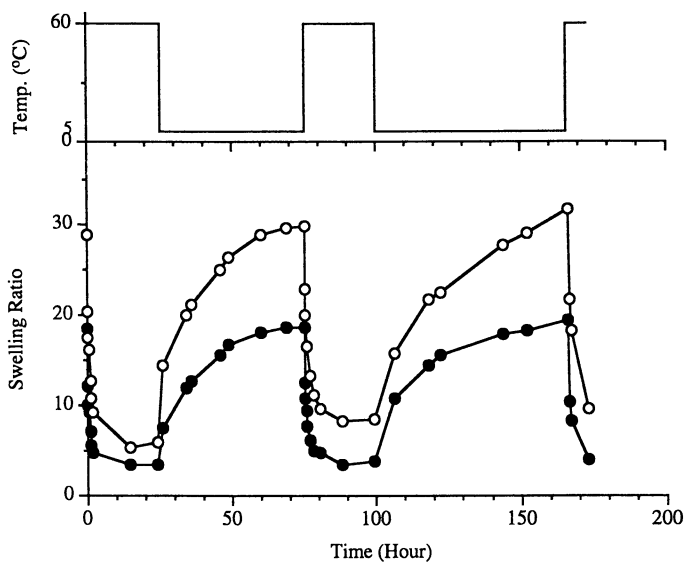


Figure 8. Temperature-dependent swelling and shrinking of sucrogels. Sucrogels were made of MACS-PPGM copolymer with the molar ratio of 2:3 and the concentration of DMAC was either 0.5 mole% (O) or 5.0 mole% (●). DMACS was used as a crosslinking agent.

**Degradation of Thermoreversible Hydrogels.** Degradation of MACS-PPGM sucrogels in acidic (pH 2) and basic (pH 12) solutions was examined. Sucrogels degraded much faster in the basic condition than in the acidic condition. Sucrogels degraded completely within 2 h in a pH 12 solution, while it took about 20 days for 80% degradation in a pH 2 solution (Fig. 9). The difference in degradation rates is most likely due to the intrinsic labile property of ester linkage by base and subsequent formation of anions. The electrostatic repulsion by the formed anions caused the swelling of the partially degraded hydrogel, which in turn made the base-catalyzed hydrolysis easier.

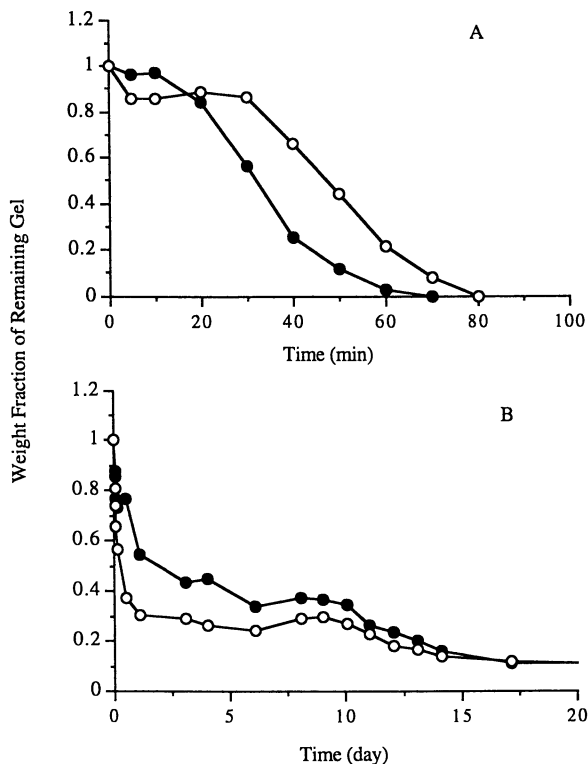


Figure 9. Degradation of sucrogel in basic solution (pH 12.0) (A) and in acidic solution (pH 2.0) (B). The sucrogels were made of MACS-PPGM (●) and MLS-PPGM (○) copolymers. The molar ratio of monomers was 1:1 and the sucrogels were formed using DMACS as crosslinking agent.

## Conclusion

Four sucrose monomers were synthesized by regioselective modification of sucrose. These sucrose monomers were copolymerized with hydrophobic monomers to produce inverse thermoreversible sucrogels. Thermoreversible sucrogels exhibited reversible volume changes as the temperature was varied, and the thermoreversible process was reproducible. The thermosensitive sucrogels were degraded in both acidic and basic conditions. These degradable, thermoreversible sucrogels are expected to find various applications in diverse fields including controlled drug delivery and biotechnology.

## Acknowledgments

This study was supported by the Sugar Association, Inc.

## References

1. Kataoka, K.; Koyo, H.; Tsuruta, T. *Macromolecules*, **1995**, 28: 3336-3341.
2. Allcock, H.R.; Ambrosio, A.M.A. *Biomaterials*, **1996**, 17: 2295-2302.
3. Yoshida, M.; Asano, M.; Kumakura, M. *Eur. Polym. J.*, **1989**, 25: 1197-1202.
4. Hoffman, A.S.; Afrassiabi, A.; Dong, L.C. *J. Controlled Release*, **1986**, 4: 213-222.
5. Shiga, T.; Hirose, Y.; Okada, A.; Kurauchi, T. *J. Appl. Polym. Sci.*, **1992**, 44: 249-253.
6. Ma, J.T.; Liu, L.R.; Yang, X.J.; De Yao, K. *J. Appl. Polym. Sci.*, **1995**, 56: 73-77.
7. Takahashi, F.; Sakai, Y.; Mitutani, Y. *J. Ferment. Bioeng.*, **1997**, 83: 152-156.
8. Lee, S.J.; Park, K. *J. Mol. Rec.*, **1996**, 9: 549-557.
9. Obaidat, A.A.; Park, K. *Biomaterials*, **1997**, 18: 801-806.
10. Yoshida, R.; Sakai, K.; Okano, T.; Sakurai, Y. *Adv. Drug Deliv. Rev.*, **1993**, 11: 85-108.
11. Park, C.-H.; Orozco-Avila, I. *Biotechnol. Progress*, **1992**, 8: 521-526.
12. Kulkarni, R.K.; Morawetz, H. *J. Polym. Sci.*, **1961**, 54: 491-503.
13. Kaczmar, B.U.; Traser, S. *Makromol. Chem.*, **1976**, 177: 1981-1989.
14. Yeoh, K.W.; Chew, C.H.; Gan, L.M.; Koh, L.L. *J. Macromol. Sci.-Chem.*, **1989**, A26: 663-680.
15. Abouhilale, S.; Greiner, J.; Riess, J.G. *Carbohydr. Res.*, **1991**, 212: 55-64.
16. Jansson, P.-E.; Kenne, L.; Schweda, E. *J. Chem. Soc. Perkin Trans.*, **1987**, 1: 377-383.



## Chapter 9

# Investigations on Cellulose-Carbanilates and Cellulose-Carbanilate-Acetates in Dilute Solutions

Kati Schmidt, Frank-Immo Hildebrandt, and Peter Zugenmaier

Institute of Physical Chemistry, Clausthal University of Technology, D-38678  
Clausthal-Zellerfeld, Germany

Two series of cellulose derivatives have been produced by a homogeneous reaction in N,N-dimethylacetamide/lithiumchloride (DMAc/LiCl) using cellulose with two different degrees of polymerization (DP) as starting materials. The first series was obtained by a carbanilation leading to cellulose-carbanilates with varying degrees of substitution (DS). The second series was derived by a peracetylation of the not fully carbanilated derivatives of the first series resulting in corresponding cellulose-carbanilate-acetates with overall DS(ov) of 3. Their dilute solution behavior has been studied by combined static and dynamic light scattering as well as by viscosimetry in two different solvents, N,N-dimethylformamide (DMF) and 2-methoxyethylacetate (EMMAc). Two remarkable results were obtained: (i) All derivatives including carbanilates with free OH-groups were dissolved on a molecular level. (ii) The investigations in EMMAc suggest the formation of a duplex molecular structure in contrast to a single molecular random coil in DMF.

Cellulosic materials differ in many ways from synthetic polymers in their solid state properties and behavior as well as in solution. The aim of our ongoing research in this field is to investigate the solution properties of different cellulose derivative/solvent-systems by variation of substituents, degree of substitution and solvent. We characterized the systems with molecular parameters such as the radius of gyration ( $\langle s^2 \rangle_z$ ), hydrodynamic radius ( $R_h$ ), molecular weight ( $M_w$ ), diffusion coefficient ( $D_z$ ), intrinsic viscosity ( $[\eta]$ ) and with structure-sensitive parameters such as the  $\rho$ -parameter ( $\rho \equiv \langle s^2 \rangle_z / R_h$ ) and the second virial coefficient ( $A_2$ ). An interpretation of these system properties leads to models on the molecular level, including single-chain characteristics

such as flexibility, helicity, stiffness of the molecules or the shape as a worm-like chain as well as supramolecular properties, e.g., aggregation or association of the macromolecules in solution.

In this paper we present the results of investigations on cellulose-carbanilates and cellulose-carbanilate-acetates in dilute solutions.

## Experimental

**Instrumentation.** Light scattering and viscosimetric measurements were carried out to determine the solution properties at a temperature of 25 °C. An ALV-light scattering instrument with an ALV-5000-correlator and a laser with a wave length of  $\lambda = 532$  nm, Coherent Compass DPSS-532/100mW, was used for combined static and dynamic light scattering investigations. Details of the method and this instrument are described elsewhere (1-3). Refractive index increments ( $dn/dc$ ) were obtained with a Brice-Phoenix differential refractometer, BP-2000-V. A low-shear-rotation-viscosimeter, Contraves LS 30, served for the viscosimetric measurements.

**Synthesis.** The cellulose-carbanilates were synthesized by a well established method in the solvent system DMAc/LiCl under homogeneous conditions (4-6). Two different cellulose materials (microcrystalline cellulose abbreviated with (A), Fluka, Avicel DP  $\approx$  200 and spruce sulfite pulp abbreviated with (H), Fluka, DP  $\approx$  600) with various DP were derivatized with phenylisocyanate as represented in Scheme 1 applying the following procedures:

*A homogeneous cellulose solution was prepared by suspending dry cellulose (6 wt % of cellulose (A); 1.5 wt % of cellulose (H)) in dry DMAc (85 wt % for cellulose (A); 89.5 wt % for cellulose (H)) and stirred for 1/2 h at 150 °C. After cooling to 100 °C dry LiCl (9 wt %) was added, the suspension was cooled to room temperature and stirred for 12 h resulting in a clear, yellow-like, viscous solution.*

*Derivatization was achieved by slowly adding pyridine (1.3 molar excess of the amount of phenylisocyanate) to the solution stirred, followed by the dropwise addition of phenylisocyanate dissolved in DMAc. The amount of phenylisocyanate was varied between 0.4 and 1.0 mol reagent per OH-group. The reaction solution was stirred for 4 h at room temperature, for 4 h at 80 °C and 12 hours at room temperature.*

*The product was isolated by precipitation of the reaction solution into a mixture of methanol and water (10 fold volume of the reaction solution). The precipitate was washed repeatedly with water and methanol and purified by reprecipitation and dried under vacuum.*

The DS, determined by elemental analysis, was controlled by the stoichiometric ratios of phenylisocyanate to the available hydroxyl-groups as represented in Figure 1. Obviously the derivatization of the cellulose with lower molecular weight (A) led to higher degrees of substitution with the use of the same amount of reagent than the one with the higher molecular weight (H).

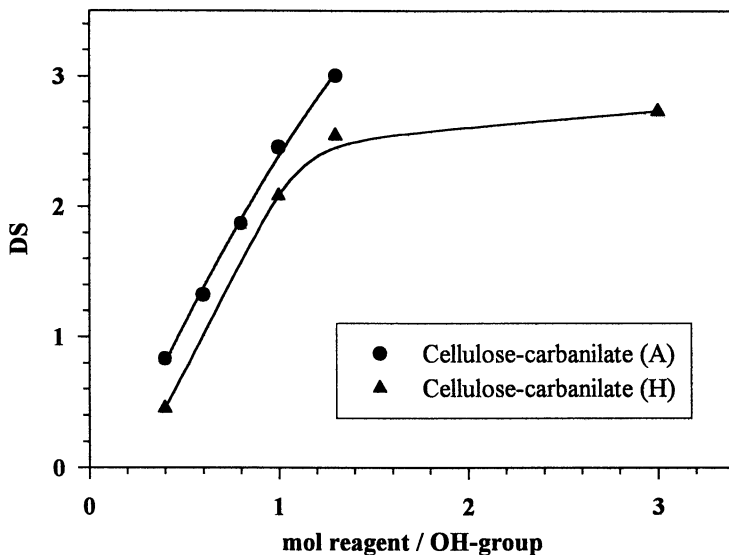


Figure 1. Degree of substitution as function of the amount of reagent in mol per OH-group of cellulose-carbanilate (A) and (H).

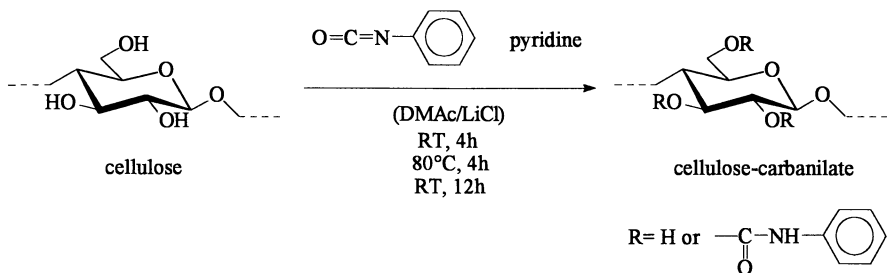
For reason of comparison 5 g of each carbanilate was peracetylated to obtain derivatives without free OH-groups by the following procedure:

*5-10 wt % of partially carbanilated cellulosic materials were dissolved or suspended (depending on DS) in pyridine. Afterwards a 10 fold excess of recently distilled acetic anhydride (in respect to the number of free OH-groups) was added into the solution stirred in drops. Stirring was continued for 4 h at 50 °C and for 12 h at room temperature. The product was isolated and purified in the same way as the carbanilates.*

All the derivatives that we made can be divided into two series (i) and (ii) with two degrees of polymerization in each series. The DS(carb) varies in each group ranging from 0.45 to 2.73:

- (i) carbanilates with free OH-groups
- (ii) carbanilates-acetates without free OH-groups and an overall DS(ov) of 3

The characterization was carried out by infrared-spectroscopy. It is commonly accepted that cellulose is dissolved on a molecular basis in DMAc/LiCl. Homogeneous reaction conditions and a similar accessibility of all OH-groups are provided (7,8). Therefore, a uniform distribution of substituents along the cellulose chain should be achieved without the appearance of blockwise substituted segments of the anhydroglucose unit (AGU).



Scheme 1. Synthesis of cellulose-carbanilates.

In principal three different types of solvents have been tested with respect to the intended investigations and an appropriate solvent/precipitant-system for the fractionation into different molecular weights.

- polar, protic: water, methanol (no solubilities were found)
- weak polar: dioxane, tetrahydrofuran (THF)
- polar, aprotic: dimethylacetamide (DMAc), dimethylformamide (DMF), dimethylsulfoxide (DMSO), acetone, chloroform ( $\text{CHCl}_3$ ).

The solubility of the derivatives strongly depends on DP, DS and the ratio of the two substituents. In general the solubility increases with increasing DS, and the carbanilate-acetates exhibit a better solubility than the corresponding carbanilates. The polar, aprotic solvents DMF, DMSO, DMAc represent good solvents for nearly all degrees of substitution. Based on these results the investigations were carried out in DMF for the purpose of a better comparison considering the solubility of nearly all derivatives, and in the solvent 2-methoxyethylacetate (EMMAc), in which many highly concentrated cellulose carbanilates show lyotropic liquid crystalline phases (9,10).

Different molecular weights were obtained by fractional precipitation using acetone, THF or DMF as solvent depending on DS and water as precipitant. Again each fraction was purified by reprecipitation. The fractionation resulted in four to as many as seven different molecular weights for a single derivative. The  $M_w$  determined in DMF of the cellulose-carbanilates (A) ranges from 15000 to 138000 g/mol, of cellulose-carbanilate-acetates (A) from 40000 to 280000 g/mol, of cellulose-carbanilates (H) from 110000 to 674000 g/mol and of cellulose-carbanilate-acetates from 64000 to 1800000 g/mol. The polydispersity  $M_w/M_n$  of the (A) derivatives varies from 1.3 to 2.2, and that of the (H) derivatives from 1.8 to 2.9, as determined by GPC-analysis. The polydispersity decreases with decreasing molecular weight.

## Results and Discussion

Some selected systems of different fractions of molecular weights were investigated in DMF and in EMMAc. Distinct differences were expected between partially and fully substituted derivatives. The solution properties of trisubstituted cellulose derivatives

such as -tricarbanilate or -trinitrate are described behaving like synthetic, linear semi-flexible polymers (11). In contrast aggregation phenomena occur with partially substituted derivatives (11-14). These general findings were tested with the described systems.

The intrinsic viscosity  $[\eta]$  was determined by means of viscosimetric measurements applying the Huggins equation:

$$\eta_{\text{red}} = [\eta] + [\eta]^2 k_H c \quad (1)$$

with  $\eta_{\text{red}} = \left( \frac{\eta_0}{\eta_S} - 1 \right) c^{-1}$  the reduced viscosity,

$k_H$ : Huggins-constant,  $c$ : polymer concentration,  
 $\eta_0$ : zero shear rate viscosity,  $\eta_S$ : viscosity of the solvent.

$M_w$ ,  $\langle s \rangle_z$ ,  $A_2$  and  $D_z$  may be obtained by combined static and dynamic light scattering while  $R_h$  can be calculated with the Stokes-Einstein law:

$$D_z = \frac{k T}{6\pi \eta_S R_h} \quad (2)$$

with  $k$ : Boltzmann constant,  $T$ : temperature.

The concentrations of the solutions were chosen below the critical overlap concentration which is given by  $c^* = 1/[\eta]$ .

Figures 2 and 3 show static and dynamic Zimm plots of cellulose-carbanilate (H) with  $DS(\text{carb}) = 2.54$  in EMMac und cellulose-carbanilate-acetate (H) with  $DS(\text{carb}) = 2.54$  ( $DS(\text{ov}) = 3$ ) in DMF as examples to prove the excellent shape of the curves and serving for the evaluation of the light scattering measurements. Surprisingly, both the trisubstituted derivatives and the systems containing some free OH-groups showed:

- a linear dependence of the scattering intensity on  $q^2$  ( $q$ : scattering vector) and concentration  $c$ ,
- excellent parallelity of the scattering curves and
- positive values of the second osmotic virial coefficient.

These observations suggest that the compounds are dissolved on a molecular level. These results are supported by the size of the molecular weight and the radius of gyration by an evaluation of the Zimm plots. However, the molecular weights and radii of gyration appear up to double in values for solutions of EMMac as compared to those of DMF.

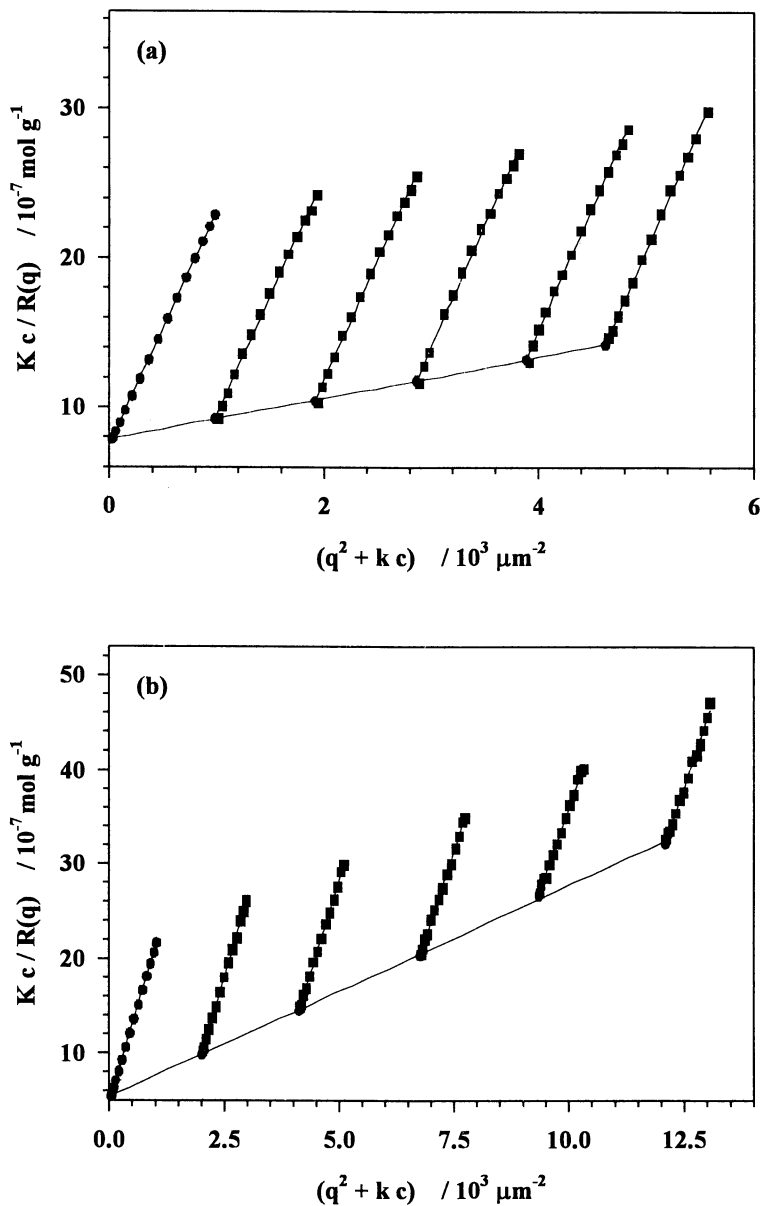


Figure 2. Static Zimm-plots of (a) cellulose-carbanilate (H),  $DS(\text{carb}) = 2.54$ , in EMMac (1. fraction), (b) cellulose-carbanilate-acetate (H),  $DS(\text{carb}) = 2.54$ , in DMF (1. fraction).

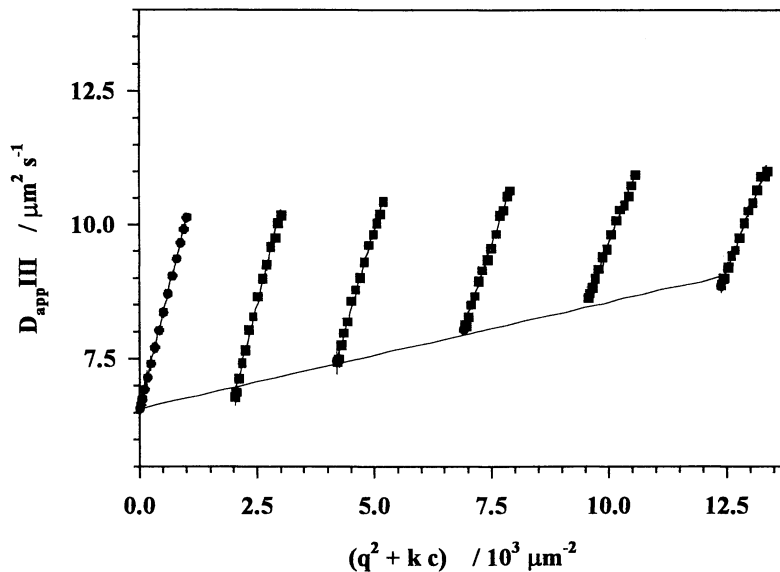


Figure 3. Dynamic Zimm-plot of cellulose-carbanilate-acetate (H), DS(carb) = 2.54, in DMF (1. fraction).

The structures of the molecules in solutions were determined by means of the particle scattering factor  $P(q)$ , but this method is limited to derivatives with a sufficient size of the radius of gyration. Details are given in (15,16), where measurements are compared with theoretical values calculated for different shapes of structures, like spheres, thin rods and coils. The Holtzer plots for cellulose-carbanilate-acetate (H) with DS(carb) = 2.73 in DMF and EMMAc and cellulose-carbanilate (H) with DS(carb) = 2.54 in EMMAc are given in Figure 4 and 5 as examples. All systems investigated reveal these results:

- the experimental data are in excellent agreement with the theoretical values of polydisperse coils,
- no principle differences are detected between fully and partially substituted derivatives and between the solvents DMF and EMMAc.

The molecular weight dependence of  $\langle s \rangle_z$ ,  $R_h$ ,  $D_z$  and  $[\eta]$  supplies further information on the structure of the molecules in solution. Mostly exponential relations are found, obeying the form (17):

$$Y = K M^{aY} \quad (3)$$

with Y:  $\langle s \rangle_z$ ,  $R_h$ ,  $D_z$ ,  $[\eta]$ , M: molecular weight.

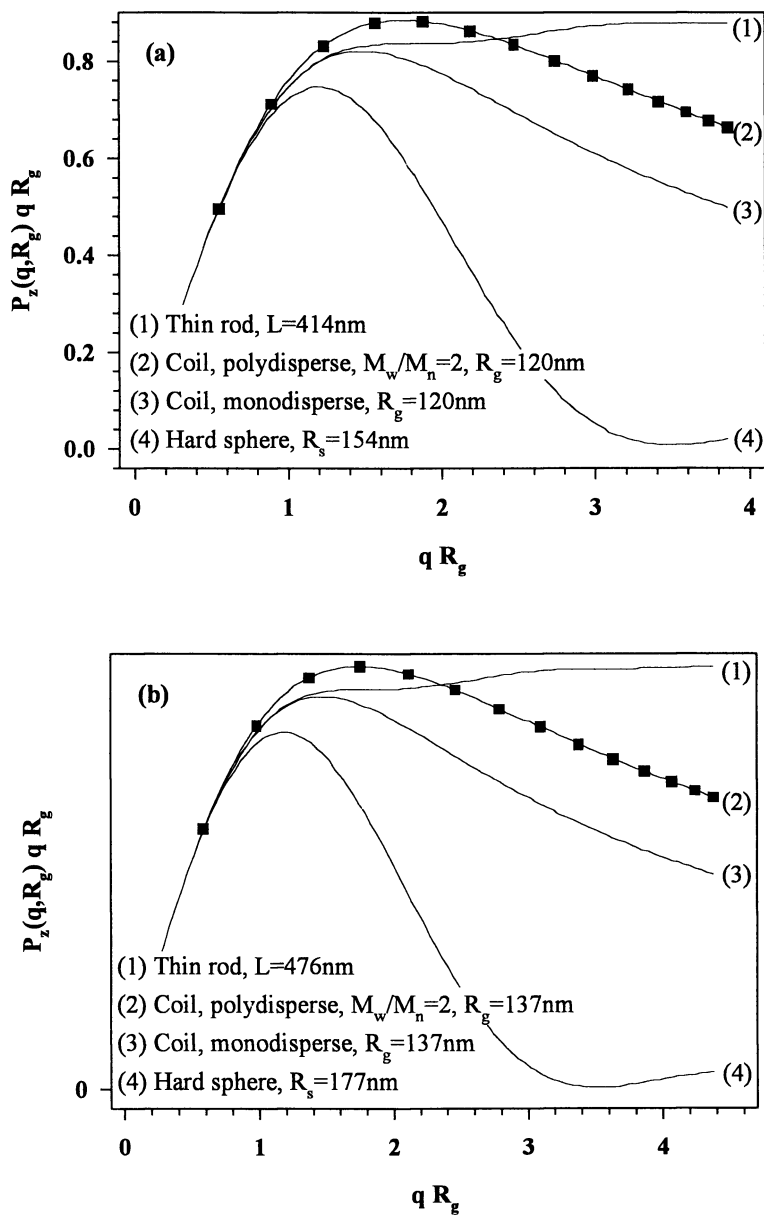


Figure 4. Holtzer-plots of cellulose-carbanilate-acetate (H),  $DS(\text{carb}) = 2.73$ , in (a) DMF and in (b) EMMac (1. fraction).



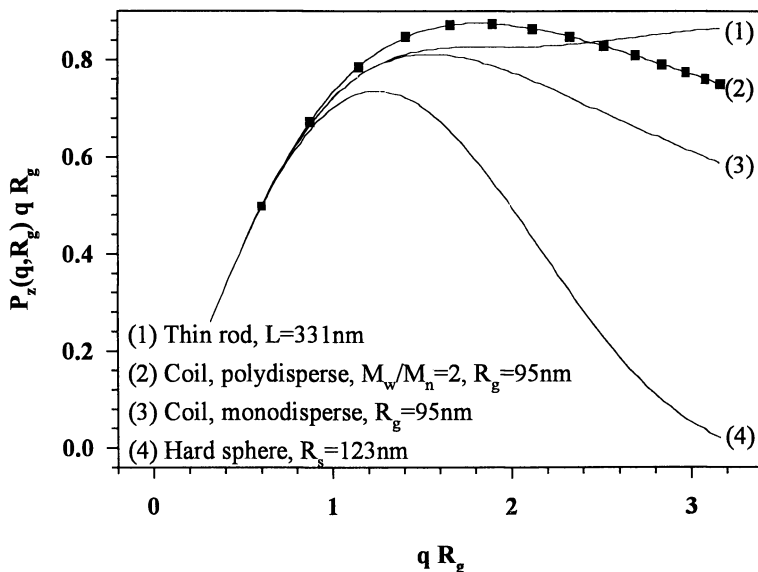


Figure 5. Holtzer-plot of cellulose-carbanilate (H),  $DS(\text{carb}) = 2.54$ , in EMMAc (1. fraction).

As an example for the systems investigated selected plots for cellulose-carbanilate-acetate (H) with  $DS(\text{carb}) = 2.73$  in DMF are shown for an evaluation of the exponents in Figure 6 and 7. The plots are basing on data given in Table I. The slopes in the double logarithmic plots represent the exponents and are summarized for all systems in Table II. The theoretically expected values are listed for different shapes of polymer structures in Table III.

Comparison of experimental and theoretical data leads to similar results for all systems investigated. The structure of flexible, linear chains and also of semi-flexible chains may be evaluated through the exponents given in Eq. (3). Further evidence on the structure in solution can be obtained by comparing theoretical values of the  $\rho$ -parameter given in Table IV and the experimental data.

Figure 8 shows the molecular weight dependence of the  $\rho$ -parameter of cellulose-carbanilate-acetate (H) with  $DS(\text{carb}) = 2.73$  in EMMAc and in DMF.

The  $\rho$ -parameters of all systems in DMF indicate linear random coils ( $\rho = 1.5$  to  $2.05$ ) and the values are almost independent of molecular weight. The systems in EMMAc exhibit slightly increasing  $\rho$ -parameters with decreasing molecular weight. In some cases, at low molecular weights, the  $\rho$ -parameters determined indicate stiff chains ( $\rho > 2$ ) as molecular shape. This evidence suggests increasing chain stiffness with decreasing molecular weight.

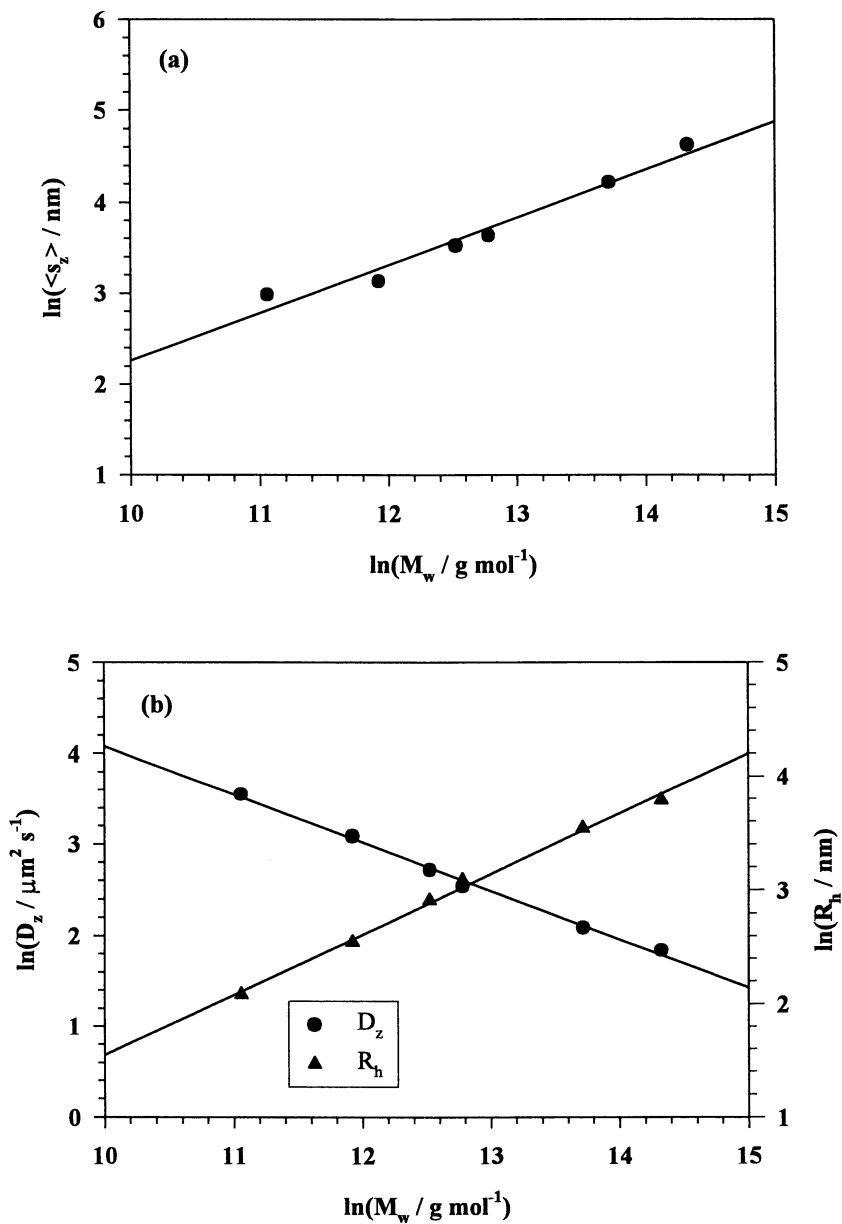


Figure 6. Molecular weight dependence of (a)  $\langle s_z \rangle$  and (b)  $D_z$ ,  $R_h$  of cellulose-carbanilate-acetate (H), DS(carb) = 2.73, in DMF.

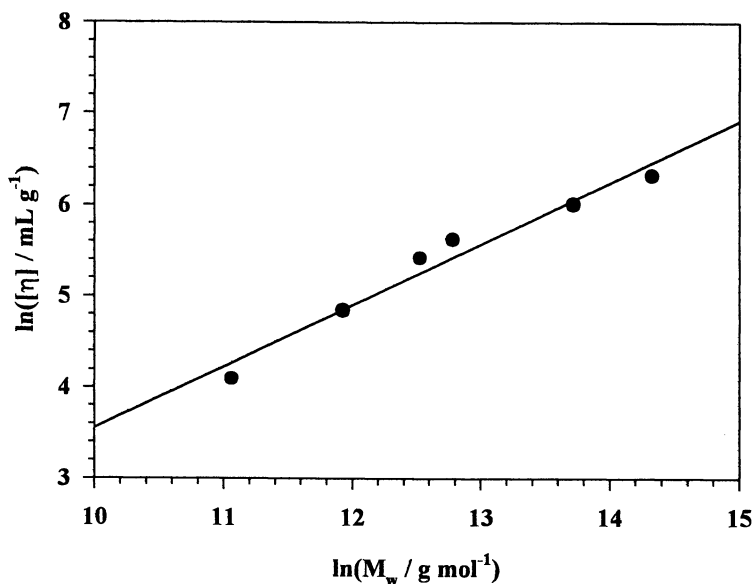


Figure 7. Molecular weight dependence of intrinsic viscosity  $[\eta]$  of cellulose-carbanilate-acetate (H),  $DS(\text{carb}) = 2.73$ , in DMF.

**Table I.  $M_w$ ,  $R_g$ ,  $R_h$ ,  $D_z$ ,  $A_2$ , and  $[\eta]$  of the Molecular Weight Fractions of Cellulose-carbanilate-acetate (H) with  $DS(\text{carb}) = 2.73$  in DMF and EMMAc.**

| <i>Cellulose-carbanilate-acetate in DMF [DS(ov) = 3]</i>   |                             |            |            |                                       |   |                               |
|--|-----------------------------|------------|------------|---------------------------------------|---|-------------------------------|
| Fraction No.   | $M_w$ / $\text{g mol}^{-1}$ | $R_g$ / nm | $R_h$ / nm | $D_z$ / $\mu\text{m}^2 \text{s}^{-1}$ | $A_2$ / $\text{mol dm}^3 \text{g}^{-2}$ | $[\eta]$ / $\text{mL g}^{-1}$ |
| 1  | 1669000                     | 101.5      | 44.1       | 6.27                                  | $4.72 * 10^{-7}$                        | 556                           |
| 2  | 910000                      | 67.7       | 34.4       | 8.05                                  | $5.14 * 10^{-7}$                        | 406                           |
| 3  | 356000                      | 37.7       | 21.9       | 12.65                                 | $5.14 * 10^{-7}$                        | 276                           |
| 4  | 276000                      | 33.7       | 18.3       | 15.09                                 | $5.68 * 10^{-7}$                        | 225                           |
| 5  | 151000                      | 22.8       | 12.7       | 21.77                                 | $5.40 * 10^{-7}$                        | 126                           |
| 6  | 64000                       | 19.7       | 8.0        | 34.66                                 | $6.13 * 10^{-7}$                        | 60                            |
| <i>Cellulose-carbanilate-acetate in EMMAc [DS(ov) = 3]</i> |                             |            |            |                                       |   |                               |
| 1  | 2323000                     | 134.8      | 90.6       | 2.34                                  | $3.21 * 10^{-8}$                        | 360                           |
| 2  | 947000                      | 67.8       | 37.3       | 5.69                                  | $3.02 * 10^{-7}$                        | 435                           |
| 3  | 509000                      | 46.2       | 25.8       | 8.22                                  | $3.89 * 10^{-7}$                        | 284                           |
| 4  | 310000                      | 36.3       | 19.1       | 11.09                                 | $4.44 * 10^{-7}$                        | 173                           |
| 5  | 194000                      | 30.3       | 14.6       | 14.48                                 | $3.30 * 10^{-7}$                        | 114                           |
| 6  | 89000                       | 22.2       | 8.6        | 24.76                                 | $3.85 * 10^{-7}$                        | 45                            |

**Table II. Exponents of the Exponential Relations between the Molecular Parameters  $R_g$ ,  $R_h$ ,  $D_z$ ,  $[\eta]$  and the Molecular Weight.**

| <i>Cellulose-carbanilate-acetates</i> [ $DS(ov) = 3$ ] |                 |                |          |          |          |              |
|--|-----------------|----------------|----------|----------|----------|--------------|
| <i>Cellulose</i>                                       | <i>DS(carb)</i> | <i>Solvent</i> | $a_{Rg}$ | $a_{Rh}$ | $a_{Dz}$ | $a_{[\eta]}$ |
| A  | 1.32            | DMF            | 0.87     | 0.91     | -0.91    | 0.86         |
| A  | 1.87            | DMF            | 0.58     | 0.56     | -0.56    | 1.03         |
| A  | 2.45            | DMF            | 0.98     | 0.55     | -0.55    | 0.65         |
| A  | 2.45            | EMMAc          | 0.64     | 0.62     | -0.62    | 0.92         |
| H  | 0.45            | DMF            | 0.53     | 0.73     | -0.73    | 0.72         |
| H  | 2.08            | DMF            | 0.59     | 0.57     | -0.57    | 0.63         |
| H  | 2.54            | DMF            | 0.56     | 0.56     | -0.56    | 0.66         |
| H  | 2.73            | DMF            | 0.53     | 0.53     | -0.53    | 0.67         |
| H  | 0.45            | EMMAc          | 0.50     | 0.74     | -0.74    | 0.52         |
| H  | 2.73            | EMMAc          | 0.55     | 0.70     | -0.70    | 0.67         |
| <i>Cellulose-carbanilates</i>                          |                 |                |          |          |          |              |
| A  | 2.45            | DMF            | 0.75     | 0.72     | -0.72    | 0.92         |
| A  | 2.45            | EMMAc          | 0.69     | 0.61     | -0.61    | 0.65         |
| H  | 2.54            | DMF            | 0.70     | 0.72     | -0.72    | 1.18         |
| H  | 2.54            | EMMAc          | 0.63     | 0.76     | -0.76    | 1.30         |

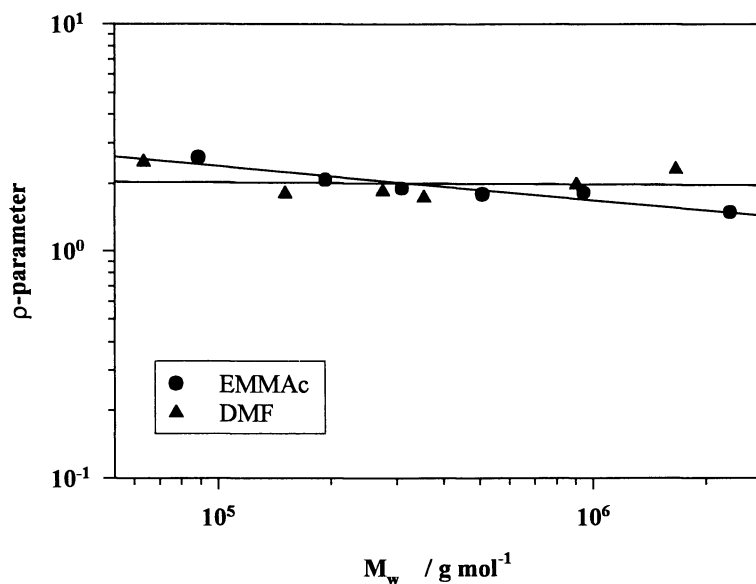


Figure 8.  $\rho$ -parameter as a function of molecular weight for cellulose-carbanilate-acetate (H),  $DS(carb) = 2.73$ , in EMMAc and in DMF.

**Table III. Predicted Exponents for Molar Weight Dependencies of Radius of Gyration  $a_{Rg}$ , Diffusion Coefficient  $a_{Dz}$ , and Intrinsic Viscosity  $a_{[\eta]}$  (9).**

| <i>Macromolecular architectures</i> |             |               |              |
|-------------------------------------|-------------|---------------|--------------|
| <i>architectures</i>                | $a_{Rg}$    | $a_{Dz}$      | $a_{[\eta]}$ |
| hard spheres                        | 0.33        | -0.33         | 0.00         |
| thin rods                           | 1.00        | 1.00          | 1.80 – 2.00  |
| flexible, linear chains             | 0.50 – 0.60 | -0.50 – -0.59 | 0.50 – 0.80  |
| semi-flexible chains <sup>a</sup>   | 0.50 – 1.00 | -0.60 – -1.00 | 0.80 – 1.60  |

<sup>a</sup> experimentally determined

**Table IV. Values of the  $\rho$ -Parameter for Different Polymer Architectures (11).**

| <i>architecture</i>           | $\rho$ -parameter |
|-------------------------------|-------------------|
| stiff chains                  | 2.20              |
| linear, random coils          | 1.50 – 2.05       |
| star branched molecules       | 1.00              |
| hard spheres                  | 0.778             |
| microgel, globular structures | 0.30 – 0.50       |

The chain stiffness may be expressed by means of different parameters, e.g., the characteristic ratio  $C_\infty$ , Kuhn-length  $l_k$  and persistence length  $l_q$ . In this work  $l_q$ ,  $l_k$ , and  $C_\infty$  were determined from static light scattering data applying the Kratky-Porod-model of worm-like chains. The unperturbed radius of gyration  $\langle s^2 \rangle_0$  of a monodisperse worm-like chain is given according to Benoît and Doty (18) by:

$$\langle s^2 \rangle_0 = \frac{L l_k}{6} - \frac{l_k^2}{4} + \frac{l_k^3}{4L} - \frac{l_k^4}{8L^2} \left( 1 - e^{-\frac{L}{l_k}} \right) \quad (4)$$

with: L: contour length of a chain.

According to Murakami et al. (19) Eq. (4) can be simplified considering polydispersity:

$$\left( \frac{M_w}{\langle s^2 \rangle_w} \right)^{1/2} = \left( \frac{3 M_L}{l_q} \right)^{1/2} \left[ 1 + \left( \frac{3 l_q M_L}{2 M_w} \right) \right] \quad (5)$$

with  $M_L = m_0 / l_0$ : linear mass density,  
 $m_0$ : molecular weight, and  
 $l_0$ : length of the repeating unit ( $l_0 = 0.515$  nm, (20-22)).

Further assuming a Schulz-Zimm distribution, the weight average of the radius of gyration can be derived from the number average of the various molecular weight fractions and polydispersity:

$$\langle s^2 \rangle_w = \langle s^2 \rangle_z \left( \frac{U+1}{U+2} \right) \quad \text{with:} \quad U = \frac{1}{\langle M_w \rangle / \langle M_n \rangle - 1} \quad (6)$$

$C_\infty$  and  $l_k$  are then given by:

$$l_k = 2 l_q \quad \text{and} \quad C_\infty = l_k / l_0 \quad (7)$$

The calculated values of selected systems are summarized in Table V leading to the following results:

- The systems in EMMac show larger values of  $l_q$ ,  $l_k$ , and  $C_\infty$  as compared to the derivatives in DMF.
- The systems containing free OH-groups exhibit lower values of  $l_q$ ,  $l_k$ , and  $C_\infty$  than the corresponding trisubstituted derivatives.
- The mixed derivatives show slightly increasing  $l_q$ ,  $l_k$ , and  $C_\infty$  with increasing DS(carb) of the carbanilate in DMF.

The solution behavior of cellulose-carbanilates and -carbanilate-acetates in various solvents can be summarized as follows:

- The solubility in different solvents is dependent on the DS, DP and the nature of the substituents. Generally the solubility improves with increasing DS and introduction of acetyl- instead of OH-groups in the given solvent.
- The results of all systems -partially and trisubstituted derivatives- indicate the existence of linear random coils in both DMF and EMMac solutions. However, a duplex structure, i.e. two molecules attached to each other, seems to be present for some of the molecules in EMMac.
- A higher chain stiffness is achieved in EMMac than in DMF for trisubstituted systems as well as for derivatives with free OH-groups.

## Conclusions

Our investigations on dilute solutions of cellulose-carbanilates and -carbanilate-acetates showed similar behavior for all derivatives. This result is unexpected with regard to partially substituted derivatives. In general aggregation phenomena are assumed to occur for partially substituted derivatives. This aggregation behavior of partially substituted derivatives is commonly explained by irregular distribution of side-groups leading to low substituted blocks along the chain which are cooperatively bonded by hydrogen bonds and the solvent is not able to break these bonds.

**Table V. Calculated Persistence Length  $l_q$ , Kuhn-length  $l_k$ , and Characteristic Ratio  $C_\infty$  of Different Derivative/Solvent-Systems.**

| <i>Cellulose-carbanilate-acetates</i> [ $DS(ac) = 3-DS(carb)$ ] |                 |                |          |          |            |
|---|-----------------|----------------|----------|----------|------------|
| <i>Cellulose</i>  | <i>DS(carb)</i> | <i>solvent</i> | $l_q/nm$ | $l_k/nm$ | $C_\infty$ |
| H   | 2.73            | EMMAc          | 11.95    | 23.90    | 46.41      |
|   |                 | DMF            | 10.27    | 20.54    | 39.88      |
| H   | 2.54            | DMF            | 8.48     | 16.96    | 32.93      |
| H   | 2.08            | DMF            | 7.41     | 14.82    | 28.76      |
| H   | 0.45            | EMMAc          | 14.19    | 28.38    | 55.11      |
|   |                 | DMF            | 8.00     | 16.00    | 31.07      |
| A   | 2.45            | EMMAc          | 11.03    | 22.06    | 42.83      |
|   |                 | DMF            | 3.64     | 7.28     | 14.14      |
| <i>Cellulose-carbanilates</i>                                   |                 |                |          |          |            |
| H   | 2.54            | EMMAc          | 8.39     | 16.78    | 32.58      |
|   |                 | DMF            | 5.59     | 11.18    | 21.71      |
| A   | 2.45            | EMMAc          | 6.14     | 12.28    | 23.84      |

An uniform distribution of the substituents along the cellulose chains was achieved by the homogeneous reaction conditions and may explain our results. Our derivatives have no lengthy segments with free OH-groups that can hydrogen bond with other chains, so irreversible, lateral aggregation is prevented.

At the present no reason or explanation can be given for the higher apparent molecular weights in EMMAc solutions. Investigations on analogous cellulose-benzoate(-acetate)-systems are in progress. They should show whether a duplex structure is also formed by these systems. It will also be of interest to learn whether those derivatives are dispersed in dilute solution as individual molecules when the degree of substitution is comparable to the present molecules.

For further investigations the appearance of larger radii of gyration and chain stiffness of the systems in EMMAc as compared to those in DMF is also of great interest. This behavior is found for trisubstituted derivatives as well as for partially substituted ones. It seems that the interaction between solvent and polymer plays a far more important role than is generally accepted not only in the lyotropic liquid crystalline state with EMMAc as solvent (9,10) rather than already in the dilute state.

## Acknowledgment

Financial support of this work by a grant from the Deutsche Forschungsgemeinschaft is gratefully acknowledged.

## References

- Bantle, S.; Schmidt, M.; and Burchard, W. *Macromolecules* **1982**, *15*, 1604.
- Peters, R. *Introduction to the Multiple Tau Correlation Technique*, supplied by ALV Lasertriebwerks GmbH, Langen, Hessen, FRG 1995.

3. Burchard, W. *Macromol. Chem., Macromol. Symp.* **1988**, *18*, 1.
4. McCormick, C. L.; Lichatowich, D. K. *J. Polym. Sci., Polym. Lett. Ed.* **1979**, *17*, 479.
5. McCormick, C. L.; Callais, P. A. *Polymer* **1987**, *28*, 2317.
6. McCormick, C. L.; Shen, T. C. In: *Macromolecular Solutions*, Eds. Seymour, R. B.; Stahl, G. S., Pergamon Press, New York 1982, p 101-107.
7. Morgenstern, B.; Kammer, H.-W. *TRIP* **1996**, *4*, 87.
8. Dawsey, T. R.; McCormick, C. L. *J. Macromol. Sci., Rev. Macromol. Chem. Phys.* **1990**, *C30*, 405.
9. Klohr, E. *Dissertation*, TU Clausthal, D-38678 Clausthal-Zellerfeld 1995.
10. Zugenmaier, P.; Derleth, C. In: *Cellulose Derivatives*, ACS Symp. Ser. 688, Eds. Heinze, T. J.; Glasser, W. G., American Chemical Society, Washington, DC 1998, p 239-252.
11. Burchard, W. *Das Papier* **1994**, *12*, 755.
12. Burchard, W. *TRIP* **1993**, *1*, 192.
13. Schulz, L.; Burchard, W. *Das Papier* **1993**, *47*, 1.
14. Schulz, L.; Burchard, W.; Dönges, R. In: *Cellulose Derivatives*, ACS Symp. Ser. 688, Eds. Heinze, T. J.; Glasser, W. G., American Chemical Society, Washington, DC 1998, p 218-238.
15. Lechner, M. D.; Gehrke, K.; Nordmeier, E. H. *Makromolekulare Chemie*, Birkhäuser Verlag, Basel, Boston, Berlin 1993.
16. Burchard, W. *Macromolecules* **1977**, *10*, 919
17. De Gennes, P. G. *Scaling Concepts in Polymer Physics*, Cornell University Press, Ithaca, NY 1979.
18. Benoît, H.; Doty, P. M. *J. Phys. Chem.* **1953**, *57*, 958.
19. Murakami, H.; Norisuye, T.; Fujita, H. *Macromolecules* **1980**, *13*, 345.
20. Wenzel, M.; Burchard, W.; Schätzel, K. *Polymer* **1986**, *27*, 195.
21. Zugenmaier, P. *J. Appl. Polym. Sci.* **1983**, *37*, 223.
22. Zugenmaier P. In: *Polysaccharide*, Ed. Burchard, W., Springer-Verlag, Heidelberg 1985, p. 260-279.



## Chapter 10

# Molten Inorganic Salt Hydrates as Cellulose Solvents

S. Fischer<sup>1</sup>, H. Leipner<sup>1</sup>, E. Brendler<sup>2</sup>, W. Voigt<sup>1</sup>, and K. Fischer<sup>3</sup>

Departments of<sup>1</sup> Inorganic Chemistry and <sup>2</sup> Analytical Chemistry,  
Technical University of Freiberg, Freiberg D-09596, Germany

<sup>3</sup> Department of Wood and Paper Science, Technical University of Dresden,  
Dresden D-01737, Germany

Molten inorganic salt hydrates can be used to dissolve cellulose. According to the salt concentration molten salt hydrates are arranged between concentrated salt solutions and anhydrous melts. As new cellulose solvents molten  $\text{LiClO}_4 \cdot 3\text{H}_2\text{O}$  and  $\text{LiI} \cdot 2\text{H}_2\text{O}$  were found. Mixtures of  $\text{LiClO}_4 \cdot 3\text{H}_2\text{O}$  with e. g.  $\text{Mg}(\text{ClO}_4)_2$  are also able to swell or dissolve cellulose. The eutectic mixture of  $\text{NaSCN}/\text{KSCN}$  with different amounts of added  $\text{LiSCN} \cdot 2\text{H}_2\text{O}$  constitutes another group of solvents. The crystallite dimensions of the regenerated cellulose II samples vary in dependence on the melt composition. The structural change of the cellulose after regenerating was confirmed by Scanning Electron Microscopy (SEM). To investigate the interactions between cellulose and molten salts solvent state  $^{13}\text{C}$ -NMR experiments were carried out.

Cellulose as a natural polymer is used for a lot of pharmaceutical products and cosmetics, e. g. carboxymethyl celluloses are important ingredients of pharmaceuticals. (1) Bead cellulose and its derivates are used for example as supports for immobilization and chromatographic purification of proteins. (2)

The dissolution of cellulose is now as ever a fundamental step for applications and the chemical analysis of the polymer. For the preparation of cellulose solutions several solvent systems are known, though most of them are mixtures of different components. They can be classified as aqueous or nonaqueous and into nonderivatizing or derivatizing. For salt solutions as aqueous and nonderivatizing solvents, such as  $\text{ZnCl}_2/\text{H}_2\text{O}$ , the effect on cellulose is already known for a long time. (3) Herewith a swelling can be observed, but the chain length is drastically shortened. Under suitable conditions (pretreatment, low level DP cellulose) it is possible to dissolve cellulose in concentrated aqueous chloride solutions or aqueous  $\text{Ca}(\text{SCN})_2$ . (4,5) Molten salt hydrates were also used as swelling agents or solvents. The dissolution of cellulose was observed in  $\text{LiSCN} \cdot 2\text{H}_2\text{O}$  and in mixtures of  $\text{NaSCN}/\text{KSCN}/\text{Ca}(\text{SCN})_2/\text{H}_2\text{O}$ . (6) However, systematic investigations of the dissolving power of molten salt hydrates for cellulose have not been carried out yet, nor is there any structural information regarding the interactions between the molten salt hydrates and the cellulose.

The aim of this work is to test hydrated salt melts in order to find new solvents for cellulose. Besides it was important to characterize the regenerated products.

## Experimental

All experiments were carried out using nonactivated cellulose (dissolving pulp) with a number average DP of 756. The salt hydrates were heated to above the melting point in a closed flask and cellulose was added without pretreatment. The mixture was stirred at constant temperature for a maximum time of two hours, after which the mixture was cooled down to room temperature. The crystallization of the melt could be observed along with the precipitation of the cellulose. The salt was removed from the polymer by washing with water. Molecular weight distribution was determined by size exclusion chromatography (SEC) after nitration according to the methods described by Fischer et. al.(7)

To obtain the  $^{13}\text{C}$ -NMR spectra at 100-140°C a Bruker DPX 400 spectrometer operating at 9.3 T which corresponds to a frequency of 100.13 MHz for  $^{13}\text{C}$  was used. Chemical shifts were recorded relative to an external DMSO- $\text{D}_6$  standard and determined for cellulose concentrations between two and four percent. Obtained chemical shifts were not corrected with respect to magnetic susceptibility.

For the X-ray analysis samples of 200 mg freeze dried cellulose were prepared. The measurements were done with a Siemens D 5000 diffractometer using Cu  $K_\alpha$  radiation. For separation of overlapping peaks the PROFILE program (DIFFRAC-AT software, SOCABIM company) and the pseudo-Voigt model were used. After this fitting procedure the crystallite dimensions were determined according to the Scherrer equation. (8)

## Results and Discussion

First of all a multitude of known pure molten salt hydrates was investigated regarding to their reaction behaviour with cellulose. It follows that the melts could be divided into five groups, depending on their observed degree of interaction with cellulose. Table I shows the different groups with an example each.

**Table I. Interaction of molten salts with cellulose**

| Group | Observed Interaction | Example   | Regenerated Cellulose Form |
|-------|----------------------|---|----------------------------|
| 1     | no reaction          | $\text{CaCl}_2 \cdot 6\text{H}_2\text{O}$           | cellulose I                |
| 2     | fine dispersion      | $\text{NaCH}_3\text{COO} \cdot 3\text{H}_2\text{O}$ | cellulose I                |
| 3     | decomposition        | $\text{MgCl}_2 \cdot 6\text{H}_2\text{O}$           | -                          |
| 4     | strong swelling      | $\text{Na}_2\text{S} \cdot 9\text{H}_2\text{O}$     | cellulose II               |
| 5     | dissolution          | $\text{LiI} \cdot 2\text{H}_2\text{O}$              | cellulose II               |

The varying reactivity of molten hydrates is also indicated by the structure of the recovered product samples. Whereas the cellulose regenerated from melts of group 1 and 2 had the Cellulose I modification, swelling and dissolution lead to a transition into modification II. This classification was important not only for the prediction of new solvents but also to find new solvent mixtures by combination of suitable melts. Consequently new pure salt melts as well as new hydrated salt mixtures were found as solvents for cellulose. They are summarized in Table II.

**Table II. New molten salts as solvents for cellulose**

| Solvent system  | Reaction temperature | Cellulose concentration |
|---|----------------------|-------------------------|
| $\text{LiI} \cdot 2\text{H}_2\text{O}$                        | 100 °C               | 0.25 %                  |
| $\text{LiClO}_4 \cdot 3\text{H}_2\text{O}$                    | 110 °C               | 5 %                     |
| $\text{NaSCN/KSCN/LiSCN/H}_2\text{O}$                         | 140 °C               | 3 %                     |
| $\text{LiClO}_4/\text{Mg}(\text{ClO}_4)_2/\text{H}_2\text{O}$ | 110 °C               | 6 %                     |

The dissolution of cellulose in these molten salts leads to transparent and fiber-free solutions that become more viscous as the cellulose dissolves. The dissolution time is ranged between 10 and 30 minutes depending on the amount of cellulose added. According to determinations of molecular weight distribution a certain decrease of the molecular mass of the regenerated products could be stated. (9)

To discover the state of the cellulose in molten salts, solutions of cellulose in  $\text{LiClO}_4 \cdot 3\text{H}_2\text{O}$  and  $\text{NaSCN/KSCN/LiSCN/H}_2\text{O}$  were studied with static light scattering. It was found that the state of cellulose does not consist of single chains but in form of agglomerates uniting 150 until 200 molecules of cellulose. This is similar to solutions of cellulose in  $\text{NMMNO} \cdot \text{H}_2\text{O}$ . (10)

Taking into account that most of the hydrated melts which act as solvents for cellulose contain  $\text{Li}^+$  ions further solubility investigations were focused on other lithium containing melts. Whereas molten  $\text{LiCl} \cdot 3\text{H}_2\text{O}$  represents a swelling agent, molten  $\text{LiNO}_3 \cdot 3\text{H}_2\text{O}$  and  $\text{LiCH}_3\text{COO} \cdot 2\text{H}_2\text{O}$  can only suspend cellulose. The view usually taken in publications is that small cations, e. g.  $\text{Li}^+$ , in combination with soft anions should have good swelling or dissolving properties. (4) This can be confirmed in the case of  $\text{LiI} \cdot 2\text{H}_2\text{O}$  and for the thiocyanate melts containing lithium ions. This assumption cannot be applied for molten  $\text{LiClO}_4 \cdot 3\text{H}_2\text{O}$ . There must exist other factors which promote the dissolution of cellulose in molten hydrates. The influence of the acidity and basicity of molten salts was already discussed. (9)

Generally the dissolution of cellulose is accompanied by a transformation from the modification I to II. This can be confirmed for the celluloses dissolved and regenerated from molten hydrates. Dependence of the crystallinity on the different salt hydrates was found. (9) The determination of the dimension of the crystalline regions is important for further applications of the regenerated polymer. Such information can be obtained from wide angle X-ray diffraction.

The crystallite dimensions were determined for cellulose regenerated from  $\text{LiClO}_4 \cdot 3\text{H}_2\text{O}$  and  $\text{NaSCN/KSCN/LiSCN/H}_2\text{O}$  melts. Comparing the crystallite values

as shown in Table III significant differences can be stated. The crystallite dimensions are smaller for cellulose reprecipitated from molten  $\text{LiClO}_4 \cdot 3\text{H}_2\text{O}$  and especially for the 002 plane a strong decrease of the crystallite size can be recognized.

**Table III. Crystallite dimensions (D) of regenerated celluloses**

| Solvent system                             | D in nm |               |       |
|--|---------|---------------|-------|
|  | 1 0 1   | 1 0 $\bar{1}$ | 0 0 2 |
| $\text{LiClO}_4 \cdot 3\text{H}_2\text{O}$ | 5.02    | 3.89          | 4.61  |
| $\text{NaSCN/KSCN/LiSCN/H}_2\text{O}$      | 7.62    | 5.65          | 8.65  |

For the characterization of both regenerated celluloses additionally Scanning Electron Microscopy (SEM) measurements were done. (Figures 1a and 1b) It is recognizable that the macroscopic shape of the two regenerated celluloses is different, too. Whereas cellulose regenerated from molten thiocyanates (Figure 1a) has a fibrous shape, cellulose precipitated from molten perchlorate (Figure 1b) is more lamellar.

For a better understanding of the chemical interactions of cellulose and molten hydrates solvent state  $^{13}\text{C}$ -NMR measurements were carried out. The  $^{13}\text{C}$ -NMR spectrum of cellulose in molten  $\text{LiClO}_4 \cdot 3\text{H}_2\text{O}$  is shown in Figure 2. The six observed peaks show that the cellulose is dissolved in the molten salt. The chemical shifts of the carbon atoms of the cellulose are compared with literature data (11) in Table IV.

**Table IV.  $^{13}\text{C}$ -NMR data of cellulose in molten  $\text{LiClO}_4 \cdot \text{H}_2\text{O}$  compared with literature data**

| Solvent system                             | $^{13}\text{C}$ -NMR chemical shift (ppm) |      |      |      |      |      |
|--|---|------|------|------|------|------|
|  | C-1                                       | C-2  | C-3  | C-4  | C-5  | C-6  |
| $\text{LiClO}_4 \cdot 3\text{H}_2\text{O}$ | 101.0                                     | 72.5 | 73.7 | 77.3 | 73.2 | 60.3 |
| $\text{LiCl/DMAc}$                         | 103.9                                     | 74.9 | 76.6 | 79.8 | 76.6 | 60.6 |
| $\text{NaOH/D}_2\text{O}$                  | 104.5                                     | 74.7 | 76.3 | 79.8 | 76.2 | 61.5 |

The observed chemical shifts of the carbon atoms are comparable with those of other nonderivatizing cellulose solvents, the small deviations are caused by differences of susceptibility of melts and conventional solvents. To get more detailed information about the interaction of cellulose and molten salt hydrates Raman measurements and  $^7\text{Li}$ -NMR investigations will be done.

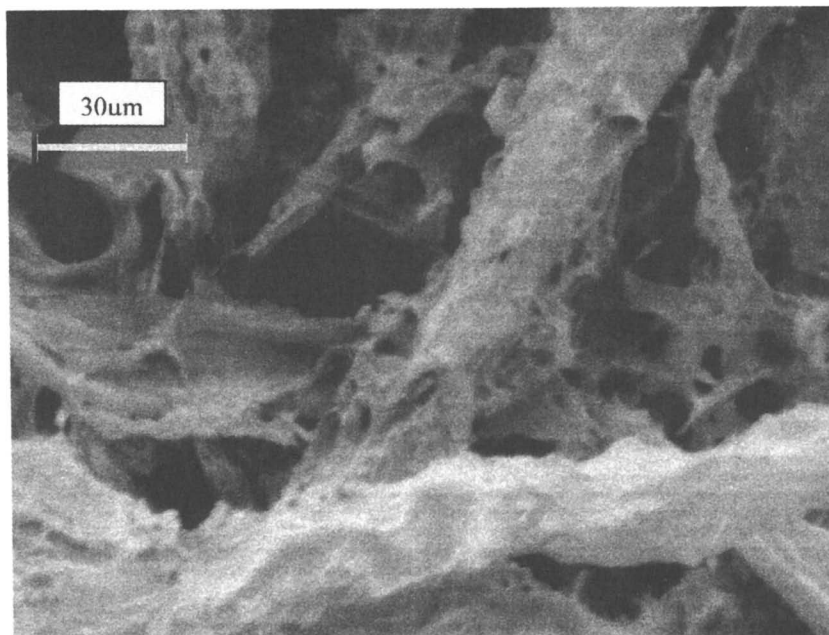


**Figure 1a.** SEM of cellulose regenerated from thiocyanates.

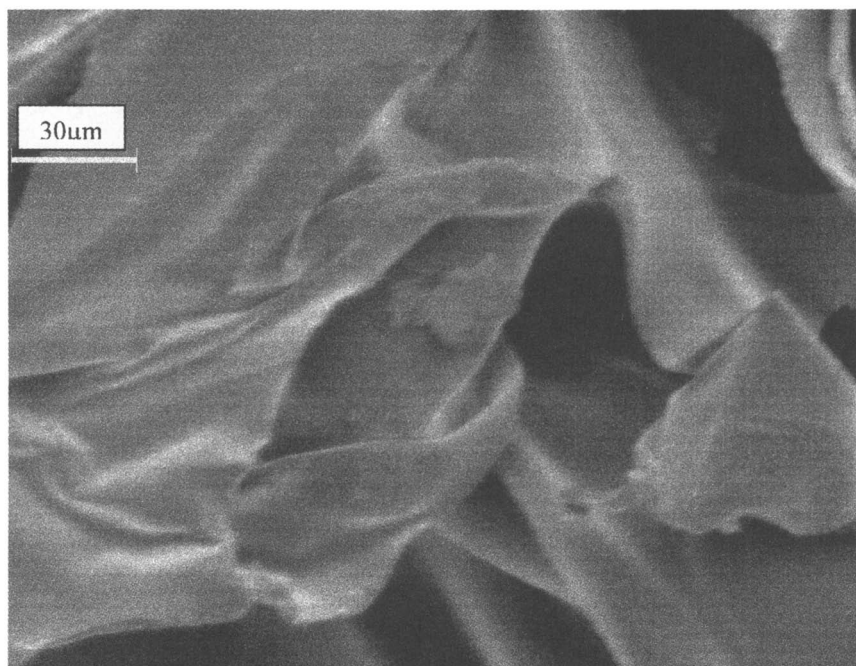


**Figure 1b. SEM of cellulose regenerated from perchlorate.**

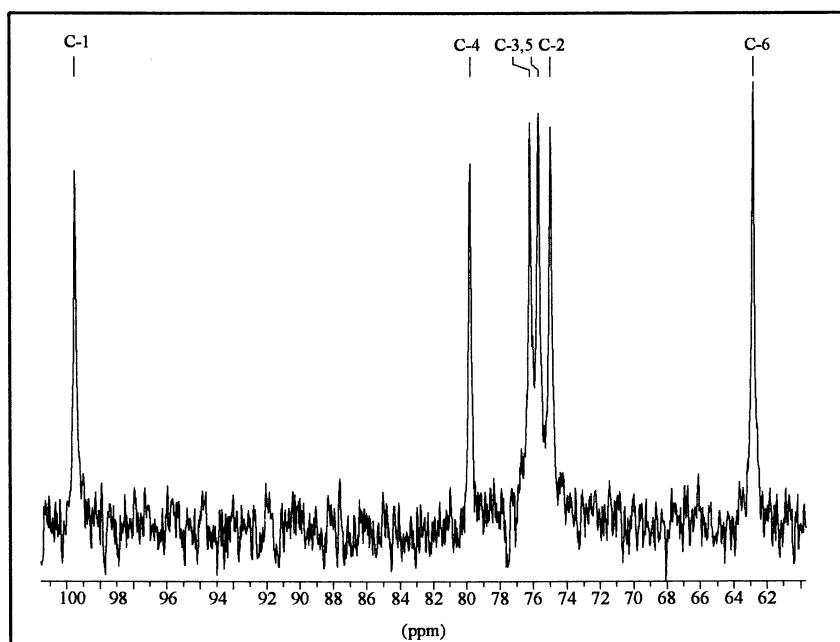


Figure 2.  $^{13}\text{C}$ -NMR spectrum of cellulose in molten  $\text{LiClO}_4 \cdot 3\text{H}_2\text{O}$  at  $110^\circ\text{C}$

**Literature Cited**

1. Bikales, N. M.; In *Cellulose and Cellulose Derivates*; Segal, L., Ed.; Part 5; Wiley-Interscience: New York, 1971, p 790
2. Boeden, H.-F.; Pommerening, K.; Becker, M.; Rupprich, C.; Holtzhauer, M.; Loth, F.; Müller, R.; Bertram, D. *J. Chromatogr.* **1991**, *552*, 389.
3. Letters, K. *Kolloid-Zeitschrift* **1932**, *LVIII*, 229.
4. Warwicker, J. O.; Jeffries, R.; Colbran, R. L.; Robinson, R. N. *Shirley Inst. Pamphlet* **1966**, *93*, 164.
5. Kuga, S. *J. Colloid Interface Sci.* **1980**, *77*, 413.
6. Lukanoff, B.; Schleicher, H.; Philipp, B. *Cell. Chem. Techn.* **1977**, *17*, 593.
7. Fischer, K.; Schmidt, I.; Hintze, H. *Das Papier* **1994**, *48*, 769.
8. Scherrer, P. *Göttinger Nachrichten* **1918**, *2*, 98.
9. Fischer, S.; Voigt, W.; Fischer, K.; Spange, S.; Vilsmeier, E. *Molten Salt Forum* **1998**, *5-6*, 477.
10. Röder, T. W. *PHD Thesis TU Dresden* **1998**.
11. Nehls, I.; Wagenknecht, W.; Philipp, B.; Stscherbina, D. *Prog. Polym. Sci.* **1994**, *19*, 29.



## Chapter 11

# Cellulosic Liquid Crystals

**Pierre Sixou**

**Laboratoire de Physique de la Matière Condensée, UMR 6622,  
Parc Valrose, 06108 Nice Cedex 02, France**

We discuss the various aspects of the mesophase formation. The following parameters are considered:

- The "rigidity" of the ordered objects (macromolecules fibrils...).
- The "chirality" which occurs at several levels: molecule, macromolecule, supramolecular organization of macromolecules or microfibrils.
- The nature of the considered phase: solution, melt, cross-linked polymers...

The next part is devoted to an illustration of these concepts in the case of a given cellulose derivative (hydroxypropylcellulose).

Some considerations concerning the influence of chemical structure on the optical properties of the mesophases are more particularly discussed.

Molecular order and related properties such as the nature and the degree of order or the dynamics of the order/disorder transition have a great importance in several fields (physics, biology...). In the case of polysaccharides and particularly of cellulose or cellulose derivatives these phenomena happen in different aspects such as the textile fiber formation or the biological membranes.

The mesophase formation is governed by various parameters. Three important factors are:

- The "rigidity" of the ordered objects (macromolecules, fibrils...)
- The "chirality" which occurs at several levels: molecule, macromolecule, and supramolecular organization of macromolecules or microfibrils...
- The nature of the considered phase: solution, melt, cross-linked polymer...

In this paper we first discuss the various aspects of the mesophases and the role of these parameters (part 1). The next part is devoted to an illustration of these concepts in the case of a given cellulose derivative (hydroxypropyl cellulose). Some considerations concerning the developed and potential applications are put forward in conclusion.

## MESOPHASE FORMATION AND RELATED PROPERTIES

The discovery of the self-ordering of cellulose derivatives (1) has stimulated considerable interest in forming mesophases of cellulose itself (2) or of polysaccharides (Gray et al (3-10), Gilbert et al (11-12), Cifferi et al (13), Porter et al (14), Suto et al (15-16), Zugenmaier et al (17), Watanabe and Miyamoto et al (18-19), Rinaudo et al (20-21), Navard et al (22)...)

### 1/ Textures

In cellulose and cellulose derivatives, the ordered phase is cholesteric (figures 1 and 2). The simplest way to characterize the existence of the anisotropic cholesteric phase in polymer melt or in solution is to use a polarizing microscope. For lyotropic liquid crystal of cellulose derivatives, solutions at high polymer concentration are anisotropic and birefringent. Below a certain critical concentration the solution becomes isotropic at constant temperature. Some cellulose derivatives are thermotropic and show an optically anisotropic phase in the melt. At higher temperatures a transition from a liquid crystal to an isotropic phase occurs. Figures 3 to 6 show typical cross-polarized micrographs. Depending on the orientation of the cholesteric axis, several types of textures are observed (figures 2 a, b, c, d)): planar, fingerprint, polygonal field... The equidistant alternating bright and dark lines (figure 3) are related to the periodicity of the helical cholesteric structure (figure 2 b). The appearance of these lines is linked to the anisotropy of polarizability due to the orientation of the molecular axis related to the direction of propagation of the light wave. Conventional cholesteric defects (figure 4) which are observed in low molar mass liquid crystals (23) are also seen in lyotropic or thermotropic cellulosic mesophases. Various behaviors like spherulites (figure 5) or interphase between two mesophases have been observed and studied in details.

### 2/ Formation of mesophases and rigidity of macromolecular chains

The cellulose derivative chains are relatively rigid. If one approximates the chain by a wormlike chain model, the obtained persistence lengths ( $q$ ) are of an order of

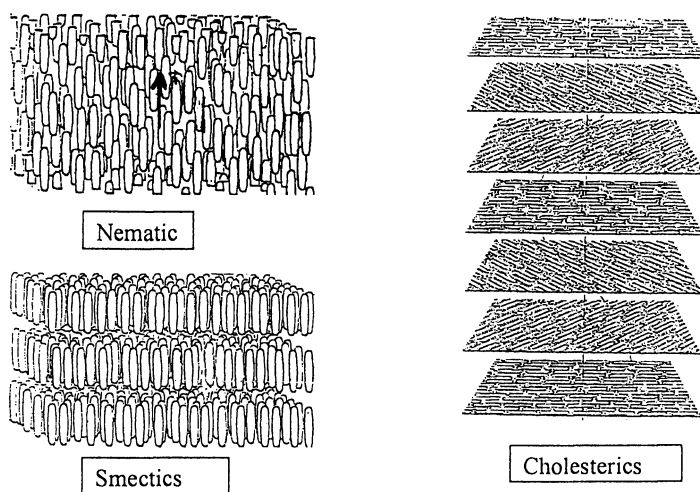


Figure 1. Schematic representation of molecules in isotropic phase and in nematic, cholesteric and smectic liquid crystal phases.

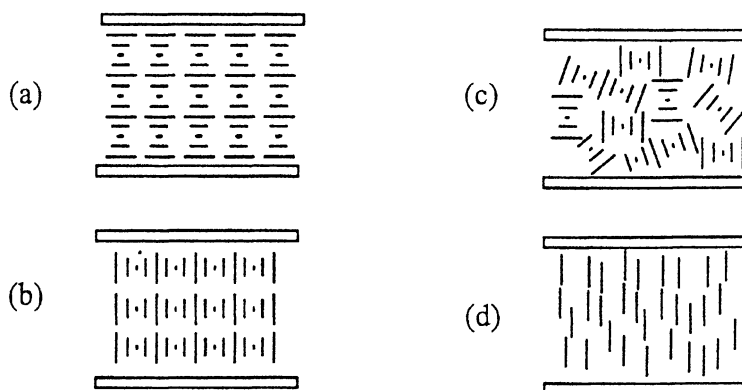


Figure 2. Cholesteric order: projection of the director  $n$ . The cholesteric pitch is called  $p$ .

- |    |                     |
|----|---------------------|
| a) | Planar texture      |
| b) | Focal conic texture |
| c) | Fingerprint texture |
| d) | Homeotropic texture |

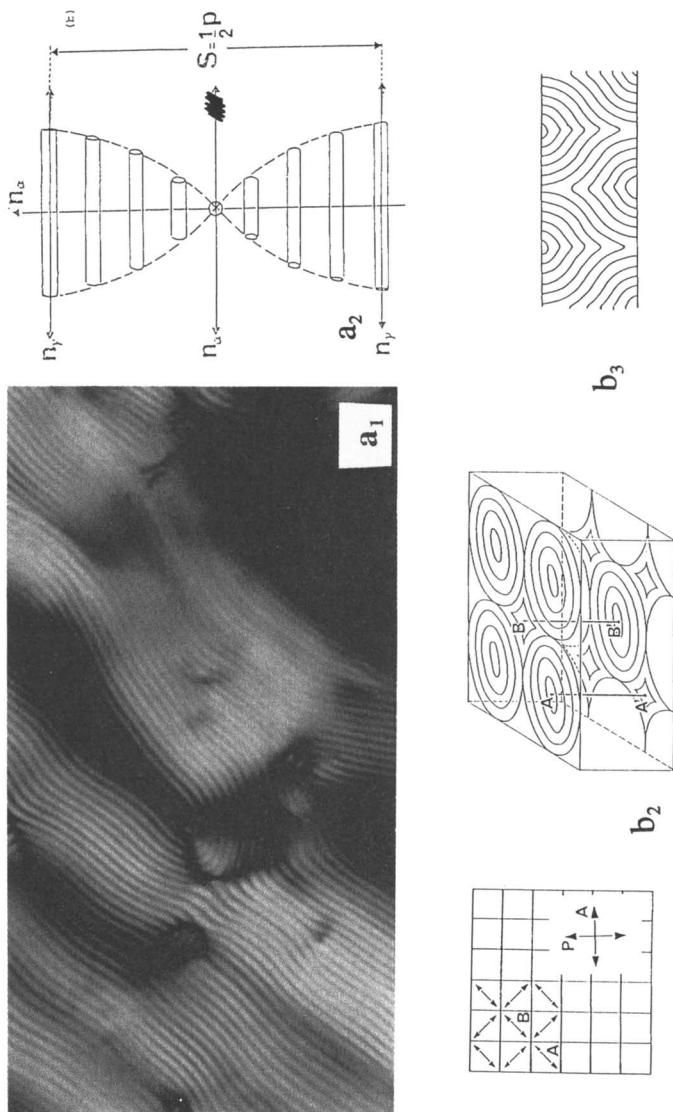


Figure 3. Typical observed textures between cross-polarizers. The black areas correspond to homeotropic orientation. The bright and dark lines (figure 3a<sub>1</sub>) are related to the refractive index modification associated to the molecular orientation (see a<sub>2</sub>). The figure b illustrates the cholesteric layers of the polygonal field texture (see ref 23 ). The figures c and d present the observations of these polygonal fields in different mesomorphic cellulosic solutions.

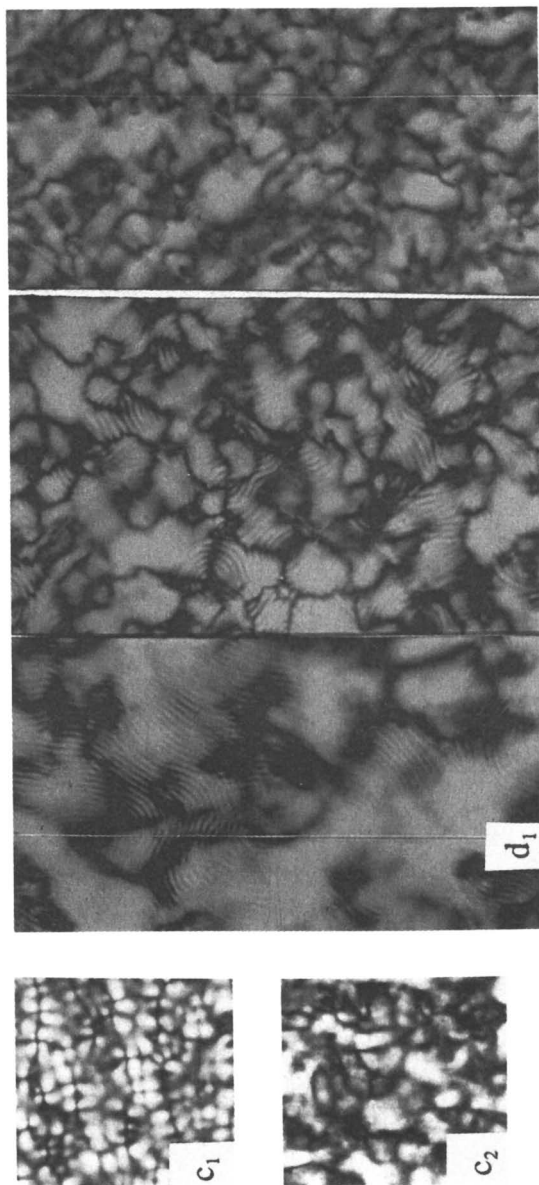


Figure 3. *Continued.*

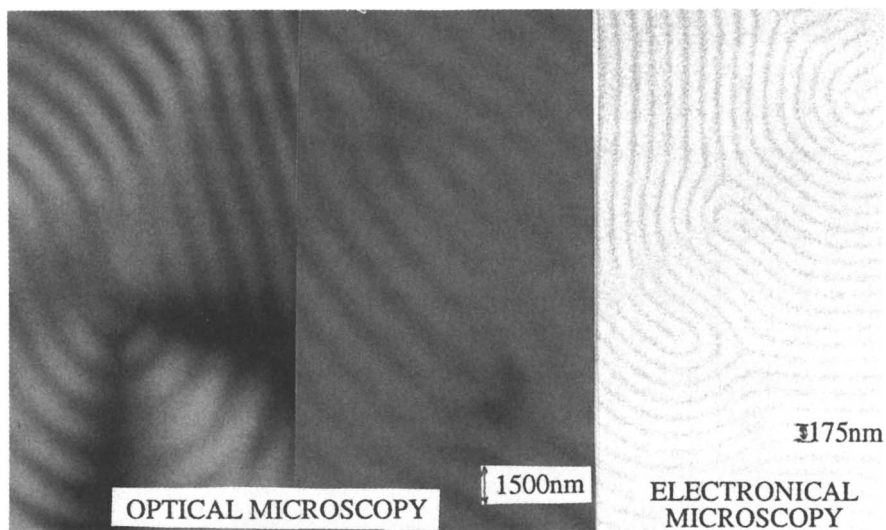


Figure 4. Conventional cholesteric defects (see ref 23) observed by optical or electronical microscopy.

magnitude of several to more than thirty monomers (i.e., more than a hundred and fifty angstroms). The persistence length of the same chain can be modified by an order of magnitude of two, depending on the solvent employed (table 1). In addition to the rigidity, steric effects and flexibility of side groups seems to influence the formation and properties of cellulosic mesophases : they allow (or not) the existence of a mesophase before crystallization, influence the onset temperature of a mesophase, and contribute to the value of the cholesteric pitch. For a given solvent, a chain in the nature of the substituent can also strongly modify the rigidity of the chain (three times) (table 2).

Intrinsic viscosity (24) and quasielastic light scattering (25) measurements have been made in many cellulose derivative / solvent systems and can be used to extract information on chain characteristics. The flexibility of semirigid polymers can be measured by the persistence length  $q$ , which correlates the direction of the first monomer unit with that of subsequent units. Physical parameters such as the radius of gyration and the end-to-end distance can be evaluated as a function of the ratio of the total contour length  $L$  divided by the persistence length.

Given a system of monodispersed wormlike chains, Yamakawa and Fujii (26) calculate the intrinsic viscosity with a method based on Kirkwood and Riseman work (27). An approximate expression of the variation of the intrinsic viscosity with the molecular weight  $M$  is given as a function of the diameter and persistence length of the molecular chain. Conversely from a measurement of the intrinsic viscosity as a function of  $M$ , a numerical fit will give both the diameter  $D$  and persistence length  $q$  (figure 6). The method has been applied to monodispersed and polydispersed cellulose derivatives. Studying the quasielastic light scattering from dilute solutions of cellulose derivatives can also test the applicability of the wormlike chain model of Yamakawa and Fujii. The experiment gives the translational diffusion coefficient  $D$  and the hydrodynamic radius  $R_0$  which is substantially smaller than the radius of gyration  $R_G$ . The results from the latter experiment are in agreement with those obtained from intrinsic viscosity.

### 3/ Phase diagrams

#### 1. Thermotropic mesophases

The transition temperature (figure 7) of the thermotropic polymer increases with degree of polymerization but attains a limiting value. This type of behavior has been theoretically predicted (28) and also observed (29) in many other mesomorphic

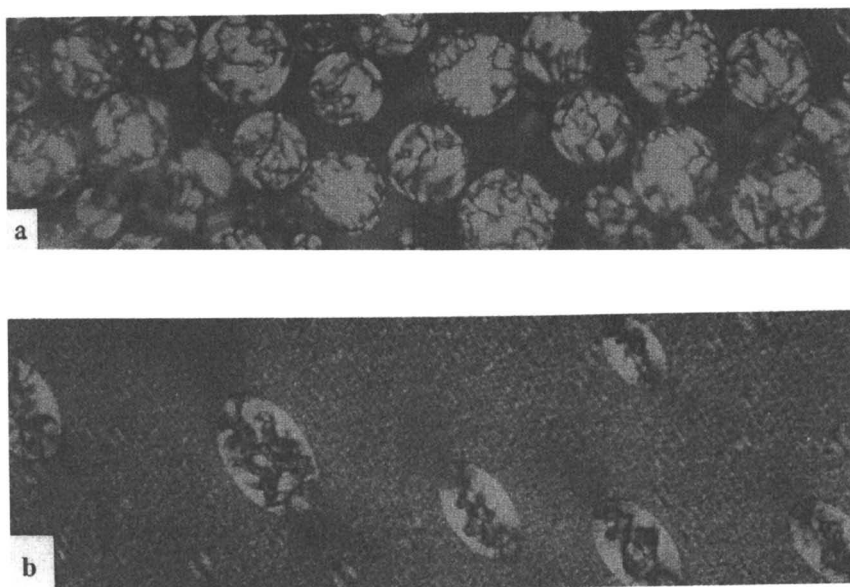


Figure 5. Optical observation of lyotropic cellulosic spherulites.

- a) Hydroxypropylcellulose/water solution.
- b) Deformation of spherulites by a flow.
- c) Organization inside a spherulite: just after preparation of the solution (left)
- d) Organization inside a spherulite: several hours after preparation (right).
- e) Lyotropic solution of a mixture of mesomorphic solution: organization of the second polymer outside of the spherulite.
- f) Spherulite with high pitch mesomorphic organization.



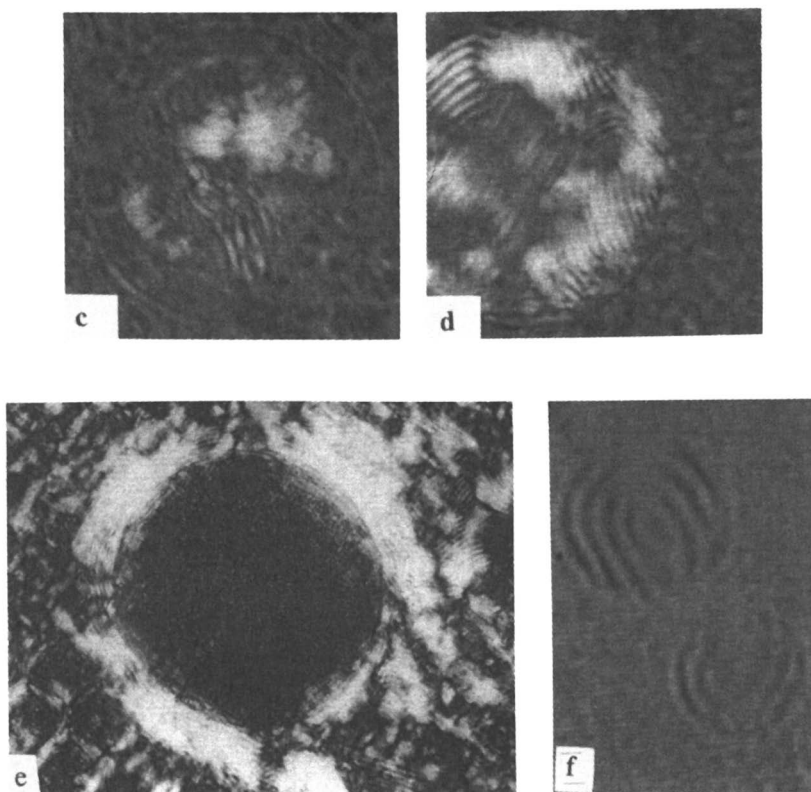


Figure 5. *Continued.*

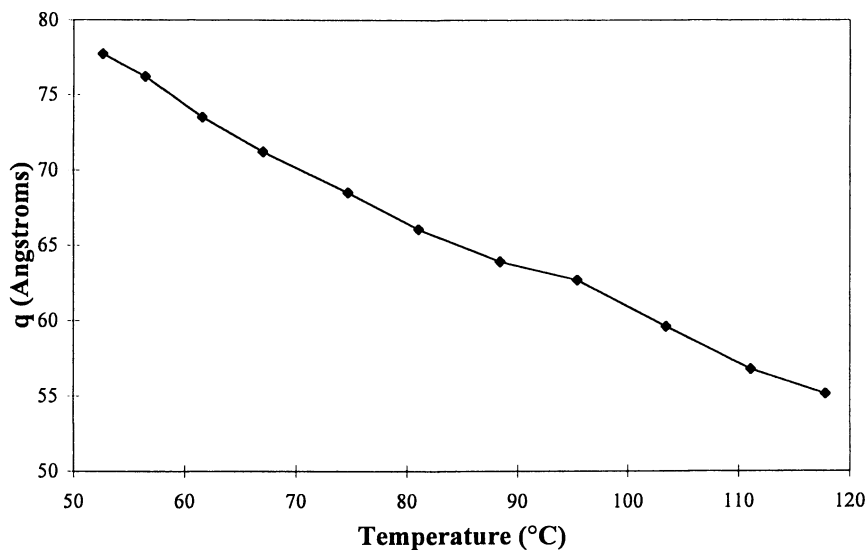


Figure 6. Persistence length and hydrodynamic radius as function of temperature (Tricarbanilate/solution)

Table 1: Influence of the solvent on the persistence length

| Solvent              | q( Angstroms) |
|----------------------|---------------|
| Dimethyl acetamide   | 66            |
| Acetone              | 57            |
| Trifluoroacetic acid | 55            |
| Dichloromethane      | 39            |
| Trichloromethane     | 35            |
| Tetachloromethane    | 35            |

Table 2: Influence of the polymer nature on the persistence length.  
The solvent is acetone in the three cases.

| Polymer                  | q( Angstroms) |
|--------------------------|---------------|
| Cellulose tricarbanilate | 154           |
| Cellulose nitrate        | 155           |
| Cellulose diacetate      | 57            |

polymers (polyesters, polyisocyanates...). In cellulosic mesophases the presence of hydroxyl groups raises the temperature of isotropic behavior. The persistence lengths of the two compounds are comparable.

## 2. Lyotropic mesophases

Lyotropic cellulose mesophases can be observed in a large variety of solvents with derivatives that can be thermotropic (ethylcellulose, hydroxypropylcellulose, acetoxypropylcellulose, etc.) or not (cellulose acetate). Figure 8 shows examples of a phase diagram of a mixture consisting of cellulose derivatives dissolved in an ordinary organic solvent. The anisotropic phase is separated from the isotropic one via a two-phase coexistence region. The size of the two-phase gap depends on parameters such as temperature, molecular weight, polydispersity, etc. A linear decrease in the transition temperature (here, temperature for complete disappearance of the anisotropic phase) with decreasing polymer concentration is observed in "inert" solvents. The earliest theories for phase separation of polymeric liquid crystals were calculated based on a model of long rigid rods. Onsager showed that a tendency to order occurs owing to steric hindrance of the rods. Flory calculated the entropy of a rigid rod system on a lattice. The rigid rod model was extended to semirigid chains by introducing a parameter representing the proportion of aligned neighboring monomers (30). These theories have been applied to interpret experimental phase diagrams in cellulose derivative systems. Problems arise from ill-defined biphasic separation in the experiments. Furthermore, many cellulose derivatives form cholesteric phases and are thought to have helical or ribbon like conformations.

In the case of strongly interacting solvents with specific interactions such as hydrogen bonding, a curvature in the plotted transition temperature is found.

The lyotropic mesophase prepared from polymer dissolution in a mixture of solvents is an interesting case (31). At a given polymer concentration, the organization of macromolecules is governed by the surface of the droplets and intermolecular interactions. It can be varied by changes in the relative proportions of the solvents. Concerning the predicted theoretical phase diagrams, rodlike solvents were also explored as well as ternary systems. Unfortunately the comparison with experiment is difficult particularly in the case of hydrogen bonding solvents. The figure 9 shows the case of HPC ( $M_w=60000$ )/water system (curve a). At room temperature the solution is isotropic below 45% (g/g) and anisotropic for the higher concentrations. For these latter concentrations a gel is observed when the temperature is raised. The gel appearance temperature can be modified by adding a second polymer (curves b, c, d, e, f).

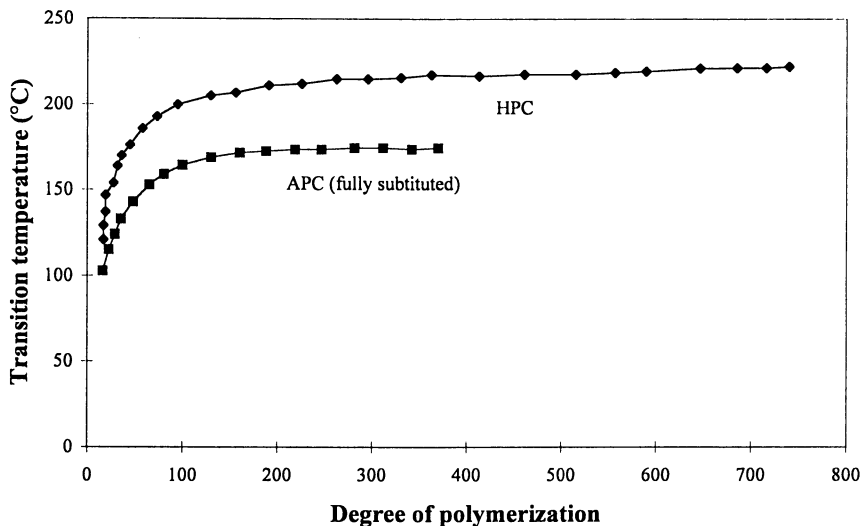


Figure 7. Transition temperature versus degree of polymerization for two thermotropic polymers: Hydroxypropyl cellulose and Acetoxypopyl cellulose (fully substituted).

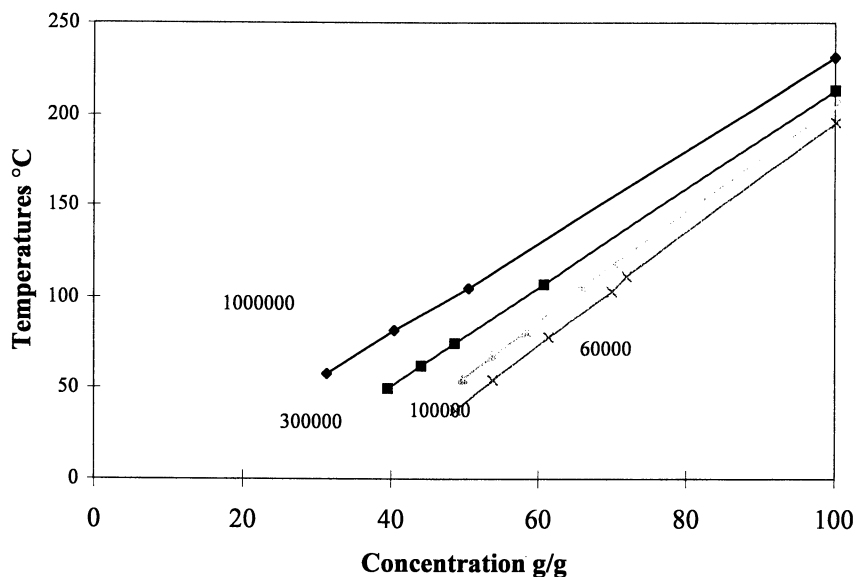


Figure 8. Phase diagram of Hydroxypropylcellulose/ Dimethylacetamide system.

- a)  $M_w = 1000000$
- b)  $M_w = 300000$
- c)  $M_w = 100000$
- d)  $M_w = 60000$

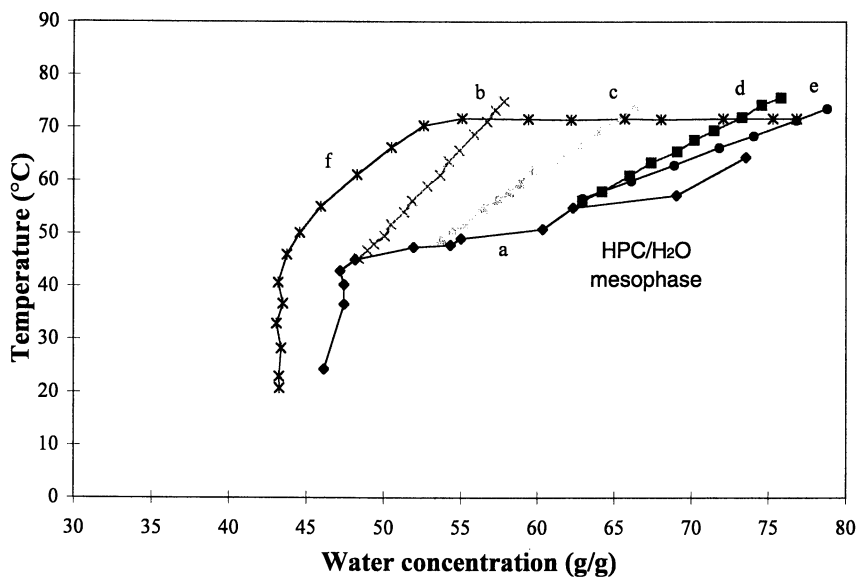


Figure 9 Phase diagram of HPC ( $M_w=60000$ )/water system (curve a). Modification of the gel temperature appearance by adding a second polymer (curves b, c, d, e, f).

b)  $M_w\text{HPC} = 60000$ ,  $M_w\text{PVP} = 10000$ . The relative HPC/PVP concentrations (g/g) are 50/50

a)  $M_w\text{HPC} = 60000$ ,  $M_w\text{PVP} = 10000$ . The relative HPC/PVP concentrations (g/g) are 55/55

b)  $M_w\text{HPC} = 60000$ ,  $M_w\text{PVP} = 10000$ . The relative HPC/PVP concentrations (g/g) are 65/35

c)  $M_w\text{HPC} = 60000$ ,  $M_w\text{PVP} = 40000$ . The relative HPC/PVP concentrations (g/g) are 65/35

d)  $M_w\text{HPC} = 60000$ ,  $M_w\text{PVP} = 10000$ . The relative HPC/PVP concentrations (g/g) are 10/90

### 3. Mixtures of mesophases

Mixtures of flexible and mesomorphic cellulose polymers were also studied (32). Segregation is observed as in flexible polymer systems at high relative degree of polymerization and can be followed more easily when one of the components is itself anisotropic. The thermodynamic stability of a mixture of two cellulosic mesomorphic polymer has been studied (33). Incompatibility is the rule in most cases, especially for high molecular masses of the constituents, unless specific interactions exist between the different constituents. Ternary experimental phase diagrams present several zones: isotropic, isotropic/isotropic biphasic, anisotropic/isotropic biphasic, anisotropic/anisotropic biphasic, anisotropic. Phase diagrams can be calculated from the free energy of mixing. An expression has been derived which includes several terms: the entropy of mixing, the isotropic interactions, the entropy of chain conformation and the contribution of anisotropic interactions. The first two terms are characteristic of non-mesomorphic polymer mixtures, while the last one represents additional contributions related to chain rigidity and liquid crystal properties (34). The crystallization kinetics (spherulitic growth rate, crystallization time and size of the spherulites) of semicrystalline polymer blended with mesomorphic cellulose derivative polymer has been studied (35).

### 4/ Order parameter

Interest has been revived in the model of stiff chains described by a string with bending elasticity to explain nematic ordering in polymer systems. This model using the wormlike chain has been employed to foresee the phase diagrams as well the order parameters (30, 28).

In the model, the stiff chain is represented by a curve  $r(s)$ . The persistence length is given by  $q = \epsilon/kT$ . The bend elasticity favors conformations of constant curvature. By introducing an anisotropic interaction  $uS (3(\cos^2\Phi(s)-1)/2)$  and an order parameter  $S = \langle 3(\cos^2\Phi(s)-1)/2 \rangle$ , a first-order nematic isotropic transition can be found. Here  $\Phi(s)$  is the angle of the chain at contour length  $s$  to the director and  $u$  is an effective mean field parameter, which tends to align the chains. The relevant parameters of the model are then  $q/L$  and  $uq/kT$ ,  $L$  being the degree of polymerization. Two methods were used to solve the free energy. A numerical calculation of the distribution function for a given chain conformation (and therefore the free energy) was made possible by using theories developed for flexible chains. In the pure polymer, the transition temperature is shown to increase as  $L$  or  $q$  is increased. A large "induced rigidity" or extension of the polymer chain at the transition was also predicted. For comparison, a Landau-de-Gennes expansion of the free energy, valid near the transition temperature

$$F = F_0 + AS^2 + BS^3 + CS^4$$

was also calculated (30). The coefficients A, B, C are given in the parameters of the wormlike chain. The transition temperatures are in good agreement with the former calculations. In both calculations at low  $L/q$ , the order parameter tends to the 0.43 of rigid rods. NMR can be used to obtain the order parameter of the cholesteric phase. The local order can be studied by orientation of solvent molecule in lyotropic solutions (36) (figure 10). It is expected, because of the order parameter, a splitting of resonance lines and a difference between chemical shielding in anisotropic and isotropic solution. These effects can be studied with different nuclei ( $C^{13}$ , F...) and with different experimental conditions (for example with and without rotation). By a systematic study of spectra it can be shown that the spectrum can be separated onto two parts: one which is caused by molecules in anisotropic environments and the other by molecules in an isotropic environment. The order parameters obtained by  $C^{13}$ , F splitting and chemical shift are in reasonable agreement with predicted values.

### 5/ Flow and rheology

Cellulosic mesophases are strongly modified by a flow field. Rheo-optic studies can be performed in order to describe the way whose cholesteric phase reorganizes to nematic after orientation by a strong shear. Band textures are observed. An unwinding of the supermolecular structure occurs and uniaxial orientation of the macromolecules, induced by a sufficient shear flow, is achieved and leads to a nematic like continuous phase. Band textures appear (37) after a very short time following cessation of the shear stress and after the occurrence of a longer relaxation process. The higher the shear rate is, the faster the macroscopic texture vanishes. In the case of lyotropic solutions, when the solvent is allowed to evaporate, the shear-induced structure can be frozen and an analysis of the optical texture has been proposed. Very beautiful textures are also found in fibers and threads.

The phase transition modification of mesomorphic polymers in elongational flow can be studied theoretically (38). The case of cholesteric polymers isn't easy due to the unwinding of supramolecular helicoidal structure. In the presence of flow on nematic polymers, Landau-de-Gennes expansion of free energy in the order parameter shows that the transition is shifted to lower polymer concentrations and the biphasic gap disappears at sufficiently high strain rates.

Rheological properties have also been studied (39) (figure 11). It has been observed for some concentrations a decrease of the viscosity when the polymer concentration increases and on the other hand that the first difference of normal stress becomes negative for a certain range of shear stress. This effect had been noticed in the case of different lyotropic cellulose derivatives and in their mixtures.

### 6/ Optical properties

At high concentrations, solutions of cellulose derivatives are iridescent, a characteristic of cholesteric liquid crystals. Selective reflection of light is caused by the helical order present in a cholesteric phase. For a planar texture, a cholesteric phase with right-handed pitch will reflect left-handed circular polarized light at a certain wavelength  $\lambda_r$  given, for normal incidence, by  $\lambda_r = pn/2$  ( $p$ = helical pitch,  $n$ =refractive index). The peak of intensity of reflected light is associated with Bragg reflection in the cholesteric phase. The pitch can also be measured by different methods: apparent optical absorption, circular dichroism, and observation of the fingerprint texture by optical microscopy, ... It can thus be determined according to various parameters such as concentration, temperature, molar mass, degree of substitution... The pitch can also be measured for wavelengths outside the visible spectrum (UV, IR). Qualitative comparison was made with the theories developed for (rigid) small-molecule cholesteric phases. Effects due to the semirigidity of the chain or the helical conformation can be considered. The presence of some type of asymmetric potential in addition to the orientational interaction is taken into account. From analysis of experimental results the following conclusion can be drawn.

- On increasing the temperature, the solutions pass from blue to red (figure 12). It is the opposite of the variation found in small-molecule cholesteric phases. We conclude that anharmonic effects, important in the latter case, can be neglected in the polymers we studied. A thermally induced inversion of the twist sense has been viewed.

- The dielectric constant of the solvent does not appear to be an essential parameter. The same polymer dissolved in two solutions of different static permittivity can lead to the same value for the cholesteric pitch. Inversely, in a ternary mixture of constant static permittivity but varying proportions of the various components, the pitch varies considerably.

- The concentration of the polymer influences the magnitude of the pitch: an increase in the polymer concentration gives a decrease of the pitch.



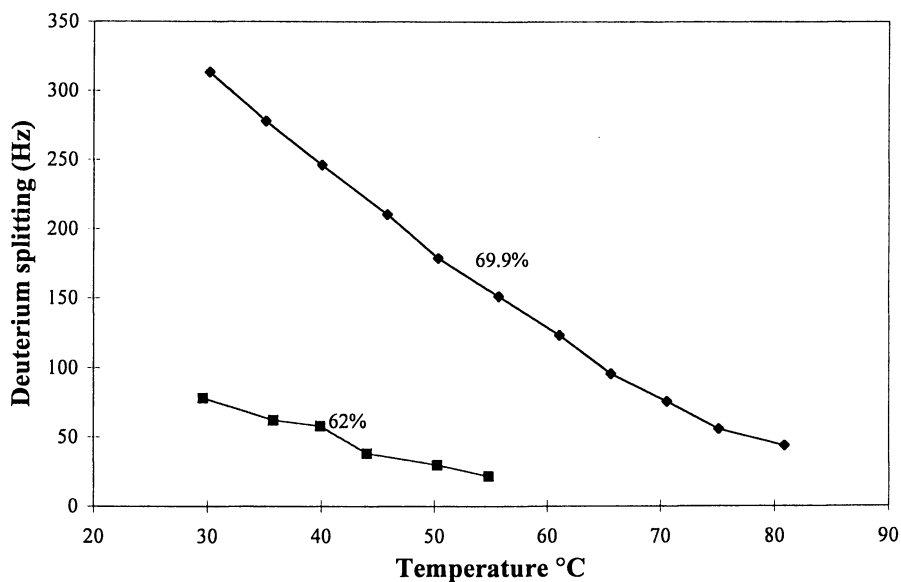


Figure 10. Deuterium splitting of 2D nucleus of HPC/D<sub>2</sub>O solutions versus temperature. Upper curve: HPC concentration = 69.9% (g/g). Lower curve: HPC concentration = 62% (g/g).

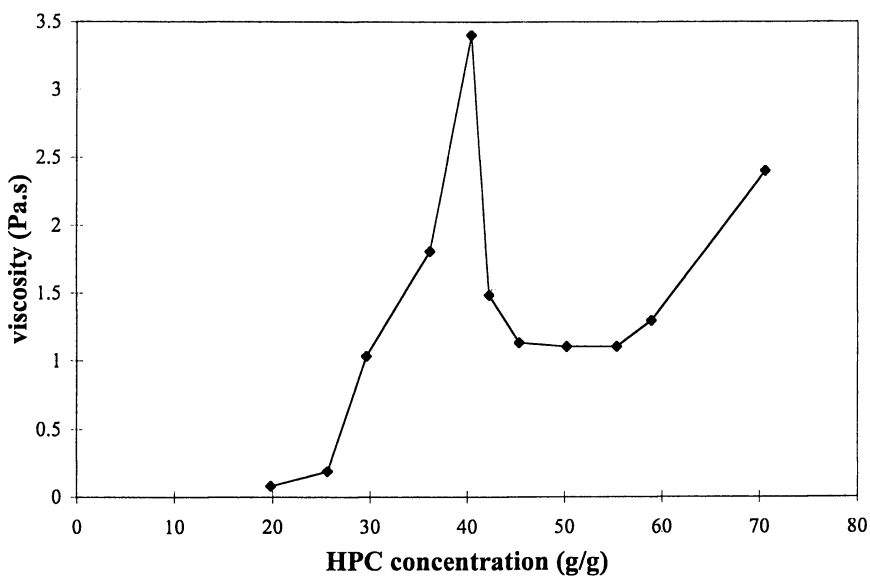


Figure 11. Shear viscosity versus concentration in HPC/water solutions.

- It appears that a relation between the pitch and the rigidity of the chains (or the concentration for the anisotropic phase appearance) is qualitatively possible. Often a larger pitch is found for chains of greater stiffness.

- The pitch also varies as a function of the molar mass of the polymer: for thermotropic cellulose derivatives, the short chain fraction shows the longest pitch.

- The effect of the molar volume of side groups on the chain appears to be important. If the substitution side chains are sufficiently cumbersome, a thermotropic film can be obtained.

- In lyotropic cellulosic mesophases the nature of solvent appears determinant on the pitch value as well as on the concentration of the mesophase appearance.

It must be also noticed that the very specific interactions between polymer-solvent (H bonds) also appear as an important factor for the pitch formation.

## **PRESENTATION OF AN EXAMPLE: MESOPHASES OF HPC AND ITS DERIVATIVES**

Hydroxypropyl cellulose (HPC) is the first derivative in which mesophase was observed. And among the cellulose derivatives it is also the most studied.

### 1/ HPC in solutions and blends

Various studies of lyotropic mesophases in different solvents, oligomers or polymers and in their mixtures were performed. The cholesteric phases are easy to obtain and can be seen as "model" for the analysis of several points such as defects, unwinding... Some previous figures illustrate some of these aspects.

### 2/ Ester derivatives of HPC

The range of temperatures where mesophases exist depends on a lot of macromolecular data (40): molar mass, degree of esterification, nature of grafted groups, etc. The larger the molar mass, the higher the clearing temperature is. For the superior molar mass (DP>50) a saturation of clearing temperature is observed. For a given molar mass, esterification is more or less extended. Glass transition decreases when the esterification degree is increasing. Temperature gap of the mesophase state is not strongly modified (around 150°C) by the number of carbons of the grafted groups. On the other hand, the number of carbons has strong influence on the optical properties (figure 13). The selective reflection can be situated in the visible or IR light spectra and between 20°C and 140°C. The higher the temperature, the stronger the cholesteric pitch

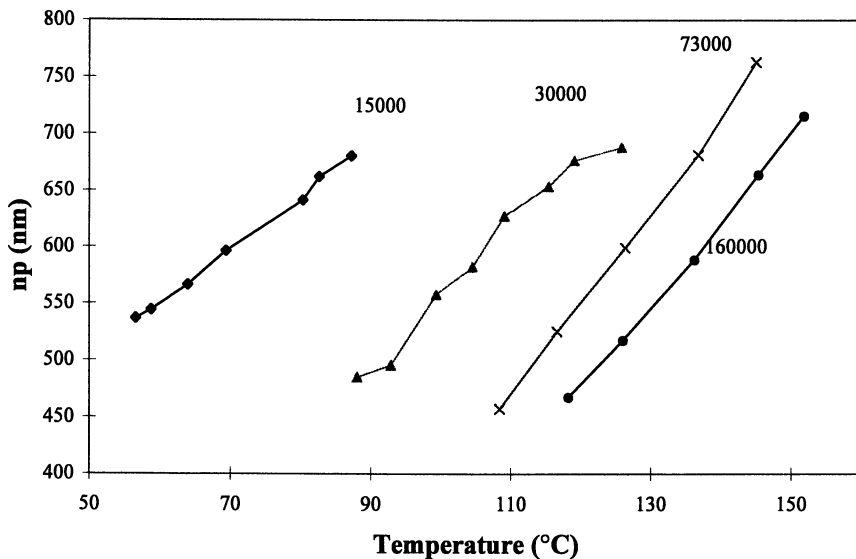


Figure 12. Pitch as function of temperature in acetoxypolypropylcellulose. The curves from left to right correspond to the following molar masses: 15000, 30000, 73000, 160000.

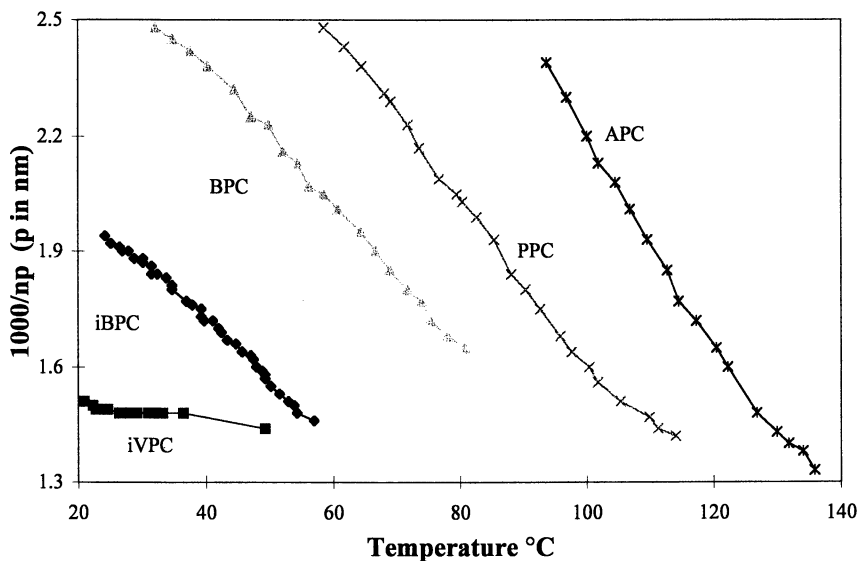


Figure 13. Pitch variation with temperature for several esters of HPC. From left to right: iVPC, iBPC, BPC, PPC, and APC. (Reproduced with permission from reference 41. Copyright 1994 Wiley.)

modification with temperature is. The absolute pitch value simply shows the steric bulk of side chains.

### 3/ Ether of HPC: mixtures and copolymers

Different ethers have been prepared (41). They are more stable than the esters for which hydrolysis of the esters linkage can occur. Like the esters, the ethers show interesting cholesteric optical properties (figure 14) : the pentyl compound is blue green at the ambient temperature and becomes red when the temperature is raised and finally, loses its color at 150°C. The butyl compound is blue at 85°C and changes its color when temperature is warmed up. The pitch variation with substitution degrees is opposite in ester and ether compounds. The higher the ether degree of substitution, the larger the pitch is. The higher the degree of esterification, the lower the pitch is. Optical properties of copolymers present an intermediate response between the two homopolymers response. The temperature range where we wish to operate selective reflection can be freely chosen and made through pertinent choice of the butyl /pentyl ratio.

Dynamical properties of selective reflection are also important. In order to reach them, a temperature jump can be quickly applied to homo or copolymers and the temporal modification of the selective reflection can be recorded. We observe that the response time of the pentyl homopolymer - and therefore its viscosity - is larger than the copolymer response time.

Miscibility of homopolymers gives us some detailed information about molecular interactions. Thermodynamical methods allow visualizing the demixtion process and its temporal dynamics. Using selective reflection can do this. It is shown that the formed mesophases obtained by the demixtion contains mainly an homopolymer but also some part of the other homopolymer.

### 4/ Mesophase containing fluorocarbon lateral chains

In order to obtain more organized and less viscous phases several esters of HPC and their homologue with fluorocarbon component can be synthesized (42). Two main observations must be retained (figure 15):

- Clearing temperature of fluorinated polymers are lower,
- The pitch of protonated ester polymer is bigger than the ether polymer one, which is itself bigger than the pitch of the fluorocarbon ester polymer (figure 16).

These observations suggest micro-segregation of end lateral chains and disentanglement which is more important in the fluorinated polymers than in the protonated ones.

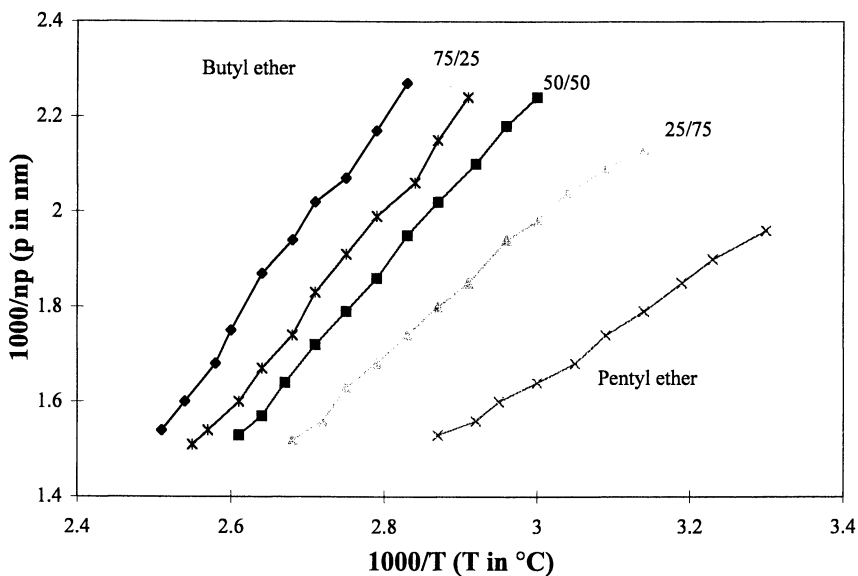


Figure 14. Pitch inverse versus temperature for butyl (left curve), pentyl (right curve) ether of HPC and copolymers (respectively 75/25, 50/50 and 25/75).

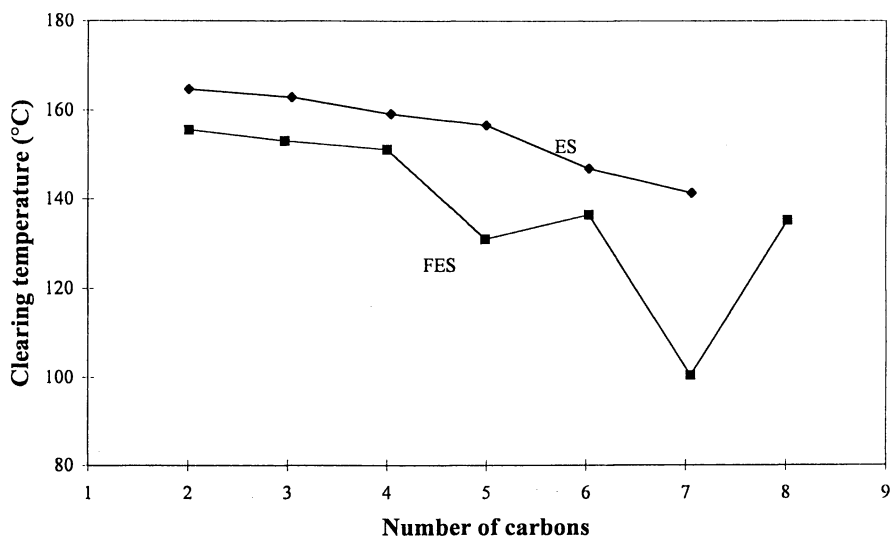


Figure 15. Clearing temperature of ester of HPC (ES) and their homologues with fluorocarbon (FES). (Reproduced with permission from reference 42. Copyright 1994 Springer-Verlag.)

## SOLID FILMS OBTAINED FROM THE MESOPHASES

The order of the mesophases strongly influences the order in solid phases (fibers, films, composites...) derived from these mesophases and thus their final properties (mechanical, optical, electrical...)

Three examples are selected in the following:

### 1/Crosslinked mesophases

Macromolecules of the ordered mesophase can be crosslinked (43). An efficient method consists in:

- substituting a part of the hydrogen bonding sites by a monofunctional chemical group,
- bounding macromolecules by bifunctional group acting on a part of free hydrogen bonding,
- achieving the substitution by monofunctional chemical groups identical to those of the first step.

This process was applied as well as esters than ethers. The networks also formed can be swollen and shrunked by solvents. The selective reflection is strongly modified in the swelling of the gel. In some cases, color disappears by swelling and appears again after solvent evaporation (figure 17). The network (swollen or not) can be also stretched. The birefringence of the film can be studied as a function of elongation using mechanical device operating in an optical microscope. Nature of bifunctional group and of lateral cellulose derivatives group has not a strong effect on birefringence. A strong effect is viewed with other parameters like: crosslinking in isotropic or anisotropic phases, bifunctional spacer concentration, stirring time. If the network, obtained by cross-linking polymers, is swollen or prepared in a nematic solvent, it is possible to obtain electro-optic effects like in PDLC (polymer dispersed liquid crystals) and PNLC (polymer network liquid crystals).

### 2/ Fibers obtained from cellulose mesophase

Structured fibers can be acquired from cellulosic mesophases. The orientation of molecules is strongly dependent on the spinning conditions. If the spinning is realized in anisotropic phase an improvement of mechanical properties is achieved. The threads show optical band structures, in some cases patterns with reminiscence of the chirality are obtained (figure 18).

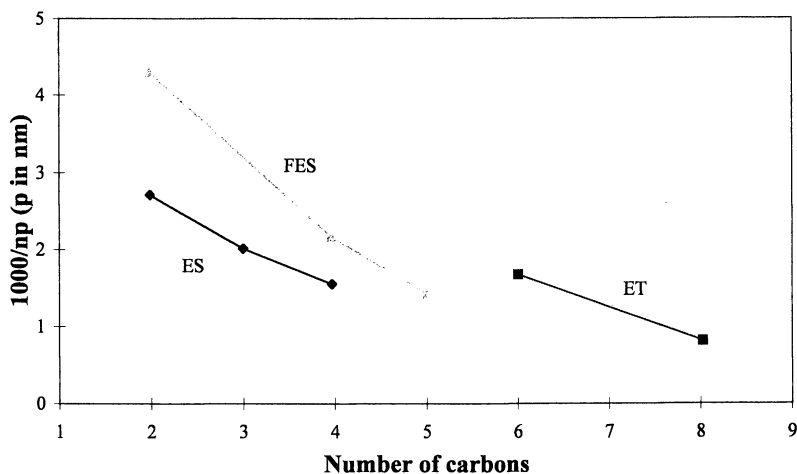


Figure 16. Pitch of ester of HPC (ES), their homologues with fluorocarbon (FES) and ether of HPC (ET) (Reproduced with permission from reference 42. Copyright 1994 Springer-Verlag.)

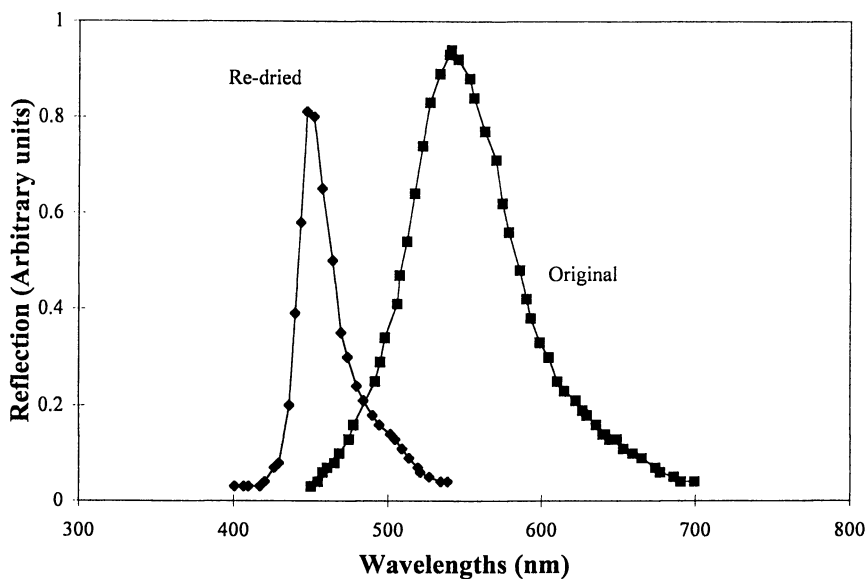


Figure 17. Reflection spectra of cross-linked HPC. Original gel before swelling (right). Gel dried again after swelling in THF (left). (Reproduced with permission from reference 43. Copyright 1995 Butterworth.)

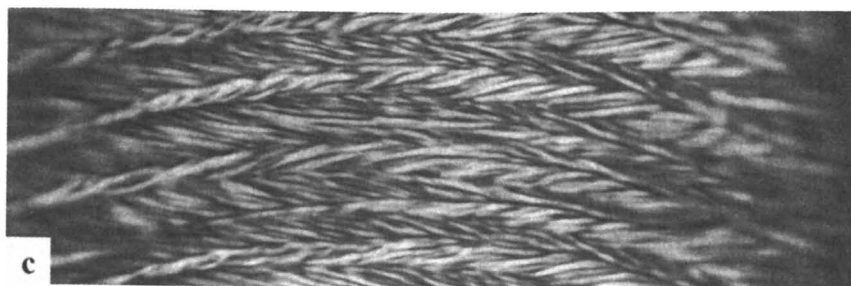
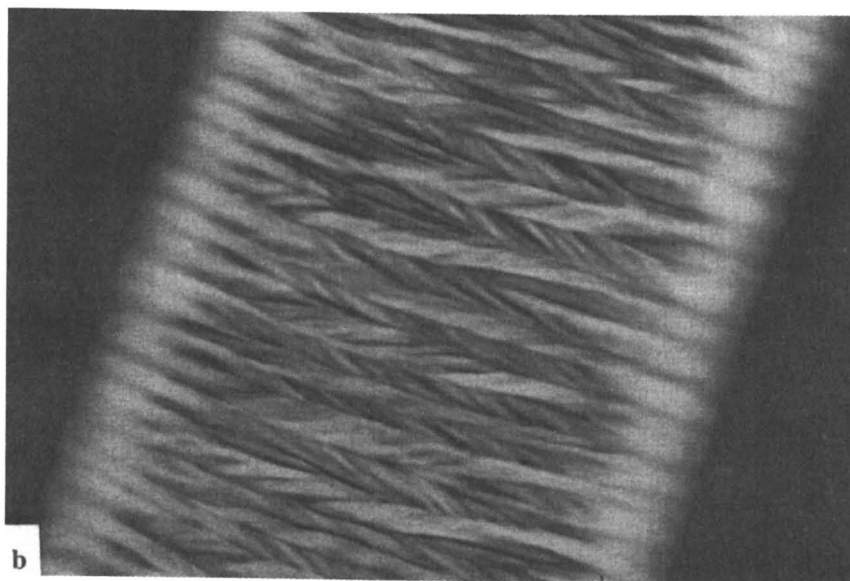
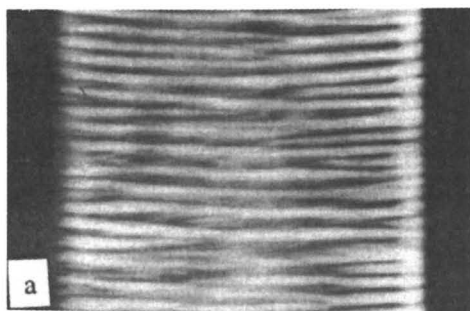


Figure 18. Observation of HPC threads and fibers.



## 2/ Solid films obtained from suspension of cellulose crystallites

Solid films can be prepared from colloidal suspensions of cellulose crystallites (44). The colloidal suspensions are prepared by acid hydrolysis of crystalline cellulose under carefully controlled conditions. At low concentration (few percents) the suspensions separate on standing into an upper isotropic phases and a lower anisotropic phase. The anisotropic phase shows cholesteric character. Furthermore this structure of the suspensions is preserved on careful drying to give a film of "paper" in which the cellulose crystallites are arranged in cholesteric order. This film can present selective reflections. The wavelength of the reflected light can be controlled to give colors across the visible spectrum and if necessary to ultraviolet and infrared wavelengths.

### **Conclusions**

The cellulosic polymers form a type of main chain liquid crystalline polymers. One of essential problems is to understand the relationship between the molecular structure and the properties of mesophases and their solids. Several experimental facts are arising:

- Both thermotropic and lyotropic behaviors in a large variety of solvents are found.
- Transition temperatures often appear at medium temperatures ( $O/100^{\circ}\text{C}$ ) and allow easy observation.
- The properties of mesophases can easily be changed by often minor modifications of the chemical structure (nature of substituent, degree of substitution, etc.).
- The cholesteric mesophases have interesting optical properties.
- The twist character of the mesophase is achieved at different scales such as oligomers, macromolecules or fibrils.

These chiral "objects" are thus often considered as good "model systems."

Several theoretical works predict the existence of mesophases and take into account the molecular structure of polymers.

At a fundamental level the answers to questions concerning several aspects of the cellulosic mesophases like kind of order in connection with chemical structure, gel cross-linking, modification of order by an external stress are still limited.

Some applications in very different fields (high modulus fibers, self-reinforced polymeric materials, thermochromic materials, electronic display devices, membranes, papers with optically variable properties, non-linear optics, materials having optical modification by swelling or with mechano and electro-optical properties... have already been realized or are being pursued.

## References

1. Werbowyj, R.S. Gray, D.G. *Mol. Cryst. Liq. Cryst.*, **1976**, *34 (Letters)*, 97.
2. Chanzy, H., Peguy, P., Chaunis, S., Monzie, P., *J. Polym. Sci. Polym. Phys. ed.*, **1980**, *18*, 1137.
3. Bhadani, S.N., Gray, D.G. *Mol. Cryst. Liq. Cryst.*, (*Letters*), **1984**, *102*, 255.
4. Bhadani, S.N., Gray, D.G., *Mol. Cryst. Liq. Cryst.*, **1983**, *99*, 29.
5. Gray, D.G., *Journal of Applied Polymer Science: Applied Polymer Symposium*, **1983**, *37*, 179.
6. Guo, I.-X., Gray, D.G., *Journal of Polymer Science: Part A: Polymer Chemistry*, **1994**, *32*, 889.
7. Gray, D.G., *Carbohydrate polymers*, **1994**, *25*, 277.
8. Gray, D.G., in *Cellulosic polymers, blends and composites*, Editor, Gilbert, D., Hanser/Gardner Publications
9. Gray, D.G., *Journal of Pulp and Paper Science*, **1989**, *15*, 3.
10. Gray D.G., in *Polym. Liq. Cryst. Polym. Sci. and Tech.*, **1985**, *Vol 28 (A)*. Blumstein ed. Plenum.
11. Hawkinson, D.E., Kohout, E., Fornes, R.E., Gilbert, R.D., *Journal of Polymer Science: Part B: Polymer Physics*, **1991**, *29*, 1599.
12. Gilbert, R.D., Patton, P.A. *Prog. Polym. Sci.*, **1983**, *9*, 115.
13. Bianchi, E. Ciferri, A. Conio, G. Lanzacecchia, L., Terbojevich. M. *Macromolecule*, **1986**, *19*, 630.
14. Kiss, G. Porter, R.S., *Mol Cryst. Liq. Cryst.*, **1980**, *60*, 267
15. Suto, S., *Journal of Applied Polymer Science*, **1989**, *37*, 2781.
16. Suto, S., Tashiro, H., Karasawa, M., *Journal of Applied Polymer Science*, **1992**, *45*, 1569.
17. Zugenmaier, P. Voihsel, M., *Macromol. Chem. Rapid Commun.*, **1984**, *5*, 245
18. Yamagishi, T., Fukuda, T., Miyamoto, T., Watanabe, J., *Mol. Cryst. Liq. Cryst.*, **1989**, *172*, 17
19. Yamagishi, T., Fukuda, T., Miyamoto, T., Watanabe, *Polym. Bull.*, **1988**, *20*, 373
20. Maret, G. Milas, M. Rinaudo, M., *Polym. Bull.*, **1981**, *4*, 291
21. Milas, M. Rinaudo, M., *Polym. Bull.*, **1983**, *10*, 27
22. Tsakalos, V.T., Navard, P., Peuvrel-Disdier, E, *Liquid Crystal*, **1996**, *21*, 663.
23. Bouligand, Y., *Solid State Physics*, **1978**, Supplement *14*, 259
24. Dayan, S., Maissa, P., Vellutini, M.J., Sixou, P., *Polymer*, **1982**, *23*, 800.
25. Fried, F., Searby, G.M., Seurin-Vellutini, M.J., Dayan, S., Sixou, P., *Polymer*, **1982**, *23*, 1755.
26. Yamakawa, H. Fujii, M., *Macromolecule*, **1973**, *6*, 407.
27. Kirkwood, F.G., Riseman, J., *J. Chem. Phys.*, **1948**, *16*, 565.
28. Sixou, P., ten Bosch, A., in *Cellulose: structure, modification, and hydrolysis*, Editor, R.A. Young, R.M. Rowell, Ed. ; Wiley, **1986**, p205-219.
29. d'Allest, J.F., Sixou, P., *Mol. Cryst. Liq. Cryst.*, **1988**, *157*, 229.
30. ten Bosch, A., Maissa, P., Sixou, P., *Phys Lett.*, **1983**, *94A*, 298.
31. Fried, F., Sixou, P., *J. Polym. Sci. Polym. Chem.*, **Ed**, **1984**, *22*, 239.
32. Maïssa, P., Seurin, M.J., Sixou, P., *Polymer Bulletin*, **1986** *15*, 257.
33. S. Ambrosino, T. Khallala, M.J. Seurin, A. ten Bosch, F. Fried, M. Maissa, P. Sixou, *J. Polym. Sci.*, **1987**, *25*, 351.
34. Maissa, P., Sixou, P., *Liquid Crystals*, **1989**, *5*, 1861.
35. S. Ambrosino, S. Murray, P. Sixou, *Polym. Networks Blends*, **1992**, *2*, 179.
36. Dayan, S., Fried, F. Gilli, J.M., Sixou, P., *J. Appl. Polym. Sci.*, **1983**, *37*, 193.
37. Fried, F., Sixou, P., *J. Polym. Sci.*, **1988**, *158B*, 163.
38. Maissa, P., ten Bosch, A., Sixou, P., *J. Polym. Sci.*, **1983**, *21*, 757.

39. Ambrosino, S., Sixou, P., *Journal of Polymer Science, Polymer Chemistry Edition*, 1994, 32, 77.
40. Rusig, I., Dedier, J., Filliatre, C., Godhino M.H., Varichon, L., Sixou, P., *Journal of Polymer Science: Part A: Polymer Chemistry*, 1992, 30, 895.
41. Russig, I., Godinho, M.H., Varichon, L., Sixou, P., Dedier, J., Filliatre, C., Martins, A.F., *Journal of Polymer Science: Polymer Physics*, 1994, 32, 1907.
42. Yamagishi, T.-A., Guittard, F., Godinho, M.H., Martins, A. F., Cambon, A., Sixou, P., *Polymer Bulletin*, 1994, 32, 47.
43. Yamagishi, T., Sixou, P., *Polymer*, 1995, 36, 2315
44. Giasson, J., Revol, J.F., Gray, D.G. *macromolecules*, 1991, 24, 1694.

## Chapter 12

# Chitosan–Pluronic Physical Interpenetrating Network: Membrane Fabrication and Protein Permeability Studies

Derrick Anderson, Tragiang Nguyen, and Mansoor Amiji

Department of Pharmaceutical Sciences, School of Pharmacy,  
Northeastern University, 110 Mugar Life Sciences Building, Boston, MA 02115

Chitosan-Pluronic<sup>®</sup> physical interpenetrating network (PIN) membranes were fabricated for potential use in microencapsulation of cells and tissues. Human serum albumin was used as a protein permeability marker to examine the permselective nature of the membranes. Scanning electron micrographs showed distinct porous surfaces and cross-sections in chitosan-Pluronic PIN membranes. The swelling studies showed that chitosan-Pluronic membranes, containing 20% (w/w) Pluronic F-108 had swollen extensively as compared to the control chitosan membranes in phosphate-buffered saline (pH 7.4) due to the porosity of the matrices. The permeability coefficient of albumin increased from  $2.7 \times 10^{-8}$  cm<sup>2</sup>/min in chitosan membrane to  $5.47 \times 10^{-7}$  cm<sup>2</sup>/min in chitosan-Pluronic PIN membrane made with 20% (w/w) Pluronic F-108. Based on the choice of Pluronic polyol and the concentration used, the results of this study clearly show that the PIN membranes can be designed for selective permeation of microencapsulated products, while restricting immune recognition elements from going inside.

Drugs with short duration of action, narrow therapeutic index, those that require site-specific delivery, or those that are difficult to formulate as a stable product can be released from transplanted cells or tissues. One of the major limitation of *in vivo* cell therapy is the potential for rejection by the host unless accompanied with chronic immunosuppressive treatment protocol (1). This could be avoided if the foreign tissue is isolated from the host immune system by a permselective membrane which allows for transfer of nutrients and cell products, but is impermeable to the immune recognition elements. Sefton and co-workers (2) have developed biocompatible microcapsules from poly(2-hydroxyethyl methacrylate) and poly(methyl methacrylate) with controlled morphology and porosity for selective permeation. A number of different cell types can be considered as candidates for microencapsulation. The use of alginate-poly(L-lysine) system for encapsulation of the  $\beta$  Islet cells by Sun and co-workers (3) was used to restore normoglycemia in diabetic rodents over an extended period of time. Recently, other cell types, including hepatocytes (4,5) and dopamine-secreting cells (6,7) have been encapsulated to

normalize metabolic deficiencies or act as a self-regulating drug delivery system. In addition, cells and tissues can be genetically engineered prior to encapsulation to release the product of interest (8,9).

Based on the need for biocompatible polymeric materials that could be used for cell or tissue encapsulation under mild conditions, we have examined the role of chitosan in this area. Chitosan, a linear copolymer of D-glucosamine, is obtained by alkaline N-deacetylation of chitin (Figure 1). Chitin is the second most abundant polymer from nature, predominantly isolated from the exoskeleton of marine crustaceans such as crabs, shrimps, and krill (10). A variety of medical and pharmaceutical applications of chitosan have been proposed based on the chemical and physical properties of the polymer (11,12). Since the  $pK_a$  of the primary amine functional group of D-glucosamine is about 6.5 (13), chitosan is positively charged in dilute acidic solutions. The cationic property of chitosan allows it to form complexes with anionic polymers by electrostatic interactions. Chitosan microcapsules have been formed by complex coacervation with a number of polyanions including sodium alginate (14,15), sodium carboxymethylcellulose (16), chondroitin sulfate (17), and poly(acrylic acid) (18).

In a previous study, we have observed that the permeability coefficient of high molecular weight compounds (e.g., vitamin B-12, Mol. wt. 1,355 daltons) through chitosan membrane was significantly lower than through cellulose (Cuprophane<sup>®</sup>) membrane (19,20). To increase the permeability of products secreted from the encapsulated cells, in the present study, we have incorporated Pluronic<sup>®</sup> polyols with chitosan prior to membrane formation. Calvo *et al.* (21) have prepared chitosan-Pluronic nanoparticles for use as mucosal vaccine delivery systems. Pluronics are poly(ethylene oxide)/poly(propylene oxide)/poly(ethylene oxide) (PEO/PPO/PEO) triblock copolymers that are available with different chain lengths of the PEO and PPO segments (Figure 1). We have fabricated chitosan-Pluronic physical interpenetrating network (PIN) by blending chitosan acetate with either Pluronic F-68 or F-108, casting the membrane, and neutralizing the acetate salt. Pluronic F-68 (PF68, Mol. wt. 8,350 daltons) has 75 ethylene oxide (EO) residues and 30 propylene oxide (PO) residues. In contrast, Pluronic F-108 (PF108, Mol. wt. 14,000 daltons) has 122 EO residues and 56 PO residues (22). The intermolecular hydrogen bonding interactions between chitosan and Pluronic polyol chains results in the formation of PIN (Figure 2). We have examined the surface and cross-section morphology and the permeability of human serum albumin through the chitosan-Pluronic PIN membranes.

## MATERIALS AND METHODS

**Materials.** Chitosan with a viscosity-average molecular weight of 750,000 daltons and a degree of deacetylation of 87.6% was obtained from Pronova Biopolymers (Raymond, WA). Pharmaceutical grade of PF68 and PF108 were kindly supplied by the BASF Corporation (Parsippany, NJ). Human serum albumin (Fraction V), purchased from Sigma Chemical Company (St. Louis, MO), was purified by equilibrium dialysis against phosphate-buffered saline (PBS, pH 7.4). Deionized distilled water (NanoPure II, Barnsted/Thermolyne, Dubuque, IO) was used to prepare all aqueous solutions. All other chemicals were of standard analytical grade and were used as received.

**Membrane Fabrication.** Chitosan was dissolved in 0.10 M acetic acid to prepare a 1.0% (w/v) solution. The polymer was purified from proteins and inorganic impurities by precipitation in 0.10 M sodium hydroxide, followed by washing with deionized distilled water, and freeze-dried. One-hundred mg of purified chitosan, dissolved in 10 ml of 0.10 M acetic acid, was allowed to spread evenly on a polystyrene petri dish. In some instances, PF68 or PF108, dissolved in 0.10 M acetic

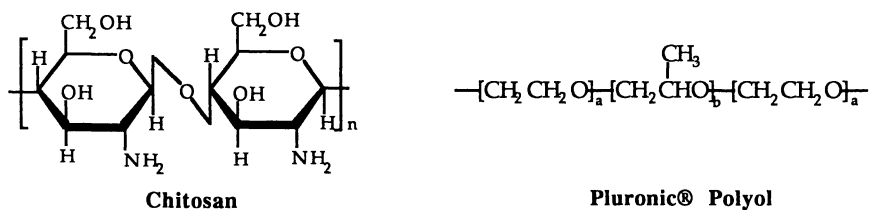


**Figure 1:** The chemical structures of chitosan and Pluronic® polyol.

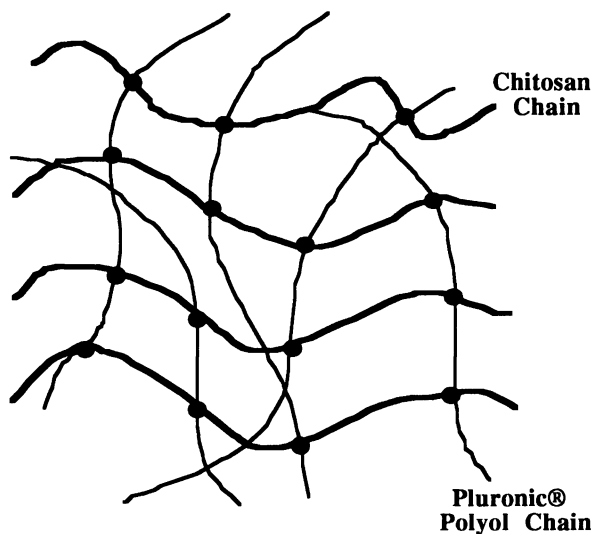


**Figure 2:** Schematic representation of the physical interpenetrating network formed by intermolecular hydrogen bonding between chitosan and Pluronic® polyol. The closed circles indicate potential points of contact between the two polymer chains.

acid, was added to the chitosan solution to give a final Pluronic concentration ranging from 10% (w/w) to 30% (w/w). After drying at room temperature for approximately 48 h, the acetate salt of chitosan was neutralized in 0.10 M sodium hydroxide. During the neutralization step, chitosan is expected to form intermolecular hydrogen bonding interactions with the Pluronic polyols leading to the formation of PIN. After extensively washing the control and chitosan-Pluronic PIN membranes in deionized distilled water, they were stored wet at 4°C.

**Scanning Electron Microscopy (SEM) Analysis.** Control and chitosan-Pluronic PIN membranes were air-dried for about 48 h. The samples were mounted on a aluminum sample mount and sputter-coated with gold-palladium. The coated samples were observed with a AMR 1000 (Amray Instruments, Bedford, MA) scanning electron microscope at 10 kV accelerating voltage. The original magnification of the surface and cross-section SEM images of the membranes were 12,500X and 5,000X, respectively.

**Equilibrium Swelling Studies.** The samples of control and chitosan-Pluronic PIN membrane were air-dried for up to 48 h. After carefully weighing the membrane samples, each was placed in 50 ml of PBS for 24 h at room temperature. Equilibrium swelling ratio ( $Q$ ) of the membranes was calculated as follows:

$$Q = W_s/W_d$$

where  $W_s$  is the weight (in grams) of the swollen membrane and  $W_d$  is the weight of the dry membrane.

**Albumin Permeability Studies.** The permeability coefficient of human serum albumin was determined through the control and chitosan-Pluronic PIN membranes using a temperature-controlled side-by-side diffusion apparatus. Fifteen ml of albumin (1.0 mg/ml) solution was placed in the donor compartment of the diffusion apparatus. The receptor compartment, separated by a pre-hydrated membrane, was filled with 15 ml of PBS. Both sides of the dialysis apparatus, maintained at 37°C, were continuously stirred to assure uniform protein distribution during the experiment. At pre-determined time intervals, 1.0 ml of the sample from the receptor compartment was removed and the absorbance of albumin at 280 nm was measured with a Shimadzu 160U (Columbia, MD) UV/VIS spectrophotometer. The concentration of albumin in the receptor compartment was calculated using the specific absorptivity of 0.58 cm<sup>2</sup>/mg (23). The permeability coefficients of albumin through the control and chitosan-Pluronic PIN membranes were calculated according to the following equation (24):

$$\ln(C_0/C_t) = PSt/IV$$

where  $C_0$  is the initial concentration of albumin in the donor compartment,  $C_t$  is the concentration at any time  $t$ ,  $P$  is the permeability coefficient (in cm<sup>2</sup>/min),  $S$  is the surface area of the membrane (1.77 cm<sup>2</sup>),  $V$  is the volume of solution in the donor compartment (15 ml), and  $l$  is the wet-thickness of the membrane (~15 μm). Plots of  $\ln(C_0/C_t)$  versus (dialysis time/membrane thickness) were constructed and the slope of the line was used to calculate  $P$ . The results represent the average permeability coefficient (± S.D.) of albumin from three independent experiments.

## RESULTS AND DISCUSSION

**SEM Analysis.** The surface and cross-section morphology of the control and chitosan-Pluronic IPN membranes, as analyzed by SEM, is shown in Figure 3. Chitosan membrane had a very smooth surface and cross-section (Fig. 3-A and B). These observations are consistent with our previous work (19) and suggest that during the air-drying process, inter- and intramolecular hydrogen bonding interactions in chitosan may result in the formation of a highly crystalline matrix. The addition of PF68 and PF108, on the other hand, resulted in the formation of porous membranes. The surface of chitosan-Pluronic PIN membranes made with PF68 (Fig. 3-C) showed distinct pores that extended into the matrix (Fig. 3-D). Chitosan-Pluronic PIN membranes made with PF108 had similar surface and cross-section morphology. Since Pluronic polyols are known to form macromolecular aggregates in aqueous solution due to the hydrophobic interactions between the PPO segments (25), we speculate that these aggregates are responsible for pore formation in these membranes. Based on the selection of Pluronic polyol with the appropriate PEO and PPO chain lengths, it may be possible to develop membranes with controlled porosity for selective permeation of microencapsulated products.

**Swelling Studies.** The degree of hydration of polymeric materials is an indirect measure of the hydrophilicity of the membrane and the mechanical strength. As shown in Table 1, the equilibrium swelling ratio of control chitosan membranes was 2.38. The ratio increased to 3.66 and 4.88 upon incorporation of 20% (w/w) PF68 and PF108, respectively. The increase by more than 51% in the equilibrium swelling ratio in chitosan-PF108 PIN membranes was probably due to the significant increase in the hydrophilicity and extensive porosity of the matrix which allows more aqueous medium to imbibe. Although the swelling ratio did continue to increase with increasing the concentration of Pluronic, the mechanical strength of the membranes was significantly compromised when the concentrations exceeded 30% (w/w).

**Table 1.** Swelling of the control and chitosan-Pluronic<sup>®</sup> physical interpenetrating network membranes<sup>a</sup>.

| Membrane Type  | Swelling Ratio           |
|----------------|--------------------------|
| Chitosan       | 2.38 ± 0.25 <sup>b</sup> |
| Chitosan-PF68  | 3.66 ± 0.50              |
| Chitosan-PF108 | 4.88 ± 0.34              |

<sup>a</sup> The swelling studies were carried out in phosphate-buffered saline (pH 7.4) with the control and chitosan-Pluronic membranes containing 20% (w/w) Pluronic polyols.

<sup>b</sup> Mean ± S.D. (n = 4).

**Permeability Studies.** Human serum albumin (Mol. wt. 68,000 daltons) was used as a model protein to investigate the permeability properties of chitosan-Pluronic PIN membranes for potential use as a material for cell or tissue encapsulation. The permeability coefficient of albumin in chitosan membrane, as shown in Table 2, was  $2.70 \times 10^{-8}$  cm<sup>2</sup>/min. In contrast, the permeability coefficient increased to  $1.03 \times 10^{-7}$  cm<sup>2</sup>/min and  $5.47 \times 10^{-7}$  cm<sup>2</sup>/min when PF68 and PF108, respectively, were incorporated at 20% (w/w). Increasing the concentration of Pluronic above 20% (w/w), however, did not have a significant effect on the permeability coefficient of albumin (Figure 4). The increased hydrophilicity and porosity of the PIN membranes



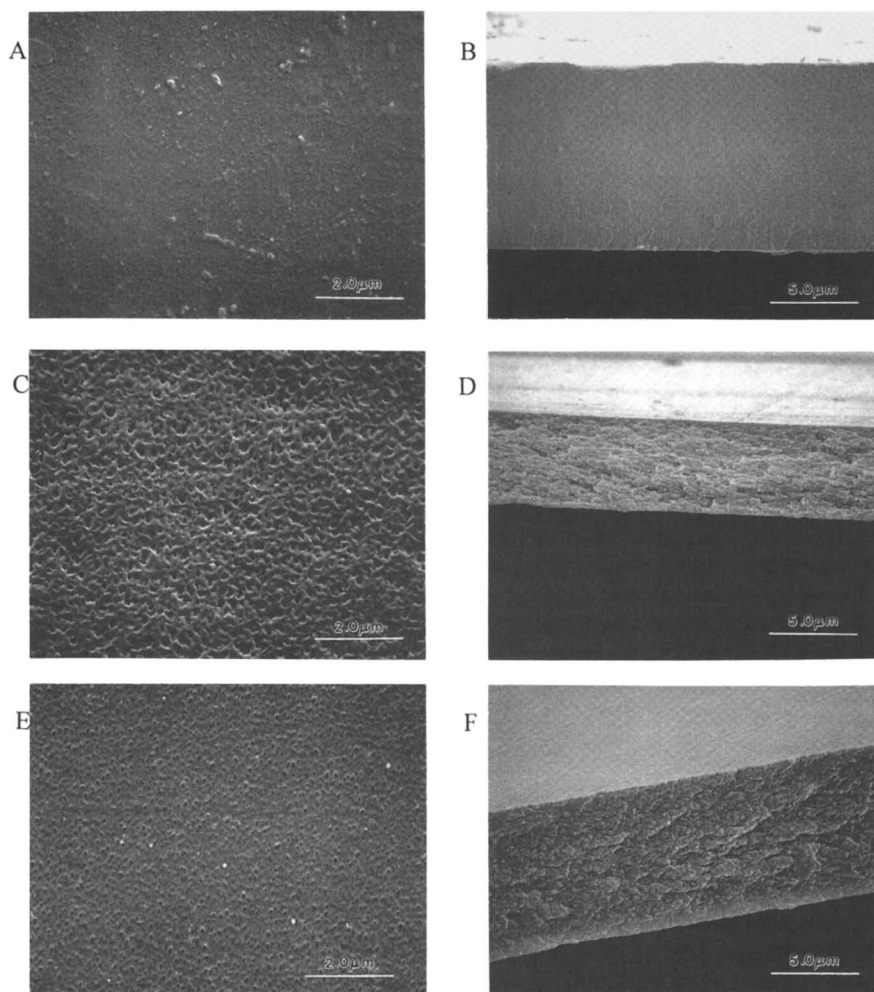


**Figure 3:** Scanning electron micrographs of the surfaces (A,C,E) and cross-sections (B,D,F) of chitosan (A,B) and chitosan-Pluronic physical interpenetrating network (PIN) membranes. The PIN membranes were formed with Pluronic F-68 (C,D) and F-108 (E,F) at 20% (w/w) concentration. Original magnification of the surface and cross-section images were 12,500X and 5,000X, respectively.

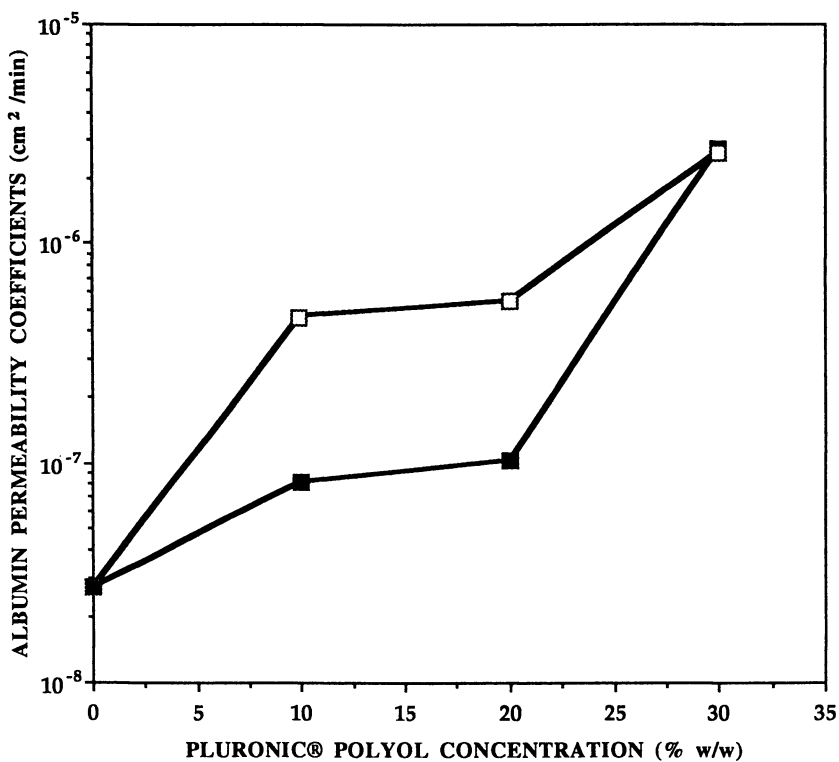


**Figure 4:** Change in the permeability coefficient of human serum albumin in chitosan-Pluronic<sup>®</sup> physical interpenetrating network (PIN) as a function of the concentration of incorporated Pluronic<sup>®</sup> polyol. The PIN membranes were made with Pluronic F-68 (■) and F-108 (□).

allowed for much rapid permeation of albumin as compared to the control. Based on the results of this study, it is possible to design chitosan-Pluronic PIN membranes with controlled pore sizes using different types of Pluronic that vary in the PEO and PPO chain lengths and the concentration of the Pluronic used in the PIN. When used for microencapsulation, these membrane will be beneficial for their selective permeation properties where it is possible for the products from the cells or tissues to diffuse out of these membranes, but the immune recognition elements would not be able to get inside.

**Table 2.** Permeability coefficients of human serum albumin through the control and chitosan-Pluronic<sup>®</sup> physical interpenetrating network membranes<sup>a</sup>.

| Membrane Type  | Permeability Coefficient<br>(cm <sup>2</sup> /min x 10 <sup>7</sup> ) |
|----------------|---|
| Chitosan       | 0.27 ± 0.05   |
| Chitosan-PF68  | 1.03 ± 0.45   |
| Chitosan-PF108 | 5.47 ± 0.56   |

<sup>a</sup> The concentration Pluronic polyols in the chitosan-Pluronic physical interpenetrating network membranes was 20% (w/w).

<sup>b</sup> Mean ± S.D. (n = 3).

## CONCLUDING REMARKS

We have fabricated chitosan-Pluronic PIN membranes for selective permeation of products from microencapsulated cells and tissues. Unlike chitosan membranes which are non-porous, the PIN membranes made with PF68 or PF108 had a porous surface and cross-section. Due to the porous nature of the PIN membranes, the permeability coefficient of albumin increased significantly as compared to the control. The results of this study show that chitosan-Pluronic PIN membranes can be designed for selective permeation of nutrients and products from microencapsulated cells, while restricting the immune recognition process. We are currently investigating the molecular weight cut-off of the PIN membranes prepared with ten different Pluronic varying in the PEO and PPO segment lengths and the concentration of the Pluronic in the PIN membrane.

## ACKNOWLEDGMENTS

This study was supported by the Northeastern University's Research and Development grant and by the Honors Program.

## REFERENCES

1. W.T.K. Stevenson and M.V. Sefton. *TRIP* **2**: 98 (1994).
2. C.A. Crooks, J.A. Douglas, R.L. Broughton, and M.V. Sefton. *J. Biomed. Mater. Res.* **24**: 1241 (1990).
3. F. Lim and A. Sun. *Science* **210**: 908 (1980).
4. H.W.T. Matthew, S.O. Salley, W.D. Peterson, D.R. Deshmukh, A. Mukhopadhyay, and M.D. Klein. *ASAIO Trans.* **37**: M328 (1991).
5. V. Dixit and G. Gitnick. *J. Biomater. Sci., Polym. Edn.* **7**: 343 (1995).
6. P. Aebischer, L. Wahlberg, P.A. Tresco, and S.R. Winn. *Biomaterials* **12**: 50 (1991).

7. E.G. Campioni, J.N. Nobrega, and M.V. Sefton. *Biomaterials* **19**: 829 (1998).
8. D. Basic, I. Vacek, and A.M. Sun. *Artif. Cells Blood Substit. Immobil. Biotechnol.* **24**: 219 (1996).
9. P.L. Chang. *Ann. NY Acad. Sci.* **831**: 461 (1997).
10. R.A.A. Muzzarelli, C. Jeuniaux, and G.W. Gooday (eds.). *Chitin in Nature and Technology*. Plenum Press, Inc. New York, NY. 1986.
11. T. Chandy and C.P. Sharma. *Biomat. Art. Cells Art. Org.* **18**: 1 (1990).
12. Y. Shigemasa and S. Minami. *Biotechnol. Genetic Engr. Revs.* **13**: 382 (1995).
13. P.M. Claesson and B.W. Ninham. *Langmuir* **8**: 1406 (1992).
14. M.M. Daly and D. Knorr. *Biotechnol. Prog.* **4**: 76 (1988).
15. B.A. Zielinski and P. Aebischer. *Biomaterials* **15**: 1049 (1994).
16. T. Yoshioka, R. Hirano, T. Shioya, and M. Kako. *Biotechnol. Bioengr.* **35**: 66 (1990).
17. H.W. Matthew, S.O. Salley, W.D. Peterson, and M.D. Klein. *Biotechnol. Prog.* **9**: 510 (1993).
18. V. Chavasit and J.A. Torres. *Biotechnol. Prog.* **6**: 2 (1990).
19. M.M. Amiji. *Biomaterials* **16**: 593 (1995).
20. M.M. Amiji. *J. Biomat. Sci., Polymer Edn.* **8**: 281 (1996).
21. P. Calvo, C. Remuñan-Lopez, J.L. Vila-Jato, and M.J. Alonso. *Pharm. Res.* **14**: 1431 (1997).
22. M. Amiji and K. Park. *Biomaterials* **13**: 682 (1992).
23. E. Brynda, N.A. Cepalova, and M. Stol. *J. Biomed. Mater. Res.* **18**: 685 (1984).
24. M.T. Qureshi, H.S. Blair, and S.J. Allen. *J. Appl. Polym. Sci.* **46**: 263 (1992).
25. M. Amiji and K. Park. *J. Appl. Polym. Sci.* **52**: 539 (1994).

## Chapter 13

# Interactions between Cyclodextrins and a Mixed Cationic Cellulose Ether: Anionic Surfactant Gelling System

Paschalis Alexandridis <sup>1</sup>, Sungsook Ahn <sup>1</sup>, and Marina Tsianou <sup>2</sup>

<sup>1</sup> Department of Chemical Engineering,  
State University of New York at Buffalo, Buffalo, NY 14260-4200

<sup>2</sup> Physical Chemistry 1, Center for Chemistry and Chemical Engineering,  
Lund University, Lund S-22100, Sweden

The intermolecular interactions in aqueous solutions containing polyelectrolytes, surfactants, and cyclodextrins were probed using rheology. The association of surfactant aggregates with the oppositely charged polymer leads to points of physical crosslinking and to a viscosity increase. Cyclodextrins can control this viscosity enhancement by forming inclusion complexes with the hydrophobic moieties of surfactants and thus disrupting the network formed by the surfactants and the polymers. We found the concentration of cyclodextrin required to "deactivate" the surfactant to be approximately double the surfactant concentration.  $\beta$ -CD is more effective than  $\alpha$ -CD in reducing the solution viscosity. The molecular recognition abilities of cyclodextrin can be exploited in modifying the solution properties and functionality of polymers.

### Introduction

Polymers that dissolve or swell in water are used in a great variety of products, e.g., cosmetics and pharmaceuticals, and in processes such as oil production and mineral processing. Most applications of water-soluble polymers arise from their solution properties, and especially from their ability to modify the rheology of an aqueous medium and/or to adsorb from solution onto particles or surfaces (1-4). Many important water-soluble polymers are obtained from natural sources, either directly, e.g., polysaccharides and proteins, or following modification, e.g., cellulose ethers and starch derivatives (5). Water-soluble cellulose derivatives like hydroxyethyl cellulose (HEC) have traditionally been used as thickeners in food and cosmetic products, as protective colloids in polymerization processes and as

thickeners in water-based paints. In order to improve their ability to impart the desired rheological properties to different industrial formulations, the HEC samples are often modified by ionic and/or hydrophobic groups (6).

In the various applications, water-soluble polymers are often used in conjunction with surfactants. The interactions between the polymer and the surfactant play an important role in these cases (7-11). Surfactant molecules, at a certain critical aggregation concentration (CAC), interact with polymers and form micelle-like aggregates with them. CAC is usually considerably lower than the critical micellization concentration (CMC) of the corresponding surfactants in the absence of polymer. The interaction has been shown to depend on the relative charge and the hydrophobicity of the polymer-surfactant pair (7,8). In the case of mixtures of an ionic polymer (polyelectrolytes) and a charged surfactant, these interactions are predominately electrostatic in nature. Association between polyelectrolytes and surfactants of the same charge is expected to be weak or even absent due to the unfavorable electrostatic repulsions, and can only occur when the polymer has a very pronounced hydrophobic nature. On the other hand, strong interactions are observed in mixtures of polyelectrolytes with oppositely charged surfactants since the complexes formed are stabilized by both electrostatic attractions and cooperative hydrophobic effects (8).

One of the consequences of the strong interaction in mixtures of oppositely charged polyelectrolyte and surfactant (e.g., a cationic polyelectrolyte and an anionic surfactant) is a pronounced enhancement of the solution viscosity and the formation of a gel based on a three-dimensional network (8,11). The crosslinks responsible for the gel are not permanent but are based on the electrostatic association between (negatively-charged) surfactant assemblies and (positively charged) polyelectrolyte chains. The ability to control the rheological properties, e.g., to form or destroy a gel on demand, is important in applications (1-4). Since the addition of a surfactant to the polymer solution results in the formation of a gel, the removal of the surfactant should have the opposite effect, i.e., destroy the gel. However, the removal of the surfactant from a formulation that contains numerous other compounds is not practical. An easier approach would be to "deactivate" the surfactant by adding an appropriate molecule to the solution. Cyclodextrins are molecules that can achieve such "deactivation".

Cyclodextrins (denoted here as CDs) are cyclic oligomers of  $\alpha$ -D-glucose;  $\alpha$ -CD and  $\beta$ -CD have six and seven glucose units, respectively. CDs are doughnut-shaped molecules with a fairly polar exterior and a nonpolar interior (cavity). CDs have been studied as "hosts" for "guest" molecules capable of entering (in whole or in part) their cavity and forming noncovalent host-guest inclusion complexes (12,13). The structure of the complex is determined by an energetic balance between maximal inclusion of guest nonpolar surface area in the host CD cavity, and optimal mutual orientation of host and guest to permit interactions of polar portions of the guest with the CD or the solvent. The molecular recognition between the host CD and the guest is thus amenable to rational design, according to specific needs. CDs and their derivatives are used in pharmaceutical formulations, personal care products, and foods, to increase or reduce the

"availability" (e.g., solubility in water) of active substances (e.g., drugs, flavors) or to stabilize/protect active substances ("molecular encapsulation") (14-16).

A number of publications have discussed the inclusion complex formation between CDs and small organic guest molecules (12). The addition of CDs to an aqueous solution of surfactant dramatically affects the physicochemical properties of the solution (12). The reason for these changes is the ability of CDs to screen the hydrophobic moieties of the surfactant molecules from contact with the surrounding aqueous media by the formation of an inclusion complex in which the hydrophobic chain of the surfactant is inserted into the CD cavity. As a consequence of complex formation, the surface tension of the surfactant solution usually increases, suggesting that neither the surfactant-CD complexes, nor the CDs are surface active. In the presence of CDs, the micelles are destroyed and the CMC is shifted towards higher concentrations (12).

Motivated from the ability of cyclodextrins to "deactivate" surfactants (in terms of their hydrophobic interactions), we explored the potential of cyclodextrins in controlling the viscosity enhancement caused by surfactants in mixtures with oppositely charged polyelectrolytes (17). In addition to the control of the rheological properties, our investigation is of general interest to formulations that contain cyclodextrins, surfactants, and associating polymers. Despite their significance, to the best of our knowledge, no studies on the interactions of cyclodextrins and mixtures of associating polymer and surfactant are available in the literature. Here we present information on the effects of cyclodextrins on the system of the cationic hydroxyethyl cellulose polymer, commercially denoted as JR400, and the anionic surfactant sodium dodecyl sulfate (SDS), that exhibits gelation in aqueous solution (18).

## Materials and Methods

**Materials.** The cationic polymer JR400 was supplied by Amerchol, Union Carbide Chemicals and Plastics Company, USA, and was used after purification by dialysis against MilliQ-treated water in a Filtron Ultraset device, followed by lyophilization. JR400 is the chloride salt of a *N,N,N*-trimethylammonium derivative of hydroxyethyl cellulose (HEC) with a molecular weight of approximately 500 000 (see Figure 1 for the nominal chemical structure of JR400) (18). An aqueous solution of 1 wt% polymer bears a charge concentration of 10 mM, and the mean contour length between charges is 20 Å. Sodium dodecyl sulfate (SDS), specially pure, was purchased from BDH Chemicals and used as received. The  $\alpha$ - and  $\beta$ -cyclodextrins were obtained from Cyclolab, Hungary, and were used without further purification.  $\alpha$ -Cyclodextrin ( $\alpha$ -CD) with six glucose units (also named cyclohexaamylose or cyclomaltohexaose) has a molecular weight of 972.9 and its solubility in water is 14.5 wt%, while  $\beta$ -cyclodextrin ( $\beta$ -CD), containing seven glucose units (cycloheptaamylose or cyclomaltoheptaose) and with molecular weight of 1135, is about ten times less soluble in water (solubility = 1.8 wt %) (13). The dimensions of the

central cavity of the cyclodextrin molecule are 4.7 - 5.3 and 6.0 - 6.5 Å for  $\alpha$ -CD and  $\beta$ -CD, respectively (15). Figure 2 shows the chemical structure and the toroidal shape of the  $\beta$ -CD molecule.

**Sample Preparation.** All samples were individually prepared by mixing concentrated stock solutions of polymer, surfactant, and  $\alpha$ - and  $\beta$ -cyclodextrins at differing ratios, in order to achieve the desired final composition. The water used was of MilliQ quality. The mixtures were homogenized by stirring, or by centrifugation in alternating directions (in the case of viscous samples), and then left to equilibrate at 25 °C for at least 1 week. After equilibration, the samples were centrifuged for at least 24 hours and the phase behavior was determined by visual inspection. All the samples discussed here were one-phase, homogeneous and clear.

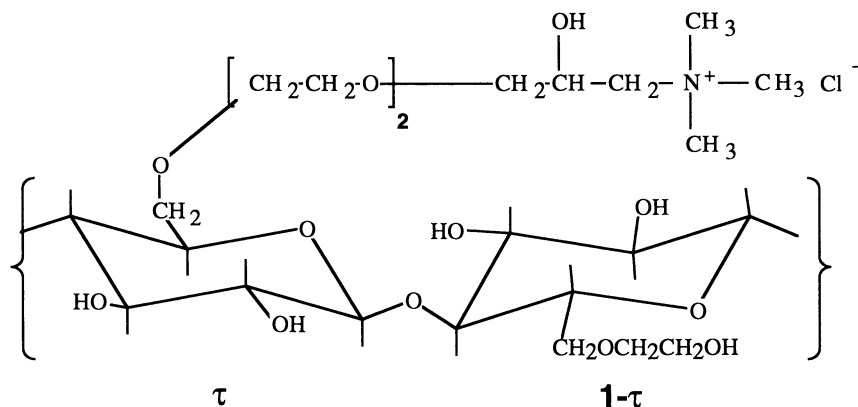
**Rheology.** Rheological measurements were conducted on a controlled stress Carri-Med CSL 100 rheometer (TA Instruments, UK), equipped with automatic gap setting. A cone and plate geometry of 4 cm (1°), or 6 cm (1°), depending on the viscosity of the sample, was used as the measuring system. The temperature in the sample chamber was controlled to within  $\pm 0.1$  °C with the aid of a Peltier plate. All rheological measurements were performed at 25 °C. The shear rate dependent measurements of the viscosity were recorded in the range 0.01 - 2000 s<sup>-1</sup>. Since most of the polymer-surfactant mixtures used in this study are highly viscous shear thinning samples, occasionally it was not possible to locate the Newtonian plateau at which the zero-shear viscosity,  $\eta_0$ , is determined. In such cases the viscosity at low shear rates is reported.

## Results and Discussion

**Increase in Solution Viscosity by the Addition of SDS to JR400.** The effect of added SDS on the JR400 solution viscosity is illustrated in Figure 3. The viscosity of 1 wt% JR400 aqueous solution is about 30 times higher than that of pure water, given the high molecular weight and polyelectrolyte nature of the polymer. A pronounced increase in viscosity, by almost three orders of magnitude, is observed when up to 2.5 mM SDS is added to the JR400 solution, indicating the formation of gels that become stronger as the SDS concentration increases. As shown in the viscosity vs shear rate plot of Figure 3a, the system behaves in a Newtonian fashion at low shear rates (less than 1 s<sup>-1</sup>), but is strongly shear-thinning at high shear rates. Indeed, most systems that form a gel based on physical association are shear-sensitive. The transition to shear-thinning occurs at lower shear rates when the SDS concentration increases. Also, the higher the SDS concentration, the more shear-thinning the gel becomes. For each SDS concentration, Figure 3a shows viscosity data collected from up and down shear rate sweeps. The two data sets are almost identical.

The zero-shear viscosity for each SDS concentration is plotted in Figure 3b. The viscosity increase appears to be exponential. The highest SDS concentration that we used is below the CMC, but above the CAC. As





$$\tau = 5.4 \text{ mol\%}$$

Figure 1. Nominal chemical structure of the cationic cellulose-ether polymer JR400.

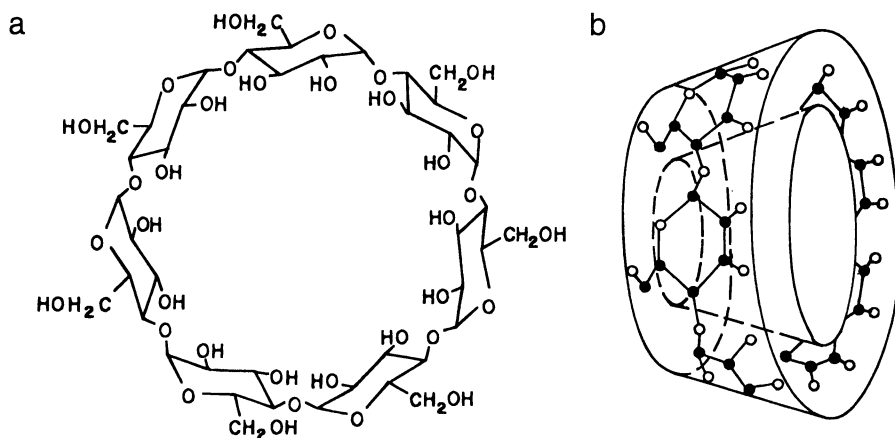


Figure 2. (a) The chemical structure and (b) the toroidal shape of  $\beta$ -cyclodextrin.

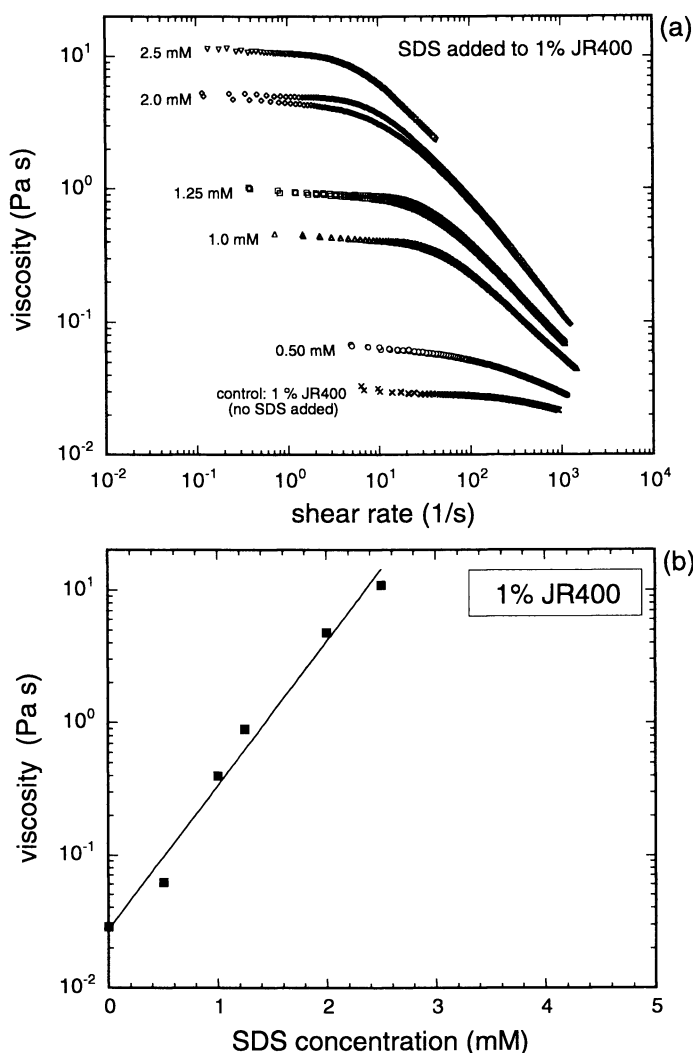


Figure 3. Viscosity enhancement in aqueous solutions of the cationic polymer JR400 effected by the addition of the anionic surfactant SDS. (a) Viscosity vs shear rate curves for different SDS concentrations at a fixed JR400 concentration (1 wt%). (b) Logarithm of zero-shear viscosity vs SDS concentration.

alluded to in the Introduction, surfactant molecules bind electrostatically to the polymer, while at the same time they tend to associate because of cooperative hydrophobic effects and to form aggregates. In doing so, they create crosslinks among the polymer chains and increase dramatically the solution viscosity. Evidence for the presence of such aggregates has been provided from fluorescence spectroscopy (19), and, more recently, from cryo-TEM (transmission electron microscopy) experiments where bilayer fragments, small vesicles and disc-like aggregates were identified. (20)

The samples with 2.5 mM SDS are clear and one-phase. Further increase on the SDS concentration does not lead to an increase in viscosity, but to a phase separation (8). The interactions in mixtures of polyelectrolytes with oppositely charged surfactants generally result in an associative phase separation and can be characterized by three distinct zones at increasing surfactant concentration (8,20): (i) a clear (or pre-precipitation) zone where the polymer is in excess, (ii) a precipitation zone, where the surfactant-to-polymer ratio is close or equal to charge neutralization (i.e. equal amounts of polymer and surfactant charges), and finally (iii) a clear resolubilization (or post-precipitation) zone, where redissolution of the complex can take place (a phenomenon which has been ascribed to the charge reversal of the complex by an excess surfactant). We have worked in the region of the phase diagram where the polymer is in excess (recall that a 1 wt% aqueous solution of the JR400 polymer bears a charge concentration of 10 mM).

**Regulation of Solution Viscosity by the Addition of CD to Mixture of SDS and JR400.** The effect of added CD on the JR400 + SDS solution viscosity is illustrated in Figure 4. Following the addition of up to 5 mM CD (twice the concentration of SDS, as discussed below) the viscosity of the mixture drops down to that of the polymer in the absence of SDS. This is a nice demonstration of the ability of cyclodextrins to "deactivate" the surfactant and destroy the gel. As in Figure 3a, the CD + SDS + JR400 system is Newtonian at low shear rates and strongly shear-thinning at high shear rates. The shear rates at which the shear-thinning transition occurs increase with increasing CD concentration (and the corresponding decrease in the concentration of "active" SDS).

The overall rheological behavior does not seem to depend on the type ( $\alpha$  or  $\beta$ ) of CD used, however there is some difference on the zero-shear viscosity. The zero-shear viscosity data for both  $\alpha$ - and  $\beta$ -CD are plotted in Figure 5 as a function of CD concentration. The reduction in viscosity appears to be exponential with CD concentration. Two important pieces of information can be obtained from Figure 5: (i) the amount of CD needed to bring the viscosity down to the JR400 level, and (ii) the relative effectiveness of  $\alpha$ - and  $\beta$ -CD.

The concentration of CD required to "deactivate" SDS is 4 to 5 mM. This is approximately double the SDS concentration (2.5 mM). This could indicate that the "effective" stoichiometric ratio for the SDS-CD complexes is 1:2 (1 guest - 2 hosts). While this ratio has been observed before, the most commonly claimed stoichiometric ratio for CD complexes is 1:1 (12,13). The CDs usually function as one-site ligands, this site being the wider rim of the cavity carrying the secondary hydroxyl groups. The substrate possesses one

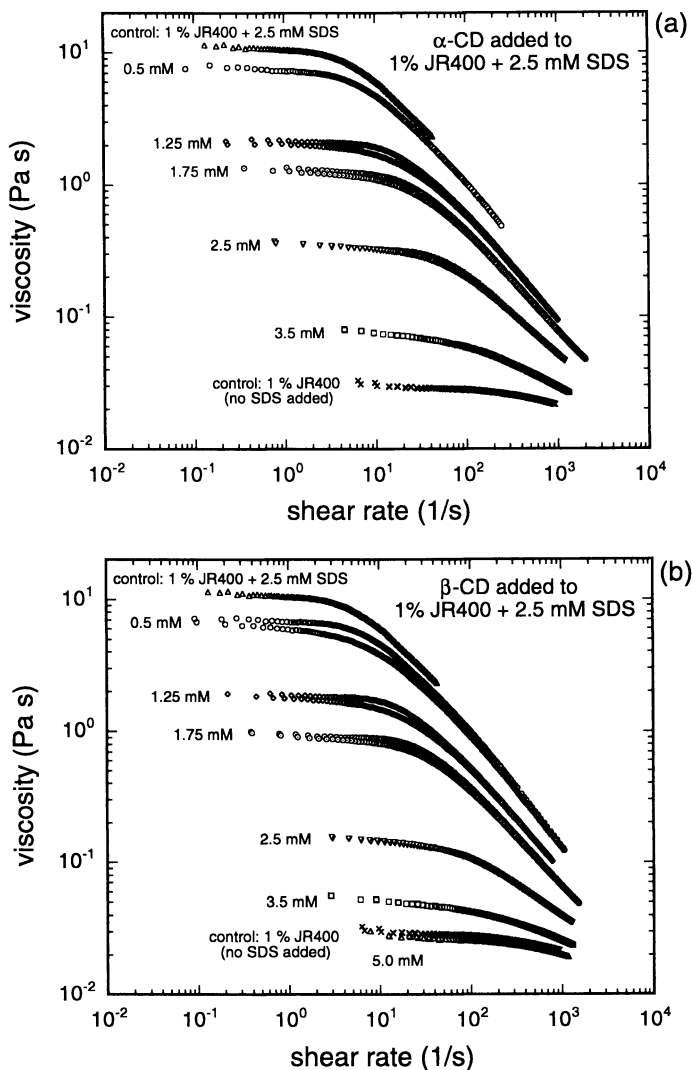


Figure 4. Viscosity decrease in aqueous solutions of the cationic polymer JR400 and anionic surfactant SDS, effected by the addition of CD. (a) Viscosity vs shear rate curves for different  $\alpha$ -CD concentrations at fixed SDS (2.5 mM) and JR400 concentration (1 wt%). (b) viscosity vs shear rate curves for different  $\beta$ -CD concentrations at fixed SDS (2.5 mM) and JR400 concentration (1 wt%).

or more binding sites, which are portions of the molecule sterically capable of insertion, whether shallowly or deeply, into the CD cavity. It is generally assumed that CD interacts with the hydrophobic moiety of the surfactant, and not with its polar headgroup (12). Indeed, in studies of surfactant-CD inclusion complex formation (including studies on the system of interest here,  $\beta$ -CD + SDS) it has been found that the predominant complex formed has a stoichiometry of 1:1 (21-24).

The discrepancy between the expected 1:1 stoichiometric ratio and the 1:2 ratio which is actually required to bring down the viscosity could be the result of a competition between polymer (or possible hydrophobic impurities which accompany the polymer) and CD for the surfactant binding site, or a result of some CD binding to a sidegroup along the polymer chain, and thus not being available for complexation with SDS.  $\alpha$ -CD is known to complex with poly(ethylene oxide), PEO (the modification used to render cellulose water soluble), but  $\beta$ -CD does not (25). The viscosity of aqueous SDS-free JR400 solution is not affected by the addition of up to 5 mM CD. We are currently looking into more detail on the origin of the apparent 1:2 SDS-CD stoichiometric ratio.

A comparison between  $\alpha$ - and  $\beta$ -CD in terms of reducing the viscosity shows that  $\beta$ -CD is more effective than  $\alpha$ -CD at concentrations above 2 mM, an indication of stronger CD-SDS binding in the case of  $\beta$ -CD. This is another contradiction to the behavior expected from CD + SDS studies which found the complexation constant involving  $\alpha$ -CD to be always higher than the corresponding value for  $\beta$ -CD (21-24). If  $\alpha$ -CD were to bind to PEO side chains of the polymer (as discussed above) at the time that  $\beta$ -CD were unable to do so, then there would be less  $\alpha$ -CD available to bind SDS, and  $\beta$ -CD would appear as binding stronger.

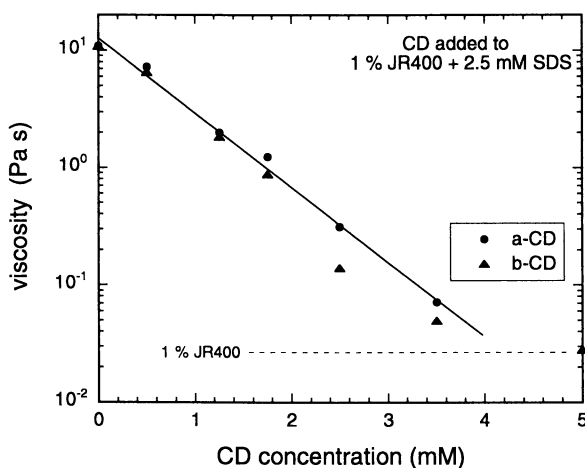


Figure 5. Logarithm of zero-shear viscosity vs CD concentration plot (for 2.5 mM SDS) that shows an exponential decrease in the JR400 + SDS solution viscosity upon the addition of CD.

The respective values of the 1:1 complexation constants for the  $\alpha$ - and  $\beta$ -CD complexes presumably reflect the geometrical dimensions of the two hosts. In terms of relative dimensions, the internal diameter and depth of  $\alpha$ -CD are 4.5 and 6 - 7 Å, respectively, whereas both these structural parameters have a value of 7 Å for the  $\beta$ -CD. Six methylene groups can be included in the  $\alpha$ -CD cavity; the other methylenes might attach to the exterior surface of the  $\alpha$ -CD molecule, which is less hydrophobic than the cavity. The large diameter of  $\beta$ -CD allows for the hydrocarbon chain to coil inside the cavity. Thus a fully extended hydrocarbon chain has more freedom of movement in the cavity of  $\beta$ -CD compared to  $\alpha$ -CD, resulting in a correspondingly lower value for the  $\beta$ -CD complexation constants (12).

### Summary and Outlook

We used rheology to probe the molecular-level interactions in aqueous solutions containing polyelectrolytes, surfactants, and cyclodextrins. We demonstrate here the ability of cyclodextrins to control the viscosity enhancement effected by surfactants mixed with oppositely charged polyelectrolyte. A schematic representation of the interactions between polyelectrolyte, surfactants, and cyclodextrins is given in Figure 6: (a) the (electrostatic) association of surfactant aggregates with the polymer leads to points of physical crosslinking and to a viscosity increase; (b) the inclusion complex formation by the hydrophobic moieties of surfactants and CD leads to micelle dissociation and a viscosity decrease. The concentration of CD required to "deactivate" the surfactant is found here to be approximately double the surfactant concentration, suggesting an "apparent" stoichiometric ratio for the SDS-CD complexes of 1:2 (1 guest - 2 hosts).  $\beta$ -CD is more effective than  $\alpha$ -CD in reducing the solution viscosity, an indication of stronger CD-SDS binding in the case of  $\beta$ -CD. Possible interaction of CD with the polymer may affect these conclusions. In fact, the effects of added CDs may help clarify the electrostatic vs hydrophobic origin of the gelation in the case of aqueous mixtures of oppositely charged polyelectrolytes and surfactants. The molecular recognition abilities of CD can be further exploited in modifying the solution properties and the functionality of polymers. We are currently investigating the effect of CDs on the solution properties of hydrophobically-modified associating polymers. The theme of our work is the coupling of the molecular recognition properties of CDs with the tailored solution properties and length/time scales afforded by polymers.

**Acknowledgments.** Financial support from the Swedish Natural Science Research Council (NFR) is gratefully acknowledged. The rheometer used in this study was financed by the Nils and Dorthi Troëdsson Research Foundation.

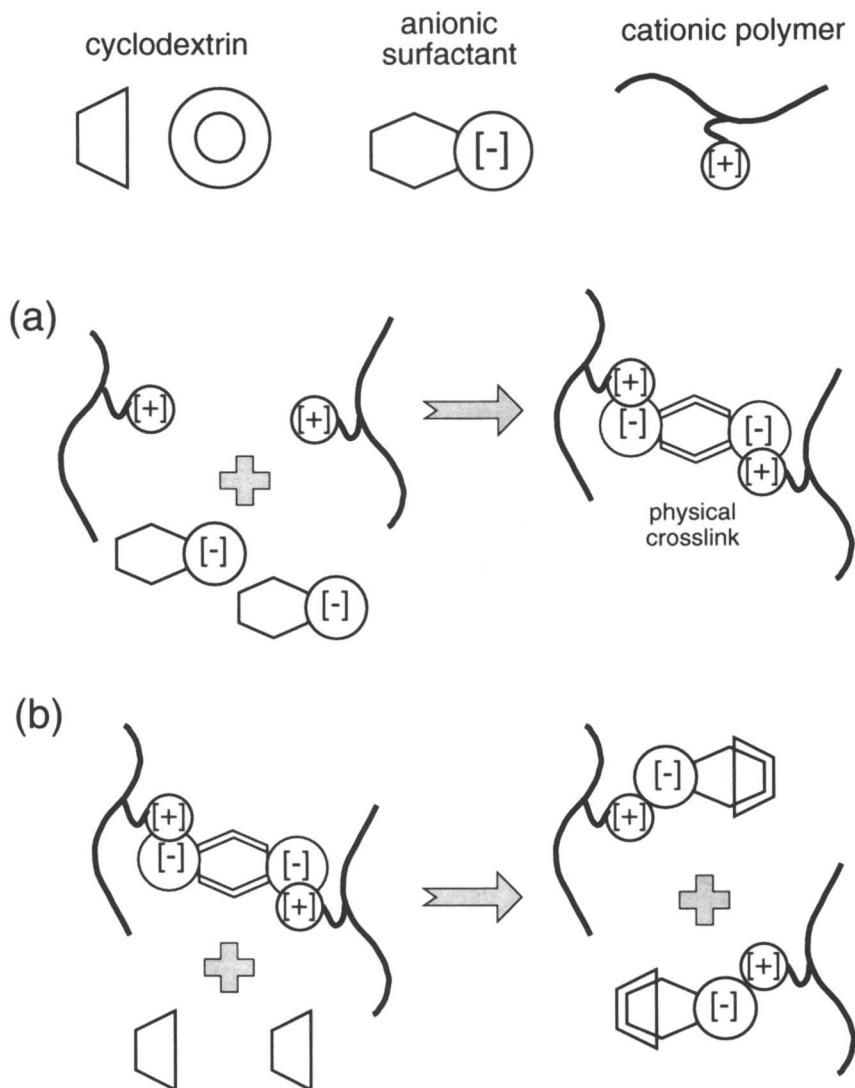


Figure 6. Schematic representation of the interactions between cationic polymers, anionic surfactants, and cyclodextrins, leading to the observed modulation of viscosity. (a) Association of surfactant micelles with the polymer, leading to a physical crosslinking and viscosity increase. (b) inclusion complex formation by cyclodextrins and (the hydrophobic moieties of) surfactants, leading to micelle dissociation and a viscosity decrease.

## Literature Cited

1. McCormick, C. L.; Bock, J.; Schulz, D. N. *Encyclopedia of Polymer Science and Engineering* **1989**, *17*, 730-784.
2. Finch, C. A., Ed. *Industrial Water Soluble Polymers*, Special Publication No. 186, The Royal Society of Chemistry, 1996.
3. Jönsson, B.; Lindman, B.; Holmberg, K.; Kronberg, B. *Surfactants and Polymers in Aqueous Solutions*. J. Wiley & Sons: Chichester, 1998.
4. Alexandridis, P. *Curr. Opin. Colloid Interface Sci.* **1996**, *1*, 490.
5. Donges, R. *Papier* **1997**, *51*, 653.
6. Iliopoulos, I. *Curr. Opin. Colloid Interface Sci.* **1998**, *3*, 493.
7. Goddard, E. D. *Colloids Surf.* **1986**, *19*, 255.
8. Goddard, E. D. *Colloids Surf.* **1986**, *19*, 301.
9. Piculell, L.; Lindman, B. *Adv. Colloid Interface Sci.* **1992**, *41*, 149.
10. Lindman, B.; Thalberg, K. *Interactions of Surfactants with Polymers and Proteins*, Goddard E. D.; Ananthapadmanabhan, K. P., Eds.; Boca Raton: CRC Press, 1993, pp. 203-276.
11. Hansson, P.; Lindman, B. *Curr. Opin. Colloid Interface Sci.* **1996**, *1*, 604.
12. Szejtli, J.; Osa, T., Vol. Eds: *Comprehensive Supramolecular Chemistry - Vol 3: Cyclodextrins*, Atwood, J. L.; Davies, J. E. D.; MacNicol, D. D.; Vögtle, F., Exec. Eds; Pergamon, Oxford, 1996.
13. Connors, K. A. *Chem. Rev.* **1997**, *97*, 1325.
14. Hedges, A. R. *Chem. Rev.* **1998**, *98*, 2035.
15. Loftsson, T.; Brewster, M. E. *J. Pharm. Sci.* **1996**, *85*, 1017-1025.
16. Thompson, D. O. *Critical Reviews in Therapeutic Drug Carrier Systems* **1997**, *14*, 1.
17. Tsianou, M.; Alexandridis, P. *Langmuir* **1999**, submitted for publication.
18. Goddard, E. D.; Leung, P. S. *Polym. Prepr.* **1982**, *23*(1), 47.
19. Winnik, F. M.; Regismont, S. T. A. *Colloids Surf. A* **1996**, *118*, 1.
20. Goldraich, M.; Schwartz, J. R.; Burns, J. L.; Talmon, Y. *Colloids Surf. A* **1997**, *125*, 231.
21. Funasaki, N.; Yodo, H.; Hada, S.; Neya, S. *Bull. Chem. Soc. Jpn.* **1992**, *65*, 1323.
22. Junquera, E.; Tardajos, G.; Aicart, E. *Langmuir* **1993**, *9*, 1213.
23. Wan Yunus, W. M. Z.; Taylor, J.; Bloor, D. M.; Hall, D. G.; Wyn-Jones, E. *J. Phys. Chem.* **1992**, *96*, 8979.
24. Mwakibete, H.; Bloor, D. M.; Wyn-Jones, E. *Langmuir* **1994**, *10*, 3328.
25. Harada, A. *Adv. Polym. Sci.* **1997**, *133*, 141.



# Interaction between Chitin Derivatives and Surfactants

J. Desbrières and M. Rinaudo

Centre de Recherches sur les Macromolécules Végétales, CNRS, affiliated with  
Joseph Fourier University, BP 53, 38041 Grenoble Cedex 9, France

This paper demonstrates the interesting properties of alkylated chitosans in aqueous solution; especially in dilute solution, at a concentration lower than the critical overlap concentration, a large increase of the viscosity is observed due to interchain hydrophobic interactions; in some conditions, a gel-like behaviour is obtained. The interactions depend on the net charge of the polyelectrolyte, on the temperature, on the external salt concentration but mainly on the number and length of grafted alkyl chains.

Then, interfacial properties of carboxymethylchitin in the presence of cationic surfactant were examined. It is shown that the efficiency to decrease the surface tension is influenced by the surfactant concentration and the degree of substitution of the polyelectrolytes. The critical aggregation concentration of the surfactant in presence of carboxymethylchitin with a DS = 1.1 is 100 times lower than the critical micellar concentration of the surfactant alone. It is attributed to strong cooperative associations between the chitin derivative and the oppositively charged surfactant forming an electrostatic hydrophobic complex as demonstrated by conductivity and fluorescence measurements. It is shown that even at a concentration in surfactant as low as  $10^{-5}$  mol/L, a viscoelastic interfacial film is formed which may be of importance for applications in foam or emulsion stabilization.

Chitin is one of the most important natural polysaccharides; it is usually found in the composition of crustacean shells (1). This polysaccharide consists of a linear chain of  $\beta$  1 $\rightarrow$ 4 D-glucosamine units N-acetylated on the C-2 position. The most common derivative prepared is the chitosan, coming from the partial deacetylation of the chitin.

When the degree of acetylation (DA) is lower than 0.5, chitosan becomes soluble in acidic aqueous solution; it behaves as a cationic polyelectrolyte; the most important applications are under this form. In addition, this polymer is biodegradable and often used for biological application such as drug release. An other advantage of chitosan is that the C-2 position of the glucosamine unit can be specifically modified. This property was used to prepare the alkylated derivatives (2).

The residual -OH functions are able to be modified; the carboxymethylation of chitin with high degree of acetylation was performed to obtain an anionic polymer with a controlled charge density characterized by the degree of substitution (DS) (3).

These different polymers were investigated previously in our laboratory and very interesting properties in aqueous solutions were demonstrated such as associative characteristics depending on the degree of alkylation, on the pH, on the temperature or on the ionic strength (4). But, also their tensioactive properties were studied as well as their interactions with ionic surfactants (5).

This paper will describe briefly the synthesis, the characterization and the properties of some of these chitin derivatives. Our main objective is to discuss the role of the charge density and that of the stiffness of the polymeric backbone on the interfacial properties in relation with the degree of interaction between oppositely charged surfactants and polyelectrolytes.

### Experimental.

Chitin extracted from crab shell was carboxymethylated in the presence of NaOH, monochloroacetic acid and in an isopropanol/water medium (6). The degree of substitution (DS) was determined by potentiometric titration; the degree of acetylation (DA) was determined by infrared and/or nmr as described previously for characterization of chitosan (7). The characteristics of the two samples tested were :

-CMCh (A) DS=1.1 DA=0.85  $C_i=3.86 \times 10^{-3}$  equiv./g.  $\lambda=1.52$

-CMCh (B) DS=0.7 DA=0.7  $C_i=2.84 \times 10^{-3}$  equiv./g.  $\lambda=0.96$

where  $C_i$  is the ionic capacity of CMCh expressed as the number of charge per gram of polymer,  $\lambda$  being the charge parameter which characterizes a polyelectrolyte (8). Their molecular weights  $M_w$  were around 140,000 (5). These samples were kindly provided by V.Babak (Ineos, Moscow).

Chitosan was a commercial sample from Protan (Norway) carefully purified before use. The residual DA was 0.12 and the molecular weight determined from viscosity measurements was  $M_v=300,000$ . This sample was alkylated by reductive amination on the C-2 position using a  $C_{12}$  aldehyde. The degree of alkylation ( $\tau$ ) and the length of the alkyl chain are controlled by the experimental synthesis conditions (2). In this paper, the alkylchitosan is named  $CC_{12}$  derivative with  $\tau$  equal 0.04 (or 4 alkyl chain per 100 monomeric units).

The surfactant used was a cationic tetradecyltrimethylammonium bromide (TTAB). All the experiments were performed in absence of external salt for conductivity and surface tension determinations. The stoichiometric ratio  $Z=[TTAB]/[CMCh]$  was expressed in terms of the ratio of ionic concentrations.

The physical properties in the bulk were investigated by conductivity to determine the degree of interaction ( $\theta$ ) between the polyelectrolyte and ionic surfactants forming ion pairs. The conductimeter is a Tacussel Type CD 78, the frequency is 250 Hz and the temperature is controlled at  $25 \pm 0.1^\circ\text{C}$ . The fluorescence spectroscopy was used to demonstrate the existence of hydrophobic domains in the presence of pyrene as a probe on a Perkin Elmer LS-50B spectrophotometer; the results are expressed by the ratio of the intensities of the first and third peaks of the fluorescence spectrum of pyrene in chitin derivative solutions ( $R=I_1/I_3$ ); this ratio reflected the hydrophobicity of the environment and as example, it equals 1.78 in water but 0.60 in hexane.

The viscosity measurements were performed in the dilute regime with a Low shear 30 from Contraves in the range of  $10^{-2}$  to  $128 \text{ s}^{-1}$ . The surface tension was determined using different equipments; at equilibrium, the measurements are obtained with the Wilhelmy plate method with K-10 tensiometer from Krüss (Germany); this technique gives us the surface tension as a function of the surfactant concentration added. This study allows to get the CMC for the surfactant and the critical aggregation concentration CAC in the presence of polyelectrolytes. Preliminary results concerning the kinetics of adsorption at the air/aqueous solution interface were obtained using a dynamic drop tensiometer (Traker) produced by I.T. Concept (France). This equipment also allows to determine the viscoelastic properties of the interfacial film (9). For the dynamic experiments, the sinusoidal fluctuation of the drop volume was fixed at a frequency of  $0.125 \text{ s}^{-1}$ . It is possible to determine the absolute value of the complex modulus  $E$  and the phase angle  $\phi$  between changes in surface tension and the changes in surface area.

## Results and discussion.

In this paper two aspects of behavior of chitin derivatives having amphiphilic character will be considered; the bulk properties of alkylchitosans having the alkyl chains covalently grafted randomly on the chitosan chain; these polymers are soluble in acidic solution but the properties depend on the balance between electrostatic repulsions controlled by the pH and hydrophobic attractions.

Then, the second aspect covered will be the electrostatic interaction between negatively charged chitin derivatives and a cationic surfactant. The objective is to relate the degree of interaction between polyelectrolyte/surfactant and the tensioactive properties.

### A. Bulk properties.

Alkylchitosan synthesis was previously described; the alkylation is controlled by the stoichiometry of the reaction and the length of the alkyl chain of the aldehyde used for the chemical modification (2).

When the polymer is dissolved in acidic conditions, if the alkyl chain is longer than 6, non-Newtonian character of the solution appears and a large increase of the viscosity is observed compared to the parent polymer. The increase of the viscosity in the Newtonian plateau depends on the degree of alkylation  $\tau$ , on the length of the alkyl chain and on the polymer concentration. An example of the experimental data is given in Figure 1. In some conditions, a gel-like character was shown by dynamic rheology;

the elastic modulus becomes larger than the viscous contribution ( $G' > G''$ ) especially when external salt is added, when the temperature increases or when the net charge of the polymer decreases by increasing the pH (4). These characteristics are due to the amphiphilic character of the alkylchitosan and also probably to the local stiffness of the polymeric chain (characterized by  $L_p$ , the intrinsic persistence length of chitosan estimated to  $50 \text{ \AA}$  (10)). As shown, only 1 to 4 % of alkylation (expressed per monomeric unit) gives a crosslink effect (4). The existence of hydrophobic domains was proved from fluorescence experiments in presence of pyrene; over a critical concentration (lower than the overlap concentration of the polymer) when the viscosity of the alkylated derivatives increases, hydrophobic domains are formed in the bulk as shown by the decrease of the ratio  $R=I_1/I_3$  of the intensities of the first and third peaks of fluorescence spectrum of the pyrene (4).

The influence of the stiffness of the polymers on these properties is under investigation in our laboratory. The important fact is that the reaction of alkylation is performed in homogeneous conditions giving a regular distribution of the hydrophobic chains.

On the opposite, when an ionic surfactant is added to the oppositely charged polymer a continuous decrease of the viscosity is observed at least for low  $Z$  ratios when the surfactant forms ion pairs as discussed later (Figure 2); in these experimental conditions, the net charge of the polymer is reduced and probably not regularly along the chains and over all the chains; a phase separation is also observed for low  $Z$  ratios (for  $Z < 0.3$  when  $C_p = 10^{-3}$  monomol./L). In the same conditions, strong interfacial modifications are obtained i.e. a strong decrease of the surface tension; in that respect, for the same content in alkyl chain as demonstrated previously, the electrostatic complex is much more efficient than the covalent alkylated derivative (5).

## **B. Interfacial properties.**

### **B-1. Equilibrium properties.**

The surface tension and the properties of the interfacial film are under investigation in connection with the mechanism of interaction between negatively charged carboxymethylchitins with different DS and cationic surfactant (TTAB). Figure 3 demonstrates the role of the polyelectrolyte in solution to reduce the surface tension and that of the charge density; the lower the DS the lower the efficiency. A surface tension around  $40 \text{ mN/m}$  is obtained for 100 times less surfactant molecules in the presence of CMCh(A) than in absence; the minimum surface tension for the complex is larger than the value obtained with the surfactant alone. For much higher surfactant concentrations, the curve of surface tension in presence of polyelectrolyte superimpose with the curve obtained with surfactant alone as previously shown on other systems (11). These data were obtained under equilibrium conditions after 24 hours. The curves given in Figure 3 are shown to be independent of the polymer concentration at least for  $C_e = 10^{-4}$  and  $10^{-3}$  equiv./L for the two DS (with  $C_p \times DS = C_e$ ); from this, it is concluded that the important factor to fix the CAC is not  $Z$  but the concentration of surfactant.

Figure 3 allows to determine a CAC around a concentration of surfactant  $C_s = 10^{-5}$  mol./L for DS=1.1 that increases to  $10^{-3}$  for DS=0.7. The stronger interaction with the

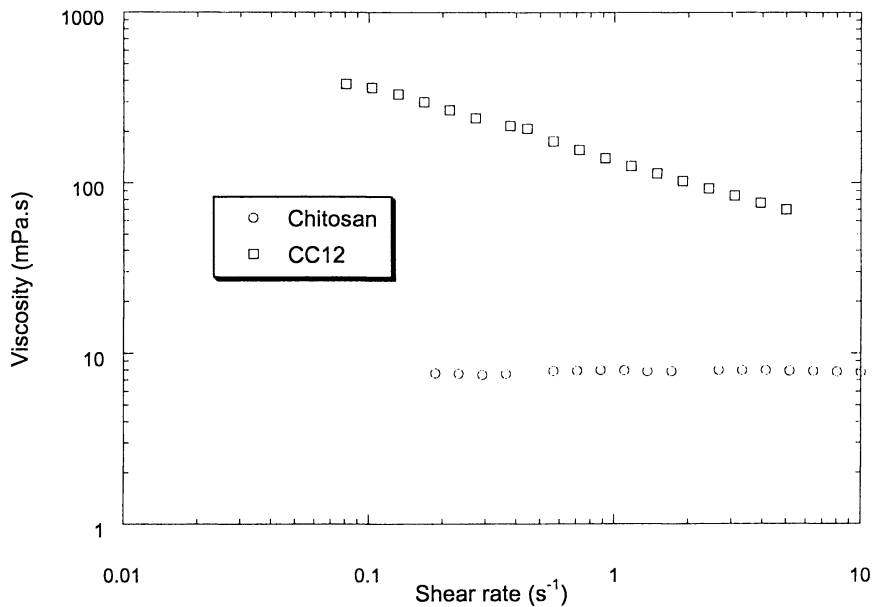


Figure 1. Viscosity of a solution of chitosan (o) and  $C_{12}$  alkylchitosan ( $\square$ ) as a function of the shear rate. Solvent : acetic acid 0.3M;  $T=20^{\circ}C$ ; polymer concentration : 1.5 mg/mL.

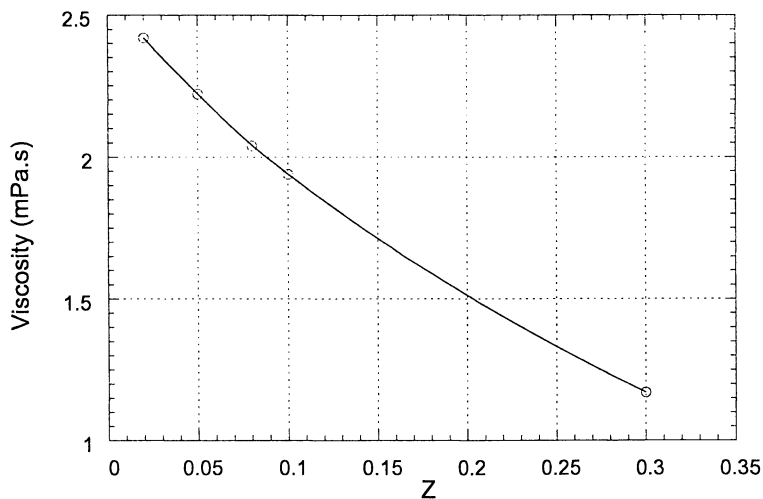


Figure 2. Change of the viscosity of a dilute solution of CMCh (A) on addition of TTAB (the TTAB concentration is expressed by Z). Polymer concentration :  $2 \times 10^{-3}$  monomol/L.

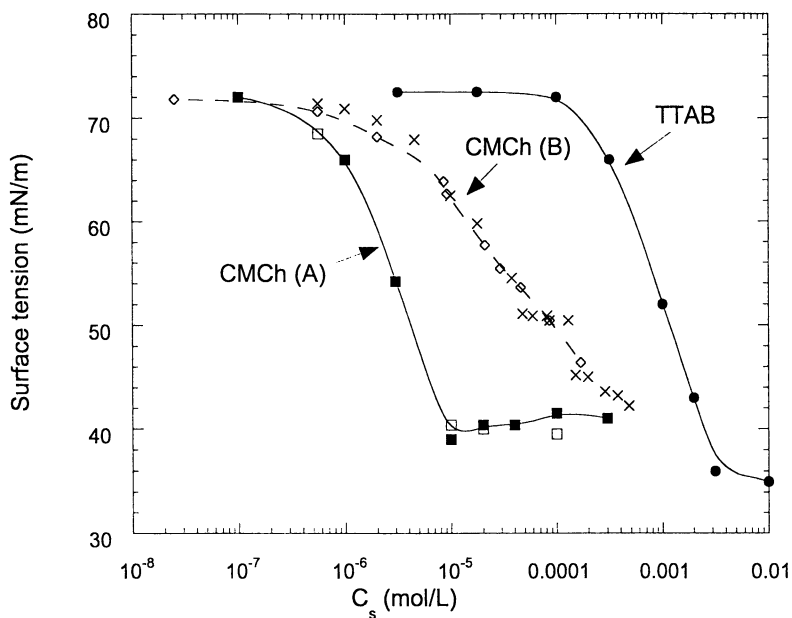


Figure 3. Variation of the surface tension on addition of TTAB (the TTAB concentration is expressed by  $C_s$  mol/L). Influence of the charge density of carboxymethylchitins (DS=1.1 and DS=0.7). Polymer concentrations for each system is  $C_e = 10^{-4}$  and  $10^{-3}$  equiv./L.

higher DS (1.1) is attributed to the cooperative interaction between the surfactant and the polyelectrolyte. This conclusion allows to predict that a minimum polymer concentration in the range of  $10^{-5}$  monomol/L is needed to reach the CAC for DS=1.1 This regime of very small addition of surfactant is the important domain for all the interfacial mechanisms in relation with stabilization of foam and emulsions.

The conductivity and fluorescence variations were followed for progressive additions of surfactant in water or in a polymer solution. First, the CMC of the surfactant in water was determined from the crossover point of the two straight lines giving the variation of the conductivity of the solution for progressive additions of surfactant; the data are given in Figure 4,a; the CMC of TTAB equals  $3.62 \times 10^{-3}$  mol./L (or 1.22g/L) at 25°C in good agreement with the literature data ( $3.5 \times 10^{-3}$  mol./L at 30°C) (12); this value is in agreement with the plateau obtained in surface tension (Figure 3) and the transition obtained in fluorescence (Figure 4,b). The ratio of the two slopes of conductivity straight lines gives a fraction of free counterions (f) characterizing the degree of aggregation of surfactant molecules; here  $f = 0.3$ . The variation of the conductivity of aqueous solutions of CMCh(A) for progressive additions of surfactant is given in Figure 5. The shape of the conductivity curve obtained is more complex than for surfactant alone and the curves were analyzed taking into account the additivity of the mobility of free ionic species. Considering Figures 4a and 5, one can write respectively for the initial slope of each conductivity curve for additions of TTAB solution :

$$- \text{ for surfactant alone added in water : } p_0 = k (\lambda_{TA} + \lambda_{Br}) \quad [1]$$

- for the mixture surfactant/polymer when surfactant is progressively added in a polymer solution prepared at a given concentration :

$$p_1 = k(\lambda_{TA} + \lambda_{Br}) + k \theta (\lambda_{Na} - \lambda_{TA} - f(\lambda_p + \lambda_{Na})) \quad [2]$$

where  $\lambda_i$  is the mobility of the ion  $i$ ,  $\theta$  the degree of association between chitin derivative and the surfactant and  $k$  is a constant .

Then, from the slopes, it follows :

$$p_1 / p_0 = 1 + (\theta / p_0) (\lambda_{Na} - \lambda_{TA} - f(\lambda_p + \lambda_{Na})) \quad [3]$$

The term  $f(\lambda_p + \lambda_{Na})$  can be calculated assuming  $f$  given by Manning theory (13) in which the transport coefficient  $f = 0.57$  and  $0.91$  respectively for DS = 1.1 and 0.7 and  $\lambda_p$  for the polyion is taken equal to  $40 \Omega^{-1} \text{ cm}^2 \text{ equiv}^{-1}$ . This term  $f(\lambda_p + \lambda_{Na})$  is also determined experimentally from the slope of the conductivity when the polymer is added in a given volume of water. The value of  $\lambda_{TA}$  was found equal to  $33.55 \Omega^{-1} \text{ cm}^2 \text{ equiv}^{-1}$ . First, the initial slope up to a specific value of  $Z$ ,  $Z_a$ , is compared to that of surfactant added in water; this gives a determination of the degree of association of surfactant with the carboxylic sites ( $\theta$ ) which corresponds to the fraction of ion pairs formed in the complex. The experimental data obtained for  $C_p = 10^{-3}$  monomol./L are the following:

|            |        |              |                 |
|------------|--------|--------------|-----------------|
| - CMCh (A) | DS 1.1 | $Z_a = 0.75$ | $\theta = 0.9$  |
| - CMCh (B) | DS 0.7 | $Z_a = 0.65$ | $\theta = 0.55$ |

Then, it was shown that the degree of association  $\theta$  is independent on the polymer concentration; the values of  $\theta$  are much larger than the calculated values predicted from electrostatic theory;  $(1 - f)$  should be 0.43 and 0.09 respectively for the two CMChitin derivatives. The first conclusion is that for the larger DS, a very cooperative interaction

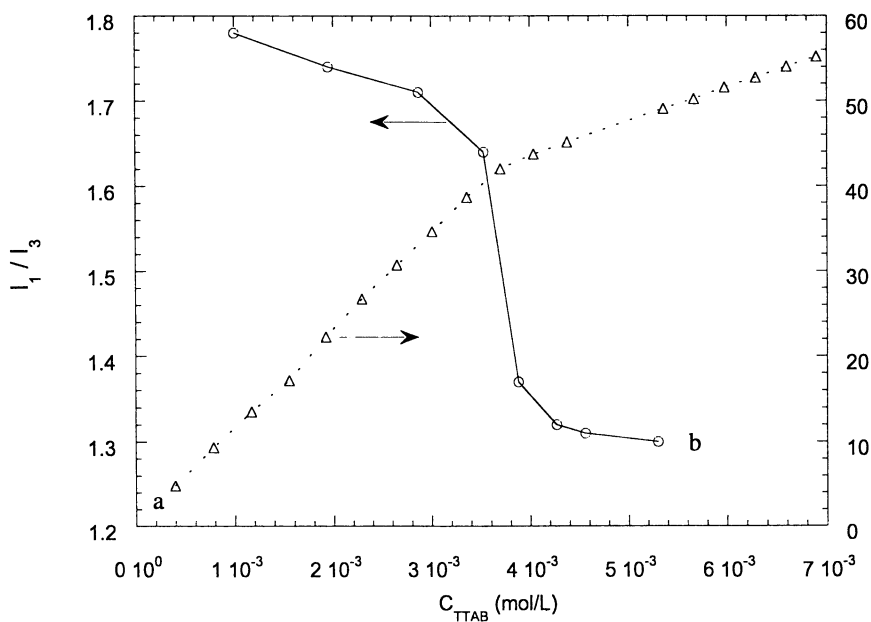


Figure 4. (a) Change of the conductivity on addition of an aqueous solution of TTAB in water ( $\Delta$ ). Determination of the CMC. (b) Variation of the fluorescence ratio  $I_1/I_3$  in the same conditions (o).



with formation of a very large fraction of ion pairs is shown reducing the net charge of the polymer. For small additions of surfactant, the polyelectrolyte is nearly saturated with surfactant giving a very hydrophobic complex which decreases strongly the surface tension.

The average net charge of the polyelectrolytes per monomeric unit decreases and following their solubility; a partial phase separation occurs around  $Z=0.3$  for CMCh(A) at a polymer concentration of  $10^{-3}$  monomol./L. The phase separation is less pronounced for the lower DS in the same polymer concentration range in relation with the lower degree of association of surfactant, then a larger net charge for the complex formed. The CAC determined by surface tension measurement for DS=1.1 (Figure 3) is given by  $[TA] = 10^{-5}$  mol./L for  $C_e = 10^{-4}$  and  $10^{-3}$  equiv./L i.e.  $Z = 0.1$  and  $0.01$  respectively; these  $Z$  values correspond to the first part of the conductivity curves and then to a high degree of association and an absence of phase separation. This cooperative complex formation was largely investigated by Osada and coll. (14) in relation with the distance between ionic sites along the polymer and the length of the alkyl chains of surfactants.

In the intermediate zone, the degree of precipitation first increases, then decreases with a partial redissolution for CMCh (A). In the range of concentration covered for CMCh (B) no true precipitation was observed.

For the two polymers tested, the last part of the conductivity curves (over  $Z_b$  as marked in Fig. 5) presents the same slope as that obtained for the surfactant alone in the micellar regime. From this, one concludes that for larger  $Z$  ratios, independent micelles of surfactant are formed with the same degree of aggregation as for surfactant alone. From the crossover which limits this last part ( $Z_b$ ), one determines the CMC of the surfactant in presence of polyelectrolytes; the concentration of surfactant added to get this crossover increases in direct relation with the polymer concentration (Table 1). From this, one determined the fraction of surfactant ( $F$ ) fixed per ionic site of the polyelectrolyte which lies between 0.7- 0.8 for the two polymers independently of the polymer concentration.

After formation of these micelles the surface tension decreases and becomes equal to that of surfactant alone. In addition, in the zone of sharp decrease of the surface tension, a large decrease of the fluorescence ratio  $R$  is observed due to the hydrophobic complex formed (Figure 6).

From these results it is clear that the large binding efficiency of the polyelectrolytes is related to a cooperative association of large hydrophobic cations forming a surface active complex. The cooperativity depends directly on the charge density of the polyelectrolyte which explains the difference observed between the two systems in surface tension efficiency.

## **B-2. Dynamic interfacial properties.**

With the dynamic drop tensiometer, one can follow the kinetics of organization of the air/water interface; also, when the small droplet is subjected to sinusoidal oscillations of its volume, viscoelastic properties of the interfacial film can be measured. The surface

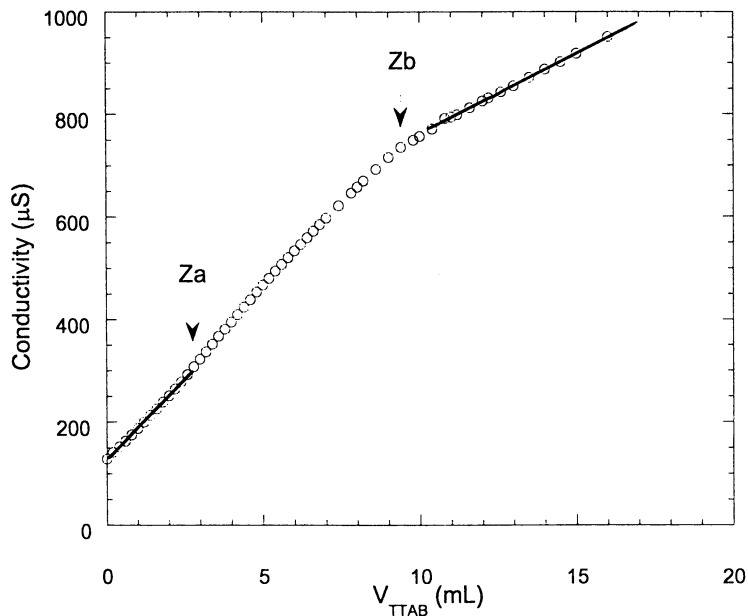


Figure 5. Change of the conductivity on addition of surfactant in a solution of CMCh (A). Polymer concentration :  $2 \times 10^{-3}$  monomol/L.

**Table 1.** Apparent CMC of surfactant (TTAB) in presence of polyelectrolytes.

| Polymer concentration monomol. L <sup>-1</sup> | Apparent CMC (mol/L)  | $\Delta \text{CMC}/C_p = F$ |
|--|-----------------------|-----------------------------|
| <b>CMCh (A)</b>                                |                       |                             |
| 0  | $3.6 \times 10^{-3}$  | -                           |
| $1 \times 10^{-3}$                             | $4.4 \times 10^{-3}$  | 0.73                        |
| $2 \times 10^{-3}$                             | $5.4 \times 10^{-3}$  | 0.82                        |
| $3 \times 10^{-3}$                             | $5.9 \times 10^{-3}$  | 0.7                         |
| <b>CMCh (B)</b>                                |                       |                             |
| 0  | $3.6 \times 10^{-3}$  | -                           |
| $x \times 10^{-3}$                             | $4.18 \times 10^{-3}$ | 0.82                        |
| $3 \times 10^{-3}$                             | $5.14 \times 10^{-3}$ | 0.73                        |

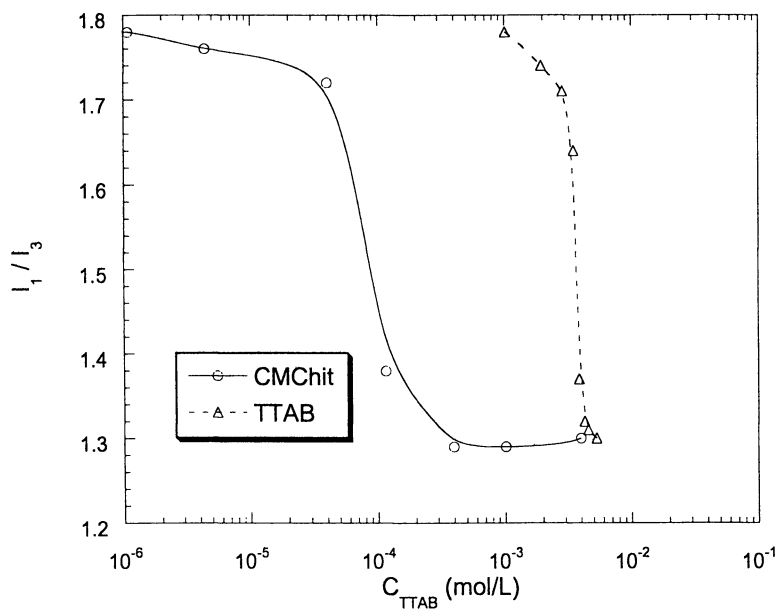


Figure 6. Change of the pyrene fluorescence ratio  $R$  on addition of surfactant: ( $\Delta$ ) in water ; ( $\circ$ ) in a CMCh (A) solution ( $C_p = 10^{-3}$  monomol/L).

viscoelasticity of polyelectrolyte/surfactant systems was recently discussed in the literature (15).

The dynamic tension data concern the kinetics; the measurements were performed with surfactant at different concentrations, and then for a fixed surfactant concentration at a given polymer concentration. The rate of decrease of the surface tension is slowed down in the presence of polymer as reflected by Figure 7 for  $[TA]=10^{-3}$  mol/L; the decrease of the surface tension is slower for the higher DS. This confirms that the equilibrium surface tension measurements takes a long time (Figure 3 was taken after 24 hours).

The second type of data concerns the viscoelastic characteristics; the complex modulus  $E$  is determined directly, as well as the phase angle  $\delta$  with  $\tan \delta = E''/E'$ , in terms of the elastic component  $E'$  and the viscous component  $E''$  respectively.

The characterization of dynamic properties of surfactant solutions is delicate; in a range of concentrations,  $10^{-4}$  up to  $2 \times 10^{-2}$  mol/L, a low modulus in the range of 3 mN/m at  $0.125 \text{ s}^{-1}$  is obtained. In the presence of polyelectrolytes at a fixed surfactant concentration, the modulus increases largely corresponding to the stabilization of the interfacial film. The values obtained for different TA concentrations are given in Table 2. From these data, it follows that the moduli are nearly equal for the two polymers :  $E \approx 25-42$  mN/m as soon as the TA concentration is larger than  $10^{-5}$  mol/L ( around the CAC). The viscous contribution appears to be larger for the DS=1.1 compared with DS=0.7; this may be related to the electrostatic repulsion that exists between the charged molecules in the interfacial film: the residual charge for DS 1.1 is 0.1 per monomeric unit whereas for DS 0.7 it is 0.3; then the repulsion is larger for DS= 0.7. Nevertheless it is important to note that these measurements are never performed under equilibrium conditions due to the slow kinetics and the technical principle of the device. The apparent surface tension measured in the same conditions does not show a large variation due to the DS; as shown previously in Figure 3, this is partly due to a change in the kinetics with the DS. This dynamic technique gives a rapid determination of the efficiency of the polyelectrolyte and especially of its role in the stabilization of the interfacial film. Complementary experiments are needed to relate the interfacial characteristics with the charge density but also with the stiffness of the polymeric chains.

## Conclusion.

In the first part of this paper, the synthesis and characterization of alkylated chitosan are briefly described. The homogeneous repartition of alkyl chains along the polymeric backbone and the control of the density of grafting allow to control of the balance between electrostatic repulsions and hydrophobic attractions. Then, with 1 to 4 percent of monomeric units modified with C12 or C14 alkyl chains, a large increase of viscosity occurs; a gel-like behaviour may also be observed in some thermodynamic conditions. As demonstrated earlier, the solutions are non-Newtonian and their rheological

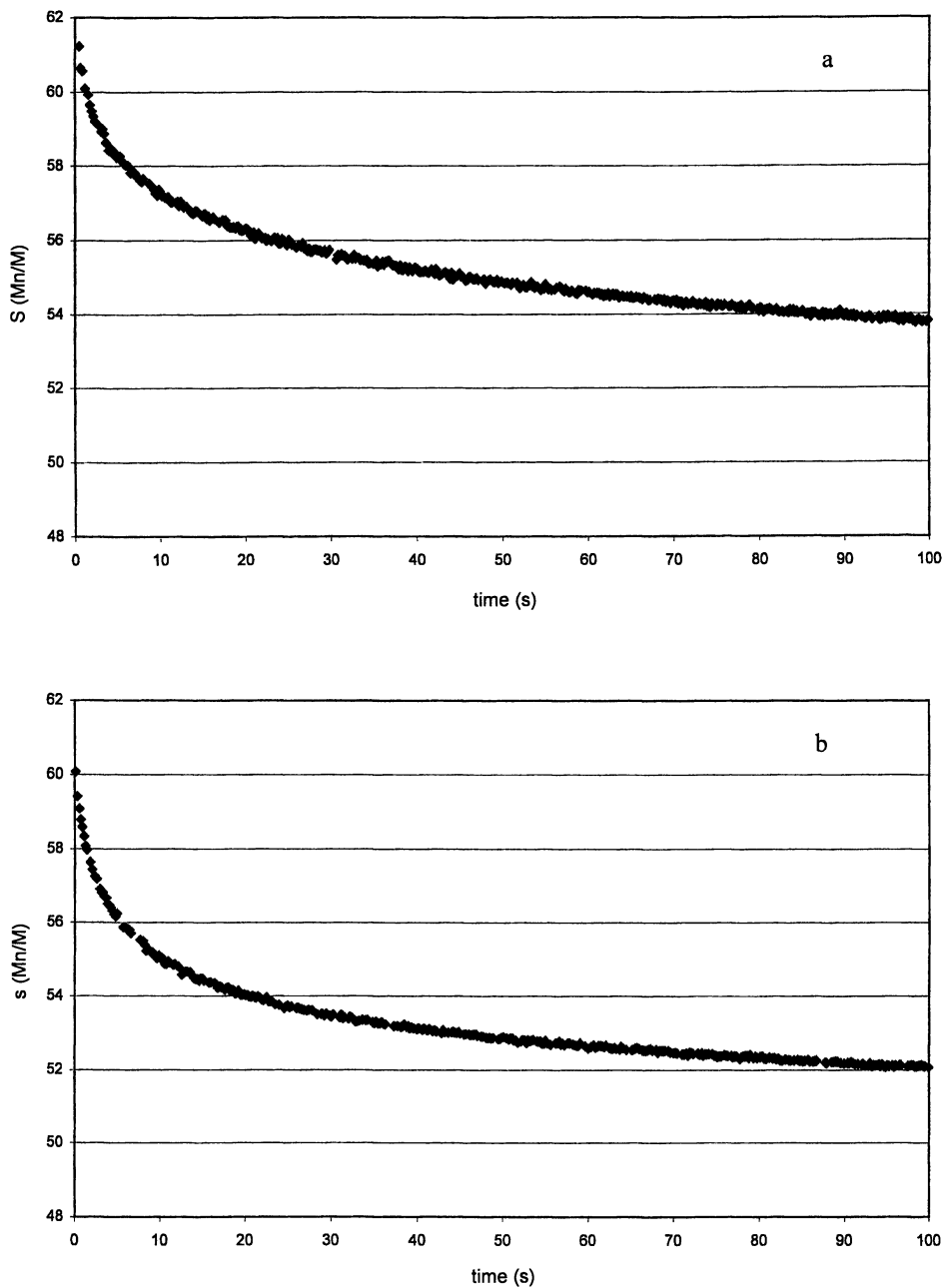


Figure 7. Evolution of the surface tension ( $\sigma$ ) with time : (a) for the CMCh(A)/TA mixture; (b) for the CMCh(B)/TA mixture.  $C_p = 10^{-3}$  monomol./L ;  $C_s = 10^{-3}$  mol./L.

**Table 2.** Viscoelastic properties of interfacial films of CMCh in presence of different concentrations of TTAB (the polymer concentration equals  $10^{-3}$  monomol/L).

a) CMCh (A) DS=1.1

|              |           |           |           |           |
|--------------|-----------|-----------|-----------|-----------|
| [TA] (mol/L) | $10^{-5}$ | $10^{-4}$ | $10^{-3}$ | $10^{-2}$ |
| E (mN/m)     | 34.5      | 42.8      | 31        | 31.2      |
| $\delta$     | 22.5      | 18        | 23        | 38        |

b) CMCh (B) DS=0.7

|              |           |           |           |           |
|--------------|-----------|-----------|-----------|-----------|
| [TA] (mol/L) | $10^{-5}$ | $10^{-4}$ | $10^{-3}$ | $10^{-2}$ |
| E (mN/m)     | 29        | 39.4      | 41.4      | 42        |
| $\delta$     | 18        | 7.8       | 7.4       | 6.5       |

characteristics depend on external salt concentration, pH and temperature. These polymers have a small effect on the surface tension due to their moderate hydrophobicity but for air/liquid interfacial properties, the polyelectrolyte characteristics for the surfactant-polymer complex formation are the most efficient. When a cationic surfactant is mixed with carboxymethylchitin a cooperative interaction occurs depending on the degree of substitution of the carboxymethylchitins used. The surface tension efficiency is related to the fraction of ion pairs formed characterizing the polyelectrolyte complex. The CAC obtained is very low and confirms that a cooperative hydrophobic complex is formed.

Preliminary results are given concerning the kinetics of adsorption of the surfactant or of the complex. It is demonstrated that a viscoelastic film is formed for a concentration of surfactant as low as to  $10^{-5}$  mol/L. The rheological properties of the interfacial films also depend on the degree of substitution i.e. on the degree of packing of the surfactant molecules fixed on the polymer at the interface. All the results concern the domain of polymer and surfactant diluted solutions.

**Acknowledgements.** V.Babak and his coworkers are thanked for the gift of the two samples and for experimental data of surface tension. L.Lamalle is acknowledged for his technical assistance.

**References.**

- 1 R.A.A. Muzzarelli, M.G. Peter, "Chitin Handbook" . Atec, Grottammare,Italy (1997).
2. J. Desbrières, C. Martinez, M. Rinaudo, *Int. J. Biol. Macromol.* **19**, 21-28 (1996).
3. M. Rinaudo, P. Le Dung, M. Milas in "Advances in chitin and chitosan", Ed. C.J. Brine, P.A. Sandford, J.P. Zikakis. Elsevier, 516-525 (1992).
4. J. Desbrières, M. Rinaudo, L. Chtcheglova, *Macromol. Symp.* **113**, 135-149 (1997).
5. J. Desbrières, M. Rinaudo, V. Babak, G.A. Vikhoreva, *Polym. Bull.* **39**, 209-215 (1997).
6. G.A. Vikhoreva, I.N. Gorbacheva, L.S. Gal'braich, *Fibre Chemistry* **26**, 326 (1994).
7. P. Le Dung, M. Milas, M. Rinaudo, J. Desbrières, *Carbohydr. Polym.* **24**, 209-214 (1994). (1996).
8. S. Lifson , A. Katchalsky, *J. Polym. Sci.*,**13**,43-55 (1954)
9. J. Benjamins, A. Cagna, E.M. Lucassen-Reynders, *Colloids and surfaces A.* **114**, 245-254 (1996)
10. M. Rinaudo, M. Milas, P. Le Dung, *Int. J. Biol. Macromol.* **15**, 281-285 (1997).
11. A. Asnacios, D. Langevin, J.F. Argillier, *Macromolecules* **29**, 7412-7417 (1996).
12. E. Pramaura, E. Pelizzi in "Surfactants in analytical chemistry", vol. 31, Wilson & Wilson's, NY (1996).
13. G.S. Manning in "Polyelectrolytes", Edit : E.Sélégny, M. Mandel, U.P. Strauss. Reidel, Dordrecht-Holland , Vol.1, 9-37 (1974).
14. H. Okuzaki, Y. Osada, *Macromolecules* **28**, 4554-4557 (1995).
13. S.T.A. Regismond, F.M. Winnik, E.D. Goddard, *Colloïds and Surfaces A.* **119**, 221-228 (1996)

## Chapter 15

# Influence of Cationic Cellulose Structure on Interactions with Sodium Dodecyl Sulfate

Melissa Manuszak Guerrini<sup>1</sup> and William H. Daly

Macromolecular Studies Group, Chemistry Department,  
Louisiana State University, Baton Rouge, LA 70803-1804

Polymer and surfactant interactions have been a subject of intense research due to industrial applications utilizing a polymer-surfactant system, such as cosmetic formulation. We have prepared mono and diquaternary aminoalkylcarbonyl cellulose derivatives by amidation of methylcarboxymethyl cellulose followed by quaternization with either iodomethane or hydroxypropyl trimethylammonium chloride. The interactions of these cationic polymers with sodium dodecyl sulfate (SDS) have been studied by precipitation, surface tension and foam stability, and the results compared with those of Polyquaternium 10.

Polymeric quaternary ammonium salts (polyquats) have a variety of uses in cosmetic formulations due to their solubility in both aqueous and aqueous-alcoholic media. Polyquats have been used as thickeners, emulsifiers, fixatives or film formers, and as additives in formulations to improve combing of hair, manageability, body, curl retention and substantivity of ingredients to keratin (1,2). The particular application of a polymer depends on the polymer's ability to adsorb at an interface, stabilize dispersions, emulsify, and confer the preferred rheology by means of a three dimensional network (2). Cationic ingredients are substantive to hair keratin due to the low isoelectric point of hair (pH = 3.67) (3). However, the high affinity of some cationic polymers has limited their use due to soiling (build up) and resistance to removal by anionic surfactants (1).

Electrostatic forces largely dominate the interactions between polyelectrolyte and surfactant with hydrophobic interactions playing a secondary role in complex

<sup>1</sup> Current address: Université Pierre et Marie Curie, Laboratoire de Chimie Macromoléculaire, UMR 7610, Tour 44, 4 place Jussieu, 75252 Paris, France.



formation (4-7). Complexation of polyelectrolytes and oppositely charged surfactants begins at a surfactant concentration, which is much lower than the critical micelle concentration (CMC) for the free surfactant (7). This surfactant concentration which first results in complexation is the critical aggregation concentration (CAC) (8). In particular, for the case of a cationic polymer and anionic surfactant, it has been shown that the polymer-surfactant complex cannot co-exist with free micelles if precipitation of the complex is observed (9-11). The region of maximum precipitation for the complex has been shown to occur near stoichiometric charge neutralization (*i.e.* when the polymer-surfactant charge ratio is approximately 1:1) (9-11). Furthermore, it has been shown that addition of excess amount of anionic surfactant results in the resolubilization of the precipitated complex (9-11).

Goddard and coworkers have studied the system of Polyquaternium 10 and SDS extensively (4,9-17). The results of these studies show that the components form strong polymer surfactant complexes, which are highly surface active despite the fact that Polyquaternium 10 by itself is only slightly, surface active. From surface tension studies (4,9,12,13,17), it was determined that a cationic polymer and SDS, like many uncharged polymer and SDS mixtures, exhibit an interaction zone (18-21). However, the interaction zone for the cationic polymer and SDS was shifted to much lower surfactant concentrations than for uncharged polymers and SDS (13). From these studies, no interaction was detected between the parent (uncharged) polymer, hydroxyethyl cellulose, and SDS by surface tension method (4,12,13,17,22). The essential features of the surface tension plots of Polyquaternium 10 and SDS are: a) a synergistic lowering of the surface tension at very low concentrations of SDS which implies the formation of a highly surface active polymer - surfactant complex; b) the persistence of a low surface tension even in the zone of high precipitation; and c) coincidence with the surface tension curve of SDS solution in the micellar region (4,12). Goddard and coworkers (12) have explained this phenomenon as being the result of changes in surface-active species present at the interface due to the progressive uptake of the SDS by the polymer. An increase in foaming power of these solutions, which is a direct consequence of the increased surface activity of the Polyquaternium 10 - SDS complex formed, was also observed (9).

The effect of polymer - SDS complexation on foam stability has recently been studied using cationic and nonionic polymers (9,23-25). These studies indicate that the formation of surface-active complexes has a profound effect on both stability and foamability of SDS solutions. Foam stability of solutions containing oppositely charged polymer surfactant pairs is increased because the polymer surfactant pairs interact strongly and enhance the adsorption of both components at the liquid/bubble interface (*i.e.* plateau borders) (23-25). The effects on foam stability are also dependent upon surfactant concentration. Below the CAC for the surfactant, polyelectrolytes are adsorbed at the liquid/bubble interface and stabilize films initially by double layer repulsion, then by polymer bridging with time as the film thins and the walls of the lamellae approach each other (25). Below the CAC, overlapping polymer layers prevent film rupture. Above the CAC, a dense polymer-surfactant complex that is strongly adsorbed at the liquid - bubble interface stabilizes foam by formation of a gel-like network. Increased stability is attributed to the formation of this network along with the accompanying changes in ionic strength (25).

## Experimental

**Materials.** Sodium dodecyl sulfate, 99%, was obtained from Sigma<sup>®</sup> Chemical Company (St. Louis, MO) and used without further purification. Polyquaternium 10, UCARE Polymer JR-400 (DS = 0.50), was obtained from Amerchol Corporation (Edison, NJ). The sample was dissolved in distilled, deionized water, dialyzed in a cellulose acetate dialysis tube having a 6-8,000 Dalton cutoff against distilled, deionized water to remove impurities and lyophilized. Carboxymethyl cellulose, sodium salt (MW = 250,000 g/mol., DS = 0.70) was obtained from Aldrich Chemical Company (St. Louis, MO) and used without further purification.

Mono and diquaternary ammoniumalkylcarbamoyl cellulose derivatives were prepared with defined charge densities in which the quaternary nitrogen is located at the sites of carboxymethylation of the starting polymer (NaCMC) (26,27). The degrees of substitution of the starting material (NaCMC), methylcarboxymethyl cellulose derivative (MCMC) and the aminoamide derivative (CMCNED) were determined by refluxing the dried derivatives in glacial acetic acid and conductrimetrically titrating with 0.1 N perchloric acid/dioxane solution. The degrees of substitution are as follows: NaCMC (DS = 0.70), MCMC (DS = 0.69) and CMCNED (DS = 0.57) (28,29). Nuclear magnetic resonance (NMR) analyses were performed using Bruker 200AC and AM400 NMR spectrometers. For CMCNED: <sup>1</sup>H NMR (D<sub>2</sub>O)  $\delta$ , ppm: 3.25-4.50 (broad peaks of anhydroglucose ring)  $\delta$ , 2.45 (s), 2.75 (overlapping triplets); <sup>13</sup>C NMR (D<sub>2</sub>O)  $\delta$ , 102.5 (C1 of anhydroglucose ring), 60.1 (C6 of anhydroglucose ring), 56.7, 56.1, 43.6, 43.2, 35.9, 34.4; 177.9 (amide carbonyl). Infrared spectra were obtained with a Perkin Elmer 1700X series Fourier transform infrared (FTIR) spectrometer at 4 cm<sup>-1</sup> resolution and 10 to 25 scans. For CMCNED; FTIR (cm<sup>-1</sup>), KBr pellets: 3436 (s, O-H stretch), 2923 (w, C-H stretch), 1651 (amide I band, shoulder), 1593 (s, amide II band), 1113 and 1061 (s, C-O-C stretch). Elemental analysis were conducted by Oneida Research Services, Inc.: CMCNED; Calculated 41.27% C; 4.65% N; Found 43.14% C; 4.57% N.

2-N,N,N-Trimethylammoniummethyl carbamoyl cellulose chloride (MQNED) was prepared from the corresponding N,N-dimethylaminoethyl carbamoyl cellulose by quaternization with methyl iodide followed by ion-exchange with 1.0 M sodium chloride in a cellulose acetate dialysis tube with a 6-8,000 Dalton cutoff. Treatment of N,N-dimethylaminoethyl carbamoyl cellulose with N,N,N-trimethylammonium-3-chloro-2-propanol (Quat 188) yielded the diquaternary derivative, 3-N,N,N-trimethylammonium - 2 - hydroxypropyl -N',N'-dimethylammoniummethyl carbamoyl-methyl cellulose chloride (DQNNED) (26,27). The polymers were dialyzed against distilled, deionized water and the purified solutions were lyophilized. The degrees of quaternary substitution determined by titrating with sodium dodecyl sulfate are as follows: MQNED (0.97 meq/g) and DQNNED (1.96 meq/g). For DQNNED: <sup>1</sup>H NMR (D<sub>2</sub>O),  $\delta$ , (ppm): 3.25-4.5 (anhydroglucose ring, broad, overlapping peaks), 4.5 (m, broad), 3.6 (d), 3.5-3.4 (d,s overlapping), 3.1 (s), 2.9 (s).

**Precipitation Studies.** Pseudo phase diagrams were prepared for the following system: SDS / Polymer / water by addition of a concentrated polymer solution (0.1 - 3%) to a

solution of SDS. The samples were stirred, placed in an oven at 60°C for 8 hours, and allowed to cool slowly. The appearance of the liquid and precipitate was judged visually following the method of Goddard and Hannan (9,11).

**Surface Tension.** Solutions were prepared by addition of a concentrated polymer solution (0.1-3%) to a solution of SDS. The solutions were stirred and allowed to equilibrate 24 hours. Surface tension measurements were obtained using a Kruss K14 tensiometer using the Wilhelmy plate method at  $20 \pm 0.5$  °C. The tensiometer was calibrated with distilled, deionized water. All surface tension measurements were made in triplicate and error bars are based upon these measurements.

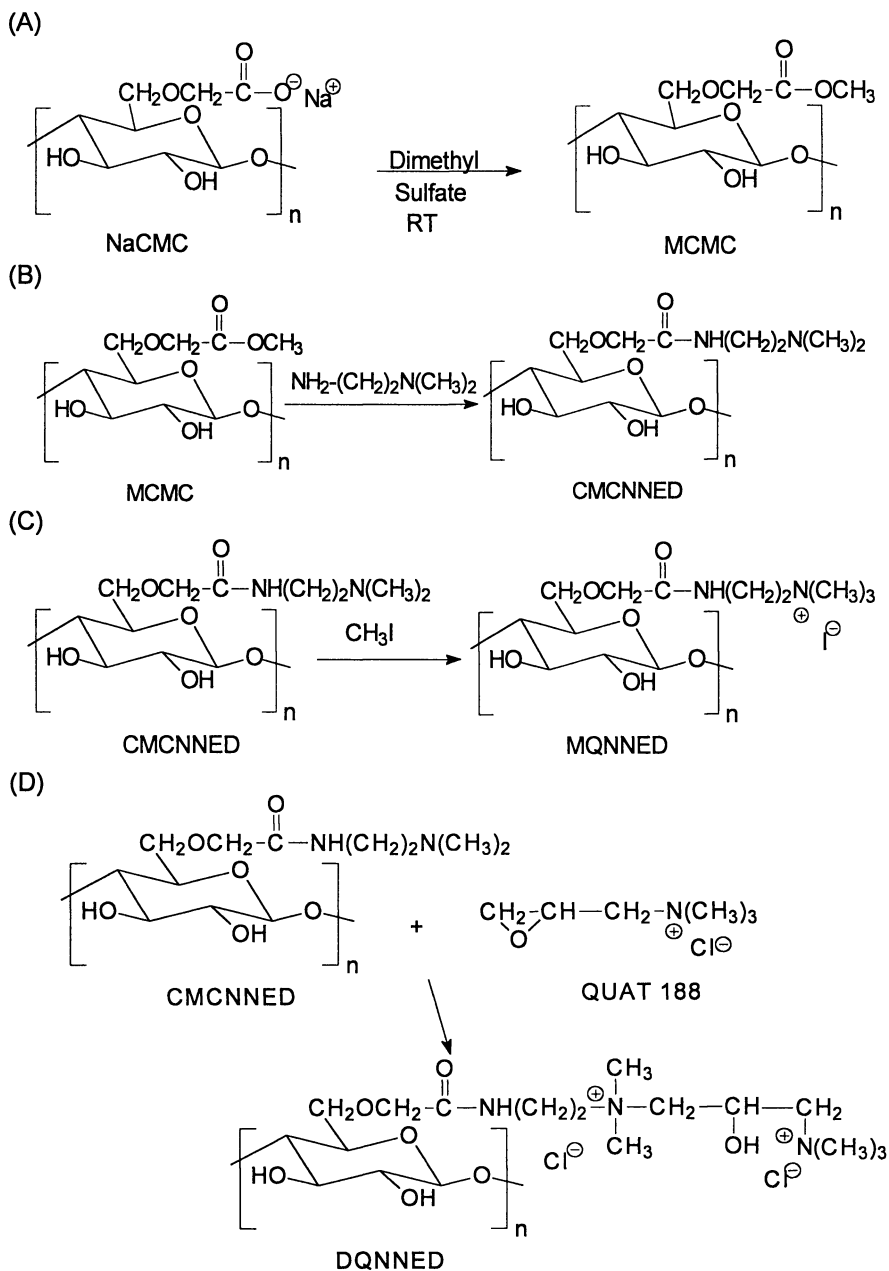
**Foam Stability.** 10 ml of each polymer - SDS solution was prepared, placed in a glass-stoppered 25 ml graduated cylinder and allowed to equilibrate 24 hours. The cylinder was inverted ten times through an arc of 180 degrees. The initial volume of foam produced was recorded and additional measurements were made at 30 minutes, 1, 6, and 24 hours following the method of Goddard and Hannan (9).

## Results and Discussion

We have prepared new mono and diquatarnary ammoniumalkylcarbamoyl cellulose derivatives with defined charge densities in which the quaternary nitrogen is located at the sites of carboxymethylation of the starting polymer (Scheme 1) (26-28). These model polymers have been used to determine the changes in surface tension, foamability and foam stability resulting from complexation with SDS. The changes in surface tension produced by these polymer-surfactant complexes have been compared with the behavior of the Polyquaternium 10 - SDS complex (30). Polyquaternium 10 is a quaternized hydroxyethyl cellulose derivative in which the cationic moiety is attached via a hydroxypropyl group to poly(oxyethylene) spacer groups that provide flexibility independent of the cellulose chain.

**Precipitation Studies with SDS.** The complexation of Polyquaternium 10 and two aminoalkylcarbamoyl cellulose graft co-polymers with SDS was studied by precipitation above and below the critical micelle concentration (CMC) of SDS, 2.4 mg/ml (31-34). The pseudo phase diagrams of SDS / water / Polymer (Figures 1-3) show the formation of clear solutions at low concentrations of SDS. Increases in solution viscosity were observed along with formation of turbid or hazy solutions, precipitates and gels as the percentage of SDS was increased. At high surfactant concentrations, resolubilization of the polymers was observed. These results are in agreement with previous studies of complexation of anionic surfactants and Polyquaternium 10 (9,11).

The complexation of cationic polymers with anionic surfactants proceeds via charge neutralization (11),  $P^{n+} + nD^- \rightarrow PD_n$  where P is the cationic polymer containing n cationic charges per residue molecular weight and D<sup>-</sup> is the anionic surfactant containing one anionic charge per residue molecular weight. Theoretical charge neutralization occurs at a 1: 1 ratio of cationic and anionic charges resulting in



**Scheme 1** Aminoalkylcarbamoyl cellulose derivatives. (A) reaction of NaCMC to form MCMC ester; (B) reaction of MCMC ester to form CMCNNE; (C) reaction of CMCNNE to form MQNNE; and (D) reaction of CMCNNE to form DQNNE

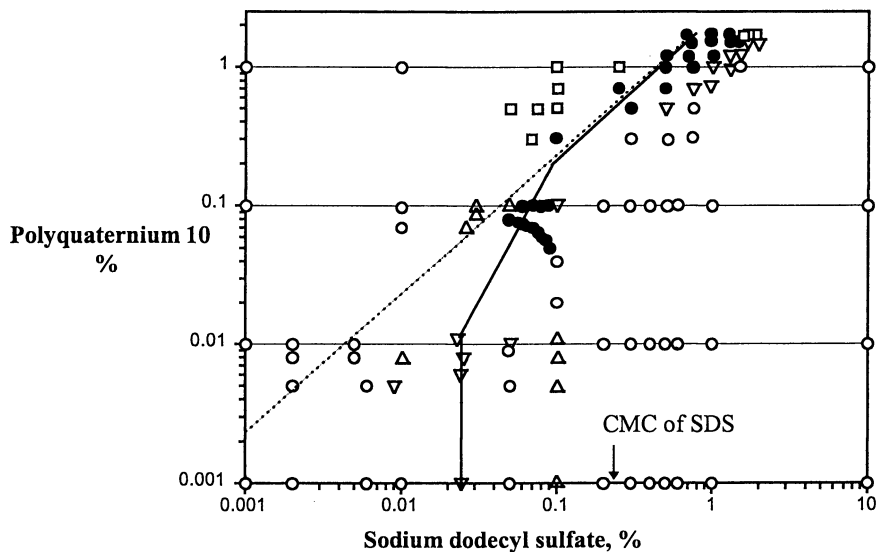


**Figure 1** Pseudo-phase diagram of the system Polyquaternium 10 / SDS / water. Symbols indicate: O clear solution; ● precipitate; ▽ slight precipitate; Δ hazy solution; □ gel; - - - - - theoretical charge neutralization weight ratio 2.3:1; and ——— compositions containing the maximum amount of precipitate.

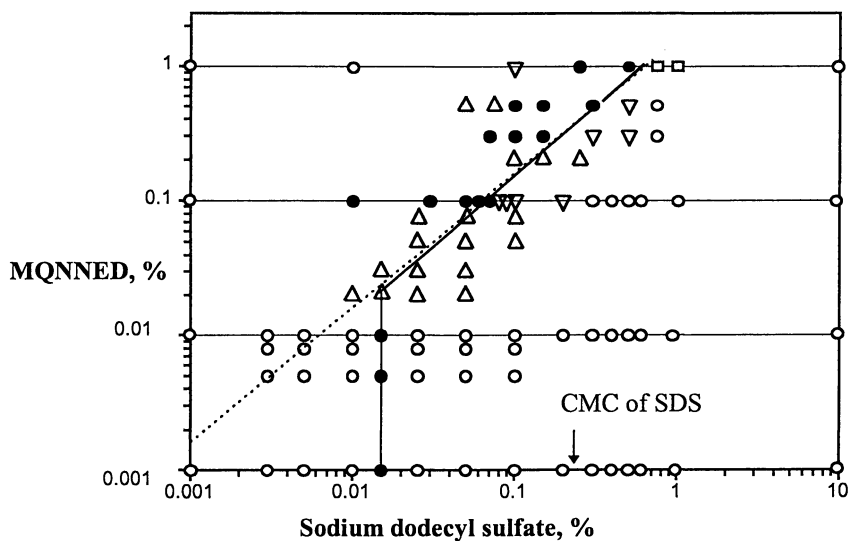


**Figure 2** Pseudo-phase diagram of the system MQNED / SDS / water. Symbols indicate: O clear solution; ● precipitate; ▽ slight precipitate; Δ hazy solution; □ gel; - - - - - theoretical charge neutralization weight ratio 1.6:1; and ——— compositions containing the maximum amount of precipitate.

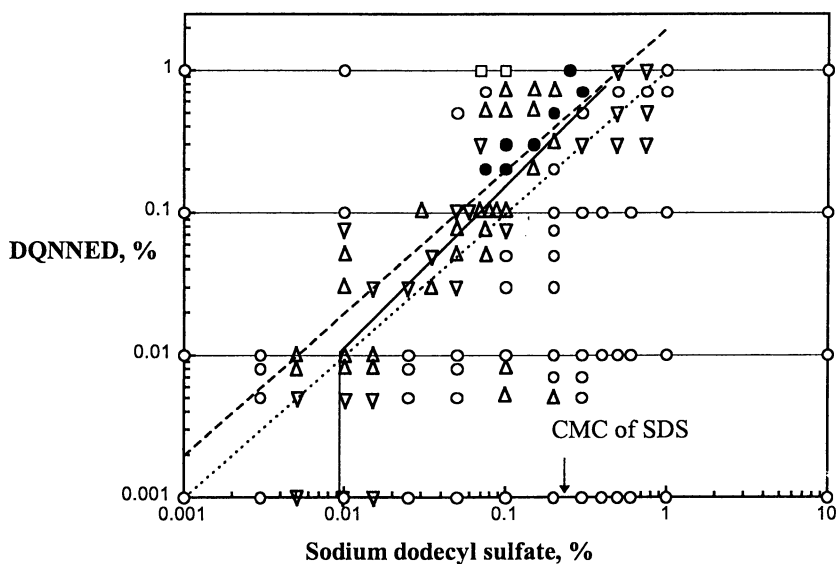


**Figure 3** Pseudo-phase diagram of the system DQNNED / SDS / water. Symbols indicate: O clear solution; ● precipitate; ▽ slight precipitate; Δ hazy solution; □ gel; - - - - theoretical charge neutralization weight ratio 2.0 : 1; ..... theoretical charge neutralization weight ratio 1.0 : 1; and ——— compositions containing the maximum amount of precipitate

maximum precipitation of the polymer. For Polyquaternium 10, the charge density or average residue molecular weight per cationic charge is 689 g/mol while the charge density of SDS is 288 g/mol. Therefore, theoretical charge neutralization should occur at a weight ratio of 2.3: 1 as represented by the dotted line in Figure 1. Comparison of the compositions containing the maximum amount of precipitated material with the theoretical charge neutralization ratio for this system (Figure 1 solid line vs. dotted line) indicates that this relationship holds true for concentrations of polymer and surfactant  $\geq 0.200$  and 0.100%, respectively. At polymer concentrations  $< 0.200\%$ , the concentration of SDS necessary to precipitate the Polyquaternium10-SDS complex is independent of polymer concentration. This result agrees with results observed previously for this system (9,11).

The average molecular weight per cationic charge for MQNED is approximately 467 g/mol. Therefore, theoretical charge neutralization should occur at a weight ratio of 1.6: 1 as represented by the dotted line in Figure 2. The results for this system (Figure 2 solid line vs. dotted line) indicate that this relationship holds true for concentrations of polymer and surfactant  $\geq 0.020$  and 0.015%, respectively. At polymer concentrations  $\leq 0.010\%$ , the concentration of SDS necessary to precipitate the MQNED-SDS complex is independent of polymer concentration.

The average molecular weight per cationic charge for DQNNED is approximately 569 g/mol. Since the graft on DQNNED contains two cationic charges, two theoretical charge neutralization weight ratios can be calculated. The first weight ratio, 2.0: 1, is related to the addition of one SDS molecule per two cationic charges as represented by the dashed line in Figure 3. The second weight ratio, 1 : 1, is related to the addition of two SDS molecules per two cationic charges as represented by the dotted line in Figure 3. The results indicate that maximum precipitation of the DQNNED-SDS complex occurs between these two theoretical charge neutralization lines. Therefore, for concentrations of polymer and surfactant  $\geq 0.010\%$ , the DQNNED-SDS complex precipitates maximally when approximately 1.5 SDS molecules neutralize the charge of the 2 cationic sites. At low polymer concentrations ( $< 0.010\%$ ) the concentration of SDS necessary to precipitate the DQNNED-SDS complex is independent of polymer concentration.

When the observed maximum precipitation patterns for the three systems are compared (Figures 1-3 solid lines), the results indicate that the polymers precipitate at their respective theoretical charge neutralization ratio when the concentrations of polymer are  $\geq 0.010$ , 0.020 and 0.200% for DQNNED, MQNED and Polyquaternium 10, respectively. However, at polymer concentrations  $\leq 0.010\%$ , the limiting SDS concentration necessary to precipitate increases as the structure of the polymer is varied: DQNNED-SDS  $<$  MQNED-SDS  $<$  Polyquaternium 10-SDS. Therefore, when precipitation is independent of polymer concentration, a polyelectrolyte containing two cationic charges per residue will precipitate at a lower percent SDS than its monoquaternary analog, and a monoquat closely related with the backbone will precipitate before a monoquat attached to a flexible spacer arm.

**Surface Tension Studies.** Using the Wilhelmy plate method, surface tension was studied as a function of surfactant concentration at a fixed polymer concentration of

0.1% (for a discussion of the effects at various polymer concentrations see reference 30). Polyquaternium 10 itself is only slightly surface active at the air/water interface (see inset curve Figure 4). This result agrees with a previously published result by Goddard and Hannan (9). The complex formed by association of SDS with Polyquaternium 10 is highly surface active as shown by the decrease in surface tension (Figure 4). This effect is especially pronounced at low concentrations of surfactant. This reduction in surface tension continues despite onset of precipitation of the polymer surfactant complex. Surface tension increases when the complex is maximally precipitated out of solution. Decreases in surface tension are observed again as the concentration of SDS is increased further resulting in resolubilization of the Polyquaternium 10 - SDS complex. Eventually, at high concentrations of SDS, surface tension of the polymer - SDS system coincides with that of SDS alone. The lowering of the surface tension has been attributed to modification of the polymer by adsorption of SDS anions at the cationic sites (9). However, any synergistic effect is difficult to describe as the slope of the surface tension plots in the presence of polymer is governed by the free SDS monomer concentration, the activity of the polymer - surfactant complex and the amount of precipitate formed.

The effect of complexation of SDS with the slightly surface active diquaternary polymer (DQNNED) on surface tension is shown (Figure 5). The behavior of this system proved to be similar to that of the Polyquaternium 10 - SDS system. Initially, at low concentrations of surfactant and 0.1% DQNNED, surface tension decreased markedly relative to the surface tension of SDS. The reduction in surface tension continues despite onset of precipitation of the DQNNED - SDS complex. Surface tension increases when the complex is maximally precipitated out of solution. Decreases in surface tension are observed again as the concentration of SDS is increased further resulting in resolubilization of the DQNNED - SDS complex. Eventually, at high concentrations of SDS, surface tension of the polymer - SDS system coincides with that of SDS alone. The reduction in surface tension continued despite precipitation of the DQNNED-SDS complex and eventually coincided with the curve for SDS.

For the system MQNNED - SDS (Figure 6) large decreases in surface tension at low concentration of SDS were observed. However, this system, in contrast to the two previous systems, does not exhibit an increase in the surface tension when the MQNNED-SDS complex is maximally precipitated out of solution. The surface tension of this system is always lower than that of SDS except when the two curves eventually coincide at high concentrations of SDS. This change in surface tension behavior of the MQNNED - SDS complex may be related to the distance of the quaternary nitrogen from the cellulose backbone. Goddard and coworkers (11) have studied the effects of complexation of various vinyl polycations on the surface tension behavior of SDS. The results indicated that cationic charge centers located near the polymeric backbone result in much lower surface tension values in the precipitation zone than observed for other quaternary derivatives.

Regardless of polymer architecture, the solutions that contained 0.1% polymer and SDS were more effective in reducing surface tension than SDS alone. We propose, at a fixed concentration of cationic polymer, that addition of increasing



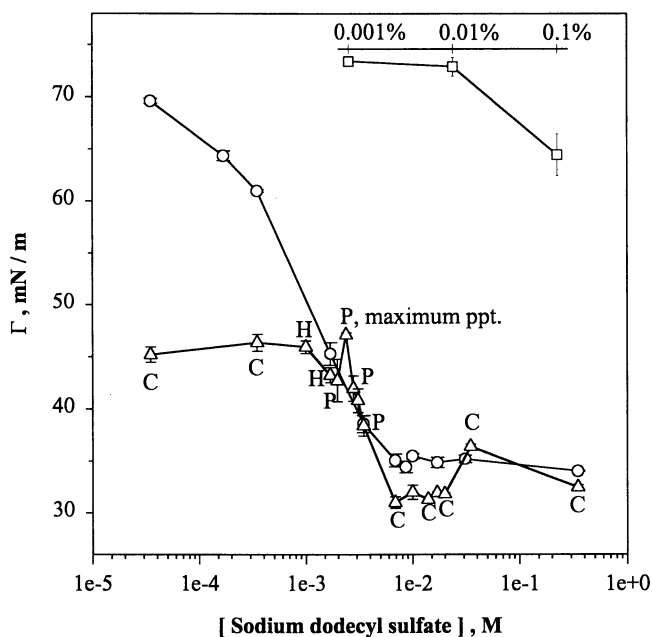


**Figure 4** Surface tension plot of Polyquaternium 10 - SDS complexes. Symbols indicate: ( O ) SDS alone; ( □ ) Polyquaternium 10 alone; ( Δ ) 0.1% Polyquaternium 10 - SDS complex; Letters indicate: C = clear solution; H = hazy solution; SP = slight precipitate; and P = precipitate.

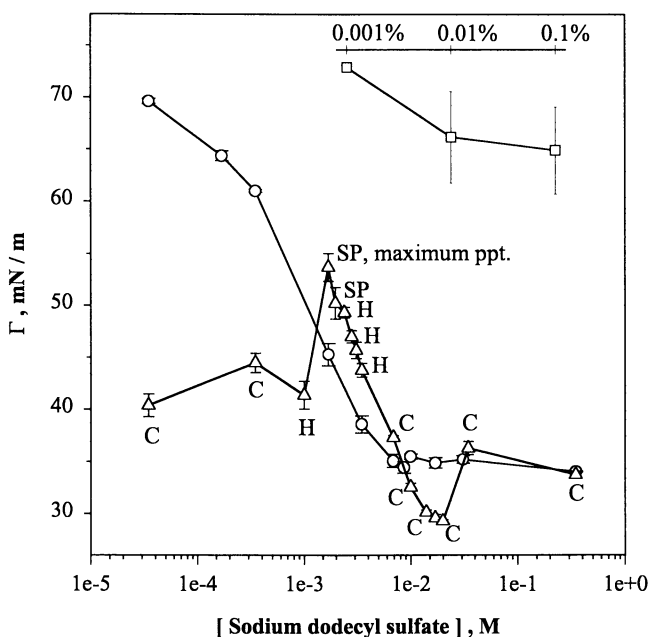


**Figure 5** Surface tension plot of DQNNED - SDS complexes. Symbols indicate: ( O ) SDS alone; ( □ ) DQNNED alone; ( Δ ) 0.1% DQNNED - SDS complex; Letters indicate: C = clear solution; H = hazy solution; SP = slight precipitate; and P = precipitate.

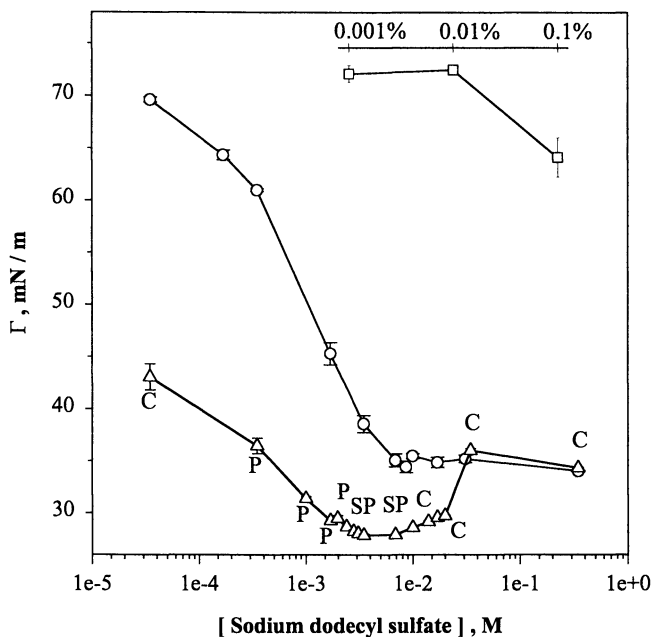


**Figure 6** Surface tension plot of MQNNE D - SDS complexes. Symbols indicate: ( O ) SDS alone; ( □ ) MQNNE D alone; ( Δ ) 0.1% MQNNE D - SDS complex; Letters indicate: C = clear solution; H = hazy solution; SP = slight precipitate; and P = precipitate.

amounts of surfactant results in further decreases in surface tension as the air/liquid interface becomes saturated until the SDS : polymer ratio approaches a stoichiometric balance. Upon neutralization by SDS, the polymer-surfactant complex precipitates maximally and surface tension increases slightly. Beyond this point of maximum precipitation, surface tension again begins to decrease as the partitioning of the surfactant between the polymer - surfactant complex and free micelles in solution controls the surface tension of the liquid. Surface tensions of the polymer - surfactant solutions eventually coincide with the surface tension of SDS as the precipitated complex is resolubilized by formation of polymer bound micelles and free micelles. The dip in the surface tension curves at the CMC of SDS indicates that a more surface-active component is being solubilized in the surfactant micelles.

### Foam Stability.

**Independent Foamability of SDS and Polymers.** The intrinsic foaming of solutions of the polymers and SDS was studied in order to determine a baseline for foam height (35,36). The results (Table I) indicate that Polyquaternium 10 produces a small amount of foam. Neither MQNED nor DQNED produced any foam, indicating an absence of intrinsic surface activity. Therefore, significant enhancement in foaming and foam stability of SDS in the presence of these cationic polymers may be attributed to the formation of polymer - surfactant complexes, stabilization, or enhancement of the adsorbed surfactant layer by the presence of the polymer.

**Table I: Intrinsic Foam Height Produced by Polymer or SDS Solutions**

| Polyquat 10<br>% | SDS<br>% | t=0<br>( mm ) | t=0.5 hr<br>( mm ) | t=1 hr<br>( mm ) | t=6 hrs<br>( mm ) | t=24 hrs<br>( mm ) |
|------------------|----------|---------------|--------------------|------------------|-------------------|--------------------|
| 0                | 10       | 117.5         | 92.5               | 87.0             | 69.0              | 0                  |
| 0                | 1        | 84.0          | 72.5               | 57.5             | 44.5              | 16.0               |
| 0                | 0.1      | 93.0          | 66.0               | 47.5             | 34.5              | 9.0                |
| 0                | 0.01     | 4.0           | 2.0                | 0.5              | 0                 | 0                  |
| 0                | 0.001    | 1.5           | 1.0                | 0                | 0                 | 0                  |
| 1                | 0        | 6.0           | 4.0                | 3.5              | 3.0               | 0                  |
| 0.1              | 0        | 9.5           | 2.5                | 1.5              | 0.5               | 0                  |
| 0.01             | 0        | 3.0           | 1.0                | 1.0              | 0                 | 0                  |
| 0.001            | 0        | 0             | 0                  | 0                | 0                 | 0                  |

**Influence of Polymers on Foam Stability of SDS.** In our studies (35,36) the concentrations of polymer and SDS were varied from 0.001 - 1% and 0.001 - 10%, respectively. Foam stability of the solutions was determined over the course of 24 hours. Semi logarithmic plots of foam height *versus* time for each of the solutions were approximately linear. This observation suggested that the rate of foam collapse may be modeled by 1<sup>st</sup> order kinetics and the slope of the plot (*i.e.* the half-life) may be used to define the foam decay process. The half-lives ( $t_{1/2}$ ), surface tension ( $\Gamma$ )

(30) and specific viscosity ( $\eta_{sp}$ ) for each of the solutions were determined (for a detailed discussion see reference (36)).

Comparison of the half-life data indicated that foam stability was greatest for a solution containing 0.1% Polyquaternium 10 - 0.01% SDS (Table II). For solutions containing 0.001 - 0.01% SDS and 0.001 - 0.1% Polyquaternium 10, foam stability, as judged by  $t_{1/2}$ , increased as surface tension decreased and specific viscosity increased. This result agrees with previous results showing that increasing bulk viscosity (37) and decreasing surface tension (38-41) produce more stable foams. Increasing the viscosity by addition of polymer decreases the rate of liquid drainage in the lamellae thereby increasing foam stability (37,42,43). The lowering of surface tension as stability is increased is a result of bridging across a lamella by polymer molecules, which stabilize the foam (25). All solutions containing 1% Polyquaternium 10 showed a reduction in foam stability compared to the solutions containing similar amounts of surfactant. Foam generation may be a problem with such high viscosity systems as these systems may be viscoelastic. Two factors, polymer aggregation and ionic shielding, may be contributing to this phenomenon.

In the case of MQNED, the half-life data (Table III) indicated that foam stability was greatest for the solution containing 0.01% MQNED and 0.1% SDS. The half-life of 156 hours exceeds that observed for the optimum stabilization conditions using Polyquaternium 10. For most of the solutions studied, the specific viscosity increased and surface tension decreased as the concentration of MQNED was increased; two exceptions at 0.001% SDS, 1% MQNED and 0.1% SDS, 1% MQNED were noted (35,36). In contrast to the data obtained with Polyquaternium 10 (Table II), the most stable foam for MQNED was observed in the region where there is a stoichiometric excess of SDS relative to the polymer additive (compare the position of these data points on the respective phase diagrams Figures 1 and 2). Maximum foam stability was observed near phase separation regardless of rigidity of the cellulose graft for a monoquaternary-substituted polymer.

Half-life data for DQNNED (Table IV) indicated that foam stability was greatest for the solution containing 0.01% DQNNED and 0.1% SDS. This system is in the region where there is a stoichiometric excess of SDS relative to the polymer additive (Figure 3). The half-life of 33 hours was less than those observed with either of the monoquaternary polymers. The same solution containing MQNED had a half-life 4.7 times greater than the half-life for DQNNED. Clearly, introduction of a second positive charge on the substituent did not contribute to increased foam stability. Solutions containing the lowest concentrations of SDS exhibited half-lives of less than 30 minutes (35,36). Additionally, two solutions did not foam, probably due to the strong binding of the SDS by DQNNED.

These results differ from the work of Goddard and Hannan (9) who showed that after 30 minutes maximum foam stability was produced by solutions containing the maximal amount of precipitated material. Our results appear to indicate that maximal foam stability after 24 hours occurs in those solutions nearest phase separation (compare results Tables II-IV with pseudo-phase diagrams Figures 1-3). This observation appears to be consistent with the findings of Ross and Nishioka (44-47) who state that high surface activity is a precursor of phase separation. The

**Table II: Half-life, Surface Tension and Specific Viscosity for Polyquaternium 10 - SDS Systems.**

| Polyquaternium 10<br>(%) | SDS<br>(%) | $t_{1/2}$<br>(hours) | $\Gamma$<br>(mN / m) | $\eta_{sp}$        |
|--------------------------|------------|----------------------|----------------------|--------------------|
| 0                        | 0.001      | < 0.50               | 69.60                | - 0.001            |
| 0.001                    | 0.001      | 55.49                | 64.80                | - 0.001            |
| 0.01                     | 0.001      | 25.01                | 59.93                | 0.003              |
| 0.1                      | 0.001      | 85.20                | 45.21                | 1.380              |
| 1                        | 0.001      | 19.25                | 54.35                | 22.150             |
| 0                        | 0.01       | 0.77                 | 61.00                | - 0.005            |
| 0.001                    | 0.01       | 1.48                 | 58.80                | - 0.001            |
| 0.01                     | 0.01       | 26.20                | 51.50                | 0.002              |
| 0.1                      | 0.01       | 116.23               | 46.36                | 1.840              |
| 1                        | 0.01       | 73.62                | 41.00                | 77.800             |
| 0                        | 0.1        | 19.25                | 38.60                | 0.007              |
| 0.001                    | 0.1        | 0.58                 | 31.40                | - 0.001            |
| 0.01                     | 0.1        | 4.81                 | 33.16                | - 0.140            |
| 0.1                      | 0.1        | 9.63                 | 38.38                | N / D <sup>1</sup> |
| 1                        | 0.1        | N / D <sup>2</sup>   | N / D <sup>2</sup>   | N / D <sup>2</sup> |
| 0                        | 1          | 25.17                | 35.20                | 0.050              |
| 0.001                    | 1          | 9.63                 | 37.66                | 0.580              |
| 0.01                     | 1          | 19.25                | 38.37                | 0.580              |
| 0.1                      | 1          | 31.82                | 36.39                | 0.250              |
| 1                        | 1          | 9.63                 | 39.40                | 43.850             |
| 0                        | 10         | 23.07                | 34.00                | 1.096              |
| 0.001                    | 10         | 9.63                 | 33.71                | 0.924              |
| 0.01                     | 10         | 9.63                 | 34.53                | 0.970              |
| 0.1                      | 10         | 9.63                 | 32.49                | 1.790              |
| 1                        | 10         | 6.42                 | 32.46                | 33.430             |

<sup>1</sup>N/D this solution contained precipitated material and could not be determined by Ubbelohde viscometry <sup>2</sup>N/D this solution was a gel; therefore no determinations could be made.

**Table III: Half-life, Surface Tension and Specific Viscosity  
for MQNED - SDS Systems**

| MQNED<br>(%) | SDS<br>(%) | $t_{1/2}$<br>(hours) | $\Gamma$<br>(mN/m) | $\eta_{sp}$        |
|--------------|------------|----------------------|--------------------|--------------------|
| 0            | 0.001      | < 0.50               | 69.60              | - 0.001            |
| 0.001        | 0.001      | 2.41                 | 72.82              | - 0.001            |
| 0.01         | 0.001      | 1.13                 | 61.24              | 0.033              |
| 0.1          | 0.001      | 1.60                 | 43.04              | 0.210              |
| 1            | 0.001      | < 0.50               | 50.73              | 1.760              |
| 0            | 0.01       | 0.77                 | 61.00              | - 0.005            |
| 0.001        | 0.01       | 3.85                 | 53.58              | - 0.001            |
| 0.01         | 0.01       | 3.85                 | 45.54              | 0.046              |
| 0.1          | 0.01       | 21.71                | 36.46              | 0.200              |
| 1            | 0.01       | 25.37                | 32.77              | 1.870              |
| 0            | 0.1        | 19.25                | 38.60              | 0.007              |
| 0.001        | 0.1        | 35.92                | 31.34              | - 0.022            |
| 0.01         | 0.1        | 156.54               | 31.13              | 0.020              |
| 0.1          | 0.1        | 30.51                | 27.86              | 0.280              |
| 1            | 0.1        | 24.50                | 29.88              | N / D <sup>1</sup> |
| 0            | 1          | 25.17                | 35.20              | 0.050              |
| 0.001        | 1          | 61.51                | 38.36              | 0.024              |
| 0.01         | 1          | 19.25                | 37.21              | 0.075              |
| 0.1          | 1          | 19.25                | 36.01              | 0.240              |
| 1            | 1          | 37.68                | 30.68              | N / D <sup>1</sup> |
| 0            | 10         | 23.07                | 34.00              | 1.096              |
| 0.001        | 10         | 9.63                 | 34.80              | 0.850              |
| 0.01         | 10         | 9.63                 | 34.36              | 0.880              |
| 0.1          | 10         | 4.81                 | 34.33              | 1.080              |
| 1            | 10         | 4.81                 | 31.87              | 4.240              |

<sup>1</sup> N/D this solution contained precipitated material and could not be determined by Ubbelohde viscometry.

**Table IV: Half-life, Surface Tension and Specific Viscosity for DQNNED - SDS Systems**

| DQNNED<br>(%) | SDS<br>(%) | $t_{1/2}$<br>(hours) | $\Gamma$<br>(mN/m) | $\eta_{sp}$        |
|---------------|------------|----------------------|--------------------|--------------------|
| 0             | 0.001      | < 0.50               | 69.60              | - 0.001            |
| 0.001         | 0.001      | < 0.50               | 73.15              | - 0.049            |
| 0.01          | 0.001      | < 0.50               | 72.68              | 0.020              |
| 0.1           | 0.001      | < 0.50               | 40.37              | 0.319              |
| 1             | 0.001      | N / D <sup>1</sup>   | 57.98              | 2.440              |
| 0             | 0.01       | 0.77                 | 61.00              | - 0.005            |
| 0.001         | 0.01       | N / D <sup>1</sup>   | 52.20              | - 0.049            |
| 0.01          | 0.01       | 0.88                 | 61.31              | - 0.030            |
| 0.1           | 0.01       | 9.63                 | 44.48              | 0.403              |
| 1             | 0.01       | 2.75                 | 55.45              | 2.850              |
| 0             | 0.1        | 19.25                | 38.60              | 0.007              |
| 0.001         | 0.1        | 6.42                 | 31.24              | - 0.049            |
| 0.01          | 0.1        | 33.54                | 34.20              | N / D <sup>2</sup> |
| 0.1           | 0.1        | 9.63                 | 43.77              | 0.028              |
| 1             | 0.1        | 6.42                 | N / D <sup>2</sup> | N / D <sup>2</sup> |
| 0             | 1          | 25.17                | 35.20              | 0.050              |
| 0.001         | 1          | 19.25                | 36.83              | 0.013              |
| 0.01          | 1          | 19.25                | 38.26              | 0.058              |
| 0.1           | 1          | 19.25                | 36.29              | 0.086              |
| 1             | 1          | 0.51                 | 34.70              | 3.710              |
| 0             | 10         | 23.07                | 34.00              | 1.096              |
| 0.001         | 10         | 9.63                 | 33.23              | 0.950              |
| 0.01          | 10         | 19.25                | 34.27              | 1.030              |
| 0.1           | 10         | 9.63                 | 33.75              | 1.176              |
| 1             | 10         | 22.98                | 32.78              | 5.580              |

<sup>1</sup> N/D this solution did not produce any foam. <sup>2</sup> N/D this solution contained precipitated material and could not be determined by Ubbelohde viscometry.



decrease in surface tension correlates with increasing foam stability. Foaming of SDS solutions is expected to be influenced by the addition of a water-soluble polymer (9) as changes in viscosity and surface tension accompany changes in foam stability (23-25,37,42,48). Generally in regions approaching formation of stoichiometric polymer-surfactant complexes, the onset of precipitation of the complexes indicates desolvation of the polymer (46). Complex formation leads to enhanced foam stability and decreasing surface tension followed by a pronounced reduction in the solubility of the polymer complexes. At the point of maximum precipitation, the foam stability is reduced, possibly because the concentration of surface-active components is reduced due to adsorption by the polymer complex.

## Conclusions

All three polymers studied precipitate near their respective theoretical charge neutralization ratio when the concentrations of polymer and anionic surfactant are greater than 0.010%. However, at polymer concentrations less than 0.010%, a fixed concentration of sodium dodecyl sulfate is necessary to precipitate the complexes. The magnitude of the fixed concentration decreases as the charge density of the polymer increases for the polymers used in this study. The ability of these polyelectrolyte - surfactant complexes to reduce surface tension is independent of polymer architecture and dependent only upon adsorption of the surfactant species at the cationic polymer sites. Optimum performance in terms of foam produced per unit polymer concentration is achieved when neutralization of the charged polymer by oppositely charged surfactant begins to induce precipitation. Systems containing Polyquaternium 10 exhibit maximum foam stability slightly before the neutralization point. In contrast, MQNNED/surfactant adducts produce the most stable foams when a slight stoichiometric excess of surfactant is present. Increasing the charge density on the polymer, *i.e.* DQNNED, failed to enhance the contribution of the polymer additive to foam properties.

## Acknowledgments

This material is based upon work supported under a Society of Cosmetic Chemists' Graduate Research Fellowship to M. Manuszak Guerrini.

## Literature Cited

1. Robbins, C. R. *Chemical and Physical Behavior of Human Hair*; 3rd ed.; Springer-Verlag: New York, NY, 1994.
2. Lochhead, R. Y. *Cosmet. Toiletr.* **1992**, *107*, 131-156.
3. Wilkerson, V. J. *Biol. Chem.* **1935**, *112*, 329-335.
4. Goddard, E. D. *Colloids Surf.* **1986**, *19*, 301-329.
5. Bruer, M. M.; Robb, I. D. *Chem. Ind.* **1972**, *July*, 530-535.

6. Lindman, B.; Thalberg, K. ; **In:** *Interactions of Surfactants with Polymers and Proteins*; Goddard, E. D., Ananthapadmanabhan, K. P., Eds.; 1st ed.; CRC Press: Boca Raton, 1993, pp 203-276.
7. Li, Y.; Dubin, P. L. **In:** *Structure and Flow in Surfactant Solutions*; 1st ed.; American Chemical Society: Washington DC, 1994; Vol. 578, pp 320-336.
8. Chu, D.; Thomas, J. K. *J. Am. Chem. Soc.* **1986**, *108*, 6270-6276.
9. Goddard, E. D.; Hannan, R. B. *J. Coll. Int. Sci.* **1975**, *55*, 73-79.
10. Goddard, E. D.; Faucher, J. A.; Scott, R. J.; Turney, M. E. *J. Soc. Cosmet. Chem.* **1975**, *26*, 539-550.
11. Goddard, E. D.; Hannan, R. B. *J. Am. Oil Chem. Soc.* **1977**, *54*, 561-566.
12. Goddard, E. D.; Ananthapadmanabhan, K. P. *Interactions of Surfactants with Polymers and Proteins*; 1st ed.; CRC Press: Boca Raton, 1993, pp 427.
13. Goddard, E. D. *J. Soc. Cosmet. Chem.* **1990**, *41*, 23-49.
14. Goddard, E. D.; Leung, P. S. *Polym. Prepr. Am. Chem. Soc. Div. Polym.* **1982**, *23*, 47.
15. Leung, P. S.; Goddard, E. D.; Han, C.; Glinka, C. J. *Colloids Surf.* **1985**, *13*, 47-62.
16. Ananthapadmanabhan, K. P.; Leung, P. S.; Goddard, E. D. *Colloids Surf.* **1985**, *13*, 63-72.
17. Goddard, E. D.; Hannan, R. B. ; **In:** *Micellization, Solubilization, and Microemulsions*; Mittal, K. L., Ed.; 1st ed.; Plenum Press: New York, NY, 1977; Vol. 2, pp 835-845.
18. Jones, M. N. *J. Coll. Int. Sci.* **1967**, *23*, 36-42.
19. Isemura, I.; Imanishi, A. *J. Polym. Sci.* **1958**, *33*, 337-352.
20. Lange, V. H. *Kolloid Z. Z. Polymere* **1971**, *243*, 101-109.
21. Saito, S. *J. Coll. Sci.* **1960**, *15*, 283-286.
22. Goddard, E. D.; Phillips, T. S.; Hannan, R. B. *J. Soc. Cosmet. Chem.* **1975**, *26*, 461-475.
23. Lioni-Addad, S.; di Meglio, J.-M. *Langmuir* **1992**, *8*, 324-327.
24. Cohen-Addad, S.; di Meglio, J.-M. *Langmuir* **1994**, *10*, 773-778.
25. Bergeron, V.; Langevin, D.; Asnacios, A. *Langmuir* **1996**, *12*, 1550-1556.
26. Culberson, D.; Daly, W. H. *Polym. Prepr. Am. Chem. Soc. Div. Poly.* **1993**, *34*, 564-565.
27. Culberson, D.; Daly, W. H. *Polym. Mat. Sci. Eng.* **1994**, *71*, 498.
28. Culberson, D. A.; Ph.D. dissertation, Louisiana State University: Baton Rouge, 1995, pp 161.
29. Manuszak Guerrini, M. A.; Culberson, D. A.; Daly, W. H. ; US Pat. pending.
30. Manuszak Guerrini, M.; Negulescu, I. I.; Daly, W. H. *J. Appl. Polym. Sci.* **1998**, *68*, 1091-1097.
31. New, R. R. C. *Liposomes: A Practical Approach*; 1st ed.; IRL Press: New York, NY, 1990.
32. Malliaris, A.; Le Moigne, J.; Sturm, J.; Zana, R. *J. Phys. Chem.* **1985**, *89*, 2709-2713.

33. Mukerjee, P.; Mysels, K. J. *Critical Micelle Concentrations of Aqueous Surfactant Systems*; First ed.; U.S. Government Printing Office: Washington, DC, 1971; Vol. NSRDS-NBS 36.
34. Williams, R. J.; Phillips, J. N.; Mysels, K. J. *Trans. Faraday Soc.* **1955**, *51*, 728-737.
35. Manuszak Guerrini, M.; Ph.D. dissertation, Louisiana State University: Baton Rouge, 1997, pp 266.
36. Manuszak Guerrini, M.; Lochhead, R. Y.; Daly, W. H. *Colloids Surf. A*, submitted June 16, 1997.
37. Shah, D. O.; Djabbarah, N. F.; Wasan, D. T. *Coll. Polym. Sci.* **1978**, *256*, 1002-1008.
38. Schott, H. *J. Am. Oil Chem. Soc.* **1988**, *65*, 1658-1663.
39. Sita Ram Sarma, D. S. H.; Pandit, J.; Khilar, K. C. *J. Coll. Int. Sci.* **1988**, *124*, 339-348.
40. Ronteltap, A. D.; Damste, B. R.; DeGee, M.; Prins, A. *Colloids Surf.* **1990**, *47*, 269-283.
41. Prins, A.; In: *Advances in Food Emulsions and Foams*; Dickenson, E., Stainsby, G., Eds.; 1st ed.; Elsevier Applied Science: New York, NY, 1988, pp 91-122.
42. Friberg, S. E.; Blute, I.; Stenius, P. *J. Coll. Int. Sci.* **1989**, *127*, 573-582.
43. Shah, D. O. *J. Coll. Int. Sci.* **1971**, *37*, 744-752.
44. Ross, S.; Nishioka, G. *Foaming behavior of partially miscible liquids as related to their phase diagrams*; An International Conference organized by the Colloid and Surface Chemistry Group of the Society of the Chemical Industry; Brunel University, September 8-10, 1975, pp 15-29.
45. Ross, S.; Nishioka, G. *J. Phys. Chem.* **1975**, *79*, 1561-1565.
46. Ross, S.; Nishioka, G. *Colloid Polym. Sci.* **1977**, *255*, 560-565.
47. Ross, S.; Patterson, R. E. *J. Phys. Chem.* **1979**, *83*, 2226-2232.
48. Bikerman, J. J.; In: *Foams*; 1st ed.; Springer-Verlag: New York, NY, 1973, pp 33-64.

## Chapter 16

# Creaming and Rheology of Flocculated Emulsions

**Pretima Manoj, Andrew D. Watson, Annette J. Fillery-Travis,  
David J. Hibberd, and Margaret M. Robins**

**Institute of Food Research, Norwich Research Park, Colney,  
Norwich NR4 7UA, United Kingdom**

In many successful oil-in-water emulsion formulations, polymers are added to the aqueous phase. This can result in the flocculation of the oil droplets by a depletion mechanism. The flocculated droplets form a space forming structure which extends throughout the container, and if strong enough, may hold the droplets in suspension which is stable for a certain period of time. Creaming then starts with the upward movement of the droplets and proceeds by the collapse of the structure under the influence of gravity. We have found the time prior to the creaming, called the 'delay period', is affected by both the polymer and oil concentrations and consequently, is related to the strength of the flocs formed. We present here an attempt to understand the processes the emulsions undergo before and during the collapsing of the flocculated structure.

In many successful formulations, polymers are added to the aqueous phase of the emulsions to enhance the stability to creaming. However, the presence of non-adsorbing polymers in colloidal dispersions can induce phase separation and flocculation by a depletion mechanism. This behaviour has been investigated for the past two decades and various theoretical treatments have been successfully applied to this system, for instance the statistical mechanical approach of Russell and Gast (1). In this laboratory we have been investigating the formation of space-forming structures within these flocculated systems. It is thought that the presence of the structure can induce a delay time prior to the onset of creaming (2). The time delay phenomenon has already been reported by this laboratory by Parker *et al* (3) and in literature where the delay period is referred to as induction phase and transient gelation.

The presence of the delay period prior to creaming presents an interesting question which was addressed by Dickinson and co-workers (4). Does the delay originate from the rheology of the continuous phase or does the space filling structure change the dispersion rheology sufficiently to produce a yield stress effectively stopping flow or creaming of the complete emulsions? To address these questions, these issues require an extensive rheological investigation and we present here the results of creaming and rheological measurements on related oil-in-water emulsions.

## METHODS.

**Emulsion Preparation and Characterisation:** The emulsions were prepared from a premix. An oil phase was added to a solution of the non-ionic surfactant Brij35 (polyoxyethylene 23-lauryl ether, Sigma Chemical Company) and the emulsion prepared in a Waring blender using a predetermined cycle. The resulting premix was stable to coalescence and disproportionation over the timescale of the experiments. Three oil phases were used within the experimental protocol:

*Premix 1 for visual characterisation of creaming:* Premix 1 contained n-hexadecane (Cetane -  $C_{16}H_{34}$ ; density  $773.4 \text{ kg.m}^{-3}$  at  $20^\circ\text{C}$ , Sigma Chemical Company) in a surfactant solution.

*Premix 2 for ultrasonic monitoring of creaming:* Premix 2 contained a mixture (density  $693.2 \text{ kg.m}^{-3}$  at  $20^\circ\text{C}$ ) of n-heptane ( $C_7H_{16}$ ; density  $683.8 \text{ kg.m}^{-3}$  at  $20^\circ\text{C}$ ; SLR, Fisons) and hexadecane in the volume ratio 9:1 in surfactant solution. The purpose of mixing hexadecane with heptane was to increase the creaming rate.

*Premix 3 for Viscometry:* Premix 3 contained 1-bromohexadecane (Cetyl Bromide -  $(CH_3(CH_2)_{15}Br)$ ; density  $1000 \text{ kg.m}^{-3}$  at  $20^\circ\text{C}$ ; Fluka) as the dispersed phase in a surfactant solution. The purpose of using the density-matched system was to eliminate the effects responsible for creaming of the droplets during viscometry measurements.

The experimental emulsions were prepared by diluting the premixes with a polymer solution to obtain the desired concentrations of oil and polymer. The diluent was a mixture of an aqueous solution of the high molecular weight polymer hydroxyethylcellulose (HEC, Natrosol 250HR, Aqualon, mean  $r_g$  (radius of gyration) = 58 nm) and the preservative sodium azide ( $NaN_3$ , Sigma Chemical Company). Prior to use the polymer was purified by dialysis and then freeze-dried. The polymer was dispersed and hydrated by stirring together the ingredients whilst heating to  $80^\circ\text{C}$ , then allowing the solution to cool to room temperature. After preparation:

- the Premix 1 emulsions were transferred to measuring cylinders for visual monitoring;
- the Premix 2 emulsions were transferred to measurement cells for ultrasonic monitoring;

- the Premix 3 emulsions were transferred to a double gap geometry in Bohlin rheometer for viscometry measurements.

For ease of emulsion reference, a coding system has been adopted here as follows:

- a 20% (v/v) hexadecane (Premix 1) in the presence of 0.10% (w/w) HEC (with respect to aqueous phase), is labelled as [20H:0.10];
- a 34% heptane/hexadecane (Premix 2) emulsion in presence of 0.35% (w/w) HEC (with respect to aqueous phase), is labelled as [34HH:0.35] and finally,
- a 25% (v/v) bromohexadecane (Premix 3) emulsion in presence of 0.20% (w/w) HEC (with respect to aqueous phase), is labelled as [25B:0.20].

**Droplet Size Distribution:** The droplet size distribution of the premix emulsion was measured using a Malvern Mastersizer laser diffraction sizer (fitted with a small sample handling unit). The formation of the emulsions was found to be highly reproducible giving a size distribution of volume-mean diameter ( $d_{43}$ ) of 1.91  $\mu\text{m}$  for Premix 1; 2.01  $\mu\text{m}$  for Premix 2; and 1.98  $\mu\text{m}$  for Premix 3 (Figure 1). Our previous studies using the same systems (3, 5, 6) have shown the primary size distribution to remain unchanged in the course of the experiments, *i.e.* coalescence of the droplets was negligible.

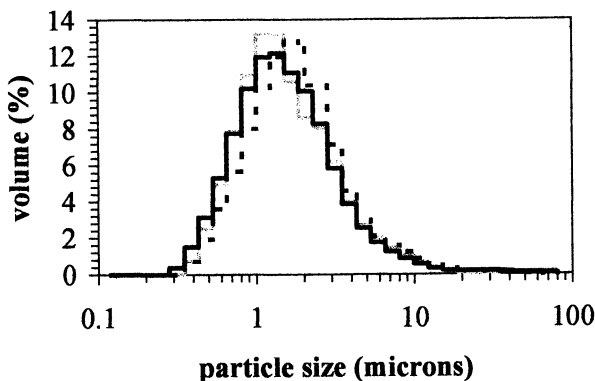


**Figure 1.** Size distributions for Bromohexadecane premix (—); Hexadecane premix (---) and Heptane/hexadecane premix (···).

### **Creaming Experiments:**

*Visual assessment of creaming:* Premix 1 dispersions and polymer diluents were poured into 100 ml measuring cylinders immediately after preparation. The cylinders were inverted ten times to ensure thorough mixing. The sample

emulsions were kept at 25°C and the movement of any creaming boundaries was followed with time. The turbidity of the serum layers below the developing creams was noted. The experiments were repeated between 3 and 5 times to obtain mean delay times. The standard deviation within each set of results was calculated to be less than 12%.

***Ultrasonic Monitor measurements:*** The IFR ultrasonic monitor (7) was used to characterise the creaming behaviour of Premix 2 emulsions by measuring the speed of ultrasound in emulsions at a series of heights of the container. The oil volume-fraction ( $\phi$ ) as a function of height was then calculated using a simple mixing theory (8). At each sampling time the validity of the calibration was verified by calculating the integrated oil volume-fraction over sample height. These oil volume-fraction profiles allowed early detection of creaming, and gave detailed information on the creaming process.

***Rheological Measurements:*** Viscosity (steady stress ( $\tau$ ) - shear rate ( $\dot{\gamma}$ )) measurements were carried out on a Bohlin Controlled Stress (CS) rheometer using a double gap geometry at 25°C. Solvent traps were used to minimise evaporation and dust settlement.

The viscometry measurements were carried out on; HEC solutions alone, emulsions without polymer and emulsions with polymer. Measurements were found to be highly consistent (<1% variation) throughout the experiments and no time dependence of the measurements was found.

## **RESULTS AND DISCUSSION:**

### **VISUAL CREAMING IN MEASURING CYLINDERS:**

***Emulsions prepared without polymer:*** Accurate visual observations were not possible due to the absence of a well-defined boundary.

***Emulsions with polymer:*** The addition of HEC (final concentration range 0.04 - 0.35% (w/w)) to Premix 1 (final oil concentration range 10 - 40% (v/v)) resulted in a significant change in the visual creaming behaviour of the emulsions, with the appearance of a rapidly creaming boundary at the base. At the onset of creaming, the boundary was characterised as either sharp or diffuse. The boundary regions in emulsions of 10% (v/v) oil volume-fraction and low HEC concentration were initially diffuse but sharpened as creaming progressed. In emulsions with high oil volume-fraction and high HEC concentration the boundary lines were sharp from the onset of creaming and creamed rapidly leaving a clear supernatant or sub-cream.

***Definition and calculation of delay time:*** Profiles of the creaming behaviour of the sample emulsions were obtained by measuring the height of the boundary between the colloid-rich fraction and the colloid-poor fraction as a function of time for each emulsion. Once started, the rate of creaming was constant (9) but a delay was

sometimes evident before creaming began. The delay could be quantified by extrapolation of the boundary height to zero movement. An example of the creaming behaviour is shown in Figure 2 for [34H:0.10] and [34H:0.35] emulsions. A delay was observed before creaming for both emulsions, the delay time being shorter for 0.1% (w/w) HEC than for 0.35% (w/w) HEC. Figure 3 represents the summary of delay times for all emulsions.

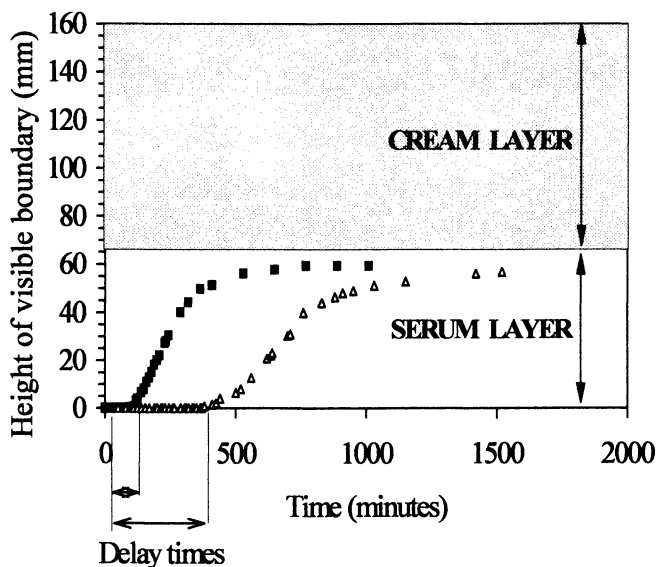


**Figure 2.** Height of visual boundaries and time at 25°C for 34% (v/v) hexadecane emulsions with ■ - 0.1% (w/w) HEC; and ▲ - 0.35% (w/w) HEC.

**Additional visual observations:** After the onset of creaming, the appearance of serums varied in their turbidity, consistent with the presence or absence of residual oil droplets. The [34H:0.35] emulsion left behind a clear layer from the start, whereas the [34H:0.10] emulsion initially left behind a turbid serum layer which cleared slowly over a period of days. The initial turbidity (after the majority of the oil had creamed rapidly to the top) gave an indication of whether the system was fully flocculated or contained floc(s) in coexistence with unflocculated droplets. Plate 1 shows [34H:0.04], [34H:0.10] and [34H:0.35] emulsions, 16 days after preparation. At 0.04% (w/w) HEC there was a boundary at approximately 47 ml, although below the boundary the system was opaque. At the higher HEC concentrations the serum layers became less opaque, and at 0.35% (w/w) HEC the serum was clear from the onset of creaming. The turbid serum layers contained droplets which creamed very slowly due to high viscosity of the HEC continuous phase. Close examination of the ultrasonic creaming data (discussed below) showed that the remaining fraction of oil



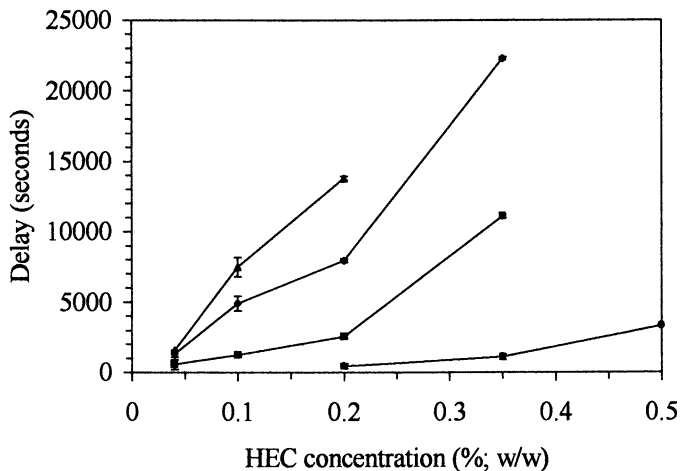


**Figure 3.** Delay times of emulsions as a function of HEC where ● - 10% (v/v) hexadecane; ■ - 25% (v/v) hexadecane; ◆ - 34% (v/v) hexadecane & ▲ - 40% (v/v) hexadecane. The error bars represent the standard deviation of the measurements on replicate samples.

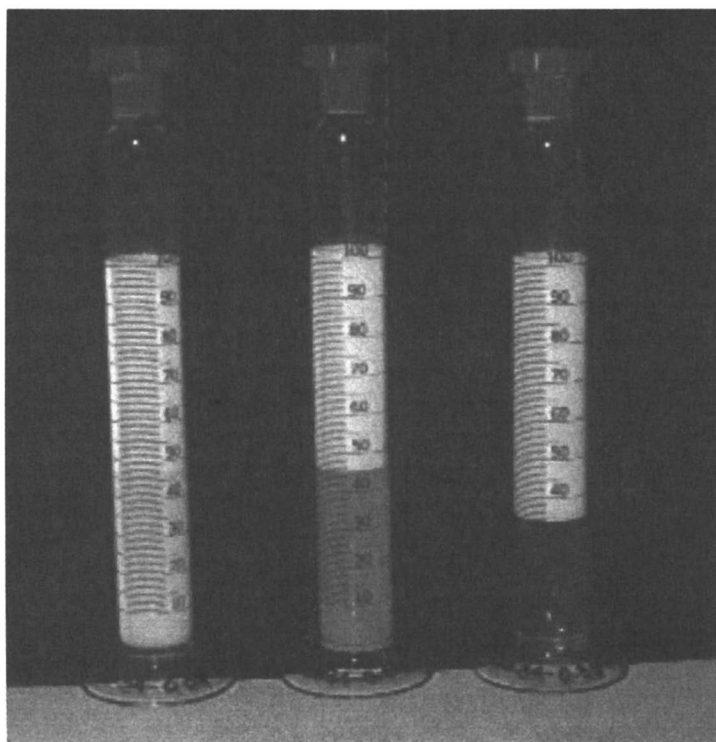


**Plate 1.** Appearance of cylinders containing 34% (v/v) hexadecane with HEC (from left to right) 0.04, 0.10 and 0.35% (w/w), after 16 days at 25°C.

was composed of individual droplets. However, at very low residual oil volume-fractions, visual observations of turbidity are more sensitive than the ultrasonic monitor to the presence of these suspended individual droplets.

### ULTRASONIC MONITORING:

An in-depth study of the creaming behaviour of emulsions without and with polymer was carried out using ultrasonic monitoring.

***Emulsions prepared without polymer:*** The ultrasonic creaming profile for 20% (v/v) heptane/hexadecane emulsion (Premix 2) in the absence of polymer is shown in Figure 4. At 0.22 day (~ 7 hours) the oil had begun to move to the top of the cell and formed a thin cream layer of approximately 80% (v/v) oil. No sharp boundary was observed in the creaming emulsions. After 4 days, the oil had cleared from the base of the cell (no oil detected at ~13 mm height from the base).

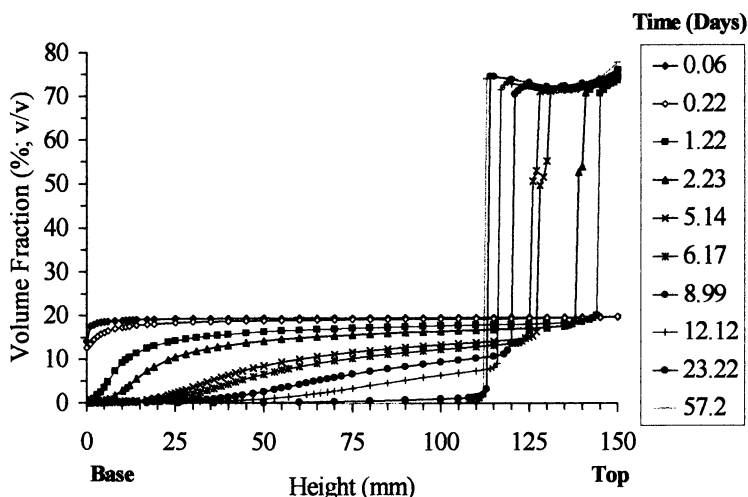


**Figure 4.** Ultrasonic creaming profiles during creaming of 20% (v/v) emulsion in the absence of polymer. Each line shows the measured variation of oil volume-fraction with height at the each sampling time.

***Emulsions prepared with polymer:*** Figure 5 shows the creaming of a [20HH:0.025] emulsion monitored using the ultrasonic technique. The profiles revealed two distinct fractions, a rapidly-moving population which creamed within a day, leaving almost half the oil behind in a slower-moving fraction. Further analysis indicated the emulsion contained two phases, a flocculated phase in coexistence with unflocculated droplets.

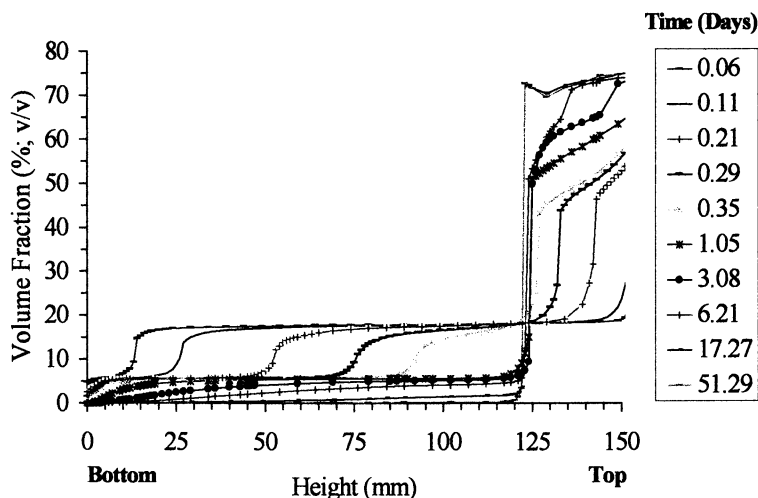


**Figure 5.** Ultrasonic creaming profiles during creaming of [20HH:0.025] emulsion, showing the coexistence between a rapidly-rising flocculated phase and a fraction of slower-moving droplets.

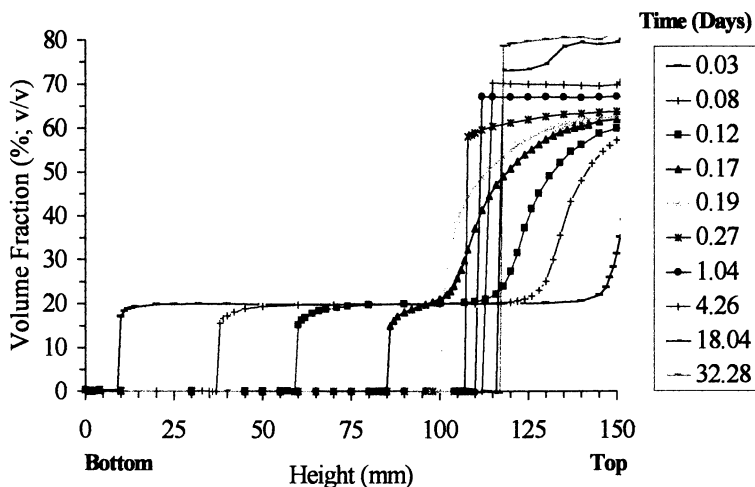
By varying the HEC concentration in the range 0.015% to 0.04% (w/w), the amount of flocculation varied in the range 1 - 98% (2). The unflocculated droplets creamed slowly, due to the increased viscosity of the polymer solution, and the serum was visually cloudy until all the oil had reached the cream layer.

Figure 6 shows the ultrasonic profiles for [20HH:0.1] emulsion. The creaming profiles showed a sharp boundary rising rapidly with time leaving a sub-cream serum containing no measurable oil. Since the serum was also visually clear, we interpreted the profiles as indicative of complete flocculation.

*Creaming behaviour of the emulsions.* We have observed two distinct modes of creaming in emulsions containing the non-absorbing polymer HEC. In **Type I creaming**, emulsions remains opaque at the base of the sample for a significant period of time whilst a concentrated cream layer develops at the top of the sample. The thickness of the cream layer gradually increases with time, and only after most of the oil has reached the cream is there any visible sign of clearing from the base of the sample, which may remain turbid. The boundary between the serum and the creaming droplets is very hazy and indistinct. This behaviour is characteristic of polydisperse emulsions in the presence of little or no polymer, where individual droplets or small aggregates move independently to the top of the container. Creaming of this type is very difficult to monitor visually but may be characterised using the IFR ultrasonic monitor (Figures 4 & 5) (7).

In **Type II creaming**, there is a clear boundary between the creaming emulsion and the serum layer at the base of the sample. Creaming occurs rapidly and the

remaining serum can be clear or turbid. Previous investigations of this behaviour (9) have suggested the presence of a high degree of flocculation within the creaming emulsion sufficient to form a space spanning structure. This type of creaming is clearly visible (Figure 6).



**Figure 6.** Ultrasonic creaming profiles during creaming of [20HH:0.10] emulsion, showing formation of a sharp boundary as the flocculated droplets rise to the cream layer.

*Phase behaviour of the emulsions* Upon increasing the HEC concentration added to a 20% (v/v) oil emulsion (3) we have observed the formation of a concentrated colloidal phase, in coexistence with a dispersed colloid-poor phase. These phases separated spatially under gravity, the colloid-rich fraction creaming rapidly in comparison with the colloid-poor fraction. Analysis of the ultrasonic creaming profiles of these emulsions showed the colloid-rich phase was composed of flocculated droplets and the colloid-poor phase consisted of individual droplets. We suggested the formation of these phases could be due to one or both of the following effects:

- Size segregation of larger droplets due to preferential flocculation;
- Phase separation which is independent of droplet size.

No significant difference was found between the size distributions of the droplets contained within each phase and we therefore concluded that phase separation was responsible, at least in part, for the observed creaming behaviour.

The flocculation behaviour of the emulsions are summarised in Figure 7 in the form of a phase diagram. The phase diagram is based on the turbidity of the serums and it shows three regimes: non-flocculated, phase coexistent and fully flocculated emulsions. The boundary between the non-flocculated and the phase coexistent region

we have denoted as the primary critical concentration (PCC) and the boundary between the phase coexistent and fully flocculated region as the secondary critical concentration (SCC). No attempt was made in this study to delineate quantitatively the boundaries between the regions, and the upper and lower limits for SCC are shown. The data are shown as solid points where the serum sub-cream layers were initially turbid, and unfilled points where the serum was clear from the onset of creaming.

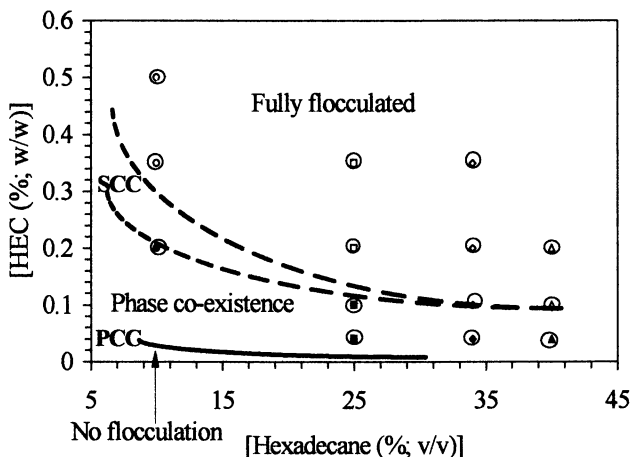


**Figure 7.** Phase diagram of hexadecane - HEC emulsions based on initial turbidity of serums left behind after creaming at 25°C (closed symbols - cloudy serum; open symbols - clear serum) in association with the existence of delay period (O). The HEC concentration is the total concentration in the continuous phase.

**Mechanism of delay** Figure 7 also shows the systems exhibiting a delay time significantly greater than zero. Delays were observed within both the phase coexistent and the fully flocculated regions. Within the phase coexistent region a prerequisite of delay was the presence of a sharp boundary upon creaming. We propose two hypotheses for the existence of the observed delay in creaming:

- The viscous nature of the continuous phase reduces the rate of flocculation and the delay is simply the timescale to form flocs which cream rapidly; or
- There is the rapid formation of a space-spanning flocculated structure of sufficient “compressive strength” to withstand buoyancy forces. We speculate that the eventual collapse of such a network could be due to coarsening of the structure by droplet rearrangement.

We will consider each of these hypotheses in turn.

- **Is the delay due to slow flocculation?** The variation of delay time with HEC concentration for each oil volume-fraction is shown in Figure 3. For a particular HEC concentration the viscosity of the continuous phase is constant and the

droplet encounter rate, and hence the rate of flocculation, would be expected to increase with volume-fraction. Thus a *decrease* in delay time would be expected upon increasing the oil volume-fraction if the observed delay time is the consequence of relatively slow flocculation. For all the HEC concentrations used in this study the delay time was found to *increase* with increasing oil volume-fraction. This result contradicts the hypothesis of slow flocculation particularly when the delay times observed within this study far exceed the characteristic timescale of droplet diffusion and encounter rates. The sharp boundary would require that the flocs all creamed at the same rate, and it seems unlikely that they would have a monodisperse effective size distribution.

- *Is the delay phase due to rearrangement and collapse of a flocculated space-spanning structure?* In our previous studies, and in common with other workers, we have identified the formation of a sharp creaming boundary to be symptomatic of a flocculated, space-spanning structure creaming as a single entity (9). The form of the ultrasonic creaming profiles supports this interpretation. Upon creaming the oil droplets ascended the container at an uniform rate producing a sharp discontinuity in volume-fraction. There was no broadening of the boundary that might suggest movement of separate aggregates with varying speed.

We therefore hypothesise that the observed delay is due to the formation of the space-spanning structure. Such a hypothesis implies:

[1] the presence of a yield stress or compressibility in the network;

[2] the delay time represents the time for the diffusion of the droplets to rearrange to a channelled structure. If droplet diffusion was to be the controlling factor in the delay time, then a relationship between the delay time and an “effective viscosity” of the medium is to be expected (5, 19). As a first approximation, the mean field theory describes an “effective viscosity”,  $\eta_e$ , that takes account of the droplet volume-fraction,  $\phi$ :

$$\eta_e = \eta_0 \left( 1 - \frac{\phi}{\phi_m} \right)^{\frac{-5\phi_m}{2}} \quad [1]$$

where  $\eta_0$  is the viscosity of the continuous phase and  $\phi_m$  the maximum packing oil volume-fraction. Figure 8 shows the delay time and estimated  $\eta_e$  of each emulsion. The interesting point about this correlation is that an expression that is analogous to a single droplet diffusion rate allowed for the  $\phi$  dependence in the rearrangement time.

This relationship, and the search for the existence and quantification of yield stress prompted a detailed study of emulsion rheology.

## **VISCOMETRY EXPERIMENTS:**

*Flow behaviour of polymer solutions:* The viscosity - shear rate profiles for aqueous HEC solutions in the concentration range of 0.005% to 0.5% (w/w) are shown in Figure 9. In the concentration range 0.005% to 0.35% (w/w) the apparent polymer solution viscosity was essentially independent of shear rate (*i.e.* Newtonian).

At 0.5% (w/w) HEC the apparent viscosity ( $\eta_a$ ) showed appreciable dependence on shear rate. At low shear rates,  $\eta$  remained constant at a fixed

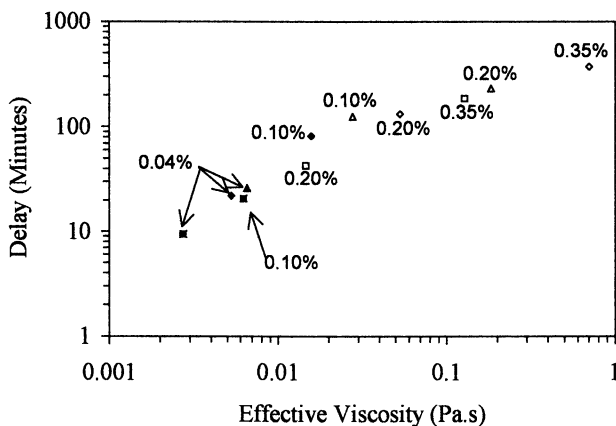


**Figure 8.** Measured delay time and the estimated effective viscosity of 25% (square), 34% (diamond) & 40% (triangle) (v/v) oil emulsions in presence of 0.04%; 0.10%; 0.20% & 0.35% (w/w) HEC. Filled and unfilled symbols represent cloudy and clear serums respectively seen after creaming.

maximum value - the *zero shear viscosity*,  $\eta_0$  - but at higher shear rates, shear thinning was observed. Shear thinning can be rationalised in terms of polymer entanglement where the rate of disentanglement exceeds the rate at which the new entanglement form and this leads to a reduction in the cross-link density and, in consequence, the viscosity. The polymer coil overlap critical concentration ( $C^*$ ) was calculated to be approximately 0.28% (w/w).

***Flow behaviour of emulsions in the absence of polymer:*** The apparent viscosities determined for the emulsion systems in the absence of HEC are shown in Figure 10. The flow behaviour was Newtonian in character at dispersed phase volume-fractions ranging from 10% to 34%. At 40% (v/v) oil the emulsion exhibited shear thinning, and was therefore identified as non-Newtonian.

***Flow behaviour of emulsions with polymer:*** The flow behaviour of emulsions in the presence of HEC were studied for oil volume-fractions of 10% to 40% (v/v) and polymer concentrations of 0.005% to 0.5% (w/w). As an example, Figure 11 represents the flow curves of 25% (v/v) Bromohexadecane emulsions in the presence of HEC polymer.

***Rheological properties of emulsions:*** Emulsions with no polymer, and polymer solutions alone exhibit Newtonian behaviour. But emulsions with polymer exhibit non-Newtonian or shear thinning behaviour. The shear thinning profiles suggest the break-up of a space-spanning structure of aggregated droplets into individual droplets at high shear rates. The concentration of polymer in emulsions is

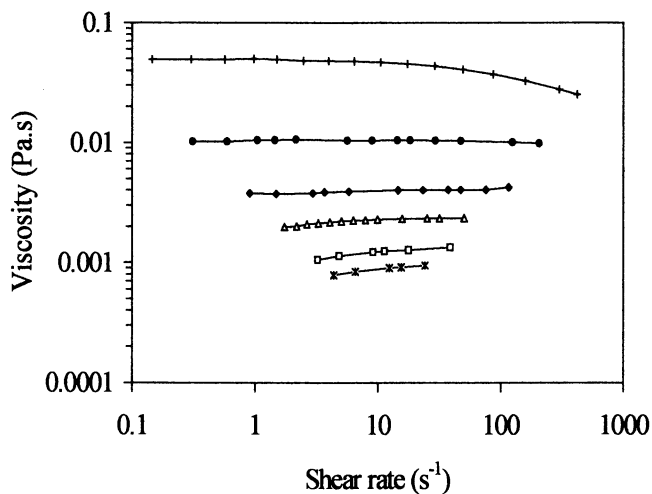


**Figure 9.** Viscosity - Shear rate profiles for HEC polymer solutions at 25°C (+ 0.5%; ● 0.35%; ◆ 0.2%; △ 0.1%; □ 0.04% and \* 0.005% (w/w) HEC).

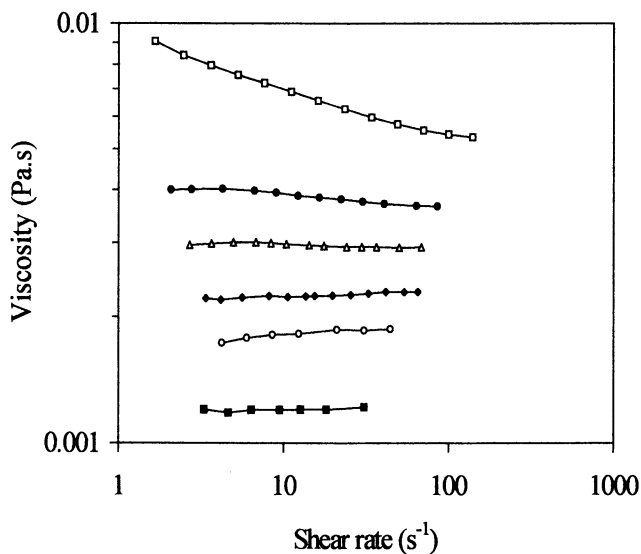


**Figure 10.** Viscosity - Shear rate profiles of Bromohexadecane emulsions with no polymer at 25°C (□ -40%; ● -34%; △ -30%; ◆ -25%; ○ -20% and ■ -10% (v/v)).



an important factor. There is a critical polymer concentration ( $C_0$ ) below which the depletion effect is insignificant and the emulsions with polymer are generally Newtonian (Figure 10). Above  $C_0$  the dispersions are generally non-Newtonian, indicating a structure break up at high shear rates. The  $C_0$  for the 25% (v/v) Bromohexadecane emulsions is 0.04% (w/w) polymer, which is in agreement with the PCC value obtained from the creaming data. This holds true for emulsions containing other oil volume-fractions.

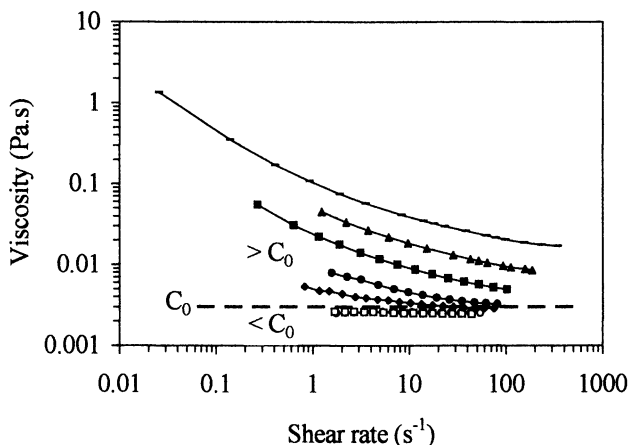


**Figure 11.** Viscosity - Shear rate profiles of 25% (v/v) Bromohexadecane emulsions with (○ -- 0.005%; □ - 0.01%; ◆ - 0.025%; ● - 0.04%; ■ - 0.1%; ▲ - 0.25%; - - 0.35% (w/w)) HEC polymer at 25°C

**Yield Stress:** Our second hypothesis postulates that during the delay period, the flocs interconnect with one another to form a space-spanning structure capable of resisting the buoyancy of the droplets. If true, this would imply the presence of a yield stress within the structure. By yield stress, we adopt a working definition as given by Nguyen and Boger (10, 11); that below a certain critical stress, the yield stress, a material may not flow, but deforms plastically like a solid, with a strain recovery upon the removal of the stress. Above the yield stress, the material flows as a fluid with some viscosity. A yield stress, regarded as a point of transition between solid-like and liquid-like behaviour, in depletion-flocculated *particulate* dispersions has been reported by several investigators (12, 13, 14, 15).

**Determination of Yield Stress** There are a number of models which may be used for the derivation of the dynamic yield stress for non-Newtonian systems which show pseudoplastic flow. The non-linearity of the observed flow behaviour negates the use of the Bingham model (16). Other alternatives were investigated, for example, the Casson model (17) :

$$\tau^{1/2} = \tau_c^{1/2} + \eta_c^{1/2} \dot{\gamma}^{1/2} \quad [2]$$

where  $\tau$  is shear stress,  $\dot{\gamma}$  is shear rate,  $\tau_c$  is Casson yield stress and  $\eta_c$  is Casson viscosity. The models were found to be unstable with respect to changes in number of data points used. Fits tended to be poor for the low shear rate end of the data, translating into significant errors in yield stress estimates (6). We propose the simple, if inelegant, strategy of extrapolating from the lowest two reliable readings at the linear shear stress axis to obtain an upper bound for the yield stress. This strategy takes no account of possible radical changes in behaviour at the very lowest shear rate values. It is, however, independent of any modelling assumptions. Figure 12 gives an example for a few emulsions, showing how yield stress can be obtained by the “eye” method.

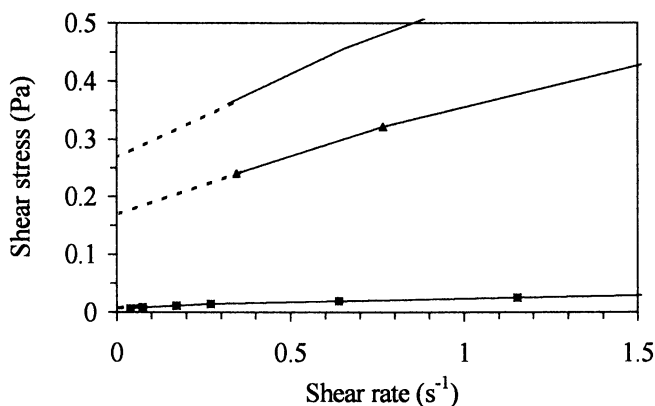


**Figure 12.** Determination of Yield Stress by “eye” method. (— - 40 % (v/v) Bromohexadecane with 0.5% (w/w) HEC; ▲- 34% (v/v) Bromohexadecane - 0.5% (w/w) HEC and ■ - 25% (v/v) Bromohexadecane - 0.1% (w/w) HEC).

Yield stress estimates do rise with increased oil volume-fraction and HEC concentration, in line with what might be expected for a true yield stress system. However, this rise may simply reflect the decreased curvature with both oil volume-fraction and HEC concentration shown by the flow curves at the lowest accessible shear rates. In view of many uncertainties and the small magnitude of the upper band at the yield stress - the largest is 0.26 Pa for [40B:0.5] emulsion as determined ‘by eye’ - we cannot claim with confidence to have fully quantified a yield stress value. It is possible that the measurement of very low dynamic yield stress values is, in fact, inappropriate, in the context of flow, due to technical difficulties.

In addition, we speculate that at very low stresses, the particulate nature of the system may become significant, in which case physical features not apparent at high stresses may come into play. Yield stress values as low as  $10^{-2}$  Pa have been quoted in the literature (18) as having a role in the properties of weak particle gels.

*Phase diagram of emulsions showing delay period & flow behaviour:* A summary of the delay period data and the flow behaviour of the emulsion systems as a function of polymer concentration and oil volume-fraction is shown in the phase diagram (Figure 13). One should be aware that the state of flocculation and presence of a delay period have been determined for hexadecane emulsions, and the rheological behaviour refers to the bromohexadecane emulsions. No attempt has been made to quantify the exact form of the phase boundaries (see Figure 13) between non-flocculated, phase coexistent and fully flocculated regions and hence these are represented as hatched regions. Shear thinning behaviour was observed within the phase coexistent and fully flocculated regions.

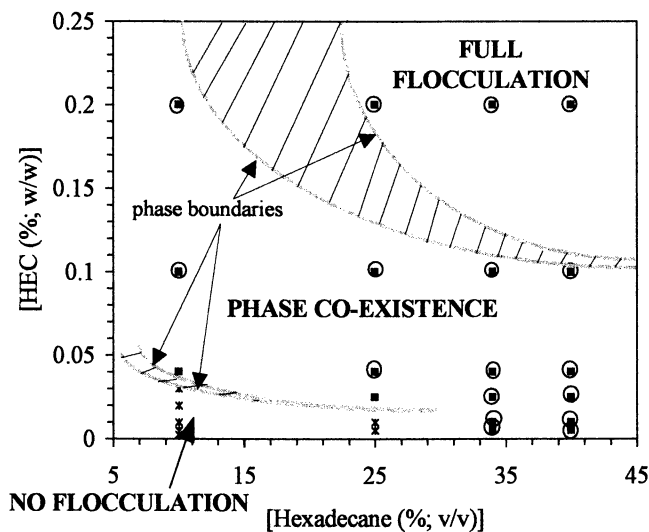


**Figure 13.** Summary of flocculation, creaming and flow behaviour for emulsions as a function of HEC and oil concentration. The state of flocculation and the presence of a delay period were determined for hexadecane-in-water emulsions, the rheological measurements were conducted on 1-bromohexadecane emulsions. Shear thinning behaviour is denoted by the symbol ■ and Newtonian behaviour by the symbol \*. The presence of a delay time greater than 20 minutes is shown by the symbol ○.

A significant delay period occurs for each oil volume-fraction at polymer concentrations higher than the initial appearance of shear thinning. This is consistent with the formation of structure within the flocculated emulsions which increases in 'strength' upon increasing the polymer concentration.

Figure 8 showed a simple correlation between the observed delay time and an estimated "effective viscosity" for the emulsions. A similar relationship is obtained using a measured viscosity, as in Figure 14. As before, the data for different  $\phi$  collapse onto a simple relationship, showing that similar factors contribute to the rearrangement time as the flow behaviour of the emulsions. A more detailed rheological study, using dynamic measurements, is in progress.

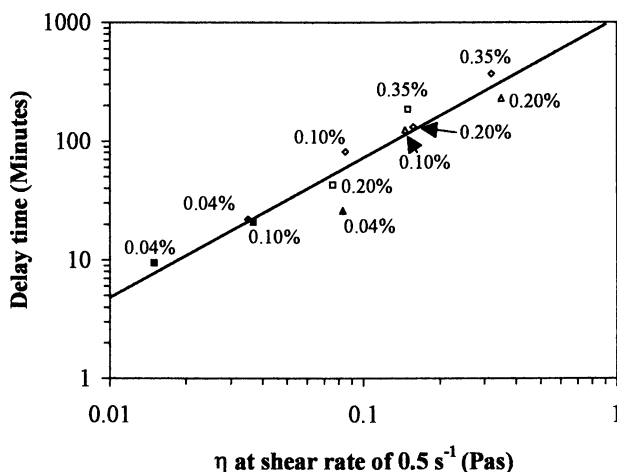


**Figure 14.** Correlation of delay time and viscosity at the shear rate of  $0.5 \text{ s}^{-1}$  for 25% (v/v) (squares), 34% (v/v) (diamonds) and 40% (v/v) (triangles) oil emulsions in presence of 0.04%, 0.10%, 0.20% and 0.35% (w/w) HEC. Filled and unfilled symbols represent cloudy and clear serums respectively seen after creaming.

## CONCLUSIONS.

- Experiments on a series of depletion-flocculated emulsions showed that the degree of flocculation, type of creaming, creaming rate and delay before creaming were dependent on the oil volume-fraction and polymer concentration.
- With increasing HEC the polydisperse emulsions creamed firstly as individual droplets; then as two fractions - a flocculated phase in coexistence with individual droplets; and finally as a fully flocculated structure with a constant boundary rate.
- Delays before creaming were observed in the fully-flocculated emulsions and in the partially-flocculated emulsion at high oil volume-fraction.
- The formation of a space-spanning structure of flocculated droplets occurs within the phase-coexistent and fully flocculated regions of the polymer/emulsion phase diagram. The origin of this structure is depletion flocculation of the oil droplets.
- Coincident with the formation of the structure, significant shear-thinning behaviour is observed in the steady-state rheology of the emulsion.
- It is not possible to determine an good estimate of the dynamic yield stress from these measurements due to instability in the fit of the commonly used models at low shear stress. The best estimates of the yield stress obtained within the constraints suggest that the value required to resist buoyancy of the network and contribute to the observed delay period prior to creaming is very low.
- The delay time appears to be related to the viscosity of the emulsions, implying similar factors in rearrangement as in flow.

## ACKNOWLEDGEMENTS.

The authors would like to acknowledge funding from the BBSRC under the ROPA scheme and the Institute's Competitive Strategic Grant.

## References

1. Gast, A. P.; Hall, C. K. and Russell, W. B., *Faraday Disc. Chem. Soc.*, No. 76, pp. 189-201; *Abstracts of Papers of the ACS* **1983**, *186*, 80. Gast, A. P.; Russell, W. B. and Hall, C. K., *J. Colloid Interface Sci.* **1986**, *1*, 161.
2. Fillery Travis, A. J.; Gunning, P. A.; Hibberd, D. J.; and Robins, M. M., *J. Colloid Interface Sci.* **1993**, *159* (1), 189-197.
3. Parker, A.; Gunning, P.A.; Ng, K., and Robins, M. M., *Food Hydrocolloids* **1995**, *9* (4), 333-342.
4. Dickinson, E.; Golding, M. and Povey, M. J. W., *J. Colloid Interface Sci.* **1997**, *185*, 515.
5. Manoj, P.; Watson, A.; Hibberd, D. J.; Fillery-Travis, A. and Robins, M., Part I. *J. Colloid Interface Sci.* **1998**, *207*, 283-293.
6. Manoj, P.; Watson, A.; Hibberd, D. J.; Fillery-Travis, A. and Robins, M., Part II. *J. Colloid Interface Sci.* **1998**, *207*, 294-302
7. Howe, A. M.; Mackie, A. R. and Robins, M. M., *J. Disp. Sci. Tech.* **1986**, *7* (2), 231-243.
8. Urick, R. J., *J. Appl. Phys.* **1947**, *18*, 983-987.
9. Robins, M. M., *ACS Symposium Series* **1991**, *448*, 230-246.
10. Nguyen, Q. D. and Boger, D. V., *Annu. Rev. Fluid Mech.* **1992**, *24*, 47.
11. Cheng, D. C. H., *Rheologica Acta* **1986**, *25* (5), 542.
12. Liang, W.; Tadros, Th. F. and Luckham, P. F. *J. Colloid Interface Sci.* **1993**, *155*, 156.
13. Liang, W.; Tadros, Th. F. and Luckham, P. F., *J. Colloid Interface Sci.* **1993**, *158*, 152.
14. Liang, W.; Tadros, Th. F. and Luckham, P. F., *J. Colloid Interface Sci.* **1993**, *160*, 183.
15. Buscall, R.; McGowan, I. J. and Mumme-Young, C. A., *Faraday Disc. Chem. Soc.* **1990**, *90*, 115.
16. Pal, R., *Encyclopaedia of Emulsion Technology*; Marcel Dekker: New York, 1996, Vol. 4.; Chapter 3, pp. 93.
17. Casson, N., *Rheology of Disperse Systems*; Pergamon Press Ltd., London, 1959, pp 84.
18. Van Vliet, T. and Walstra P., *Food Colloids*; Royal Society of Chemistry Special Publication No. 75, Great Britain, 1989, pp. 206.
19. Ball, R. C. and Richmond, P., *Phys. Chem. Liq.* **1980**, *9*, 99-116.

## Chapter 17

# Building Aqueous Viscosity through Synergistic Polymer–Polymer Interactions

James V. Gruber and Peter N. Konish<sup>1</sup>

Amerchol Corporation, 136 Talmadge Road, Edison, NJ 08818–4051

The rheology of aqueous solutions containing a hydrophobically-modified, cationic cellulose ether, **2**, blended with amylose, **3**, a linear polyglycan obtained from potato starch, was examined. The viscosity of solutions containing 0.5, 1.0 and 2.0 weight percent **2** optimally blended with amylose concentrations of 0.12, 0.25 and 0.5 weight percent, respectively, were investigated under controlled shear and stress. The mixtures show indications of building yield at increasing concentrations of **2** and are pseudo-plastic at high shear. The storage and loss moduli were examined as well and indicate that **2** and **3** interact synergistically to form gels at the higher concentrations of **3** employed. The data continues to support a hypothesis reported earlier suggesting that mixtures of **2** and **3** interact through a non-covalent crosslinking mechanism where the hydrophobic groups attached to **2** intercalate into the interior of the helix formed by the amylose, a so-called “Lariat Complex”.

It is the nature of polymers to interact either synergistically or antagonistically with other polymers when they are intimately mixed.<sup>1</sup> That is, when one polymer species is blended with another, the two materials may either have a molecular affection for one another, or they may be repelled by one another. In truth, this description is simplistic as portions of various copolymers may attract while other regions repel. It is often difficult to predict these interactions in advance. Part of the difficulty arises from the fact that polymers can assume various configurations, e.g., random, helical, loose or tight coils, pleated sheets, folds, etc. It thus becomes necessary to predict in a more 3-

<sup>1</sup> Current address: Mane, USA, 60 Dermarest Drive, Wayne, NJ 07479.

dimensional sense whether interactions will be cooperative or repulsive.

When interacting polymers are dissolved in a solvent, these attractions and repulsions are further compounded by solvation effects. Water is a particularly tricky solvent which can control and manipulate the 3-dimensional structure of polymers through strong hydrogen bonding and hydrophobic effects. In addition, water can transmit electrostatic effects and polymer counter-ions which can further influence polymer morphology and polymer/polymer interactions.

Regardless of these difficulties, efforts to better understand aqueous polymer/polymer interactions have continued to develop and several classic aqueous polymer/polymer synergisms have attracted research attention. These include, for example, the interaction of xanthan gum with gluco- or galactomannans,<sup>2</sup> *k*-carrageenan with galactomannans<sup>3</sup> and poly(acrylic acid) with poly(ethylene oxide).<sup>4</sup>

Cairns, et al., in describing the synergistic study of binary polysaccharide gels, developed conceptual models of various types of polysaccharide/polysaccharide interactions, Figure 1.<sup>5</sup> Within a polymer/polymer network, synergistic interactions can be described as either: a) single polymer networks containing a second polymer, b) interpenetrating networks, c) phase-separated networks or d) coupled networks. Distinguishing one type of interaction from another is not always straightforward.

Coupled networks are a particularly interesting form of polymer networking because in a solvated system certain portions of one of the polymer chains must have a particular affection (stronger than the powerful forces of hydration) for a portion of the other polymer chain. Sometimes these effects can be a manifestation of a common ion shared by both polymers. More intriguingly, the effect can be driven by hydrophobic properties inherent in certain regions of each polymer. Regardless of the source of the synergism, the points of attachment are referred to as junction zones.<sup>5</sup> When junction zones develop in aqueous polymer solutions, the effects can be quite pronounced. A particularly well known example of a synergistic aqueous rheological viscosity response can be seen in the interaction of xanthan gum with guar, a polygalactomannan.<sup>6,7</sup> The nature of the junction zone in this classic example is still being debated.

Recently, we reported on a new type of synergistic polysaccharide/polysaccharide interaction which is an extension of Cairns' coupled network.<sup>8</sup> This network occurs when a water-soluble, hydrophobically-modified, cationic cellulose ether (Polyquaternium-24), **2**, is blended with solubilized potato amylose, **3**, a nearly linear polyglucan. The synergistic interaction of these two polysaccharides has potential applications in the development of surfactant-free emulsions and skin lotions.<sup>9</sup> We wish to expand our discussion on this unique synergistic polymer/polymer system by examining some of the rheological properties of solutions containing these two polymers. This discussion, we feel, further supports our hypothesis that these two polymers interact through a newly described junction zone which develops when the amylose coils in a helical configuration around the hydrophobic groups of the cationic cellulose ether.

## Experimental

**Materials.** The formation of the Polyquaternium-24/amylose complex has been described elsewhere.<sup>8</sup> In summary, an aqueous solution of Polyquaternium-24 heated

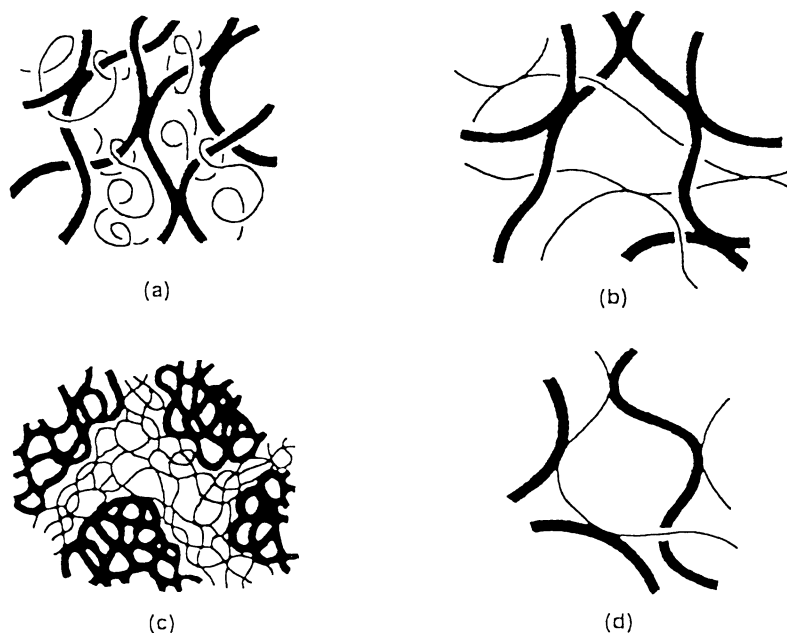


Figure 1. Types of binary polysaccharide gel-structure. Polysaccharide *A* [■], polysaccharide *B* [—]: (a) single polymer network containing the second polymer within the gel, (b) interpenetrating networks, (c) phase-separated networks, (d) coupled network “Reprinted from *Carbohydrate Polymers*, 160, Cairns, P.; Miles, MJ.; Morris, VJ.; Brownsky, GJ, X-Ray Fibre-Diffraction Studies of Synergistic, Binary Polysaccharide Gels, 411-423, 1987, with permission from Elsevier Science”.



to 90 °C is carefully blended with a solution of potato amylose also at 90 °C (the amylose must be hydrated at higher temperatures, near 110 °C in a pressure tube or a pressure cooker prior to blending), such that the resultant mixture composes 1.0 part Polyquaternium-24, 0.25 part amylose, and enough deionized water to bring the mixture to 100 parts. The hot mixture is then placed into a 2-gallon water bath heated to 90 °C and the temperature is allowed to cool slowly overnight by removing the power to the bath. This slow cooling allows the polymer complex to form its optimum solution viscosity. Xanthan gum was obtained from Aldrich and was used as received.

**Equipment.** All rheological studies were conducted on either a Bohlin VOR rheometer using a C25 cup-and-bob or a Double Gap (DG) 24/27 cup-and-bob, or a Bohlin CS rheometer using a CP 4/40 cone and plate or a Double Gap (DG) 40/50 cup and bob. The temperature was maintained at a constant 30 °C during the measurements. The viscosity measurements were averaged over 40 seconds with a small 0.1 second delay between measurements. To establish the linear viscoelastic region of the polymer complexes in a dynamic test, the solutions were subjected to a stress sweep at a fixed frequency of 1 Hz. The resulting spectra indicated that a controlled stress of 20 Pa would be sufficient to run the resulting dynamic analysis. All the rheological data was subsequently transferred to Microsoft Excel 7.0 for graphing.

## Results and Discussion

A summary of our initial empirical observations on the complex between amylose and Polyquaternium-24 can be found in Table I.<sup>8</sup> From these observations, we proposed a

**Table I. Summary of empirical data on interactions of Polyquaternium-24 and amylose.**

| Observation  | Implication   |
|--|---|
| <ul style="list-style-type: none"> <li>No effect from Polyquaternium-10, 1</li> </ul>  | <ul style="list-style-type: none"> <li>Hydrophobe required for synergism</li> </ul>   |
| <ul style="list-style-type: none"> <li>Synergism develops on cooling</li> <li>Pseudoplastic</li> </ul>   | <ul style="list-style-type: none"> <li>Thermoreversibility</li> <li>Typical for polysaccharide solutions</li> </ul>                     |
| <ul style="list-style-type: none"> <li>Inhibits amylose retrogradation</li> <li>Ratio of amylose to hydrophobe is approximately 1:2</li> </ul> | <ul style="list-style-type: none"> <li>Amylose is not “free” to complex</li> <li>Two hydrophobic groups per amylose molecule</li> </ul> |

mechanism of junction zone formation which requires the amylose to wrap itself around two adjacent hydrophobic groups on the Polyquaternium-24, Figure 2. We euphemistically refer to this type of junction zone as a “Lariat Complex”. The empirical data in Table I is consistent with the proposed junction zones, but does not

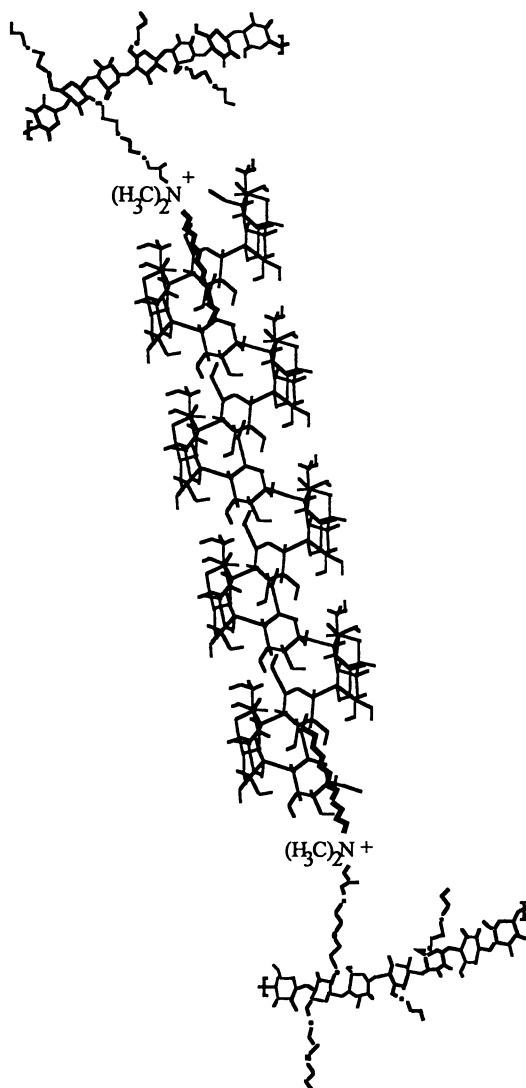
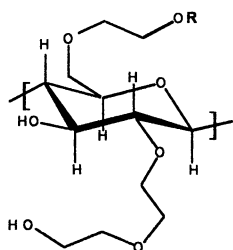


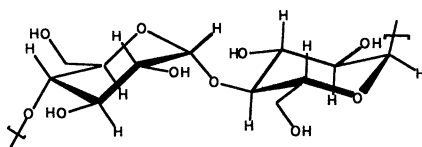
Figure 2. Proposed junction zones for the complex between Polyquaternium-24 and amylose, a "Lariat Complex" (Reprinted with permission from *Macromolecules* 1997, 30, 5361-5266. Copyright 1997 American Chemical Society).

establish this as the only possible mechanism. The possibility of phase separation could not be entirely ruled out from these studies. In addition, recent work employing the Polyquaternium-24/amylose complex to develop surfactant-free emulsions suggested that the combination of these two polymers in aqueous solution imparts a yield point to the aqueous solution.<sup>9</sup> Attempts to build such formulations from Polyquaternium-24 alone failed in a matter of days, whereas emulsion formulations which contained both polymers were stable at elevated temperatures for up to six months.

Rheological investigation of gelation phenomena is a useful technique to glean additional information about the characteristics of polymer blends. We examined the rheological behavior of solutions containing Polyquaternium-24, **2**, amylose, **3**, and the combination of **2** and **3**. A graph of viscosity and shear stress verses shear rate is



(1)  $R=CH_2CH(OH)CH_2N(CH_3)_3Cl$   
Polyquaternium-10



(3) amylose

(2)  $R=CH_2CH(OH)CH_2N(CH_3)_2(CH_2)_{11}CH_3Cl$   
Polyquaternium-24

shown in Figure 3. From the graph it is immediate apparent that the combination of the two polymers creates significant viscosity (solutions of 0.25% amylose are very low in viscosity, nearly equivalent to unadulterated water-data not shown). The appearance of the small deflection at low shear rate in the viscosity curve of the combined polymers is indicative of the formation of a network between the two polymer components. In addition, in examining the resulting shear stress curve for the polymer combination, one notes two apparent peaks. We suggest the peak corresponding to point A represents the maximum extension of the amylose helices with increasing shear rate and that point B may represent the eventual linear comingling of the two polymer systems under high shear. As can be seen in Figure 4, however, the system is thixotropic suggesting that the amylose helices never completely detach from the cellulose ether hydrophobes. The synergistic complex of the amylose and Polyquaternium-24 requires more time to recover from stress than a typical 0.5% xanthan solution, indicated by the separation of the forward and reverse viscosity curves. Once the shearing force is removed from the system, the amylose helices recoil and viscosity rebuilds.

Figure 5 demonstrates that, as expected, the rheological properties of solutions containing **2** and **3** are concentration dependent. A complex formed using 0.5% Polyquaternium-24 and 0.12% amylose (i.e., half the typical concentrations)

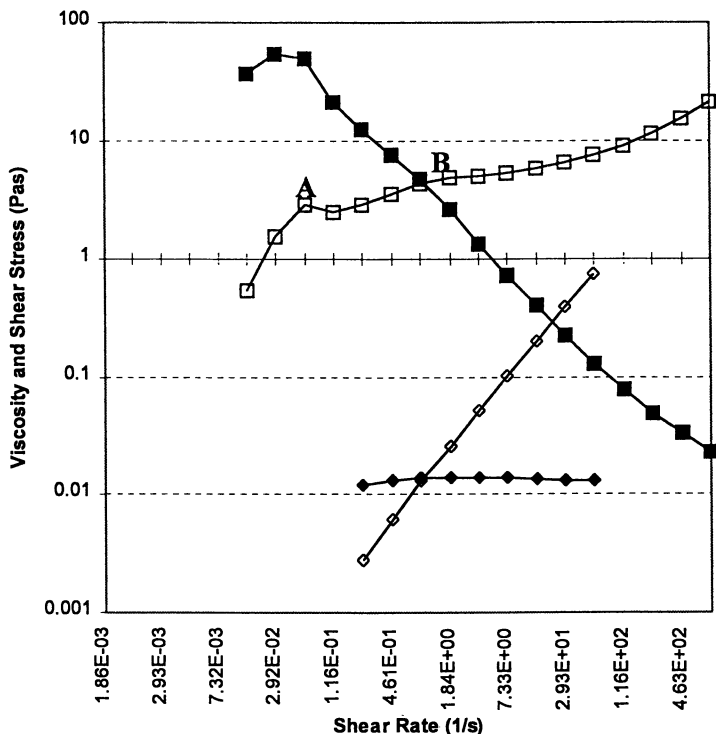


Figure 3. Viscosity (closed points) and shear stress (opened points) verses shear rate for 1% Polyquaternium-24, 0.25% amylose and the combination of 1% Polyquaternium-24/0.25% amylose.

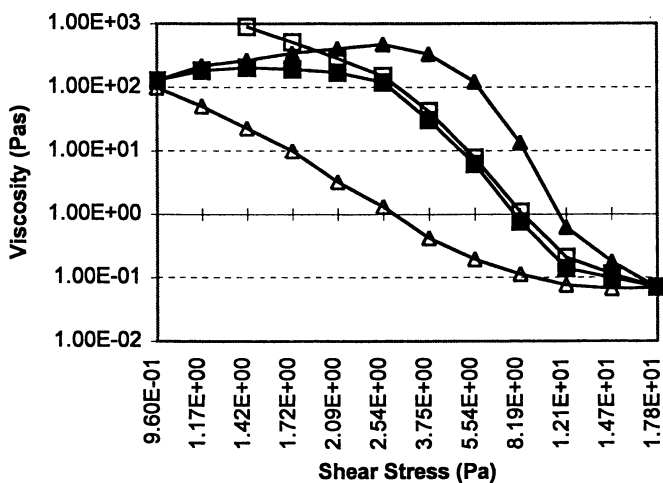


Figure 4. Thixotropy curve for a 1% Polyquaternium-24/0.25% amylose complex ( $\blacktriangle$ -up,  $\triangle$ -down) and a curve of a 0.5% xanthan solution ( $\blacksquare$ -up,  $\square$ -down).

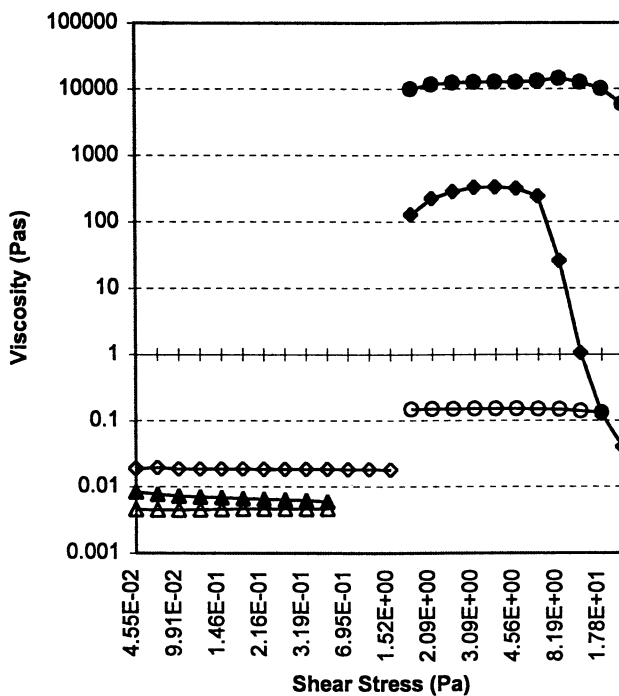


Figure 5. Viscosity versus shear stress curves for a 2% Polyquaternium-24/0.5% amylose mixture (●), a 1% Polyquaternium-24/0.25% amylose mixture (◆), a 0.5% Polyquaternium-24/0.12% amylose mixture (▲) and the three polymer concentrations without added amylose (corresponding open symbols).

builds very little viscosity, being only slightly greater in viscosity than 0.5% Polyquaternium-24 alone. A solution of 2.0% Polyquaternium-24 and 0.5% amylose has even greater viscosity (on the order of kilopascals) and the stress range over which the complex displays Newtonian behavior is also increased.

Perhaps the most significant information on the complex can be obtained from examination of the complex under dynamic mechanical conditions. Figure 6 shows that for both the 1.0% Polyquaternium-24/amylose complex and the 2.0% Polyquaternium-24/amylose complex, the storage modulus,  $G'$  (a measure of the elastic component of the system) exceeds the loss modulus,  $G''$  (a measure of the viscous component of the system). Such dynamic modulus curves are indicative of gelation although the crossover of  $G'$  with  $G''$  for the 1% polymer solution suggests that this mixture is more characteristic of a pseudogel.<sup>10,11</sup>

In the case of the 2% polymer mixture, the storage modulus exceeds the loss modulus over the whole range of frequencies examined. This type of behavior can be ascribed to strongly crosslinked gels. However, covalent crosslinking in this system is

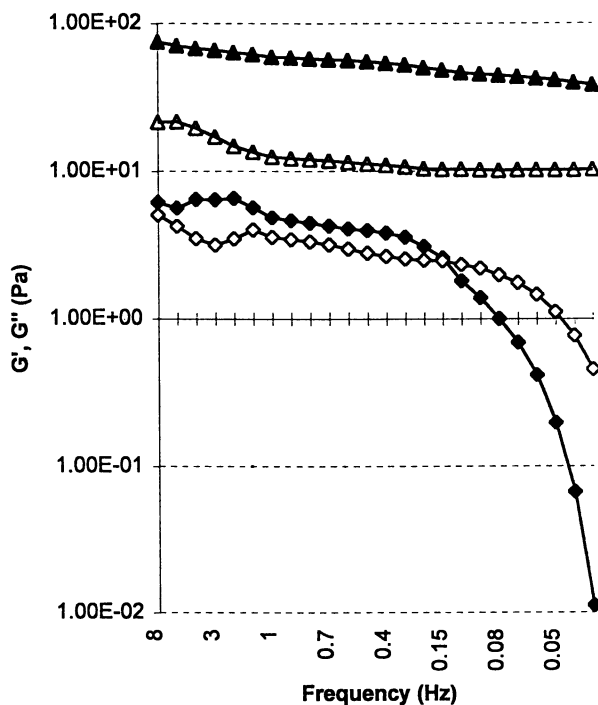


Figure 6. Storage modulus,  $G'$ , (closed symbols) and loss modulus,  $G''$ , (open symbols) for 1.0% Polyquaternium-24/0.25% amylose ( $\blacklozenge$ ) and 2.0% Polyquaternium-24/0.5% amylose ( $\blacktriangle$ ).

unlikely so the crosslinking must be attributable to a non-covalent mechanism. Because such viscosity enhancement was not noted for a cationic polymer similar to Polyquaternium-24 that does not contain hydrophobic substituents, i.e., Polyquaternium-10, 1, we feel that the mechanism is not electrostatic in nature and must, therefore, be related to some type of interaction between the amylose and the hydrophobes on the Polyquaternium-24.<sup>8</sup> It is well known that amylose will complex hydrophobic molecules via an inclusion mechanism, therefore, the junction zone proposed in Figure 2 seems to be the most likely possible candidate.

## Conclusions

The data presented above continues to support our observation that Polyquaternium-24 and amylose interact synergistically to form weak gels. While the data does not prove conclusively that this synergistic interaction occurs via the helical crosslinking complex we propose, it does lend further evidence to this suggestion. Additional proof will need to come from more extensive x-ray diffraction studies or perhaps from intermolecular NOE NMR experiments which may demonstrate either the presence of the amylose  $\alpha$ -helix in the complex, or intermolecular NOEs between the amylose glucose monomers and the cellulose ether hydrophobes. Such information would be useful to further establish the nature of the interaction between these two unique polysaccharides. Establishment of the nature of the interaction, however, has not prevented us from exploring the use of the binary polymer synergism in the development of novel surfactant-free cosmetic formulations.

## Literature Cited

- 1) Gruber, J. V. In *Polysaccharide-Based Polymers in Cosmetics*; Goddard, E. D.; Gruber, J. V. eds., Principles of Polymer Science and Technology in Cosmetics and Personal Care. Marcel Dekker, New York. 1999 (In press), pp 325-389.
- 2) Schorsch, C.; Garnier, C.; Doublier, J-L. *Carbohydr. Polym.* **1997**, *34*, 165-175.
- 3) Turquois, T.; Rochas, C.; Taravel, FR. *Carbohydr. Polym.* **1992**, *17*, 263-268.
- 4) Back, D. M.; Clark, E.M.; Ramachandran, R. In *Polyethers, Ethylene Oxide Polymers*. Kroschwitz, J.I.; Howe-Grant, M. eds., Kirk-Othmer Encyclopedia of Chemical Technology 4<sup>th</sup> ed., Vol. 19. New York: John Wiley & Sons, 1996, pp 700-722.
- 5) Cairns, P.; Miles, M. J.; Morris, V. J. Brownsky, G. J. *Carbohydr. Polym.* **1987**, *160*, 411-423.
- 6) Goycoolea, F. M.; Richardson, R. K.; Morris, E. R.; Gidley, M. J. *Macromolecules* **1995**, *28*, 8308-8320.
- 7) Chandrasekaran, R.; Radha, A. *Carbohydr. Polym.* **1997**, *32*, 201-208.
- 8) Gruber, J. V.; Konish, P. N. *Macromolecules* **1997**, *30*, 5361-5366.
- 9) Konish, P. N.; Gruber, J. V. *J. Cosmet. Sci.* **1998**, *49*, 335-342.
- 10) Clark, A. H.; Ross-Murphy, S. B. *Structural and Mechanical Properties of Biopolymer Gels*. Clark, A. H.; Kamide, K.; Ross-Murphy, S. eds., *Adv. Polym. Sci.* **1987**, *83*, 57-192.
- 11) Kavanagh, G. M.; Ross-Murphy, S. B. *Prog. Polym. Sci.* **1998**, *23*, 533-562.

## Chapter 18

# Ultrasonic Techniques to Characterize Concentrated Colloidal Dispersions

D. J. Hibberd, M. J. Garrood, J. M. Leney, and M. M. Robins

Institute of Food Research, Norwich Research Park, Colney,  
Norwich NR4 7UA, United Kingdom

The principles and applications of ultrasonic techniques to colloidal dispersions are described. The techniques are arranged as a hierarchy, showing firstly the major effects, requiring comparatively simple apparatus, and then more sophisticated techniques where complex theories and sensitive instrumentation are required. Applications to model suspensions and emulsions are shown, with reference to non-ideal food dispersions.

Many foods and pharmaceutical products are concentrated dispersions, whose properties are critically dependent on the colloidal structure. There is a need for non-intrusive techniques to characterise such systems. In many cases it is desirable to monitor colloidal properties on-line during processing. The important properties include the dispersed phase concentration and state, the particle size distribution of the dispersed phase, and whether aggregation (flocculation) has occurred. Further information on the structure of the dispersion, such as the composition of the particle surfaces, would also be of value in the control of product quality.

In principle ultrasonic techniques can be used to determine all these properties of dispersions, and without the dilution needed for most alternative techniques. When ultrasound is propagated through a colloidal dispersion, the beam is attenuated by a number of mechanisms, depending on the contrast in thermophysical properties between the dispersed and continuous phases. Here we summarise the principal effects of dispersion composition and structure on the propagation of ultrasound, showing a hierarchy from the major phenomena to more subtle effects requiring sensitive instrumentation. The instrumentation required for each application is also described.



## First-Order Effect: Dispersion Composition

**Characterisation of Creaming or Sedimentation** In most dispersions, the overall composition is the dominating influence on the propagation of ultrasound. Each component contributes to the velocity and attenuation of the wave by an amount that depends on the volume fraction and the characteristics of propagation in the isolated component. In many cases, there is significant contrast in the velocity of ultrasound between the dispersed and continuous phases, and simple mixing theory can be used to estimate the velocity through a dispersion of known volume fraction (1). Conversely, a measurement of the velocity through a dispersion can be used to measure the particle volume fraction reasonably accurately, provided the ultrasonic velocity (and density) of each phase is known.(2). This technique has been applied very successfully to monitor the vertical distribution of dispersed phase in dispersions that are sedimenting or creaming in a gravitational field (3,4).

Figure 1a shows the oil concentration profiles measured ultrasonically for an emulsion during creaming. Each line represents a vertical scan of over 80 data points collected at a particular sample age. Initially, the line (dashed) was horizontal, showing uniform composition. After a few days the oil had begun to move up the sample cell, forming a concentrated cream layer at the top. As time progressed the base slowly cleared of oil droplets, which all collected in the cream layer (dotted line). The emulsion was visually uniform for 14 days, but the ultrasonic instrument detected droplet movement between one and two days. The emulsion contained polydisperse droplets, and the smaller fraction creamed more slowly than the larger droplets, maintaining opacity at the base even though the majority of the droplets had already moved towards the top. The form of the creaming profiles allowed the effective hydrodynamic size distribution of the droplets to be estimated (5), and the resulting size distribution is shown in Figure 1b. The effective hydrodynamic size distribution was very similar to that measured at the start of the experiment, using a Malvern Mastersizer, and shown in Figure 1c. The ultrasonic instrument is thus able to determine the effective size distribution of creaming (or sedimenting) particles in concentrated dispersions. This can be used to detect droplet coalescence, or aggregation due to added flocculants. Figure 2a shows creaming profiles for the oil-in-water emulsion shown in Figure 1, but after the addition of 0.02%w/w hydroxyethyl cellulose (HEC). The hydrodynamic size distribution of the creaming particles is shown in Figure 2b. The form of the profiles, and the derived size distribution, showed two distinct populations of droplets in the emulsions, corresponding to individual droplets and small flocs. At certain concentrations non-adsorbing polymers, such as HEC in the presence of a surfactant, cause partial flocculation of the droplets, which is readily detected and quantified using the ultrasonic instrument (4).

At higher polymer concentrations the emulsion was fully flocculated, and the creaming behaviour, shown in Figure 3, indicated that the droplets moved as if they were part of a single network, with a sharp lower boundary. The behaviour of the network is the subject of an associated paper in the current volume (6).

**Crystallisation Processes** The contrast in ultrasonic velocity between phases in dispersions can also be used to detect crystallisation. In general, when a material

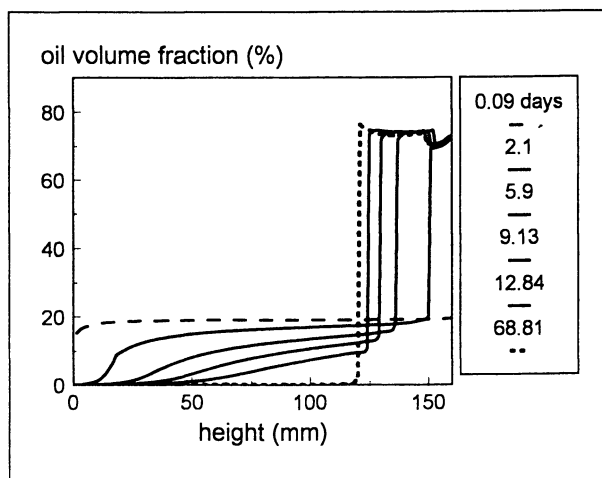


Figure 1a. Profiles of oil volume fraction with height during creaming of an alkane-in-water emulsion, obtained using the IFR ultrasonic sedimentation/creaming monitor.

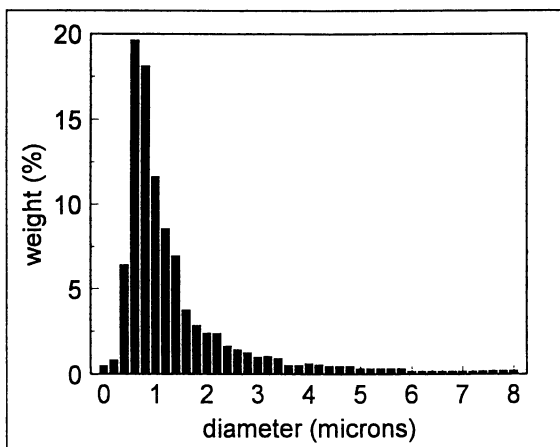


Figure 1b. The hydrodynamic droplet size distribution derived from the creaming data of Figure 1a.

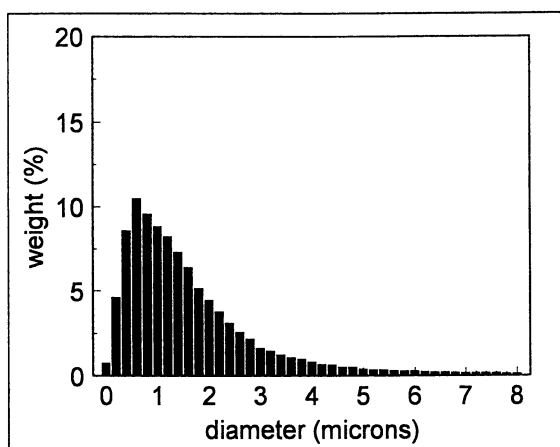


Figure 1c. The droplet size distribution measured by the Mastersizer light diffraction sizer.

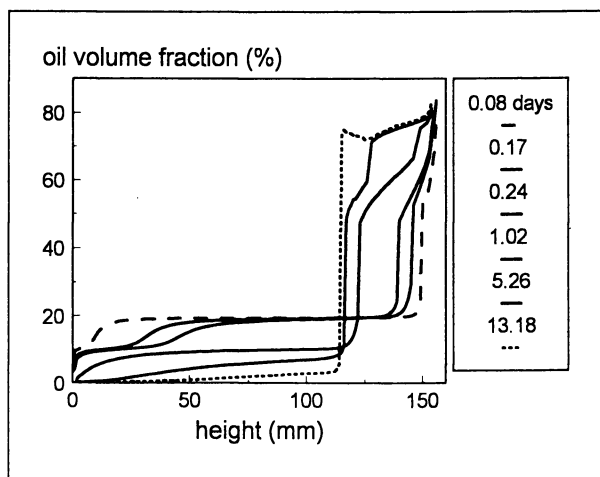


Figure 2a. Profiles of oil volume fraction with height during creaming of an alkane-in-water emulsion in the presence of 0.02%w/w hydroxyethyl cellulose.

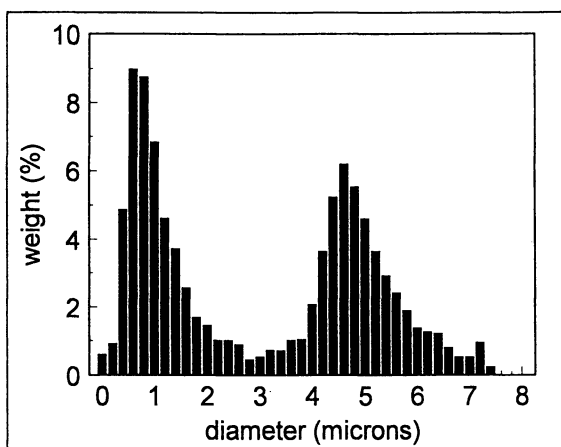


Figure 2b. The hydrodynamic droplet size distribution derived from the creaming data in Figure 2a, showing flocs and individual droplets.

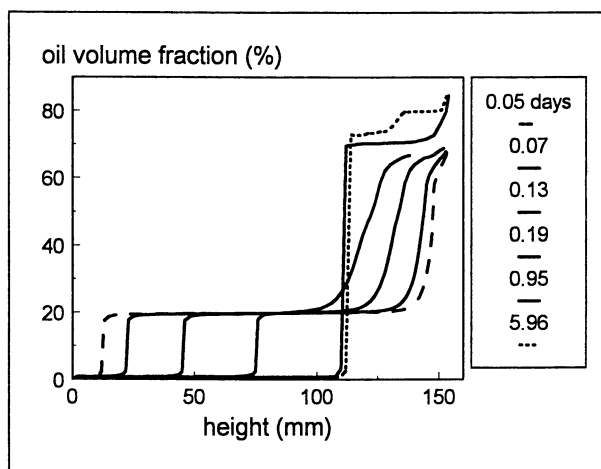


Figure 3. Profiles of oil volume fraction with height during creaming of an alkane-in-water emulsion in the presence of 0.04%w/w hydroxyethyl cellulose showing collective movement of the flocculated droplets.

solidifies its ultrasonic velocity is significantly higher than in the liquid state, and measurement of the velocity is a simple method to determine the degree of crystallinity (7).

Figure 4 shows an application of ultrasonic velocimetry to monitor crystallisation in honey, a super-saturated solution of fructose in glucose. The liquid honey solution was seeded with a small amount of fructose crystals and the ultrasonic velocity measured over a period of 72 days. The data show the changes in ultrasonic velocity during the crystallisation process. With associated calibration experiments using samples of known crystallinity, the data in Figure 4 can be converted to values of crystal concentration. In the case of natural products such as honey it is also important to allow for variations in moisture in the samples, and to collect data from a wide range of sources in order to confirm absolute crystallinity values. However, the simplicity of this application makes it particularly suitable for an industrial environment.

**Instrumentation Required** To apply either of these techniques to a dispersion requires a measure of the velocity of ultrasound through the material. The simplest techniques determine the time-of-flight for a pulse of ultrasound to propagate from a transmitting transducer, through the sample and be received by a second transducer (2). A variant on this method uses a single transducer for both transmission and reception, with a reflector at the far side of the sample (8). The technique requires timing electronics, and good temperature control. If absolute values of velocity are required, then the instrument needs calibration using fluids of known velocity.

### Ultrasonic Spectroscopy

**Second-Order Effect: Dispersion Composition and Particle Size.** A much more sophisticated application of ultrasonic methods involves measuring the velocity and the attenuation of ultrasound of known frequency as it propagates through a dispersion. The variation with frequency of the ultrasonic velocity and attenuation in a simple dispersion are related to the concentration of dispersed phase, its particle size distribution and a number of thermophysical parameters of both phases. In principle, measurement of the ultrasonic properties provides information on the volume fraction and particle size of the dispersed particles.

The theory most commonly used to relate ultrasonic properties to dispersion composition is based on the scattering of ultrasound for single particles, formulated in detail by Allegra and Hawley (9). Essentially, the theory considers the loss mechanisms in operation when an ultrasonic wave travelling in a liquid medium (the continuous phase) encounters a (spherical) particle of a different material. An amount of energy is converted to heat and therefore lost from the ultrasonic wave. Other losses from the straight-through wave arise from scattering of the ultrasound at oblique angles, and mode conversion to shear or surface waves. The amount of the loss, which affects both the overall attenuation and propagation speed of the wave, is dependent on the contrast between the thermal properties of the two phases, and on their differences in density and ultrasonic velocity. A key factor in the overall loss is

the particle size and the number of particles. Thus, if the relevant properties of the two phases are known, the ultrasonic propagation at a range of frequencies can be used to determine the volume fraction and size of the particles.

In practice, it is not straightforward to infer the dispersion properties from ultrasonic measurements, due mainly to uncertainty in the thermophysical properties. However, it is possible to distinguish overall differences in size distribution using ultrasonic attenuation, even for irregular, polydisperse particles. Figure 5 shows the ultrasonic spectra of suspensions of 5%w/w sucrose crystals in a saturated sucrose/glucose solution (10). The smaller crystals passed through a 25 $\mu\text{m}$  sieve, and the larger fraction passed through a 45  $\mu\text{m}$  mesh but were retained on a 32 $\mu\text{m}$  mesh sieve. Despite the high polydispersity of the samples (10), and their irregular shape resulting from grinding, there were still significant differences in their ultrasonic properties. The increases in velocity and attenuation occurred at a lower frequency for the larger particle size distribution, which is consistent with the predictions of the scattering theory, although the non-spherical particle shape and lack of thermophysical parameters precluded full application of the theory.

### Third-order Effects: Distribution of Components in a Dispersion.

**Adsorbed layers.** The application of scattering theory to a simple two-phase dispersion is highly complex, as shown above, but it is possible to detect further effects using ultrasonic techniques. Since these effects are in general of much smaller magnitude than the first- and second-order phenomena, they can only be identified in systems where the concentration, primary particle size and temperature are very well-controlled.

The basic scattering theory of Allegra and Hawley (9) has been modified by several workers (11, 12) to include a third component, a shell on the surface of the particles. This development opens the possibility to detect adsorbed layers of surfactant, or polymer, on the surfaces of particles or droplets.

Figure 6 shows the attenuation spectra from polystyrene latex suspensions in the absence and presence of adsorbed layers of non-ionic surfactant or polymer (HEC). The lines show the predicted effects, using scattering theory, if the added components were uniformly dispersed in the continuous phase (13,14). The experimental results show a higher attenuation than predicted, indicating that the distribution of the added components (on the surfaces of the particles instead of as a background) is detectable using ultrasonic techniques (14). To fit the proposed shell-core models requires considerable knowledge of the thermophysical properties of the layers, which is not currently available. However, the data are shown as preliminary evidence that such layers are detectable and clearly more work is needed on a wide range of systems to be confident of the results.

**Flocculation.** A related third-order effect is the distribution of particles in the dispersions. If particles become flocculated, the majority of them are surrounded by other particles, not by continuous phase, and this is similarly predicted to affect the ultrasonic properties (12). To examine this effect, polystyrene suspensions were flocculated in two ways, both by the addition of HEC (13,14). At low polymer concentrations, the HEC was adsorbed on to the particles but insufficiently to obtain full surface coverage. The latex particles were thus flocculated by polymer bridges,

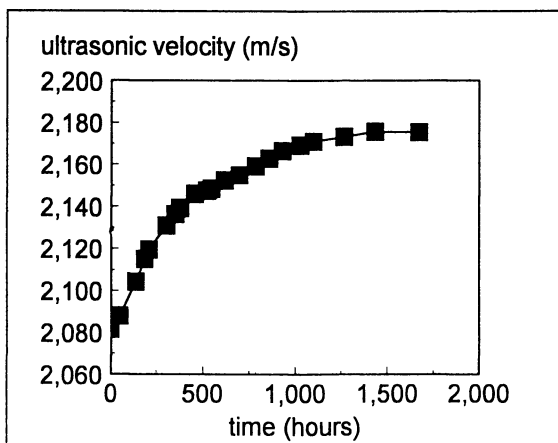


Figure 4. The ultrasonic velocity of honey during crystallisation.

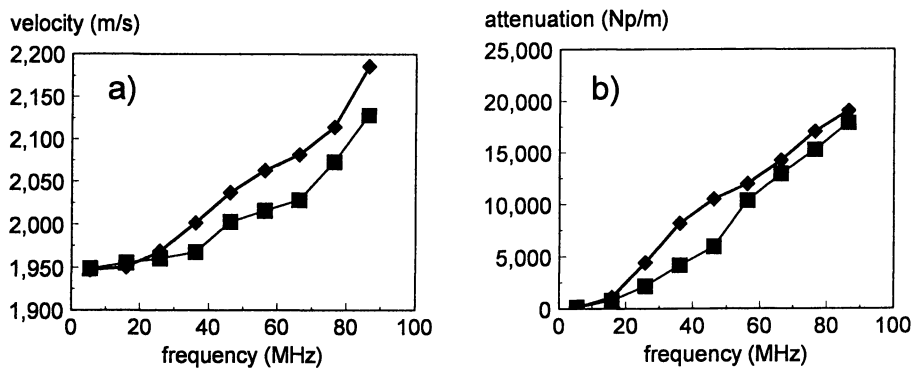


Figure 5. Ultrasonic velocity (a) and attenuation (b) spectra obtained from 5%w/w sucrose crystals dispersed in saturated sugar solution. Key: ■, crystals <25 μm diameter; ♦, crystals in diameter range 32-45 μm.



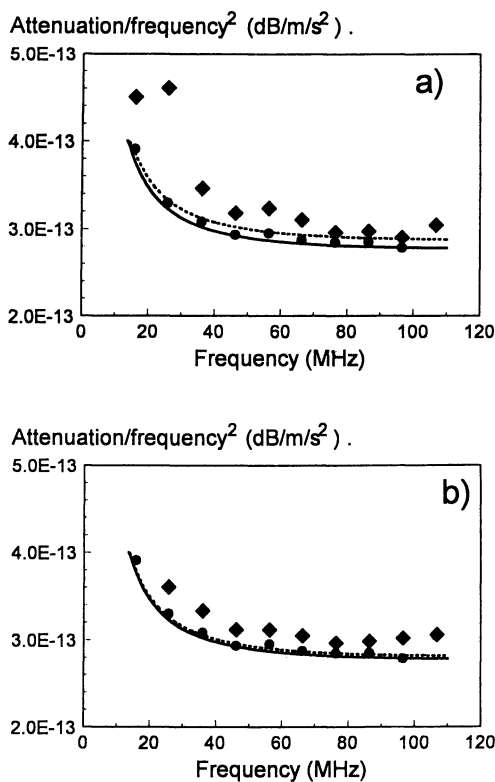


Figure 6. Measured (symbols) and theoretical (line) ultrasonic attenuation spectra for polystyrene-in-water suspension (4.388%v/v) in the presence of adsorbed layers of (a) 0.138%w/w Triton TX100 surfactant, and (b) 0.104%w/w HEC polymer. Key: • and —, bare particles; ♦ and ... , particles with adsorbed layers. The theoretical spectra almost coincide.

and the ultrasonic attenuation was affected, as in Figure 7a. Similarly, adding HEC to a polystyrene suspension in the presence of surfactant caused flocculation by a depletion mechanism, and this was also detectable using ultrasonics, as in Figure 7b. Microscopic examination and sedimentation analysis (see above) showed full flocculation in both samples (13). Although the addition of polymer to the continuous phase increases its attenuation slightly, the theoretical spectra (also shown in Figure 7) were indistinguishable, and the measured effects were only attributable to flocculation. Similar effects have been observed in oil-in-water emulsions (15,16) and some progress has been made towards applying the "shell" variation of scattering theory to the data (17).

**Instrumentation Required.** To make measurements of the ultrasonic properties for the purposes of fitting scattering theory, more sophisticated instrumentation is required than in the semi-empirical application above. As before, the temperature must be well-controlled, to at least  $\pm 0.1^\circ\text{C}$ . In addition, the ultrasonic wave must be of known frequency, and the true phase velocity and the attenuation through the sample must be measured. There are a number of ways to make these measurements and the most accurate are interferometric techniques (18). Recently, broad-band techniques have been developed (19) that propagate a spectrum of frequencies and deconvolve the time-of-flight and attenuation of each frequency component using Fourier methods. These instruments have the advantage of speed of operation, and therefore are suitable for systems where the particle size or concentration may be changing, and are less prone to temperature drift during the measurement.

The spectra shown in this paper were collected using the IFR discrete frequency spectrometer, based on the principle of coherent pulse interferometry, estimated to be accurate to 0.01% and 4% in velocity and attenuation respectively (20, 13).

## Conclusions.

Typically ultrasound travels at different velocity through the dispersed and continuous phases. The particle concentration in a dispersion can thus be inferred from its ultrasonic velocity. If velocity measurements are made as a function of height in a container, they provide a sensitive measure of sedimentation or creaming. Similarly, velocity measurements enable crystallisation from a solution or melt to be monitored non-intrusively. These simplest applications exploit first-order effects.

A more sophisticated use of ultrasonics (exploiting second order effects) involves measuring the velocity and attenuation as a function of frequency, to obtain a full spectrum. Applying theories of ultrasonic scattering in two-phase media, in principle the data can be interpreted in terms of the particle size distribution as well as its concentration. However, the difficulty in obtaining the thermophysical parameters needed for the theory precludes its rigorous application to complex dispersions such as food systems.

Third-order effects involve the distribution of components in dispersions, which can be utilised by extensions of the spectroscopic approach. We have shown that the presence of adsorbed layers of polymer or surfactant cause significant changes to the

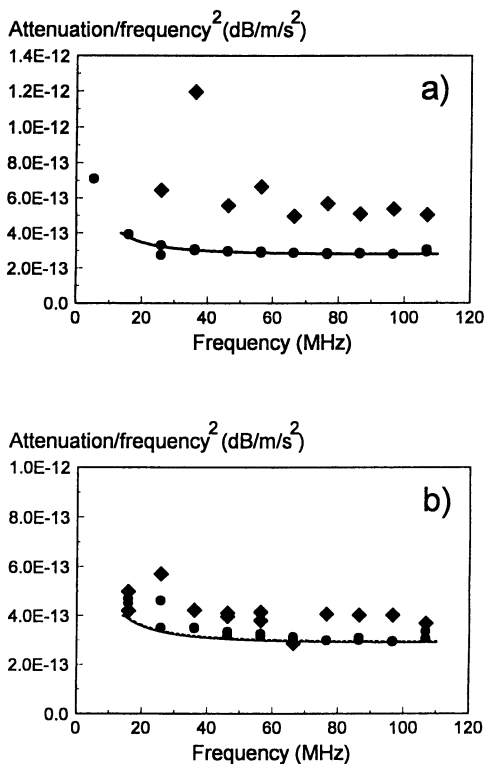


**Figure 7.** Measured (symbols) and theoretical (line) ultrasonic attenuation spectra for (a) bridged and (b) depletion flocculated polystyrene-in-water suspensions (4.388%v/v) in the presence of HEC. Key: • and —, unflocculated suspension; ♦ and ... , flocculated suspension. The theoretical spectra almost coincide.

ultrasonic properties of a suspension, and similarly that non-uniform particle distribution due to flocculation can also be detected using sensitive ultrasonic techniques. Recent theoretical developments offer the potential to model both these types of non-uniformity in terms of an effective shell around the particles, and we anticipate significant progress in this area in the future.

### Acknowledgments

The work described here was conducted at the Institute of Food Research and funded by the SERC (CASE award to DJH), BBSRC ROPA award, and a MAFF/DTI LINK project. We thank Richard Challis, Brian Robinson and Yacine Hemar for useful discussions, and our industrial partners, RHM, Dow AgroSciences and Nestle for their support.

### References

1. Urick, R. J., *J. Appl. Phys.* **1947**, *18*, 983.
2. McClements, D. J.; Povey, M. J. W., *Adv. Coll. Int. Sci.* **1987**, *27(3-4)*, 285-316.
3. Howe, A. M.; Mackie, A. R.; Robins, M. M., *J. Disp. Sci. Technol.* **1986**, *7(2)*, 231-243.
4. Fillery-Travis, A. J.; Gunning, P. A.; Hibberd, D. J.; Robins, M. M., *J. Coll. Int. Sci.* **1993**, *159(1)*, 189-197.
5. Carter, C.; Hibberd, D. J.; Howe, A. M.; Mackie, A. R.; Robins, M. M., *Prog. Colloid Polym. Sci.* **1988** *76*, 37.
6. Manoj, P.; Fillery-Travis, A. J.; Hibberd, D. J.; Watson, A. D.; Robins, M. M. This volume.
7. McClements, D. J.; Povey, M. J. W., *Int. J. Food. Sci. Tech.* **1987** *22(5)*, 491-499.
8. McClements, D. J.; Fairley, P., *Ultrasonics* **1991**, *29(1)*, 58-62.
9. Allegra, J. R.; Hawley, S. A., *J. Acoust. Soc. Am.* **1972**, *51*, 1545-1564.
10. Garrood, M. J.; Hibberd, D. J.; Towersey, P. J.; Robins, M. M. (unpublished results)
11. Anson, L.; Chivers, R. G., *J. Acoust. Soc. Am.* **1989**, *85(2)*, 535-540.
12. Hemar, Y.; Hermann, N.; Lemarechal, P.; Hocquart, R.; Lequeux, F., *J.Phys.II* **1997**, *7*, 637.
13. Hibberd, D. J., *Ph.D. thesis*, **1997**, University of East Anglia, UK.
14. Hibberd, D. J.; Robinson, B. H.; Robins, M. M., *Colloids Surfaces B:Biointerfaces* (in press).
15. McClements, D. J., *Colloids And Surfaces A-Physicochemical and Engineering Aspects* **1994**, *90(1)*, 25-35.
16. Hibberd, D. J.; Holmes, A. K.; Garrood, M. J.; Fillery-Travis, A. J.; Robins, M. M.; Challis, R. E., *J. Coll. Int. Sci.* **1997**, *193*, 77-87.

17. Chanamai, R.; Hermann, N.; McClements, D. J., *J. Coll. Int. Sci.* **1998**, *204*, 268-276.
18. Fujii, K.; Masui, R., *J. Acoust. Soc. Am.*, **1993**, *93(1)*, 276-282.
19. Challis, R. E.; Harrison, J.; Holmes, A. K.; Cocker, R., *J. Acoust. Soc. Am.* **1991**, *90(2)*, 730-740.
20. Hibberd, D. J.; Garrod, M. J.; Robins, M. M., *Proceedings of the Institute of Acoustics*, **1995**, *17(6)*, 1-12.

## Chapter 19

# Fluorescence Microscopy Study of the Sorption of Cationic Polymers on Hair

S. T. A. Regismond<sup>1</sup>, Y.-M. Heng<sup>2</sup>, E. D. Goddard<sup>3</sup>, and F. M. Winnik<sup>1,4</sup>

<sup>1</sup> Department of Chemistry and <sup>2</sup> Electron Microscopy Facility,  
McMaster University, 1280 Main Street West, Hamilton, Ontario L8S 4M1, Canada  
<sup>3</sup> 849 Buccaneer Lane, Manahawkin, NJ 08050

A fluorescent dye, 5-(4,6-dichlorotriazinyl)aminofluorescein, was attached covalently to Polymer JR400, the chloride salt of a trimethylammonium derivative of hydroxyethylcellulose ether. Fluorescence microscopy was used to monitor the adsorption of this cationic cellulose ether derivative onto hair fibers. The intensity and the pattern of fluorescent deposits along the hair surface were monitored as a function of changes in exposure time. Significant desorption of the polymer was observed upon treatment of polymer-coated hair fibers with aqueous solutions of sodium dodecylsulfate.

Water-soluble polymers have been studied extensively by fluorescence spectroscopy (1). Some experiments involve the addition of fluorescence probes to a solution, whereas others rely on fluorescent tags attached to the polymer backbone. The hydrophobic dye pyrene is often chosen in studies aimed at unraveling detailed aspects of the solution properties of polymers, especially amphiphilic polymers. Examples of pyrene-labeled cellulose ethers reported to date include neutral polymers, such as hydroxypropylcellulose ether (2)(3), hydroxyethylmethylcellulose ether (tylose) (4), hydroxypropylmethylcellulose ether (4) and polyelectrolytes, such as Polymer JR400 (5), a trimethylammonium chloride derivative of hydroxyethylcellulose ether and Quatrisoft LM200 (5), a hydrophobically-modified derivative of Polymer JR400. Pyrene, however is ill-suited for the visual demonstration of the presence of a polymer using fluorescence microscopy, since its absorption and emission spectra do not match the requirements of typical fluorescence microscopes. A dye emitting in the visible range is preferred. Fluorescein is often chosen as the chromophore, since its green emission is readily detected by fluorescence microscopy.

Fluorescent dyes have been used extensively in qualitative characterization of surface deposits on wool fibers (6)(7) and on hair (8). For example, by scanning the fluorescence intensity along a hair fiber previously exposed to aqueous polymer

<sup>4</sup> Corresponding author.

solutions containing a fluorescent dye, Weigmann et al were able to quantify the distribution of deposits on the fiber (9). However, in these fluorometric studies of polymer deposits on hair, the dye was added to the solution and free to diffuse in solution and on the keratin surface. Since the dye was not attached by a covalent bond to the polymer, the imaging experiments bring only indirect proof of the adsorption of the polymer itself. In order to eliminate this ambiguity we have prepared a fluorescently labeled cationic cellulose ether by covalent attachment of a dye. Polymer JR400 was selected as polymeric substrate, as it is known to act as an effective conditioner in commercial shampoo formulations. We report here the preparation of a labeled polymer, JR400-F, (Figure 1) and a study by fluorescence microscopy of its adsorption onto hair fibers. The intensity and the patterns of fluorescent deposits along the hair surface were monitored as a function of changes in parameters, such as exposure time and post-treatment with surfactants.

## Experimental Section

**Materials.** Water was deionized using a NANOpure water deionization system. 5-(4,6-dichlorotriazinyl)aminofluorescein was purchased from Molecular Probes (Eugene, Oregon). Sodium dodecylsulfate (SDS) was obtained from Sigma Chemicals. Triton-X100 was obtained from BDH Chemicals. Polymer JR400 was a gift from Amerchol Inc., Edison, NJ, and it was used without further purification. It is the chloride salt of a trimethylammonium derivative of hydroxyethylcellulose ether with an approximate molecular weight of 400,000 and a level of cationic substitution of about 5 wt %. The labeled polymer JR400-F was prepared by reaction of Polymer JR400 with 5-(4,6-dichlorotriazinyl)aminofluorescein (10)(11) following a procedure described for the preparation of fluorescein-labeled dextran (12). The amount of dye incorporated, determined by UV spectroscopy was  $7.4 \times 10^{-5}$  mol  $g^{-1}$  polymer or on average 1 dye for every 75 glucose units. Analysis by gel permeation chromatography (GPC) indicated that the labeled polymer has the same molecular weight as its precursor, and that all the dye was attached covalently to the polymer backbone.

**Methods.** Fluorescence spectra were recorded at room temperature on a SPEX Fluorolog 212 spectrometer equipped with a DM3000F data system. The excitation wavelength was set at 496 nm. Emission scans were recorded from 500 nm to 650 nm. Gel permeation chromatography (GPC) was performed with a system consisting of a Waters 510 HPLC pump coupled to a Waters 410 differential refractometer and a Waters Tunable 486 UV-Visible absorbance detector equipped with two Waters Ultrahydrogel columns kept at 35 °C and eluted with an aqueous sodium nitrate (0.1 M) solution at a flow rate of 0.7 mL  $min^{-1}$ . Conventional fluorescence microscopy was performed using a microscope having a HBO50 illuminator (broad band light source) and equipped with a Zeiss 20X objective (PLAN-NEOFLUAR). Images were acquired with a digital Sony 3 CCD camera and processed with Northern Exposure software. Confocal Laser Scanning Microscopy was performed using a Zeiss LSM10 laser scanning microscope (Zeiss Ltd) equipped with a Zeiss 20X objective. A HeNe laser was used to image red emissions. An Argon ion laser (488 nm) was used to image green emissions. Hair samples were mounted on clean glass slides using a non-fluorescing aqueous/dry mounting medium (Biomedica Corporation). They were covered with clean glass cover slips.

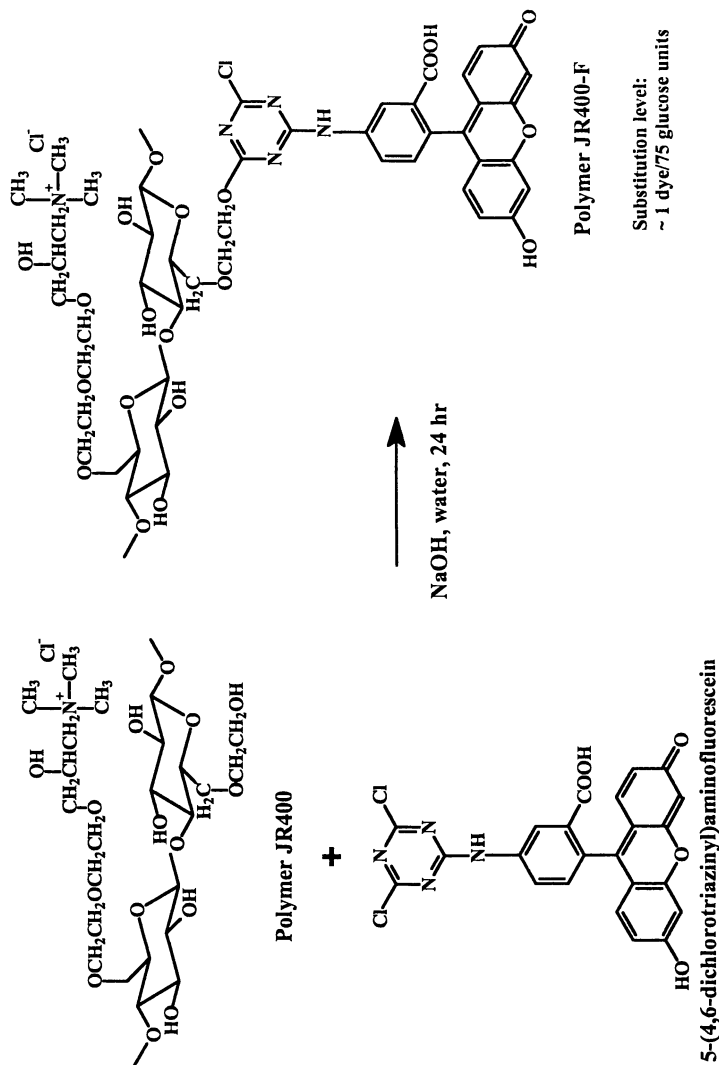


Figure 1. Synthetic scheme depicting the preparation of fluorescein-labeled Polymer JR400.



**Sample Preparation.** Tresses of black hair (7.5 cm long) tied at one end were washed by a 30 min-soaking in an aqueous solution of sodium dodecylsulfate (SDS, 5 %). They were rinsed thoroughly with hot tap water and several times with deionized water. They were then treated for 20 min in a saturated aqueous solution of Triton-X100. Subsequently, they were rinsed thoroughly with hot tap water and several times with deionized water. The tresses were then soaked in an aqueous solution of Polymer JR400-F (0.1 wt %, 30 mL) for either, 1 min, 30 min, 12 hr, or 36 hr. Two samples were gathered for each soaking period. They were rinsed with deionized water for 1 min. One sample was then allowed to dry in air, the other sample was given an additional treatment with aqueous SDS (5 wt %, 10 min), then rinsed copiously with deionized water and allowed to dry before imaging.

## Results

Fluorescein-labeled Polymer JR400 was prepared by coupling of a dichlorotriazine derivative of fluorescein (13) to Polymer JR400 in aqueous alkaline solution (Figure 1) (12). The degree of substitution was kept low, in order to ensure that the presence of the chromophore did not alter the properties of the polymer. Through the use of gel permeation chromatography, we ascertained that the molecular weight of the labeled polymer was the same as that of the parent polymer and that it was not contaminated with unreacted dye. In water, Polymer JR400-F exhibits a broad featureless emission centered at 522 nm, characteristic of the fluorescein chromophore.

A fluorescence micrograph of a hair fiber treated for 1 minute in a 0.1 wt % Polymer JR400-F aqueous solution is presented in Figure 2 (bottom) together with a fluorescence micrograph of a virgin hair fiber (Figure 2, top). The green fluorescence of the fluorescein label is easily detected on the fiber that was treated with the labeled polymer (Figure 2, bottom). It is interesting to note that the sharp demarcation of the scale edges of the cuticle is seen, suggesting enhanced deposition of the polymer between cuticular cells. This effect, which becomes more pronounced with increasing time of exposure of the hair fiber to aqueous polymer, is consistent with the known affinity of Polymer JR400 to sites of hair damage (14). A micrograph of a hair fiber soaked in aqueous Polymer JR400-F for 12 hr is shown in Figure 3 (top).

It is well established that the histological structure of a hair fiber consists of three components (Figure 4) (14)(15). The outermost region, known as the cuticle, is composed of cells that form a rather thick protective coating around the cortex consisting of spindle-shaped macrofibrils. The third component, called the medulla, is a porous region in the center of the fiber. The surface of hair and of the stratum corneum of skin consists primarily of the protein  $\alpha$ -keratin.

In a second series of fluorescent polymer deposit observations, we conducted desorption studies, in which hair fibers initially treated with aqueous Polymer JR400-F for times ranging from 1 min to 12 hr, were washed with a solution of an anionic surfactant (SDS, 5 wt %) for 10 min. This treatment resulted in complete desorption of the polymer in the case of samples treated with the polymer for times shorter than 30 min. Such fibers exhibited no green fluorescence, when viewed under fluorescence imaging conditions, while hair fibers immersed in pure water after treatment in aqueous solutions of JR400-F retained their original fluorescence. This confirms that

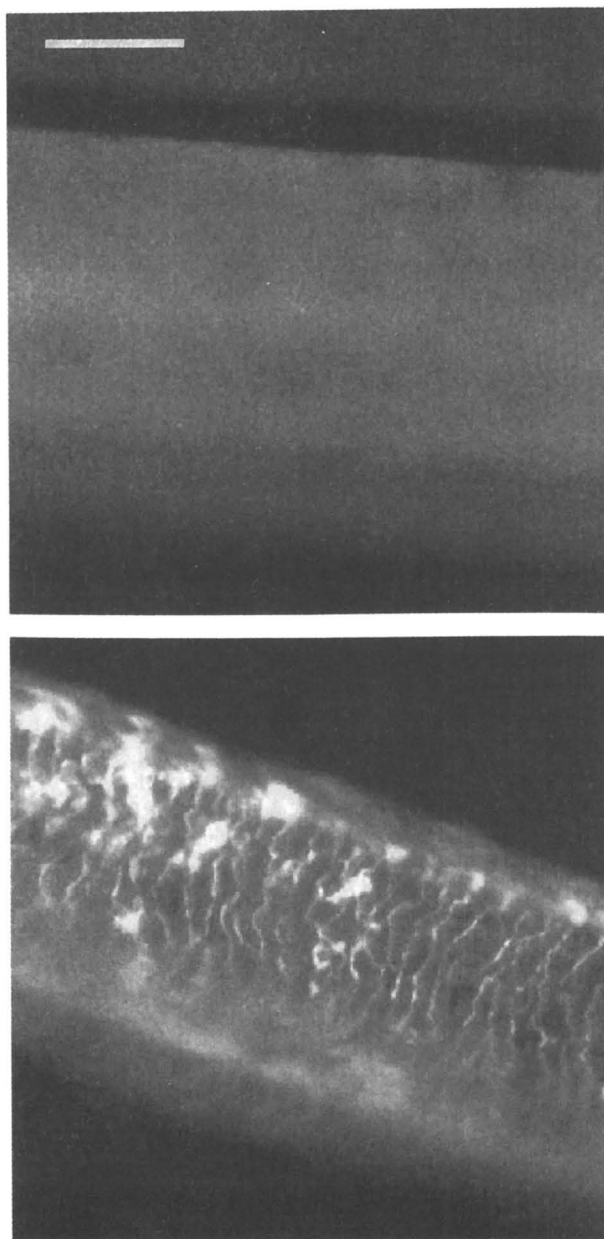


Figure 2. Fluorescence micrographs of a hair fiber treated with an aqueous solution of Polymer JR400-F (bottom) and of a virgin hair fiber (top). Scale bar = 50  $\mu\text{m}$ .

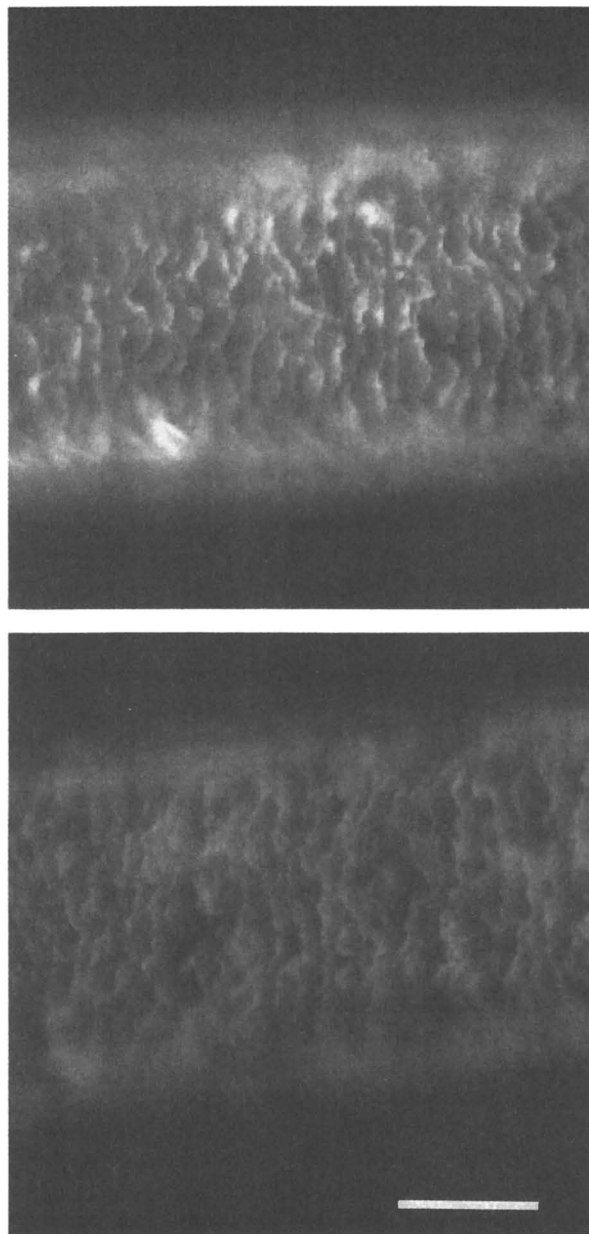


Figure 3. Fluorescence micrographs of a hair fiber treated with an aqueous solution of Polymer JR400-F (0.1 wt %); soaking time: 12 hr; top: water rinse; bottom: following treatment with aqueous SDS (5 wt %, 10 min). Scale bar = 50  $\mu\text{m}$ .

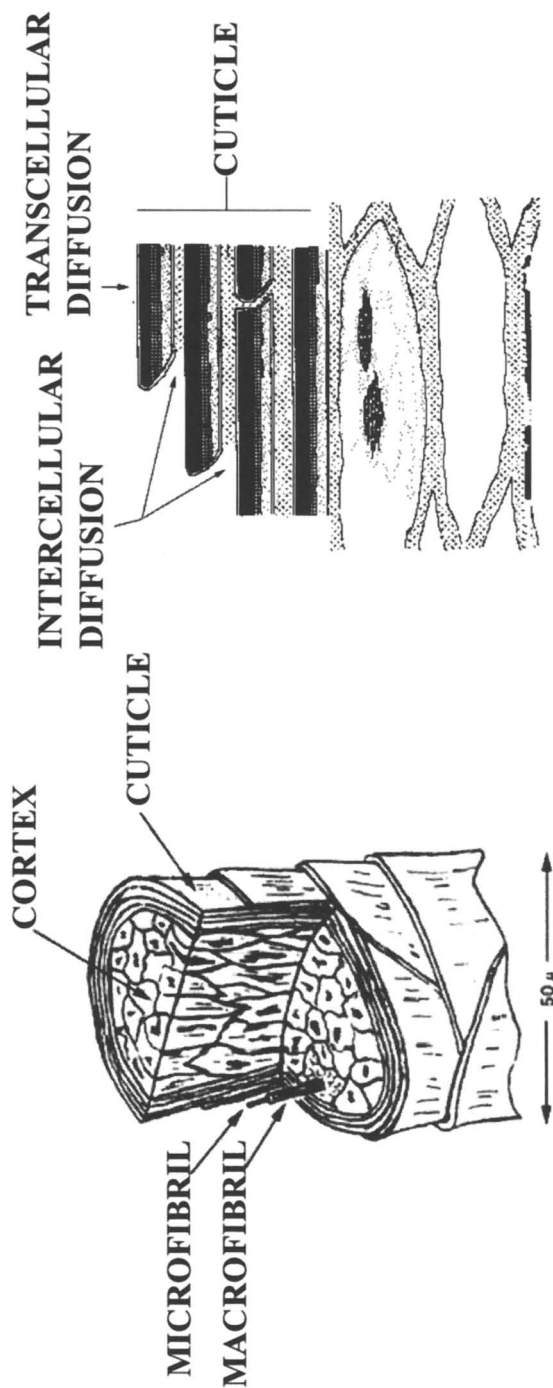


Figure 4. Histological structure of a hair fiber.

the adsorbed polymer can be displaced by SDS, but that it does not desorb in the absence of surfactant.

Fibers soaked in water for extended periods of time could not be entirely depleted of fluorescent polymer by SDS solutions, as seen in the micrograph (Figure 3, bottom) of a fiber soaked in aqueous JR400-F for 12 hrs and subsequently treated with aqueous SDS. The fluorescent patterns observed prior to surfactant wash (Figure 3, top) are easily observed, albeit with significantly weaker intensity. Cross-sections of the tip of a hair fiber soaked in a polymer solution for 36 hrs are presented in Figure 5, under normal viewing conditions (top) and under confocal imaging (bottom). In the latter case, only the plane that is in focus is observed, without interference from the layers above or below (16). The red emission arises from the natural fluorescence of keratin in the cortex of the hair fiber. This property allows imaging of structures with height differences comparable to the wavelength of the laser beam. An irregular rather thick fluorescent layer surrounds the hair surface.

## Discussion

Hair and, to some extent wool, have been traditionally viewed physicochemically speaking as 'non-reactive' fibers in the sense that materials known to be sorbed by them were generally considered to be located on their surface, i.e. physically adsorbed. In particular, cationic agents especially surfactants, and more recently, certain polymers, were considered to be surface deposited because of the well-known conditioning they conferred to the fibers. Indeed, their presence on the surface had been demonstrated by many methods, including surface free-energy measurements (17)(18), ESCA analysis (19), and indirect methods, such as gel permeation chromatography (20). The mechanism of uptake has been ascribed to electrostatic forces in view of the known low value of the isoelectric point of hair and wool (pH ca 4.0) (21) and, because of their relatively hydrophobic nature, to a hydrophobic contribution (16)(17).

While the conditioning phenomenon itself will be largely a surface process, the view that uptake of cationic conditioning agents is exclusively a surface phenomenon, that is simple adsorption, has progressively been challenged. Thus, early results involving the use of sectioning and staining procedures (22) had demonstrated definite penetration of hair by the conditioning agent cetyltrimethylammonium bromide (CTAB) which represents a molecule of considerable size. More persuasive evidence of the existence of penetration paths in hair was provided in the work of Woodward (23) using radiotagged polymers, such as poly(ethylene imine) (PEI) of molecular weight as high as 60,000. This approach was extended by Goddard and co-workers on a series of cationic hydroxyethylcellulose ethers of even higher molecular weights, ranging from 150,000 to 700,000 daltons. The observed uptake values, approaching 1 % by weight, far exceeded the amounts required for external monolayer coverage of the hair fibers (24). These observations prompted these authors to postulate a diffusion process by these macromolecules into hair fibers, swollen by the water of the contacting phase. It has been reported that hair fibers can imbibe as much as 30 % of their own weight of water (14). In harmony with the postulate of a diffusion process, uptake values in the above series of polymers were found to decrease with increasing molecular weights, the opposite of what would be expected for a simple adsorption

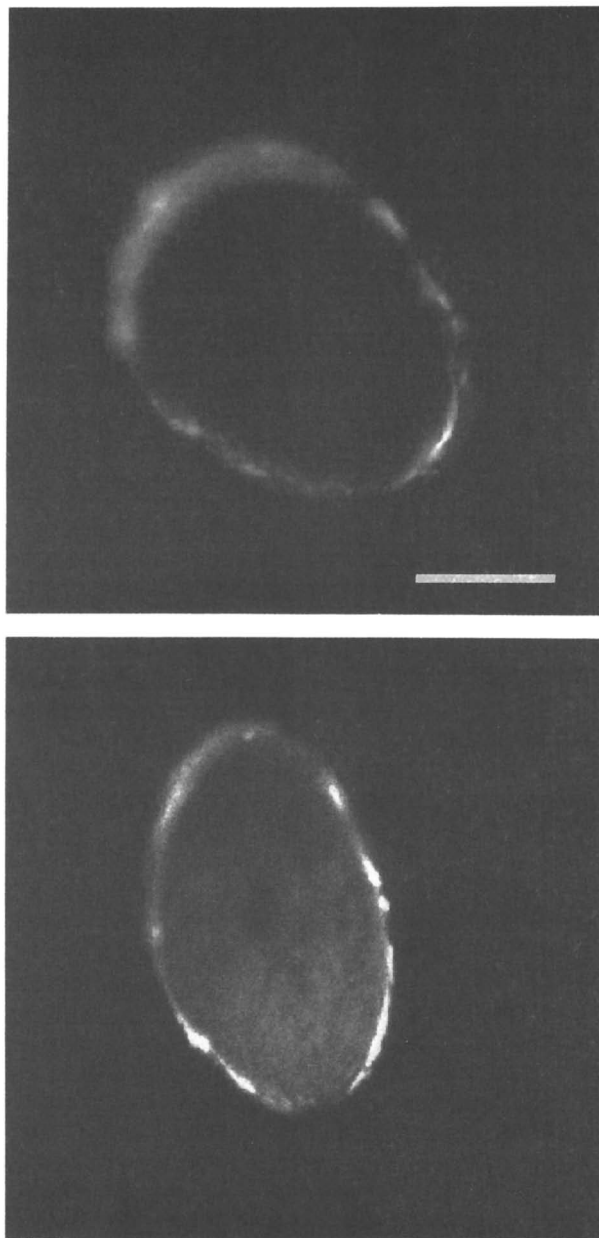


Figure 5. Cross-sections of the top of a hair fiber treated with Polymer JR400 (0.1 wt %, 12 hr); top: normal viewing conditions; bottom: confocal imaging. Scale bar = 50  $\mu\text{m}$ .

process. Furthermore, desorption of presorbed polymers was found to be very limited (25). The above results and interpretation have received support from subsequent studies, including (a) further radiotracer studies involving poly-(dimethyldiallylammonium chloride (Merquat polymers) (26), (b) various solution depletion study methods, such as colloid titration of cationic hydroxyethylcellulose ethers (27), electrometric titration of cationic starch (28), and gel permeation chromatography studies of Merquats (29), (c) a fluorescent dye disclosing method (30), and (d) electron probe microanalysis (EPMA) for silicon in dimethicone polymers (18).

The fluorescence imaging experiments described here do not give undeniable evidence for the penetration of Polymer JR400 into the hair fiber. However, several observations support such a process in highly water-swollen fibers. Particularly suggestive of such a penetration is the cross-sectional view of fibers soaked in aqueous Polymer JR400-F for 36 hrs (Figure 5) which displays a polymer coating thicker than monolayer coverage. Additionally, the fact that polymer deposited on hair after prolonged contact between hair and aqueous polymer solution is only partially desorbed from the fiber surface also suggests such a penetration.

## Conclusions

We have investigated the adsorption of a fluorescently-labeled cationic derivative of hydroxyethylcellulose ether onto hair fibers by fluorescence microscopy. The method provides a visual demonstration of the deposition of polymer. It can be applied to the study of the interactions of hair and 'real' shampoo formulations, thus affording a direct study of these complex colloidal systems. Future investigations include probing the extent of polymer adsorption in the presence of surfactant, and polymer penetration into the hair fiber under highly swollen conditions. Also of interest is an evaluation of the technique in the quantitative analysis of the amount of polymer deposited on hair.

## Acknowledgements

This work was supported by a research grant of the Natural Science and Engineering Council of Canada to FMW.

## Literature Cited

1. Anghel, D. F.; Alderson, V.; Winnik, F. M.; Mizusaki, M; Morishima, Y., *Polymer* 1998, 39, 3035 and references therein.
2. Winnik, F. M.; Winnik, M. A.; Tasuke, S.; Ober, C. K., *Macromolecules* 1987, 20, 38.
3. Winnik, F. M., *Macromolecules* 1987, 20, 2745.
4. Winnik, F. M., in *Hydrophilic Polymers, Performance with Environmental Acceptability*, Glass, J. E.; Ed, *Advances in Chemistry Series 248*, American Chemical Society, Washington DC 1996, chapter 22.
5. Winnik, F. M.; Regismond, S. T. A.; Goddard, E. D., *Langmuir* 1997, 13, 141.
6. Garcia-Dominguez, J.; Julia, M. R.; de la Maza, A.; Pujol, J. M.; Sanchez, J., *J. Soc. Dyers Color.*, 1976, 92, 433.

7. Rothery, F. R.; White, M. A., *J. Soc. Dyers Color.* **1983**, *99*, 11.
8. Gottschalk, H.; Hohm, G.; Kaminski, H., *Proc. Internat. Wool Text. Res. Conf.*, Aachen, 1975, Vol III, 349.
9. Weigmann, H.-D.; Kamath, Y. K.; Ruetsch, S. B.; Bussch, P.; Tessman, H., *J. Soc. Cosmet. Chem.* **1990**, *41*, 379.
10. Blakeslee, D., *J. Immunological Methods*, **1977**, *17*, 361.
11. The procedure described for the labeling of dextran, reported in ref 9 was adopted. Full synthetic details will be reported elsewhere.
12. De Belder, A. N.; Granath, K., *Carbohydr. Res.* **1973**, *30*, 375.
13. Dudman, W. F.; Bishop, C. T., *Can. J. Chem.* **1968**, *46*, 3079.
14. Robbins, C. R., *Chemical and Physical Behavior of Human Hair*, 2nd Ed., Springer Verlag, New York, NY, 1988.
15. Swift, J. A., *Fundamentals of Hair Science*, Cosmetic Science Monographs, 1, Micelle Press, Dorset, UK, 1997.
16. Wilson, T., *Confocal Microscopy*, Academic Press, New York, 1990.
17. Weigmann, H. D.; Kamath, Y. K., *Cosmetics & Toiletries* **1981**, *101*, 37.
18. Yahagi, K., *J. Soc. Cosmet. Chem.* **1992**, *43*, 275.
19. Goddard, E. D.; Harris, W. C., *J. Soc. Cosmet. Chem.* **1987**, *38*, 233.
20. Blanco, B.; Durost, B. A., Myers, R. R., *J. Soc. Cosmet. Chem.* **1997**, *48*, 127.
21. Wilkerson, V. *J. Biol. Chemistry* **1935**, *112*, 329.
22. Scott, G. V.; Robbins, C. R.; Barnhurst, J. D., *J. Soc. Cosmet. Chem.* **1969**, *20*, 135.
23. Woodard, J. *J. Soc. Cosmet. Chem.* **1972**, *23*, 593.
24. Goddard, E. D.; Hannan, R. B.; Faucher, J. A., *Proc. 7th Internat. CID Meeting, Moscow*, **1976**, 580.
25. Faucher, J. A.; Goddard, E. D.; Hannan, R. B., *Text. Res. J.* **1977**, *47*, 616.
26. Sykes, A. R.; Hammes, P. A. *Drug Cosmet. Ind.* **1980**, 62.
27. Hutter, J. M.; Clarke, M. T.; Just, E. K.; Lichtin, J. L.; Sakr, A., *J. Soc. Cosmet. Chem.* **1991**, *42*, 87.
28. Van, Nguyen, N.; Cannell, D. W.; Mathews, R. A.; Oei, H. H. Y., *J. Soc. Cosmet. Chem.* **1992**, *43*, 259.
29. Blanco, B.; Durost, B. A.; Myers, R. R. *J. Soc. Cosmet. Chem.* **1969**, *48*, 127.
30. Weigmann, H. D.; Kamath, Y. K.; Ruetsch, S. B.; Busch, P.; Tessman, H., *J. Soc. Cosmet. Chem.* **1990**, *41*, 379.



## Chapter 20

# Small-Angle Neutron Scattering on Neutral and Cationic Guar Galactomannan

M. R. Gittings<sup>1</sup>, J. Lal<sup>2</sup>, P. J. Dérian<sup>1</sup>, and C. Marques<sup>1</sup>

<sup>1</sup> Complex Fluids/CNRS Laboratory, Rhodia Inc., CN 7500, Cranbury, NJ 08512-7500

<sup>2</sup> IPNS Laboratory, Argonne National Laboratory, 9700 South Cass Avenue, Argonne, IL 60439

We investigate the local structure of aqueous solutions of guar, a naturally occurring polysaccharide. Small-angle neutron scattering (SANS) results are presented for both the native neutral polymer and for salt solutions of a cationically modified guar in D<sub>2</sub>O based systems. The intermediate wavevector range of the neutron spectra carries a signature of a Gaussian or nearly Gaussian chain with a decay close to  $q^{-2}$ . A crossover to a smaller slope at higher wavevectors, indicative of a local rigidity, was observed for all. The chain structure revealed by SANS is independent of temperature in the range of 9-50°C.

Guar is a naturally occurring polysaccharide known mostly for its ability to noticeably increase solution viscosity at relatively low concentrations. Naturally occurring forms of this neutral polymer as well as its derivatives (*i.e.* having cationic or hydrophobic substitutions) have applications that span a broad range of industries including cosmetics, pharmaceutical, food and oil industries. In the cosmetic industry, for example, it is used as a skin protective agent (1) and as a conditioner in shampoos (2). In pharmaceuticals, on the other hand, its presence is known to influence digestion in chickens (3) and also to control nutrition in camels (4). Randomly distributed galactose units along a mannose backbone at the approximate ratio of 1 galactose unit to 1.6 mannose units insure good polymer solubility in water through steric effects (Figure 1a). However, it is believed that the random nature of the substitution leads to inter- and intrachain association through the guar chain segments which are galactose-poor (5,6). These interactions are noncovalent and form stable intersegmental junction zones which can span several sugar units along the backbone. These associated regions have important consequences for the structure of the chains and for the physical behavior of the solution. In particular, aggregates are often presumed to be present even in dilute solutions and make the physical characterization of the polymer by common light-scattering measurements ambiguous (7,8).

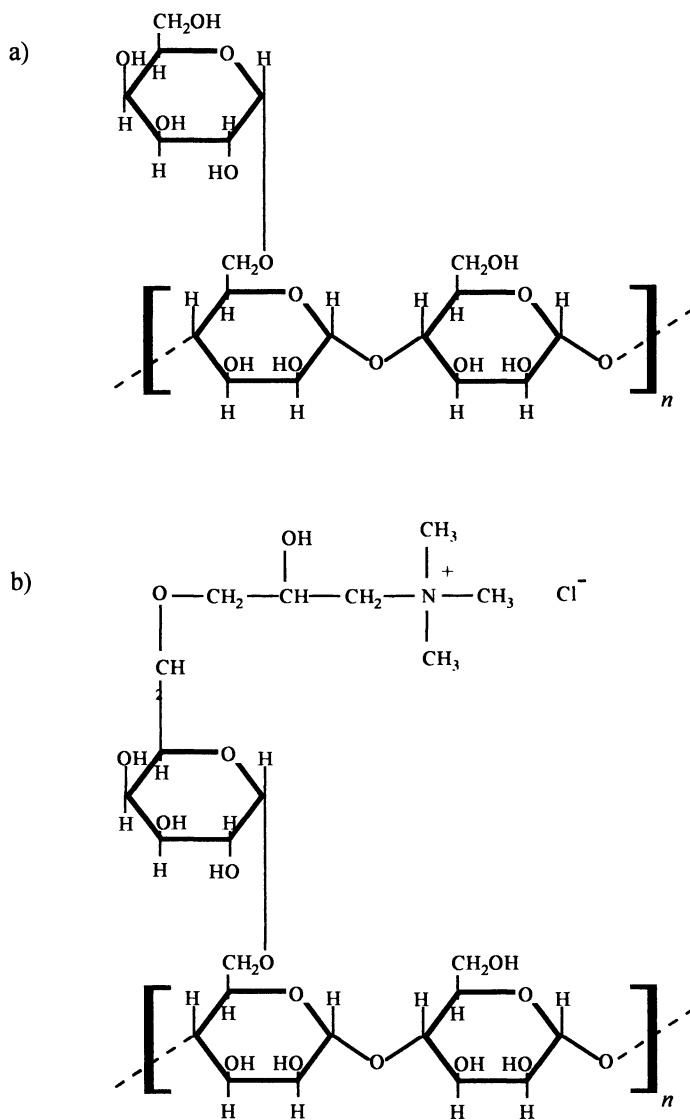


Figure 1. Molecular structure of (a) neutral and (b) cationic forms of guar. Note that the galactose units are randomly distributed at a ratio of 1 for every 1.6 mannose units. Also, the quaternary propylammonium is randomly attached to 14% of the mannose and galactose units.

In this study, small-angle neutron studies were performed on the native (neutral) form of guar and on cationic guar, a modified form of neutral guar more commonly used in cosmetic applications. Our particular sample has quaternary propylammonium groups distributed randomly along the chain (Figure 1b). The measurements on cationic guar were performed in the presence and absence of 0.1 M NaCl, with the focus of work being on the former. For a monovalent salt in water, the electrostatic screening length (Debye length) equals  $0.304/c^{1/2}$  giving 9.6 Å for 0.1 M NaCl. This is approximately twice the length of a sugar unit along the backbone (5.4 Å) (9). It was hoped that this salt concentration would be high enough to effectively eliminate long-range electrostatic repulsion while retaining enough short range repulsion to hinder formation of inter- and intrachain associations. SANS measurements were performed on solutions at concentrations greater than the overlap concentration. Such concentrated systems were necessary to increase the signal-to-noise ratio allowing reasonable statistics to be obtained within a 12-24 hour timeframe. Also, to increase the scattering contrast between polymer and solvent, D<sub>2</sub>O was used as the solvent. It is known for other molecules, however, that H<sub>2</sub>O is a somewhat better solvent than D<sub>2</sub>O (10) which may have some effect on the conformation of the polymer in solution. This fact must be remembered when comparing to H<sub>2</sub>O-based systems.

## Background

Scattering experiments provide information on the conformation of macromolecules in solution. Real space features with a characteristic dimension of  $l$  can be determined from the scattering spectra at wavevectors of  $q \sim 1/l$ . Moreover, the mass density of the macromolecules often follows a power-law distribution, leading also to power-law forms of the scattered intensity. For instance, the characteristic chain dimension of polymer chains ( $R$ ) increases with the polymerization index ( $N$ ) to a certain power,  $R \sim N^{1/D_f}$ , where  $D_f$  is the fractal dimension (11). In the case of Gaussian chains,  $D_f=2$  and the intensity scattered at intermediate wavevectors ( $a^{-1} \gg q \gg R^{-1}$  where  $a$  is the monomer length) decays as  $I(q) \sim q^{-D_f} = q^{-2}$ . On the other hand, the intensity scattered by rigid rod molecules ( $D_f=1$ ) has a slower decay— $I(q) \sim q^{-1}$ . A polymer molecule will often appear flexible at large lengthscales (intermediate wavevectors), but more rigid at local lengthscales (large wavevectors) since the monomers and their connections between each other provide some intrinsic rigidity to the backbone. Thus, the scattering profiles of polymer chains exhibit a crossover from larger to smaller fractal dimensions with increasing wavevector indicating a change in apparent rigidity at the different lengthscales.

## Experimental Method

Guar was obtained in its unmodified (neutral) and cationic form from Rhodia Inc. Both polymers were purified by centrifugation to remove insoluble impurities, precipitated with isopropyl alcohol, and dried under vacuum. The final moisture content of the powder was ~8.7%. The intrinsic viscosity,  $[\eta]$ , of neutral guar

solutions at room temperature was determined to be 21 dl/g. For the cationic polymer, quaternary propylammonium groups (which remain fully ionized in aqueous solutions without pH adjustment) are randomly attached to fourteen percent of the sugar units on the chain backbone. The intrinsic viscosity of the cationic guar depends on the salt concentration, ranging from 454 dl/g without added salt to 16.2 dl/g in 0.5 M NaCl (at room temperature). Such variations in the intrinsic viscosity are typical for polyelectrolytes (12). The overlap concentration, estimated from  $c^* \sim 4/[\eta]$ , corresponds to 0.19 g/dl and 0.25 g/dl (upper bound) for the neutral and cationic guar, respectively. D<sub>2</sub>O (99.9% pure) obtained from Cambridge Isotope Laboratories was filtered (with a hydrophilically modified PTFE Millipore filter, 0.2 μm) directly into clean glass vials with screw cap tops. The solutions were made by adding the guar powder to the filtered D<sub>2</sub>O and manually shaking to disperse the powder. They were then rotated on a spinning wheel at a low speed for 1-2 days at room temperature to allow for full dissolution of the polymer. After dissolution, the solutions were stored at 6 °C except during neutron scattering runs. The NaCl was added to the D<sub>2</sub>O and solubilized prior to adding cationic guar. The concentrations were 0.25%, 0.46%, 0.70%, and 1.1% (by weight) for the neutral guar in D<sub>2</sub>O and 0.25%, 0.46%, 0.65%, and 0.91% (by weight) for the cationic guar in 0.1 M NaCl in D<sub>2</sub>O. A 0.46% cationic guar solution in the absence of salt was also prepared.

Small-angle neutron scattering measurements were performed using the time-of-flight small-angle diffractometer at the Intense Pulsed Neutron Source (IPNS) in Argonne National Laboratory. The details of the instrument setup and operation are described elsewhere (13). Large sample cells with a 5 mm pathlength were used since guar scatters weakly in D<sub>2</sub>O. Data from  $q$  values ranging from 0.00494 Å<sup>-1</sup> to 0.247 Å<sup>-1</sup> were collected over 12 hours (for concentrations greater than 0.25%) and 24 hours (for concentrations of 0.25% and for the solvents without polymer). All measurements were taken at 25°C except for 2 runs on 0.46% neutral guar solutions at 9.5°C and 50°C. All data were treated according to methods used by Argonne National Laboratory which correct for solvent and parasitic scattering and place the data on an absolute level using standards. Within the range of polymer concentrations studied here, the amount of H<sub>2</sub>O in the bulk (from exchange of hydrogen along the polymer chain with deuterium in the bulk and from residual moisture in the guar powder) is less than 0.1%.

## Results and Discussion

The intensity values for the neutral and cationic guar solutions are plotted in absolute terms in Figure 2 normalized by concentration. Error bars are not shown in order to make the graph more readable, but vary from approximately ± 5% at intermediate wavevectors to ± 10% at high wavevectors. Data at wavevectors above 0.13 Å<sup>-1</sup> are omitted since incoherent scattering effects are more significant there. The data collapse onto a single curve at wavevectors above 0.01 Å<sup>-1</sup> for the neutral guar and 0.02 Å<sup>-1</sup> for the cationic guar. The curves do not show a well-defined plateau at the lowest measured wavevectors indicating that neutrons are probing the internal structure of the molecule (at dimensions  $\ll R$ ). In general, the data show two slopes. This feature is more easily seen when the data for each concentration are

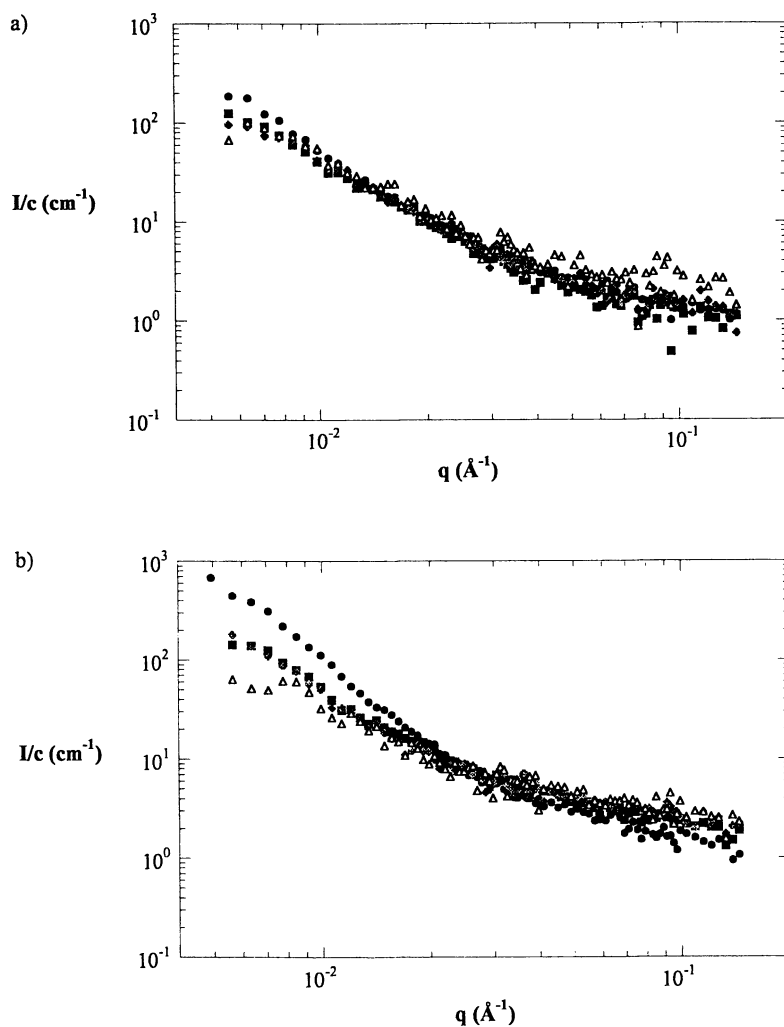


Figure 2. Neutron scattering spectra for (a) neutral guar in  $D_2O$  [(●) 1.1%; (■) 0.70%; (◆) 0.46%; (△) 0.25% concentration by weight] and (b) cationic guar in  $D_2O$ -based 0.1 M NaCl [(●) 0.91%; (■) 0.65%; (◆) 0.46%; (△) 0.25% concentration by weight].

plotted separately and in different manners. An example is shown in Figure 3 for neutral guar at 0.46% concentration. Figure 3a shows the data plotted in the same way as in Figure 2. Neglecting the first few data points (which are at the limits of the capabilities of the instrument), two lines were fit through the data giving slopes of -2.0 and -1.0 at the lower and higher ends of the neutron spectra, respectively. These slopes represent the fractal dimension of the polymer and indicate a crossover from a more flexible structure at larger lengthscales to a more rigid structure at smaller lengthscales. Reinforcing this finding, Figure 3b shows a Kratky plot where  $Iq^2$  vs.  $q$  is plotted on linear scales. The plot shows a flat region at lower wavevectors indicating  $q^{-2}$  behavior and an increase in the slope at high wavevectors indicating a change to smaller power law behavior. For comparison, lines with power law behavior of  $q^{-2}$  and  $q^{-1}$  are also shown. Plotted in this way, such crossovers are clearly seen for all of the samples, both neutral and cationic, although the exact power law behavior varies somewhat. Moreover, the crossovers appear independent of concentration for each guar, giving  $0.033 \pm 0.005 \text{ \AA}^{-1}$  for neutral guar and  $0.025 \pm 0.002 \text{ \AA}^{-1}$  for cationic guar. It is reasonable that the crossover point for the cationic guar occurs at lower wavevectors than for neutral guar. This represents a larger "rigid" lengthscale for the cationic guar and suggests that some local repulsion still exists even in 0.1 M NaCl. Also, the cationic guar has a larger average monomer size due to the attachment of charge groups to the backbone, making the polymer in a steric sense even more rigid.

Data at other guar concentrations were analyzed similarly and are summarized in Table I. The correlation factors describing the quality of the fitted data are 0.98 or greater at intermediate wavevectors. At higher wavevectors the data are more difficult to fit, with correlation factors ranging from 0.74 (for the 0.25% neutral guar solution) to 0.97. Note that some of the slopes at higher wavevectors are not reported; the measured slopes are less than one giving a fractal dimension that has no physical meaning within the framework of the power law discussed earlier. With some variability, the neutral guar displays a fractal dimension of  $\sim 2$  at low wavevectors ( $0.006 \text{ \AA}^{-1} \leq q \leq 0.03 \text{ \AA}^{-1}$ ) and  $\sim 1$  in the range  $0.03 \text{ \AA}^{-1} \leq q \leq 0.13 \text{ \AA}^{-1}$ . Thus, neutral guar exhibits Gaussian behavior at intermediate lengthscales and rigid rod behavior at smaller lengthscales, displaying the signature of a random walk polymer with local rigidity.

**Table I.** Summary of power law behavior for neutral and cationic guar.

| <i>Neutral Guar in D<sub>2</sub>O</i> |                                      |                              | <i>Cationic Guar in 0.1 M NaCl (D<sub>2</sub>O-based)</i> |                                      |                              |
|---------------------------------------|--------------------------------------|------------------------------|---|--------------------------------------|------------------------------|
| <i>Guar concentration n (wt. %)</i>   | <i>slope in intermediate q range</i> | <i>slope in high q range</i> | <i>Guar concentration (wt. %)</i>                         | <i>slope in intermediate q range</i> | <i>slope in high q range</i> |
| 1.1%                                  | -2.26                                | -1.04                        | 0.91%   | -2.89                                | -1.04                        |
| 0.70%                                 | -2.01                                | -0.98                        | 0.65%   | -2.04                                | ----                         |
| 0.46%                                 | -2.03                                | -1.01                        | 0.46%   | -2.18                                | ----                         |
| 0.25%                                 | -1.94                                | ----                         | 0.25%   | -1.84                                | ----                         |

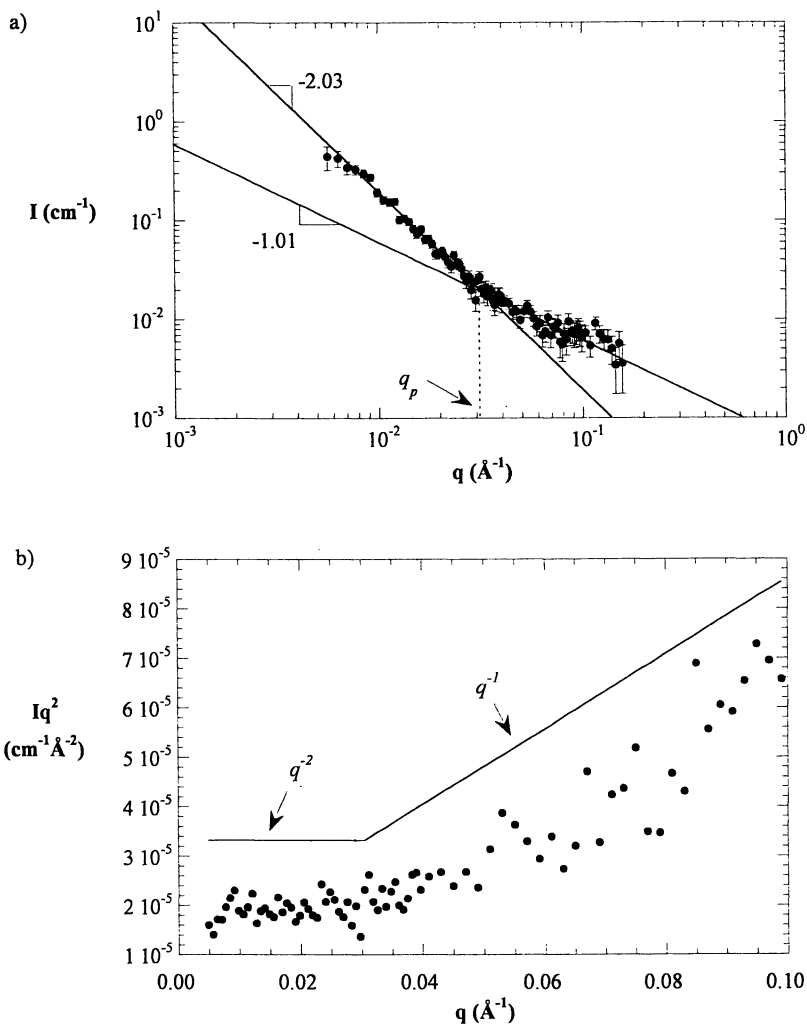


Figure 3. Neutron scattering spectrum for 0.46% neutral guar in D<sub>2</sub>O. a) Logarithmic plot of  $I$  vs.  $q$ ; b) Linear plot of  $Iq^2$  vs.  $q$  (Kratky plot). Lines showing  $q^{-2}$  and  $q^{-1}$  power law behavior are also shown.

The cationic guar data vary more widely in the wavevector range  $0.006 \text{ \AA}^{-1} \leq q \leq 0.13 \text{ \AA}^{-1}$ , with a slope close to 3 at the highest concentration that decreases with the polymer concentration. While electrostatic effects may encourage some swelling at the lowest concentration, the total increase in the ion concentration from contributions due to the polymer is less than 3%. This small increase is not expected to reduce long range repulsion significantly enough to completely account for such large changes in the polymer conformation. Hence, the large slope at the highest concentration may indicate increased interaction among chains, perhaps due to incomplete polymer dissolution. Both the 0.91% cationic guar solution and the 1.1% neutral guar solution exhibited some elastic qualities making polymer dissolution more difficult. Considering these factors, no definite concentration dependence in the fractal dimension can be ascertained.

The slopes for cationic guar in the higher- $q$  region are less than 1 except at the highest concentration. The absence of a clear  $q^{-1}$  regime might be due to the charged nature of the polymer. Not only are charged monomers more bulky structurally, but counterion contributions to the scattering profile may mask the signature of local rigidity. Figure 4 makes this statement more clear. It shows the neutral and cationic guar at 0.46% concentration plotted together and includes all measured  $q$  values, even those above  $0.13 \text{ \AA}^{-1}$  where the signal-to-noise ratio is considerable. At intermediate wavevectors ( $0.01 \text{ \AA}^{-1} \leq q \leq 0.03 \text{ \AA}^{-1}$ ) the data coincide whereas at large wavevectors ( $q \geq 0.03 \text{ \AA}^{-1}$ ) the data diverge. Typically, all intensity profiles will eventually flatten out to zero slope at high enough wavevectors as the neutrons probe molecular rearrangements within the monomer itself.

Polysaccharides are weak scatterers of neutrons mostly because of the exchange of hydrogens along the backbone with deuterium in the bulk. This not only reduces the contrast between the polymer and solvent, but it also increases the total amount of incoherent scattering. Thus, in order to get good scattering statistics, the data must be collected for long time periods, making the experiments more difficult. Recall that the data in this study were collected for 12 to 24 hours both for the sample and solvent. Up to this point, incoherent scattering was not subtracted from the measured data. To estimate the error from incoherent scattering one must include the presence of hydrogen from the polymer and from residual moisture in the guar powder before addition to water. Estimates reveal a small increase in the slopes extracted from data at intermediate wavevectors (up to 2%), but a moderate increase at high wavevectors (up to 22%). Also, the effect on the crossover position is minimal (~1%). Hence, even though incoherent scattering increases with guar concentration, the crossover position stays the same. Thus, the change in slopes in the intensity data is not a manifestation of improper background subtraction, but rather an intrinsic characteristic of the guar chain.

Regardless of the type of guar or the concentration, a change in the fractal dimension from a number greater than one at intermediate wavevectors to approximately one at higher wavevectors is usually associated with a persistence length of the polymer. This length represents a contiguous portion of the chain where the directional orientation the monomers at either end of this portion becomes uncorrelated (14). The wormlike chain is often used as a polymer model when the



fractal dimension changes from 2 to 1. For an ideal wormlike chain, the crossover in the scattered intensity ( $I$ ) from intermediate to high wavevectors has been shown by des Cloizeaux (15) to obey

$$I = C \left( \frac{2}{3} \frac{1}{q^2} + \frac{l_p \pi}{q} \right). \quad (1)$$

Here  $l_p$  denotes the persistence length and  $C$  is a constant. Note that the intensity as written here has two asymptotes at high and low- $q$  values with a crossover point,  $q_p$ , at

$$q_p = \frac{2}{3\pi l_p}. \quad (2)$$

Within the framework of this model,  $l_p$  was found to be approximately 7 Å for neutral guar at 0.46% which is slightly larger than the length of a sugar molecule along the backbone, 5.4 Å (9). A similar calculation on the neutral guar data at 0.7% concentration gives a persistence length of approximately 6 Å.

The values obtained here for the persistence length seem surprisingly small. Polystyrene chains, for example, have been reported to have a persistence length of  $\sim 9$  Å (16). However, the reported persistence lengths are usually extracted by fitting the lower and middle  $q$ -range of the scattering spectra, typically from zero wavevectors to the end of the plateau region in the  $q^2 I(q)$  representation. The lowest of our scattered data belong already to the plateau. Moreover, we do observe a clear crossover from the plateau to the next linear regime, allowing for the use of the asymptotic form equation (1). The differences in numbers are certainly to be attributed to differences in the extraction methods, and not to differences in the properties of the chains. For instance, considering the steric hindrance of the mannose units and the high frequency of galactose side chains, the persistence length of guar is expected to be larger than the persistence length of polystyrene. Indeed, if we estimate the value of  $q_p$  for polystyrene from the data in reference 17, and compare it with our results, we would be lead to a persistence length of guar 2-2.5 times larger than that of polystyrene.

Other techniques also yield different values for the persistence length. Robinson *et al.* (7), for instance, find a value of  $\sim 37$  Å for neutral guar in H<sub>2</sub>O using intrinsic viscosity measurements. These measurements probe global properties of the solution and, hence, are affected by the molecular weight and polydispersity as well as by inter- and intra-chain interactions. Extrapolations to infinite dilution may rule out inter-chain interactions, but intra-chain interactions may still be present. Hence, the intrinsic viscosity would be higher than in the absence of these interactions, leading to a higher-than-real persistence length. Alternatively, small-angle neutron scattering probes the local features of the polymer.

In addition to the SANS studies previously discussed, a measurement was performed on cationic guar in the absence of salt (at 0.46% (by wt.) concentration) to show the extent of screening in the 0.1 M NaCl case. Figure 5 shows that the characteristic features are still present in the absence of salt, but the crossover point is

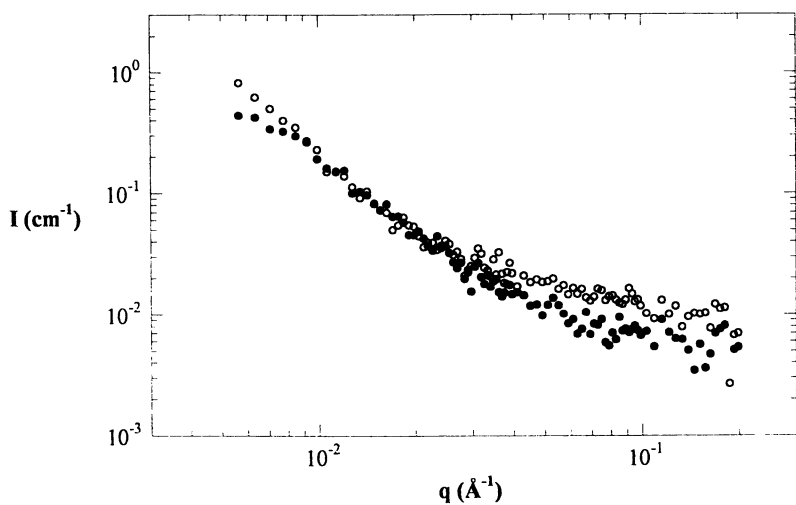


Figure 4. Comparison of neutron scattering spectra for 0.46% neutral guar in  $\text{D}_2\text{O}$  (●) and 0.46% cationic guar in  $\text{D}_2\text{O}$ -based 0.1 M NaCl (○).

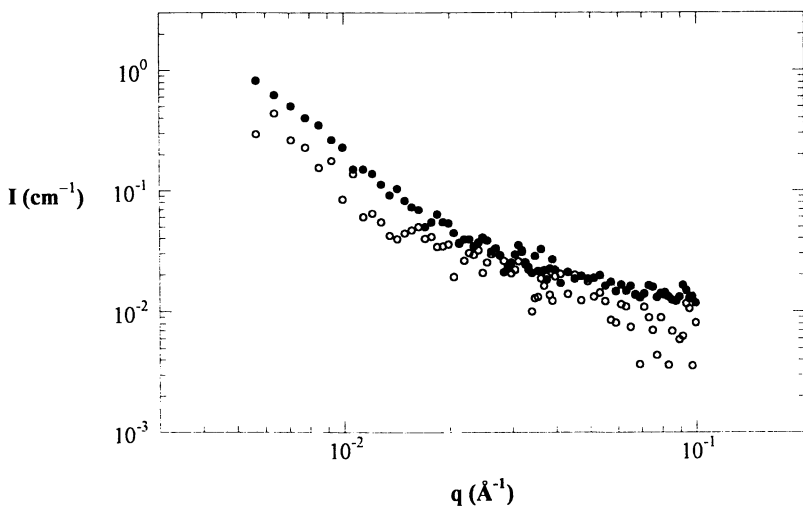


Figure 5. Comparison of 0.46% cationic guar in presence (●) and absence (○) of 0.1M NaCl.

shifted to lower  $q$  values as expected for a polymer with the persistence length increased by electrostatic repulsion. Indeed, without salt the crossover occurs approximately between  $0.013 \text{ \AA}^{-1}$  and  $0.020 \text{ \AA}^{-1}$ , as compared to  $\sim 0.025 \text{ \AA}^{-1}$  in the presence of  $0.1 \text{ M NaCl}$ . This corresponds to a 40-100% increase in the persistence length, which is somewhat lower than would be expected from an Odijk calculation. In Figure 5, the scattering intensities of the two samples differ slightly. This may simply reflect increased scattering from the electrolyte surrounding the guar molecule which also may increase the signal-to-noise ratio for that sample, giving less scattered data.

In the last part of the study, the influence of temperature on the conformation of the polymer was investigated (Figure 6). Three temperatures were investigated,  $9.5^\circ\text{C}$ ,  $25^\circ\text{C}$ , and  $50^\circ\text{C}$ , and no difference in the static organization of the polymer was detected within the available  $q$  range of the instrument. In fact, the collapse of the data at each temperature suggests rather good reproducibility of all the results, despite some scatter in the data.

## Conclusion

Small-angle neutron scattering experiments were performed on concentrated neutral and cationic guar solutions, the latter in the presence of salt. Here we reported, to our knowledge, the first measurements on the local structure of such a system. The polymer was found to have a conformation close to that for a Gaussian chain at

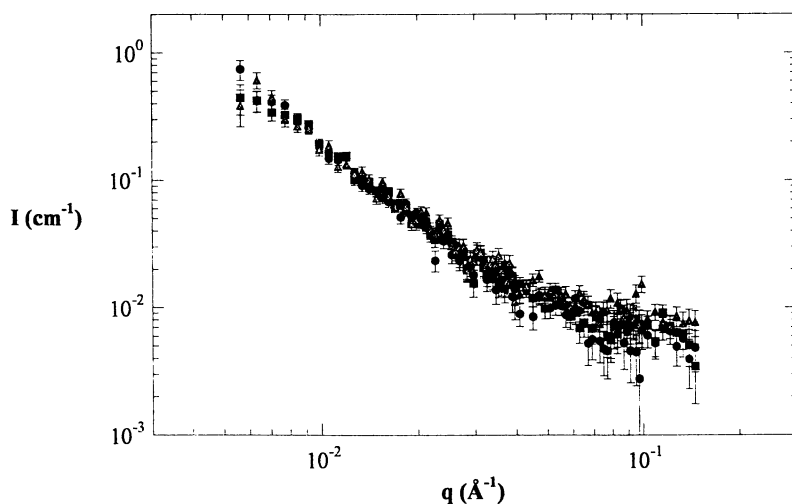


Figure 6. Temperature dependence of neutron scattering spectra for 0.46% neutral guar in  $\text{D}_2\text{O}$ : (●)  $9.5^\circ\text{C}$ ; (■)  $25^\circ\text{C}$ ; (▲)  $50^\circ\text{C}$ .

intermediate lengthscales. The scattering profiles are typical of those for polymers with intrinsic rigidity, with a  $q^{-1}$  slope at high wavevectors. Crossovers from the two regions occur at roughly the same  $q$  values, around  $0.033 \pm 0.005 \text{ \AA}^{-1}$  for neutral guar and  $0.025 \pm 0.002 \text{ \AA}^{-1}$  for cationic guar. Electrostatic effects on the cationic guar were partially screened in the presence of salt, but appeared strong enough to influence the scattered intensity at the higher end of the measured  $q$  range. Incoherent scattering does not appear to strongly affect the results. Last, the static properties of the neutral polymer do not change within temperature range  $9.5^\circ\text{C}$  to  $50^\circ\text{C}$ .

### Acknowledgments

We thank Animesh Goswami and Olivier Anthony for many useful discussions and for purifying the guar. We also thank Anthony Homack and Denis Wozniak for help with sample preparation and instrument operation and Jeanne Chang and Christian Robelin for intrinsic viscosity measurements. Last, we are grateful to Martin In, Robert Prud'homme, and Redouane Borsali for valuable discussions.

We gratefully acknowledge the financial support of Rhodia, Inc. Also, this work has benefited from the use of the Intense Pulsed Neutron Source at Argonne National Laboratory. This facility is funded by the U.S. Department of Energy, BES-Materials Science, under Contract W-31-109-Eng-38.

### Literature Cited

1. Pugliese, P.; Himes, G.; Wielinga, W. *Cosmetics and Toiletries* **1990**, *105*, pp. 105-111.
2. Brode, G. L.; Goddard, E. D.; Harris, W. C.; Salensky, G. A. In *Cosmetic and Pharmaceutical Applications of Polymers*; Gebelein, C. G.; Cheng, T. C.; Yang, V. C., Eds.; Plenum Press: New York, 1991; pp. 117-128.
3. Yasar, S.; Forbes, J. M. *Brit. Poultry Sci.* **1997**, *38*, pp. S44-S45.
4. Nagpal, A. K.; Rai, A. K. *Indian J. of Animal Sciences* **1993**, *63*, pp. 580-581.
5. Morris, E. R. *Brit. Polym. J.* **1986**, *18*, pp. 14-21.
6. Molyneux, P. In *Water-Soluble Polymers: Synthesis, Solution Properties, and Applications*; S. W. Shalaby, S. W.; McCormick, C. L.; Butler, G. B., Eds. *ACS Symposium Series*; 1991, **467**; pp. 232-248.
7. Robinson, G.; Ross-Murphy, S. B.; Morris, E. R. *Carbohydr. Res.* **1982**, *107*, pp. 17-32.
8. Vijayendran, B. R.; Bone, T. *Carbohydr. Polym.* **1984**, *4*, pp. 299-313.
9. Morris, E. R.; Ross-Murphy, S. B. *Techniques in Carbohydrate Metabolism* **1981**, *B310*, 1-46.
10. Gripon, C.; Legrand, L.; Rosenman, I.; Vidal, O.; Robert, M. C.; Boué, F. *J. of Crystal Growth* **1997**, *117*, pp. 238-247.
11. de Gennes, P. G. *Scaling Concepts in Polymer Physics*; Cornell University Press: London, 1979.
12. Rubinstein, M.; Colby, R. H. *Phys. Rev. Letters* **1994**, *73*, pp. 2776-2779.
13. Thiyagarajan, P.; Epperson, J. E.; Crawford, R. K.; Carpenter, J. M.; Klippert, T. E.; Wozniak, D. G. *J. Appl. Cryst.* **1997**, *30*, pp. 280-293.
14. Higgins, J. S.; Benoît, H. C. *Polymers and Neutron Scattering*, Clarendon Press: Oxford, 1994.
15. des Cloizeaux, J. *Macromolecules* **1973**, *6*, pp. 403.
16. Brûlet, A.; Boué, F.; Cotton, J. P. *J. Phys. II France* **1996**, *6*, pp. 885-891.

## Chapter 21

# Applications of Gel Permeation Chromatography with Multi-Angle Light Scattering to the Characterization of Polysaccharides

D. Richard White, Jr.

Food and Beverage Analytical Department, The Procter & Gamble Company,  
Winton Hill Technical Center, 6210 Center Hill Road, Cincinnati, OH 46224

Gel permeation chromatography with multi-angle light scattering (GPC-MALS) is a useful technique for the characterization of polysaccharides. Polysaccharides are typically polydisperse, exhibiting a wide range in molecular weight, sequence, and structure. Industrial polysaccharides find use in pharmaceuticals and cosmetics, as well as in foods, beverages, detergents, textiles, paper and paint, to name a few. Industrial polysaccharides include, but are not limited to, such materials as native and modified starches, dextrans, dextrans, glucans, pullulans, modified celluloses, pectins, carrageenans, and gums from microbial and plant seed sources. Information as to size, structure and conformation is useful in order to better understand solution behavior, intra- and intermolecular interactions, rheology, and function. GPC-MALS permits the determination of molar mass and size from the measurement of scattered light as a function of angle. This chapter illustrates the use of the technique for the characterization of some important industrial polysaccharides.

The primary advantage of combining light-scattering with size-exclusion chromatography is that it allows for the absolute determination of molar mass and mean square radius, without the need to calibrate the column with standards, which oftentimes are not available. The first of two key principles is that the amount of light scattered is proportional to both the molecular weight ( $M_w$ ) and concentration ( $c$ ) of polymer (1),

$$R(\theta) = K * M_w c P(\theta) [1 - 2A_2 M_w c P(\theta)] \quad (1)$$

where  $R(\theta)$  is termed the “excess Rayleigh Ratio” and is the excess light scattered above that of the pure solvent.  $A_2$  is the second-order virial coefficient which accounts for non-ideal scattering due to solute-solute and solute-solvent interactions.  $A_2$  can often be neglected in dilute solutions and/or solutions of lower molar mass polymers. The proportionality constant or optical constant,  $K^* = 4\pi^2(\text{dn}/\text{dc})^2 n_0^2 N_A^{-1} \lambda_0^{-4}$ , includes several known and constant terms:  $n_0$  is the refractive index of the solvent,  $N_A$  is Avogadro’s number,  $\lambda_0$  is the vacuum wavelength of incident light. The refractive index increment ( $\text{dn}/\text{dc}$ ) is the change in the refractive index of the solution with respect to the change in concentration of polymer in the limit of zero concentration. For co-polymers and for polymers with molar masses below about  $10^3 \text{ g mol}^{-1}$ , the value of  $\text{dn}/\text{dc}$  may vary significantly with molecular weight. However, for most homopolymers of higher molar mass, the value of  $\text{dn}/\text{dc}$  is essentially constant over the range of masses measured. Thus, it may be determined by making ancillary refractive index measurements of solutions of the bulk polymer at varying concentration. It can also be computed “on the fly” during a chromatographic run if the mass injected is accurately known and there is 100 percent recovery from the column.

The second key principle is that the variation in the scattered light with angle depends on the mean square radius of the molecule. This is reflected in the “scattering function”,  $P(\theta)$ ,

$$P(\theta) = 1 - (2k \sin \theta/2)^2 \langle r_g^2 \rangle / 3 \quad (2)$$

where  $k = 2\pi n_0 / \lambda_0$ . It is important to note that  $P(\theta) \rightarrow 1$  as  $\theta \rightarrow 0$ . The mean square radius,  $\langle r_g^2 \rangle (= \sum r_i^2 m_i / M_i)$ , is the sum of the square of the equilibrium distances between scattering centers and the center of mass of the polymer. Hence,  $\langle r_g^2 \rangle$  is related to the distribution of mass within the molecule and is not generally a measure of the molecule’s external geometry. The square-root is termed the root-mean-square radius,  $r_g$ , although it is often erroneously called the “radius of gyration.” It is also important to note that  $r_g$  is not the hydrodynamic radius, but has the distinct advantage of revealing information about a molecule’s internal structure so that one can make inferences as to conformational shape, degree of branching, etc. Combining equations 1 and 2 in the fashion of Zimm (2) yields what is referred to as the Zimm formalism of the Rayleigh-Debye-Gans approximation. In vertically polarized light,

$$K^*c/R(\theta) = 1/M_w P(\theta) + 2A_2c \quad (3)$$

The second term on the right of Equation 3,  $A_2c$ , is retained to account for non-ideality at higher concentration and/or in the case of higher molar mass polymers. As previously mentioned,  $A_2c$  can often be neglected. At the limit of zero angle and zero concentration where  $P(\theta)$  is unity, the function  $K^*c/R$  is exactly equivalent to the reciprocal molecular weight.

In Gel Permeation Chromatography (GPC) it is assumed that each chromatographic slice contains molecules of a single, or at least very narrow band, molecular weight,  $M_i$ . Therefore, once data have been processed, the effective mass moments can be calculated over the entire peak from the following relations:

$$\begin{aligned}
 \text{weight-average,} & \quad M_w = \sum c_i M_i / \sum c_i \\
 \text{number average,} & \quad M_n = \sum c_i / (\sum c_i / M_i) \\
 \text{"Z" average,} & \quad M_z = \sum c_i M_i^2 / (\sum c_i M_i) .
 \end{aligned}$$

The weight-average molecular weight ( $M_w$ ) is the parameter directly measured by light-scattering. It is the sum of the products of the concentration and molecular weight at each slice, divided by the total concentration,  $c$  ( $= \sum c_i$ ). The number average molecular weight ( $M_n$ ) tends to weigh more heavily the lower molecular weight species and is more closely related to that which would be determined by measurement of colligative properties such as osmometry. On the other hand, the Z-average molecular weight ( $M_z$ ), tends to weigh more heavily the higher molecular weights and is more closely related to that determined by sedimentation equilibrium and ultracentrifugation experiments, for example. The ratio of the  $M_w$  to  $M_n$  or  $M_z$  is often used as an estimate of relative polydispersity of a polymer.

The corresponding quantities for the mean square radii are written in an analogous fashion as:

$$\begin{aligned}
 \langle r_g^2 \rangle_w &= \sum \langle r_g^2 \rangle_i c_i / \sum c_i \\
 \langle r_g^2 \rangle_n &= (\sum \langle r_g^2 \rangle_i c_i / M_i) / (\sum c_i / M_i) \\
 \langle r_g^2 \rangle_z &= (\sum \langle r_g^2 \rangle_i c_i M_i) / (\sum c_i M_i) .
 \end{aligned}$$

In GPC, it can usually be assumed that the concentration in each slice of the chromatogram is so small that the second virial coefficient is negligible. Thus, for each slice of the chromatogram, one can plot  $K^*c/R(\theta)$  vs.  $\sin^2(\theta/2)$  to yield an intercept which is the reciprocal molecular weight for that slice. Correspondingly, the slope of the plot at the intercept permits the determination of the mean square radius for that slice. Figure 1 is a Debye Plot using the Zimm formalism ( $K^*c/R$ ) for a representative slice of a narrow band pullulan polysaccharide. The nominal  $M_w$  of this material from the manufacturer (Polymer Laboratories, Amherst, MA) is 404,000 g mol<sup>-1</sup>. Taking the slice at maximum concentration (maximum RI signal) and plotting  $K^*c/R(\theta)$  vs  $\sin^2(\theta/2)$  for 3 angles (approximately 45°, 90°, and 135°) yields  $M_w = 449,000$  g mol<sup>-1</sup> and  $r_g = 13$  nm.

## Experimental

The experimental setup consisted of a Waters (Milford, MA) 2690 solvent delivery system with built-in degasser, a thermostatted sample compartment, injector, and column oven. A 0.1  $\mu\text{m}$  in-line filter was added between the pump and injector. The columns were Waters ultrahydrogel 2000 and 250 in series, thermostatted to 45 °C. Mobile phase was either 0.025 M phosphate buffer with added 0.05 M NaCl, or 0.1 M LiCl for charged polysaccharides (such as the carrageenans), shown to inhibit gel formation. Samples were prepared in the mobile phase to contain from 1 - 3 mg mL<sup>-1</sup>. Typically, the polysaccharides were dissolved by stirring at 50 °C. For the starch, samples (~5 mg mL<sup>-1</sup>) were microwave solubilized at 130 °C for 10 minutes. Samples were coarsely filtered through 5 $\mu\text{m}$  syringe-tip filters prior to analysis. The pump flow rate was 0.5 mL/min and the injection volume was 100  $\mu\text{L}$ . The detectors

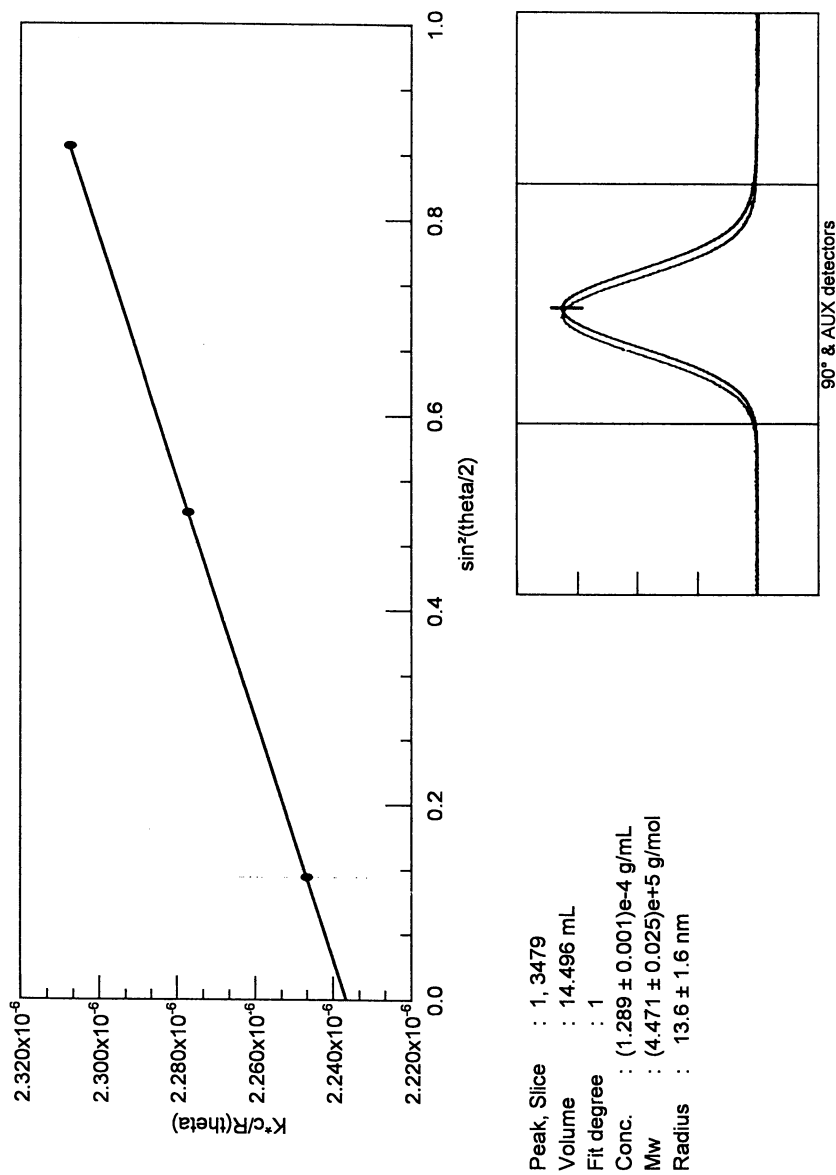


Figure 1. Debye Plot (Zimm Formalism) for a Representative Slice of a Narrow Band Pullulan Polysaccharide.



consisted of a MiniDAWN (Wyatt Technology, Inc., Santa Barbara, CA) which is a 3-angle laser light scattering detector capable of making measurements at fixed angles approximately 45, 90, and 135 degrees, and an Optilab interferometric refractive index detector (Wyatt Technology, Inc.) which operates at the same wavelength as the MiniDAWN, in this case 690 nm. The software was ASTRA version 4.5 (Wyatt Technology, Inc.). Calibration of the RI detector and measurements of  $dn/dc$  were accomplished with DNDC software version 5.2 (Wyatt Technology, Inc.).

The first step before making measurements is to calibrate the detectors. As with all transducers, it is necessary to relate the signal output, in this case Volts, to the physical quantity of interest. In the case of the RI detector it is the refractive index change,  $dn$ , that must be measured as a function of the voltage output. This is accomplished by making RI measurements on accurately prepared solutions for which the quantity  $dn/dc$  is already known. The quantity  $dn$  can then be calculated for each solution by multiplying the concentration,  $c$ , by  $dn/dc$ . The slope of a plot of  $dn$  vs. the measured voltage output yields the calibration constant for the detector. Once the calibration constant is determined, then with a knowledge of  $dn/dc$  for a sample polymer, it is possible to calculate the concentration at any point in the run as the polymer elutes through the detectors. To calibrate the RI detector, solutions of NaCl (0.1 to 0.6 mg/mL) were passed through the RI detector via syringe pump. Voltage readings were taken when the signal had reached a stable plateau.

For the light-scattering detector, one would like to relate the signal output (Volts) to the Rayleigh ratio,  $R(\theta)$ . This is accomplished by measuring the signal at the  $90^\circ$  detector while passing solvent with a well-characterized  $R(\theta)$  through the light scattering flow cell. Toluene is a good choice because it has a high Rayleigh factor relative to most common solvents. Once the  $90^\circ$  diode is calibrated, the final step is to normalize the diodes at the other angles to that of the  $90^\circ$  signal. This is necessary because of differences in the light scattered due to the geometry of the cell, the refractive index of the cell material, and the refractive index of the solvent in which measurements will be made. For this reason, normalization must be carried out in the solvent that will be used to make the final measurements. Normalization coefficients for the low angle and the high angle are determined by measuring the signal produced by a monodisperse, isotropic scatterer in the solvent to be used. In our case, the solvent was water and bovine serum albumin (BSA,  $M_w \sim 69,000$ ) was a suitable polymer for normalization. BSA's small radius ( $< 10\text{nm}$ ) ensures that the angular dependence of scattering is very small, i.e.,  $P(\theta) \sim 1$ .

## Results and Discussion

The polymers studied here were limited to a relatively few commercially available polysaccharides for illustrative purposes. All the polysaccharides chosen were rather well behaved in terms of solubility and stability in the aqueous mobile phases employed.

**Pullulans.** Pullulans are water-soluble extracellular polysaccharides synthesized by *Aureobasidium pullulans* (3, 4), a common and widespread fungus; they are prepared by fermentation. The chemical structure varies according to the substrate and strain of

microorganism used, as well as the chemical fractionation and purification methods employed. Nevertheless, pullulan is currently accepted to be a water-soluble, neutral glucan, which consists of linear chains of malto-triosyl units, linked together by 1→6 alpha-D-linkages. It is a flexible, odorless, tasteless material and its film forming properties make it an ideal coating for foods and drugs. Pullulan is non-nutritive in that it is not degraded by *in vivo* digestive enzymes. It is commercially available in narrow molecular weight ranges and has been recommended for column calibration in size-exclusion chromatography by Kato (3) and Fishman (5). Seven narrow molecular weight pullulans (Polymer Laboratories, Amherst, MA) were analyzed separately. Three concentration levels were used so that the mass on column ranged from 0.1 to 0.3 mg for a 100  $\mu$ L injection. Figure 2 is an overlay of the GPC chromatograms for the seven polymers. Both refractive index and light-scattering signals vs. elution volume are illustrated. The three concentrations are apparent from the relative magnitude of the RI signals. Comparison of the relative intensity between the LS and RI signals highlights the dependence of scattering on molar mass as well as concentration. Note that the LS signal is much higher for the larger, early eluting polymers in spite of their lower concentration. Superimposed on the chromatograms are the calculated point-by-point  $M_w$  values across each polymer band. If each polymer were truly monodisperse these would be horizontal lines and one would expect to see a stair-step like pattern. As observed here, there is a slight slope downward within each band indicating some polydispersity. Table I is a summary of the results obtained. Calculated results for the average  $M_w$  agree reasonably well with the nominal values from the manufacturer, although about 10% higher. It is noteworthy that the range of polydispersity values is essentially the same as that obtained by Fishman (5), who used differential RI detection, a different set of chromatographic columns, sodium chloride mobile phase, and a smaller injection volume (20  $\mu$ L). The  $dn/dc$  values for the pullulan standards were obtained from the known mass injected on column and by assuming 100 percent recovery. Although there was quite a bit of uncertainty in the  $r_{g,z}$  values obtained, the range is close to values given in the literature (3, 5). The inability to calculate a reasonable  $r_{g,z}$  for the smaller  $M_w$  polymers probably reflects the lower limit of molecular radius for which one can realize a measurable angular dependence,  $P(\theta)$ . That limit appears to be about 10 nm for  $\lambda = 690$  nm.

**Table I. Summary of  $M_w$  and  $r_{g,z}$  Results for Seven Commercial Pullulan Standards**

| $M_w$ (nominal) | $M_w$ (calc) | $M_w/M_n$ | $dn/dc$ (mL/g) | $r_{g,z}$ (nm) | $r_{g,z}$ (nm)* |
|-----------------|--------------|-----------|----------------|----------------|-----------------|
| 11,800          | 13,230       | 1.10      | 0.133          | —              | 3               |
| 22,800          | 24,760       | 1.15      | 0.136          | —              | 5               |
| 47,300          | 54,850       | 1.04      | 0.137          | —              | 7               |
| 112,000         | 115,200      | 1.04      | 0.138          | —              | 12              |
| 212,000         | 230,200      | 1.06      | 0.133          | 10-21          | 17              |
| 404,000         | 455,700      | 1.04      | 0.133          | 18             | 25              |
| 788,000         | 817,400      | 1.08      | 0.136          | 30             | 37              |

\*data interpolated from (3, 5)

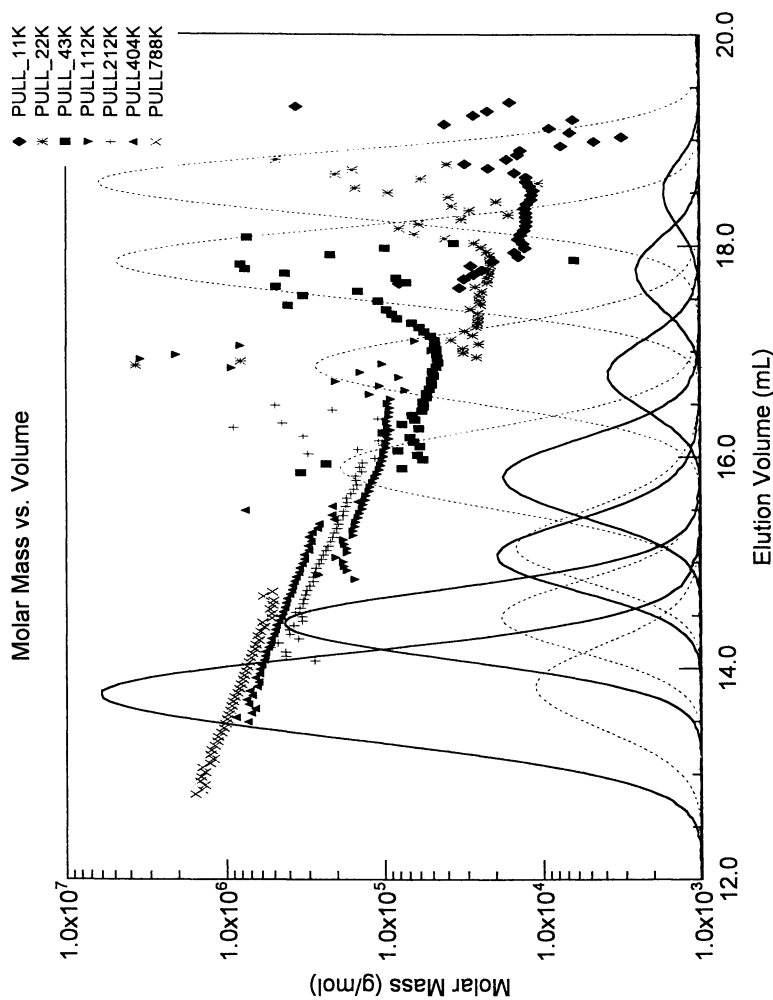


Figure 2. GPC-LS-RI Overlay of Seven Pullulan Standards with Molar Mass Superimposed (—) LS Signal, (---) RI Signal.

**Dextrans.** Dextrans are contiguous alpha 1→6 glucosidic linkages in the main chains, with variable amounts of alpha 1→2, 1→3, or 1→4 branch linkages (6). Dextrans are found anywhere sucrose is found and, as such, are often unwanted contaminants in sucrose refineries, sugary foods, and other sucrose preparations. When synthesized in the mouth by *Streptococcus mutans*, dextrans form dental plaque. Purified dextrans and their derivatives have found valuable uses as blood plasma substitutes, anticoagulants, antilipemics (sulfate esters), and anti-ulcer therapeutics, all of which require very specific molecular weight ranges to be effective. Figure 3 shows GPC-RI chromatograms obtained from a series of dextrans available commercially (Sigma, St. Louis, MO). It is readily apparent how much more broadly these polymers are distributed relative to the pullulans. Whereas the average peak elution volume for the pullulans was ~2 mL, the dextrans elute in ~4-5 mL volume. Table II gives a comparison of calculated molecular weights with the nominal  $M_w$  given by the manufacturer; all agree to within 10%. Again,  $dn/dc$  values were obtained by assuming 100 percent column recovery. The polydispersity numbers agree well with Fishman (5) and the calculated radii range for the highest  $M_w$  dextrans encompasses that in the literature. Note that the calculated molecular weights superimposed on the chromatogram exhibit a smooth trend downward, with overlap between adjacent peaks. In contrast with the narrower band pullulans, this is characteristic of broad, polydisperse polymers.

**Table II. Summary of  $M_w$  and  $r_{g,z}$  Results for Five Commercial Dextran Standards**

| $M_w$ (nominal) | $M_w$ (calc) | $M_w/M_n$ | $dn/dc$ (mL/g) | $r_{g,z}$ (nm) | $r_{g,z}$ (nm)* |
|-----------------|--------------|-----------|----------------|----------------|-----------------|
| 19,500          | 21,470       | 1.31      | 0.134          | —              | 4               |
| 41,000          | 43,290       | 1.34      | 0.134          | —              | 6               |
| 74,400          | 68,210       | 1.69      | 0.134          | —              | 8               |
| 167,000         | 169,800      | 2.20      | 0.146          | 12             | 12              |
| 580,000         | 539,300      | 2.15      | 0.134          | 19             | 22              |

\*Data interpolated from (3, 5)

**Dextrins.** Unlike pullulan and dextran, which are synthesized from smaller molecules by bacterial enzymes, dextrins are hydrolysis products of larger polysaccharide material, specifically starch (7). The result is a range of D-glucose polymers, linked by alpha 1→4 bonds, typically referred to as dextrin, or maltodextrin when the “dextrose equivalent” is less than 20, corresponding to a degree of polymerization (DP) greater than about 5 glucose units. Dextrins have a variety of uses as absorbents, binders, bulking agents, adhesives, films, conditioners, thickeners, or as foundation for make-up, and face powders. Dextrins are also used as an aid to spray-drying, or encapsulation to provide new dosage forms, tasteless or controlled-release drugs, and food flavors. Figure 4 is a plot of differential molar mass calculated from GPC-MALS of a commercial maltodextrin which nominally contained oligosaccharides in the range 5 to 30 DP, corresponding to a maximum molecular weight of about 5000 g

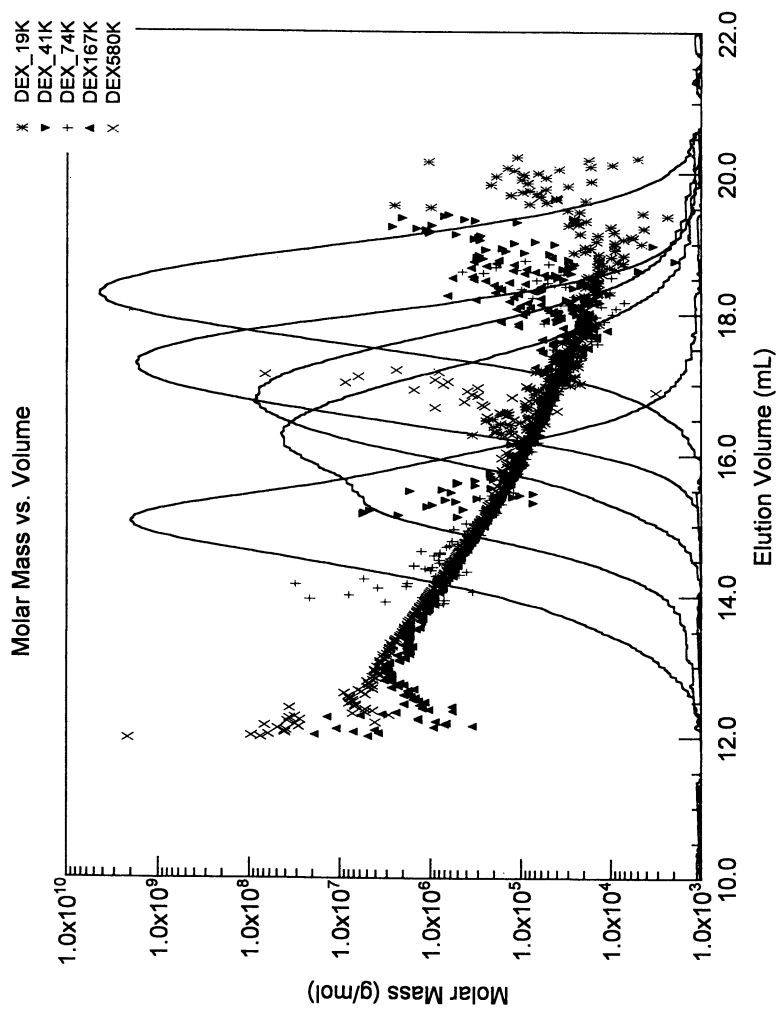


Figure 3. GPC-RI Overlay of Five Dextran Standards with Molar Mass Superimposed.

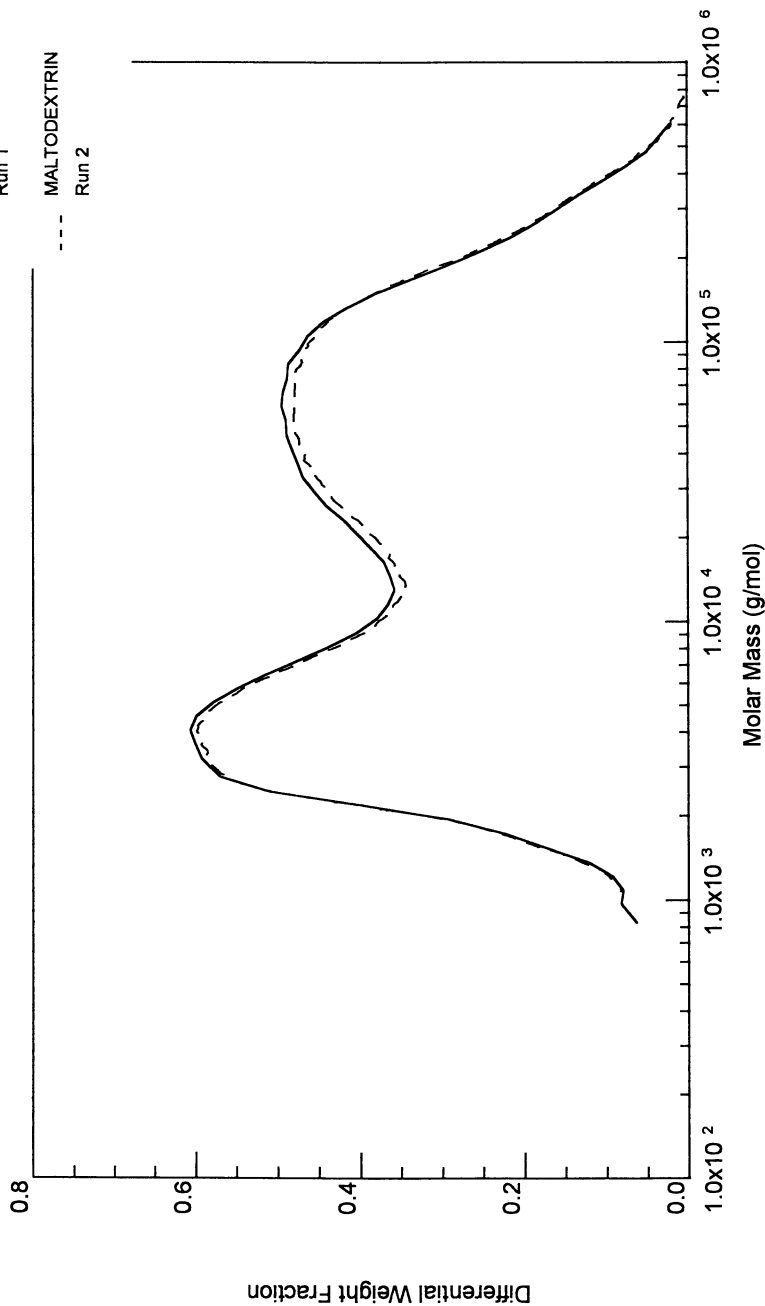


Figure 4. Differential Molar Mass Plot for a Commercial Maltodextrin (—) Run 1, (---) Run 2.

$\text{mol}^{-1}$ . It can be seen that in addition to the material in the molecular weight range of a few thousands, there is a significant amount of material in the higher range of 100,000 to roughly half a million, unexpected for a DP 30 dextrin. This is likely an indication of "left-over" high molecular weight material from incomplete hydrolysis. This information would likely be missed by conventional detection methods but could be important in terms of the functional properties of this material.

**Gums.** Gums are hydrophylic polysaccharides that are particularly known for their water thickening and gelling properties; also termed hydrocolloids. Hydrocolloid gums are usually classified in terms of their origin. For example, seed gums arise from the endosperm of seeds or other ground plant products. Plant gums fall into the general category of extracts isolated from land plant sources, such as pectin. These should be distinguished from other extract gums derived from seaweed sources such as alginates or carrageenans. Bacterial gums are fermentation products such as xanthan and gellan. Animal gums are also extract gums but derived from animal sources and protein based, an example being gelatin.

**Xanthan.** Xanthan gum is one of the most versatile gums, used extensively in foods, pharmaceuticals, and personal care products. It is a bacterial gum derived from *Xanthomonas campestris* (8). Its main chain is 1 $\rightarrow$ 4-beta-D-glucopyranosyl units, identical to cellulose. However, every other unit in the main chain is substituted with a trisaccharide unit of beta-D-mannopyranosyl linked 1 $\rightarrow$ 4 to a beta-D-glucopyranosyluronic acid, and linked 1 $\rightarrow$ 2 to a 6-acetyl, alpha-D-mannopyranosyl unit. The molecular weight is probably about 2 million, although much higher molecular weights have been reported (9). Although xanthan is anionic, pH has almost no effect on its viscosity. Xanthan is a thickener that is stable to heat and shear. It is a high molecular weight, rod-like molecule which forms aggregates through hydrogen bonding and polymer entanglement. These networks dissociate when stress is applied giving xanthan its pseudoplastic properties. There is much controversy as to changes in the structure with changing solution conditions. Single, double and even triple helical structures have been proposed. Xanthan's pseudoplastic property improves the flow properties of many viscous liquid products. It provides lubricity to heavy creams, is compatible with other gums and starches, and works synergistically to increase viscosity.

**Guaran.** Guaran is the purified polysaccharide from guar gum, which in turn is derived from the endosperm of guar seeds, and is therefore a seed gum (10). It is a polymer of D-galactose and D-mannose with a mannan backbone, that is a linear chain of 1 $\rightarrow$ 4 beta-D-mannopyranosyl units with every other unit being substituted with a 1 $\rightarrow$ 6 alpha-D-galactopyranosyl unit. The polymer is neutral, and forms very high viscosity, pseudoplastic (shear thinning) solutions at low concentrations. It is often used in combination with other gums.

**Carrageenans.** Carrageenans are sulfated algal polysaccharides and are heteropolymers with alternating alpha 1→3 D- and beta 1→4 D-galactans (11). There are conformational differences between the non-gelling lambda form and the gel-forming kappa and iota forms. Carrageenan has diverse industrial applications including its use in creams, toothpaste, shampoos, pharmaceutical and industrial suspensions, etc. There is also some anticoagulant activity and some evidence of inducing growth of new connective tissue.

**Gellan.** Gellan is an anionic polysaccharide from *Pseudomonas elodea* (10). It finds use mostly in food applications. Its gelling properties are highly dependent on cation concentration. It is used in synergy with other gums, mono- and oligosaccharides, often in sugary foods.

Figure 5 is an overlay of GPC-LS chromatograms of the four gums investigated. Following the recommendation by Lecacheux (12), we used 0.1 M LiCl as the mobile phase to avoid potential gel formation. Each of the gums were made up at roughly the same concentrations, so one can readily see from this plot the relative molecular size as indicated by the intensity of the light scattering signals and the order of elution. Xanthan is obviously the largest polymer, followed by guar, then κ-carrageenan, and finally gellan. Some peak deformity in the xanthan and significant tailing of the xanthan and guar may indicate less than optimum chromatographic conditions. Table III summarizes the results obtained. The dn/dc value for xanthan

**Table III. Summary of  $M_w$  and  $r_{g,z}$  Results for Some Commercial Gums**

| Gum           | $M_w$ ( $\times 10^{-6}$ g mol <sup>-1</sup> ) (lit.)* | $M_w/M_n$ (lit.)* | dn/dc (mL/g) | $r_{g,z}$ (nm) (lit.)* |
|---------------|--|-------------------|--------------|------------------------|
| xanthan       | 4.87 ± 2.8 (2.2, 7)                                    | 1.06              | 0.141        | 228 ± 15               |
| guar          | 1.98 ± 2   | 1.16              | 0.14         | 113 ± 3                |
| gellan        | 0.298 ± 0.02<br>(0.15-0.56)                            | 1.58              | 0.133        | 70 ± 5                 |
| κ-carrageenan | 0.495 ± 0.03 (0.468),<br>(0.34-0.58), (0.42)           | 1.53              | 0.115        | 73 ± 3 (60)            |

\*data from (9, 12, 13)

was taken from the literature (9). The dn/dc value of 0.133 for gellan was obtained by assuming 100 percent column recovery and was considered reasonable. However, the value obtained for guar in this manner was less than 0.1, an unreasonable value for polysaccharides in aqueous media, and probably a result of poor column recovery. Because a dn/dc value for guar could not be found in the literature, a value close to that of xanthan was chosen. The  $M_w$  obtained for xanthan was within the range of those reported in the literature (9). The apparent molecular weight may be solution dependent due to changes in the solution conformation of xanthan. The radius of xanthan was estimated to be over 0.2 micron, which is quite large and may necessitate the inclusion of a second virial coefficient in Equation 3, although this was not investigated. Thus, the absolute accuracy of these calculated results may be questionable. The  $M_w$  for guar was higher than expected, as the literature would seem



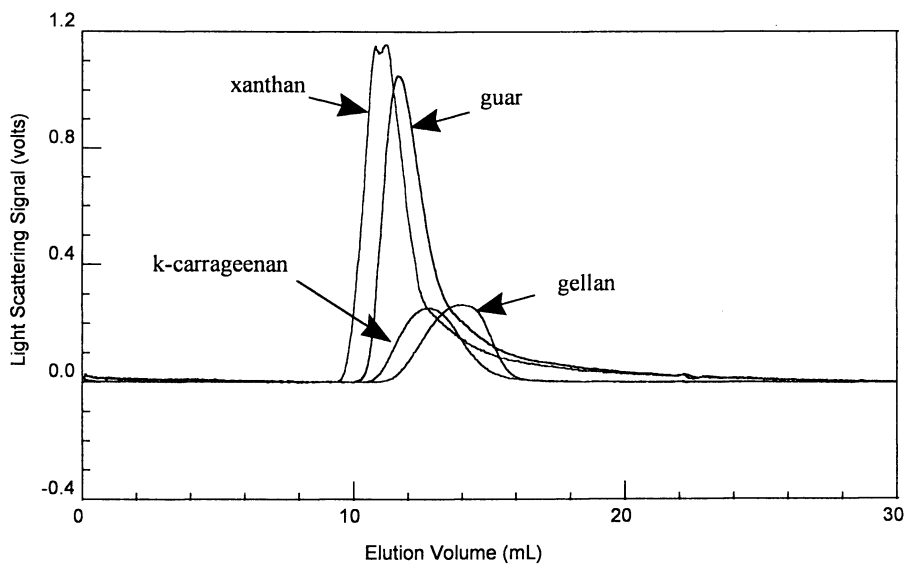


Figure 5. GPC-LS Overlay of Four Commercial Gums.

to suggest a  $M_w$  in the 200,000 range. Both the  $M_w$  and the radius were about half that of xanthan. The polydispersity numbers for xanthan and guar were relatively low. The results for gellan and  $\kappa$ -carrageenan were very much in line with expected results.

**Starch.** Starch is the principle food-reserve polysaccharide in plants and serves as the main carbohydrate in the diet of man and animals. It is a mixture of two polysaccharides, both being D-glucans. Amylose, which normally comprises 20-30% of starch, is a linear  $\alpha$ -D-1 $\rightarrow$ 4 glucan with a DP of several thousand and a molecular weight probably under 1 million (14-16). Amylose is thought to be a random coil in neutral solution. Amylopectin is 70-80% of starch and is also an  $\alpha$ -D-1 $\rightarrow$ 4 glucan, but with  $\alpha$ -D-1 $\rightarrow$ 6 branch points. Most uses of starch capitalize on its high viscosity and gel-forming properties. Physical and chemical modifications, such as partial hydrolysis to dextrans, conversion to ester, ether derivatives, or amino derivatives can have profound effects on starch behavior. Figure 6 shows GPC-LS chromatograms for a purified potato amylopectin and a soluble potato starch (Sigma, St. Louis, MO). Note the relative monodispersity of the amylopectin relative to the starch. Examination of the calculated molecular weight vs. elution volume for the two materials shows a region early in the elution where the slopes overlap; here presumably only amylopectin is eluting from the column. For the intact starch, there is a point at which the slope departs from that of the pure amylopectin, implying co-elution of lower molecular weight material. The slope decreases more rapidly with elution volume, probably as the linear amylose makes up more of the eluting material. It should be kept in mind that molecules are separated in size-exclusion based on their hydrodynamic volume. Thus, one would expect the molecular weight of linear molecules to drop off more rapidly with elution volume than that of compact, highly branched molecules. It is also useful to examine a log-log plot of radius vs. molecular weight (Figure 7). For a highly branched molecule approximating a sphere, one would expect that the radius would increase as a cube root of the molecular weight. Thus, the slope of  $\log r_g$  vs.  $\log M_w$  would approach 0.33. On the other hand, for a rigid rod the radius should increase linearly with molecular weight and the slope would be  $\sim 1$ . For a random coil the radius would increase as approximately the square-root of  $M_w$ , yielding a slope in the log-log plot of  $\sim 0.5$ . It is noteworthy that the average slope for the purified amylopectin is 0.35, close to expected for the branched polymer. For the starch, the slope is nearer to 0.5, reflecting perhaps the random coil behavior contributed by the amylose portion. Results are summarized in Table IV. Using a  $dn/dc$  value of 0.146 mL/g (17), an average  $M_w$  of  $2.4 \times 10^6$  g mol $^{-1}$  with a corresponding radius of 39 nm was obtained for the potato starch. These values agree quite well with the  $2.0 \times 10^6$  g mol $^{-1}$  and 39 nm, respectively, reported by Fishman (16) who took a similar approach. For the amylopectin, the  $M_w$  was estimated to be about  $10^7$  g mol $^{-1}$  with a radius of 60 nm. Although the high  $M_w$  and  $r_{g,z}$  for the amylopectin are undoubtedly pushing the capability limits of the 3-angle Mini-DAWN detector, the results of the replicate analyses shown here give an appreciation for the repeatability that can be obtained.

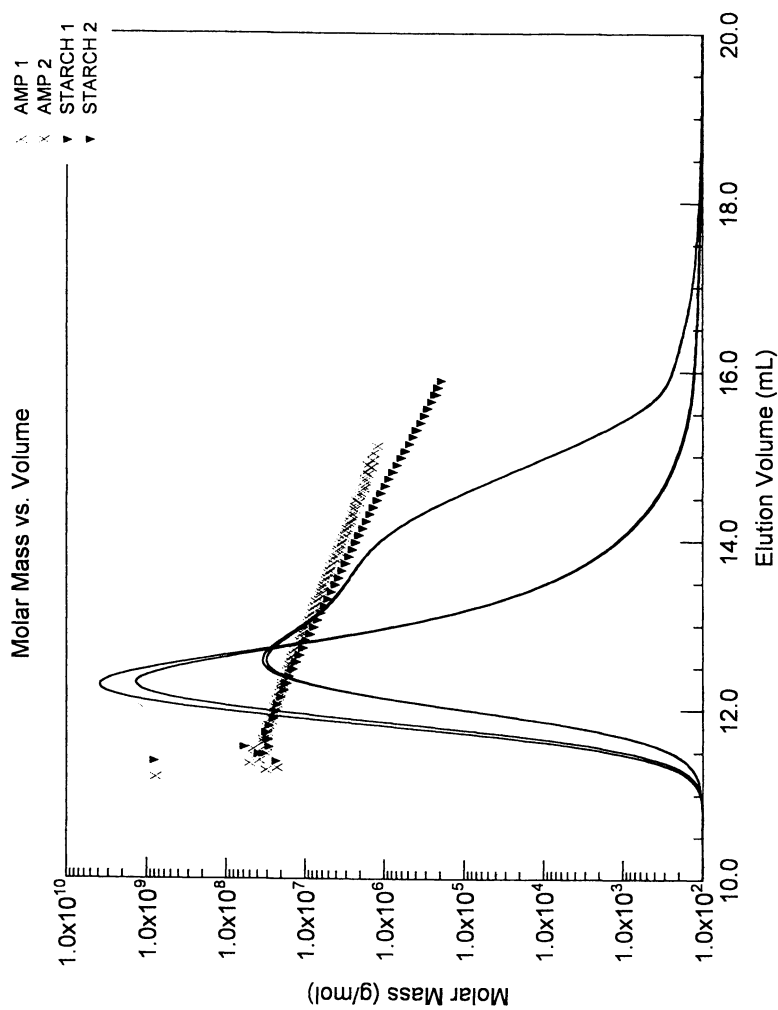


Figure 6. GPC-LS Overlay of Commercial Potato Amylopectin (X) and Soluble Potato Starch (▼) with Molar Mass Superimposed .

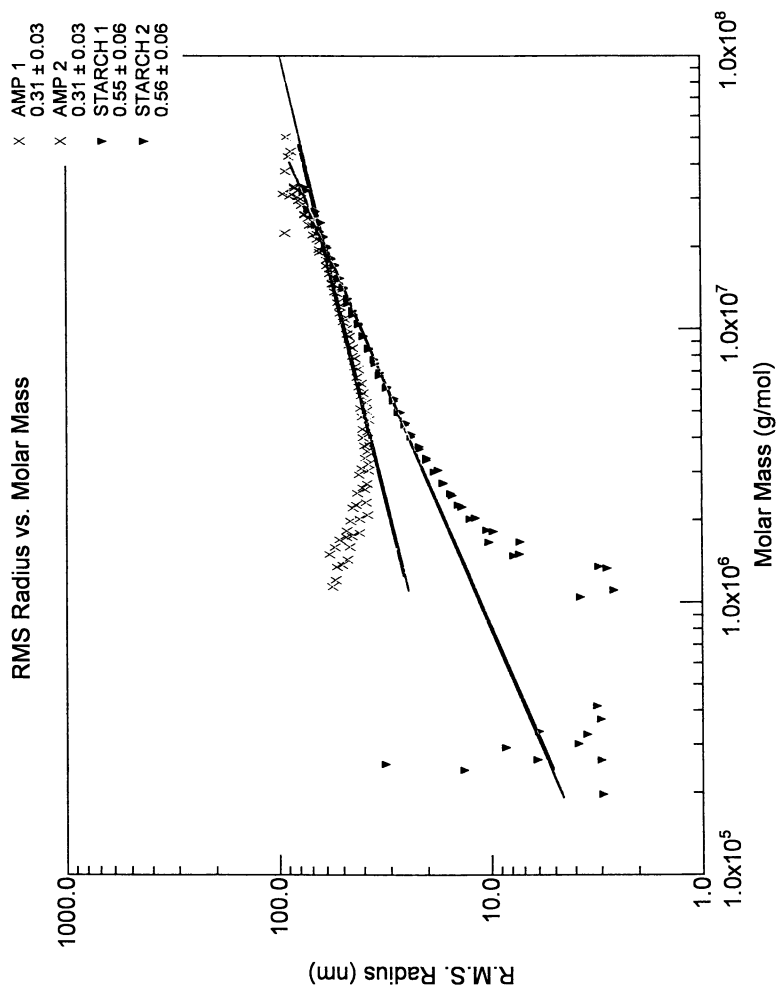


Figure 7. Log-Log Plot of Root Mean Square Radius vs. Molar Mass for Amylopectin (X) and Starch (▼).

**Table IV. Summary of  $M_w$  and  $r_{gz}$  Results for Replicate Analysis of Potato Amylopectin and Soluble Potato Starch**

| sample              | $M_w$ ( $\times 10^{-6}$ g mol <sup>-1</sup> ) | $M_w/M_n$ | dn/dc (mL/g) | $r_{gz}$ (nm) |
|---------------------|--|-----------|--------------|---------------|
| amylopectin (run 1) | 10.48  | 2.24      | 0.146        | 58            |
| amylopectin (run 2) | 10.04  | 2.45      | 0.146        | 57            |
| starch (run 1)      | 2.30   | 3.46      | 0.146        | 39            |
| starch (run 2)      | 2.47   | 3.25      | 0.146        | 39            |

## Conclusion

We have shown here some basic light-scattering principles and application of the technique to a variety of polysaccharides. To summarize, GPC-MALS is a technique that permits the estimation of absolute molecular weight and radius of polysaccharides without the need for column calibration methods or standards. The technique is suitable for characterizing a wide variety of industrial polysaccharides. The results obtained are of comparable accuracy to those obtained by other methods. GPC-MALS is a useful tool for the characterization and quality control of polysaccharides of industrial importance, particularly where functional properties are dependent on molecular size or conformation.

## Acknowledgements

The author thanks his colleagues, Ms. Pat Hudson of the Procter & Gamble Co. for her assistance in the laboratory, and Ms. Helena Soini of the Procter & Gamble Co. for providing the microwave-solubilized starch samples. Appreciation is also expressed to Dr. Ron Myers of Wyatt Technology, Inc. for helpful comments.

## Literature Cited

- Wyatt, P. J. *Analytica Chimica Acta*, **1993**, 272, 1.
- Zimm, B. H. *J. Chem. Phys.* **1948**, 16, 1093.
- Kato, T.; Tokrya, T.; Takohoski, A. J. *J. Chromatogr.* **1983**, 256, 61.
- Tsujisaka, Y.; Mitsuhashi, M. In *Industrial Gums: Polysaccharides and Their Derivatives*, 3<sup>rd</sup> ed.; Whistler, R. L.; BeMiller, J. N. Eds.; Academic Press, San Diego, CA, 1993, pp 447-460.
- Fishman, M. L.; Damert, W. C.; Phillips, J. G.; Barford, R. A. *Carbohydrate Res.* **1987**, 160, 215.
- DeBelder, A.N. In *Industrial Gums: Polysaccharides and Their Derivatives*, 3<sup>rd</sup> ed.; Whistler, R. L. and BeMiller, J. N. Eds.; Academic Press, San Diego, CA, 1993, pp 400-425.
- Chronakis, I. S., *Crit. Rev. Food Sci.*, **1998**, 38, 599.
- Kang, K. S.; Pettitt, D. J. In *Industrial Gums: Polysaccharides and Their Derivatives*, 3<sup>rd</sup> ed.; Whistler, R. L.; BeMiller, J. N. Eds.; Academic Press, San Diego, CA, 1993, pp 341-397.

9. Lecacheux, D.; Mustiere, Y.; Panaras, R.; Brigand, G. *Carbohydrate Polymers* **1986**, 6, 477.
10. Maier, H., Anderson, M, Karl, C., Magnuson, K., Whistler, R. L. In *Industrial Gums: Polysaccharides and Their Derivatives*, 3<sup>rd</sup> ed.; Whistler, R. L.; BeMiller, J. N. Eds.; Academic Press, San Diego, CA, 1993, pp 181-226.
11. Therkelsen, G. H. In *Carrageenan*; Whistler, R. L. and BeMiller, J. N. Eds.; Industrial Gums: Polysaccharides and Their Derivatives; Academic Press, San Diego, CA, 1993, Vol. 3; pp 145-180.
12. Lecacheux, D.; Panaras, R.; Brigand, G.; Martin, G. *Carbohydrate Polymers* **1985**, 5, 423.
13. Viebke, C.; Borgstrom, J.; Piculell, L. *Carbohydrate Polymers* **1995**, 27, 145
14. Whistler, R. L.; Daniel, J. R. In *Food Chemistry*, 2<sup>nd</sup> ed.; Fennema, O.R. Ed.; Marcel-Dekker, New York, NY, 1985; pp 112-120.
15. Hanselmann, R.; Burchard, W.; Ehrat, M.; Widmer, H. M. *Macromolecules* **1996**, 29, 3277.
16. Fishman, M. L.; Rodriguez, L.; Chau, H. K. *J. Agric. Food Chem.* **1996**, 44, 3182.
17. Yu, L. P.; Rollings, J. E. *J. Appl. Polym. Sci.* **1987**, 35, 1085.

## Chapter 22

# Capillary Electrophoresis in Starch Analysis

H. A. Soini<sup>1</sup> and M. V. Novotny<sup>2</sup>

<sup>1</sup> Procter & Gamble Company, Miami Valley Laboratories, Food and Beverage Technology Division, P. O. Box 538707, Cincinnati, OH 45253

<sup>2</sup> Department of Chemistry, Indiana University, Bloomington, IN 47405

A fast and quantitative capillary electrophoresis - iodine affinity method (CE-IA) has been developed for the determination of amylopectin and amylose in different starches. The method is linear, reproducible and specific for starch components in presence of other polysaccharides. For the oligosaccharide composition and branching studies in starches, a sensitive capillary electrophoresis separation method with laser-induced fluorescence detection (CE-LIF) was used. The CE-LIF technique demonstrated high separation efficiency for small oligosaccharide branching changes in modified starches. A combination of these two CE methods made it feasible to efficiently characterize native and modified starches.

Starch and starch-derived materials are versatile, non-toxic polymeric ingredients used in foods, cosmetics and pharmaceutical formulations. Paper surfaces, packaging materials and adhesives also commonly contain starch or modified starch components. Starch is a naturally abundant and relatively inexpensive raw material. Starch consists of extremely large polydisperse anhydro glucose homopolymers of amylopectin and amylose. They are arranged in crystalline and amorphous regions within the starch granules inside plant cells. The molecular weight of amylopectin, the major component of starch (75-82 % w/w), can reach up to  $2 \times 10^8$  daltons. Amylopectin is highly branched through  $\alpha$ -(1-6)-linkages between its glucose units in addition to linear  $\alpha$ -(1-4)-linked backbones. Amylose (18-25 % w/w) is pre-dominantly linear,  $\alpha$ -(1-4)-linked glucopyranose polymer. It is also known to contain minor amounts of  $\alpha$ -(1-6)-branches(1). The average molecular weight of amylose is  $10^6$  daltons(1,2). Genetically modified waxy maize, rice and potato starch consisting solely of amylopectin has been found a favorable base material for chemically modified starches. Chemical modification can enhance starch properties which can be especially beneficial in non-food industrial applications(3). It is known that the physical characteristics of starches vary not only with the botanical source, but also by

the crop year, with environmental conditions, and geographical origin(4). Starch structures are still today being extensively studied through different bulk state physical measurements such as rheology(5), viscometry (6), differential scanning calorimetry (7) and X-ray crystallography(8). Physicochemical methods include spectrophotometry(9), <sup>1</sup>H-NMR (10), size-exclusion HPLC with MALS (multi-angle light scattering)(8) and HPLC with pulsed amperometric detection (HPLC-PAD)(11).

It is important to develop fast and specific methods to assess the qualities of starch materials for the particular uses. Starch functionalities in particular industrial uses are strongly dependent on the physical and chemical properties of these biopolymers. Therefore, it is important to understand their structural details. Capillary electrophoresis (CE) has previously demonstrated extremely high separation efficiency in the separation of polydisperse polysaccharide mixtures(12-14). Detection sensitivity and specificity of measurements could be achieved through fluorescent labeling and LIF (laser-induced fluorescence) detection. In this paper, we report several fast and practical uses of CE in chemical characterization of the native and modified starches from different botanical sources. A simple and reproducible quantitative method to determine soluble amylose and amylopectin quantities in starch materials has been developed. The combined use of CE iodine affinity and visible- wavelength detection improved measurement specificity within short analysis times compared to the traditional methods. The method has been adapted from the less quantitative methodology reported by Brewster *et al.* (15). CE of the fluorescently labeled oligosaccharides (using CE-LIF) has been developed for determination of the characteristic branching patterns in the derived oligosaccharide maps.

## Experimental

**Materials:** Lugol potassium iodide/iodine solution, Trizma base, maltotriose (DP 3, degree of polymerization), maltotetraose (DP 4), maltoheptaose (DP 7), amylopectin, rice starch, potato starch, hydrochloric acid and isoamylase (EC 3.2.1.68) from *Pseudomonas amyloclavata* were obtained from Sigma Chemical Co. (St. Louis, MO). Maltodextrins (hydrolyzed starch) were obtained from Grain Processing Corporation (Muscatine, IA). Sodium phosphate (UltraPure Bioreagent) and sodium acetate were from JT Baker (Phillipsburg, NJ) and sodium citrate buffer solution, 20 mM, pH 6 for HPCE, was from Fluka BioChemika (Buchs, Switzerland). APTS (aminopyrene trisulfonate) was purchased from Molecular Probes (Eugene, OR). Sodium cyanoborohydride (1M in THF) was from Aldrich (Milwaukee, WI).

**Equipment:** Hewlett-Packard 3D Capillary Electrophoresis with detection at visible wavelength (560 nm) was used for the iodine affinity separations. UV/VIS spectra were collected at the range of 300-600 nm. Sulfonic acid-coated, 50  $\mu$ m, i.d. x 50 cm, capillary (Microsolv CE, Scientific Resources) was used with the run buffer of 10 mM sodium citrate, pH 6.0, 1.3 mM iodine - 4 mM potassium iodide. The run voltage was 22 kV at a capillary temperature of 30 °C. The detector was connected to the negative ground. BioFocus LIF<sup>2</sup> (Bio-Rad) with Argon-ion laser at 488 nm excitation wavelength was used for the oligosaccharide mapping. Uncoated capillaries (50  $\mu$ m, i.d. x 50 cm, Supelco) were used with Trizma-phosphate, pH 2.5, buffer. The run voltage was -22 kV (detector at the positive ground).

**Sample solubilization:** Starch samples (2 mg/ml) were dissolved by boiling in 5 mM phosphate buffer, pH 5.0, for 30 min. For the CE-iodide affinity measurement samples



were filtered through 0.45  $\mu\text{m}$  Acrodisc (HT Tuffryn) filters from Gelman Sciences (Ann Arbor, MI).

**Enzyme hydrolysis:** Enzyme solution was diluted with 0.025 M sodium acetate (25  $\mu\text{l}$  solution in 2 ml 0.025 M sodium acetate, pH 3.7). To 300  $\mu\text{l}$  of sample solution, 780 U of isoamylase were added. The samples were incubated for 20 h at 37  $^{\circ}\text{C}$ . Hydrolysis was stopped by boiling the sample for 5 min.

**Mild acid hydrolysis:** In this hydrolysis, 20  $\mu\text{l}$  of 2 M hydrochloric acid was added to a 300  $\mu\text{l}$  sample. Incubation was repeated as in the enzyme hydrolysis.

**Fluorescent tagging:** To 25  $\mu\text{l}$  of sample, 2  $\mu\text{l}$  of APTS solution (80  $\mu\text{g}/\mu\text{l}$ ) and 5  $\mu\text{l}$  of sodium cyanoborohydride were added. Samples were incubated at 55  $^{\circ}\text{C}$  for 1.5 hours. The reaction was stopped by adding 20  $\mu\text{l}$  of water. Samples were frozen at -20  $^{\circ}\text{C}$  until analyzed, and diluted with water prior to analysis.

## Results and Discussion

**Determination of Amylopectin and Amylose by Capillary Electrophoresis.** The capillary electrophoresis-iodine affinity method with the visible wavelength detection (15) has been modified for the quantitation of bulk amylopectin and amylose in aqueous starch solutions. Iodine complexation with linear oligosaccharides as the colorful red, purple and blue complexes is a well-known phenomenon (16). A traditional method for the determination of amylose is a colorimetric measurement after iodide addition. However, the method is not specific for amylose in the presence of amylopectin. In particular, longer oligosaccharide branches in amylopectin bind iodine and emit at visible wavelength, overlapping with the amylose emission range. Polyiodide rods have been found as the complexing species in iodine-iodide ( $\text{I}_2/\text{I}^-$ ) containing solutions (17,18). When  $\text{I}_2/\text{I}^-$  -buffer is used as a separation electrolyte in the electric field, negatively charged polyiodides form inclusion complexes with the linear amylose and the oligosaccharide branches of amylopectin inside the capillary. Polyiodide-oligosaccharide complexes emit light at a visible-wavelength range of 400-700 nm. The emission maximum is dependent on the ratio of iodine-iodide concentrations (18). Recently Hong *et al.* (19) proposed that the dynamic equilibrium between polyiodides complexing with shorter oligosaccharides was faster than equilibrium between polyiodides and longer oligosaccharides. Consequently, complexation with longer oligosaccharides (DP >30) was more stable than with shorter chains (DP 20-30). Therefore, amylose-iodide complexes remained negatively charged for a longer time than the amylopectin-iodide complexes. This resulted in a migration time difference for amylopectin and amylose bands against the fast electroosmotic flow toward the detector, as shown in Fig. 1. At the wavelength of 560 nm, both amylose- and amylopectin-iodide complexes could be detected. Quantitation of amylopectin at 560 nm proved relatively independent from the small variations in the oligosaccharide composition, as illustrated in Fig. 2 with different maltodextrin fractions. However, at this wavelength the sensitivity of detection was about five times higher for amylopectin than for amylose (data not shown).

**Validation:** The detection limit for amylopectin was about 0.2 mg/ml and for amylose, 1 mg/ml. Peak areas were linearly related in the concentration range of 2- 6 mg/ml for amylopectin and amylose. The measurements were specific for amylose and amylopectin in the presence of cellulose, pectin, carrageenan, alginate and  $\beta$ -cyclodextrin. Small

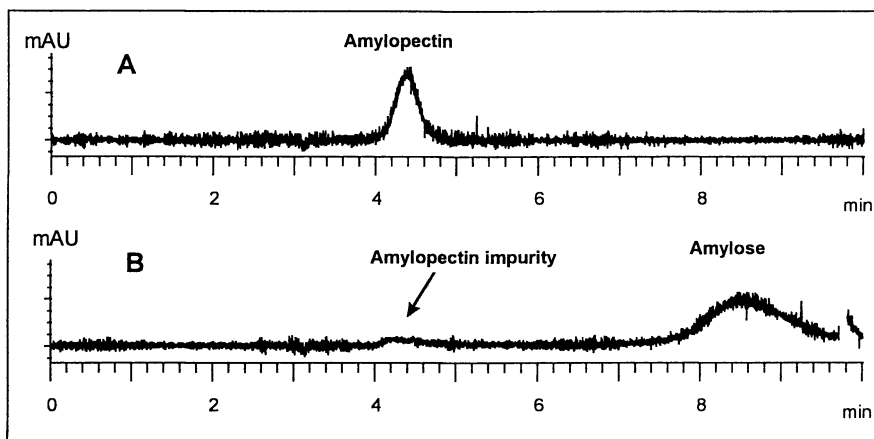


Figure 1. Iodine affinity capillary electrophoretic separation of amylopectin and amylose standards, with detection at 560 nm. Sulfonic acid-coated (50  $\mu\text{m}$ , i.d.  $\times$  50 cm) capillary was used with the run buffer of 10 mM sodium citrate (pH 6) and 1.3 mM iodine-4 mM potassium iodide. The applied voltage was 22 kV, at a capillary temperature of 30  $^{\circ}\text{C}$ . A: Potato amylopectin standard; B: Potato amylose standard isolated from potato starch.

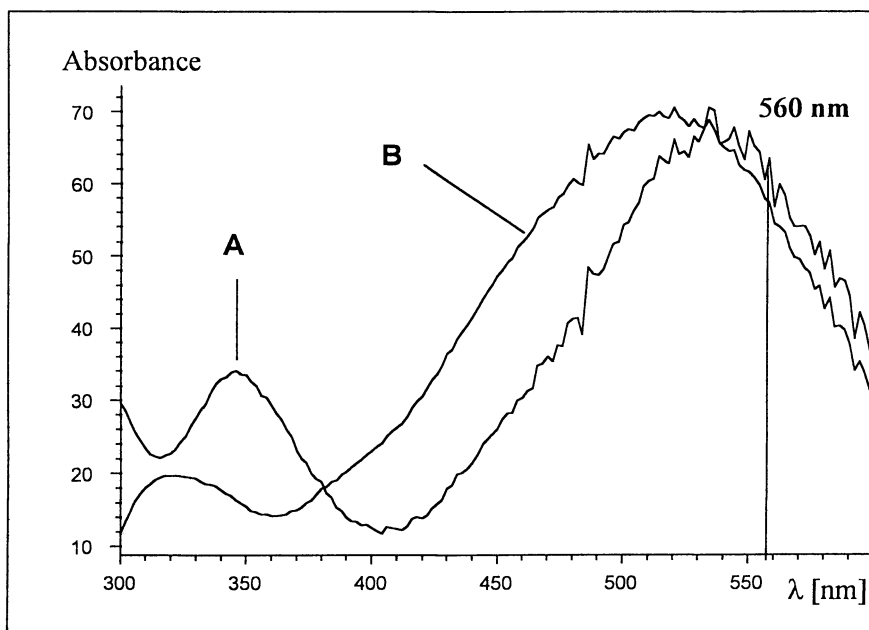


Figure 2. UV/VIS spectra for maltodextrins with different oligosaccharide compositions. A: long oligosaccharides (larger than DP 30); B: short oligosaccharides (smaller than DP 25).

oligosaccharides ( $DP < 8$ ) were not detected, as expected from the previous findings (19). Maltodextrin with a low degree of hydrolysis (DE-5) was detected just before the amylopectin band. Selected validation data are shown in the Table I. The method was proven to be fast and efficient, for example, in the determination of purity of the standard potato amylose isolated from potato starch by recrystallization with thymol (Fig. 1). Compositions of starch from potato and rice were determined, as shown in Fig. 3.

**Table I. Summary of the Validation Data for Determination of Amylopectin and Amylose by CE-Iodide Affinity Method in Starch**

|   | <b>Amylopectin<br/>Peak Area</b> | <b>Amylose<br/>Peak Area</b> |
|---|----------------------------------|------------------------------|
| Repeatability (run-to-run)<br>RSD* % (n=4)    | 4.3                              | 1.5                          |
| Reproducibility (day-to-day)<br>RSD* % (n=10) | 4.6                              | 7.2                          |

\* Relative Standard Deviation

**Oligosaccharide Mapping.** Recently, several reports in food science have linked the fine structures of amylopectin and amylose to important functional parameters such as dough pasting(20) and texture of cooked rice(21). Therefore, analytical methodologies addressing the detail structures, such as branching characteristics of amylopectin and chain-length distribution of amyloses, are of major interest in the other starch formulation applications. One of the analytical challenges in polysaccharide analysis, in addition to large molecular weights and polydispersity, is a lack of chromophores for optical detection in the targeted molecules. Also, despite the almost unlimited availability of starches and many polysaccharides, one has to work with relatively dilute analytical solutions, since large molecular sizes limit solubility. Additionally, in recrystallization at higher concentrations (especially for amylose), the subsequent generation of gel networks is complicating the starch solution dynamics(1). In waxy starch solutions, recrystallization and gelling are less problematic than in the amylose-containing starches(3). Modified starches have been developed for industrial uses partly to overcome the solution state difficulties associated with unmodified starches.

A highly sensitive and specific fluorescent aminopyrene (APTS) tag(22) containing the negative sulfonate groups has provided the necessary detection sensitivity for oligosaccharides derived from dilute polysaccharide solutions. The reductive amination derivatization is shown in Scheme 1. Calibration of the glucose oligosaccharide migration times was facilitated by using the fluorescently tagged linear maltodextrin mixtures as a calibration ladder. In Fig. 4, we show a maltodextrin DE-5 calibration mixture. Reproducibility of migration times was typically better than 1%, approximately 3-5% for the peak areas, and 0.4-0.7% for various adjacent peak area ratios (RSD, n=5).

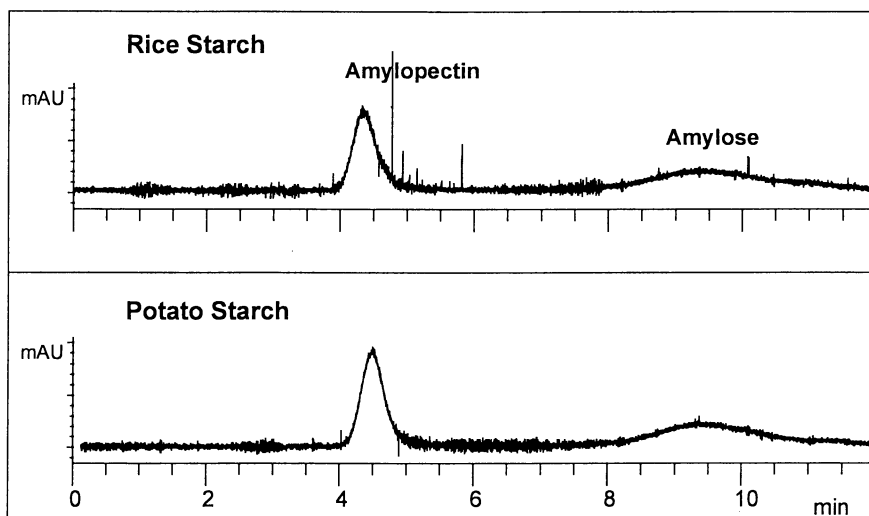
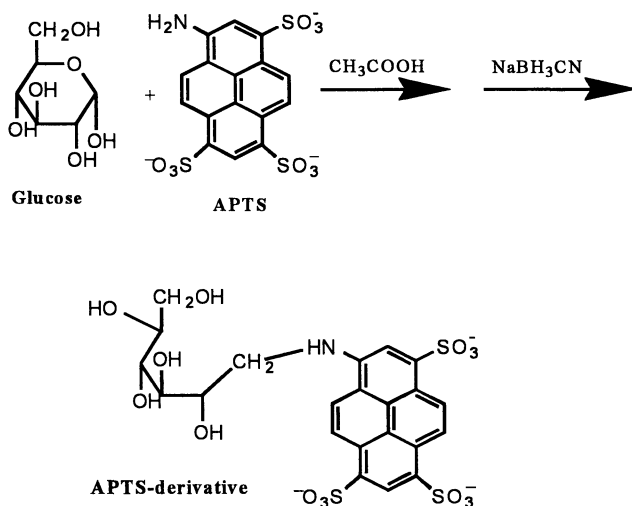


Figure 3. Amylopectin and amylose determined in potato and rice starch. Conditions as in Fig. 1.

A response decrease has been observed due to the increasing molecular size of oligosaccharides (23). The response for maltotetraose (M.W. 640) was about twice the response for maltoheptaose (M.W. 1120). This was analogous to the response loss observed in the HPLC -PAD (pulsed amperometric detection) determinations of oligosaccharides (11,24). The oligosaccharide maps can be utilized as "fingerprints" characteristic for certain manufacturing batches, and as manufacturing specifications for polysaccharide raw materials. Characteristic branching fingerprints (after isoamylase digest) of a modified waxy maize and modified waxy maize containing additional corn syrup solids, using APTS as a fluorescent tag are shown in Fig. 5. Repeatability in measuring the branching patterns was 5 % (RSD,  $n = 4$ ) when calculated as peak areas of DP 12 and DP 20 oligosaccharides.

**Scheme 1. Fluorescent Tagging of the Reducing End of the Carbohydrate through Reductive Amination and Aminopyrenesulfonate (APTS) Tagging**



Sample preparation procedures may effect the results of oligosaccharide compositions. Different oligosaccharide patterns may be obtained due to a random degradation during solubilization. An increasing time and temperature contribute to starch leaking from the starch granules during solubilization. The botanical origin influences the order in which the amylopectin and amylose are arranged within their crystalline or amorphous regions inside the starch granules(3), contributing further to the differential dissolution patterns. Other matrix effects, such as the amounts of proteins and lipids, can influence the sample preparation as well. Therefore, optimization and control of the sample preparation conditions for each application are important for reproducible results.

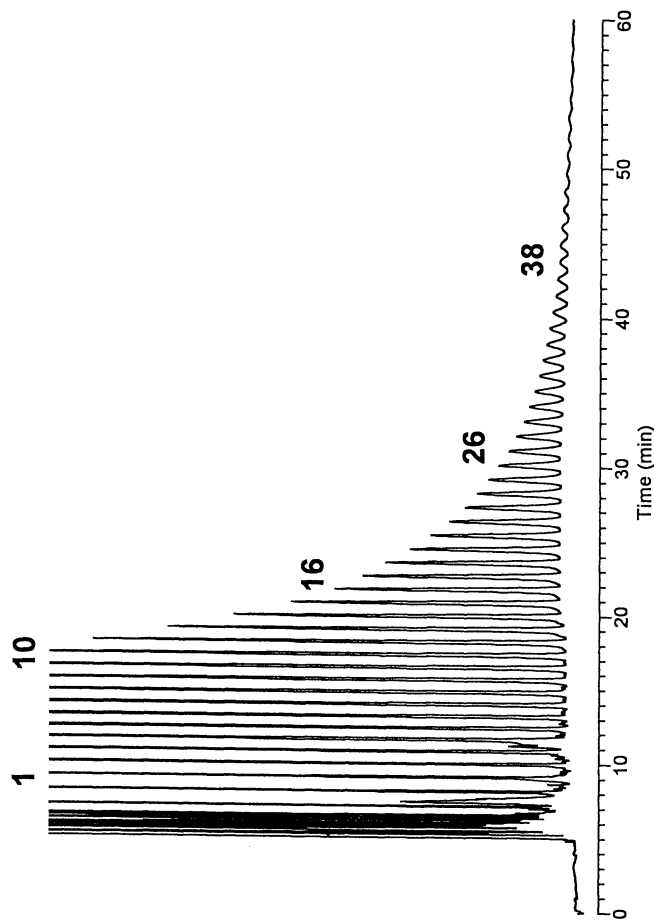


Figure 4. Maltodextrin mixture as the standard ladder for the oligosaccharides from glucose (DP 1) to DP 45. Capillary uncoated, 50  $\mu\text{m}$ , i.d. x 50 cm. The run buffer: Trizma-phosphate buffer, pH 2.5, run voltage -22 kV. APTS fluorescent tag. LIF detection at  $\lambda_{\text{ex}}$  488 nm and  $\lambda_{\text{em}}$  520 nm.

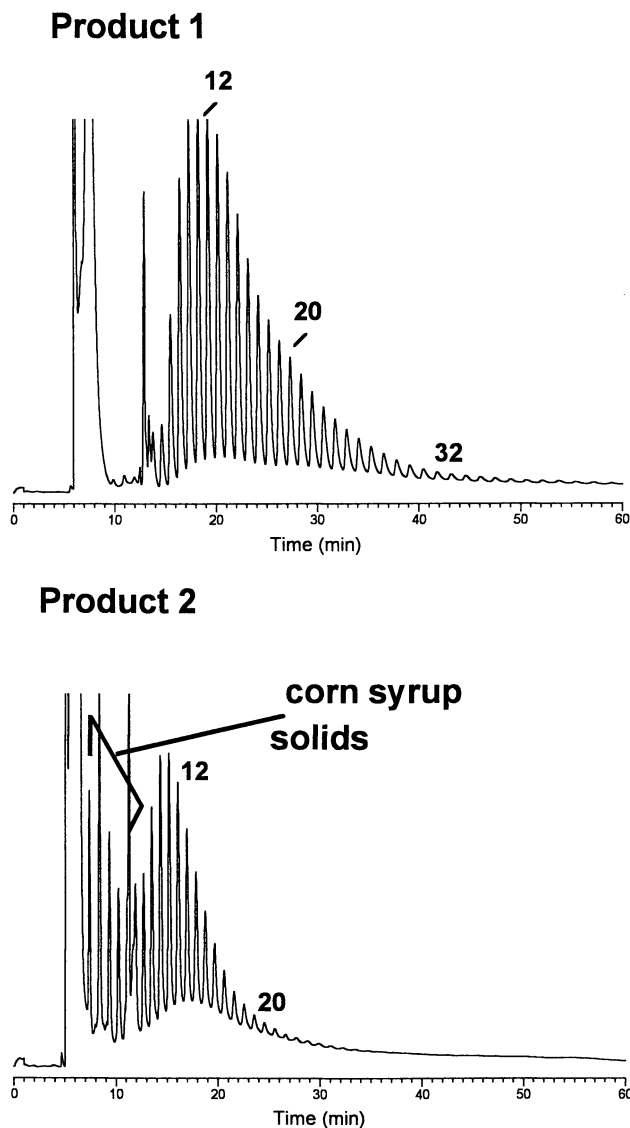


Figure 5. Modified waxy maize (100 % amylopectin) branching patterns derived after the isoamylase digest from two different products. A: chemical modification B: chemical modification and spiking with corn syrup solids. Capillary electrophoresis conditions as in Fig.4.

The oligosaccharide branching patterns can be used effectively as a precise quality control tool in evaluation of starch raw materials. The batch- and source-originated variations can be monitored by comparing oligosaccharide maps derived from isoamylase digests. Fig.6 demonstrates the oligosaccharide branching patterns of two differently manufactured chemically modified starches. Cross-linked starches are

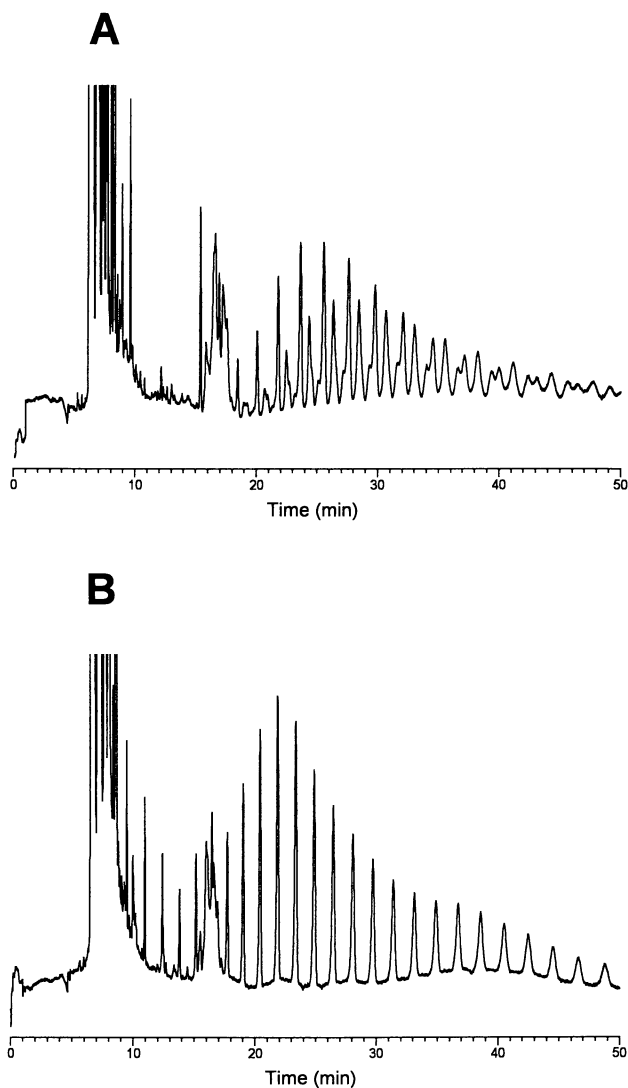


Figure 6. Branching patterns of the isoamylase digests from proprietary cross-linked and modified starches, A and B. Capillary electrophoresis conditions as in Fig.4.



known to be sparingly soluble (< 0.2 mg/ml) in aqueous solutions. This is an additional case for the use of high detection sensitivity mediated through the CE-LIF detection.

## Conclusions

The quantitative iodine affinity mode of CZE can be reliably used as a fast screening method to measure the amylopectin and amylose amounts and ratios in different starches. Mapping of the oligosaccharide degradation profiles and branching patterns in starch polysaccharides has also been proven effective due to the CE-LIF method. Fluorescent tagging has provided sufficient sensitivity and specificity for the detection in dilute working solutions. The high separation efficiency of this method has facilitated detection of characteristic, secondary branching patterns in modified starches.

## Acknowledgements

The authors thank Ms. Jennifer Ramos-Galluzzi for her input in the method development and Ms. Lois Boekley for her assistance in sample preparation. This study has been partially supported by Grant CHE-9321431 from the National Science Foundation.

## References

- Hood, L.F. in *Food Carbohydrates*, Chapter 13, Lineback D.R.; Inglett, G.E., Eds.; AVI Publishing Company, Westport, CT, **1982**, pp. 217-237
- Whistler, R.L.; BeMiller, J. N. *Carbohydrate Chemistry for Food Scientists*, Chapter 6, Eagan Press, St. Paul, MN, **1997**, pp. 117-151
- Eliasson, A.-C.; Gudmundsson, M. in *Carbohydrates in Food*, Chapter 10, Eliasson, A.-C., Ed., Food Science and Technology Series, vol. 74, Marcel Dekker, Inc., New York, NY, **1996**, pp. 431-503.
- Banks, W.; Greenwood, C.T. *Starch and its Components*, Edinburgh University Press, Edinburgh, UK, **1975**
- Cesàro, A. *J. Food Engineering* **1994**, *22*, 27-42
- Betancur, A.D.; Chel, G.L. *J. Agric. Food Chem.* **1997**, *45*, 4237-4241
- Karkalas, J.; Ma, S.; Morrison, W.R.; Pethrick, R.A. *Carbohydr. Res.* **1995**, *68*, 333-247
- Mua, J.P.; Jackson, D.S. *J. Agric. Food Chem.* **1997**, *45*, 3840-3847
- Morrison, W.R.; Laignelet, B. *J. Cereal Sci.* **1983**, *1*, 9-20
- Nilsson, G.S.; Bergquist, K.-E.; Nilsson, U.; Gorton, L. *Starch/Stärke* **1996**, *48*, 352-357
- Koizumi, K.; Fukuda, M.; Hizukuri, S. *J. Chromatogr.* **1991**, *585*, 233-238
- Novotny, M.V.; Sudor, J. *Electrophoresis*, **1993**, *14*, 373-389
- Stefansson, M.; Novotny, M.V. *Anal. Chem.* **1994**, *66*, 1134-1140
- Stefansson, M.; Novotny, M.V. *Carbohydr. Res.* **1994**, *258*, 1-9

15. Brewster, J.D.; Fishman, M.L. *J.Chromatogr.A* **1995**, *693*, 382-387
16. McCready, R.M.; Hassid, W.Z. *J.Am.Chem.Soc.* **1943**, *65*, 1154-1157
17. Teitelbaum, R.C.; Ruby, S.L.; Marks, T.J. *J.Am.Chem.Soc.* **1980**, *102*, 3322-3328
18. Yu, X.; Houtman, C.; Atalla, R.H. *Carbohydr.Res.* **1996**, *292*, 129-141
19. Hong, M.; Soini, H.A.; Novotny, M.V., *submitted for publication*
20. Jane, J.-L.; Chen, F.-F. *Cereal Chem.* **1992**, *69*, 60-65
21. Reddy, K.R.; Zakiuddin, S.; Bhattacharya, A.; Bhattacharya, K.R. *Carbohydr.Polym.* **1993**, *22*, 267-275
22. Evangelista, R.A.; Liu, M-S.; Chen, F-T. A. *Anal.Chem.* **1995**, *67*, 2239-2245
23. Chmelik, J.; Chmelikova, J.; Novotny, M.V. *J.Chromatogr.A* **1997**, *790*, 93-100
24. Koch, K.; Anderson, R.; Åman, P. *J.Chromatogr.A.*, **1998**, *800*, 199-206

# Author Index

- Ahn, Sungsook, 187  
Alexandridis, Paschalis, 187  
Amiji, Mansoor, 178  
Anderson, Derrick, 178  
Baglioni, Piero, 46  
Borie, D., 1  
Bowersock, T. L., 1  
Brendler, E., 143  
Ceccato, Massimo, 46  
Daly, William H., 214  
Dérian, P. J., 287  
Desbrières, J., 199  
Dohba, T., 85  
Edge, Stephen, 98  
Fillery-Travis, Annette J., 234  
Fischer, K., 143  
Fischer, S., 143  
Garrod, M. J., 262  
Gittings, M. R., 287  
Goddard, E. D., 276  
Gruber, James V., 252  
Guerrini, Melissa Manuszak, 214  
Heng, Y.-M., 276  
Hibberd, David J., 234, 262  
Hildebrandt, Frank-Immo, 127  
Jo, Seongbong, 113  
Konish, Peter N., 252  
Lal, J., 287  
Leipner, H., 143  
Leney, J. M., 262  
Loftsson, Thorsteinn, 24  
LoNostro, Pierandrea, 46  
Manoj, Pretima, 234  
Marques, C., 287  
Másson, Már, 24  
Murata, Jun-ichi, 15  
Nguyen, Tragiang, 178  
Nishi, Norio, 68, 85  
Novotny, M. V., 317  
Ohya, Yuichi, 15  
Ouchi, Tatsuro, 15  
Park, H., 1  
Park, Kinam, 1, 113  
Regismond, S. T. A., 276  
Rinaudo, J., 199  
Robins, Margaret M., 234, 262  
Sakairi, Nobuo, 68, 85  
Schmidt, Kati, 127  
Siger, L., 1  
Sixou, Pierre, 151  
Soini, H. A., 317  
Staniforth, John N., 98  
Steele, D. Fraser, 98  
Suckow, M. A., 1  
Takahashi, K., 85  
Tamura, H., 85  
Taylor, A., 1  
Tobyn, Michael J., 98  
Tokura, Seiichi, 68, 85  
Tsianou, Marina, 187  
Turek, J. J., 1  
Van Horne, D., 1  
Voigt, W., 143  
Watson, Andrew D., 234  
White, D. Richard, Jr., 299  
Winnik, F. M., 276  
Zugenmaier, Peter, 127

# Subject Index

## A

### Acetazolamide

- effect of PVP concentration on aqueous solubility, 37*f*
- eye drop solutions, 38
- inclusion complex with HP $\beta$ CD, 38
- mean IOP lowering activity, 39*f*
- release through semipermeable cellophane membrane, 39*f*
- solubility in aqueous HP $\beta$ CD solutions, 28*f*
- solubility in eye drop solutions, 39*f*

### Acetoxypropylcellulose, pitch as function of temperature, 169*f*

### Acetylation, chitin and chitosan, 200

### Acrylamide derivatives, thermosensitive hydrogels, 114

### Activation energy, different compounds and carbon atoms, 63*f*

### Adsorbed layers, modified scattering theory, 269

#### Aeroflow particle flow data, MCC and SMCC powders, 102*f*

### Aggregate formation, cross-links among polymer chains, 193

### Aggregation, detection, 263

### Aggregation behavior, partially substituted derivatives, 140

### Air–water interface, kinetics of organization, 207–210

### Albumin permeability studies, chitosan–Pluronic PIN membranes, 181

### Alginate

- difficulty with sterilization, 13
- polyionic block structures, 4

### Alginate microparticles

- boiling, 12
- electron microscopy, 5–6
- production, 4–5
- vaccine delivery, 1–14

### Alkylchitosans

- bulk properties, 201–202
- interfacial properties, 202–210
- properties in solution, 199–213
- viscosity as function of shear rate, 203*f*

### Aminoalkylcarbamoyl cellulose derivatives, reaction schemes, 218*f*

### Ammoniumalkylcarbamoyl cellulose derivatives, complexation with SDS, 217

### Amphiphilic character, chitin derivatives, 201–202

### Amylopectin

- CE–IA analysis and separation, 317–328
- potato and rice starch, 322*f*
- validation data for CE–IA method in starch, 321*t*

### Amylose

- CE–IA analysis and separation, 317–328
- colorimetric measurement after iodide addition, 319
- potato and rice starch, 322*f*
- structure, 257*f*
- validation data for CE–IA method in starch, 321*t*

### Amylose–iodide and amylopectin–iodide complexes, migration time difference, 319

### Antibody response, rabbits immunized with PTE microparticles, 12

### Antigens

- encapsulation in alginate microparticles, 1–14
- microencapsulation, 3–4

### Antihormification agent, silicon dioxide combined with MCC, 98

### Anti-PTE IgA activity, rabbit nasal lavage samples, 10*f*

### Anti-PTE IgG activity

- mouse sera of microparticles, 8*t*
- rabbit serum samples, 10*f*

### Apparent CMC, TTAB in presence of polyelectrolytes, 208*t*

### Aqueous polymer–polymer interactions and synergisms, 253

### Aqueous stability, drugs in CD solutions, 28

### Aqueous viscosity, building through synergistic polymer–polymer interactions, 252–261

### Attenuation spectra, polystyrene latex suspensions with adsorbed layers, 269

## B

### $\beta$ -galactosidase activity

- assay, 19
- effective genetic transfection, 21–23
- expression, 15

### B lymphocytes, stimulated antigen-specific, 3

### Bioavailability, drug–CD–polymer formulations, 43

### Bioavailability study, dexamethasone eye drop solution, 40

### Biocompatible microcapsules, controlled morphology and porosity, 178

### Boiling, alginate microparticles, 12

- Bordetella bronchiseptica*, kennel cough, 3
- Boundary, creaming emulsion and serum layer, 241–242
- Branching patterns  
 isoamylase digests from starches, 326*f*  
 modified waxy maize, 325*f*  
 quality control tool in evaluation of starch raw materials, 326
- Bromohexadecane emulsions, viscosity–shear rate profiles, 246*f*, 247*f*
- C**
- Caffeine–MT complex, kinetics of formation, 62
- Cairns' coupled network, extension to polysaccharide–polysaccharide interaction, 253
- Calcium chloride dihydrate–methanol–water system, chitin solubility, 85
- Capillary electrophoresis (CE)  
 $\alpha$ -CD-linked chitosan, 78–80  
 determination of amylopectin and amylose, 319–321
- Capillary electrophoresis–iodine affinity method (CE–IA), starch analysis, 317–328
- Capillary electrophoresis–laser-induced fluorescence detection (CE–LIF), starch analysis, 317–328
- Carbon spin–lattice relaxation rate measurement, dynamic properties of PEG–MT and MT, 51
- Carboxymethylated CD derivative, synthesis of CD-linked chitosan, 69
- Carboxymethylchitins, equilibrium properties, 202
- Carrageenan(s), characterization, 310
- $\kappa$ -Carrageenan,  $M_w$  and  $r_{r,g}$  results, 310*t*
- Cataract surgery,  
 dexamethasone–HP $\beta$ CD–polymer co-complex, 40
- Cationic cellulose ether, fluorescently labeled, 277
- Cationic cellulose structure, influence on interactions with SDS, 214–233
- Cationic guar  
 electrostatic effects, 298  
 presence and absence of NaCl, 296*f*
- Cationic polymers, sorption on hair fiber, 276–286
- Cavity orientation, initial threading, 54
- Cellular recognition devices, multiantennary sugar chain, 15
- Cellulose  
 $^{13}\text{C}$ -NMR spectrum in molten  $\text{LiClO}_4 \cdot 3\text{H}_2\text{O}$ , 149*f*  
 dissolution in molten salt hydrates, 144–146  
 regenerated from perchlorate, 148*f*  
 regenerated from thiocyanates, 147*f*  
 use in pharmaceutical and cosmetic products, 143
- Cellulose II, compactibility of MCC, 107
- Cellulose carbanilate(s)  
 calculated properties in solution, 141*t*  
 degree of substitution, 129*f*  
 dilute solutions, 127–142  
 Holtzer plot, 135*f*  
 static Zimm plots, 132*f*  
 synthesis, 128–130
- Cellulose carbanilate acetates  
 calculated properties in solution, 141*t*  
 dilute solutions, 127–142  
 dynamic Zimm plot, 133*f*  
 Holtzer plots, 134*f*  
 MW dependence in DMF, 136*f*  
 MW fractions in DMF and EMMAC, 137*t*  
 static Zimm plots, 132*f*
- Cellulose chains, distribution of substituents, 141
- Cellulose crystallites, solid films prepared from colloidal suspensions, 175
- Cellulose derivatives  
 characterization in polymer melt or solution, 152  
 phases, 161  
 solution properties, 130–131
- Cellulose in molten  $\text{LiClO}_4 \cdot \text{H}_2\text{O}$ ,  $^{13}\text{C}$ -NMR data, 146*t*
- Cellulose polymers, flexible and mesomorphic mixtures, 164
- Cellulose solvents, molten inorganic salt hydrates, 143–150
- Cellulosic liquid crystals, mesophase formation, 151–177
- Cellulosic mesophases, structured fibers, 172
- Cellulosic polymers, molecular structure and properties, 175
- Chain structure, flexible and semiflexible, 135
- Charge density  
 carboxymethylchitins, 204*f*  
 magnitude of fixed concentration, 231
- Charge neutralization  
 average MW per cationic charge, 221  
 complexation of cationic polymers with anionic surfactants, 217, 221  
 maximum precipitation patterns, 221
- Chemical characterization, MCC and SMCC, 103
- Chemical shifts, cellulose in molten  $\text{LiClO}_4 \cdot 3\text{H}_2\text{O}$ , 146

- Chitin**  
 adsorption of dyes, 87  
 characterization, 85  
 chemical structure, 88*f*  
 preparation of inclusion foams, 85–97  
 solubility, 87  
 solvent systems, 88*t*
- Chitin derivatives**  
 amphiphilic character, 201–202  
 interaction with surfactants, 199–213
- Chitin foam**  
 preparation, 86  
 time course of release  
 amido black 10B at different pHs, 94*f*  
 amido black 10B in SDS aqueous solution, 92*f*  
 aniline violet and brilliant green, 90*f*  
 congo red and amido black 10B, 91*f*  
 Eriochrome Black T and Eriochrome Blue Black B, 95*f*
- Chitin gel, preparation, 86**
- Chitosan**  
 carrier of DNA in gene delivery, 15–23  
 CD-linked, 68–84  
 cell or tissue encapsulation under mild conditions, 179  
 chemical structure, 88*f*, 180*f*  
 polyelectrolyte complexes with DNA, 16  
 properties in solution, 199–213  
 SEM micrographs, 183*f*  
 viscosity as function of shear rate, 203*f*
- Chitosan–Pluronic PIN membranes**  
 albumin permeability studies, 181  
 fabrication, 179–181  
 permeability coefficients of human serum albumin, 184*f*, 185*t*  
 physical interpenetrating network, 178–186  
 schematic representation, 180*f*  
 swelling, 182*t*
- Chlorambucil**  
 degradation pathways in CD solutions, 29*f*  
 degradation rates in HP $\beta$ CD solutions, 29*f*
- Cholesteric defects, optical and electron microscopy, 156*f***
- Cholesteric optical properties, HPC ethers, 170**
- Cholesteric order, schematic representation, 153*f***
- Cholesteric phase**  
 characterization in polymer melt or solution, 152  
 optical properties, 166–168
- Cholesteric polymers, unwinding of supramolecular helicoidal structure, 165**
- Cluster effect, biological recognition by carbohydrate–receptor binding, 15**
- Colloidal dispersions, ultrasonic characterization techniques, 262–275**
- Commercial gums, GPC–LS overlay, 311*f***
- Compacted powders**  
 properties of MCC and SMCC, 103–105  
 XRD analyses of failed compacts of MCC and SMCC, 106*f*, 107*f*
- Compaction simulator, behavior of MCC and SMCC, 109–110**
- Complex formation, enhanced foam stability, 231**
- Complexation constants, geometrical dimensions of hosts, 196**
- Complexation efficacy approaches, 31**  
 CD in drug and cosmetic formulations, 24  
 drug–CD solution, 43
- Concentrated colloidal dispersions, ultrasonic characterization techniques, 262–275**
- Conditioning agents, penetration of hair, 283, 285**
- Conductivity**  
 addition of surfactant in solution of CMCh, 208*f*  
 aqueous solution of TTAB, 206*f*  
 carbosymethylchitins and cationic surfactant, 205
- Controlled release,  $\alpha$ -CD-linked chitosan beads, 78**
- Correlation times over all carbons ( $\tau_c$ )**  
 calculation, 57–59  
 molecular necklace, 59  
 temperature dependence, 59–62
- Cosmetics industry**  
 applications of guar, 287  
 CD-linked chitosan, 80  
 polysaccharides, 299  
 use of polyquats, 214
- Coupled networks, polymers in solvated system, 253**
- Coupling reactions, chitosan with CD, 68**
- Creaming**  
 appearance of cylinders, 239*f*  
 characterization, 263  
 emulsions, 249*f*  
 flocculated emulsions, 234–251  
 visual, 237–240
- Creaming profiles, oil-in-water emulsion, 263**
- Critical aggregation concentration (CAC), surfactant molecules, 188**
- Critical micellization concentration (CMC), surfactant molecules, 188**
- Cross-linked HPC, reflection spectra, 173*f***
- Cross-linked mesophases, formation and characteristics, 172**

- Cross-linking density, swelling of hydrogels, 119
- Cross-linking mechanism, noncovalent, 261
- Cross-polarizers, typical observed textures, 154*f*–155*f*
- Crystal(s), cellulosic liquid, 151–177
- Crystalline–amorphous orientation, MCC and SMCC, 105–108
- Crystallinity of cellulose, dependence on salt hydrates, 145
- Crystallite dimensions, regenerated celluloses, 146*t*
- Crystallization in honey, application of ultrasonic velocimetry, 268
- Crystallization process, detection, 263, 268
- Cyclodextrin (CD)
- characterization, 25–27
  - complexes and inclusion compounds, 46–47
  - dynamics of  $\alpha$ -CD–PEG adducts, 57–62
  - increasing solubility through polymers, 35–36
  - interactions with cationic cellulose ether–anionic surfactant gelling system, 187–198
  - pharmaceutical uses, 42–43
  - solubility, 25–26
  - structure, 26*f*
  - structure and dynamics, 65
  - structure and properties of  $\alpha$ -,  $\beta$ -, and  $\gamma$ -oligomers, 48*f*
  - surfactant deactivation, 188
  - threading of  $\alpha$ -CD rings around PEG, 65
- Cyclodextrin complexation
- drug diffusion across membrane, 29
  - efficacy for small drug compounds, 31–32
  - efficacy for water-soluble polymers, 32–33
- Cyclodextrin complexes, increasing solubility through polymers, 35–36
- Cyclodextrin derivatives
- characterization, 25–27
  - solubility, 25–26
  - structure, 26*t*
- Cyclodextrin–drug complexation, presence of water-soluble polymers, 24–45
- Cyclodextrin formation, model calculation, 58*f*
- Cyclodextrin-linked chitosan
- applications, 78–80
  - different linkages, 70*f*
  - inclusion ability, 75
  - preparation, 69–72
  - preparation of beads, 72
  - solubility, 72
  - spectroscopic examination of inclusion ability, 76*f*–77*f*
  - synthesis and inclusion complexation abilities, 68–84
- $\alpha$ -Cyclodextrin (CD) and PEG in aqueous solution
- diffusion rate, 54
  - variation of absorbance with time, 53*f*
- $\alpha$ -Cyclodextrin-linked chitosan
- release of *p*-nitrophenol from beads, 79*f*
  - SEM photograph of bead, 74*f*
- $\alpha$ -Cyclodextrin–PEG adducts, dynamics, 57–62
- $\alpha$ - and  $\beta$ -Cyclodextrin-linked chitosan, preparation and physical properties, 71*t*
- $\beta$ -Cyclodextrin ( $\beta$ CD)
- chemical structure and toroidal shape, 191*f*
  - effect of drugs and HPMC polymer on aqueous solubility, 37*f*
  - effect of PVP concentration on aqueous solubility, 37*f*
- $\beta$ -Cyclodextrin-linked chitosan,  $^{13}\text{C}$ - and  $^1\text{H}$ -NMR spectra, 73*f*
- ## D
- Debye plot, representative slice of narrow band pullulan polysaccharide, 302*f*
- Delay period
- correlation with viscosity, 250*f*
  - definition and calculation, 237–238
  - emulsions, 239*f*
  - mechanism in creaming, 243–244
  - prior to creaming, 234–235
  - viscosity of emulsions, 250
- Depletion flocculation, space-spanning structure of flocculated droplets, 250
- De-threading, CD from polyrotaxane ends, 54
- Deuterium splitting, 2D nucleus of HPC–D<sub>2</sub>O solutions v. temperature, 167*f*
- Dexamethasone
- concentration in aqueous humor, 41*f*
  - eye drop formulation, 39–40
- Dextran, characterization, 306
- Dextran standards with molar mass, GPC–RI overlay, 307*f*
- Dextrin, characterization, 306, 309
- Differential dissolution patterns, amylopectin and amylose, 323
- Dilute solution behavior, cellulose derivatives, 127–142
- Dispersion
- distribution of components, 269, 272
  - velocity and attenuation of ultrasound of known frequency, 268
- Dispersion composition, influence on propagation of ultrasound, 263
- DMACS

degree of substitution, 120*f*  
<sup>1</sup>H-NMR spectra, 121*f*  
**DNA**  
 formation of polyelectrolyte complex, 19, 21  
 gene-transfer methods, 15  
 Dorzolamide, mean IOP lowering activity, 39*f*  
 Dough pasting, fine structures of amylopectin  
 and amylose, 321–326  
 DQNNED, half-life data on foam, 227  
 DQNNED–SDS systems  
 half-life, surface tension, and specific  
 viscosity, 230*t*  
 surface tension plot, 224*f*  
 DQNNED–SDS–water system, pseudo-phase  
 diagram, 220*f*  
 Drinking water, PTE in alginate microparticles,  
 1  
 Droplet coalescence, detection, 263  
 Droplet diffusion, delay time, 244  
 Droplet size distribution  
 Mastersizer light diffraction sizer, 265*f*  
 premix emulsion, 236  
**Drug(s)**  
 availability from aqueous CD formulations,  
 29–30  
 diffusion from CD solution through skin, 30*f*  
 increased solubility through complexation  
 with CD, 27–28  
 solubilization, 32–33  
**Drug–CD complexation**  
 presence of water-soluble polymers, 24–45  
 solubility, 36  
**Drug–CD–polymer co-complexes,**  
 physicochemical properties, 35  
**Drug–CD–polymer formulations, development**  
 and *in vivo* evaluations, 38–42  
**Drug formulation, diffusion across biological**  
 membrane, 24  
**Drugs from CD–polymer solutions,**  
 bioavailability, 36  
**Dye(s)**  
 chemical structures, 93*f*  
 controlled drug release, 85  
 Dye adsorption site, hydrophilic side chain, 87  
 Dye release, chitin foam, 86

## E

Elastic qualities, guar solution, 294  
 Electrophoresis, capillary, 317–328  
 Electrostatic effects  
 cationic guar, 294  
 interactions between polyelectrolyte and  
 surfactant, 214–215

Electrostatic repulsion  
 charged molecules in interfacial film, 210  
 formation of anions, 125  
**Emulsion(s)**  
 creaming behavior, 241–242  
 delay period and flow behavior, 249  
 depletion-flocculated, 250  
 flocculated, 234–251  
 phase behavior, 242–243  
 rheological properties, 245–247  
 Emulsion formulations, Polyquaternium-  
 24–amylose complex, 257  
 Equilibrium properties, alkylchitosans,  
 202–207  
 Ester linkage, intrinsic labile property, 125  
 Estradiol sublingual tablets, formulation and  
 clinical evaluation of bioavailability, 40–41  
 17 $\beta$ -Estradiol  
 concentration v. time after sublingual  
 administration, 42*f*  
 dissolution rate profiles, 42*f*  
 hormone replacement therapy, 40–41

## F

Fibers, obtained from cellulose mesophase, 172  
 Flexibility, semirigid polymers, 157  
 Flexibility of side groups, cellulosic  
 mesophases, 157  
 Flocculated emulsions, creaming and rheology,  
 234–251  
**Flocculation**  
 delay period, 243–244  
 depletion mechanism, 272  
 emulsion, 242–243, 249*f*, 263  
 ultrasonic properties, 269, 272  
**Flow**  
 cellulosic mesophases, 165  
 MCC and SMCC, 101–102  
**Flow behavior**  
 emulsions, 245, 249*f*  
 polymer solutions, 244–245  
 Fluorescein, characterization of surface  
 deposits on fibers, 276–277  
 Fluorescein-labeled Polymer JR400  
 characterization, 279  
 preparation, 278*f*  
 Fluorescence detection, starch analysis,  
 317–328  
 Fluorescence microscopy study, sorption of  
 cationic polymers on hair, 276–286  
 Fluorescence probes, water-soluble polymers,  
 276  
 Fluorescence variations, carboxymethylchitins



and cationic surfactant, 205

Fluorescent aminopyrene tag, oligosaccharide detection, 321

Fluorescent tagging  
dilute working solutions, 327  
reducing end of carbohydrate, 323*f*

Fluorocarbon lateral chains, mesophase, 170

Foam stability  
polymer–SDS complexation, 215  
solutions of polymers and SDS, 226–231

Formylmethylated CD derivative, coupling with polymeric chitosan, 71–72

Fractal dimension  
neutral guar, 292  
persistence length of polymer, 294

Fractional precipitation, cellulose carbanilates, 130

Franz diffusion cell setup, drug diffusion through skin, 30

**G**

Gel formation, oppositely charged polyelectrolyte and surfactant, 188

Gel permeation chromatography (GPC), effective mass moments over entire peak, 300–301

Gel permeation chromatography with multi-angle light scattering (GPC–MALS)  
polysaccharide characterization, 299–316  
primary advantage, 299

Gel temperature appearance, modification by adding second polymer, 163*f*

Gellan  
characterization, 310, 312  
 $M_w$  and  $r_{g,z}$  results, 310*t*

Gelling, amylose-containing starches, 321

Gene delivery, quaternary chitosan with antennary galactose residues, 15–23

Gene therapy, delivery of genes to target cells, 15

Gibbs free energy change, model calculation, 58*f*

Glaucoma, acetazolamide, 38

Guar  
cationically modified in D<sub>2</sub>O-based systems, 278–298  
conformation close to Gaussian chain, 297–298  
molecular structure of neutral and cationic forms, 288*f*  
 $M_w$  and  $r_{g,z}$  results, 310*t*  
persistence length, 295, 297

Guaran, characterization, 309

Gums, characterization, 309

**H**

<sup>1</sup>H–<sup>13</sup>C dipolar interaction, relaxation rate measurements, 57–59

Hair, sorption of cationic polymers, 276–286

Hair fiber  
aqueous solution of Polymer JR400-F, 280*f*  
aqueous solution of Polymer JR400-F and aqueous SDS, 281*f*  
desorption studies, 279, 283  
diffusion process by macromolecules, 283  
histological structure, 279, 282*f*  
surface adsorption, 283

HEC polymer solutions, viscosity–shear rate profiles, 246*f*

Helical cross-linking complex,  
Polyquaternium-24 and amylose, 261

Hexadecane–HEC emulsions, phase diagram, 243*f*

Honey, application of ultrasonic velocimetry, 268

Hormone replacement therapy, 17 $\beta$ -estradiol, 40–41

Host–guest inclusion complexes  
CD, 188–189  
MT and aqueous solution of I<sub>3</sub><sup>−</sup> or caffeine, 62, 65  
UV spectra, 64*f*

Host–guest systems  
formation, 47  
preparation of polyrotaxanes and MT, 46–67  
study of complicated biological complexes, 47

Hydrocortisone, solubility relative to PVP concentration, 33*f*

Hydrocortisone flux, through hairless mouse skin, 31*f*

Hydrocortisone HP $\beta$ CD  
effect of PVP on stability constant, 35*t*  
maximum flux through skin, 36

Hydrocortisone suspensions, solubility increase, 32–33

Hydrodynamic droplet size distribution  
creaming data, 265*f*  
flocs and individual droplets, 266*f*

Hydrogels  
environment-sensitive, 114  
thermosensitive volume change, 123*f*

Hydrogen bonding in chitosan, highly crystalline matrix, 182

Hydrophobic domains, alkylchitosans, 202

Hydrophobic effects, cross-links among polymer chains, 193

Hydrophobic molecules, amylose complex, 261

Hydroxyethylcellulose ether, cationic derivative adsorbed on hair, 276–286

Hydroxyethylcellulose polymer (JR400)  
 nominal chemical structure, 191*f*  
 solution viscosity, 190–193

Hydroxypropylcellulose (HPC)  
 clearing temperature of ester and  
 homologues with fluorocarbon, 171*f*  
 ester derivatives, 168–170  
 ether mixtures and copolymers, 170  
 mesophases, 168–170  
 pitch inverse *v.* temperature for butyl, pentyl,  
 and ether, 171*f*  
 pitch of ester, homologues, and ether, 173*f*  
 pitch variation with temperature for several  
 esters, 169*f*  
 threads and fibers, 174*f*

Hydroxypropylcellulose–dimethylacetamide  
 system, phase diagram, 162*f*

Hydroxypropylcellulose–water solutions, shear  
 viscosity *v.* concentration, 167*f*

Hypersensitive skin, CD-linked chitosan, 80

## I

Immune recognition elements, *in vivo* cell  
 therapy, 178

Immunization  
 delivery of vaccine at mucosal surfaces, 2–3  
 infectious pathogens, 1

Immunogenicity of PTE, boiling, 12

Immunosorbent assay, enzyme-linked, 7

*in vivo* testing, drug diffusion through skin, 30

Inclusion complexation  
 CD and small organic guest molecules,  
 188–189  
 CD-linked chitosan, 68–84  
 organic compounds and CD-linked chitosan,  
 75

Inclusion compound, MT and aqueous solution  
 of  $I_3^-$  or caffeine, 62, 64*f*

Inclusion foams, preparation from chitin and  
 PEG–chitin, 85–97

Independent foamability, SDS and polymers,  
 226

Induction phase, *see* Delay period

Industrial applications, polysaccharides, 299

Inflammatory disease of the eye,  
 dexamethasone, 39–40

Inorganic salt hydrates, molten, 143–150

Intensity profiles, neutral and cationic guar, 294

Interfacial film  
 CMCh, viscoelastic properties, 212*t*  
 stabilization, 210  
 surface tension, 202

Intermolecular interactions, polyelectrolytes,

surfactants, and cyclodextrins, 187–198

Intrinsic foam height, polymer or SDS  
 solutions, 226*t*

Intrinsic viscosity, cellulose derivative–solvent  
 systems, 157

Inverse thermosensitivity, synthesized  
 hydrogels, 114

Iodine affinity  
 amylopectin and amylose amounts and ratios  
 in starches, 327  
 starch analysis, 317–328

Iodine–iodide ( $I_2-I^-$ )-containing solutions,  
 separation electrolyte in electric field, 319

Ionic surfactants, viscosity, 202

## J

Junction zone  
 aqueous polymer solutions, 253  
 formation mechanism, 255  
 Polyquaternium-24–amylose complex, 256*f*

## L

*N*-Lactonoyl-1,6-hexanediamine 1, synthesis,  
 16, 18*f*

Lariat Complex  
 junction zone, 255  
 noncovalent cross-linking mechanism, 252  
 Polyquaternium-24–amylose complex, 256*f*

Lectin, interaction of conjugates, 19, 21, 22*f*

Ligands, conjugated to DNA-binding  
 compounds, 16

Light scattering, proportional to MW and  
 concentration of polymer, 299–300

Lipophilic drugs  
 biological membrane, 29–30  
 formulations, 24–25

Liquid crystals, cellulosic, 151–177

Lithium-containing melts, dissolution of  
 cellulose, 145–146

Loss modulus, Polyquaternium-24–amylose  
 complex, 260

Lubricant sensitivity, MCC and SMCC,  
 108–109

Lymphocytes, migration to other mucosal sites,  
 3

Lymphoid tissue, uptake of alginate, 12

Lyophilized chitin foam  
 SEM views, 89*f*  
 surface view, 87

Lytotropic cellulosic spherulites, optical  
 observation, 158*f*–159*f*

Lyotropic mesophases, cellulose, 161

## M

Macromolecular architectures, MW

dependence of properties, 139*t*

Macromolecular chains, rigidity, 152,157

Macroscopic shape, regenerated celluloses, 146

MACS, <sup>1</sup>H-NMR spectra, 121*f*

Magnesium stearate, MCC and SMCC,

108–109

Maltodextrin

differential molar mass plot, 308*f*

standard ladder for oligosaccharides, 324*f*

UV/VIS spectra for different oligosaccharide compositions, 320*f*

Malvern Mastersizer, effective hydrodynamic size distribution, 263

Maximum precipitation, surface tension, 226

Membrane fabrication, chitosan–Pluronic PIN membranes, 178–186

Membrane surface, aqueous diffusion layer, 29

Mesophase, mixtures, 164

Mesophase formation

cellulosic liquid crystals, 151–177

related properties, 152–168

Methazolamide in aqueous HPβCD solution, phase solubility diagram, 33*f*

Microcrystalline cellulose (MCC)

characterization of particles and compacts, 100–105

mean yield pressures and strain rate

sensitivities, 109*t*

orientation during compaction, 105–108

properties, 98–99

silicified, 98–112

tableting technology, 108–110

Microencapsulation, antigens, 3–4

Microencapsulation of cells and tissues, chitosan–Pluronic PIN membranes, 178–186

Microparticles

alginate, 1–14

bacterial load, 7

electron microscopy, 8

enzyme-linked immunosorbent assay, 8

scanning electron micrograph, 9*f*

Migration time

amylopectin and amylose bands, 319

fluorescently tagged linear maltodextrin mixtures, 321

Model drugs, controlled release, 86

Molecular cages, entrapment of ions and organic molecules, 47

Molecular motions, temperature effect, 62

Molecular necklace (MN)

CD homologues, 47

preparation for host–guest systems, 46–67 synthesis, 50*f*

Molecular recognition abilities, CD, 196

Molecular tube (MT)

α-CD condensed throughout –OH groups, 59

host–guest properties, 62

preparation for host–guest systems, 46–67

structure and dynamics, 65

synthesis, 50*f*

Molecular weights, fractionation of cellulose carbanilates, 130

Molecules in isotropic and liquid crystal phases, schematic representation, 153*f*

Molten inorganic salt hydrates

cellulose solvents, 143–150

interaction with cellulose, 144*t*

solvents for cellulose, 145*t*

Monomers used in preparation of

thermoreversible sucrogels, structures, 117*f*

Morphology, MCC and SMCC, 101

Mouse, immunization studies, 6

MQNNED, half-life data on foam, 227

MQNNED–SDS systems

half-life, surface tension, and specific

viscosity, 229*t*

surface tension plot, 225*f*

MQNNED–SDS–water system, pseudo-phase diagram, 219*f*

Mucosal immune system, linkage, 3

Mucosal immunization, oral administration of vaccines, 3

Mucosal surfaces

induction of immunity, 1–14

infectious pathogens, 1

## N

Neutral and cationic guar

comparison of neutron-scattering spectra, 296*f*

in D<sub>2</sub>O, neutron-scattering spectra, 291*f*, 293*f*

power law behavior, 292*t*

SANS, 278–298

temperature dependence of neutron-scattering spectra, 297*f*

Neutron scattering, guar, 294

Newtonian behavior, emulsions, 249*f*

Nitrophenols

chromatogram, 79*f*

inclusion complexes with α-CD-linked chitosan, 80

separation by capillary electrophoresis, 81*f*

Nonuniform particle distribution, model shell

around particles, 274  
Nutriceutical industry, CD-linked chitosan, 78

## O

Oil emulsions in presence of HEC, delay time and effective viscosity, 245*f*  
Oil volume fraction  
alkane-in-water emulsion in presence of hydroxyethyl cellulose, 266*f*  
collective movement of flocculated droplets, 267*f*  
creaming of alkane-in-water emulsion, 264*f*  
Oligosaccharide(s), cyclic, 69  
Oligosaccharide composition and branching studies, CE-LIF, 317–328  
Oligosaccharide mapping  
fine structures of amylopectin and amylose, 321–326  
manufacturing specifications, 323  
starch polysaccharides, 327  
Optical properties, solutions of cellulose derivatives, 166–168  
Oral availability, lyophilized CD complexes, 36  
Oral immunization, dilution and destruction of antigens, 1  
Oral vaccination, effectiveness, 12  
Oral vaccines, advantages and limitations to development, 3  
Order parameter, model of stiff chains, 164–165  
Organic solvents, intrinsic solubility of drugs, 31–32  
Orientation, MCC and SMCC, 105–108

## P

Parenteral immunization, limitations, 2  
Particle concentration in dispersion, ultrasonic velocity, 272  
*Pasteurella multocida*  
chickens, 3  
cultured, 8, 12  
mean colony-forming units, 11*f*  
potassium thiocyanate extract (PTE), 1  
Pasteurellosis, antigenic preparations for immunization of rabbits, 2  
PEG–chitin  
chemical structure, 88*f*  
preparation of inclusion foams, 85–97  
PEG–chitin foam  
adsorption of dyes, 87  
time course of Eriochrome Black A and Congo Red release, 96*f*

PEG–chitin gel, preparation, 86  
Penetration enhancers, dermal and other topical formulations, 30  
Penetration paths, hair, 283  
Percutaneous transport, drug–CD complexation in presence of water-soluble polymers, 24–45  
Permeability coefficients of human serum albumin, chitosan–Pluronic PIN membranes, 184*f*, 185*t*  
Permeability studies, chitosan–Pluronic PIN membranes, 182, 185  
Permeable membrane, isolation from host immune system, 178  
Persistence length  
fractal dimension, 294–295  
guar, 295, 297  
Pharmaceutical chemistry, CD-linked chitosan, 78  
Pharmaceutical functionality, SMCC, 98  
Pharmaceutical industry  
applications of guar, 287  
cyclodextrin, 25  
polysaccharides, 299  
Phase separation  
emulsions, 242–243  
mixtures of polyelectrolytes with surfactants, 193  
Polyquaternium-24–amylose complex, 257  
surfactant–polymer mixture, 207  
Phase solubility types, drug–CD complexes, 27*f*  
Physical interpenetrating network (PIN), chitosan–Pluronic, 178–186  
Plasma cells, migration to other mucosal sites, 3  
Pluronic polyol  
chemical structure, 180*f*  
permeability of products from encapsulated cells, 179  
Poly-(DL-lactide-*co*-glycolide) (DL-PLG), antigen encapsulation, 4  
Polydisperse emulsions, increasing HEC, 250  
Polyelectrolytes, interactions with charged surfactant, 188  
Polyethylene glycol (PEG), threading of  $\alpha$ -CD rings, 65  
Polyethylene glycol (PEG) chain  
binding of organic molecules and ions, 47  
length effect on threading process rate, 54  
threading kinetics of  $\alpha$ -CD units, 52–57  
Polyethylene glycol–MT,  $\tau_c(C_5)$ , 59  
Polyiodide–oligosaccharide complexes, stability, 319  
Polymer chains, relation between pitch and rigidity, 168

- Polymer conformation, influence of temperature, 297
- Polymer–polymer interactions, building aqueous viscosity, 252–261
- Polymer–surfactant complex, maximum precipitation near stoichiometric charge neutralization, 215
- Polymeric quaternary ammonium salts (polyquats), uses in cosmetics, 214
- Polyquaternium-10–SDS systems  
comparison of half-life data, 227  
interaction, 215  
surface tension and specific viscosity, 228*t*  
surface tension plot, 223*f*
- Polyquaternium-10–SDS–water system, pseudo-phase diagram, 219*f*
- Polyquaternium-24, structure, 257*f*
- Polyquaternium-24–amylose complex  
empirical data on interactions, 255*t*  
formation, 253–255
- Polyrotaxane  
formation, 48*f*  
preparation for host–guest systems, 46–67  
threaded complexes with cyclodextrin, 46–47  
transition state theory, 65
- Polysaccharide(s)  
characterization by GPC–MALS, 299–316  
inhibitory effect on denaturation of skin mucosa, 82*f*
- Polysaccharide engineering, SMCC as a pharmaceutical material, 98–112
- Polysaccharide gel structure, binary types, 254*f*
- Porosity, MCC and SMCC, 101
- Potassium thiocyanate extract (PTE), *P. multocida*, 1,4
- Potato amylopectin and potato starch  
log–log plot of root mean square radius v. molar mass, 314*f*  
 $M_w$  and  $r_{g,2}$  results for replicate analysis, 315*t*  
molar mass, GPC–LS overlay, 313*f*
- Power law behavior, neutral and cationic guar, 292
- Precipitation, maximum foam stability, 227
- Precipitation rates, stabilization by polymers, 32
- Precipitation studies, SDS, 217–221
- Processing, on-line monitoring of colloidal properties, 262
- Protein permeability studies, chitosan–Pluronic PIN membranes, 178–186
- Pullulan, characterization, 303–304
- Pullulan standards with molar mass, GPC–LS–RI overlay, 305*f*
- Pyrene fluorescence ratio, change on addition of surfactant, 209*f*
- ## Q
- Quasielastic light scattering, cellulose derivative–solvent systems, 157
- Quaternary chitosan, carrier of DNA in gene delivery, 15–23
- ## R
- $\rho$ -parameter  
function of MW for cellulose carbanilate acetates, 138*f*  
values for different polymer architectures, 139*t*
- Rabbit  
challenge studies, 8, 12  
immunization studies, 6–7  
*P. multocida* infection, 1–14
- Radius of gyration, calculation, 140
- Randomly methylated  $\beta$ CD (RM $\beta$ CD)  
characterization, 26–27  
flux from solutions through hairless mouse skin, 37*f*
- Receptor-mediated endocytosis, gene delivery, 16, 17*f*
- Recrystallization, amylose-containing starches, 321
- Regulatory status, MCC and SMCC, 110
- Re-orientational motion, activation energy, 60*f*–61*f*
- Rheology  
cellulosic mesophases, 166  
floculated emulsions, 234–251
- Rice, fine structures of amylopectin and amylose, 321–326
- Rigid rod system, polymeric liquid crystals, 161
- Rigidity, macromolecular chains, 152, 157
- ## S
- Salmonella choleraesuis* var. *kunzendorf*, swine, 3
- Scattering function, variation with angle, 300
- Scattering theory, shell–core models, 269
- SDS–CD complexes, stoichiometric ratio, 196
- Secretory IgA (sIgA), antibody isotype at mucosal sites, 2–3
- Sedimentation, characterization, 263
- Selective adsorption, CD-linked chitosan, 78
- Shampoo formulations, interactions with hair, 285

- Shear stress, Polyquaternium-24–amylose  
 complex, 258*f*, 259*f*
- Shear thinning behavior, emulsions, 249*f*
- Shell–core models, scattering theory, 269
- Silicification  
 functional improvements of SMCC over  
 MCC, 100–105  
 tensile strength and failure energy, 104
- Silicified microcrystalline cellulose (SMCC)  
 characterization of particles and compacts,  
 100–105  
 mean yield pressures and strain rate  
 sensitivities, 109*t*  
 orientation during compaction, 105–108  
 pharmaceutical functionality, 98–112  
 preparation and use, 99  
 tableting technology, 108–110
- Skin, protection from chemical penetration, 80
- Skin mucosa, denaturation inhibition by  
 polysaccharides, 80
- Small-angle neutron scattering (SANS), neutral  
 and cationic guar, 278–298
- Sodium dodecyl sulfate (SDS)  
 desorption of Polymer JR400 from hair, 279,  
 283  
 influence of cationic cellulose structure,  
 214–233  
 solution viscosity, 190–193
- Solid films  
 obtained from mesophases, 172  
 obtained from suspension of cellulose  
 crystallites, 175
- Solubility  
 drug–CD complexation in presence of water-  
 soluble polymers, 24–45  
 drugs complexed with CD, 27–28  
 drugs in solution, 34*t*
- Solubilization, random degradation, 323
- Solution behavior, cellulose carbanilates and  
 cellulose carbanilate acetates, 140
- Solution properties, cellulose  
 derivative–solvent systems, 127–142
- Solution viscosity  
 addition of SDS to JR400, 190–193  
 oppositely charged polyelectrolyte and  
 surfactant, 188  
 regulation, 193–196
- Solvent–precipitant system, fractionation of  
 cellulose carbanilates, 130
- Sorption of cationic polymers on hair,  
 fluorescence microscopy study, 276–286
- Space-forming structures, flocculated systems,  
 234
- Space-spanning structure, delay due to  
 formation, 244
- Spectroscopic approach, distribution of  
 components in dispersions, 272
- Starch, characterization, 312, 315*t*
- Starch analysis, capillary electrophoresis,  
 317–328
- Starch solution dynamics, gel networks, 321
- Static permittivity, cholesteric pitch, 166
- Steric effects, cellulosic mesophases, 157
- Sterilization, bacterial contamination of  
 antigens, 12–13
- Stiffness  
 expressed by chain parameters, 139  
 MCC and SMCC compacts, 104–105
- Storage modulus, Polyquaternium-24–amylose  
 complex, 260
- Sucrose hydrogels (sucrogels)  
 degradation in basic and acidic solution, 125*f*  
 synthesis and characterization, 113–126  
 temperature dependence of swelling and  
 swelling kinetics, 118  
 temperature-dependent swelling and  
 shrinking, 124*f*  
 thermoreversible and degradable properties,  
 113–126  
 thermosensitive volume change, 121*f*
- Sucrose monomers  
 synthesis, 114–116, 118–119  
 synthetic reaction scheme, 115*f*
- Sugar chain, multiantennary, 15
- Surface tension  
 carboxymethylchitins and cationic surfactant,  
 202  
 evolution with time, 211*f*  
 foam stability, 227  
 fraction of ion pairs formed, 212  
 function of surfactant concentration at fixed  
 polymer concentration, 221–226  
 polyelectrolyte–surfactant complexes, 231  
 variation on addition of TTAB, 204*f*
- Surfactants  
 increased solubilizing effect, 32  
 interaction with chitin derivatives, 199–213  
 micelle-like aggregates with polymers, 188
- Surfactant aggregates, association with  
 oppositely charged polymer, 187–198
- Surfactant–CD inclusion complex formation,  
 1:1 stoichiometry, 193–195
- Swelling profiles, temperature-dependent,  
 119–122
- Swelling studies, chitosan–Pluronic PIN  
 membranes, 182
- Synergistic interaction, polymers, 252–261

## T

- Tablet formulations, MCC, 98
- Tablet strength  
 compaction pressure, 108  
 SMCC, 99
- Tableting technology, MCC and SMCC,  
 108–110
- Tensile strength, compacts of MCC and SMCC,  
 103–104
- Tensile strength and failure energies, MCC and  
 SMCC, 104*t*
- Tensile test load–deflection data, compacts of  
 MCC and SMCC, 105*f*
- N*-[Tetragalactose antenna]-1,6-hexanediamine  
 3, synthesis, 16–17, 18*f*
- Textures, cellulose and cellulose derivatives,  
 152
- Thermodynamic stability, cellulosic  
 mesomorphic polymer mixture, 164
- Thermoresponsive hydrogels,  
 copolymerization, 122
- Thermoreversible hydrogels  
 degradation, 118, 125  
 synthesis, 116  
 synthesis and characterization, 113–126
- Thermosensitive sucrogels, copolymerization,  
 122
- Thermosensitivity, type of sucrose monomers,  
 122
- Thermotropic cellulose derivatives, relation  
 between pitch and rigidity, 168
- Thermotropic mesophases, behavior, 157, 161
- Thermotropic polymers, transition temperature  
*v.* degree of polymerization, 162*f*
- Thioxtropy curve, Polyquaternium-24–amylose  
 complex, 258*f*
- Threading process  
 $\alpha$ -CD and PEG mixture, 65  
 kinetics, 47, 52–57  
 thermodynamic parameters, 55–57
- Threading time  
 concentration of  $\alpha$ -CD and PEG, 58*f*  
 detectable increment in absorbance, 52  
 variation as function of temperature, 53*f*
- TM-chitosan–galactose conjugate, synthesis,  
 19, 20*f*, 21
- Transient gelation, *see* Delay period
- Triamcinolone acetamide flux, through  
 cellophane membrane, 31*f*
- Tricarbanilate solution, persistence length and  
 hydrodynamic radius, 160*f*
- Turbidity, serum layer, 238–240

## U

- Ultrasonic attenuation, differences in size  
 distribution, 269
- Ultrasonic attenuation spectra  
 bridging and depletion flocculated  
 polystyrene-in-water with HEC, 273*f*  
 polystyrene-in-water suspension with  
 adsorbed layers, 271*f*  
 sucrose crystals dispersed in saturated sugar  
 solution, 270*f*
- Ultrasonic characterization techniques,  
 application to colloidal dispersions,  
 262–275
- Ultrasonic monitoring  
 creaming behavior of emulsions, 240–244  
 creaming profiles, 240*f*, 241*f*, 242*f*
- Ultrasonic properties, theory, 268–269
- Ultrasonic scattering, two-phase media, 272
- Ultrasonic spectroscopy, dispersion  
 composition and particle size, 268–269
- Ultrasonic velocity  
 honey during crystallization, 270*f*  
 sucrose crystals dispersed in saturated sugar  
 solution, 270*f*  
 supersaturated solution of fructose in  
 glucose, 268

## V

- Vaccination, standard methods, 2
- Vaccine delivery, alginate microparticles, 1–14
- Viscoelastic characteristics, surfactant–polymer  
 mixture, 210
- Viscoelastic film, surfactant concentration, 212
- Viscosity  
 addition of SDS to JR400, 190–193  
 alkylchitosans, 201  
 aqueous solutions of JR400 and SDS, 194*f*  
 building through synergistic  
 polymer–polymer interactions, 252–261  
 correlation with delay time, 250*f*  
 dilute solution of CMCh and TTAB, 203*f*  
 foam stability, 227  
 Polyquaternium-24–amylose complex, 257,  
 258*f*, 259*f*
- Viscosity enhancement  
 aqueous surfactant–polymer solutions, 192*f*  
 CD, 189  
 inclusion complexes, 187–198  
 polyelectrolyte, surfactants, and  
 cyclodextrins, 196

Visual creaming, in measuring cylinders,  
237–240

## W

Water, dissolved interacting polymers, 253

Water-soluble polymers

applications, 187–189

CD complexation efficacy, 32–33

foaming of SDS solutions, 231

fluorescence probes, 276

presence of drug–CD complexation, 24–45

Wet granulation, tensile strength of resulting  
tablets, 108

Wool fiber, surface adsorption, 283

Wormlike chains

approximation model, 152, 157

calculation of properties, 139–140

fractal dimension, 294–295

monodispersed system, 157

## X

Xanthan

characterization, 309

$M_w$  and  $r_{g,z}$  results, 310*r*

## Y

Yield stress

determination, 247–248

determination by “eye” method, 248*f*

flocculation during delay period, 247–249

oil volume fraction and HEC concentration,  
248

## Z

Zero-shear viscosity

$\alpha$ - and  $\beta$ -CD, 193

v. CD concentration plot, 195*f*

Zimm formalism, representative slice of narrow  
band pullulan polysaccharide, 302*f*